

The Great Observatories All-Sky LIRG Survey: *Herschel* Image Atlas and Aperture Photometry¹

Jason K. Chu¹, D. B. Sanders¹, K. L. Larson^{1,2}, J. M. Mazzarella², J. H. Howell², T. Díaz-Santos^{2,3}, K. C. Xu⁴, R. Paladini⁴, B. Schulz⁴, D. Shupe⁴, P. Appleton⁴, L. Armus², N. Billot⁵, B. H. P. Chan², A. S. Evans^{6,7}, D. Fadda², D. T. Frayer⁷, S. Haan⁷, C. M. Ishida⁸, K. Iwasawa⁹, D.-C. Kim⁷, S. Lord¹⁰, E. Murphy⁷, A. Petric¹¹, G. C. Privon¹², J. A. Surace¹³, E. Treister¹²

ABSTRACT

Far-infrared (FIR) images and photometry are presented for 201 Luminous and Ultraluminous Infrared Galaxies [LIRGs: $\log(L_{\text{IR}}/L_{\odot}) = 11.00 - 11.99$, ULIRGs: $\log(L_{\text{IR}}/L_{\odot}) = 12.00 - 12.99$], in the Great Observatories All-Sky LIRG Survey (GOALS) based on observations with the *Herschel Space Observatory* Photodetector Array Camera and Spectrometer (PACS) and the Spectral and Photometric Imaging Receiver (SPIRE) instruments. The image atlas displays each GOALS target in the three PACS bands (70, 100, and 160 μm) and the three SPIRE bands (250, 350, and 500 μm), optimized to reveal structures at both high and low surface brightness levels, with images scaled to simplify comparison of structures in the same physical areas of $\sim 100 \times 100 \text{ kpc}^2$. Flux densities of companion galaxies in merging systems are provided where possible, depending on their angular separation and the spatial resolution in each passband, along with integrated system fluxes (sum of components). This dataset constitutes the imaging and photometric component of the GOALS *Herschel* OT1 observing program, and is complementary to atlases presented for the *Hubble Space Telescope* (Evans et al. 2017, in prep.), *Spitzer Space Telescope* (Mazzarella et al. 2017, in prep.), and *Chandra X-ray Observatory* (Iwasawa et al. 2011, 2017, in prep.). Collectively these data will enable a wide range of detailed studies of AGN and starburst activity within the most luminous infrared galaxies in the local Universe.

Subject headings: atlases — galaxies: active — galaxies: interactions — galaxies: starburst — galaxies: structure — infrared: galaxies

¹Institute for Astronomy, University of Hawaii, 2680 Woodlawn Drive, Honolulu, HI 96822; jasonchu@ifa.hawaii.edu, sanders@ifa.hawaii.edu

²Infrared Processing & Analysis Center, MS 100-22, California Institute of Technology, Pasadena, CA 91125; bchan, jhhowell, klarson, lee, mazz@ipac.caltech.edu, fadda@discovery.saclay.cea.fr

³Nucleo de Astronomía de la Facultad de Ingeniería, Universidad Diego Portales, Av. Ejercito Libertador 441, Santiago, Chile; tanio.diaz@mail.udp.cl

⁴NASA Herschel Science Center, MS 100-22, California Institute of Technology, Pasadena, CA 91125; apple, bschulz, cxu, paladini, shupe@ipac.caltech.edu

⁵Observatoire de l'Université de Genève, 51 chemin des Maillettes, 1290 Versoix, Switzerland; billot@iram.es

⁶Department of Astronomy, University of Virginia, Charlottesville, VA 22904-4325; aevans@virginia.edu

⁷National Radio Astronomy Observatory, 520 Edgemont Road, Charlottesville, VA 22903-2475; dfrayer, dkim, emurphy@nrao.edu, sebhaha@gmail.com

⁸Department of Physics and Astronomy, University of Hawaii at Hilo, Hilo, HI, 96720; cishida@hawaii.edu

⁹ICREA and Institut del Ciències del Cosmos (ICC), Universi-

1. Introduction

The Great Observatories All-Sky LIRG Survey (GOALS, Armus et al. 2009), combines both imaging and spectroscopic data for the complete sample of 201 Luminous Infrared Galaxies (LIRGs:

tat de Barcelona (IEEC-UB), Martí i Franquès 1, 08028 Barcelona, Spain; kazushi.iwasawa@icc.ub.edu

¹⁰SETI Institute; slord@seti.org

¹¹Canada France Hawaii Telescope Corp., Concepción, Chile; petric@cfht.hawaii.edu

¹²Instituto de Astrofísica, Facultad de Física, Pontificia Universidad Católica de Chile, Casilla 306, Santiago 22, Chile; gprivon, etreiste@astro.puc.cl

¹³Spitzer Science Center, MS 314-6, California Institute of Technology, Pasadena, CA 91125; jason@ipac.caltech.edu

¹Based on *Herschel Space Observatory* observations. *Herschel* is an ESA space observatory with science instruments provided by European-led Principal Investigator consortia and with important participation from NASA.

$\log(L_{\text{IR}}/L_{\odot}) > 11.0$) selected from the IRAS Revised Bright Galaxy Sample (RBGS, Sanders et al. 2003). The full RBGS contains 629 objects, representing a complete sample of extragalactic sources with IRAS 60 μm flux density, $S_{60} > 5.24 \text{ Jy}$, covering the entire sky above a Galactic latitude of $|b| > 5^{\circ}$. The median redshift of objects in the GOALS sample is $\langle z \rangle = 0.021$, with a maximum redshift of $z_{\text{max}} = 0.0876$. As the nearest and brightest 60 μm extragalactic objects, they represent a sample that is the most amenable for study at all wavelengths.

The primary objective of the GOALS multi-wavelength survey is to fully characterize the diversity of properties observed in a large, statistically significant sample of the nearest LIRGs. This allows us to probe the full range of phenomena such as normal star formation, starbursts, and active galactic nuclei (AGN) that power the observed far-infrared emission, as well as to better characterize the range of galaxy types (i. e. normal disks, major and minor interactions/mergers, etc.) that are associated with the LIRG phase. A secondary objective is to provide a data set that is ideally suited for comparison with LIRGs observed at high redshifts.

GOALS currently includes imaging and spectroscopy from the *Spitzer*, *Hubble*, *GALEX*, *Chandra*, *XMM-Newton*, and now *Herschel* space-borne observatories, along with complementary ground-based observations from ALMA, Keck, and other telescopes. The GOALS project is described in more detail at <http://goals.ipac.caltech.edu/>.

Due to limitations in angular resolution, wavelength coverage, and sensitivity of pre-*Herschel* (IRAS, ISO, Spitzer, AKARI) far-infrared (FIR) data, the spatial distribution of FIR emission within the GOALS sources, and the total amount of gas and dust in these systems, are poorly determined. The *Herschel* data will allow us for the first time to directly probe the critical FIR and submillimeter wavelength regime of these infrared luminous systems, enabling us to accurately determine the bolometric luminosities, infrared surface brightnesses, star formation rates, and dust masses and temperatures on spatial scales of 2 – 5 kpc within the GOALS sample.

This paper presents imaging and photometry for all 201 LIRGs and LIRG systems in the IRAS RBGS that were observed during our GOALS *Herschel* OT1 program. A more complete description of the GOALS sample is given in §2. The data acquisition is described in §3 and data reduction procedures are discussed in §4. The image atlas is presented in §5, and photomet-

ric measurements are given in §6. Section 7 contains a discussion of basic results, including comparisons with prior measurements, and a summary is given in §8. A reference cosmology of $\Omega_{\Lambda} = 0.72$, $\Omega_m = 0.28$ and $H_0 = 70 \text{ km sec.}^{-1} \text{ Mpc}^{-1}$ is adopted, however we also take into account local non-cosmological effects by using the three-attractor model of Mould et al. (2000).

2. The GOALS Sample

The IRAS RBGS contains a total of 179 LIRGs ($\log(L_{\text{IR}}/L_{\odot}) = 11.0\text{--}11.99$), and 22 ultra-luminous infrared galaxies (ULIRGs: $\log(L_{\text{IR}}/L_{\odot}) \geq 12.0$); these 201 objects comprise the GOALS sample (Arribas et al. 2009), a statistically complete flux-limited sample of infrared-luminous galaxies in the local universe. In addition to the *Herschel* observations reported here, the GOALS objects have been the subject of an intense multi-wavelength observing campaign, including VLA 20 cm (Condon et al. 1990, 1996), millimeter wave spectral line observations of CO(1→0) emission (Sanders et al. 1991), sub-millimeter imaging at 450 μm and 850 μm (Dunne et al. 2000), near-infrared images from 2MASS (Skrutskie et al. 2006), optical and K-band imaging (Ishida 2004), as well as space-based imaging from the *Spitzer Space Telescope* (IRAC and MIPS, Mazzarella et al. 2017, in prep), *Hubble Space Telescope* (ACS, Evans et al. 2017, in prep.), *GALEX* (NUV and FUV, Howell et al. 2010), and the *Chandra X-ray Observatory* (ACIS, Iwasawa et al. 2011, 2017 in prep). Extensive spectroscopy data also exist on the GOALS sample, such as in the optical (Kim et al. 1995) and with *Spitzer* IRS in the mid-infrared (Stierwalt et al. 2013). *Herschel* PACS spectroscopy was obtained in Cycles 1 and 2 targeting the [C II] 157.7 μm , [O I] 63.2 μm , and [O III] 88 μm emission lines and the OH 79 μm absorption feature for the entire sample, as well as the [N II] 122 μm line in 122 GOALS galaxies (Díaz-Santos et al. 2013, 2014, 2017 in prep). In addition, *Herschel* SPIRE FTS spectroscopy were obtained to probe the CO spectral line energy distribution from $J = 4 \rightarrow 3$ up to $J = 13 \rightarrow 12$ for 93 of the GOALS objects (Lu et al. 2014, 2015, 2017, submitted), as well as the [N II] 205 μm emission line for 122 objects Zhao et al. (2013, 2016).

Out of the original list of 203 GOALS systems, two were omitted from our *Herschel* sample, making for a final tally of 201 objects. IRAS F13097–1531

(NGC 5010) was part of the original RBGS sample of Sanders et al. (2003), however due to a revision in the redshift of the object it was much closer than thought. This caused the resulting far-IR luminosity to drop significantly below the LIRG threshold of $10^{11} L_{\odot}$. The other object we excluded from our sample is IRAS 05223+1908, which we believe is a young stellar object (YSO), due to the fact that its spectral energy distribution (SED) peaks in the submillimeter part of the spectrum.

Table 1 presents the basic GOALS information. Column 1 is the index number of galaxies in the GOALS sample, and correspond to the same galaxies in Tables 2, 3, and 4. Column 2 is the IRAS name of the galaxy, ordered by ascending RA. Galaxies with the “F” prefix originate from the *IRAS* Faint Source Catalog, and galaxies with no “F” prefix are from the Point Source Catalog. Column 3 is a list of common optical counterpart names. Columns 4 and 5 are the *Spitzer* 8 μm centers of the system in J2000 from Mazzarella et al. (2017). For galaxy systems with two or more components, the coordinate is taken to be the geometric midpoint between the component galaxies. Column 6 gives the angular diameter distance to the galaxy in Mpc, from Mazzarella et al. (2017). Column 7 is the map size used in the atlas, denoting the physical length of a side in each atlas image in kpc. Column 8 is the systemic heliocentric redshift of the galaxy system, and Column 9 is the measured heliocentric radial velocity in km sec^{-1} , that corresponds to the redshift. Both of these columns take into account cosmological as well as non-cosmological effects (see Mould et al. 2000). Finally Column 10 is the indicative 8–1000 μm infrared luminosity in $\log(L_{\text{IR}}/L_{\odot})$ of the entire system from Armus et al. (2009). Similar to Columns 8 and 9, the L_{IR} values in Table 1 take into account the effect of the local attractors to D_A , than one would normally obtain from pure cosmological effect.

TABLE 1
BASIC GOALS DATA

#	IRAS Name	Optical Name	Right Ascension	Declination	D_A	Map Size	Redshift	Velocity	L_{IR}
—	—	—	HH : MM : SS	DD : MM : SS	Mpc	kpc	—	km s ⁻¹	$\log\left(\frac{L}{L_\odot}\right)$
(1)	(2)	(3)	(4)	(5)	(6)	(7)	(8)	(9)	(10)
1	F00073+2538	NGC 23	00 : 09 : 53.36	+25 : 55 : 27.7	63.3	100	0.01523	4566	11.12
2	F00085-1223	NGC 34, Mrk 938	00 : 11 : 06.56	-12 : 06 : 28.2	81.5	100	0.01962	5881	11.49
3	F00163-1039	Arp 256, MCG-02-01-051/2	00 : 18 : 50.37	-10 : 22 : 05.3	111.4	150	0.02722	8159	11.48
4	F00344-3349	ESO 350-IG 038, Haro 11	00 : 36 : 52.49	-33 : 33 : 17.2	85.4	100	0.0206	6175	11.28
5	F00402-2349	NGC 232	00 : 42 : 49.32	-23 : 33 : 04.3	91.3	150	0.02217	6647	11.44
6	F00506+7248	MCG+12-02-001	00 : 54 : 03.88	+73 : 05 : 05.9	67.7	100	0.0157	4706	11.50
7	F00548+4331	NGC 317B	00 : 57 : 39.72	+43 : 47 : 47.7	74.1	100	0.01811	5429	11.19
8	F01053-1746	IC 1623, Arp 236	01 : 07 : 47.54	-17 : 30 : 25.6	82.2	100	0.02007	6016	11.71
9	F01076-1707	MCG-03-04-014	01 : 10 : 08.93	-16 : 51 : 09.9	134.8	100	0.03349	10040	11.65
10	F01159-4443	ESO 244-G012	01 : 18 : 08.27	-44 : 27 : 51.9	87.7	100	0.02104	6307	11.38
11	F01173+1405	CGCG 436-030	01 : 20 : 02.63	+14 : 21 : 42.3	82.2	100	0.03123	9362	11.69
12	F01325-3623	ESO 353-G020	01 : 34 : 51.26	-36 : 08 : 14.4	82.2	100	0.016	4797	11.06
13	F01341-3735	RR 032, ESO 297-G011/012	01 : 36 : 23.76	-37 : 19 : 51.9	72	100	0.01732	5191	11.16
14	F01364-1042		01 : 38 : 52.79	-10 : 27 : 12.1	191.1	150	0.04825	14464	11.85
15	F01417+1651	III Zw 035	01 : 44 : 30.56	+17 : 06 : 09.0	112.6	100	0.02794	8375	11.64
16	F01484+2220	NGC 695	01 : 51 : 14.34	+22 : 34 : 56.0	130.4	100	0.03247	9735	11.68
17	F01519+3640	UGC 01385	01 : 54 : 57.78	+36 : 55 : 07.9	76.9	100	0.01875	5621	11.05
18	F02071-1023	NGC 838	02 : 09 : 31.84	-10 : 09 : 30.7	53.3	130	0.01285	3851	11.05
19	F02070+3857	NGC 828	02 : 10 : 09.53	+39 : 11 : 24.7	73.6	100	0.01793	5374	11.36
20	F02114+0456	IC 214	02 : 14 : 00.77	+05 : 10 : 13.8	122.4	175	0.03022	9061	11.43
21	F02152+1418	NGC 877	02 : 17 : 56.46	+14 : 31 : 58.2	52.9	75	0.01305	3913	11.10
22	F02203+3158	MCG+05-06-036	02 : 23 : 20.47	+32 : 11 : 33.6	135.7	100	0.03371	10106	11.64
23	F02208+4744	UGC 01845	02 : 24 : 07.97	+47 : 58 : 11.9	65	100	0.01561	4679	11.12
24	F02281-0309	NGC 958	02 : 30 : 42.84	-02 : 56 : 20.5	77.6	100	0.01914	5738	11.20
25	F02345+2053	NGC 992	02 : 37 : 25.46	+21 : 06 : 02.8	56.4	50	0.01381	4141	11.07
26	F02401-0013	NGC 1068	02 : 42 : 40.72	-00 : 00 : 47.9	15.8	50	0.00379	1137	11.40
27	F02435+1253	UGC 02238	02 : 46 : 17.46	+13 : 05 : 44.6	88.5	100	0.02188	6560	11.33
28	F02437+2122		02 : 46 : 39.13	+21 : 35 : 10.4	94.4	50	0.02331	6987	11.16
28	F02437+2123 ^a	2MASX J02464505+2133234	02 : 46 : 45.05	+21 : 33 : 23.5	94.4	50	0.02331	6987	11.16
29	F02512+1446	UGC 02369	02 : 54 : 01.79	+14 : 58 : 26.0	127.7	100	0.03188	9558	11.67
30	F03117+4151	UGC 02608	03 : 15 : 01.47	+42 : 02 : 08.6	95.5	100	0.02334	6998	11.41
30	F03117+4151 ^a	UGC 02612	03 : 15 : 14.58	+41 : 58 : 50.0	95.5	100	0.02334	6998	11.41
31	F03164+4119	NGC 1275	03 : 19 : 48.18	+41 : 30 : 42.0	72.4	100	0.01756	5264	11.26
32	F03217+4022		03 : 25 : 05.37	+40 : 33 : 32.2	95.5	100	0.02337	7007	11.33
33	F03316-3618	NGC 1365	03 : 33 : 36.40	-36 : 08 : 25.9	17.7	65	0.00546	1636	11.00
34	F03359+1523		03 : 38 : 47.07	+15 : 32 : 54.1	141.8	100	0.0354	10613	11.55
35	F03514+1546	CGCG 465-012	03 : 54 : 15.95	+15 : 55 : 43.4	90.1	75	0.02222	6662	11.20
35	F03514+1546 ^a	CGCG 465-011	03 : 54 : 07.67	+15 : 59 : 24.3	90.1	75	0.02222	6662	11.20
36	03582+6012		04 : 02 : 32.47	+60 : 20 : 40.0	123.5	100	0.03001	8997	11.43
37	F04097+0525	UGC 02982	04 : 12 : 22.68	+05 : 32 : 49.1	72.3	100	0.0177	5305	11.20
38	F04118-3207	ESO 420-G013	04 : 13 : 49.70	-32 : 00 : 25.3	49.8	50	0.01191	3570	11.07
39	F04191-1855	ESO 550-IG 025	04 : 21 : 20.04	-18 : 48 : 48.4	130	100	0.03209	9621	11.51
40	F04210-4042	NGC 1572	04 : 22 : 42.81	-40 : 36 : 03.1	85.1	100	0.02038	6111	11.30
41	04271+3849		04 : 30 : 33.09	+38 : 55 : 47.8	77.8	100	0.01881	5640	11.11
42	F04315-0840	NGC 1614	04 : 33 : 59.95	-08 : 34 : 46.6	65.7	100	0.01594	4778	11.65
43	F04326+1904	UGC 03094	04 : 35 : 33.81	+19 : 10 : 18.0	100.9	100	0.02471	7408	11.41
44	F04454-4838	ESO 203-IG001	04 : 46 : 49.55	-48 : 33 : 30.6	212	100	0.05291	15862	11.86
45	F04502-3304	MCG-05-12-006	04 : 52 : 04.96	-32 : 59 : 26.0	78.3	100	0.01875	5622	11.17
46	F05053-0805	NGC 1797	05 : 07 : 44.84	-08 : 01 : 08.7	61.6	100	0.01481	4441	11.04

TABLE 1—Continued

#	IRAS Name	Optical Name	Right Ascension	Declination	D_A	Map Size	Redshift	Velocity	L_{IR}
—	—	—	HH : MM : SS	DD : MM : SS	Mpc	kpc	—	km s ⁻¹	$\log\left(\frac{L}{L_{\odot}}\right)$
(1)	(2)	(3)	(4)	(5)	(6)	(7)	(8)	(9)	(10)
46	F05053-0805 ^a	NGC 1799	05 : 07 : 44.59	-07 : 58 : 09.0	61.6	80	0.01481	4441	11.04
47	F05054+1718	CGCG 468-002	05 : 08 : 20.46	+17 : 21 : 57.8	75.1	100	0.01819	5454	11.22
48	05083+2441		05 : 11 : 27.46	+24 : 45 : 41.1	94.8	100	0.02307	6915	11.26
49	F05081+7936	VII Zw 031	05 : 16 : 46.39	+79 : 40 : 12.9	216.2	200	0.05367	16090	11.99
50	05129+5128		05 : 16 : 55.96	+51 : 31 : 56.9	113.7	100	0.02743	8224	11.42
51	F05189-2524		05 : 21 : 01.45	-25 : 21 : 46.2	172	100	0.04256	12760	12.16
52	F05187-1017		05 : 21 : 06.53	-10 : 14 : 46.2	115.4	100	0.02827	8474	11.30
53	05368+4940	MCG+08-11-002	05 : 40 : 43.70	+49 : 41 : 41.6	80.6	100	0.01916	5743	11.46
54	F05365+6921	NGC 1961	05 : 42 : 04.55	+69 : 22 : 42.8	57.5	100	0.01312	3934	11.06
55	F05414+5840	UGC 03351	05 : 45 : 48.03	+58 : 42 : 03.6	63.9	100	0.01486	4455	11.28
56	05442+1732		05 : 47 : 08.49	+17 : 33 : 29.1	77.4	100	0.01862	5582	11.30
57	F06076-2139		06 : 09 : 45.84	-21 : 40 : 28.3	153.3	100	0.03745	11226	11.65
58	F06052+8027	UGC 03410	06 : 14 : 13.75	+80 : 27 : 47.1	56.9	100	0.01308	3921	11.10
59	F06107+7822	NGC 2146	06 : 18 : 37.82	+78 : 21 : 24.0	17.4	50	0.00298	893	11.12
60	F06259-4708	ESO 255-IG007	06 : 27 : 22.39	-47 : 10 : 49.4	160.3	100	0.03879	11629	11.90
61	F06295-1735	ESO 557-G002	06 : 31 : 46.45	-17 : 38 : 00.7	89.5	100	0.0213	6385	11.25
62	F06538+4628	UGC 03608	06 : 57 : 34.41	+46 : 24 : 10.6	90.4	100	0.02135	6401	11.34
63	F06592-6313		06 : 59 : 40.26	-63 : 17 : 52.4	99.4	100	0.02296	6882	11.24
64	F07027-6011	AM 0702-601	07 : 03 : 26.33	-60 : 16 : 02.7	132.6	150	0.03132	9390	11.64
65	07063+2043	NGC 2342	07 : 09 : 15.04	+20 : 37 : 10.7	75	110	0.0176	5276	11.31
66	F07160-6215	NGC 2369	07 : 16 : 37.73	-62 : 20 : 36.4	46.6	70	0.01081	3240	11.16
67	07251-0248		07 : 27 : 37.62	-02 : 54 : 54.8	338.2	200	0.08756	26249	12.39
68	F07256+3355	NGC 2388	07 : 28 : 46.38	+33 : 50 : 22.9	59.7	220	0.01379	4134	11.28
69	F07329+1149	MCG-02-20-003	07 : 35 : 43.44	+11 : 42 : 34.8	72	100	0.01625	4873	11.13
69	F07329+1149 ^a	NGC 2416	07 : 35 : 41.53	+11 : 36 : 42.1	72	100	0.01625	4873	11.13
70	08355-4944		08 : 37 : 01.87	-49 : 54 : 30.0	112.1	100	0.0259	7764	11.62
71	F08339+6517		08 : 38 : 23.18	+65 : 07 : 15.2	83.1	100	0.01911	5730	11.11
72	F08354+2555	NGC 2623	08 : 38 : 24.11	+25 : 45 : 16.5	81.1	100	0.01851	5549	11.60
73	08424-3130	ESO 432-IG006	08 : 44 : 28.07	-31 : 41 : 40.5	72.1	100	0.01616	4846	11.08
74	F08520-6850	ESO 060-IG016	08 : 52 : 31.28	-69 : 01 : 57.0	191.8	100	0.04632	13885	11.82
75	F08572+3915		09 : 00 : 25.35	+39 : 03 : 54.0	235.7	200	0.05835	17493	12.16
76	09022-3615		09 : 04 : 12.69	-36 : 27 : 01.5	241.4	200	0.05964	17880	12.31
77	F09111-1007		09 : 13 : 37.69	-10 : 19 : 24.6	221.4	200	0.05414	16231	12.06
78	F09126+4432	UGC 04881	09 : 15 : 55.10	+44 : 19 : 54.0	164.7	150	0.03953	11851	11.74
79	F09320+6134	UGC 05101	09 : 35 : 51.59	+61 : 21 : 11.9	163.8	100	0.03937	11802	12.01
80	F09333+4841	MCG+08-18-013	09 : 36 : 34.02	+48 : 28 : 18.8	109.8	150	0.02594	7777	11.34
81	F09437+0317	Arp 303, IC 0563/4	09 : 46 : 20.70	+03 : 03 : 30.4	89.3	150	0.02	5996	11.23
82	F10015-0614	NGC 3110	10 : 03 : 59.57	-06 : 29 : 08.5	75.2	95	0.01686	5054	11.37
83	F10038-3338	ESO 374-IG 032	10 : 06 : 04.65	-33 : 53 : 06.1	145.9	130	0.0341	10223	11.78
84	F10173+0828		10 : 20 : 00.24	+08 : 13 : 32.8	203.5	200	0.04909	14716	11.86
85	F10196+2149	NGC 3221	10 : 22 : 19.98	+21 : 34 : 10.6	63.9	80	0.01371	4110	11.09
86	F10257-4339	NGC 3256	10 : 27 : 51.30	-43 : 54 : 14.0	38.2	50	0.00935	2804	11.64
87	F10409-4556	ESO 264-G036	10 : 43 : 07.51	-46 : 12 : 44.1	95.9	100	0.02101	6299	11.32
88	F10567-4310	ESO 264-G057	10 : 59 : 01.70	-43 : 26 : 25.2	80.5	100	0.0172	5156	11.14
89	F10565+2448		10 : 59 : 18.15	+24 : 32 : 34.2	147.6	100	0.0431	12921	12.08
90	F11011+4107	MCG+07-23-019	11 : 03 : 53.98	+40 : 51 : 00.4	147.6	100	0.03452	10350	11.62
91	F11186-0242	CGCG 011-076	11 : 21 : 10.26	-02 : 59 : 20.8	110.5	100	0.0249	7464	11.43
92	F11231+1456	IC 2810	11 : 25 : 47.31	+14 : 40 : 21.2	146	200	0.034	10192	11.64
93	F11255-4120	ESO 319-G022	11 : 27 : 54.18	-41 : 36 : 51.7	77.4	100	0.01635	4902	11.12

TABLE 1—Continued

#	IRAS Name	Optical Name	Right Ascension HH : MM : SS	Declination DD : MM : SS	D_A Mpc	Map Size kpc	Redshift —	Velocity km s ⁻¹	L_{IR} $\log\left(\frac{L}{L_{\odot}}\right)$
(1)	(2)	(3)	(4)	(5)	(6)	(7)	(8)	(9)	(10)
94	F11257+5850	NGC 3690, Arp 299	11 : 28 : 32.35	+58 : 33 : 43.3	49.7	100	0.01032	3093	11.93
95	F11506-3851	ESO 320-G030	11 : 53 : 11.73	-39 : 07 : 49.0	40.3	50	0.01078	3232	11.17
96	F12043-3140	ESO 440-IG058	12 : 06 : 51.78	-31 : 56 : 52.8	107	100	0.0232	6956	11.43
97	F12112+0305		12 : 13 : 46.02	+02 : 48 : 42.2	295.1	200	0.07332	21980	12.36
98	F12116+5448	NGC 4194	12 : 14 : 09.71	+54 : 31 : 35.5	42.3	50	0.00834	2501	11.10
99	F12115-4656	ESO 267-G030	12 : 14 : 12.81	-47 : 13 : 42.5	93	100	0.01849	5543	11.25
99	F12115-4656 ^a	ESO 267-G029	12 : 13 : 52.28	-47 : 16 : 25.4	93	100	0.01849	5543	11.25
100	12116-5615		12 : 14 : 22.08	-56 : 32 : 32.7	121.3	100	0.0271	8125	11.65
101	F12224-0624		12 : 25 : 03.90	-06 : 40 : 52.1	118.7	100	0.02636	7902	11.36
102	F12243-0036	NGC 4418	12 : 26 : 59.74	-00 : 53 : 32.1	36.3	60	0.00727	2179	11.19
103	F12540+5708	UGC 08058, Mrk 231	12 : 56 : 14.25	+56 : 52 : 24.8	176.8	150	0.04217	12642	12.57
104	F12590+2934	NGC 4922	13 : 01 : 24.89	+29 : 18 : 39.6	105.9	100	0.02359	7071	11.38
105	F12592+0436	CGCG 043-099	13 : 01 : 50.28	+04 : 20 : 00.8	162.6	150	0.03748	11237	11.68
106	F12596-1529	MCG-02-33-098	13 : 02 : 20.02	-15 : 46 : 01.8	76.3	100	0.01592	4773	11.17
107	F13001-2339	ESO 507-G070	13 : 02 : 52.42	-23 : 55 : 17.8	101.5	100	0.0217	6506	11.56
108	13052-5711		13 : 08 : 18.73	-57 : 27 : 30.3	101.6	100	0.02123	6364	11.40
109	F13126+2453	IC 0860	13 : 15 : 03.49	+24 : 37 : 07.6	55.6	100	0.01116	3347	11.14
110	13120-5453		13 : 15 : 06.37	-55 : 09 : 22.5	135.5	120	0.03076	9222	12.32
111	F13136+6223	VV 250a	13 : 15 : 32.82	+62 : 07 : 37.4	133.1	150	0.03107	9313	11.81
112	F13182+3424	UGC 08387	13 : 20 : 35.37	+34 : 08 : 22.2	105	100	0.0233	6985	11.73
113	F13188+0036	NGC 5104	13 : 21 : 23.09	+00 : 20 : 33.2	87.5	100	0.01861	5578	11.27
114	F13197-1627	MCG-03-34-064	13 : 22 : 21.73	-16 : 43 : 06.2	79.5	100	0.01654	4959	11.28
115	F13229-2934	NGC 5135	13 : 25 : 44.02	-29 : 50 : 00.4	59.3	100	0.01369	4105	11.30
116	13242-5713	ESO 173-G015	13 : 27 : 23.79	-57 : 29 : 21.8	33.3	50	0.00973	2918	11.38
117	F13301-2356	IC 4280	13 : 32 : 53.40	-24 : 12 : 25.5	79.8	100	0.01631	4889	11.15
118	F13362+4831	NGC 5256	13 : 38 : 17.52	+48 : 16 : 37.2	122.1	100	0.02782	8341	11.56
119	F13373+0105	Arp 240, NGC 5257/8	13 : 39 : 55.34	+00 : 50 : 09.5	103.8	150	0.02261	6778	11.62
120	F13428+5608	UGC 08696, Mrk 273	13 : 44 : 42.12	+55 : 53 : 13.1	160.6	100	0.03778	11326	12.21
121	F13470+3530	UGC 08739	13 : 49 : 13.94	+35 : 15 : 26.2	78.7	90	0.01679	5032	11.15
122	F13478-4848	ESO 221-IG010	13 : 50 : 56.92	-49 : 03 : 18.8	61.6	100	0.01034	3099	11.22
123	F13497+0220	NGC 5331	13 : 52 : 16.32	+02 : 06 : 18.0	145.2	100	0.03304	9906	11.66
124	F13564+3741	Arp 84, NGC 5394/5	13 : 58 : 35.80	+37 : 26 : 20.5	57.3	100	0.01161	3482	11.08
125	F14179+4927	CGCG 247-020	14 : 19 : 43.27	+49 : 14 : 11.9	114.1	100	0.02574	7716	11.39
126	F14280+3126	NGC 5653	14 : 30 : 10.44	+31 : 12 : 55.8	58.8	70	0.01188	3562	11.13
127	F14348-1447		14 : 37 : 38.29	-15 : 00 : 24.2	330.3	300	0.08273	24802	12.39
128	F14378-3651		14 : 40 : 59.04	-37 : 04 : 32.0	276.4	200	0.06764	20277	12.23
129	F14423-2039	NGC 5734	14 : 45 : 10.02	-20 : 53 : 30.9	65.2	110	0.01375	4121	11.15
130	F14547+2449	VV 340a, Arp 302	14 : 57 : 00.51	+24 : 36 : 45.2	146.5	155	0.03367	10094	11.74
131	F14544-4255	IC 4518A/B	14 : 57 : 43.27	-43 : 07 : 56.3	77.5	100	0.01589	4763	11.23
132	F15107+0724	CGCG 049-057	15 : 13 : 13.07	+07 : 13 : 32.1	63.7	80	0.013	3897	11.35
133	F15163+4255	VV 705	15 : 18 : 06.24	+42 : 44 : 41.5	169.2	200	0.03984	11944	11.92
134	15206-6256	ESO 099-G004	15 : 24 : 57.98	-63 : 07 : 29.4	129.3	100	0.02928	8779	11.74
135	F15250+3608		15 : 26 : 59.42	+35 : 58 : 37.8	228.1	150	0.05516	16535	12.08
136	F15276+1309	NGC 5936	15 : 30 : 00.85	+12 : 59 : 22.1	65.3	100	0.01336	4004	11.14
137	F15327+2340	Arp 220, UGC 09913	15 : 34 : 57.23	+23 : 30 : 11.3	84.8	140	0.01813	5434	12.28
138	F15437+0234	NGC 5990	15 : 46 : 16.41	+02 : 24 : 55.6	62.8	80	0.01281	3839	11.13
139	F16030+2040	NGC 6052	16 : 05 : 12.87	+20 : 32 : 33.0	75.2	90	0.01581	4739	11.09
140	F16104+5235	NGC 6090	16 : 11 : 40.84	+52 : 27 : 27.2	129.2	100	0.02984	8947	11.58
141	F16164-0746		16 : 19 : 11.75	-07 : 54 : 03.0	121.3	100	0.02715	8140	11.62

TABLE 1—Continued

#	IRAS Name	Optical Name	Right Ascension HH : MM : SS	Declination DD : MM : SS	D_A Mpc	Map Size kpc	Redshift	Velocity km s ⁻¹	L_{IR} $\log\left(\frac{L}{L_{\odot}}\right)$
(1)	(2)	(3)	(4)	(5)	(6)	(7)	(8)	(9)	(10)
142	F16284+0411	CGCG 052-037	16 : 30 : 54.89	+04 : 04 : 41.3	112.8	100	0.02449	7342	11.45
143	16304-6030	NGC 6156	16 : 34 : 52.55	-60 : 37 : 08.0	47	75	0.01088	3263	11.14
144	F16330-6820	ESO 069-IG006	16 : 38 : 12.64	-68 : 26 : 42.3	193.6	200	0.04644	13922	11.98
145	F16399-0937		16 : 42 : 40.11	-09 : 43 : 13.7	121.4	100	0.02701	8098	11.63
146	F16443-2915	ESO 453-G005	16 : 47 : 30.21	-29 : 20 : 14.2	96.4	140	0.02088	6260	11.37
147	F16504+0228	NGC 6240	16 : 52 : 58.90	+02 : 24 : 03.3	110.5	100	0.02448	7339	11.93
148	F16516-0948		16 : 54 : 23.72	-09 : 53 : 20.9	102.3	100	0.02253	6755	11.31
149	F16577+5900	NGC 6286, Arp 293	16 : 58 : 27.81	+58 : 56 : 47.5	83.9	100	0.01835	5501	11.37
150	F17132+5313		17 : 14 : 20.45	+53 : 10 : 31.6	210.1	200	0.05094	15270	11.96
151	F17138-1017		17 : 16 : 35.68	-10 : 20 : 40.5	81.2	100	0.01734	5197	11.49
152	F17207-0014		17 : 23 : 21.97	-00 : 17 : 00.7	182.1	175	0.04281	12834	12.46
153	F17222-5953	ESO 138-G027	17 : 26 : 43.35	-59 : 55 : 55.2	94.3	100	0.02078	6230	11.41
154	F17530+3447	UGC 11041	17 : 54 : 51.82	+34 : 46 : 34.2	75	100	0.01628	4881	11.11
155	F17548+2401	CGCG 141-034	17 : 56 : 56.65	+24 : 01 : 02.0	89.8	100	0.01983	5944	11.20
156	17578-0400		18 : 00 : 28.61	-04 : 01 : 16.3	67	100	0.01404	4210	11.48
157	18090+0130		18 : 11 : 35.91	+01 : 31 : 41.3	126.6	125	0.02889	8662	11.65
158	F18131+6820	NGC 6621, Arp 81	18 : 12 : 57.46	+68 : 21 : 38.7	92.4	100	0.02065	6191	11.29
159	F18093-5744	IC 4687	18 : 13 : 39.56	-57 : 44 : 00.9	76.7	100	0.01735	5200	11.62
160	F18145+2205	CGCG 142-034	18 : 16 : 37.26	+22 : 06 : 42.6	83.2	100	0.01868	5599	11.18
161	F18293-3413		18 : 32 : 41.10	-34 : 11 : 27.0	83	100	0.01818	5449	11.88
162	F18329+5950	NGC 6670A/B	18 : 33 : 36.00	+59 : 53 : 20.3	122.4	100	0.0286	8574	11.65
163	F18341-5732	IC 4734	18 : 38 : 25.75	-57 : 29 : 25.4	71.2	100	0.01561	4680	11.35
164	F18425+6036	NGC 6701	18 : 43 : 12.52	+60 : 39 : 11.6	60.8	100	0.01323	3965	11.12
165	F19120+7320	VV 414, NGC 6786, UGC 11415	19 : 10 : 59.19	+73 : 25 : 04.2	107.5	100	0.02511	7528	11.49
166	F19115-2124	ESO 593-IG008	19 : 14 : 31.15	-21 : 19 : 06.3	201.8	150	0.04873	14608	11.93
167	F19297-0406		19 : 32 : 22.30	-04 : 00 : 01.1	335.1	200	0.08573	25701	12.45
168	19542+1110		19 : 56 : 35.78	+11 : 19 : 04.9	260.1	200	0.06496	19473	12.12
169	F19542-3804	ESO 339-G011	19 : 57 : 37.60	-37 : 56 : 08.4	85.3	100	0.0192	5756	11.20
170	F20221-2458	NGC 6907	20 : 25 : 06.58	-24 : 48 : 32.9	49.1	60	0.01064	3190	11.11
171	20264+2533	MCG+04-48-002	20 : 28 : 31.98	+25 : 43 : 42.3	63.6	75	0.0139	4167	11.11
172	F20304-0211	NGC 6926	20 : 33 : 06.13	-02 : 01 : 38.9	85.7	100	0.01961	5880	11.32
173	20351+2521		20 : 37 : 17.73	+25 : 31 : 37.5	141.3	100	0.0337	10102	11.61
174	F20550+1655	CGCG 448-020, II Zw 096	20 : 57 : 24.01	+17 : 07 : 41.6	150	100	0.0361	10822	11.94
175	F20551-4250	ESO 286-IG019	20 : 58 : 26.78	-42 : 39 : 00.5	177.4	100	0.043	12890	12.06
176	F21008-4347	ESO 286-G035	21 : 04 : 11.11	-43 : 35 : 36.1	76.4	100	0.01736	5205	11.20
177	21101+5810		21 : 11 : 29.28	+58 : 23 : 07.9	161.2	100	0.03904	11705	11.81
178	F21330-3846	ESO 343-IG013	21 : 36 : 10.73	-38 : 32 : 37.8	82.6	100	0.01906	5714	11.14
179	F21453-3511	NGC 7130	21 : 48 : 19.54	-34 : 57 : 04.7	70.4	100	0.01615	4842	11.42
180	F22118-2742	ESO 467-G027	22 : 14 : 39.97	-27 : 27 : 50.3	74.7	100	0.0174	5217	11.08
181	F22132-3705	IC 5179	22 : 16 : 09.13	-36 : 50 : 37.2	50.2	50	0.01141	3422	11.24
182	F22287-1917	ESO 602-G025	22 : 31 : 25.48	-19 : 02 : 04.0	104.7	100	0.02504	7507	11.34
183	F22389+3359	UGC 12150	22 : 41 : 12.21	+34 : 14 : 56.8	89.6	100	0.02139	6413	11.35
184	F22467-4906	ESO 239-IG002	22 : 49 : 39.84	-48 : 50 : 58.3	175.6	100	0.04303	12901	11.84
185	F22491-1808		22 : 51 : 49.35	-17 : 52 : 24.9	302.2	200	0.07776	23312	12.20
186	F23007+0836	NGC 7469, IC 5283, Arp 298	23 : 03 : 16.84	+08 : 53 : 00.9	68	100	0.01632	4892	11.65
187	F23024+1916	CGCG 453-062	23 : 04 : 56.55	+19 : 33 : 07.1	103.7	100	0.0251	7524	11.38
188	F23128-5919	ESO 148-IG002	23 : 15 : 46.75	-59 : 03 : 15.8	182.4	100	0.0446	13371	12.06
189	F23135+2517	IC 5298	23 : 16 : 00.67	+25 : 33 : 24.3	112.7	100	0.02742	8221	11.60
190	F23133-4251	NGC 7552	23 : 16 : 10.81	-42 : 35 : 05.5	23.2	50	0.00536	1608	11.11

TABLE 1—*Continued*

#	IRAS Name	Optical Name	Right Ascension HH : MM : SS (4)	Declination DD : MM : SS (5)	D_A Mpc (6)	Map Size kpc (7)	Redshift — (8)	Velocity km s ⁻¹ (9)	L_{IR} $\log\left(\frac{L}{L_{\odot}}\right)$ (10)
—	—	—	—	—	—	—	—	—	—
(1)	(2)	(3)							
191	F23157+0618	NGC 7591	23 : 18 : 14.89	+06 : 34 : 17.8	69.1	90	0.01653	4956	11.12
192	F23157-0441	NGC 7592	23 : 18 : 22.19	-04 : 24 : 57.4	101	100	0.02444	7328	11.40
193	F23180-6929	ESO 077-IG014	23 : 21 : 04.59	-69 : 12 : 54.1	171.5	100	0.04156	12460	11.76
194	F23254+0830	NGC 7674, HCG 96	23 : 27 : 57.73	+08 : 46 : 51.0	119.4	100	0.02892	8671	11.56
195	23262+0314	NGC 7679	23 : 28 : 46.62	+03 : 30 : 41.4	71.3	100	0.01714	5138	11.11
195	23262+0314 ^a	NGC 7682	23 : 29 : 03.91	+03 : 31 : 59.9	71.3	100	0.01714	5138	11.11
196	F23365+3604		23 : 39 : 01.32	+36 : 21 : 08.2	253.3	200	0.06448	19331	12.20
197	F23394-0353	MCG-01-60-022	23 : 42 : 00.91	-03 : 36 : 54.4	92.4	100	0.02324	6966	11.27
197	F23394-0353 ^a	MCG-01-60-021, Mrk 933	23 : 41 : 46.04	-03 : 39 : 42.3	92.4	100	0.02324	6966	11.27
198	23436+5257		23 : 46 : 05.44	+53 : 14 : 01.7	139.3	100	0.03413	10233	11.57
199	F23444+2911	Arp 86, NGC 7752/3	23 : 47 : 01.73	+29 : 28 : 16.2	71.1	100	0.01708	5120	11.07
200	F23488+1949	NGC 7771	23 : 51 : 13.55	+20 : 07 : 41.2	58.5	200	0.01427	4277	11.40
201	F23488+2018	Mrk 331	23 : 51 : 22.73	+20 : 34 : 55.4	73.8	100	0.01848	5541	11.50

NOTE.—The column descriptions are (1) The row reference number. (2) The IRAS name of the galaxy, ordered by ascending RA. Galaxies with the “F” prefix originate from the *IRAS* Faint Source Catalog, and galaxies with no “F” prefix are from the Point Source Catalog. (3) Common optical counterpart names to the galaxy systems. (4) — (5) are the *Spitzer* 8 μ m centers of the system in J2000 (see Mazzarella et al. 2017). These *Herschel* atlas images are centered on these coordinates. For widely separated systems, the coordinate is taken to be half way between the component galaxies. (6) The angular diameter distance to the galaxy in Mpc, from Mazzarella et al. (2017). (7) The map size used in the atlas, denoting the physical length of a side in each atlas image, in kpc. (8) The non-relativistic redshifts as reported by NED, which also corresponds to the heliocentric velocity (Column 9), and includes both cosmological and non-cosmological effects. (9) The measured heliocentric radial velocity corresponding to the redshift in Column 8 in km/sec from Armus et al. (2009), which includes both cosmological and non-cosmological effects. (10) The indicative infrared luminosity, measured in $\log(L/L_{\odot})$ of the entire system, from Armus et al. (2009). These values take into account the effect of the local attractor to the distances than one would normally obtain from pure cosmological effects.

^aThese are very widely separated galaxy pairs that required two *Herschel* PACS observations.

3. *Herschel Space Observatory* Observations

The *Herschel Space Observatory* (Pilbratt et al. 2010) imaging observations of the GOALS sample took place between the dates of March 2011 through June 2012, through our Cycle 1 open time observing program OT1_dsanders_1 (PI: D. Sanders, Program ID #1279). A total of 169 galaxy systems were observed by the Photoconductor Array Camera and Spectrometer (PACS, Poglitsch et al. 2010) instrument in imaging mode under our proposal, with data from the remaining 32 galaxy systems from other guaranteed time (GT) or open time key programs (KPOT) obtained from the Herschel Science Archive (HSA). In addition we observed 160 targets with the Spectral and Photometric Imaging Receiver (SPIRE, Griffin et al. 2010), with the remaining 41 targets from other GT and KPOT programs extracted from the HSA. In total, 84.9 hours of observations were completed under our specific GOALS program, with 61.6 hours for PACS and 23.3 hours for SPIRE.

Broad-band imaging were obtained in the three PACS bands at $70\text{ }\mu\text{m}$, $100\text{ }\mu\text{m}$, and $160\text{ }\mu\text{m}$, and the three SPIRE bands at $250\text{ }\mu\text{m}$, $350\text{ }\mu\text{m}$, and $500\text{ }\mu\text{m}$. The normalized filter transmission curves are shown in Figure 1. Each SPIRE band has two curves associated with the filter, corresponding to the point source responsivity (solid) and extended source responsivity (dashed), which is important since some of the objects in our sample are extended even at SPIRE wavelengths (i. e. the LIRG IRAS F03316–3618/NGC 1365).

Within the GOALS sample there are eight systems consisting of widely separated pairs where two separate PACS observations were needed, but only one SPIRE observation was made since its field of view was larger. These galaxies are denoted in both Tables 1 and 2, giving a total of $201 + 8 = 209$ observation datasets. We note for the galaxy system IRAS F07256+3355 which has three components, only two are visible in the PACS imagery, due to the smaller field of view of PACS. The third component (NGC 2385) is far to the west and still within SPIRE’s larger field of view. Using the SPIRE fluxes as a rough proxy for infrared luminosity strength, NGC 2385 contributes very little to the overall infrared luminosity of the system. IRAS F23488+1949 also has a third component (NGC 7769) to the NNW in the SPIRE images, but is outside of the PACS scan area. However from the SPIRE fluxes NGC 7769 appears to have a moderate contribution to the system’s infrared luminosity. In

sum we achieved a very high degree of coverage and completeness for each GOALS object with *Herschel*.

3.1. Photoconductor Array Camera and Spectrometer (PACS) Observations

The Photoconductor Array Camera and Spectrometer (PACS, Poglitsch et al. 2010) is one of three far infrared instruments onboard the *Herschel Space Observatory* and covers a wavelength range between $60 - 210\text{ }\mu\text{m}$. In the photometer mode it can image two simultaneous wavelength bands centered at $160\text{ }\mu\text{m}$, and at either $70\text{ }\mu\text{m}$ or $100\text{ }\mu\text{m}$. These three broad bands are referred to as the blue channel ($60 - 85\text{ }\mu\text{m}$), green channel ($85 - 130\text{ }\mu\text{m}$) and red channel ($130 - 210\text{ }\mu\text{m}$). For any given observation, the blue camera observes at either $70\text{ }\mu\text{m}$ or $100\text{ }\mu\text{m}$, while the red camera only observes at $160\text{ }\mu\text{m}$. A dichroic beam-splitter with a designed transition wavelength of $130\text{ }\mu\text{m}$ directs the incoming light into the blue and red cameras, and a filter in front of the blue camera selects either the blue or green band.

The detectors for both the blue and red cameras comprise a filled bolometer array of square pixels that instantaneously samples the entire beam from the telescope’s optics. The layout of the blue camera’s focal plane consists of 4×2 subarrays, with 16×16 pixels in each subarray. Similarly the red camera consists of 2×1 subarrays with 16×16 pixels each. On the sky each bolometer pixel subtends an angle of $3''.2 \times 3''.2$ and $6''.4 \times 6''.4$ for the blue and red cameras respectively. There exists gaps between each of the subarrays in both cameras, which must be filled in by on-sky mapping techniques (i. e., scan mapping). Both the blue and red cameras were designed to image the same $3''.5 \times 1''.75$ field of view on the sky at any given instant.

In the photometer mode there are two astronomical observing templates (AOT) available, in addition to a PACS/SPIRE parallel observing mode. For our *Herschel* GOALS program we used the scan map technique for all of our astronomical observing requests (AOR), which is ideal for mapping large areas of the sky and/or targets where extended flux may be present. Our scan map observations involve slewing the telescope at constant speed along parallel lines separated by $15''$ from each other, perpendicular to the scan direction. Two example PACS observation footprints are shown in Figure 2 panels (a) and (c), overlaid on images from the Digital Sky Survey (DSS). The area

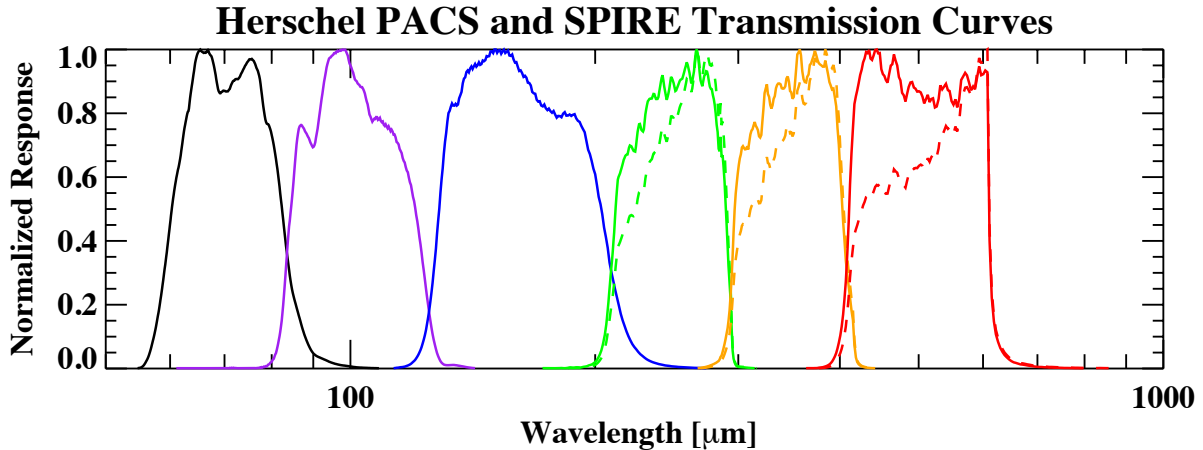


Fig. 1.— The normalized filter transmission curves for our *Herschel* data. From left to right are the PACS 70 μm , 100 μm , 160 μm channels, followed by the SPIRE 250 μm , 350 μm , and 500 μm channels. For the SPIRE bands, the point source response is shown with a solid curve, while the extended source response is shown with a dashed curve. Note the large difference in response for the SPIRE 500 μm transmission curve.

of maximum coverage is the inner region centered on the red box, where the requested observation is centered. For the GOALS observations we chose to observe 7 scan legs in each scan and cross-scan using the 20''/sec scan speed, with scan leg lengths ranging between 3–6' depending on the size of the target. At this scan speed the beam profiles for each wavelength have mean FWHM values of 5''.6, 6''.8, and 11''.3 for the 70 μm , 100 μm , and 160 μm channels respectively.

Before each PACS photometer observation is a 30 sec. chopped calibration measurement between two internal calibration sources (the calibration block), followed by 5 sec. of idle for telescope stability before the science observation is executed. As the telescope is scanned across the sky during science observations, all of the bolometer pixels are read out at a frequency of 40 Hz, even during periods where the telescope was turning around for the next scan leg. However due to satellite data-rate limitations, all PACS data are averaged over four frames effectively downampling the data to 10 Hz. The result is a data timeline of the flux seen by each detector pixel as a function of time (and by extension position on the sky) as the telescope is scanned over the target field.

In order to accurately reconstruct the image, two scan map AORs at orthogonal angles are required. This is because as the telescope scans a field, the offsets of each bolometer subarray, and even each pixel, may be different from its neighbor resulting in stripes

or gradients in the final reconstructed map. However if the same field is scanned in two orthogonal directions, many of these map artifacts can be successfully removed, by virtue of multiple different bolometers sampling each patch of the sky. Furthermore in order to maximally sample a given sky pixel by as many bolometer pixels as possible, we chose our scan angle to be 45° and 135° with respect to the detector array. The orthogonal scans similarly help remove drifts in the bolometer timelines, which are time-dependent variations in the detector or subarray offsets, caused by for example cosmic ray hits and other instrument effects. For our survey the typical PACS scan duration is about 200 sec., however larger maps with deeper coverage can be as long as \sim 1900 sec. Since two scans are needed for each target in the blue and green filter, there are two pairs of scan and cross-scan in the red channel, giving us better sensitivity. Unfortunately due to unforeseen consequences, several galaxy components in IRAS F02071–1023 and IRAS F07256+3355 had sufficient coverage by only one of the scans, which resulted in more noise along the scan direction around the target.

Since by definition all of the objects in the GOALS sample have an *IRAS* 60 μm flux of at least 5.24 Jy, the galaxies or galaxy systems are bright enough such that only one repetition was needed for each PACS scan and cross scan. With one pair of scan and cross-scan observations, we achieved a 1- σ point source sensitivity of approximately 4 mJy in the central area, and ap-

proximately 8 mJy averaged over the entire map for both blue and green observations. By combining all four red channel scans and cross-scans we achieved a $1-\sigma$ point source sensitivity of about 6 mJy in the central area, and about 12 mJy averaged over the entire map. On the other hand the extended flux sensitivities for one repetition (one scan and cross-scan pair) are 5.3 MJy sr $^{-1}$, 5.2 MJy sr $^{-1}$, and 1.7 MJy sr $^{-1}$ for the 70 μm , 100 μm , and 160 μm channels respectively.

3.2. Spectral and Photometric Imaging Receiver (SPIRE) Observations

The Spectral and Photometric Imaging Receiver (SPIRE, Griffin et al. 2010) is a submillimeter camera on *Herschel* that operates between the 194–671 μm wavelength range. In the imaging mode, it can simultaneously observe in three different broad bandpasses ($\lambda/\Delta\lambda \sim 3$), centered at 250 μm , 350 μm , and 500 μm . Similar to PACS, SPIRE images a field by scan mapping, where the instrument field of view ($4' \times 8'$) is scanned across the sky to maximize the spatial coverage. The three detector arrays use hexagonal feedhorn-coupled bolometers, with 139, 88, and 43 bolometers for the PSW (250 μm), PMW (350 μm), and PLW (500 μm) channels respectively. The beam profiles for each wavelength have mean FWHM values of 18''.1, 25''.2, and 36''.6 for the 250 μm , 350 μm , and 500 μm photometer arrays, and mean ellipticities of 7%, 12%, and 9% (the beam shape changes slightly as a function of off-axis angle).

There are three main observing modes available: point source photometry, field/jiggle mapping, and scan mapping. For our observing program (dsanders_OT1_1) we chose the scan-map mode at a scan rate of 30''/sec., since it gave the best data quality and also larger field of view for the final map than the other two mapping modes. Nominal scan angles of 42.4° and 127.2° with respect to the detector arrays were used to maximize sky coverage by as many detectors as possible, and to minimize the effect of individual bolometer drift during data processing. Like PACS, two scans are needed for data redundancy as well as cross-linking, however the scan and cross-scan with SPIRE are observed within a single AOR. Within our program, the vast majority of our targets were observed in the small map mode (~ 150 targets), while the rest were taken in the large map mode (~ 20 targets). The typical scan durations are ~ 170 sec. for small maps ($\sim 5' \times 5'$ guaranteed map coverage area), and up to ~ 2200 sec. for large maps. In Figure 2

panels (b) and (d) we show two example observations using SPIRE. The top panel shows a small map mode observation, while the bottom panel shows a large map mode observation. In both cases the SPIRE detector is scanned over the target coordinate (shown by the red box) from the top left to the bottom right, and then from the top right to the bottom left.

Due to the extremely sensitive design of the *Herschel* optics and SPIRE instrument, only one repetition was observed for every target in our observing program. The SPIRE instrument has a confusion limit of 5.8, 6.3, and 6.8 mJy beam $^{-1}$ for the 250 μm , 350 μm , and 500 μm channels, which is defined as the standard deviation of the flux density in the limit of zero instrument noise (Nguyen et al. 2010). On the other hand the instrument noise is about 9, 7.5, and 10.8 mJy beam $^{-1}$ at 250 μm , 350 μm , and 500 μm for one repetition (scan and cross-scan) at the nominal scan speed of 30''/sec. Since many of our targets have extended features, SPIRE's $1-\sigma$ sensitivities to extended flux are at the 1.4 MJy sr $^{-1}$, 0.8 MJy sr $^{-1}$, and 0.5 MJy sr $^{-1}$ levels for 250 μm , 350 μm , and 500 μm for one repetition. These flux levels are already dominated by confusion noise, and is more than enough to detect any cold dust components in our sample.

3.3. Observing Log

Table 2 below lists the observing log for our data sample. Column 1 is the galaxy reference number, and column 2 is the IRAS name of the galaxy, ordered by ascending RA. Column 3 is the common optical counterpart names to the galaxy systems. Columns 4 – 7 are the observation IDs for PACS imaging. Blue corresponds to a wavelength of 70 μm , while green corresponds to 100 μm . Each blue and green observation pair simultaneously observes the red 160 μm channel. Two orthogonal observations are made at each wavelength to reduce imaging artifacts. We note that four galaxies in our sample do not have 100 μm observations available since they were from other programs that did not observe them: IRAS F02401-0013 (NGC 1068), IRAS F09320+6134 (UGC 05101), IRAS F15327+2340 (Arp 220), and IRAS F21453-3511 (NGC 7130). Column 8 is the PACS observation duration for each scan and cross-scan, unless otherwise noted. We note these are *not* exposure times, but instead the amount of time for each scan and cross-scan. Columns 9 – 10 are the observation dates (in YYYY-MM-DD) for each pair of PACS scan and cross-scan, unless otherwise noted, while column 11

is the Program ID of the PACS program from which the data were obtained. We list the PID corresponding to each number in Table 2's caption. The bulk of the data ($\sim 80\%$) are from OT1_sanders_1, with most of the remaining data from KPGT_esturm_1 and KPOT_pvanderw_1. Column 12 is the SPIRE observation ID which includes all three $250 \mu\text{m}$, $350 \mu\text{m}$, and $500 \mu\text{m}$ observations. The scans and cross-scans for each target is combined into one observation. Column 13 is the SPIRE observation duration, which is similar to the PACS duration. Column 14 is the SPIRE observation date, and column 15 is the PID of the SPIRE program from which the data were obtained, similar to the PACS PID column.

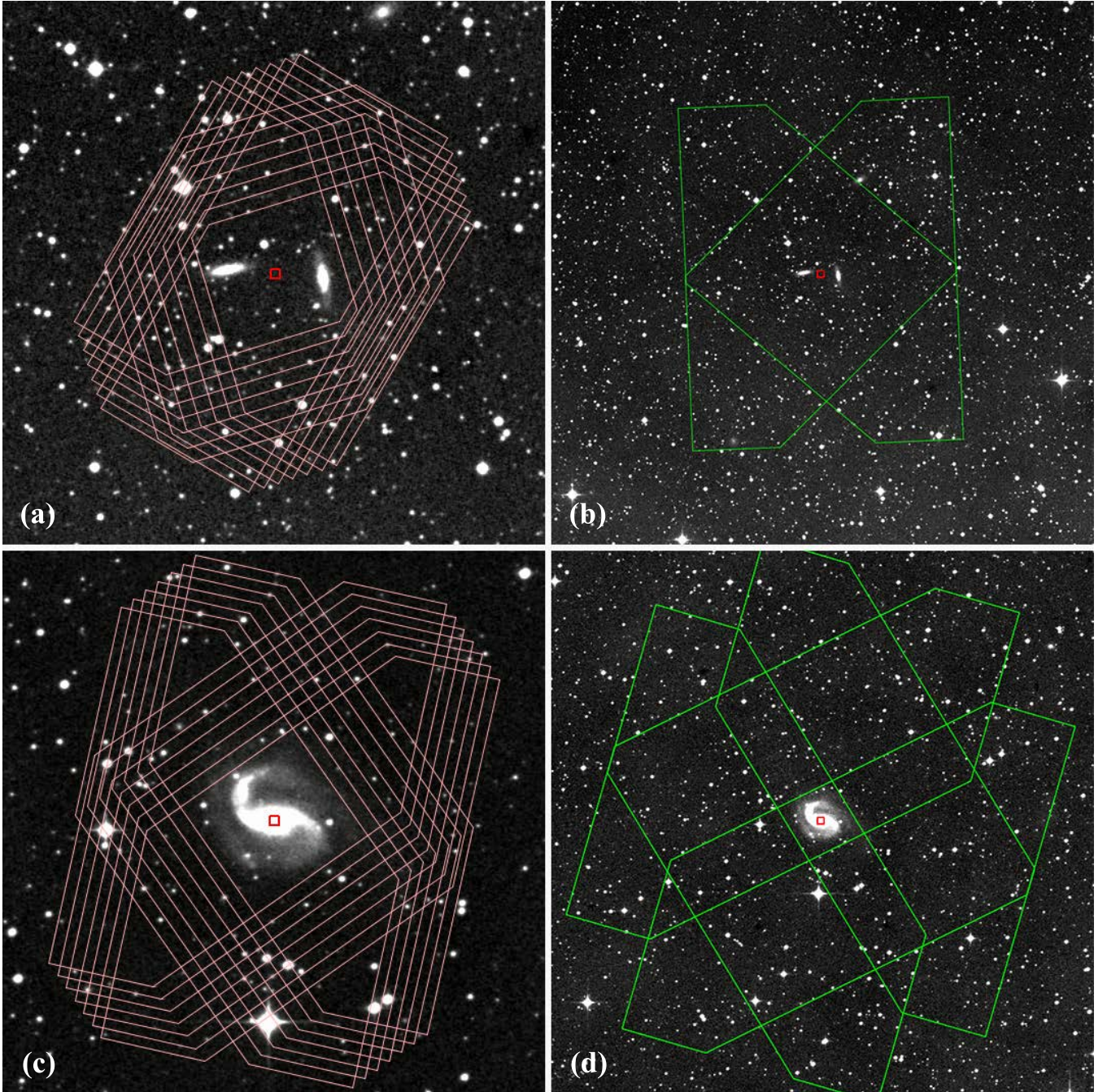


Fig. 2.— The PACS and SPIRE observation footprints for two galaxies, IRAS F18145+2205 (CGCG 142-034) in the top row, and IRAS F20221-2458 (NGC 6907) on the bottom. These figures were generated using HSPOT, the Herschel observation planning tool, while the background images used are from DSS. The red box in each panel indicates the central coordinate for each observation. The PACS observations are shown in panels (a) and (c), which show a $9' \times 9'$ field of view around the target coordinate. Each scan leg in one direction is repeated several times (nominally 7 times) for maximal coverage of the source galaxy (or galaxies). The SPIRE observations are shown in panels (b) and (d), and have a $25' \times 25'$ field of view, which is much larger than the PACS field of view. Panel (b) shows a small map scan, while the bottom panel shows a large map scan.

TABLE 2
HERSCHEL OBSERVATION LOG

#	IRAS Name	Optical Name	(3)	PACS						SPIRE					
				Blue 1 Obs. ID (4)	Blue 2 Obs. ID (5)	Green 1 Obs. ID (6)	Green 2 Obs. ID (7)	Duration (sec.)	Blue Obs. Date (8)	Green Obs. Date (9)	PACS PID ¹ (10)	Obs. ID (11)	Duration (sec.)	Obs. Date (12)	PID ¹ (13)
1	F00073+2538	NGC 23		1342225471	1342225472	1342225469	1342225470	198	2011-07-24	2011-07-24	1	1342234681	169	2011-12-18	1
2	F00085-1223	NGC 34, Mrk 938		1342212463	1342212464	1342212465	1342212466	276	2011-01-10	2011-01-10	3	1342199384	445	2010-06-29	3
3	F00163-1039	Arp 256, MCG-02-01-051/2		1342212700	1342212701	1342212702	1342212703	485	2011-01-15	2011-01-15	2	1342234694	169	2011-12-18	1
4	F00344-3349	ESO 350-JG 038, Haro 11		1342210636	1342210637	1342197713	1342197714	65 ^b	2010-12-01	2010-06-04	10	1342199386	307	2010-06-29	10
5	F00402-2349	NGC 232		1342238073	1342238074	1342237438	1342237439	240	2012-01-21	2012-01-13	1	1342234699	1217	2011-12-18	1
6	F00506+7248	MCG+12-02-001		1342237174	1342237175	1342237172	1342237173	198	2012-01-11	2012-01-11	1	1342199365	169	2010-06-29	4
7	F00548+4331	NGC 317B		1342213944	1342213945	1342213946	1342213947	347	2011-02-08	2011-02-08	2	1342238255	169	2012-01-27	1
8	F01053-1746	IC 1623, Arp 236		1342212754	1342212755	1342212846	1342212847	65	2011-01-16	2011-01-18	2	1342199388	169	2010-06-29	2
9	F01076-1707	MCG-03-04-014		1342225341	1342225342	1342225343	1342225344	198	2011-07-23	2011-07-23	1	1342234709	169	2011-12-18	1
10	F01159-44443	ESO 244-G012		1342225365	1342225366	1342225363	1342225364	198	2011-07-23	2011-07-23	1	1342234726	169	2011-12-18	1
11	F01173+1405	CGCG 436-030		1342238031	1342238090	1342238088	1342238089	198	2012-01-20	2012-01-21	1	1342237499	169	2012-01-14	1
12	F01325-3623	ESO 353-G020		1342225351	1342225352	1342223353	1342223354	198	2011-07-23	2011-07-23	1	1342234721	169	2011-12-18	1
13	F01341-3755	RR 032, ESO 297-G011/012		1342213629	1342213630	1342213631	1342213632	485	2011-02-01	2011-02-01	2	1342234720	169	2011-12-18	1
14	F01364-1042			1342238034	1342238035	1342238036	1342238037	198	2012-01-20	2012-01-20	1	1342236227	169	2012-01-02	1
15	F01417+1651	III Zw 035		1342238021	1342238022	1342238023	1342238024	198	2012-01-20	2012-01-20	1	1342237555	307	2012-01-15	1
16	F01484+2220	NGC 695		1342238017	1342238018	1342237464	1342237465	198	2012-01-20	2012-01-13	1	1342238266	169	2012-01-27	1
17	F01519+3640	UGC 01385		1342237168	1342237169	1342237166	1342237167	198	2012-01-11	2012-01-11	1	1342238260	169	2012-01-27	1
18	F02071-1023	NGC 838		1342238855	1342238856	1342238853	1342238854	303	2012-02-09	2012-02-09	1	1342237533	1324	2012-01-14	
19	F02070+3857	NGC 828		1342237468	1342237469	1342237469	1342237493	198	2012-01-13	2011-07-28	1	1342239822	169	2012-03-01	1
20	F02114+0456	IC 214		1342238796	1342238798	1342238799	1342238797	240	2012-02-08	2012-02-08	1	1342238274	169	2012-01-27	1
21	F02152+1418	NGC 877		1342238869	1342238870	1342238867	1342238868	240	2012-02-09	2012-02-09	1	1342238267	1217	2012-01-27	1
22	F02203+3158	MCG+05-06-036		1342238772	1342238773	1342223874	1342223875	347	2011-07-10	2011-07-10	2	1342238262	169	2012-01-27	1
23	F02208+4744	UGC 01845		1342237995	1342237996	1342237997	1342237998	198	2012-01-19	2012-01-19	1	1342239799	169	2012-02-29	1
24	F02281-0309	NGC 958		1342238801	1342238802	1342223580	1342223581	198	2012-02-08	2011-07-03	1	1342238277	169	2012-01-27	1
25	F02345+2053	NGC 992		1342238873	1342238874	1342238871	1342238872	198	2012-02-09	2012-02-09	1	1342238230	169	2012-03-01	1
26	F02401-0013	NGC 1068		1342189194	1342189195	909	2010-01-12	2010-01-12	8	1342189425	1076	2010-01-17	8
27	F02435+1253	UGC 02238		1342238792	1342238793	1342238794	1342238795	198	2012-02-08	2012-02-08	1	1342238270	169	2012-01-27	1
28	F02437+42122			1342238875	1342238876	1342238876	1342238880	198	2012-02-09	2012-02-09	1	1342239829	307	2012-03-01	1
28	F02437+2123 ^a	2MASX J02464505+2133234		1342238877	1342238878	1342238881	1342238882	198	2012-02-09	2012-02-09	1	
29	F02512+4446	UGC 02369		1342223858	1342223859	1342223860	1342223861	347	2011-07-10	2011-07-10	2	1342238231	169	2012-03-01	1
30	F03117+4151	UGC 02608		1342241466	1342241467	1342241466	1342241465	198	2012-03-15	2012-03-15	1	1342238219	169	2012-03-01	1
30	F03117+4151 ^a	UGC 02612		1342241649	1342241651	1342241650	1342241652	198	2012-03-17	2012-03-17	1	
31	F03164+4119	NGC 1275		1342216022	1342216023	1342204217	1342204218	153	2011-03-14	2011-09-09	2	1342203614	307	2010-08-24	2
32	F03217+4022			1342248716	1342248717	1342248714	1342248715	198	2012-07-26	2012-07-26	1	134223950	169	2012-03-01	1
33	F03316-3618	NGC 1365		1342222495	1342222496	1342222497	1342222498	1217	2011-06-11	2011-06-11	3	1342201436	999	2010-07-14	3

TABLE 2—Continued

#	IRAS Name	Optical Name	PACS						SPIRE					
			Blue 1 Obs. ID (1)	Blue 2 Obs. ID (2)	Green 1 Obs. ID (3)	Green 2 Obs. ID (4)	Duration (sec.)	Blue Obs. Date (5)	Green Obs. Date (6)	PACS PID ¹ (7)	Obs. ID (8)	Duration (sec.)	Obs. Date (9)	SPIRE PID ¹ (10)
34	F03359+1523		1342248700	1342248701	1342248698	1342248699	198	2012-07-26	2012-07-26	1	1342239948	307	2012-03-01	1
35	F03514+1546	CGCG 465-012	1342241695	1342241696	1342241693	1342241694	198	2012-03-18	2012-03-18	1	1342239946	169	2012-03-01	1
35	F03514+1546 ^a	CGCG 465-011	1342248702	1342248703	1342248704	1342248705	198	2012-07-26	2012-07-26	1
36	035824-6012		1342242575	1342242576	1342242573	1342242574	198	2012-03-28	2012-03-28	1	1342239801	169	2012-02-29	1
37	F04097+0525	UGC 02982	1342249943	1342249944	1342250109	1342250110	198	2012-08-20	2012-08-23	1	1342239338	169	2012-03-01	1
38	F04118-3207	ESO 420-G013	1342237452	1342237453	1342237450	1342237451	198	2012-01-13	2012-01-13	1	1342227719	169	2011-09-01	1
39	F04191-1855	ESO 550-JG 025	1342241947	1342241948	1342241945	1342241946	198	2012-03-20	2012-03-20	1	1342239857	169	2012-03-01	1
40	F04210-4042	NGC 1572	1342237422	1342237423	1342241686	1342241687	198	2012-01-12	2012-03-18	1	1342227720	169	2011-09-01	1
41	0427+3849		1342243496	1342243497	1342243494	1342243495	198	2012-03-24	2012-03-24	1	134222906	169	2011-09-21	1
42	F04315-0840	NGC 1614	1342243096	1342243097	1342243410	1342243411	198	2012-03-21	2012-03-24	1	1342203628	169	2010-08-24	4
43	F04326+1904	UGC 03094	1342241971	1342241972	1342241973	1342241974	198	2012-03-20	2012-03-20	1	134223944	169	2012-03-01	1
44	F04454-4838	ESO 203-JG001	1342240271	1342240272	1342240273	1342240274	198	2012-03-04	2012-03-04	1	1342227722	307	2011-09-01	1
45	F04502-3304	MCG-05-12-006	1342238887	1342238888	1342238889	1342238890	198	2012-02-09	2012-02-09	1	1342229337	169	2011-09-22	1
46	F05053-0805	NGC 1797	1342242528	1342242529	1342242526	1342242527	198	2012-03-28	2012-03-28	1	1342227717	169	2011-09-01	1
46	F05053-0805 ^a	NGC 1799	1342242523	1342242524	1342242522	1342242525	198	2012-03-28	2012-03-28	1
47	F05054+1718	CGCG 468-002	1342242680	1342242681	1342242678	1342242679	198	2012-03-29	2012-03-29	1	1342227711	169	2011-09-01	1
48	05083+2441		1342241327	1342241328	1342217496	1342217497	198	2012-03-13	2011-03-30	1	1342229551	169	2011-09-23	1
49	F05081+7936	VII Zw 031	1342242561	1342242562	1342242559	1342242560	198	2012-03-28	2012-03-28	1	1342229130	169	2011-09-21	1
50	05129+5128		1342242748	1342242749	1342242746	1342242747	198	2012-03-30	2012-03-30	1	1342229110	307	2011-09-21	1
51	F05189-2524		1342242080	1342242081	1342242082	1342242083	198	2012-03-20	2012-03-20	1	1342203532	169	2010-08-24	4
52	F05187-1017		1342242516	1342242517	1342242518	1342242519	198	2012-03-28	2012-03-28	1	134223929	169	2012-03-01	1
53	05368+4940	MCG+08-11-002	1342242752	1342242753	1342242750	1342242751	198	2012-03-30	2012-03-30	1	1342229112	169	2011-09-21	1
54	F05365+6921	NGC 1961	1342242565	1342242566	1342242563	1342242564	240	2012-03-28	2012-03-28	1	1342227442	1217	2011-09-02	1
55	F05414+5840	UGC 03351	1342242738	1342242739	1342242740	1342242741	198	2012-03-30	2012-03-30	1	1342229115	169	2011-09-21	1
56	05442+1732		1342242668	1342242669	1342242666	1342242667	198	2012-03-29	2012-03-29	1	1342229553	169	2011-09-23	1
57	F06076-2139		1342242546	1342242547	1342242544	1342242545	198	2012-03-28	2012-03-28	1	1342227695	307	2011-09-01	1
58	F06052+8027	UGC 03410	1342242734	1342242735	1342242732	1342242733	198	2012-03-30	2012-03-30	1	1342229131	583	2011-09-21	1
59	F06107+7822	NGC 2146	1342194051	1342194053	1342194052	1342194054	1934	2010-04-07	2010-04-07	5	1342191186	2167	2010-02-25	5
60	F06259+4708	ESO 255-JG007	1342236648	1342236649	1342236647	1342236646	198	2012-01-06	2012-01-06	1	1342226643	307	2011-08-16	1
61	F06295-1735	ESO 557-G002	1342242713	1342242714	1342242711	1342242712	198	2012-03-29	2012-03-29	1	1342227706	169	2011-09-01	1
62	F06538+4628	UGC 03608	1342242777	1342242778	1342242779	1342242780	198	2012-03-30	2012-03-30	1	134222949	169	2011-09-23	1
63	F06592-6313		1342233607	1342233608	1342233605	1342233606	198	2011-12-05	2011-12-05	1	1342229669	169	2011-09-23	1
64	F07027-6011	AM 0702-601	1342233595	1342233596	1342233597	1342233598	198	2011-12-05	2011-12-05	1	1342229671	169	2011-09-23	1
65	07063+2043	NGC 2342	1342231560	1342231561	1342231562	1342231563	198	2011-10-29	2011-10-29	1	1342230778	169	2011-10-10	1
66	F07160-6215	NGC 2369	1342233603	1342233604	1342233601	1342233602	198	2011-12-05	2011-12-05	1	1342229670	169	2011-09-23	1

TABLE 2—Continued

#	IRAS Name	Optical Name	PACS						SPIRE						
			Blue 1 Obs. ID (1)	Blue 2 Obs. ID (2)	Green 1 Obs. ID (3)	Green 2 Obs. ID (4)	Duration (sec.)	Blue Obs. Date (5)	Green Obs. Date (6)	PACS PID ¹ (7)	Obs. ID (8)	Duration (sec.)	Obs. Date (9)	SPIRE PID ¹ (10)	
67	07251-0248	NGC 2388	1342242707	1342242708	1342242709	1342242710	198	2012-03-29	2012-03-29	1	1342230794	307	2011-10-11	1	
68	F07250+3355	NGC 2388	1342244897	1342244898	1342244899	1342244896	303	2012-04-24	2012-03-30 ^c	1	1342239477	1324	2011-09-22	1	
69	F07329+1149	MCG+02-20-003	1342242701	1342242702	1342242700	1342242699	1342242700	198	2012-03-29	2012-03-29	1	1342239463	583	2011-09-22	1
69	F07329+1149 ^a	NGC 2416	1342242698	1342242697	1342242697	1342242695	198	2012-03-29	2011-05-04 ^d	1	1342239478	307	2011-08-20	1	
70	08355-4944		1342256690	1342256691	1342256691	1342256793	1342256794	198	2011-08-17	2011-08-24	1	1342239120	307	2011-09-21	1
71	F08339+6517		1342252800	1342252801	1342252802	1342252803	198	2012-10-08	2012-10-08	1	1342239174	169	2010-10-10	4	
72	F08354+2555	NGC 2623	1342232226	1342232227	1342232228	1342232229	198	2011-11-11	2011-11-11	1	1342239174	169	2010-10-10	4	
73	08424-3130	ESO 432-IG006	1342233390	1342233391	1342233391	1342233392	1342233393	198	2011-12-01	2011-12-01	1	1342230798	169	2011-10-11	1
74	F08520-6830	ESO 060-IG016	1342236932	1342236932	1342236933	1342236934	1342236935	198	2012-01-07	2012-01-07	1	1342236637	307	2011-08-16	1
75	F08572+3915		1342244254	1342244255	1342244255	1342244254	198	2012-04-13	2011-11-11	1	1342230749	445	2011-10-10	6	
76	09022-3615		1342233591	1342233592	1342233592	1342233593	1342233594	198	2011-12-05	2011-12-05	1	1342230799	445	2011-10-11	6
77	F09111-1007		1342233398	1342233399	1342233399	1342233398	198	2011-12-02	2011-12-02	1	1342245553	307	2012-05-11	1	
78	F09120+4432	UGC 04881	1342232391	1342232392	1342232392	1342232393	1342232394	198	2011-11-17	2011-11-17	1	134224571	169	2012-05-11	1
79	F09320+6134	UGC 05101	1342220800	1342220801	1342220801	1342220801	198	2011-04-29	2011-04-29	7	134224962	169	2010-09-21	7	
80	F09333+4841	MCG+08-18-013	1342209451	1342209451	1342209452	1342209453	1342209454	403	2011-11-17	2011-11-17	2	1342230740	307	2011-10-10	1
81	F09437+0317	Arp 303, IC 0563/4	1342211138	1342211139	1342211140	1342211141	485	2011-05-16	2011-05-16	2	1342245559	169	2012-05-11	1	
82	F10015-0614	NGC 3110	1342247307 ^e	1342247308 ^e	1342247308 ^e	1342247305 ^e	198	2012-06-23	2012-06-23	1	134223843	169	2011-12-18	1	
83	F10038-3338	ESO 374-IG 032	1342237954	1342237954	1342237955	1342233370	1342233371	198	2012-01-06	2011-12-01	1	1342234831	307	2011-12-17	1
84	F10173+0828		1342246207	1342246208	1342246208	1342246209	1342246210	198	2012-05-27	2012-05-27	1	1342247235	307	2012-06-22	1
85	F10196+2149	NGC 3221	1342231649	1342231650	1342231651	1342231651	198	2011-10-30	2011-10-30	1	1342246110	169	2012-06-03	1	
86	F10257-4339	NGC 3256	1342211183	1342211184	1342211184	1342211185	1342211186	262	2010-07-24	2010-12-16	2	134220126	307	2010-12-16	2
87	F10409-4556	ESO 264-G036	1342237950	1342237950	1342237951	1342237952	1342237953	198	2012-01-06	2012-01-06	1	1342236204	169	2012-01-02	1
88	F10567+4310	ESO 264-G057	1342237948	1342237948	1342237949	1342237949	1342237947	198	2012-01-06	2012-01-06	1	1342236203	169	2012-01-02	1
89	F10565+2448		1342233408	1342233409	1342233409	1342233410	1342233411	198	2011-12-02	2011-12-02	1	1342234869	445	2011-12-18	6
90	F11011+4107	MCG+07-23-019	1342233414	1342233415	1342233415	1342233412	1342233413	198	2011-12-02	2011-12-02	1	1342247231	169	2012-06-22	1
91	F11186-0242	CGCG 011-076	134223691	134223691	134223692	134223693	134223694	198	2011-07-04	2011-07-04	1	134223862	169	2011-12-18	1
92	F11231+1456	IC 2810	134223678	134223678	134223679	1342233458	1342233459	198	2011-07-04	2011-06-22	1	134222886	169	2011-06-20	1
93	F11255+4120	ESO 319-G022	1342237944	1342237944	1342237945	1342237945	1342237943	198	2012-01-06	2012-01-06	1	1342234822	169	2011-12-17	1
94	F11257+4850	NGC 3690, Arp 299	1342210600	1342210601	1342211104	1342211105	485	2010-11-30	2010-12-13	2	1342219344	459	2010-06-29	2	
95	F11106-3851	ESO 320-G030	1342237940	1342237941	1342237941	1342237938	134223694	198	2012-01-06	2012-01-06	1	134220129	169	2010-07-09	4
96	F12043-3140	ESO 440-IG058	1342231936	1342231936	1342231937	1342225087	1342225088	198	2012-01-06	2011-08-01	1	1342236196	169	2012-01-02	1
97	F12112+0305		1342223929	1342223929	1342223930	1342223612	1342223613	198	2011-07-11	2011-07-03	1	1342234880	169	2011-12-18	1
98	F12116+5448	NGC 4194	1342233545	1342233546	1342233546	1342235145	1342235146	198	2011-12-04	2011-12-25	1	1342230869	169	2011-10-11	1
99	F12115-4656	ESO 267-G030	1342234409	1342234410	1342234411	1342234412	198	2011-12-16	2011-12-16	1	1342234819	583	2011-12-17	1	
99	F12115-4656 ^a	ESO 267-G029	1342234413	1342234414	1342234414	1342234416	198	2011-12-16	2011-12-16	1	1342234819	583	2011-12-17	1	
											

TABLE 2—Continued

#	IRAS Name	Optical Name	PACS						SPIRE					
			Blue 1 Obs. ID (4)	Blue 2 Obs. ID (5)	Green 1 Obs. ID (6)	Green 2 Obs. ID (7)	Duration (sec.)	Blue Obs. Date (8)	Green Obs. Date (9)	PACS PID ¹ (11)	Obs. ID (12)	Duration (sec.)	Obs. Date (13)	SPIRE PID ¹ (15)
100	12116-5615		1342227110	1342227111	1342227112	1342227113	198	2011-08-23	2011-08-23	1	1342226974	169	2011-08-20	1
101	F12224-0624	NGC 4418	1342224336	1342224337	1342224338	1342224339	198	2011-07-17	2011-07-17	1	1342234887	307	2011-12-18	1
102	F12243-0036	UGC 08058, Mrk 231	1342224340	1342224341	1342224163	1342224164	240	2011-07-17	2011-07-14	1	1342234883	1217	2011-12-18	1
103	F12540+5708	UGC 4922	1342199861	1342199862	1342206704	1342206705	65	2010-07-05	2010-10-18	2	1342201218	169	2010-07-26	2
104	F12590+2934	NGC 4922	1342233366	1342233367	1342233012	1342233013	198	2011-12-01	2011-11-25	1	1342234903	307	2011-12-18	1
105	F12592+0436	CGCG 043-099	1342224902	1342224903	1342224904	1342224905	198	2011-07-28	2011-07-28	1	1342234886	307	2011-12-18	1
106	F12596-1529	MCG-02-33-098	1342234383	1342234384	1342234381	1342234382	198	2011-12-15	2011-12-15	1	1342234810	169	2011-12-17	1
107	F13001-2339	ESO 507-G070	1342236638	1342236639	1342236640	1342236641	198	2012-01-06	2012-01-06	1	1342234813	169	2011-12-17	1
108	13052-5711		1342227110	1342227110	1342227117	1342227118	198	2011-08-23	2011-08-23	1	1342226971	169	2011-08-20	1
109	F13126+2453	IC 0860	1342235337	1342235338	1342234367	1342234368	198	2011-12-03	2011-12-15	1	1342234902	169	2011-12-18	1
110	13120-5453		1342227288	1342227289	1342227286	1342227287	198	2011-08-24	2011-08-24	1	1342227280	445	2011-08-20	6
111	F13136-6223	VV 250a	1342209024	1342209025	1342209026	1342209027	347	2010-11-04	2010-11-04	2	1342229508	307	2011-09-22	1
112	F13182+3424	UGC 08387	1342235368	1342235369	1342233010	1342233011	198	2011-12-25	2011-11-25	1	1342198191	169	2010-06-12	4
113	F13188+0036	NGC 5104	1342234375	1342234376	1342234373	1342234374	198	2011-12-15	2011-12-15	1	1342236168	169	2012-01-01	1
114	F13197-1627	MCG-03-34-064	1342236913	1342236914	1342236915	1342236912	198	2012-01-07	2012-01-07	1	1342236178	169	2012-01-01	1
115	F13229-2934	NGC 5135	1342237916	1342237917	1342237918	1342237919	198	2012-01-06	2012-01-06	1	1342202248	169	2010-08-07	4
116	13242-5713	ESO 173-G015	1342237930	1342237931	1342237928	1342237929	198	2012-01-06	2012-01-06	1	1342203562	169	2010-08-23	4
117	F13301-2356	IC 4280	1342237910	1342237911	1342237912	1342237913	198	2012-01-06	2012-01-06	1	1342236191	169	2012-01-02	1
118	F13362+4831	NGC 5256	1342233497	1342233498	1342233463	1342233464	198	2011-12-03	2011-12-15	1	1342232709	169	2011-11-09	1
119	F13373+0105	Arp 240, NGC 5278	1342213606	1342213607	1342213608	1342213609	485	2011-02-01	2011-02-01	2	1342234798	169	2011-12-17	1
120	F13428+5608	UGC 08696, Mrk 273	1342208444	1342208445	1342210433	1342210433	153	2010-11-09	2010-11-18	2	1342201217	307	2010-07-26	2
121	F13470+3530	UGC 08739	1342234227	1342234227	1342234224	1342234224	198	2011-12-05	2011-12-05	1	1342236144	169	2012-01-01	1
122	F13478-4848	ESO 221-1G010	1342227128	1342227129	1342227130	1342227131	198	2011-08-23	2011-08-23	1	1342238293	169	2012-01-28	1
123	F13497+0220	NGC 5331	1342213598	1342213599	1342213600	1342213601	347	2011-02-01	2011-02-01	2	1342236165	169	2012-01-01	1
124	F13564+3741	Arp 84, NGC 5394/5	1342211285	1342211286	1342211287	1342211288	550	2010-12-17	2010-12-17	2	1342236140	1253	2012-01-01	1
125	F14179+4927	CGCG 247-020	1342235552	1342235553	1342234361	1342234362	198	2011-12-15	2011-12-15	1	1342232717	169	2011-11-09	1
126	F14280+3126	NGC 5653	1342234240	1342234241	1342233523	1342233524	198	2011-12-05	2011-12-03	1	1342236146	169	2012-01-01	1
127	F14348-1447		1342236610	1342236611	1342236612	1342236613	198	2012-01-06	2012-01-06	1	1342238301	445	2012-01-28	6
128	F14378-3651		1342238053	1342238054	1342225403	1342225404	198	2012-01-20	2011-07-24	1	1342238295	445	2012-01-28	6
129	F14423-2039	NGC 5734	1342237184	1342237185	1342237186	1342237187	240	2012-01-12	2012-01-12	1	134222731	1217	2011-09-01	1
130	F14547+2449	VV 340a, Arp 302	1342235382	1342235383	1342235384	1342235385	198	2011-12-25	2011-12-25	1	1342234779	169	2011-12-17	1
131	F14544-4255	IC 4518A/B	1342225308	1342225309	1342225306	1342225307	198	2011-07-23	2011-07-23	1	1342240003	169	2012-03-02	1
132	F15107+0724	CGCG 049-057	1342236624	1342236625	1342236626	1342236627	198	2012-01-06	2012-01-06	1	1342203077	169	2010-08-15	4
133	F15163+4255	VV 705	1342234242	1342234243	1342234244	1342234245	198	2011-12-05	2011-12-05	1	1342229532	169	2011-09-22	1
134	F15206-6256	ESO 099-G004	1342238067	1342238068	1342238065	1342238066	198	2012-01-20	2012-01-20	1	1342229209	169	2011-09-22	1

TABLE 2—Continued

#	IRAS Name	Optical Name	PACS						SPIRE					
			Blue 1 Obs. ID (4)	Blue 2 Obs. ID (5)	Green 1 Obs. ID (6)	Green 2 Obs. ID (7)	Duration (sec.)	Blue Obs. Date (8)	Green Obs. Date (9)	PACS PID ¹ (10)	Obs. ID (11)	Duration (sec.)	Obs. Date (12)	SPIRE PID ¹ (15)
135	F15250+3608		1342235398	1342235399	1342235401	1342235401	198	2011-12-25	2011-12-25	1	1342234775	445	2011-12-17	6
136	F15276+1309	NGC 5936	1342236904	1342236905	1342236902	1342236903	198	2012-01-07	2012-01-07	1	1342238324	169	2012-01-28	1
137	F15327+2340	Abp 220, UGC 09913	1342189033	1342189034	293	2010-01-06	2010-01-06	8	1342188687	619	2009-12-29	8
138	F15437+0234	NGC 5990	1342235290	1342235291	1342235292	1342235293	198	2011-07-22	2011-07-22	1	1342238312	169	2012-01-28	1
139	F16030+2040	NGC 6052	1342235429	1342235430	1342235427	1342235428	198	2011-07-24	2011-07-24	1	1342239560	169	2011-09-23	1
140	F16104+5235	NGC 6090	1342233360	1342233361	1342233358	1342233359	198	2011-12-01	2011-12-01	1	1342239529	307	2011-09-22	1
141	F16164-0746		1342241414	1342241415	1342262221	1342262222	198	2012-03-14	2013-01-28	1	1342239568	169	2011-09-23	1
142	F16284+0411	CGCG 052-037	1342241365	1342241366	1342241367	1342241368	198	2012-03-14	2012-03-14	1	1342239572	169	2011-09-23	1
143	16304-6030	NGC 6156	1342241537	1342241538	1342241539	1342241540	198	2012-03-16	2012-03-16	1	1342239213	169	2011-09-22	1
144	F16330-6820	ESO 069-IG006	1342241669	1342241670	1342241667	1342241668	198	2012-03-17	2012-03-17	1	1342230810	169	2011-10-11	1
145	F16399-0937		1342238822	1342238823	1342238824	1342238825	198	2012-02-09	2012-02-09	1	1342239188	169	2011-09-22	1
146	F16443-2915	ESO 453-G005	1342241448	1342241449	1342241450	1342241451	198	2012-03-15	2012-03-15	1	1342229199	169	2011-09-22	1
147	F16504+0228	NGC 6240	1342213938	1342213939	1342213936	1342213937	71	2011-02-08	2011-02-08	2	1342203586	332	2010-08-23	2
148	F16516-0948		1342238828	1342238829	1342238826	1342238827	198	2012-02-09	2012-02-09	1	1342229189	169	2011-09-22	1
149	F16577+5900	NGC 6286, Atp 293	1342209331	1342209332	1342209333	1342209334	485	2010-11-10	2010-11-10	2	1342229148	169	2011-09-21	1
150	F17132+5313		1342233435	1342233436	1342233434	1342233434	198	2011-12-15	2011-12-15	1	1342229150	307	2011-09-21	1
151	F17138-1017		1342241454	1342241455	1342241456	1342241457	198	2012-03-15	2012-03-15	1	1342229190	169	2011-09-22	1
152	F17207-0014		1342241373	1342241374	1342241375	1342241376	198	2012-03-14	2012-03-14	1	1342203587	169	2010-08-23	4
153	F17222-5953	ESO 138-G027	1342241671	1342241672	1342241673	1342241674	198	2012-03-17	2012-03-17	1	1342229216	169	2011-09-22	1
154	F17530+3447	UGC 11041	1342231901	1342231902	1342231903	1342231904	198	2011-11-05	2011-11-05	1	1342229169	169	2011-09-22	1
155	F17548+2401	CGCG 141-034	1342231911	1342231912	1342231912	1342231910	198	2011-11-05	2011-11-05	1	1342229175	169	2011-09-22	1
156	F17578-0400		1342241377	1342241378	1342241379	1342241380	198	2012-03-14	2012-03-14	1	1342229187	169	2011-09-22	1
157	18090+0130		1342241357	1342241358	1342231115	1342231116	198	2012-03-13	2011-10-18	1	1342229185	169	2011-09-22	1
158	F18131+6820	NGC 6621, Atp 81	1342212029	1342212030	1342212031	1342212032	403	2010-12-16	2010-12-16	2	1342220865	169	2011-05-13	1
159	F18093-5744	IC 4687	1342207063	1342207064	1342207065	1342207066	485	2010-09-21	2010-10-25	2	1342204955	169	2010-10-25	4
160	F18145+2205	CGCG 142-034	1342231915	1342231916	1342231913	1342231914	198	2011-11-05	2011-11-05	1	1342229176	169	2011-09-22	1
161	F18293-3413		1342240663	1342240664	1342240661	1342240662	198	2012-03-06	2012-03-06	1	1342204954	169	2010-09-21	4
162	F18329-5950	NGC 6670A/B	1342235433	1342232434	1342235330	1342235331	198	2011-11-17	2011-12-25	1	1342229139	169	2011-09-21	1
163	F18341-5732	IC 4734	1342241541	1342241542	1342241543	1342241544	198	2012-03-16	2012-03-16	1	1342229222	169	2011-09-22	1
164	F18425+6036	NGC 6701	1342232435	1342232436	1342235328	1342235329	198	2011-11-17	2011-12-25	1	1342229137	169	2011-09-21	1
165	F19120+7320	VV 414, NGC 6786, UGC 11415	1342220812	1342220813	1342220814	1342220815	403	2011-04-29	2011-04-29	2	1342220623	169	2011-05-08	1
166	F19115-2124	ESO 593-IG008	1342216478	1342216479	1342216476	1342216477	198	2011-03-21	2011-03-21	1	1342215995	169	2011-03-13	1
167	F19297-0406		1342241615	1342241616	1342241617	1342241618	198	2012-03-16	2012-03-16	1	1342230837	445	2011-10-11	6
168	19542+1110		1342244232	1342244233	1342244234	1342244235	198	2012-04-12	2012-04-13	1	1342230847	169	2011-10-11	1
169	F19542-3804	ESO 339-G011	1342216466	1342216467	1342216464	1342216465	198	2011-03-20	2011-03-20	1	1342230821	169	2011-10-11	1

TABLE 2—Continued

#	IRAS Name	Optical Name	PACS						SPIRE					
			Blue 1 Obs. ID (4)	Blue 2 Obs. ID (5)	Green 1 Obs. ID (6)	Green 2 Obs. ID (7)	Duration (sec.)	Blue Obs. Date (8)	Green Obs. Date (9)	PACS PID ¹ (10)	Obs. ID (11)	Duration (sec.)	Obs. Date (12)	SPIRE PID ¹ (13)
170	F20221-2458	NGC 6907	1342232508	1342232509	1342217433	1342217434	240	2011-11-19	2011-03-30	1	1342230828	1217	2011-10-11	1
171	20264+2533	MCG+04-48-002	1342244230	1342244231	1342244228	1342244229	198	2012-04-12	2012-04-12	1	1342233320	169	2011-11-30	1
172	F20304-0211	NGC 6926	1342243832	1342243833	1342232514	1342232515	198	2012-04-06	2011-11-19	1	1342218992	169	2011-04-10	1
173	20351+2521		1342218714	1342218715	1342218716	1342218717	198	2011-04-17	2011-04-17	1	1342233323	169	2011-11-30	1
174	F20550+1655	CGCG 448-020, II Zw 096	1342243838	1342243839	1342243840	1342243841	198	2012-04-06	2012-04-06	1	1342233327	169	2011-11-30	1
175	F20551-4250	ESO 286-IG019	1342217438	1342217439	1342232496	1342232497	198	2011-03-30	2011-11-19	1	1342230815	445	2011-10-11	6
176	F21008-4347	ESO 286-G035	1342217440	1342217441	1342233498	1342233499	198	2011-03-30	2011-11-19	1	1342230813	169	2011-10-11	1
177	211011+5810		1342235326	1342235327	1342235324	1342235325	198	2011-12-25	2011-12-25	1	1342220627	169	2011-05-08	1
178	F21330-3846	ESO 343-IG013	1342243782	1342243783	1342232500	1342232501	198	2012-04-06	2011-11-19	1	1342244162	169	2012-04-12	1
179	F21453-3511	NGC 7130	1342218550	1342218551	115	2011-04-11	2011-04-11	7	1342210527	169	2010-11-23	7
180	F22118-2742	ESO 467-G027	1342234426	1342234427	1342234428	1342234429	198	2011-12-16	2011-12-16	1	1342245428	169	2012-05-06	1
181	F22132-3705	IC 5179	1342233499	13422334100	13422334101	13422334102	198	2011-12-14	2011-12-14	1	1342244158	169	2012-04-11	1
182	F22287-1917	ESO 602-G025	1342244875	1342244876	1342244877	1342244878	198	2012-04-23	2012-04-23	1	1342234670	169	2011-12-18	1
183	F22389-3359	UGC 12150	1342222924	1342222925	1342235322	1342235323	198	2011-06-22	2011-12-25	1	1342220870	169	2011-05-13	1
184	F22467-4906	ESO 239-IG002	1342233627	1342233628	1342232476	1342232477	198	2011-12-05	2011-11-18	1	1342234738	307	2011-12-19	1
185	F22491-1808		1342235609	1342235610	1342235611	1342235612	198	2011-12-26	2011-12-26	1	13422334671	445	2011-12-18	6
186	F23007+0836	NGC 7469, IC 5283, Arp 298	1342211175	1342211176	1342211177	1342211178	485	2010-12-27	2010-12-27	2	1342196915	169	2010-05-24	4
187	F23024+1916	CGCG 453-062 ^a	1342237366	1342237367	1342237364	1342237365	198	2012-01-12	2012-01-12	1	1342234765	169	2011-12-19	1
188	F23128-5919	ESO 148-IG002	13422111955	13422111956	1342209486	1342209487	71	2010-12-15	2010-11-18	2	1342209299	169	2010-11-09	2
189	F23135+2517	IC 5298	1342234090	1342234091	1342234092	1342234093	198	2011-12-14	2011-12-14	1	1342234766	169	2011-12-19	1
190	F23133-4251	NGC 7552	13422111631	13422111632	13422111633	13422111634	121	2010-12-27	2010-12-27	2	1342211028	639	2010-11-23	2
191	F23157+0618	NGC 7591	1342236592	1342236593	1342236590	1342236591	198	2012-01-06	2012-01-06	1	1342234758	169	2011-12-19	1
192	F23157-0441	NGC 7592	13422211802	13422211803	13422211804	13422211805	198	2011-05-28	2011-05-28	1	1342234750	169	2011-12-19	1
193	F23180-6929	ESO 077-IG014	1342232486	1342232487	1342233442	13422334425	198	2011-11-18	2011-12-16	1	1342234094	169	2011-10-11	1
194	F23254+0830	NGC 7674, HCG 96	1342237355	1342237356	1342237353	1342237354	198	2012-01-12	2012-01-12	1	1342234929	445	2011-12-18	9
195	23962+0314	NGC 7679	1342237347	1342237348	1342221786	1342221787	198	2012-01-12	2011-05-28	1	1342234755	583	2011-12-19	1
195	23262+0314 ^a	NGC 7682	1342237351	1342237352	1342237349	1342237350	198	2012-01-12	2012-01-12	1
196	F23365+3604		1342237856	1342237857	1342225459	1342225460	198	2012-01-05	2011-07-24	1	1342234751	583	2011-12-19	1
197	F23394-0353	MCG-01-60-022	1342221749	1342221750	1342221751	1342221752	240	2011-05-27	2012-01-12	1
198	23436+5257		1342221801	1342221802	1342221799	1342221798	240	2011-05-28	2011-05-28	1	1342236249	169	2012-01-03	1
199	F23444+2911	Arp 86, NGC 7752/3	1342223786	1342223787	1342233784	1342233785	198	2012-01-05	2012-01-05	1	1342234921	1324	2011-12-18	1
200	F23488+1949	NGC 7771	1342222930	1342222931	1342223182	1342223181	198	2011-06-22	2011-06-23	1	1342199379	169	2010-06-29	4
201	F23488+2018	Mrk 331	1342225242	1342225243	1342225240	1342225241	240	2011-07-22	2011-07-22	1	1342234682	583	2011-12-18	1

NOTE.—The column descriptions are (1) the row reference number. (2) The IRAS name of the galaxy, ordered by ascending RA. Galaxies with the “F” prefix originate from the *IRAS* Faint Source Catalog, and galaxies with no “F” prefix are from the Point Source Catalog. (3) Common optical counterpart names to the galaxy systems. (4) – (7) are the observation IDs for PACS imaging. Blue corresponds to a wavelength of 70 μm , while green corresponds to 100 μm . Each blue and green observation simultaneously observes the red 160 μm channel. Each observation needs a separate scan and cross-scan to reduce imaging artifacts. Four galaxies in our sample do not have 100 μm observations available since they were from other programs: IRAS F02401-0013 (NGC 1068), IRAS F09320+6134 (UGC 05101), IRAS F15327+2340 (Ap 220), and IRAS F214.53-3511 (NGC 7130). (8) The PACS observation duration for each scan and cross-scan, unless otherwise noted. We note these are *not* exposure times. (9) – (10) The observation dates for each scan and cross-scan, unless otherwise noted. (11) The PI of the PACS program from which the data were obtained. See PI list below. (12) The SPIRE observation ID, which includes all three 250 μm , 350 μm , and 500 μm observations. The scans and cross-scans for each target is combined into one observation. (13) The SPIRE observation duration. We note these are *not* exposure times. (14) The SPIRE observation date. (15) The PID of the SPIRE program from which the data were obtained. See PID list below.

¹PI list: 1 = OT1.sanders.1; 2 = KPGT.esturn.1; 3 = GT1.msanchez.2; 4 = KPOT.pvanderw.1; 5 = KPOT.rkennicu.1; 6 = OT1.dfarrah.1; 7 = GT1.lspinogl.2; 8 = cwilso01_1 (including KPGT); 9 = OT1.mcluver.2; 10 = KPGT.smadde01.1.

^aThese are very widely separated galaxy pairs that required two *Herschel* PACS observations.

^bGreen 1 and Green 2 have durations of 65 sec., Blue 1 has a duration of 141 sec. and Blue 2 has a duration of 153 sec.

^cGreen 2 was observed on 2012-04-24.

^dGreen 2 was observed on 2012-03-29.

^eRescheduled to replace previous PACS observations: 1342245766 1342245767 1342245764 1342245765.

4. Data Processing and Reduction

The data processing for our *Herschel* data was performed using the Herschel Interactive Processing Environment (HIPE, Ott 2010) version 14 software tool, which provides the means to download, reduce, and analyze our data. All of our data reduction routines are derived from the standard pipeline scripts found within HIPE, where the programming language of choice is Jython (a Java implementation of the popular Python language). In addition to handling the data processing, HIPE also downloads and maintains all of the instrument calibration files needed for the data processing.

4.1. PACS Data Reduction

4.1.1. Choosing a PACS Map Maker

Due to the bolometer and scanning nature of the PACS instrument, it was important to determine the best map-making software to translate the time ordered data (TOD) into an image. The PACS bolometers (indeed all bolometers) produce noise that increases as one approaches lower temporal frequencies, commonly referred to as $1/f$ noise, that must be removed by the map-maker. If this noise is left uncorrected in the time ordered data, the result would be severe striping or even gradients across the image. In addition the map making software must also remove the bolometers' common mode drift (which is a changing offset as function of time) from the TOD, termed *pre-processing*, as well as cosmic ray hits and individual bolometer drift. The PACS team released a Map-making Tool Analysis and Benchmarking report² in November 2013 with an update in March 2014 that characterized in detail the six different map making packages available to reduce PACS data. We summarize the information presented in this report below to decide upon the best map making software to use, since it was important that all of the *Herschel* data on our sample were processed uniformly.

The PACS team tested the performance of six different publicly available map-making packages: MADMap (Microwave Anisotropy Dataset mapper, Cantalupo et al. 2010), SANEPIC (Signal And Noise Estimation Procedure Including Correlation, Patanchon et al. 2008), Scanamorphos (Roussel 2013), JScanam (Jython Scanamorphos³), Tamasis (Tools for

Advanced Map-making, Analysis and SImulations of Submillimeter surveys, Barbey et al. 2011), and Unimap (Piazzo et al. 2015) (see §2 and §4 of the Map-making Tool and Analysis Benchmarking report for a description of each code). We did not consider the PACS high pass filter (HPF) reduction software, since HPF maps are background-subtracted and will miss a significant amount of extended emission outside approximately one beam area. To evaluate each of the packages, a combination of simulated and real data from PACS were used. Except in a few cases, most of our fluxes are within the Benchmarking report's "bright flux regime" of 0.3 – 50 Jy, while the "faint flux regime" is defined to be 0.001 – 0.1 Jy (see Figure 5). Below we summarize the five tests performed on each map maker from the benchmarking report:

- 1) A power spectrum analysis which tests the map maker's ability to remove noise while preserving extended fluxes over large angular sizes on the map. This tests each code's performance in removing the $1/f$ noise from the PACS data, and consequently how well gradients and stripes are removed from the maps.
- 2) A difference matrix is computed for each map maker's output, which evaluates differences in fluxes for individual sky pixels over the entire image. ($S - S_{\text{true}}$) is computed for each pixel and plotted against S_{true} , and the resulting scatter, offset, and slope is evaluated.
- 3) Each map maker's performance in point source photometry is compared to fluxes measured from the HPF maps for both bright (0.3 – 50 Jy) and faint (0.001 – 0.1 Jy) cases. Since the HPF maps produced by HIPE are designed specifically for the case of point sources, they provide the most accurate reference point source fluxes.
- 4) Extended source photometry tests each map maker's ability to recover extended flux over large areas of the map. To assess this, each code's output is compared to IRAS data on M31 from the Improved Reprocessing of the IRAS Survey (IRIS, Miville-Deschénes & Lagache 2005).
- 5) The noise characteristics each map maker introduces into the final map are evaluated. This includes statistical tests on the pixel-to-pixel variance as well as the shape of the overall distribution of fluxes in each map pixel. The noise patterns are also evaluated with

²http://herschel.esac.esa.int/twiki/pub/Public/PacsCalibrationWeb/pacs_mapmaking_report_ex_sum_v3.pdf

³This is the HIPE/PACS implementation of the Scanamorphos algo-

rithm however they both differ in many assumptions, hence why they were tested separately.

regard to how isotropic the noise appears in the maps.

Considering the results of these extensive tests, it was difficult to select the best map maker for our PACS data. We rejected the High Pass Filter method outright since many of our galaxies are easily resolved at the PACS wavelengths, and would therefore have a significant amount of extended flux missed by the HPF pipeline. We decided against using SANEPIC since it significantly overestimated the true flux for both bright and faint point source photometry. We also ruled out using Tamasis since it has a tendency to introduce more pronounced noise along the scan directions. This left us with four remaining choices: JScanam, MADMap, Scanamorphos, and Unimap. We finally decided on using JScanam to reduce all of our PACS data, as it gave the best balance between photometric accuracy and map quality. Specifically, it reproduced a power spectrum closest to the original, it had the flattest ($S - S_{\text{true}}$) vs. S_{true} plot, and it yielded the most accurate photometry for both point and extended sources in both channels.

For a small fraction of our maps where JScanam could not remove all of the image artifacts (usually gradients due to non-optimal baseline subtraction), we used Unimap to process the data, since it performed just as well as JScanam. Unlike JScanam, Unimap approaches map making differently, using the Generalized Least Square (GLS) approach, which is also known as the Maximum Likelihood method if the noise has a Gaussian distribution. For a very few cases where even Unimap did not produce optimal results, we resorted to using MADMap. This map maker requires that the noise properties of the detectors are determined *a-priori*, from which a noise filter can be generated to filter out the $1/f$ noise. Finally, despite that not all of the PACS maps were generated using the same map maker, we note that the resulting photometry from all three map makers are remarkably consistent as shown in the Benchmarking report (and addendum) from the PACS team, hence giving one the freedom to use the map maker that produces the best image quality.

4.1.2. PACS Map Making With JScanam

All of our *Herschel*-GOALS PACS data were reduced in HIPE 14 using the latest available PACS calibration version 72_0 released in December 2015. In order to alleviate the processing time for all 211 objects, we started our data processing from the Level

1 products downloaded from the HSA. These Level 1 data products have the advantage of an improved reconstruction of the actual *Herschel* spacecraft pointing, which reduces distortions on the PSF due to jitter effects. Compared to previous maps from our data processing, the new maps have slight shifts of up to $\sim 1''.5$, and slightly smaller PSFs in unresolved GOALS objects.

Since each PACS scan and cross-scan are separate observations, JScanam requires two observations each for the blue and green data. On the other hand the red channel data are observed simultaneously regardless if the blue or green filter is used, so we have four observations in the red channel. Processing for both the blue and red cameras are identical, with the red data requiring a further step of combining the two pairs of scan and cross-scan data. Below we describe the key steps in the data reduction process.

After loading each scan and cross-scan observation context from HSA into HIPE, the first step was to execute the task `photAssignRaDec` to assign the RA and declination coordinates to each pixel in each frame which allows JScanam to run faster. The next step was to remove the unnecessary frames taken during each turnaround in the scan or cross-scan using the `scanamorphosRemoveTurnarounds` task. We opted to use the default speed limit which is $\pm 50\%$ of our nominal scan speed ($20''/\text{sec.}$), so any frames taken at scan speeds below $10''/\text{sec.}$ or above $30''/\text{sec.}$ were removed. After turnaround removal the `scanamorphosMaskLongTermGlitches` task in JScanam goes through the detector timelines and masks any long term glitches.

At this point we have a detector timeline of flux detected by the bolometers as a function of time with the turnarounds and long term glitches removed. Using the `scanamorphosScanlegBaselineFitPerPixel` task, our next step is to subtract a linearly fit baseline from each bolometer pixel of every scan leg, with the intention of creating a “naive” map for source masking purposes. This is done iteratively where the most important parameter is the `nSigma` variable, which controls the threshold limit for source removal. For our data any points above `nSigma=2` times the standard deviation of the unmasked data are considered real sources, until the iteration converges.

The next step is to join the scan and cross-scan data together for a higher signal-to-noise map to create the source mask. In the `scanamorphosCreateSourceMask` task we set a `nSigma=4`, so that any emission above

4 standard deviations is masked out. At this point it is not necessary to mask out all of the faint extended emission, only the brightest regions. After the source mask is determined, they are applied to the individual scan and cross-scan timelines and the real processing begins.

With the `galactic` option set to “true” in `scana-morphosBaselineSubtraction`, we only want to remove an offset in the time ordered data over all the scan legs, and subtract it from all the frames. This is done by calculating a median offset over only the unmasked part of the data which importantly does not include any bright emission, and subtracting it from each pixel’s timeline. This is so that extended flux is treated correctly when subtracting the baseline (due to the telescope’s own infrared emission) from the signal timelines, even in cases where the emission is not concentrated in a small region. We emphasize this does not imply the subtraction of the Galactic foreground emission from our maps.

Once the baseline is removed we need to identify and mask the signal drifts produced by the calibration block observation. In previous versions of our reduction, these drifts have produced very noticeable gradients in our final maps. To do this the task `scanamorphosBaselinePreprocessing` assumes that the scan and cross-scan are orthogonal to each other, which would result in gradients in different directions. The drift removal is also based on the assumption that the drift power increases with the length of the considered time ($1/f$ noise). For this reason the first iteration removes the drift component over the longest time scale which corresponds to the entire scan (or cross-scan). After that drifts are removed over four scan legs, and finally over one scan leg, with the remaining drift in each successive iteration becoming weaker. In order to actually calculate the drift in each iteration, a single scan (or scan legs) is back projected over itself in the orthogonal direction, which transforms the generally increasing or decreasing signal drift into oscillatory drifts that cancel out on large time scales. The orthogonal back projected timeline is then subtracted from the scan timeline, and the difference which represents the drift is fitted by a line.

At this point the scan and cross-scan data have been cleaned enough to be combined. Since signal drifts were only eliminated over timescales down to one scan leg, the next step is to remove them from over time scales shorter than one scan leg. These drifts are due to for example cosmic ray hits on the PACS instruments,

which produce different effects on the time ordered data depending on which part is hit. If an individual bolometer or bolometer wall is hit, it only affects those bolometer(s). However if a cosmic ray hits the readout electronics, it introduces a strong positive or negative signal for all of the bolometers read by the electronics, which can be anything from a single bolometer to an entire detector group. These jumps typically last a few tens of seconds before settling to the previous level again, and would result in stripes across the final map if not properly removed.

To remove these individual drifts, we use the task `scanamorphosIndividualDrifts` to first measure the scan speed and calculate the size of a map pixel that can hold six subsequent samples of a detector pixel crossing it. We use a threshold of `nSigma=5` which is large enough to include the strongest drifts but still masking out the real source. Then the average flux value and standard deviation from the detector pixels crossing that map pixel is calculated, along with the number of detector pixels falling into that map pixel. Using the threshold noise value (from the calibration files), we eliminate any individual detector fluxes for that map pixel that has a standard deviation greater than the noise threshold. The missing values are then linearly interpolated, and the individual drift is subtracted from the detector timeline.

After all of the individual drifts are corrected, the time ordered data are saved and we project the timelines from both the scans and cross-scans into our final map using the `photProject` task. We use a pixel scale of $1''.6\text{ pixel}^{-1}$ for the $70\text{ }\mu\text{m}$ and $100\text{ }\mu\text{m}$ maps, and a pixel scale of $3''.2\text{ pixel}^{-1}$ for the $160\text{ }\mu\text{m}$ maps. By default the `photProject` task assumes in projection an active pixel size of $640\text{ }\mu\text{m}$, however if we ‘drizzle’ the projection we can assume smaller PACS pixels. This allows us to reduce the noise correlation between neighboring map pixels and also sharpens the PSF. We used a `pixfrac` of 0.1, which controls the ratio between the input detector pixel size and the map pixel size. At this point the $70\text{ }\mu\text{m}$ and $100\text{ }\mu\text{m}$ maps are finished. For the $160\text{ }\mu\text{m}$ data, both pairs of scan and cross-scan are identically processed separately, and then combined in the end using `photProject` again.

4.2. SPIRE Data Reduction

4.2.1. Choosing a SPIRE Map Maker

Similar to the PACS instrument, the SPIRE detectors exhibit certain effects that are characteristic to bolometers. Namely, they introduce an increasing amount of noise as the length of the considered time increases ($1/f$ noise), as well as constant and changing offsets (drifts) which could result in stripes or gradients in the final image. Therefore any map maker for SPIRE must be able to remove these instrumental effects, while preserving flux (point source and extended) and creating distortion-free maps. The SPIRE team released a Map Making Test Report⁴ in January 2014 that benchmarked in depth seven different map making codes, several of which were also present in the PACS Map Making report. The map makers that participated in the benchmarking were the Naive Mapper, Destriper in two flavors (P0 and P1), Scanamorphos, SANEPIC, and Unimap. The two flavors of the Destriper differ in the polynomial order used to subtract the baseline, where P0 corresponds to a polynomial order of 0 (i.e. the mean) and P1 corresponds to an order of 1. Two additional super-resolution map makers were also tested, however we did not consider them for processing our SPIRE data. For a summary of each map maker we refer the reader to the SPIRE Map Making Test Report.

For the Map Making Test Report, the authors tested these five map makers based on a variety of benchmarks that are very similar to the PACS Map-Making Tool Analysis and Benchmarking report. A combination of real and simulated SPIRE data were used, covering the full variety of science cases such as faint vs. bright sources, extended vs. point sources, and complex vs. empty fields. The simulated SPIRE data have the advantage of comparing each of the map makers' outputs to the "truth" image, allowing for an unbiased comparison between all of the map making codes. These simulated observations were synthesized from two different layers: a truth layer based on a real or artificial source, and a noise layer from real SPIRE observations so that both instrumental and confusion noise is accurately represented. Below we summarize the four metrics and performance results for the five possible map makers:

1) Using simulated data, the deviation of each map maker's output is compared to the original synthetic

data. To quantify the deviation from truth, a scatter plot of $(S - S_{\text{true}})$ is plotted against S_{true} , and the resulting slopes, relative deviations, and absolute deviations are compared.

2) The 2D power spectrum of each map makers' output is compared to the "truth" image. The goal here is to quantify how well $1/f$ noise is removed from the maps while leaving real fluxes (point and extended) intact, as well as how high spatial frequency (small spatial scale) fluxes are treated.

3) Using the simulated data, point source photometry from each of the map makers were compared to the "truth" images. This tests how well point source fluxes are recovered by each map maker in both the bright ($S \approx 300$ mJy) and faint ($S \approx 30$ mJy) regimes.

4) Finally, extended source photometry was tested between all the map makers using the synthetic data. A simulated exponential disk with an e -folding radius of $90''$ was used, and fluxes were measured using aperture photometry.

Using the results from these tests, we concluded that the best map maker to use was the Destriper P0 mapper. It performed remarkably well among the other map makers, especially in cases where complex extended emission is present. Although the Map Making report warned about its inability to properly remove the "cooler burp" effect, the most recent version of Destriper P0 in HIPE 14 was updated to include proper treatment of this instrument effect. On the other hand Destriper P1 compared unfavorably, especially in introducing artificial gradients in many cases. The Naive Mapper was also ruled out due to it frequently over-subtracting the background where extended emission is present. The map maker SANEPIC showed significant deviations from the "truth" map, because the code makes some incorrect assumptions about the data. Finally, although Scanamorphos can handle faint pixels very well, it showed significant deviations in the bright pixel case ($S > 0.2$ Jy). This is important since many galaxies in our sample are nearby and thus quite bright.

In HIPE 14, we used a more advanced version of the Destriper code called the "SPIRE 2-Pass Pipeline" that was released by the SPIRE instrument team. The basic pipeline processing steps and settings follow exactly that of the Destriper P0 (or P1 if the user so chooses) map maker, with the added benefit of producing exceptionally clean maps to be used in the final *Herschel* Science Archive. Specifically, the 2-Pass Pipeline mitigates residual faint tails and glitches in

⁴<http://arxiv.org/pdf/1401.2109v1.pdf>

the timeline, which if not removed can produce ringing effects. The primary aim of this pipeline is to produce maps with better detections of outliers in the TOD such as glitches, glitch tails, and signal jumps, and remove any Fourier ringing that would result from failed outlier detections. As an overview, the first pass runs a stripped down version of the pipeline using only the bare minimum tasks that excludes any Fourier analysis. This includes running the Second Level Deglitching task to produce a mask over the glitches, which is then applied back to the Level 0.5 products⁵. Then a second pass of the pipeline is executed identical to the original Destripes map maker.

4.2.2. SPIRE Map Making With 2-Pass Pipeline and Destripes P0

Our final SPIRE maps were reduced in HIPE 14 using the latest calibration version SPIRECAL_14_2 released in December 2015. Below we summarize the key data reduction steps, however a more detailed description on the photometer pipeline can be found within Dowell et al. (2010).

Our data processing begins with the Level 0 data products downloaded from HSA, which are the raw data formatted from satellite telemetry containing the readout in ADU from each SPIRE bolometer. After an observation is loaded into HIPE, the first step is to execute the Common Engineering Conversion and format it into Level 0.5 products. These products are the uncalibrated and uncorrected timelines measured in Volts, and contain all of the necessary information to build science-grade maps.

The first step in processing our data from Level 0.5 to Level 1 is to join all the scan legs and turnarounds together. The turnaround occurs when the spacecraft turns around after a scan leg to begin another scan. We opted to use the turnaround data to include as much data within our maps as possible. Next the pipeline produces the pointing information for the observation, based on the positions of the SPIRE Beam Steering Mechanism as well as the offset between SPIRE and the spacecraft itself (referred to as the Herschel Pointing Product). This results in the SPIRE Pointing Product which is used later on in the pipeline. After calculating the pointing information, the pipeline corrects for any electrical crosstalk between the thermistor-bolometer channels. The thermistors measure the tem-

perature of the array bath as a function of time so that later we may accurately subtract the instrument thermal contribution, or temperature drift from the data timelines.

The next step is the signal jump detector, which detects and removes jumps in the thermistor timelines that would otherwise cause an incorrect temperature drift correction. To do this, the module subtracts baselines and smoothed medians from the thermistor timelines to identify any jumps. After deglitching the thermistor timelines, we must deglitch any cosmic ray hits on the bolometers themselves. This is an important step since any glitches that are not removed would manifest itself as image artifacts on the final maps. The pipeline does this in two steps, where the first step is to remove glitches that occur simultaneously in groups of connected bolometer detectors. This can occur when a cosmic ray hits the substrate of an entire photometer array, and can leave an imprint of the array on the final map. The second step is to run the wavelet deglitcher on the timeline data, which uses a complex algorithm to remove glitches in Fourier space.

After deglitching the detector timelines, a low pass filter response correction is applied to the TOD. This is to take into account the delay in the electronics with respect to the telescope position along a scan, in order to ensure a match between the astrometric timeline from the telescope, and the detector timeline from the instrument. At this point we can apply the flux conversion to the detector timelines, changing the units from Volts to Jy beam⁻¹. The next step involves corrections to the timelines due to temperature drifts, which are caused by variations of the detector array bath temperatures. First, with the coolerBurpCorrection flag set to true, the pipeline flags data that were affected by the “cooler burp” effect. Observations taken during this effect, usually in the first ~8 hours of SPIRE observations, can create unusual temperature drifts. The temperature drift correction step then removes low frequency noise by subtracting a correction timeline for each detector using data and calibration information. The “cooler burp” is also removed at this stage by applying additional multiplicative factors to the correction timeline.

Next we apply a bolometer time response correction which corrects any remaining low-level slow response from the bolometers. This is done by multiplying the timelines in Fourier space by an appropriate transfer function obtained from a calibration file containing the detector time constants. After this step

⁵The Level 0.5 products are the output after running the raw satellite telemetry through the engineering pipeline.

we attach the RA and declination to the data timelines by using the SPIRE Pointing Product generated earlier. Since many of our objects are extended in nature, we must apply an additional extended emission gain correction for individual SPIRE bolometers. This is because the pipeline so far assumes uniform beams across the array, whereas in reality there exists small variations among different bolometers due to their positions on the array.

We then use the Destripes to remove striping from the final maps. Since the dominant fluxes seen by SPIRE are from the telescope itself, the science signal is very small in comparison. Therefore to isolate the science signal we must subtract out thermal contributions from the telescope. However even after doing this, there are still large differences in residual offsets between different bolometers due to variations in the thermal and electronic aspects of the system, resulting in striping. This is where the Destripes P0 comes in, which effectively takes as input SPIRE Level 1 context, and outputs destriped Level 1 timelines. To do this we first subtract a median baseline as an initial guess, then we use a polynomial order of 0 to iteratively update the offsets in the TOD for each detector until an optimal solution is found. This algorithm effectively normalizes the map background to zero, however we do include the true background using data from the *Planck* High Frequency Instrument (HFI) for the PMW and PLW arrays (see §6.2.1). After destriping we run the optional second level deglitching in order to remove any residual glitches that may still remain.

At this point the data have been processed to Level 1, and in the case of the first pass, only tasks that don't involve any manipulation in Fourier space were omitted. The resulting second level deglitching mask from the first pass of this pipeline is applied to the Level 0.5 data, and the entire process is repeated in a second pass, this time including operations in Fourier space.

The final step in our SPIRE data reduction is to project the drift-corrected, deglitched, and destriped timelines into our Level 2 science grade map. To do this we use a Naive Mapper, which simply projects the full power seen by a bolometer onto the nearest map pixel. The final map pixel scales used were 6'', 10'', and 14'' for the PSW, PMW, and PLW arrays respectively. For each instant of time on each bolometer's timeline, the measured flux is added to the total signal map and a value of 1 is added to the coverage map. Once this is done for all bolometer timelines, the total

signal map is divided by the coverage map to obtain the flux density map.

Although the 2-pass pipeline does an excellent job of removing all SPIRE image artifacts, approximately twenty of the maps still exhibited stripes and residual glitches in the final map. These maps were reprocessed by first using the SPIRE bolometer finder tool to identify the misbehaving bolometer, and then masking the affected portions in that bolometer's Level 1 timeline. The data were then rerun through the Naive Mapper to produce a clean and deglitched Level 2 science grade map.

5. The *Herschel*-GOALS Image Atlas

In the following pages in Figure 3 we present the entire *Herschel* atlas of the GOALS sample, ordered by ascending RA. The archived⁶ *Herschel* GOALS maps are in standard `*.fits` format with image units of Jy pixel⁻¹. Each page consists of six panels for the 70 μm, 100 μm, 160 μm, 250 μm, 350 μm, and 500 μm channel maps.

The IRAS name of each galaxy or galaxy system is shown at the top, along with their common names from optical catalogs. Each of the six panels are matched and have the exact same map center as well as field of view. The center coordinates of the *Herschel* atlas images are listed in Table 1. For galaxy systems with multiple components, the center coordinate is chosen to be roughly equidistant from all components. The field of view for each panel is shown on the bottom left of the 70 μm panel, and represents the physical length of one side of each panel. A scale bar also indicates the physical length of 10 kpc at the distance of the galaxy (derived from the angular diameter distance in Table 1), along with the equivalent angular distance. The circle on the bottom right of each panel represents the beam size at that wavelength. Finally the right ascension and declination coordinates are indicated in J2000 sexagesimal as well as decimal format. The sexagesimal RA coordinates have the hour portion truncated for all but the center tick mark, to keep the tick name sizes manageable.

Since many objects appear as point sources at some or all of the *Herschel* wavelengths, the morphologies of these galaxies will be dominated by the PSF at that wavelength. In the case of PACS, the PSF is characterized by a narrow circular core elongated in the

⁶<http://irsa.ipac.caltech.edu/data/Herschel/GOALS>

spacecraft z -direction, at $70\ \mu\text{m}$ and $100\ \mu\text{m}$. In addition there is a tri-lobe pattern at the several percent level at all three wavelengths, however it is strongest at $70\ \mu\text{m}$. Finally, there are knotty structured diffraction rings at the sub-percent level, again most apparent at $70\ \mu\text{m}$ and $100\ \mu\text{m}$. In the case of SPIRE, the PSF appears mostly circular, however for the brightest objects, airy rings are also visible.

In order to show as much detail in these maps, we used an inverse hyperbolic sine (asinh) stretch function to maximize the dynamic range of visible structures. Also to keep all the PACS images uniform, the background for each image was adjusted such that the background is very close to zero. The format in our *Her-schel* atlas matches that of companion image atlases from *Hubble Space Telescope*-ACS (Evans et al. 2017) and *Spitzer*-IRAC/MIPS (Mazzarella et al. 2017), allowing one to study the morphological properties of these galaxies from $0.4\ \mu\text{m}$ to $500\ \mu\text{m}$.

IRAS F00073+2538 (NGC 23)

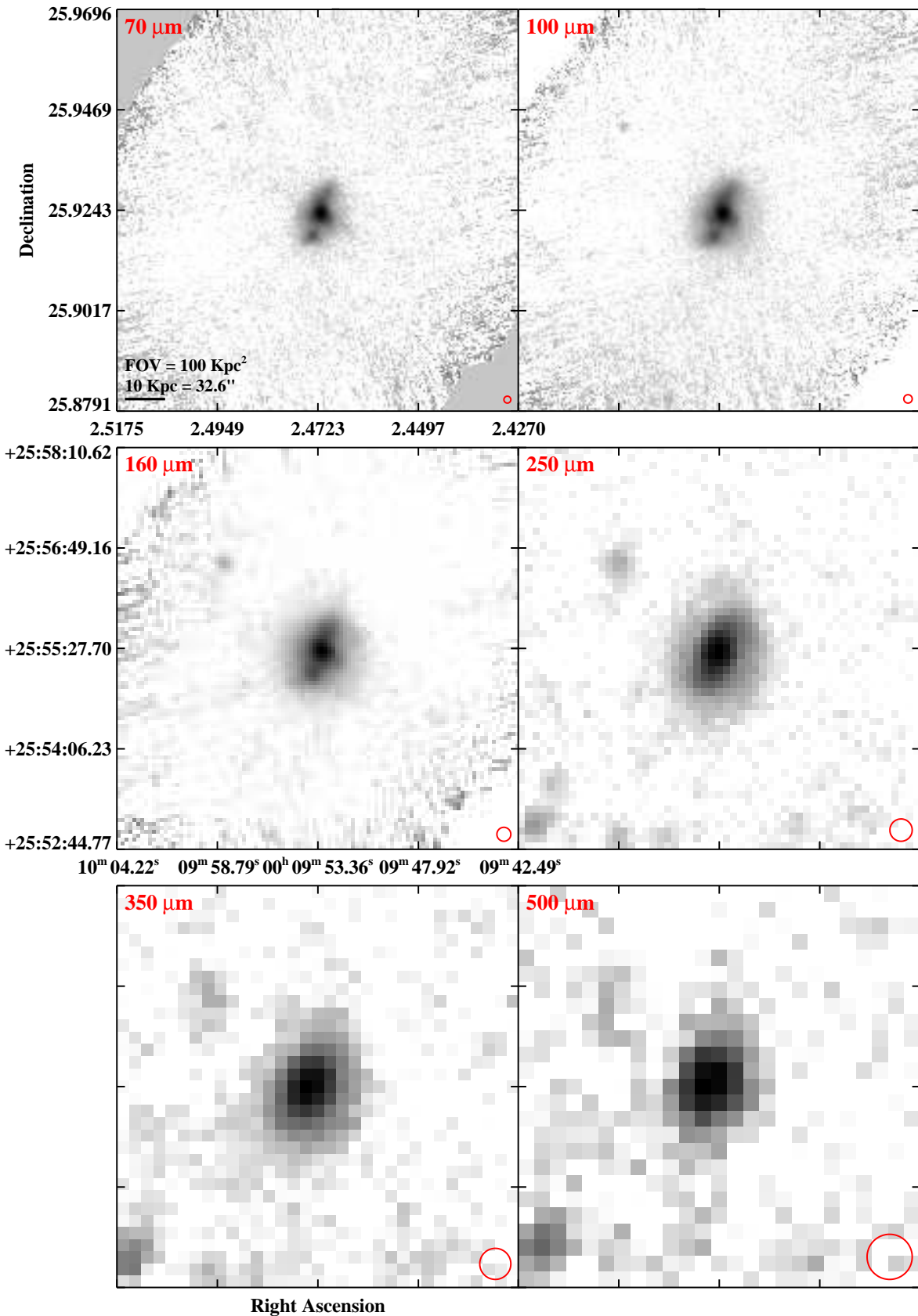


Fig. 3.— The *Herschel* GOALS atlas, displaying imagery of local LIRGs and ULIRGs in the three PACS bands and three SPIRE band. An asinh transfer function is used to maximize the dynamic range of visible structures, and a common field of view of approximately $\sim 100 \times 100 \text{ kpc}^2$ is used to facilitate comparisons across the sample and with images in the GOALS *Spitzer* atlas in Mazzarella et al. (2017). Scale bars indicate 10 kpc and the equivalent angular scale as derived from the angular diameter distance in Table 1. The beam sizes at each wavelength are indicated on the lower right of each panel. The atlas is ordered by increasing right ascension.

IRAS F00085–1223 (NGC 34/Mrk 938)

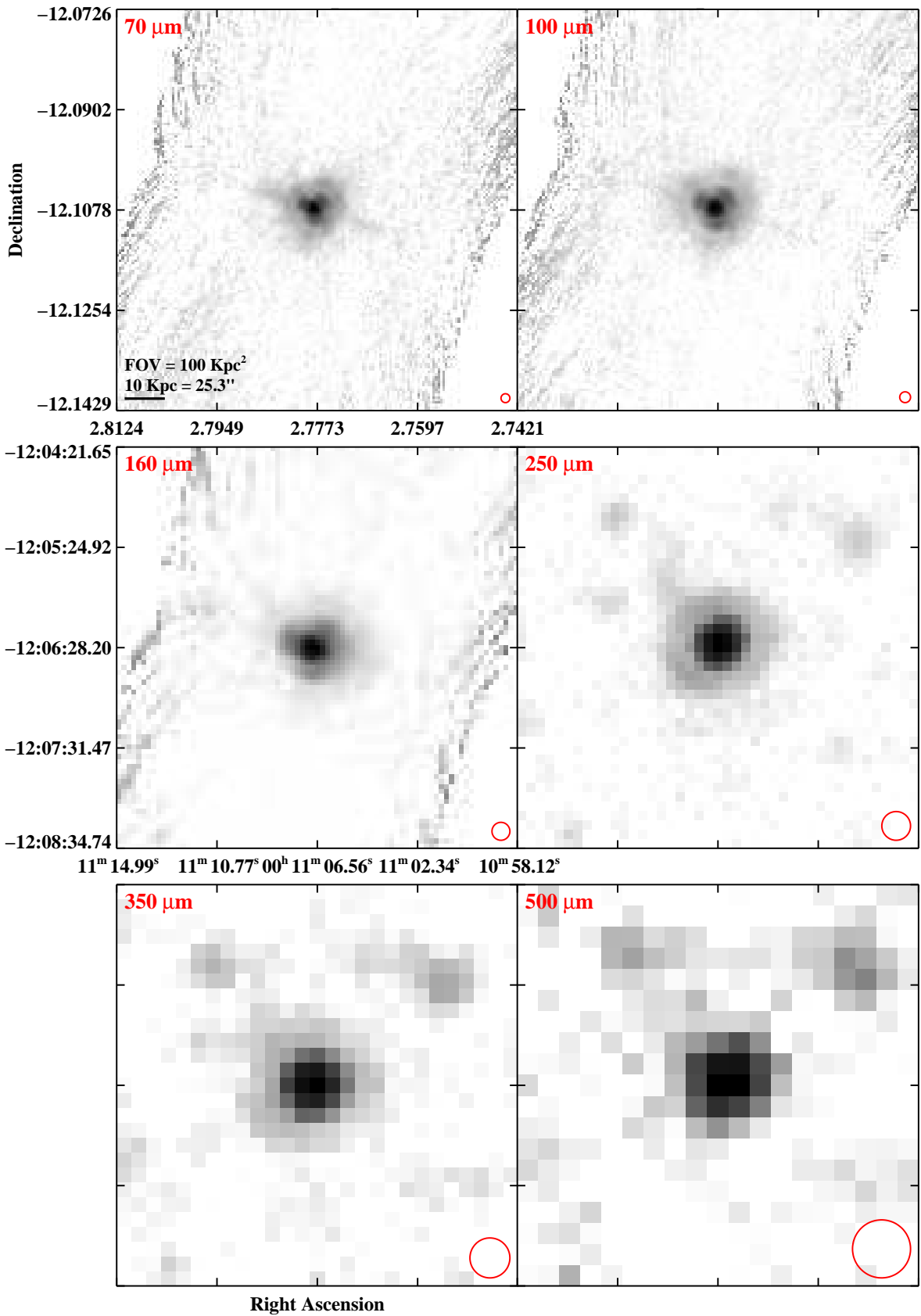


Fig. 3.— Continued (page 2 of 209).

IRAS F00163–1039 (Arp 256)

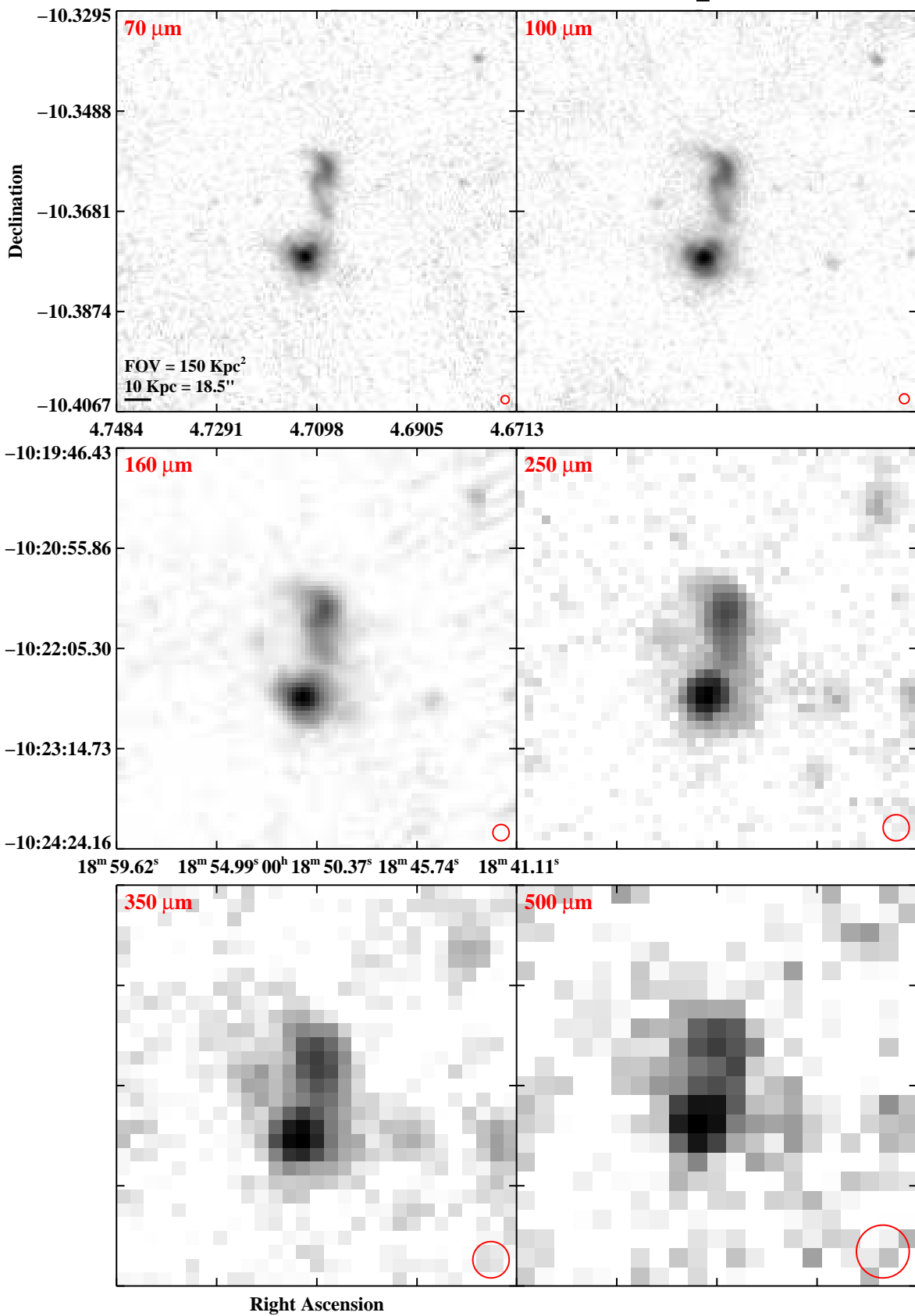


Fig. 3.— Continued (page 3 of 209).

IRAS F00344–3349 (ESO 350–IG 038/Haro 11)

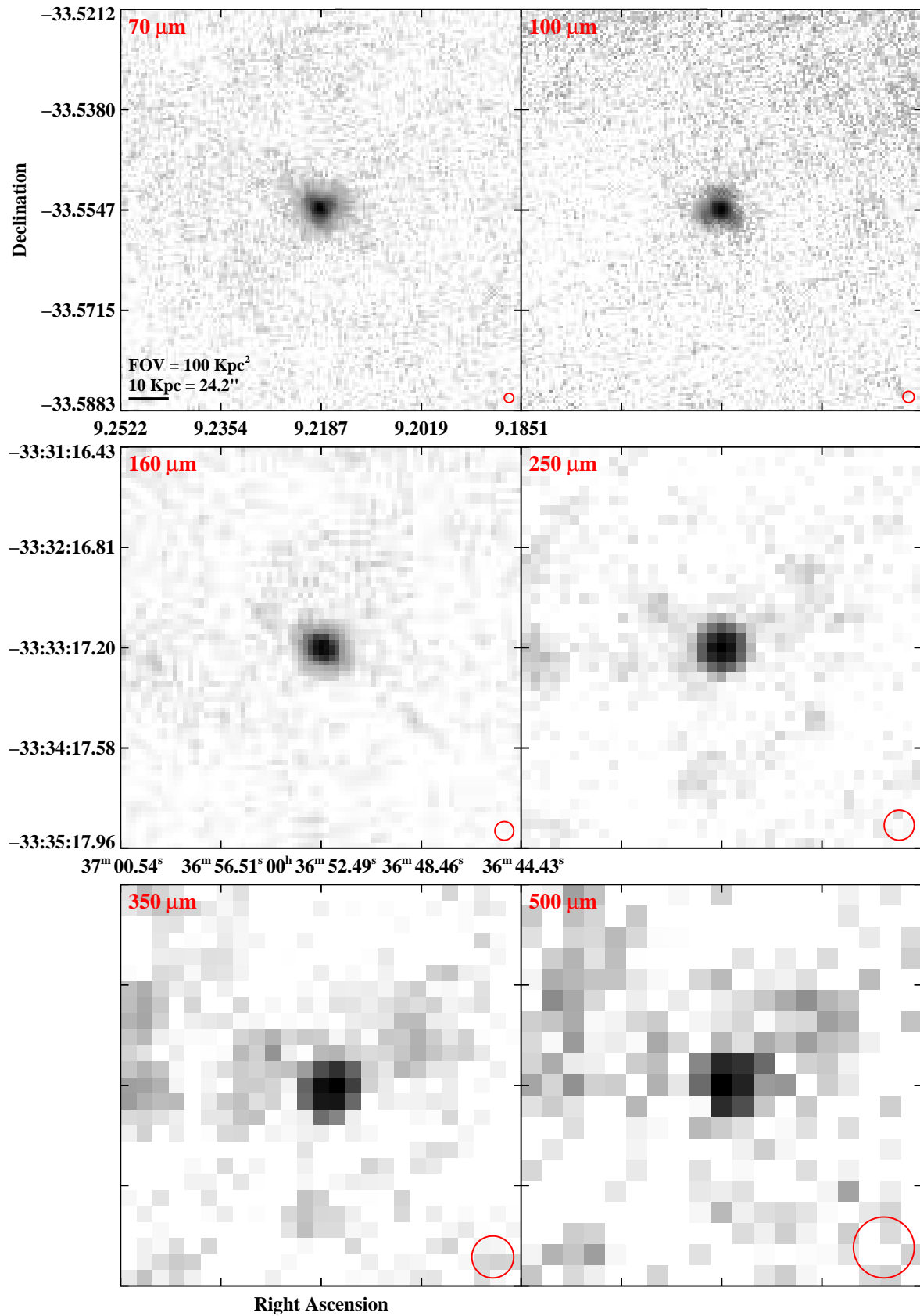


Fig. 3.— Continued (page 4 of 209).

IRAS F00402–2349 (NGC 232)

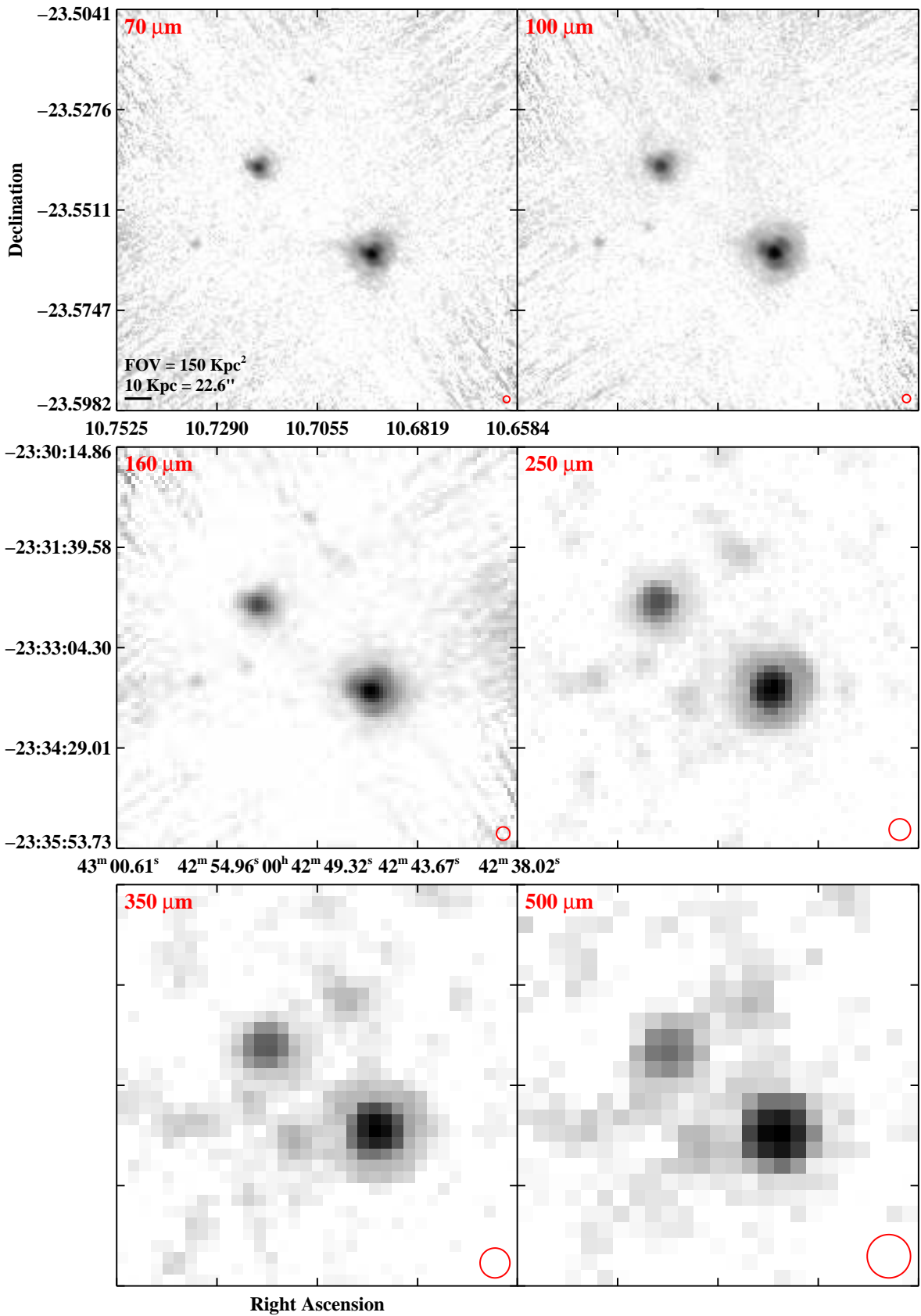


Fig. 3.— Continued (page 5 of 209).

IRAS F00506+7248 (MCG+12-02-001)

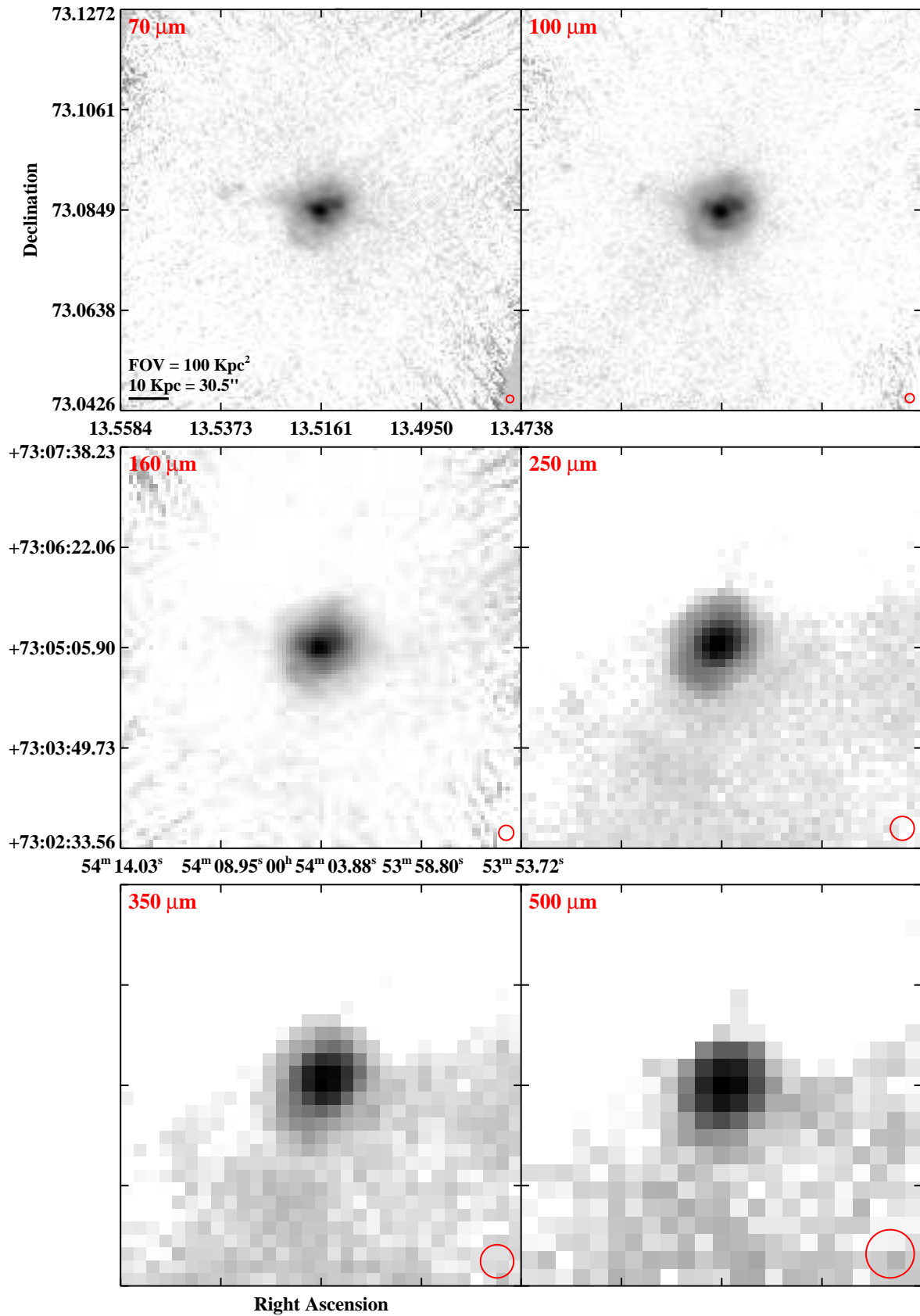


Fig. 3.— Continued (page 6 of 209).

IRAS F00548+4331 (NGC 317B)

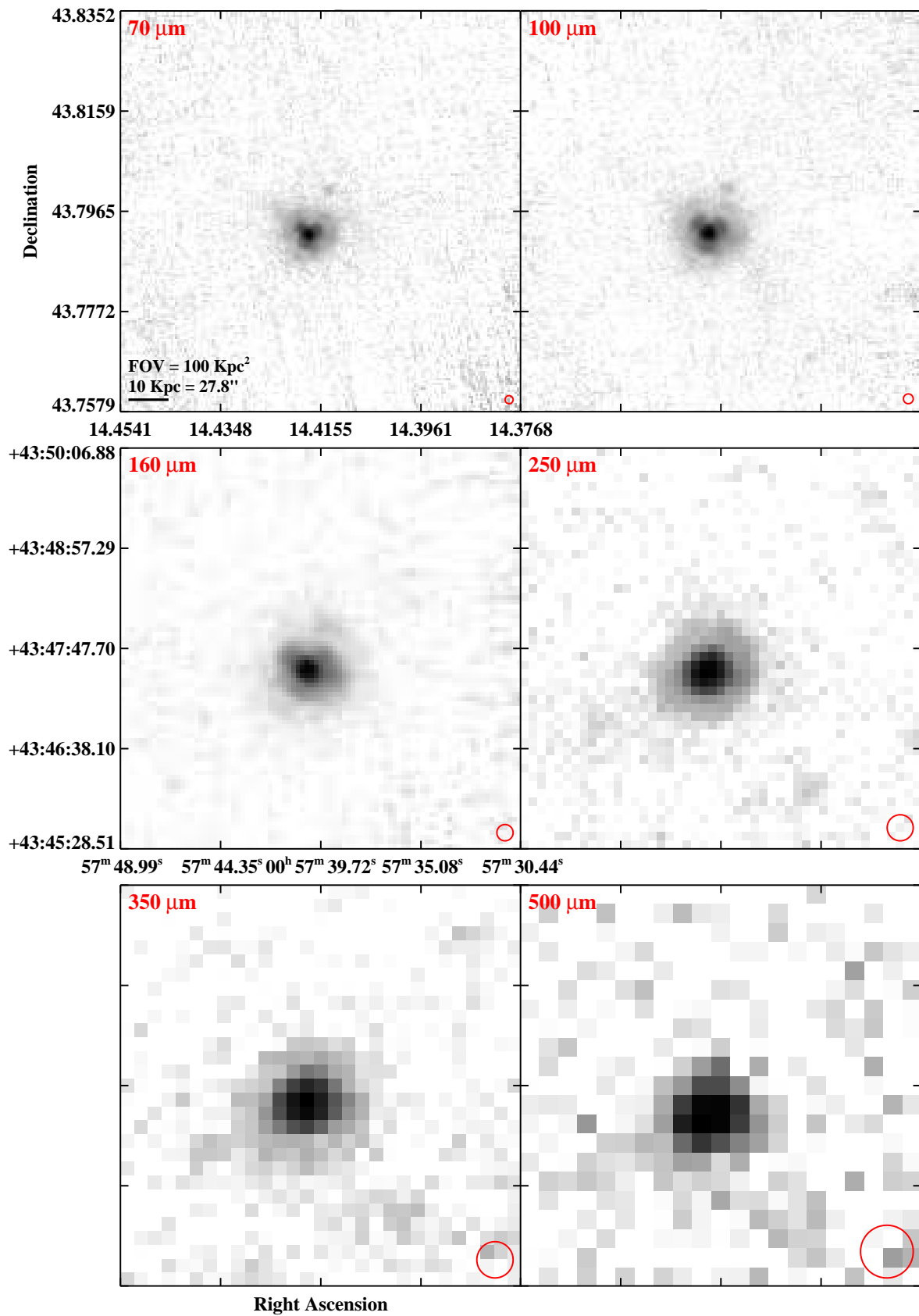


Fig. 3.— Continued (page 7 of 209).

IRAS F01053–1746 (IC 1623/Arp 236)

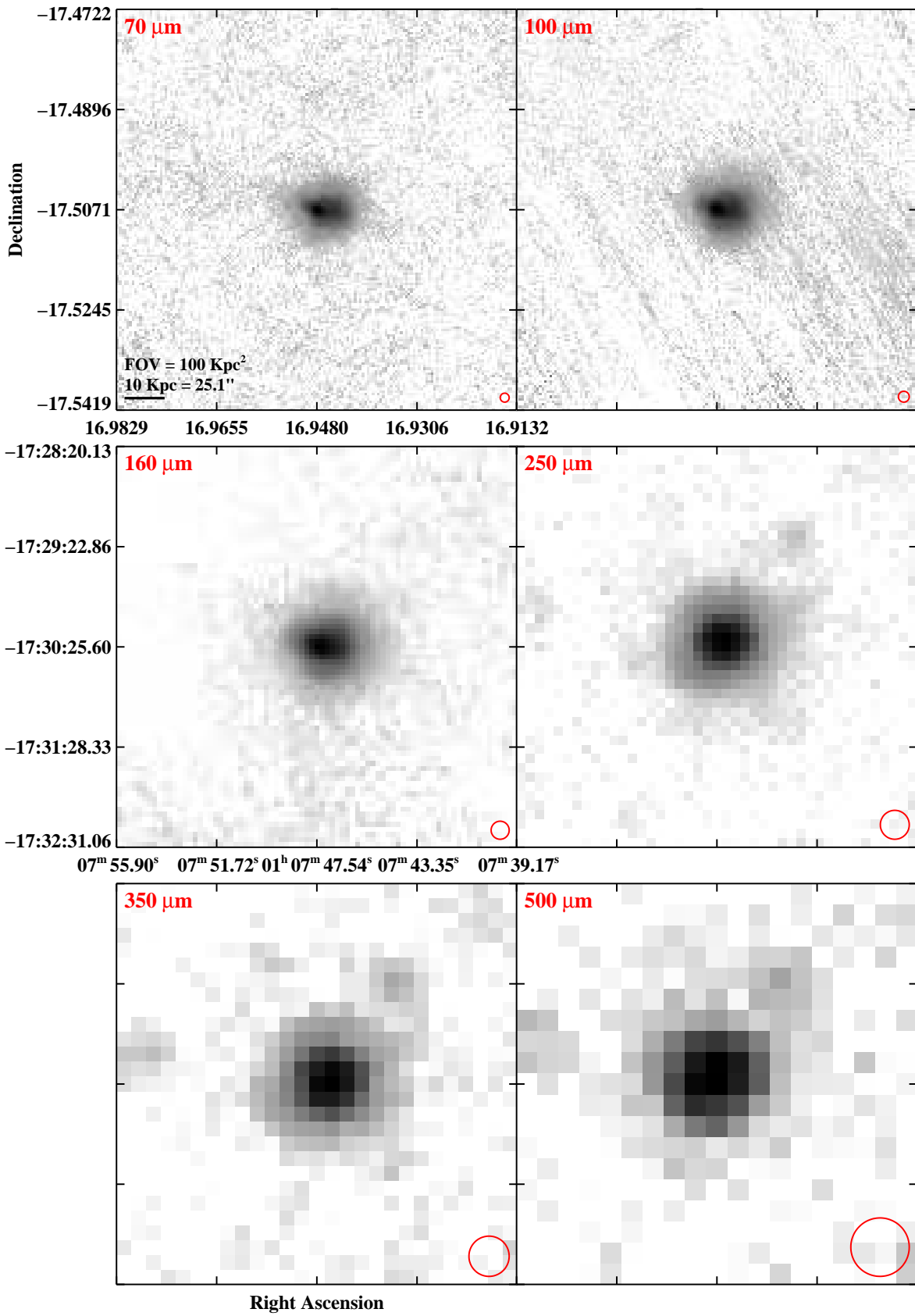


Fig. 3.— Continued (page 8 of 209).

IRAS F01076–1707 (MCG–03–04–014)

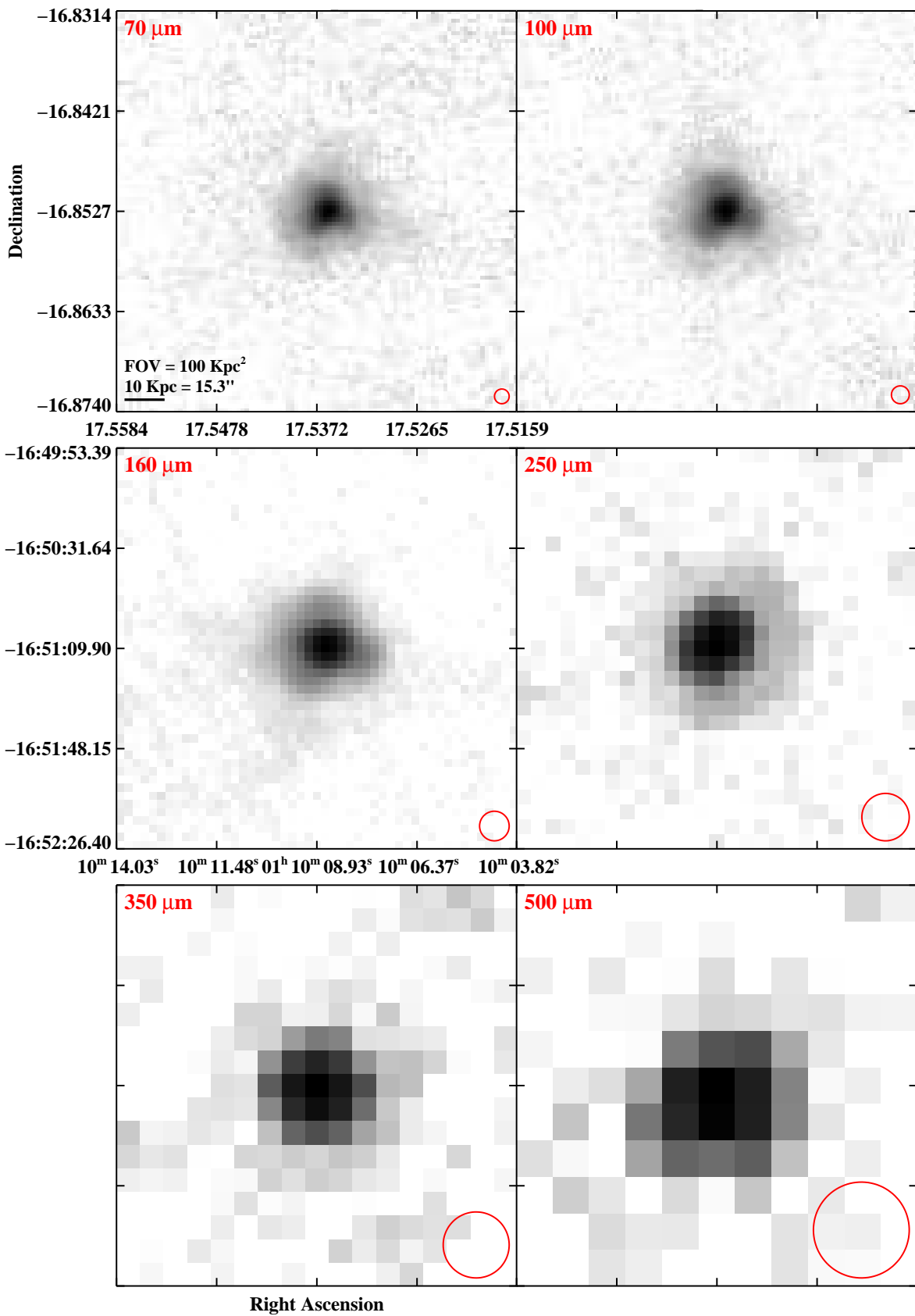


Fig. 3.— Continued (page 9 of 209).

IRAS F01159–4443 (ESO 244–G012)

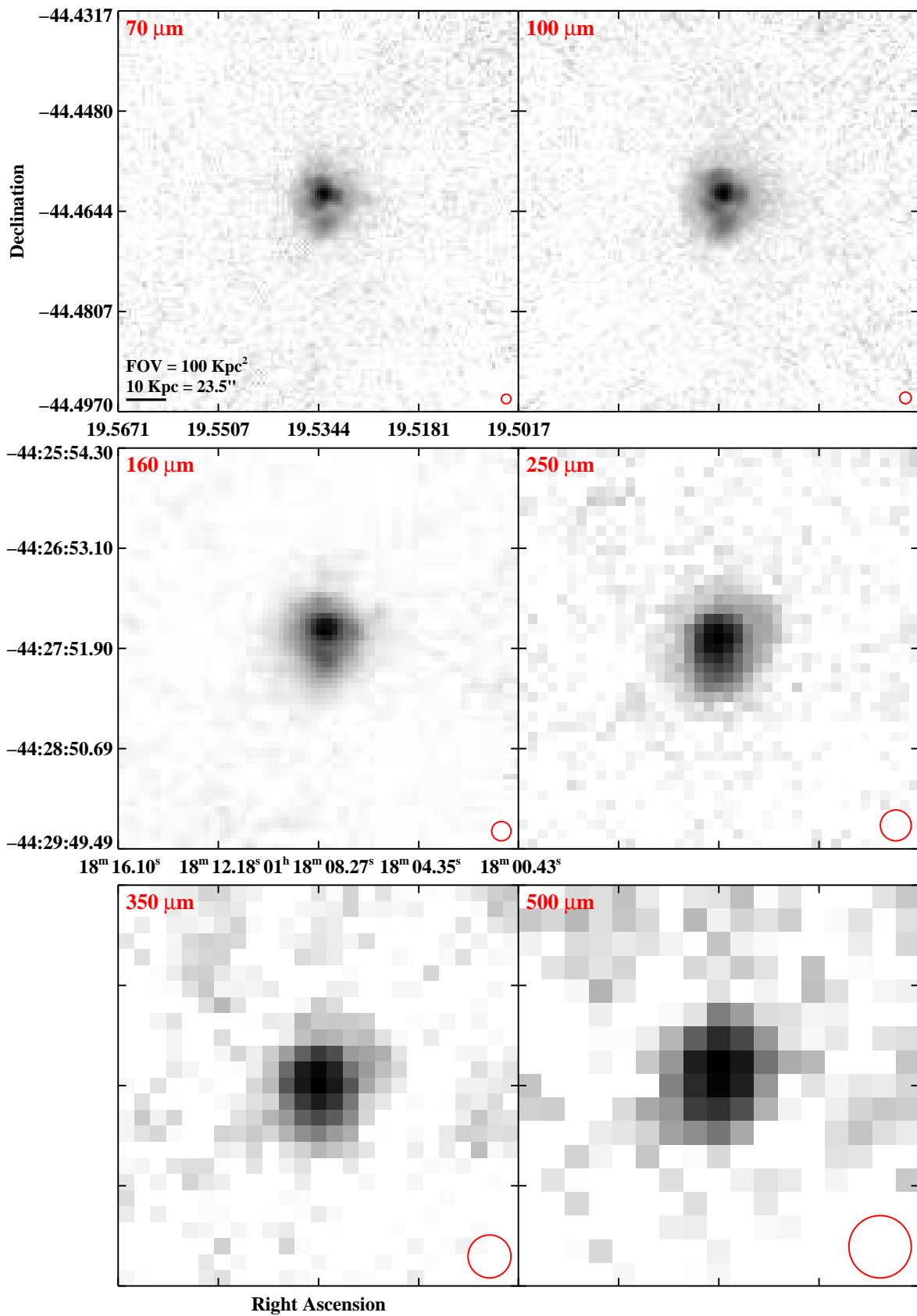


Fig. 3.— Continued (page 10 of 209).

IRAS F01173+1405 (CGCG 436-030)

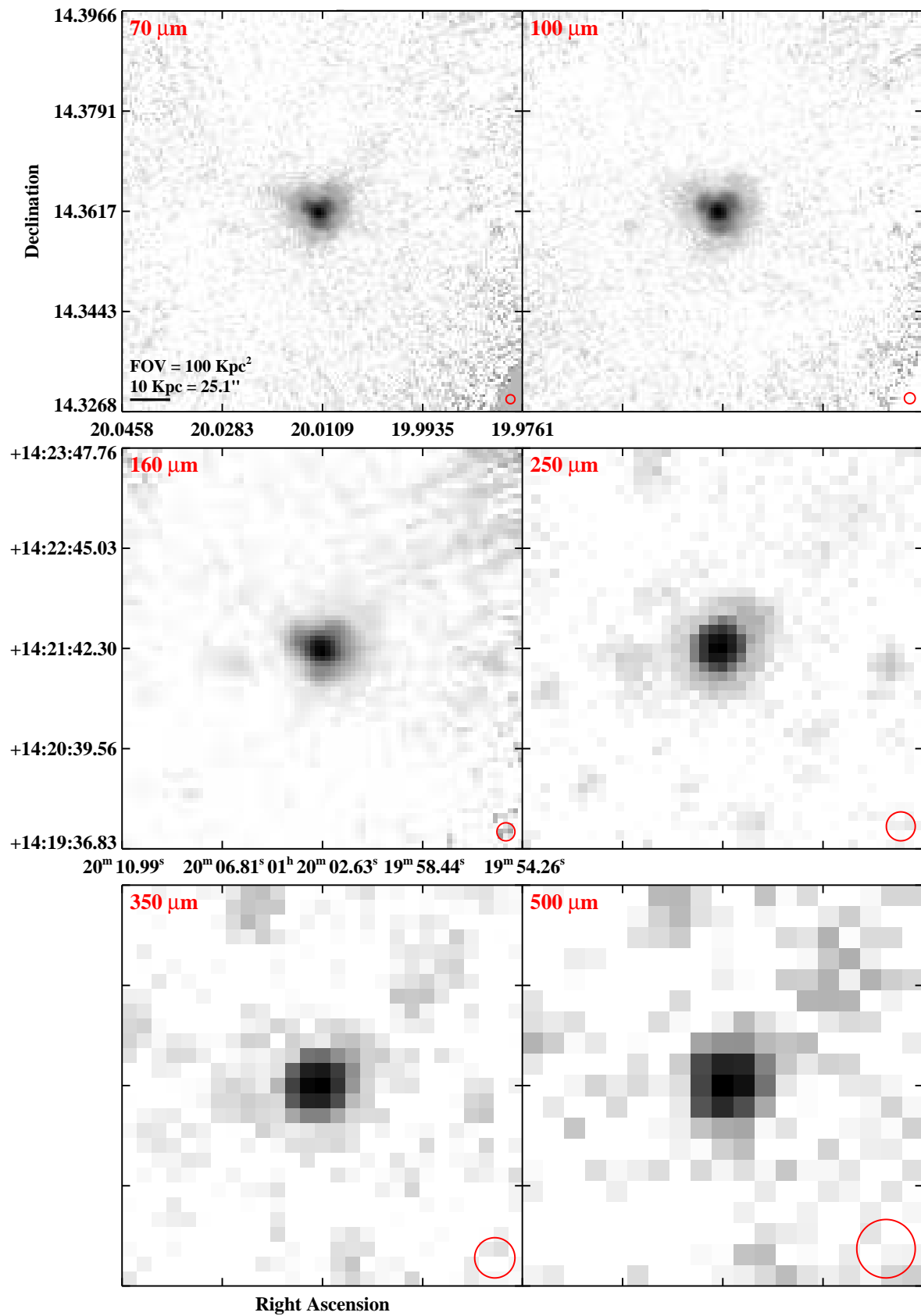


Fig. 3.— Continued (page 11 of 209).

IRAS F01325–3623 (ESO 353–G020)

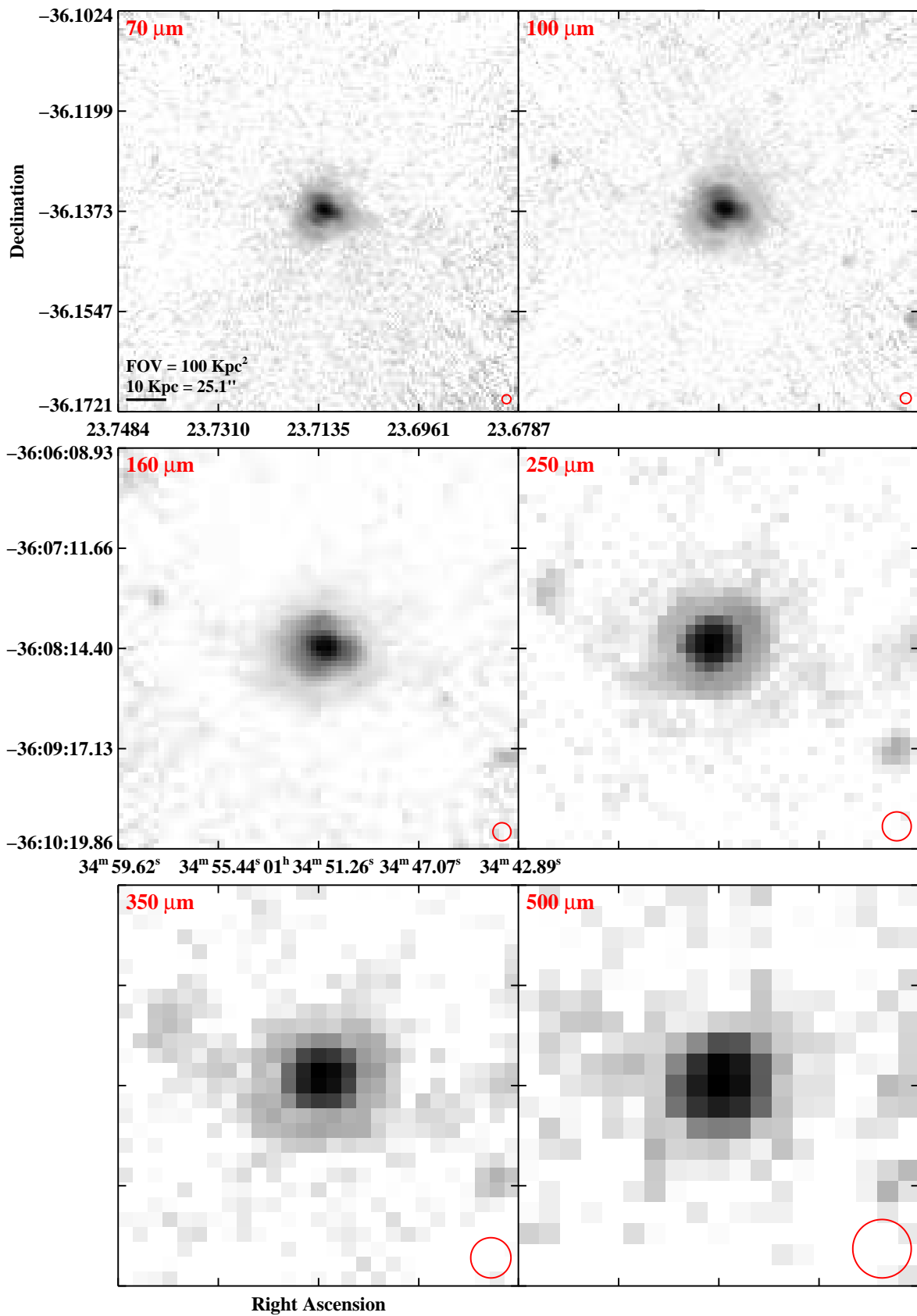


Fig. 3.— Continued (page 12 of 209).

IRAS F01341–3735 (RR 032)

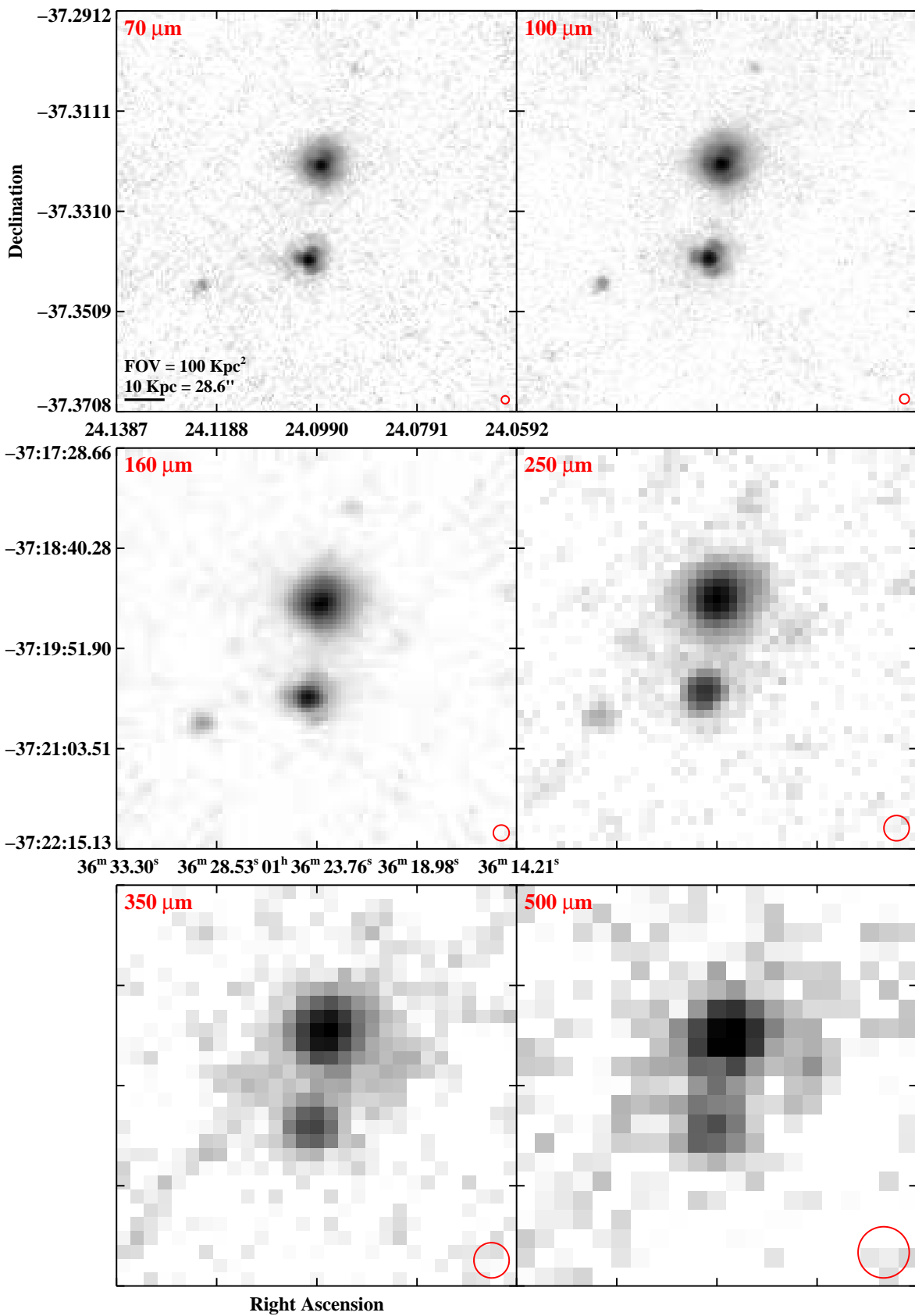


Fig. 3.— Continued (page 13 of 209).

IRAS F01364–1042

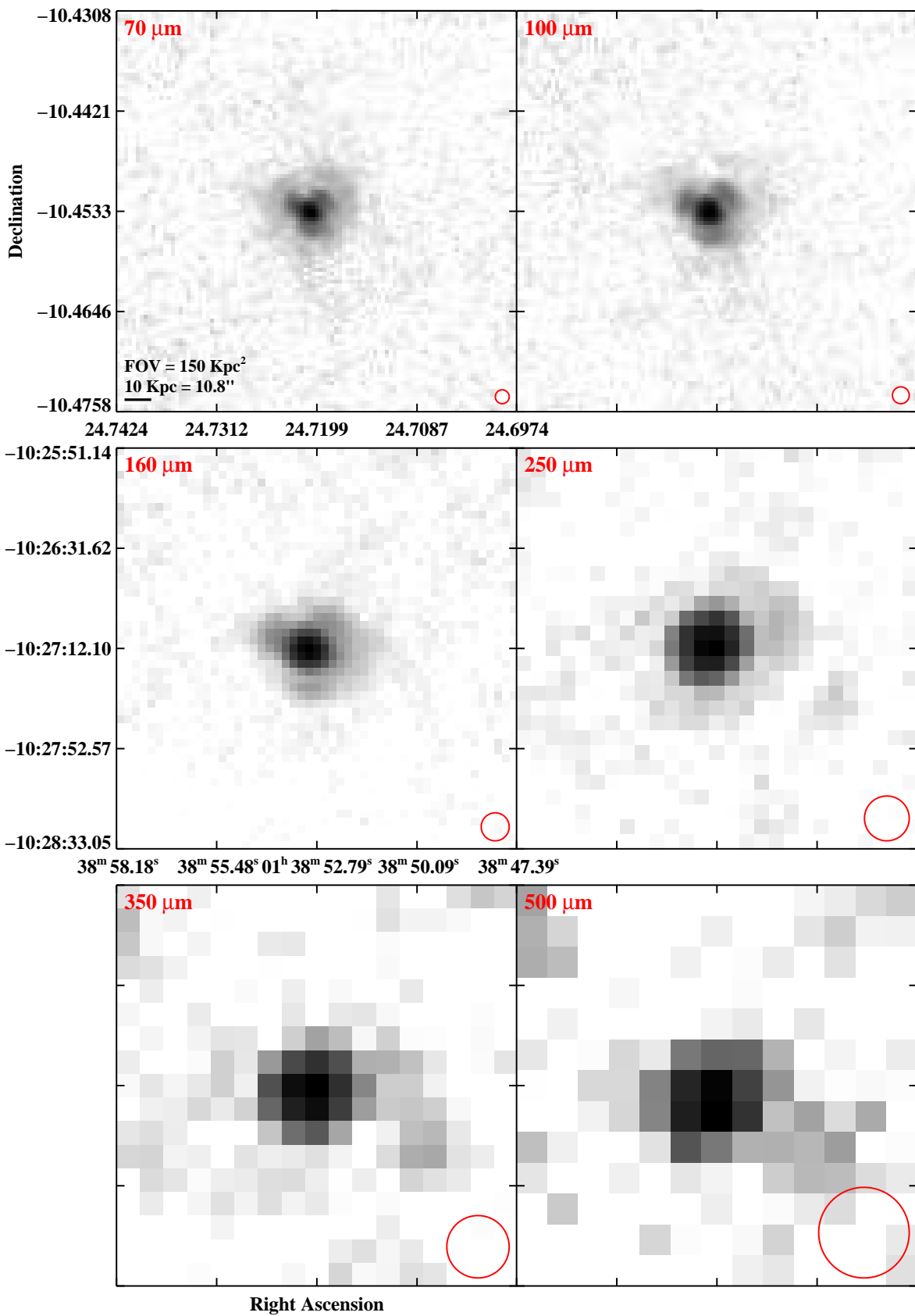


Fig. 3.— Continued (page 14 of 209).

IRAS F01417+1651 (III Zw 035)

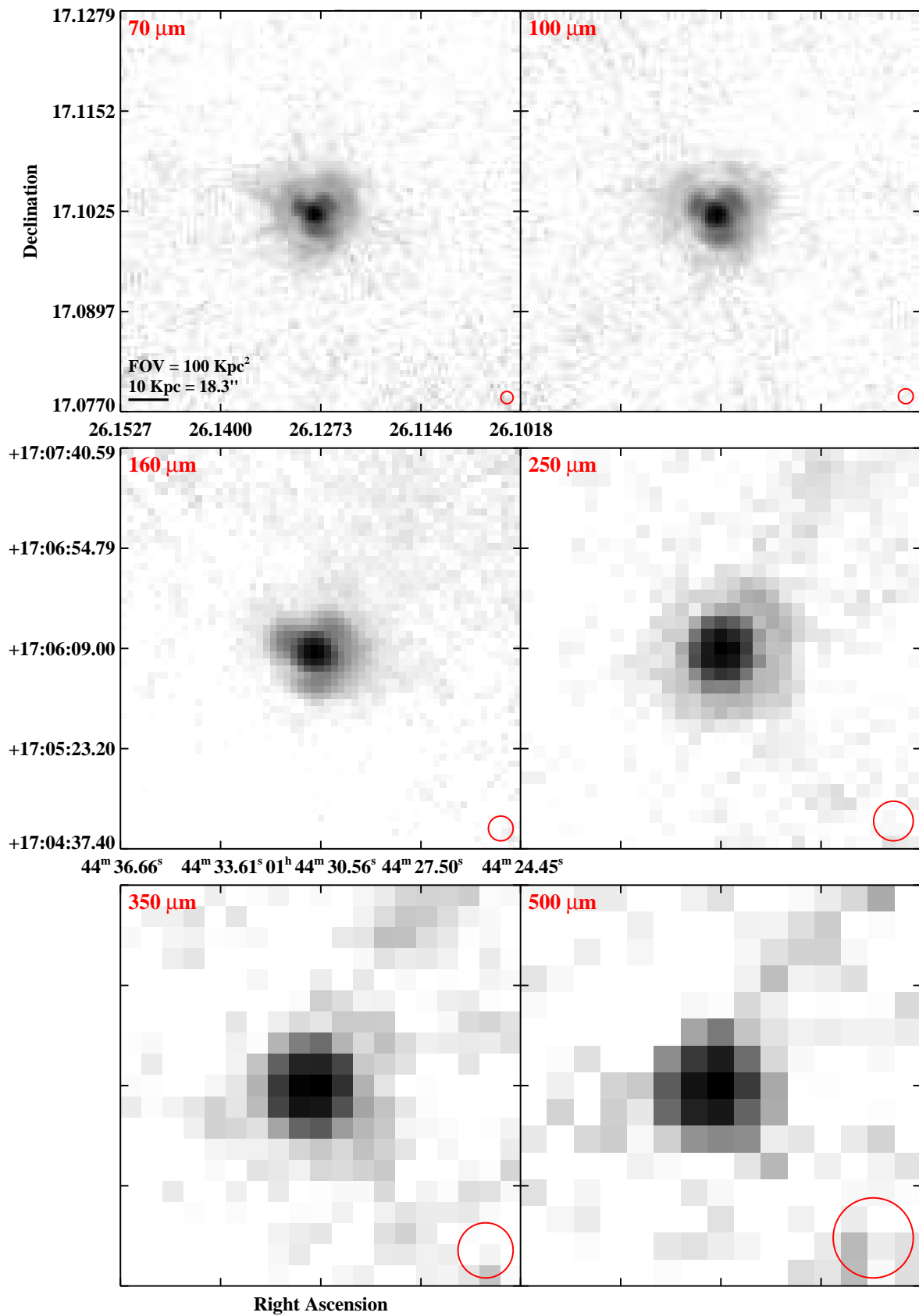


Fig. 3.— Continued (page 15 of 209).

IRAS F01484+2220 (NGC 695)

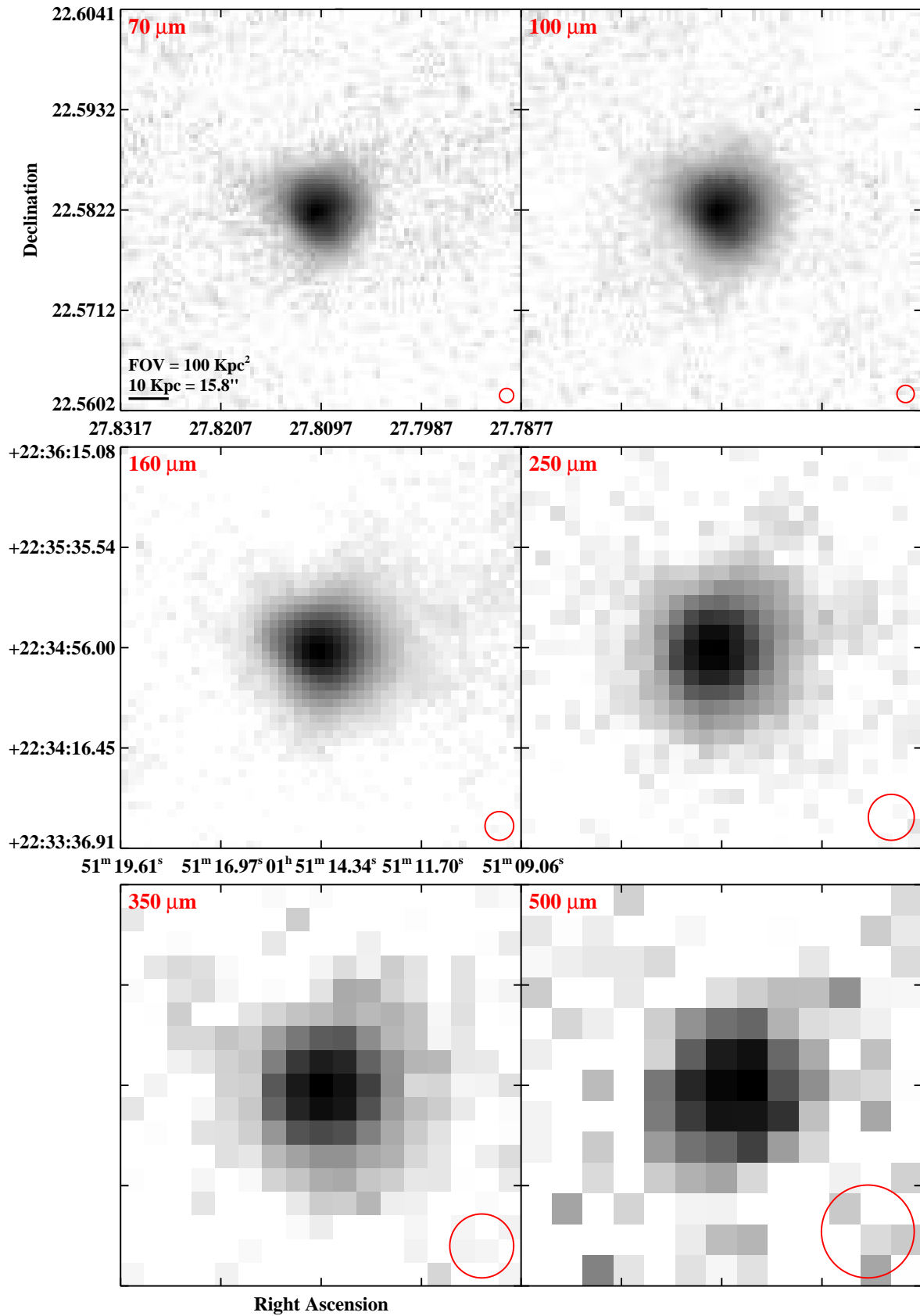


Fig. 3.— Continued (page 16 of 209).

IRAS F01519+3640 (UGC 01385)

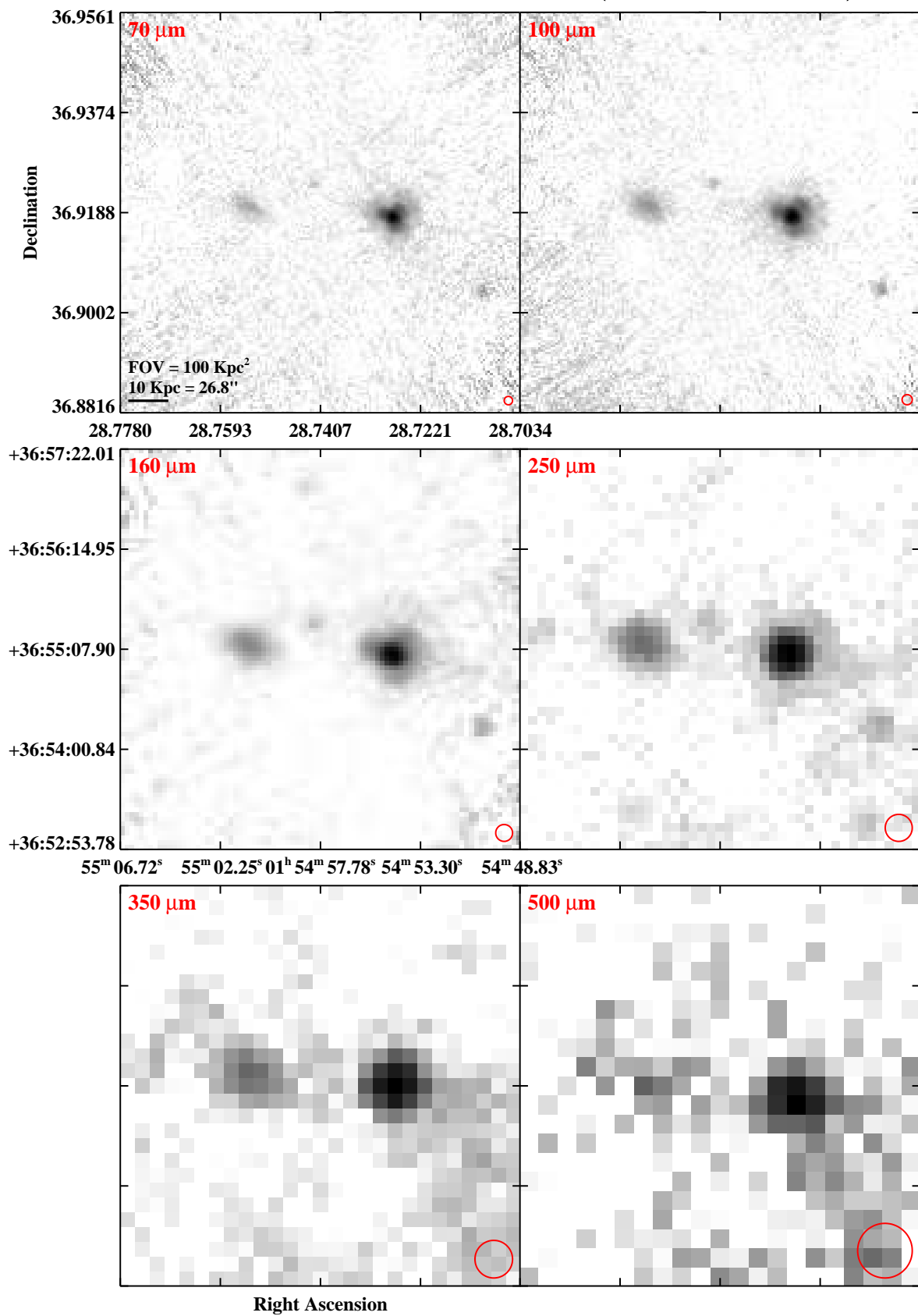


Fig. 3.— Continued (page 17 of 209).

IRAS F02071–1023 (NGC 838)

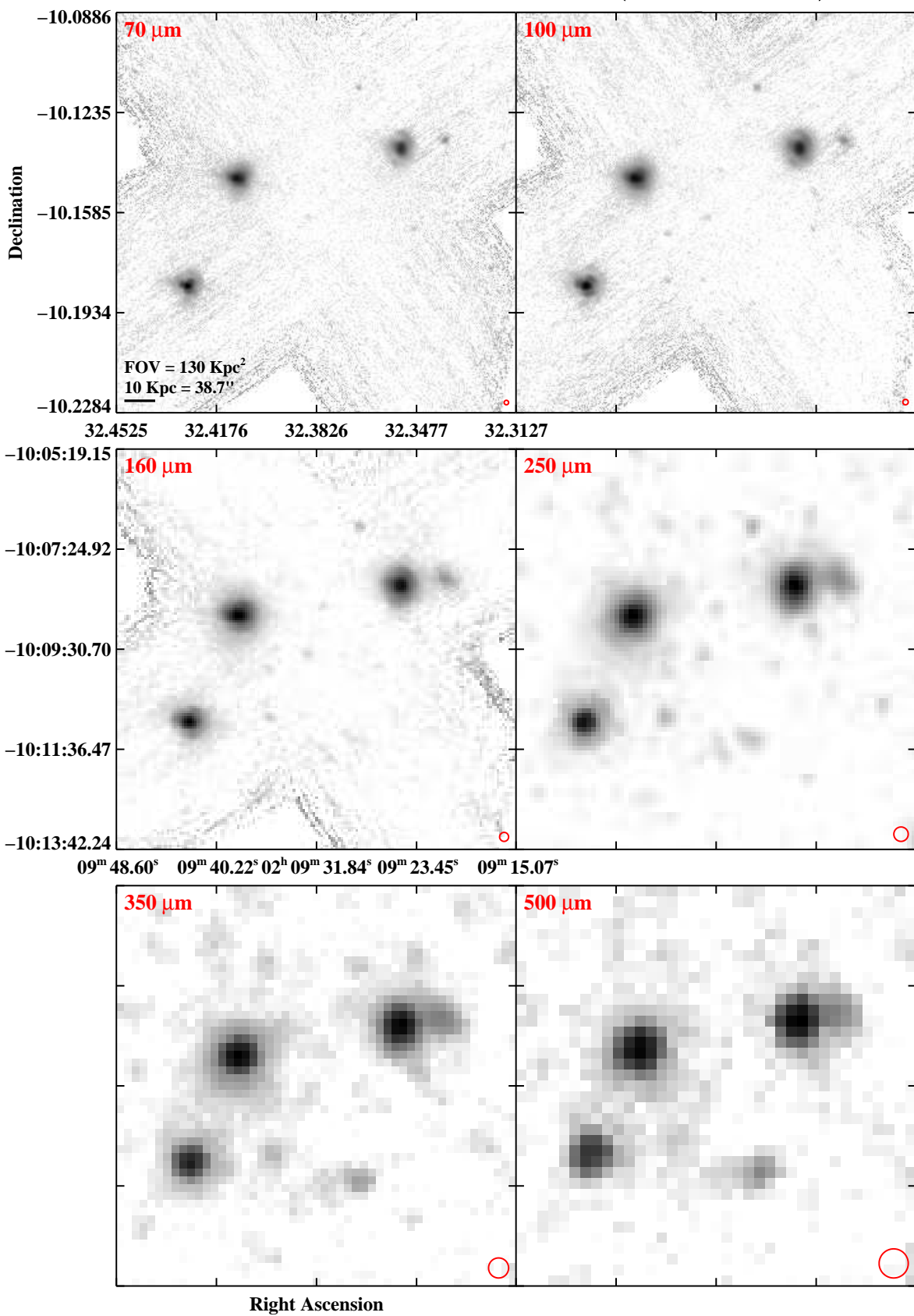


Fig. 3.— Continued (page 18 of 209).

IRAS F02070+3857 (NGC 828)

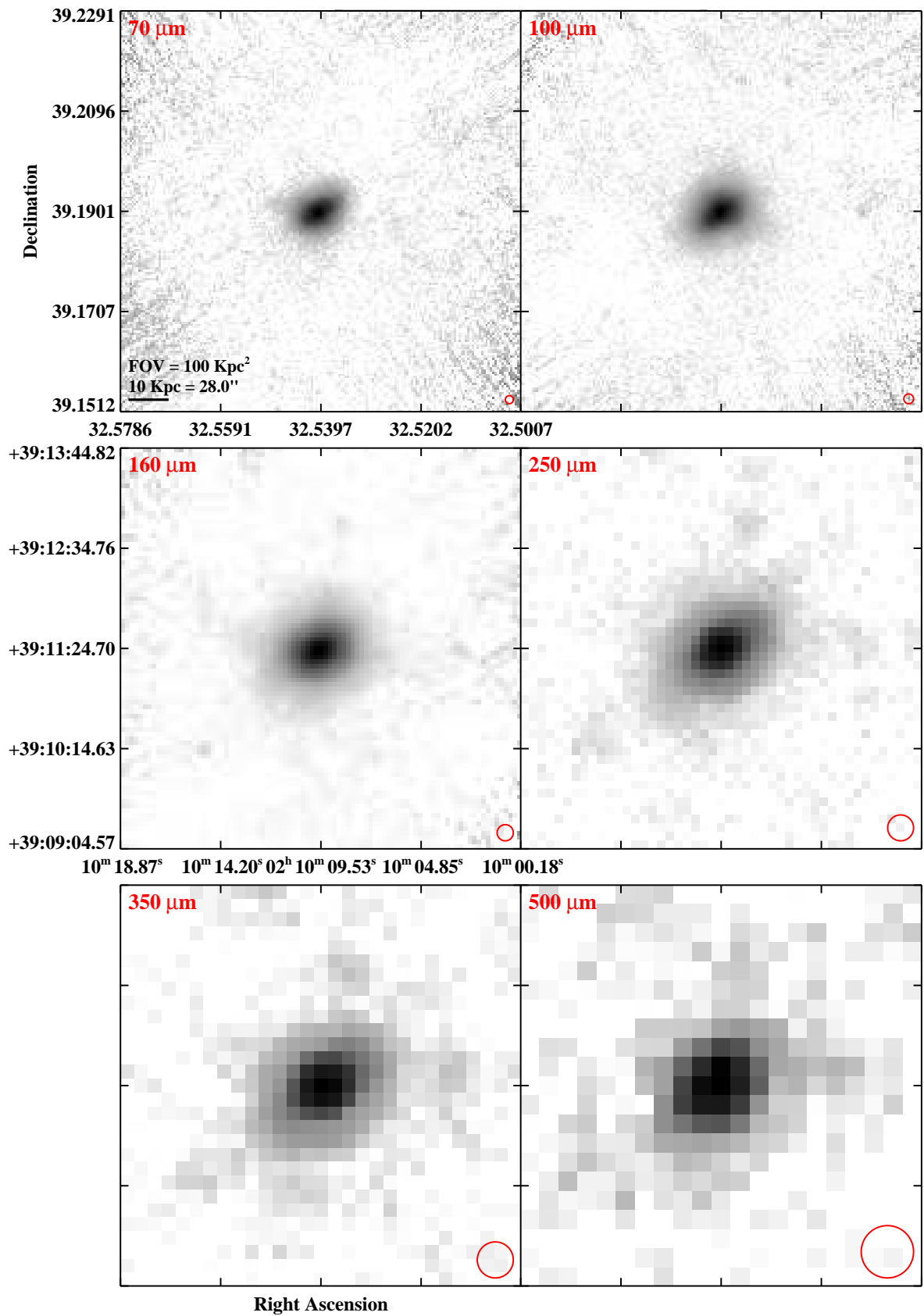


Fig. 3.— Continued (page 19 of 209).

IRAS F02114+0456 (IC 214)

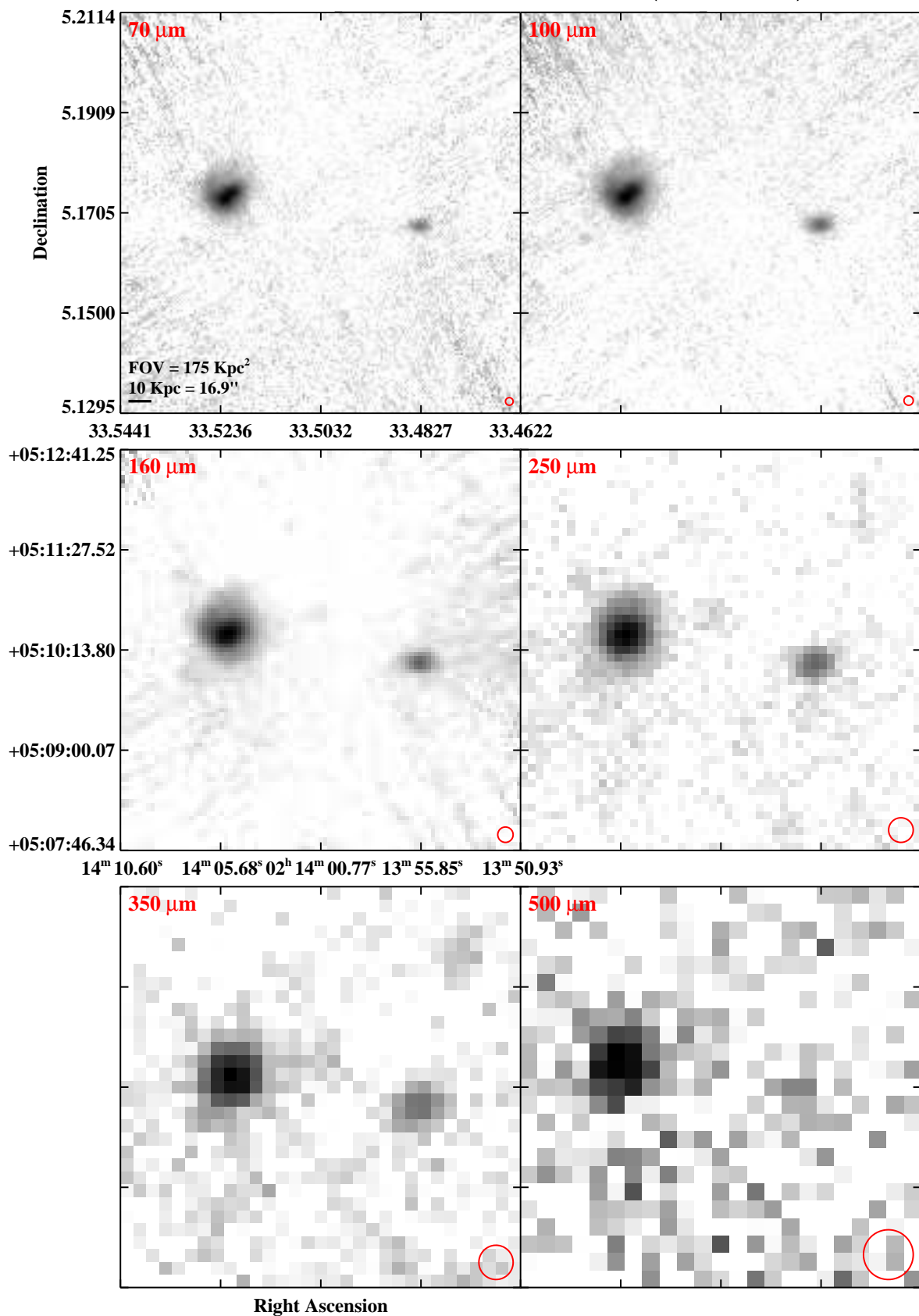


Fig. 3.— Continued (page 20 of 209).

IRAS F02152+1418 (NGC 877)

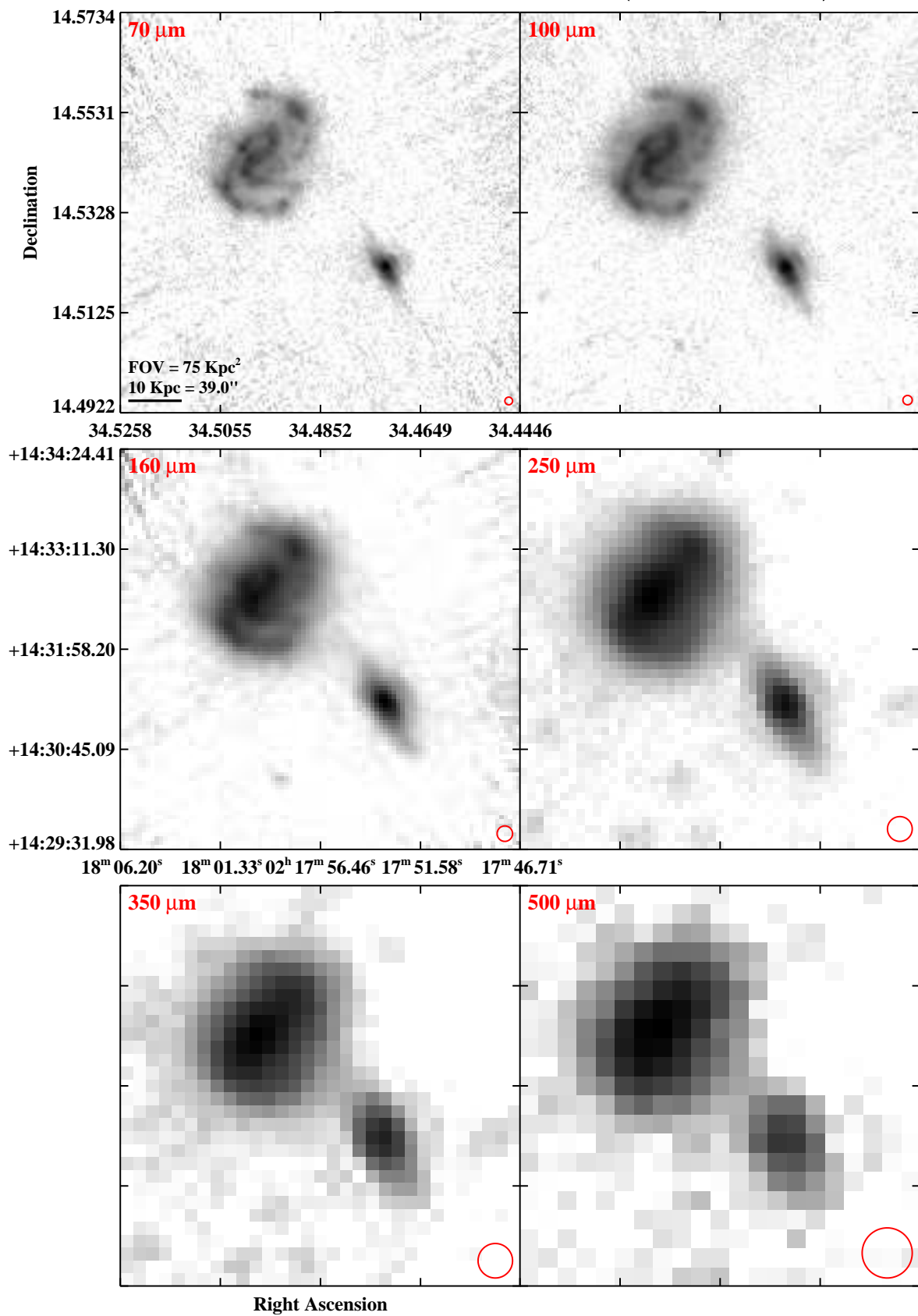


Fig. 3.— Continued (page 21 of 209).

IRAS F02203+3158 (MCG+05-06-036)

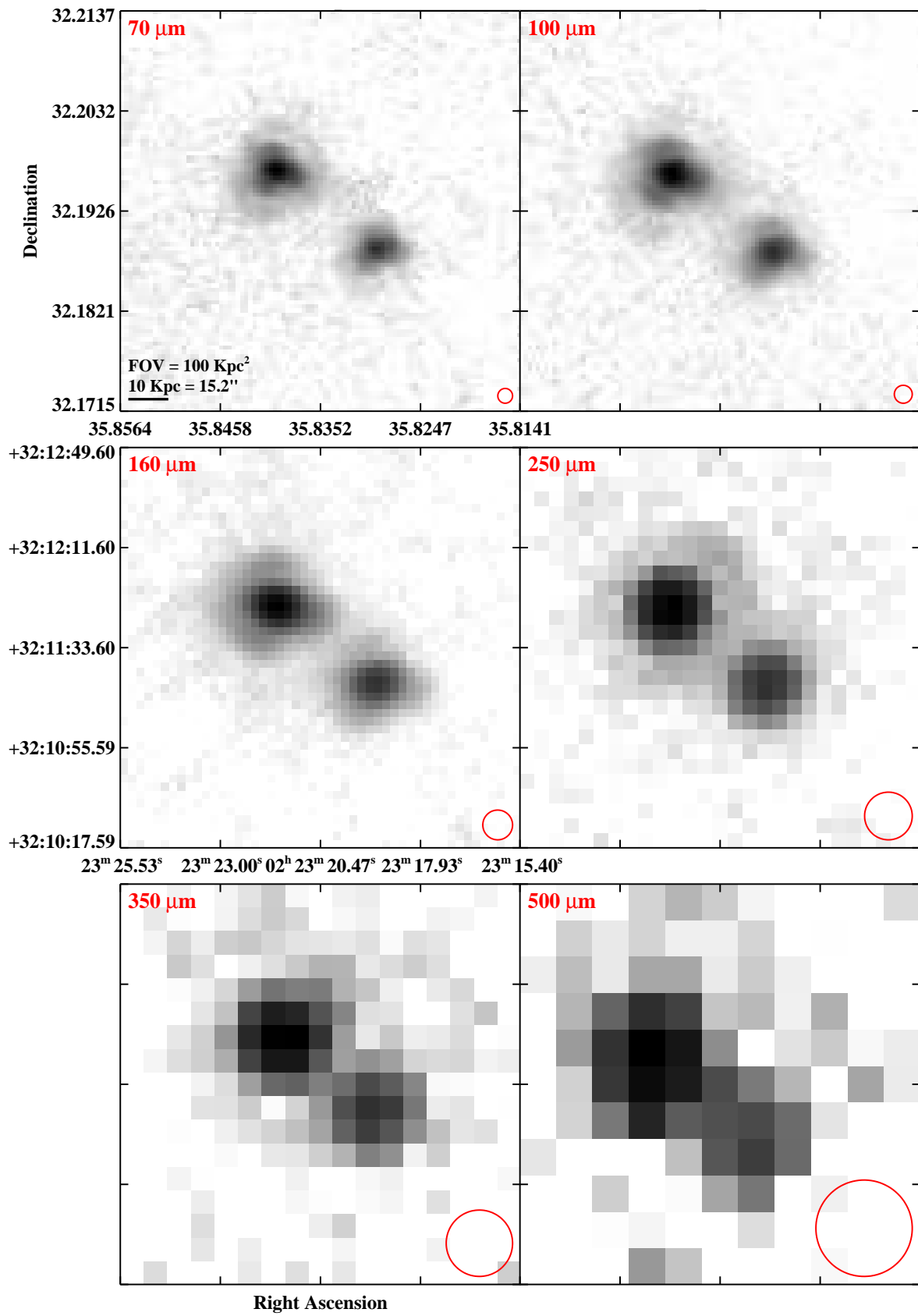


Fig. 3.— Continued (page 22 of 209).

IRAS F02208+4744 (UGC 01845)

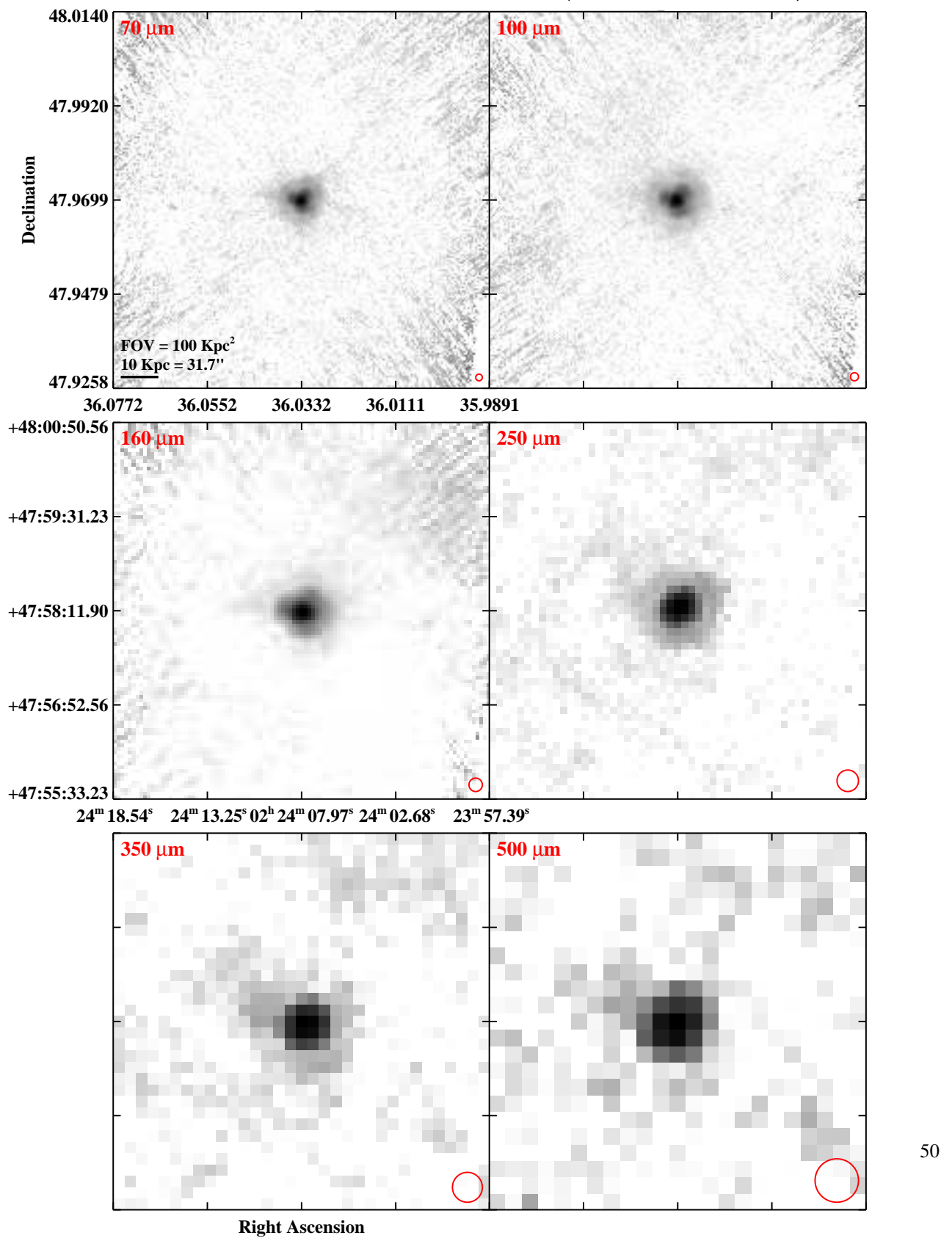


Fig. 3.— Continued (page 23 of 209).

IRAS F02281–0309 (NGC 958)

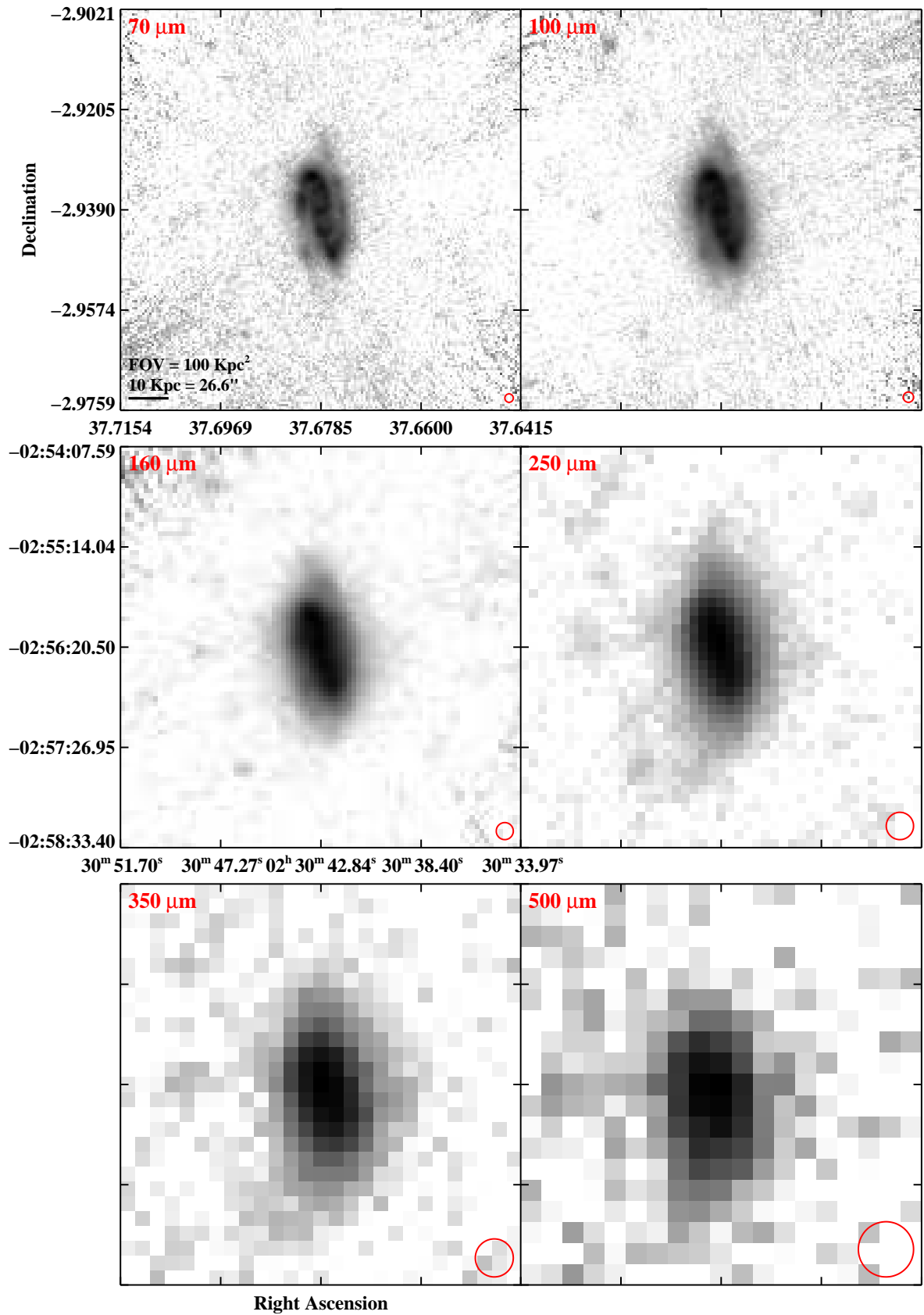


Fig. 3.— Continued (page 24 of 209).

IRAS F02345+2053 (NGC 992)

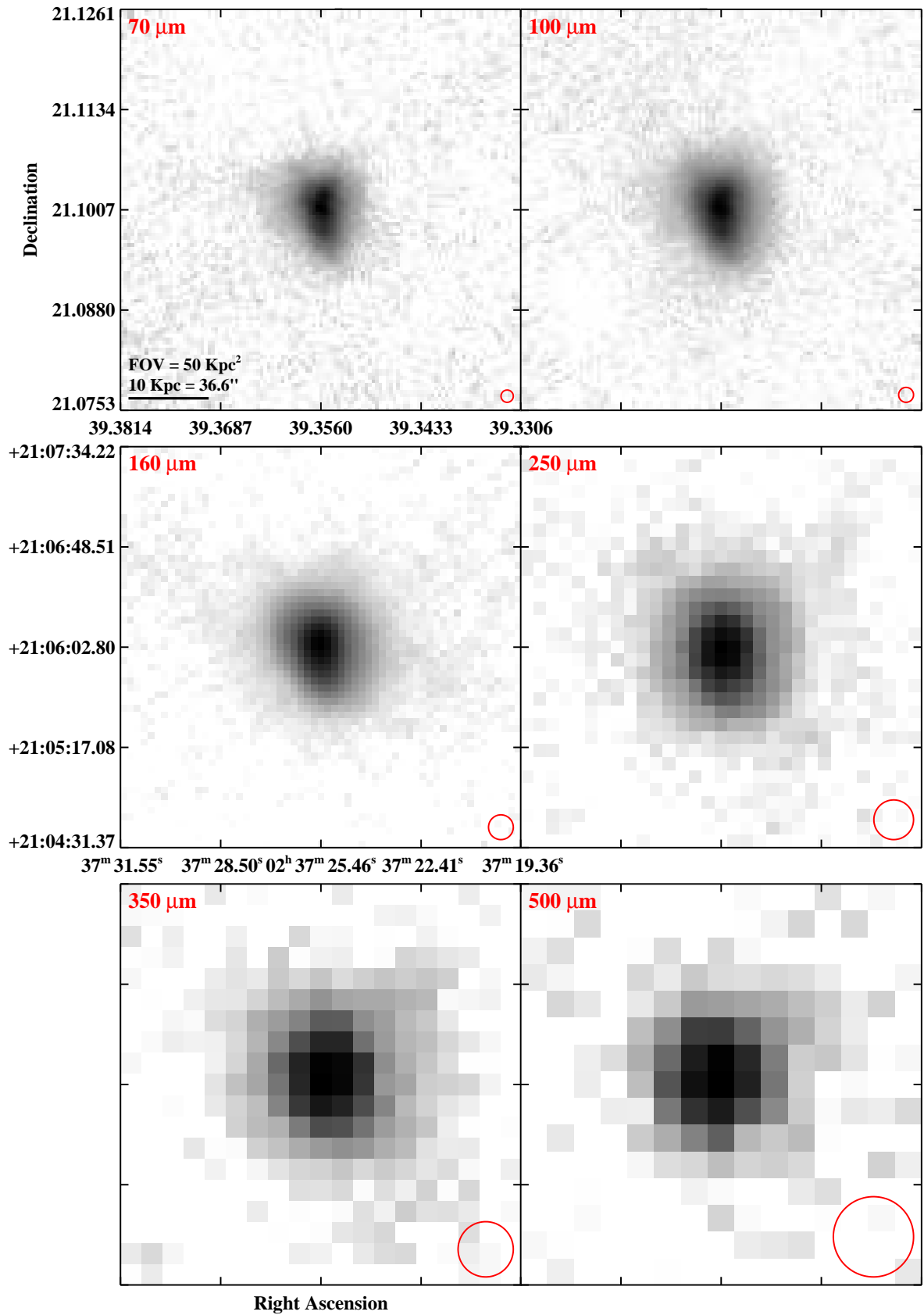


Fig. 3.— Continued (page 25 of 209).

IRAS F02401–0013 (NGC 1068)

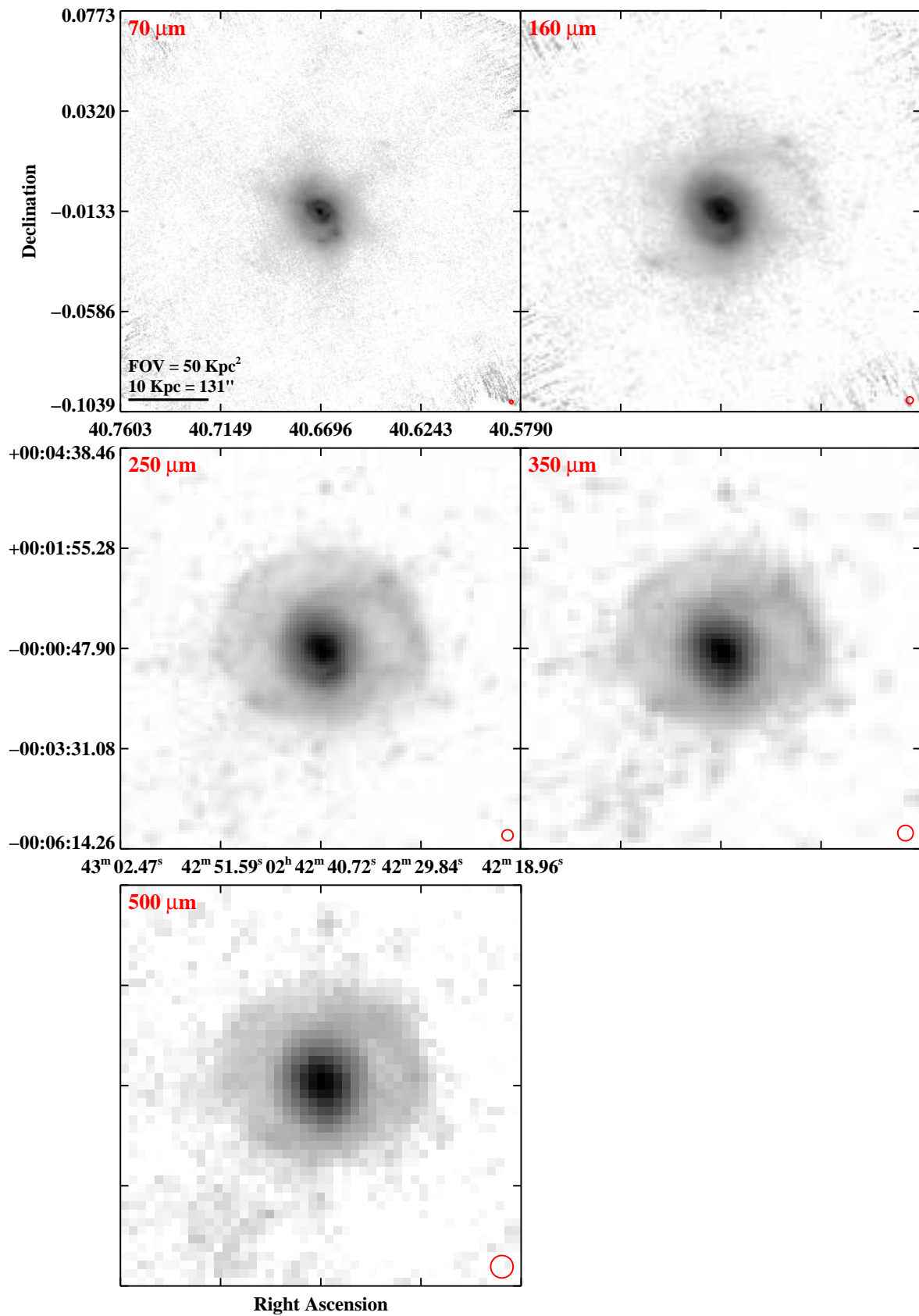


Fig. 3.— Continued (page 26 of 209).

IRAS F02435+1253 (UGC 02238)

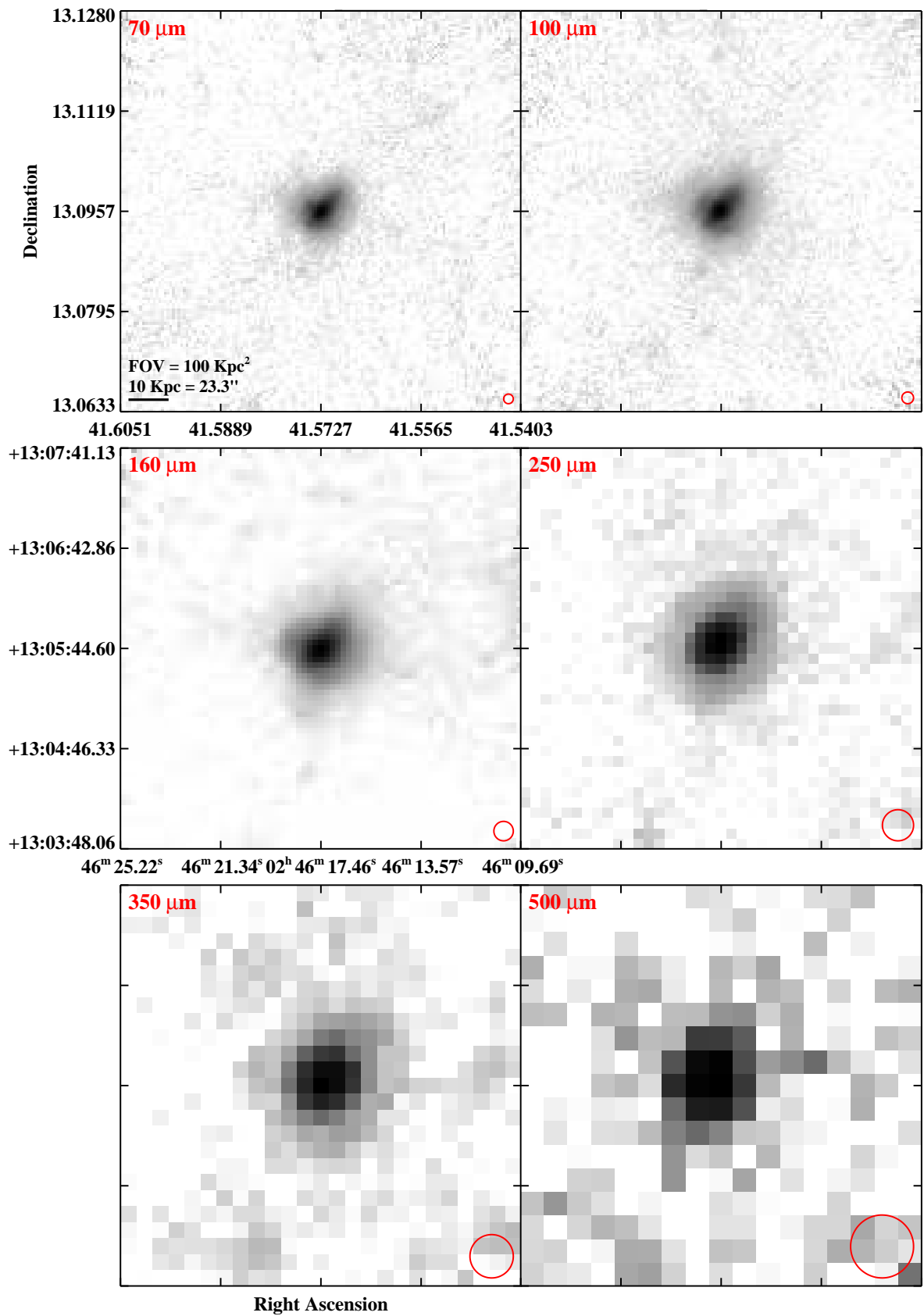


Fig. 3.— Continued (page 27 of 209).

IRAS F02437+2122

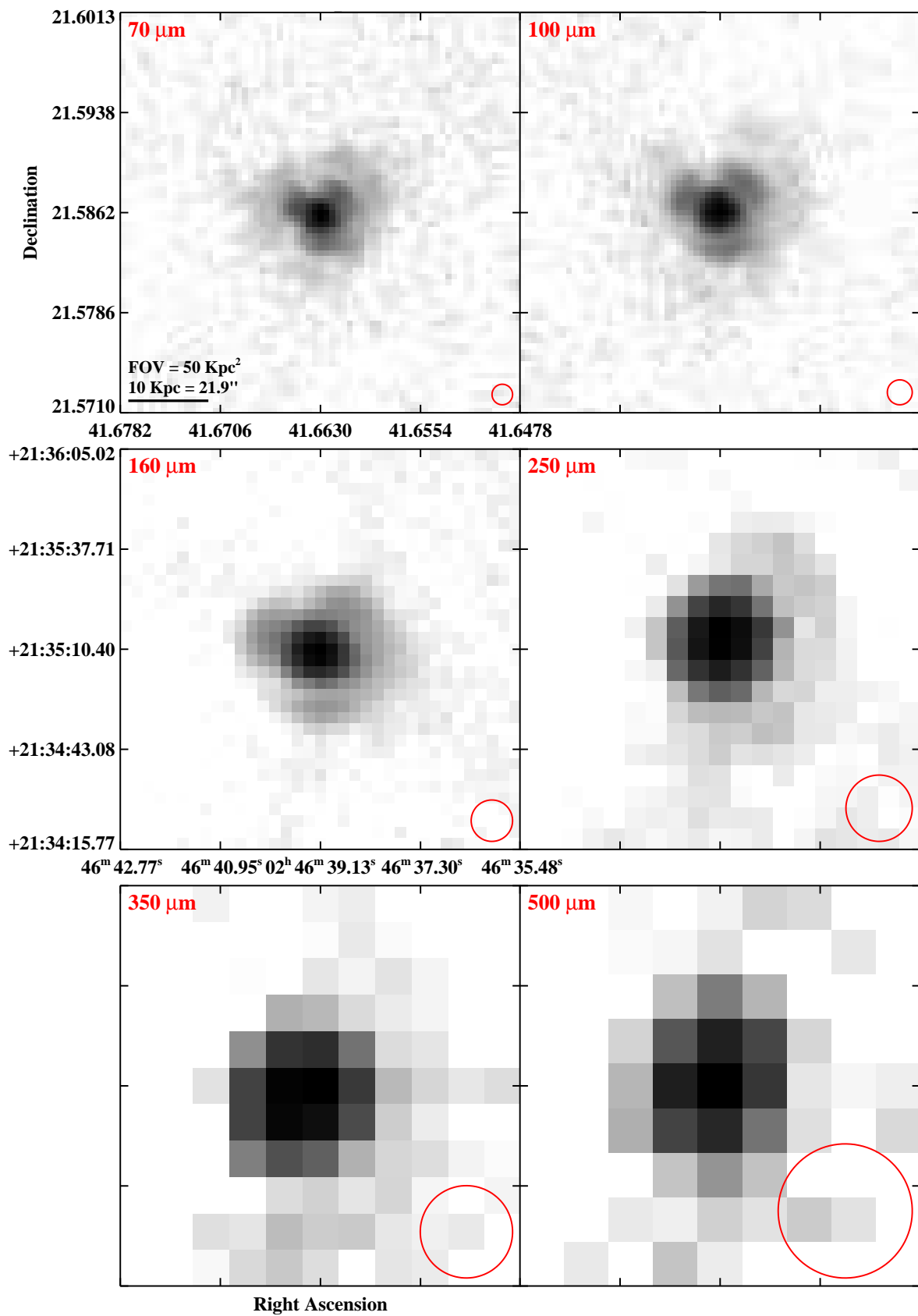


Fig. 3.— Continued (page 28 of 209).

IRAS F02437+2122 (2MASX J02464505+2133234)

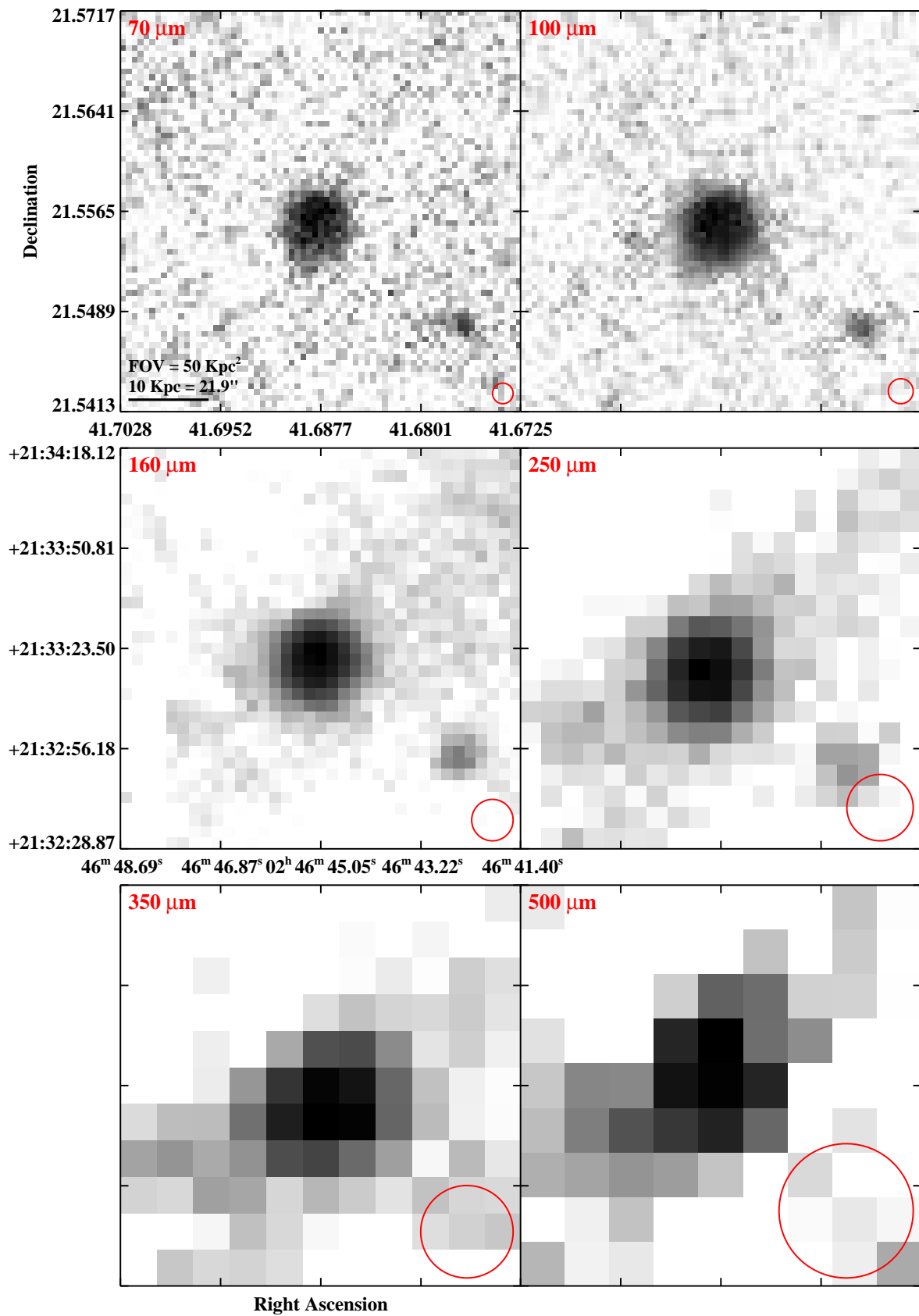


Fig. 3.— Continued (page 29 of 209).

IRAS F02512+1446 (UGC 02369)

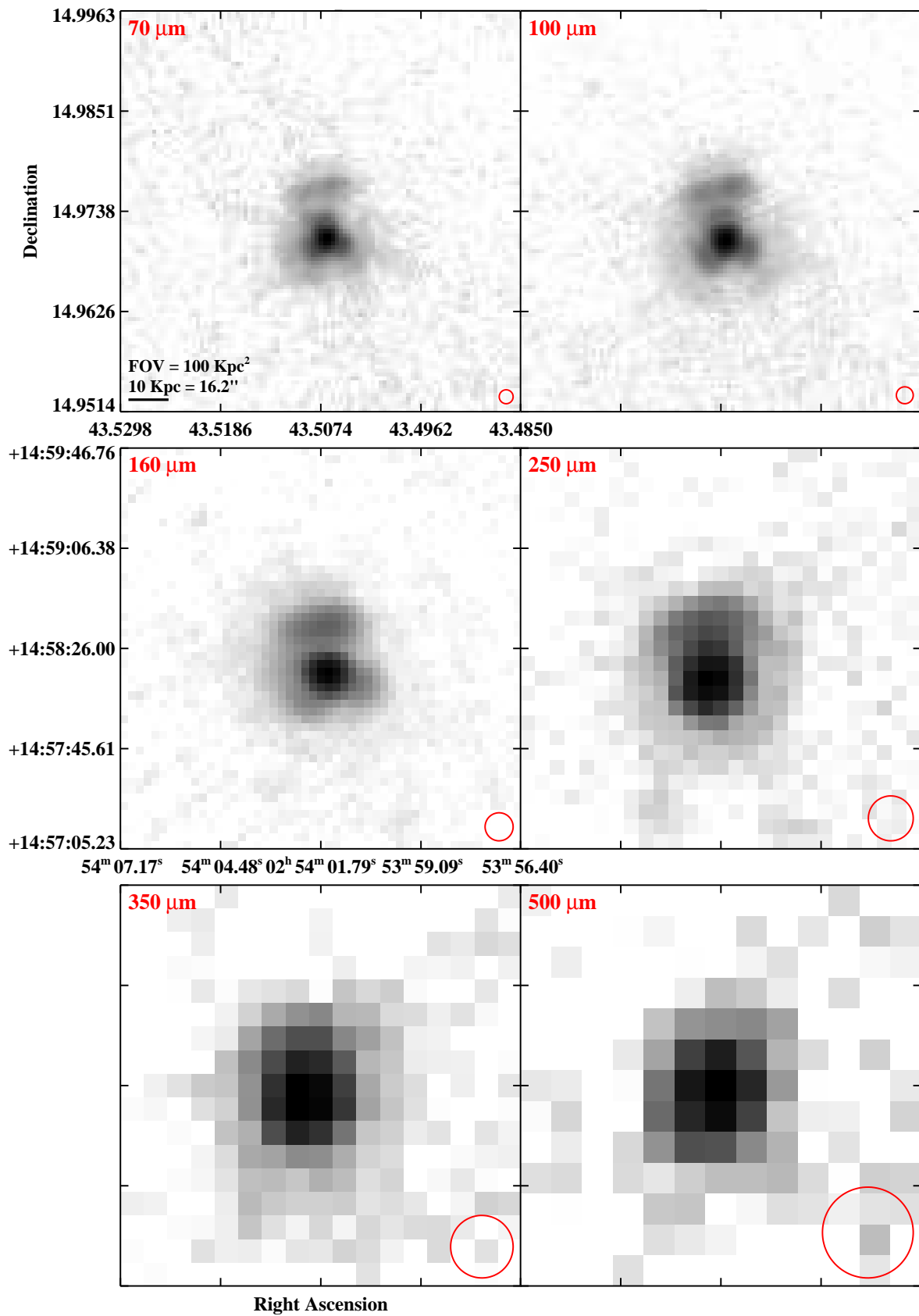


Fig. 3.— Continued (page 30 of 209).

IRAS F03117+4151 (UGC 02608)

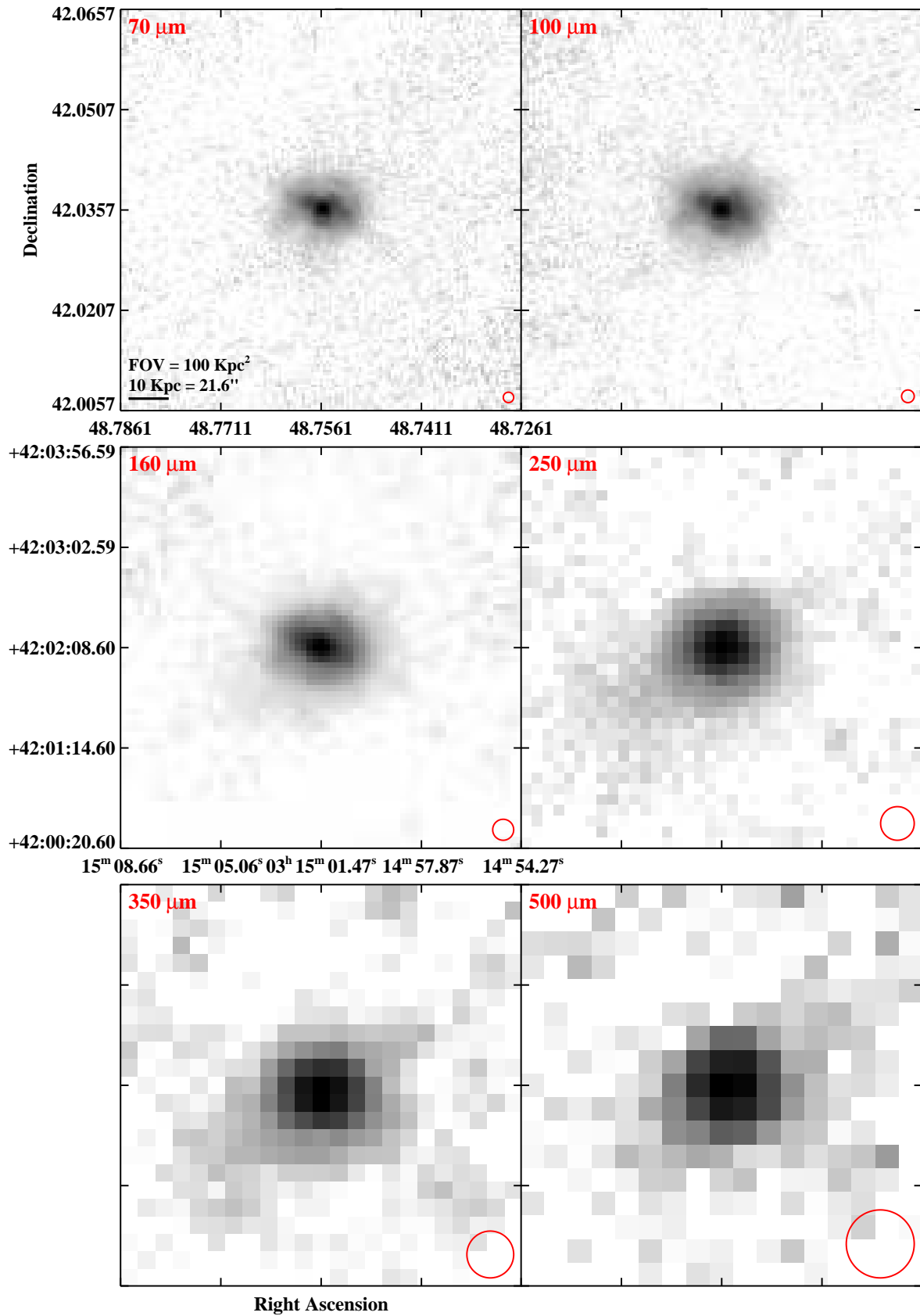


Fig. 3.— Continued (page 31 of 209).

IRAS F03117+4151 (UGC 02612)

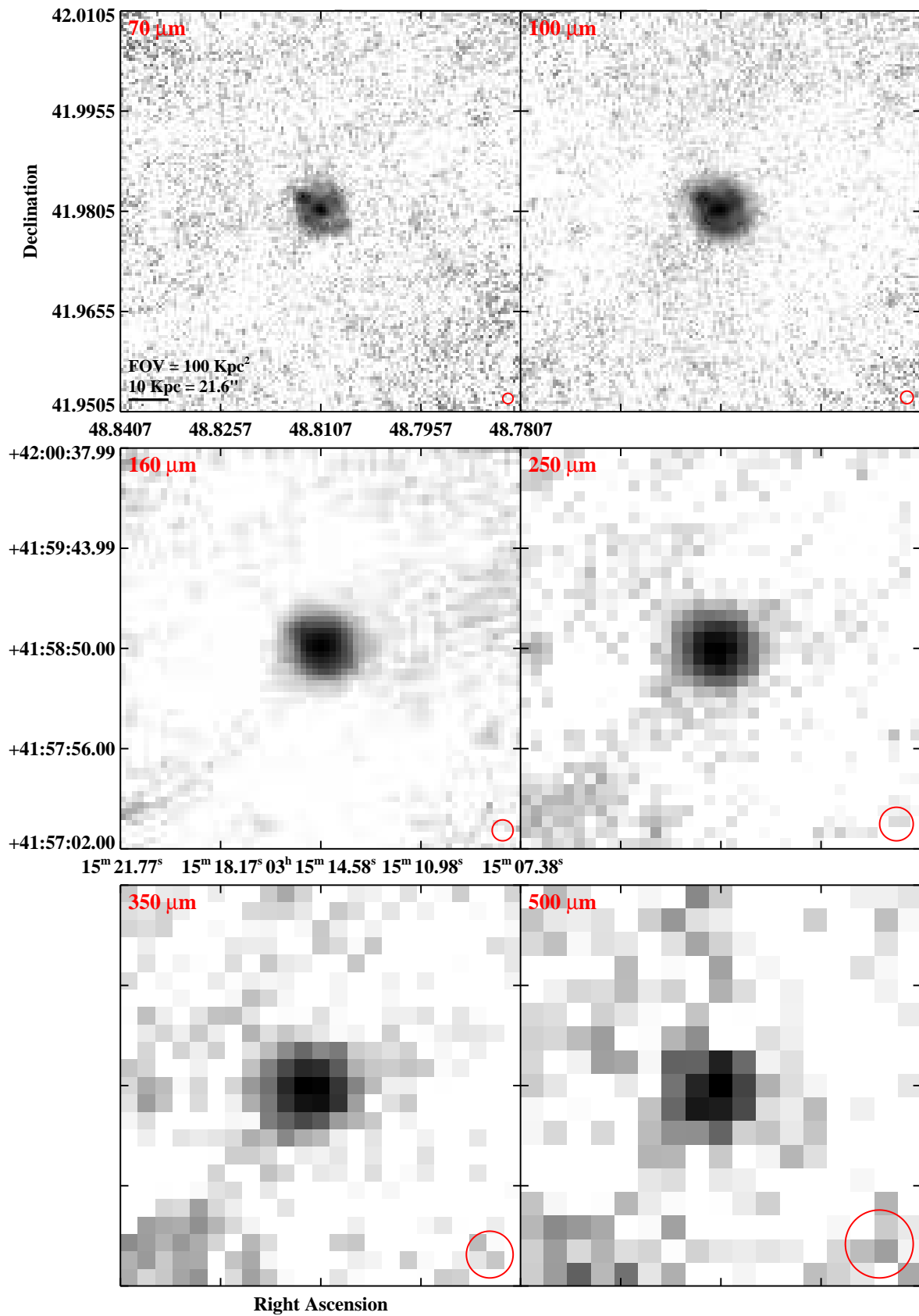


Fig. 3.— Continued (page 32 of 209).

IRAS F03164+4119 (NGC 1275)

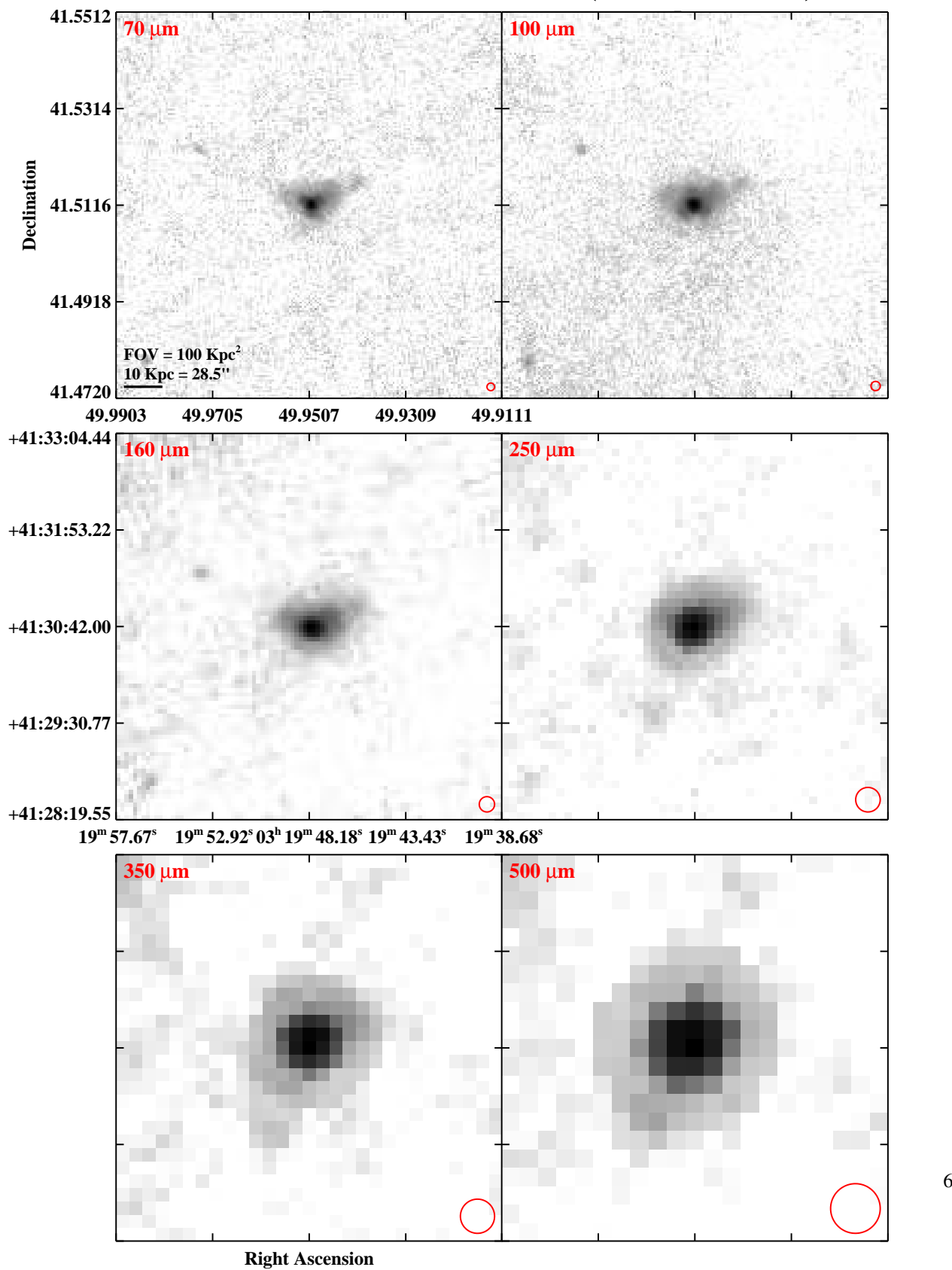


Fig. 3.— Continued (page 33 of 209).

IRAS F03217+4022

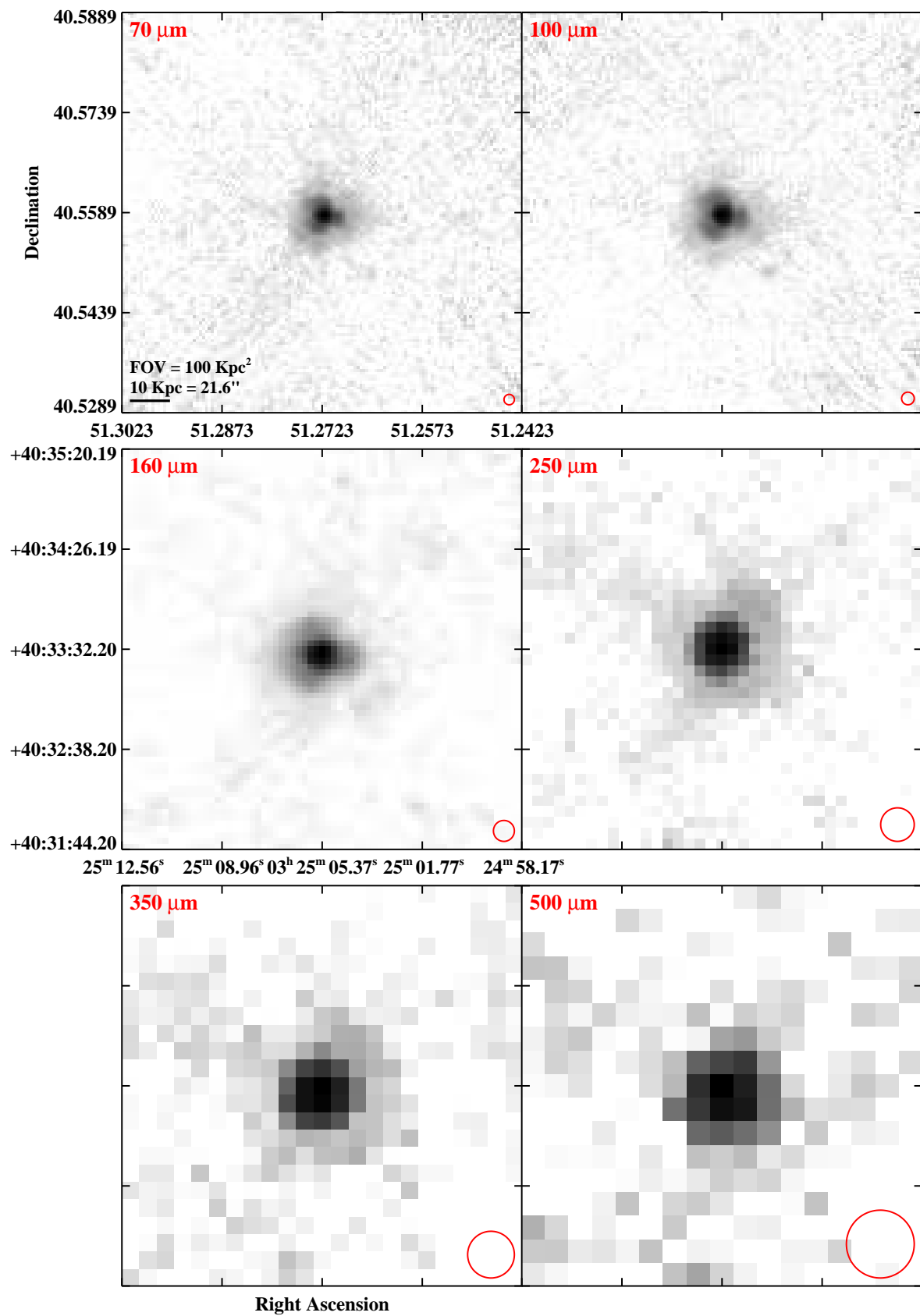


Fig. 3.— Continued (page 34 of 209).

IRAS F03316–3618 (NGC 1365)

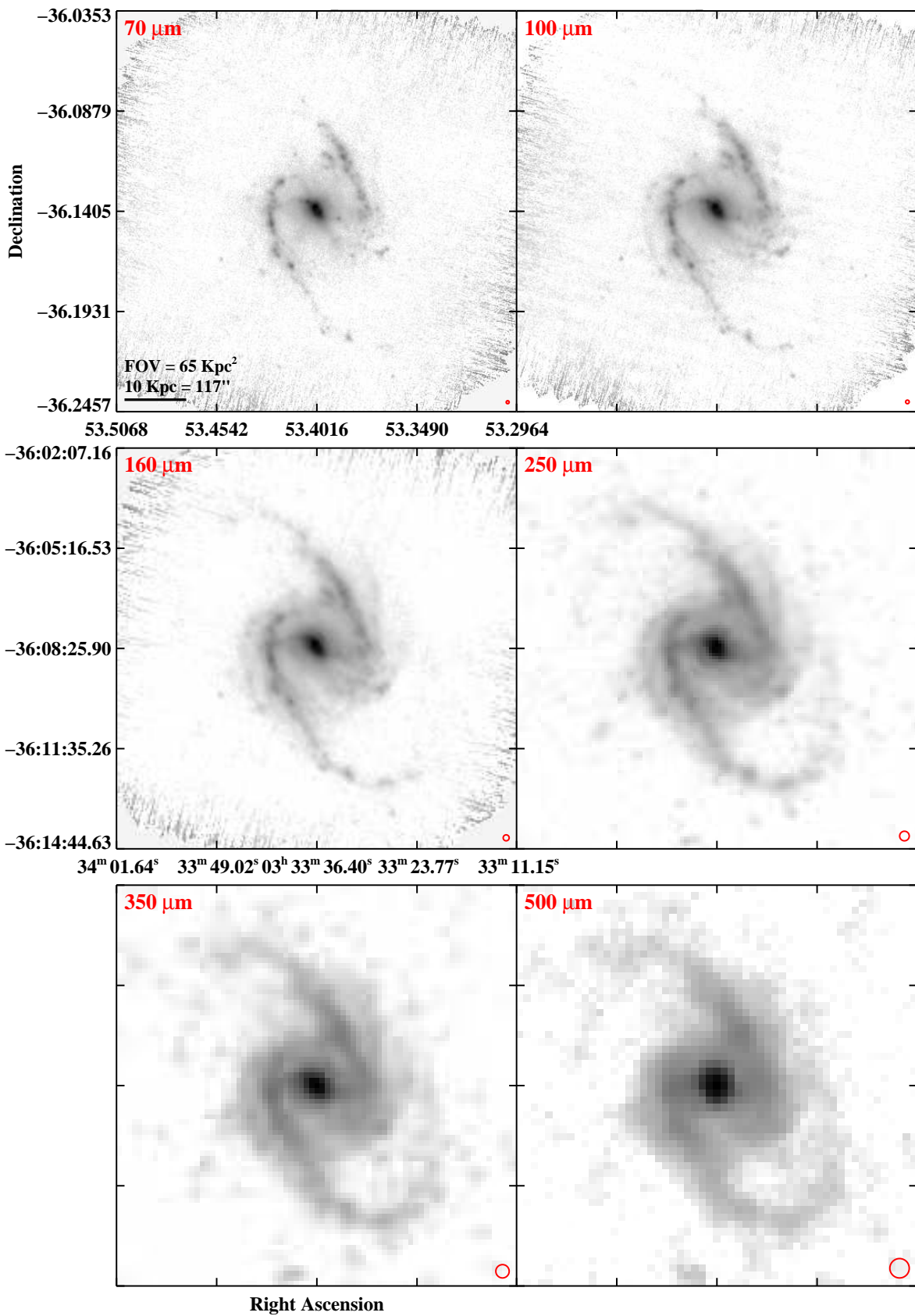


Fig. 3.— Continued (page 35 of 209).

IRAS F03359+1523

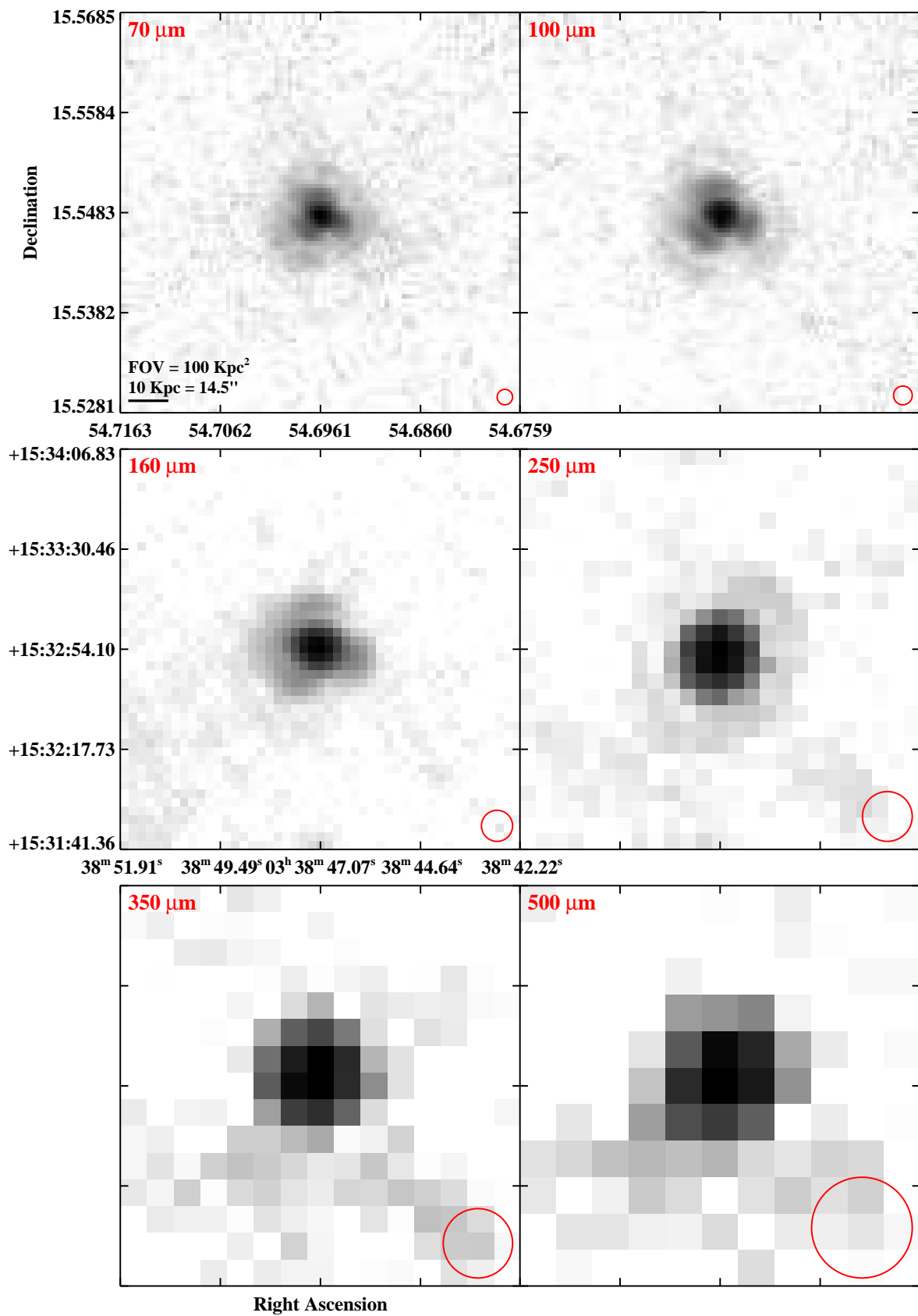


Fig. 3.— Continued (page 36 of 209).

IRAS F03514+1546 (CGCG 465-012)

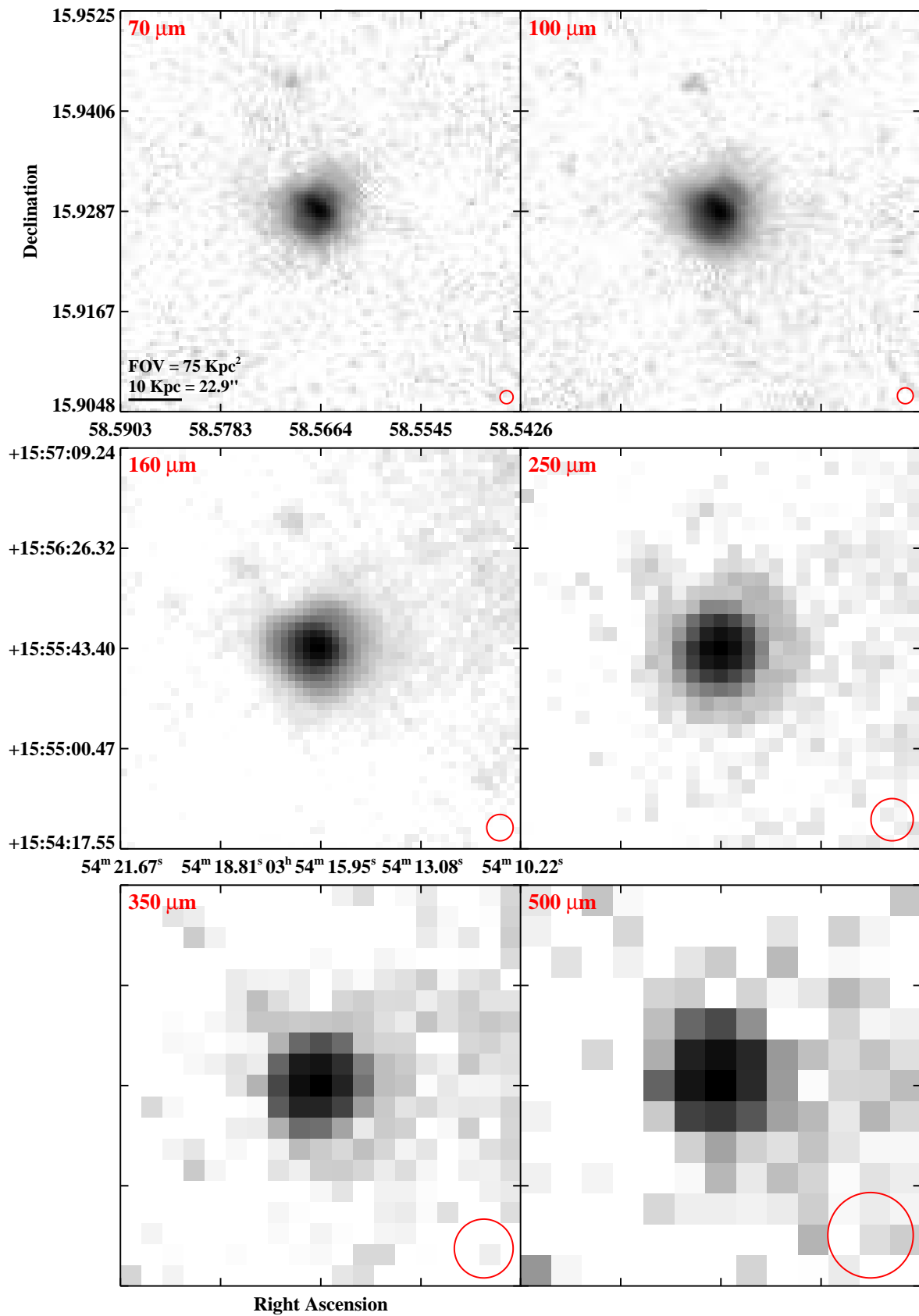


Fig. 3.— Continued (page 37 of 209).

IRAS F03514+1546 (CGCG 465-011)

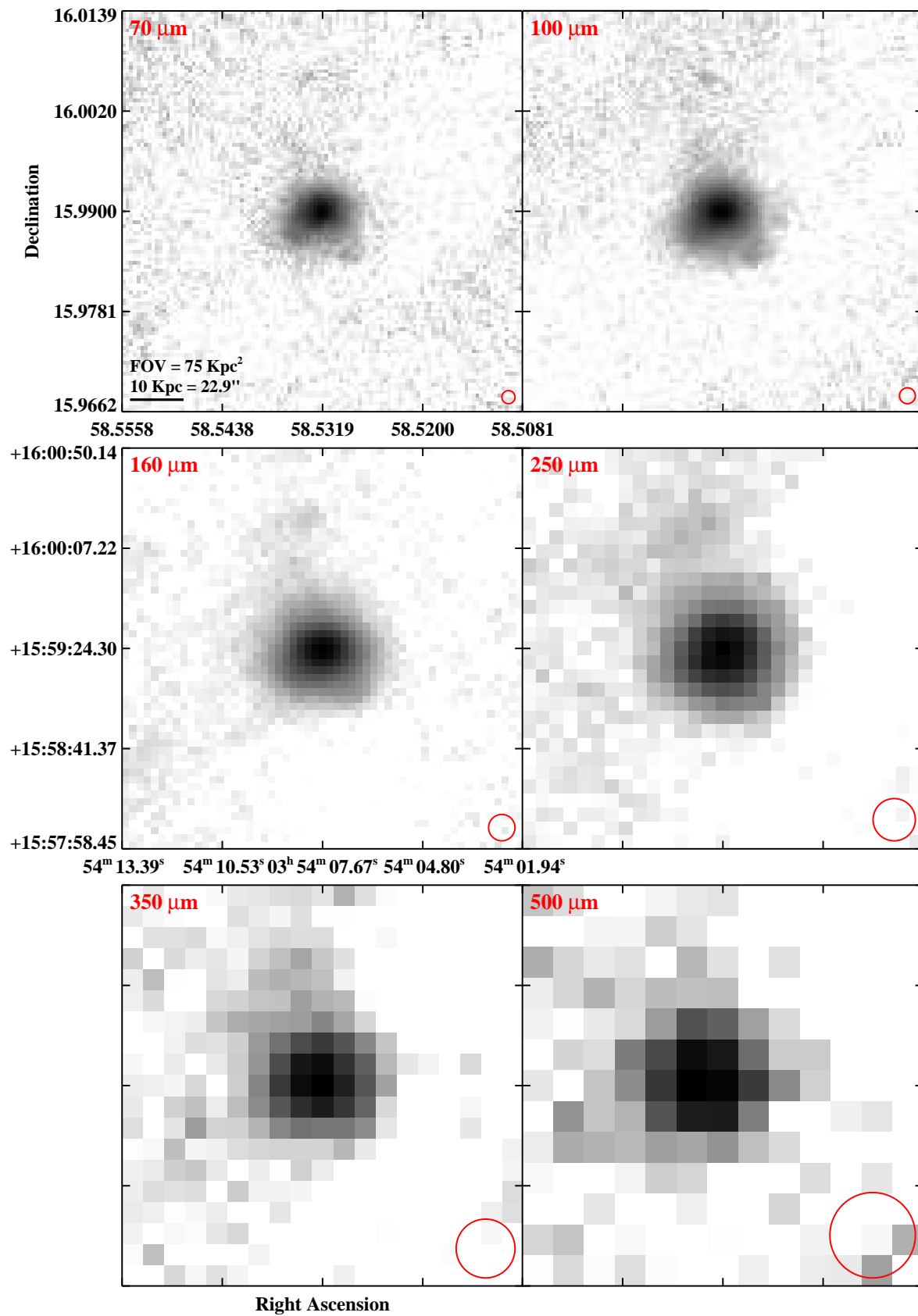


Fig. 3.— Continued (page 38 of 209).

IRAS 03582+6012

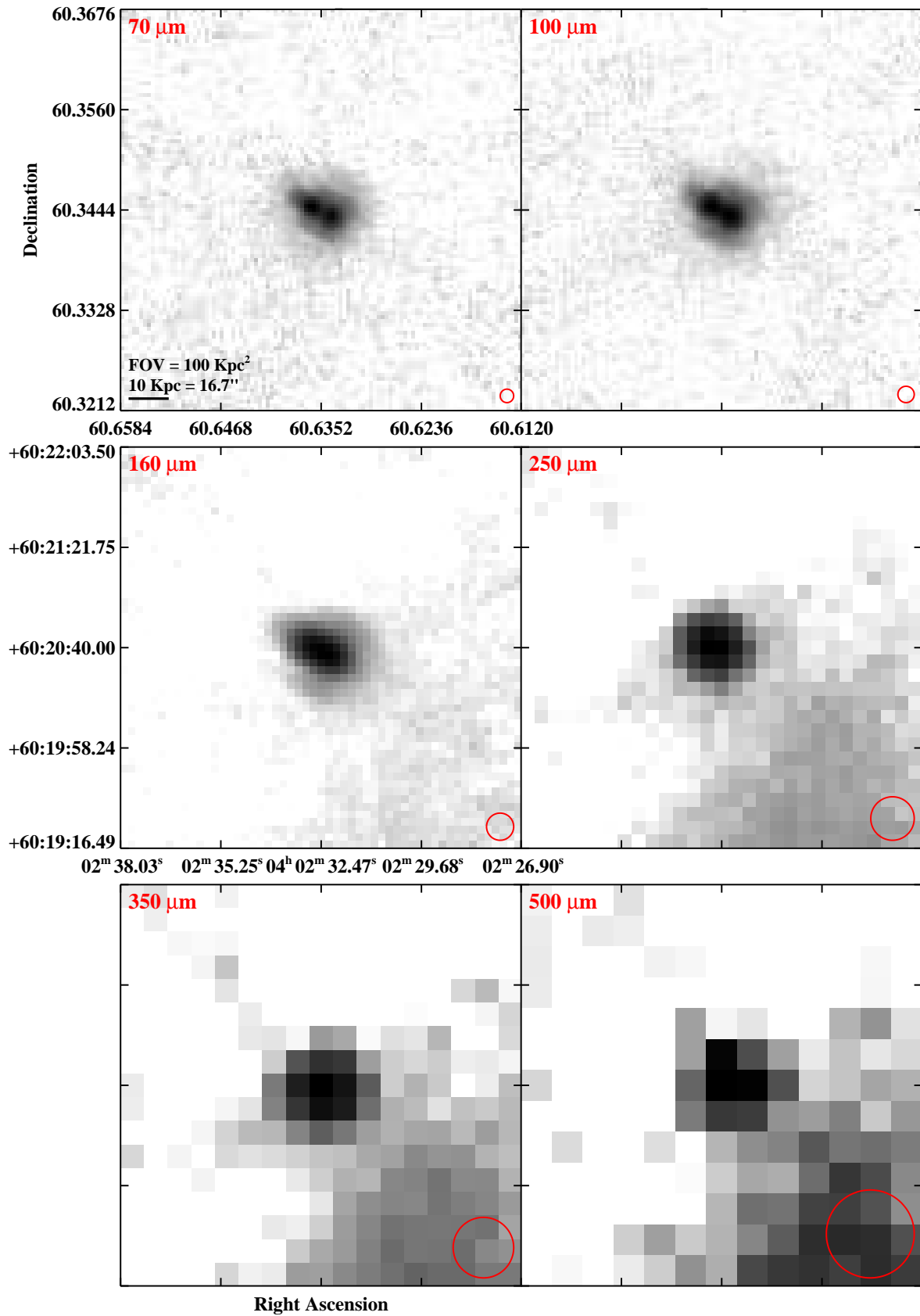


Fig. 3.— Continued (page 39 of 209).

IRAS F04097+0525 (UGC 02982)

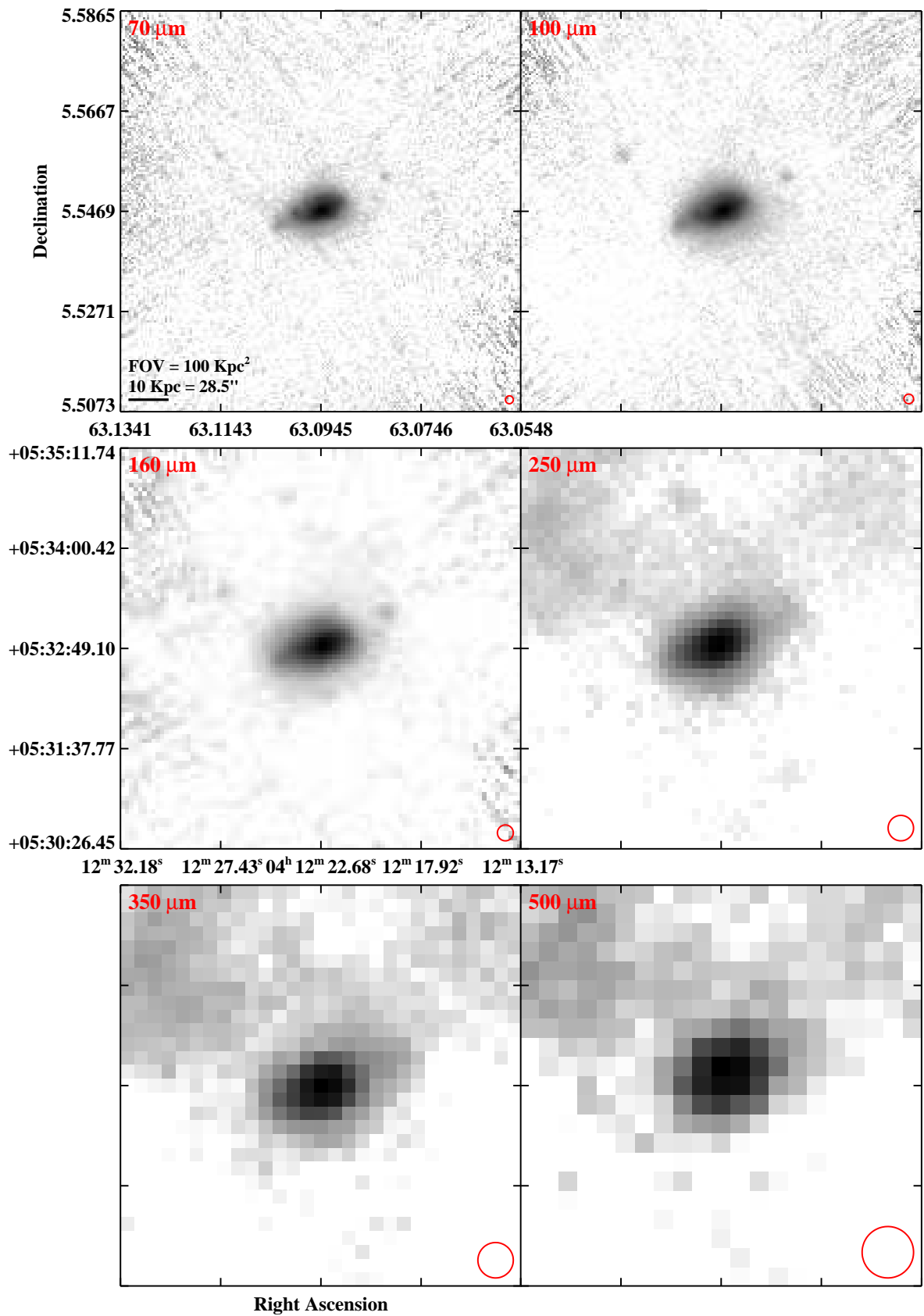


Fig. 3.— Continued (page 40 of 209).

IRAS F04118–3207 (ESO 420–G013)

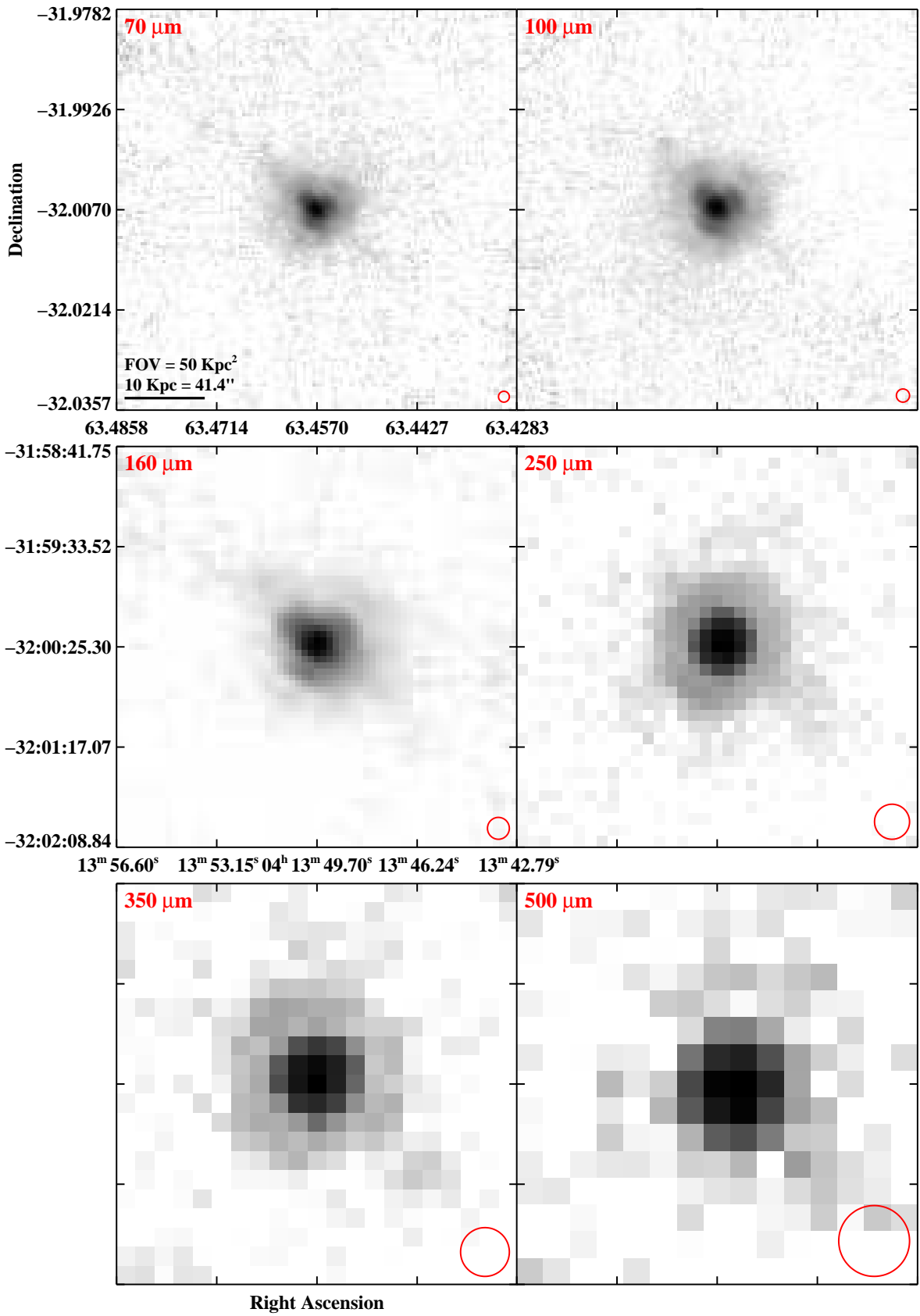


Fig. 3.— Continued (page 41 of 209).

IRAS F04191–1855 (ESO 550–IG 025)

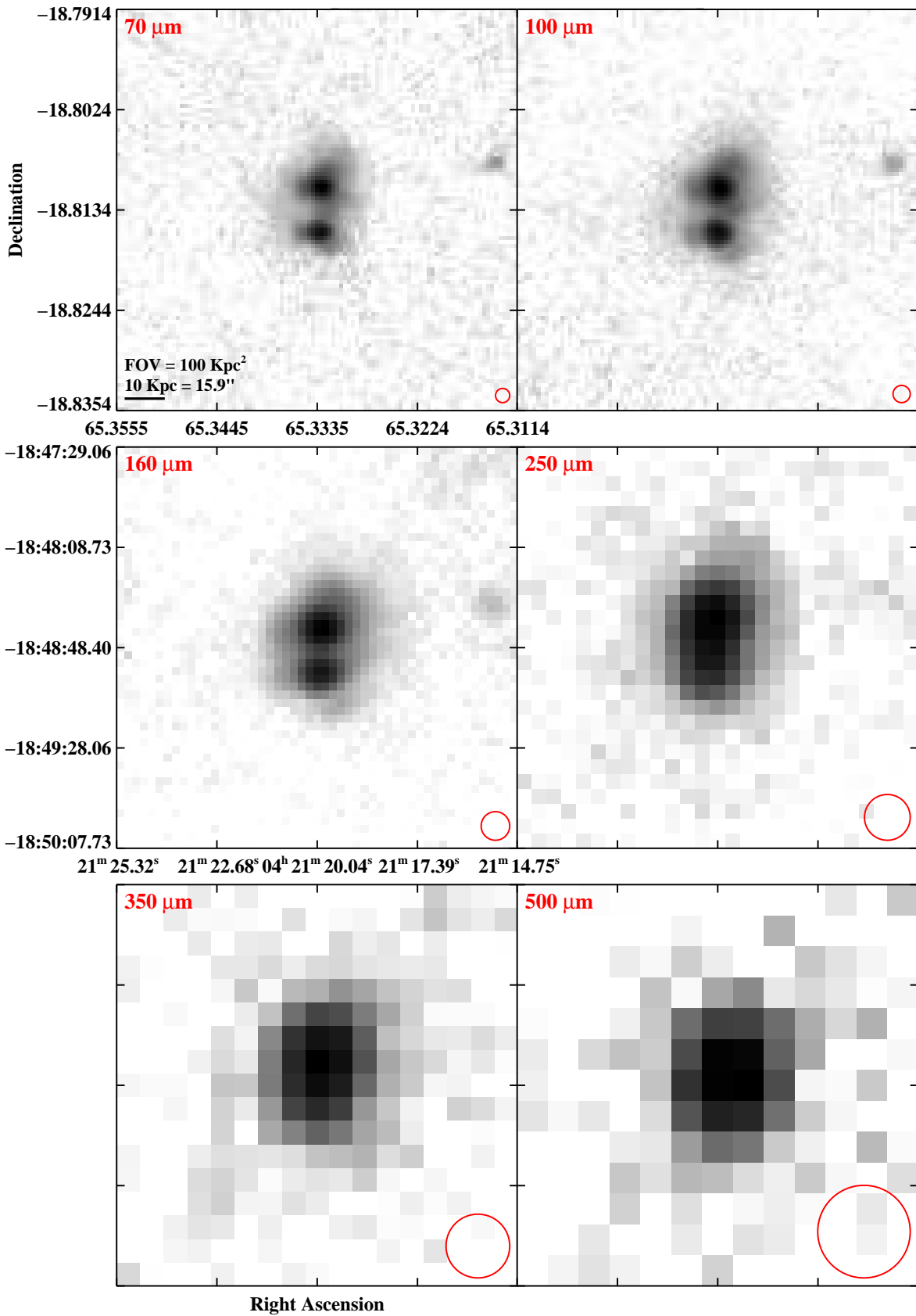


Fig. 3.— Continued (page 42 of 209).

IRAS F04210–4042 (NGC 1572)

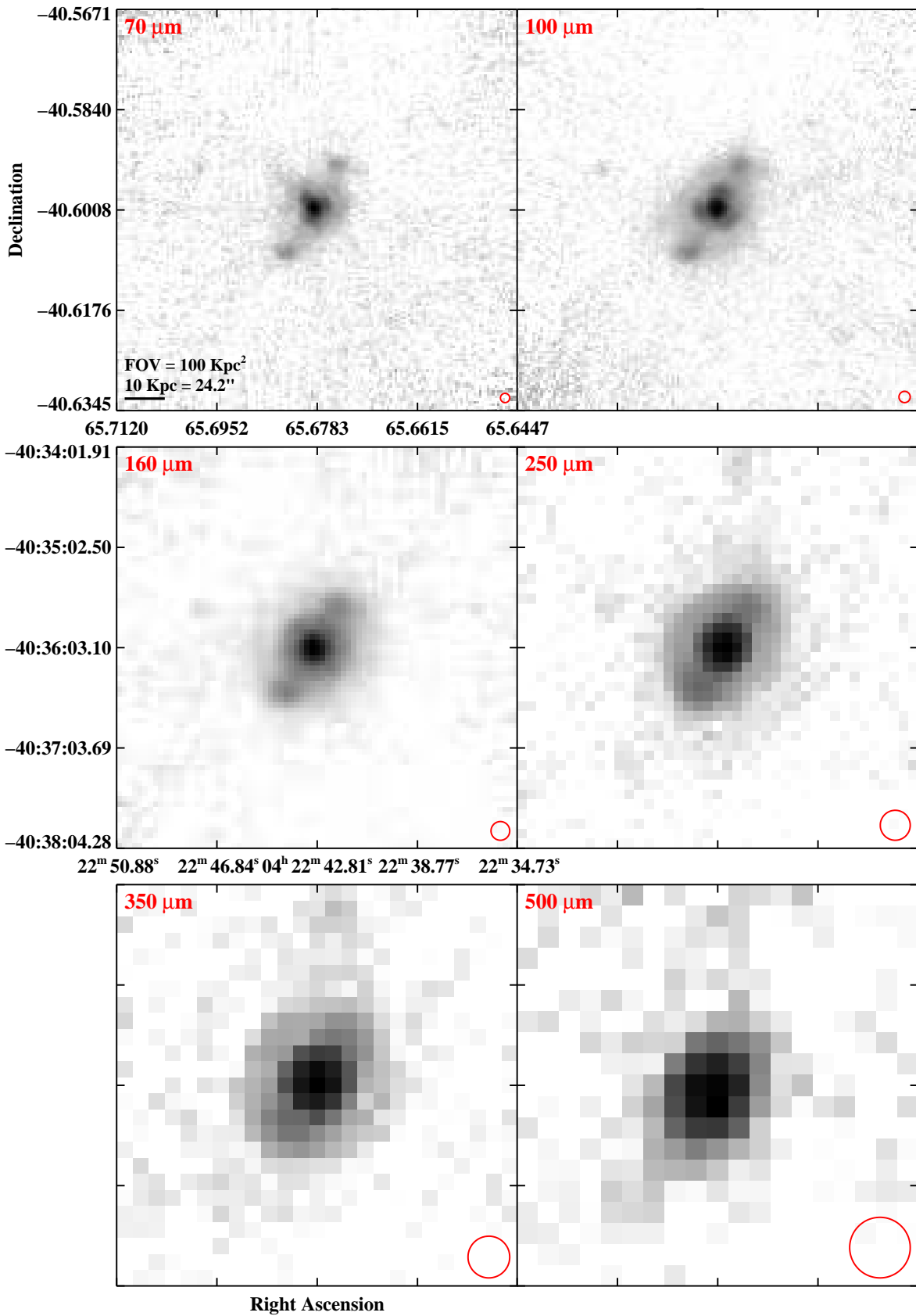


Fig. 3.— Continued (page 43 of 209).

IRAS 04271+3849

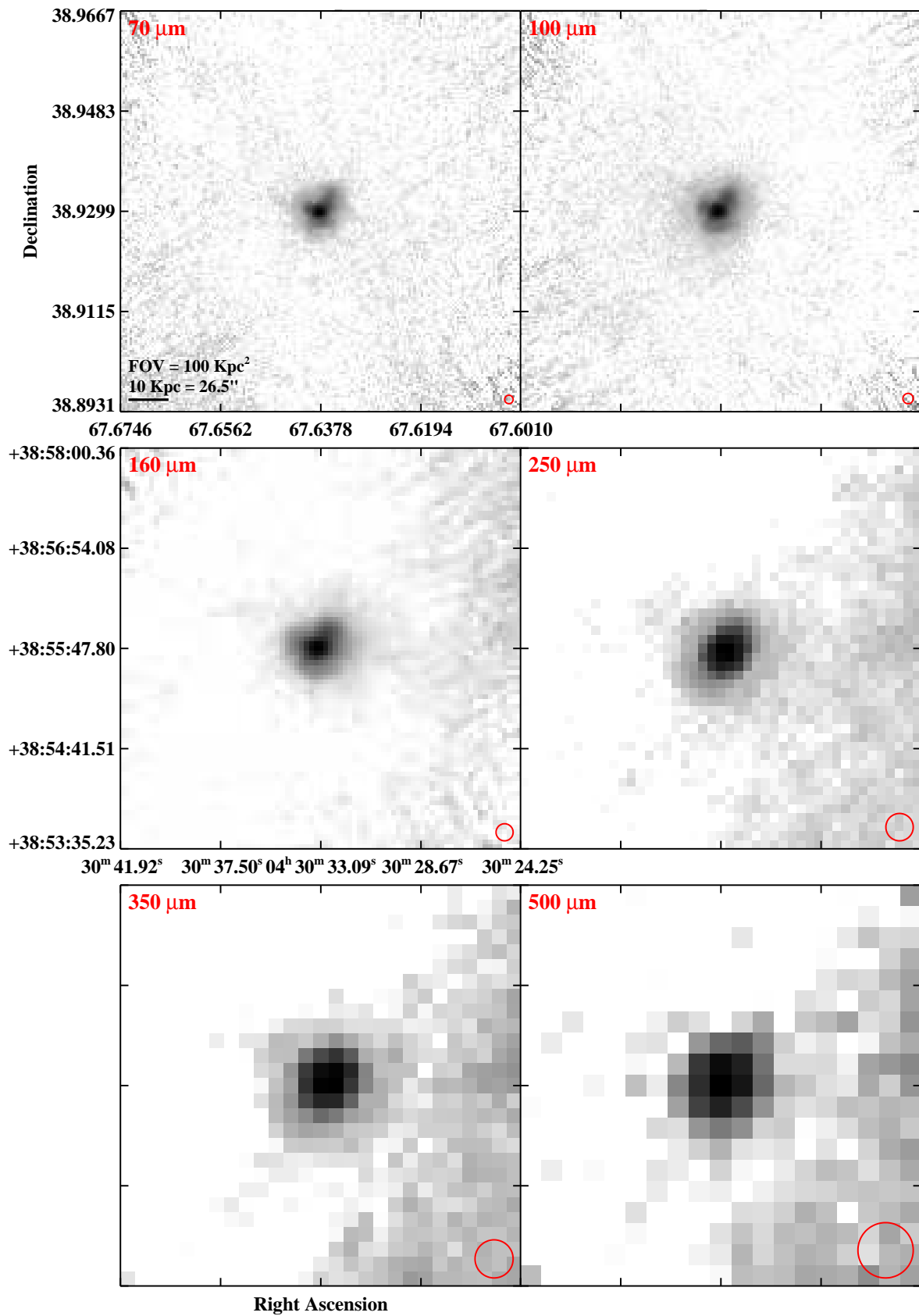


Fig. 3.— Continued (page 44 of 209).

IRAS F04315–0840 (NGC 1614)

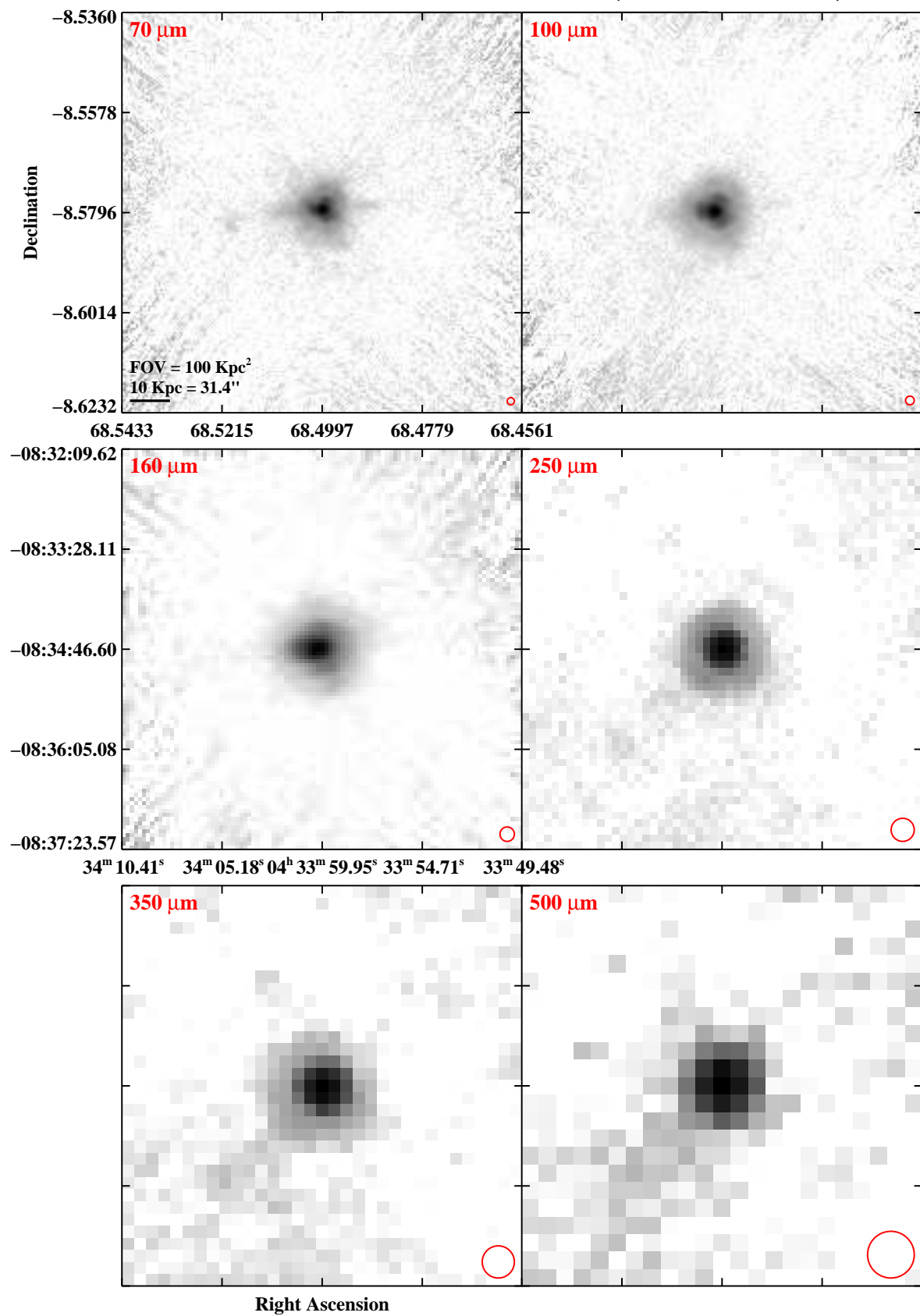


Fig. 3.— Continued (page 45 of 209).

IRAS F04326+1904 (UGC 03094)

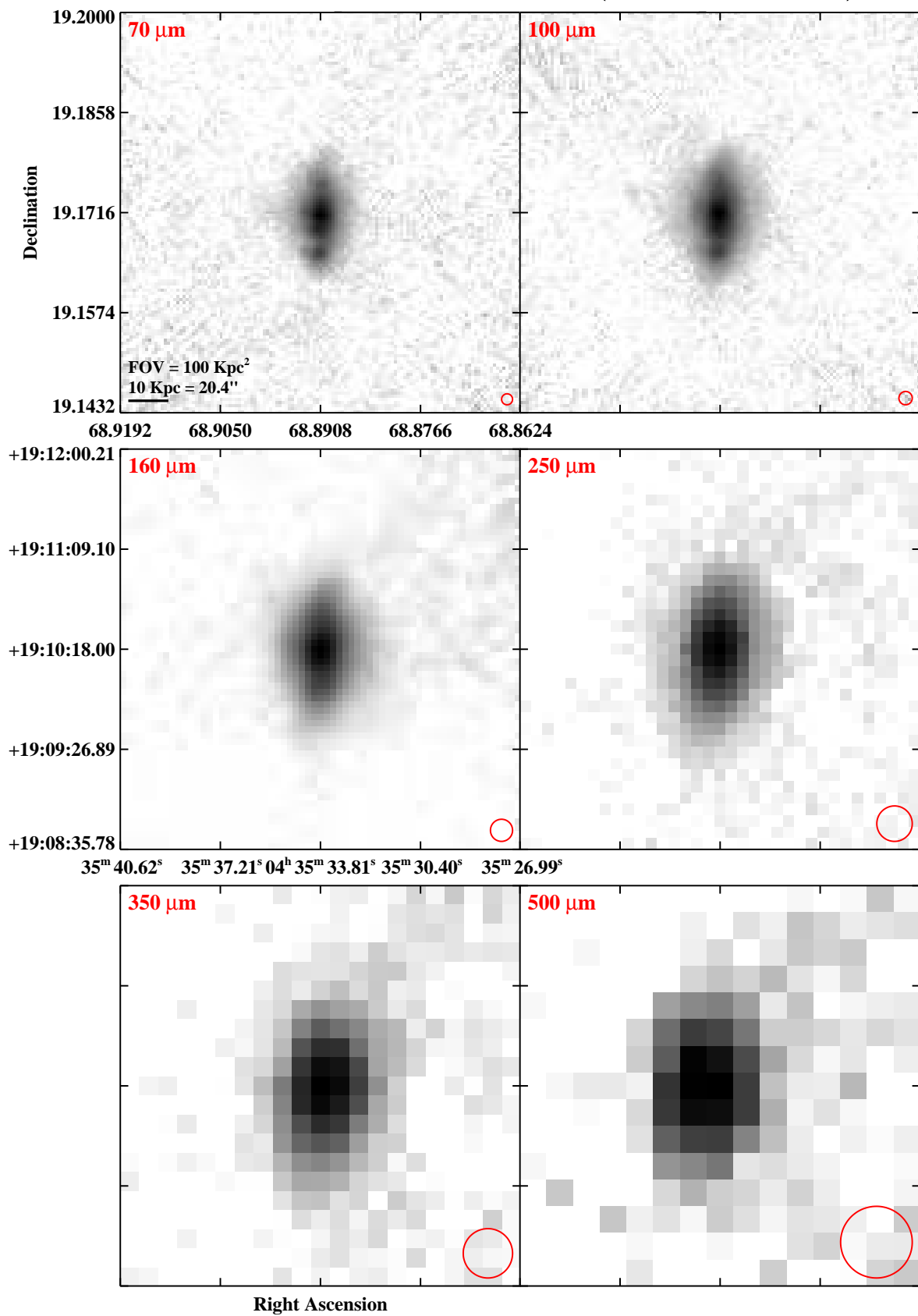


Fig. 3.— Continued (page 46 of 209).

IRAS F04454–4838 (ESO 203–IG001)

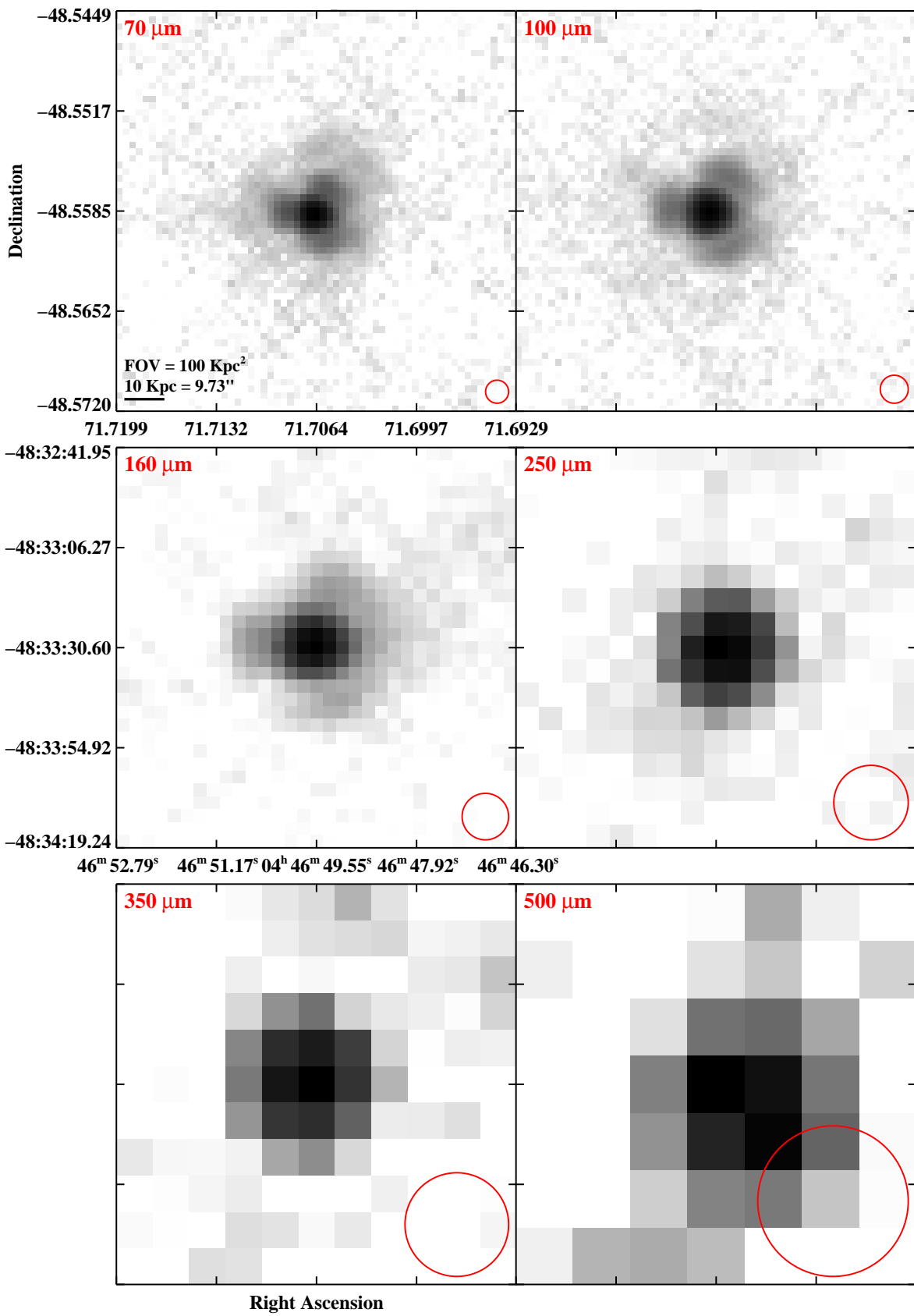


Fig. 3.— Continued (page 47 of 209).

IRAS F04502–3304 (MCG–05–12–006)

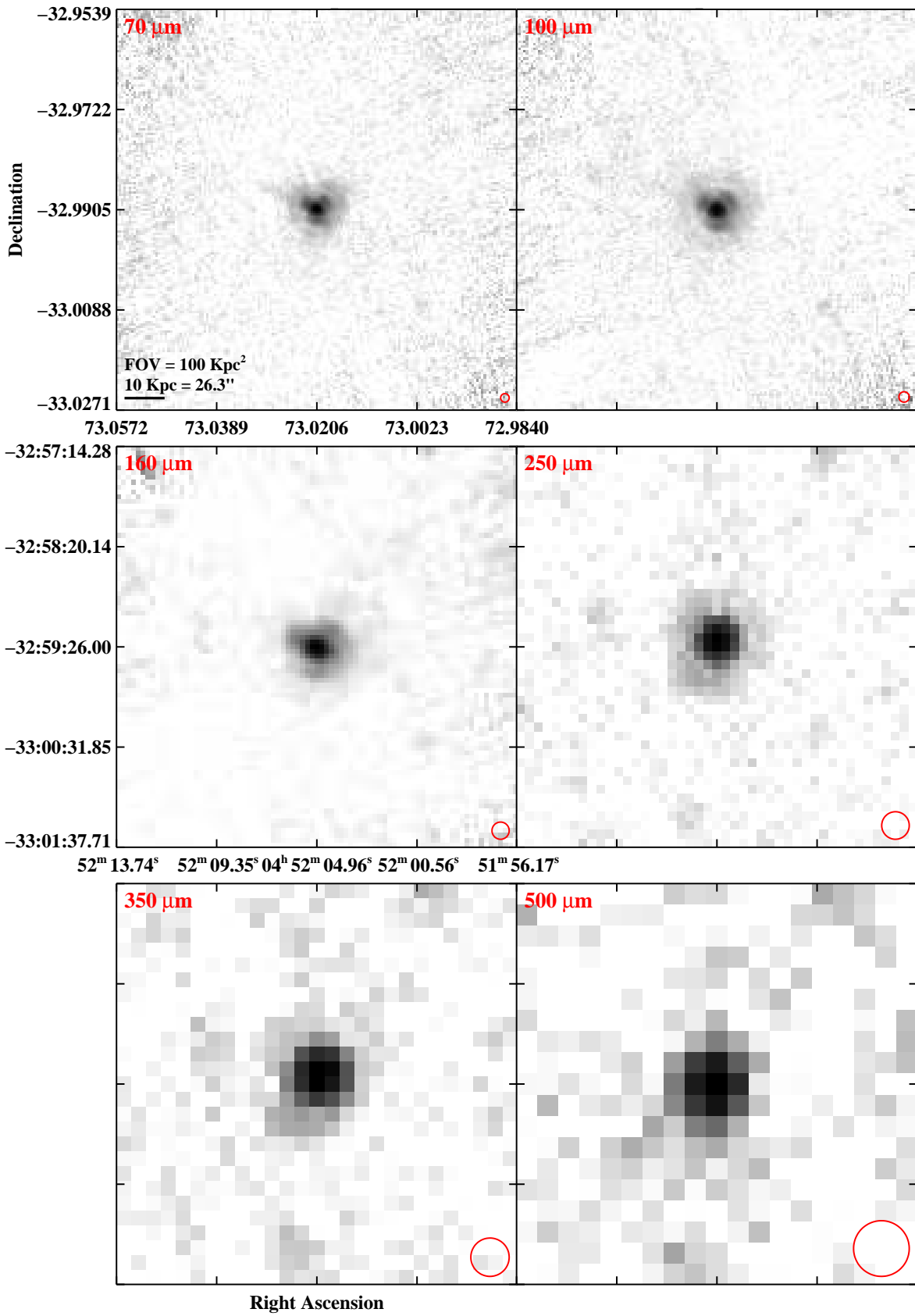


Fig. 3.— Continued (page 48 of 209).

IRAS F05053–0805 (NGC 1797)

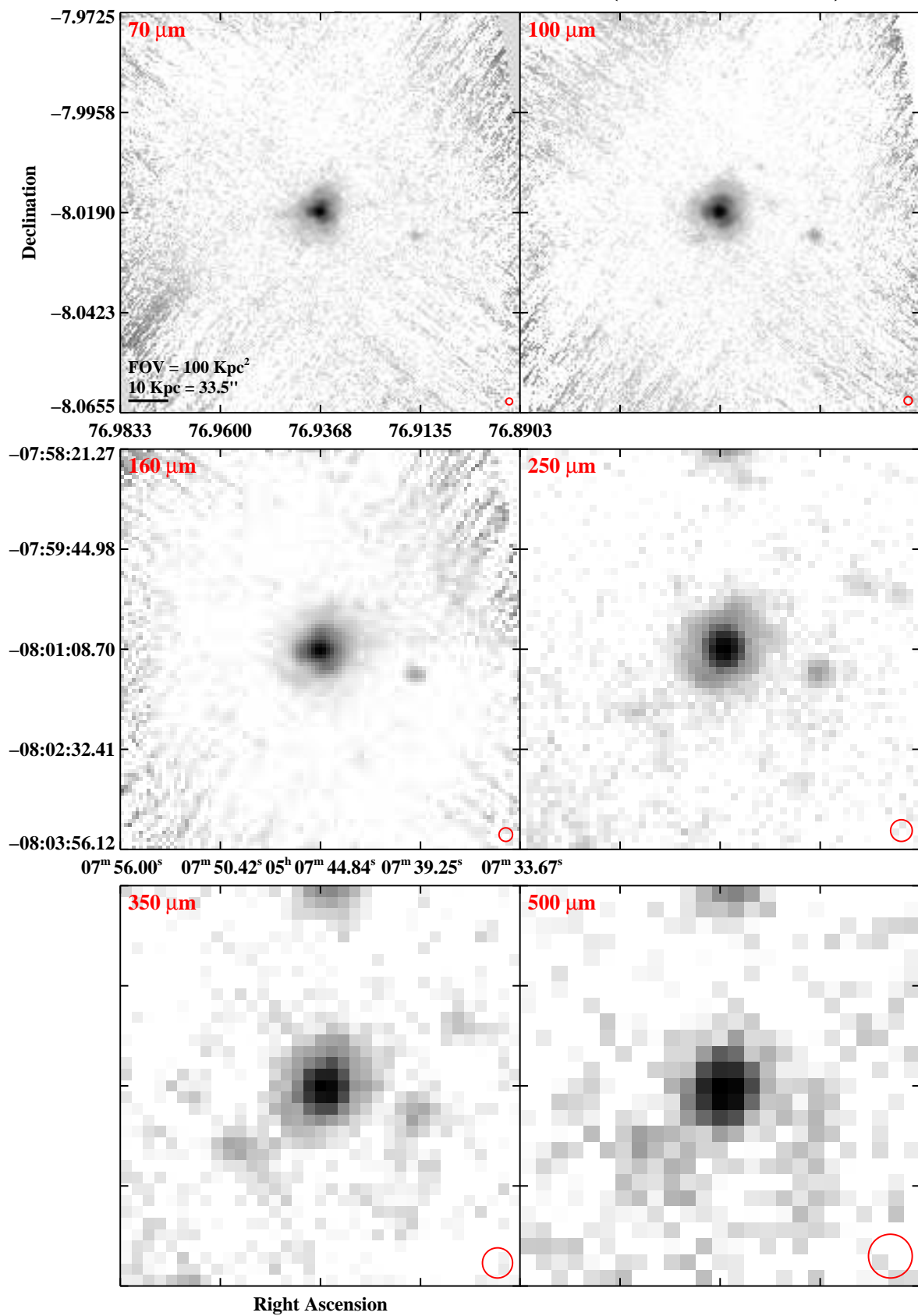


Fig. 3.— Continued (page 49 of 209).

IRAS F05053–0805 (NGC 1799)

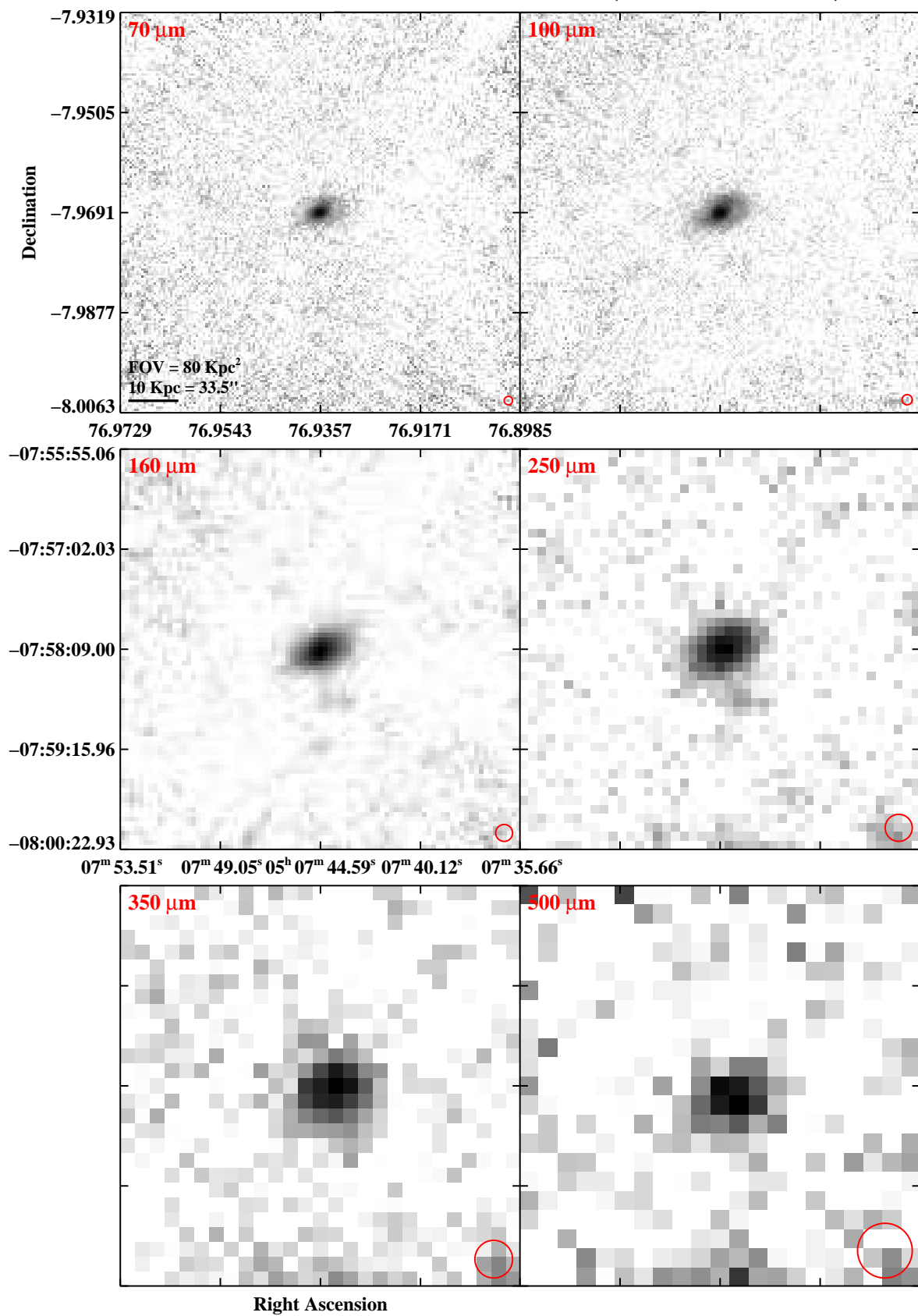


Fig. 3.— Continued (page 50 of 209).

IRAS F05054+1718 (CGCG 468-002)

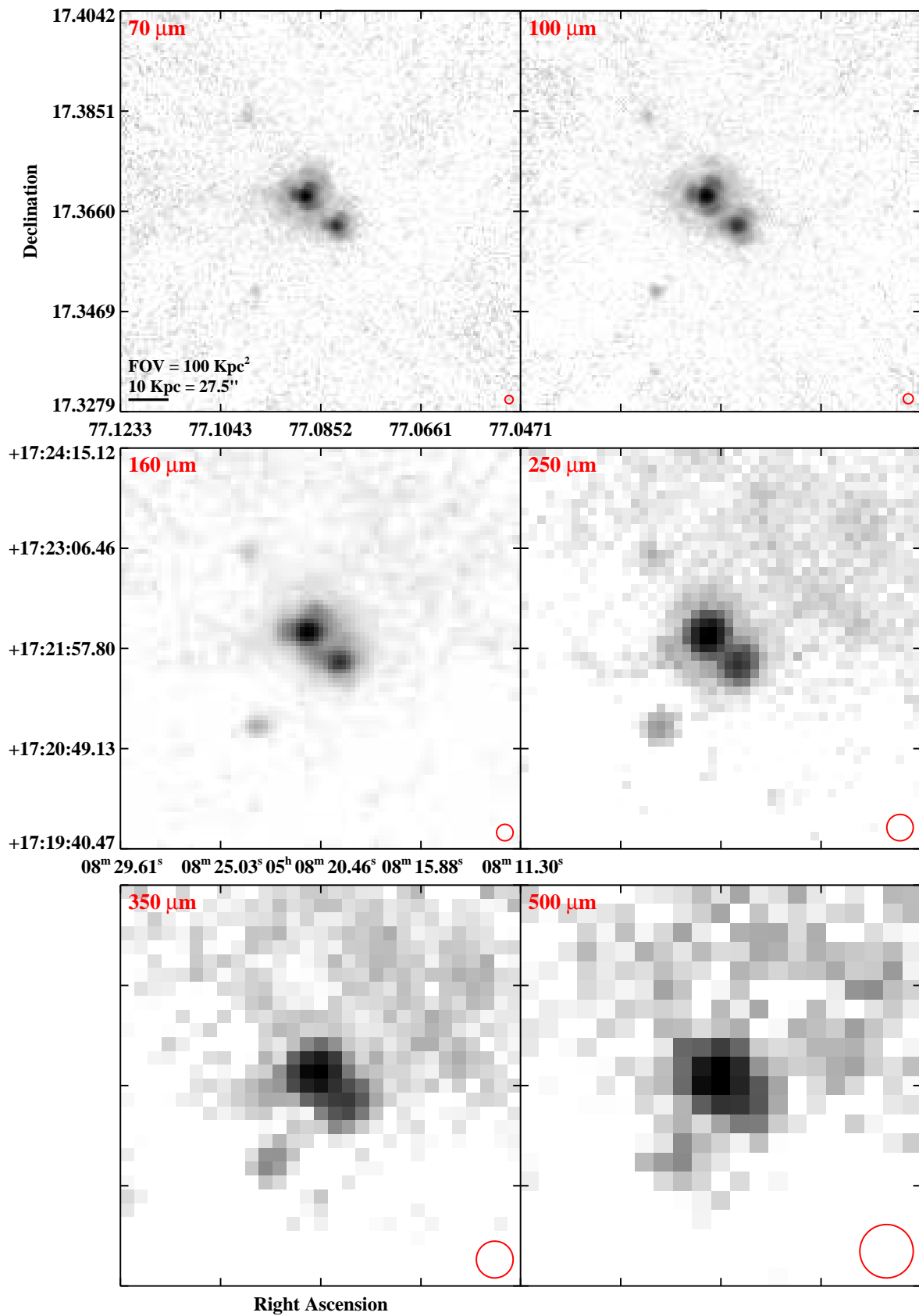


Fig. 3.— Continued (page 51 of 209).

IRAS 05083+2441

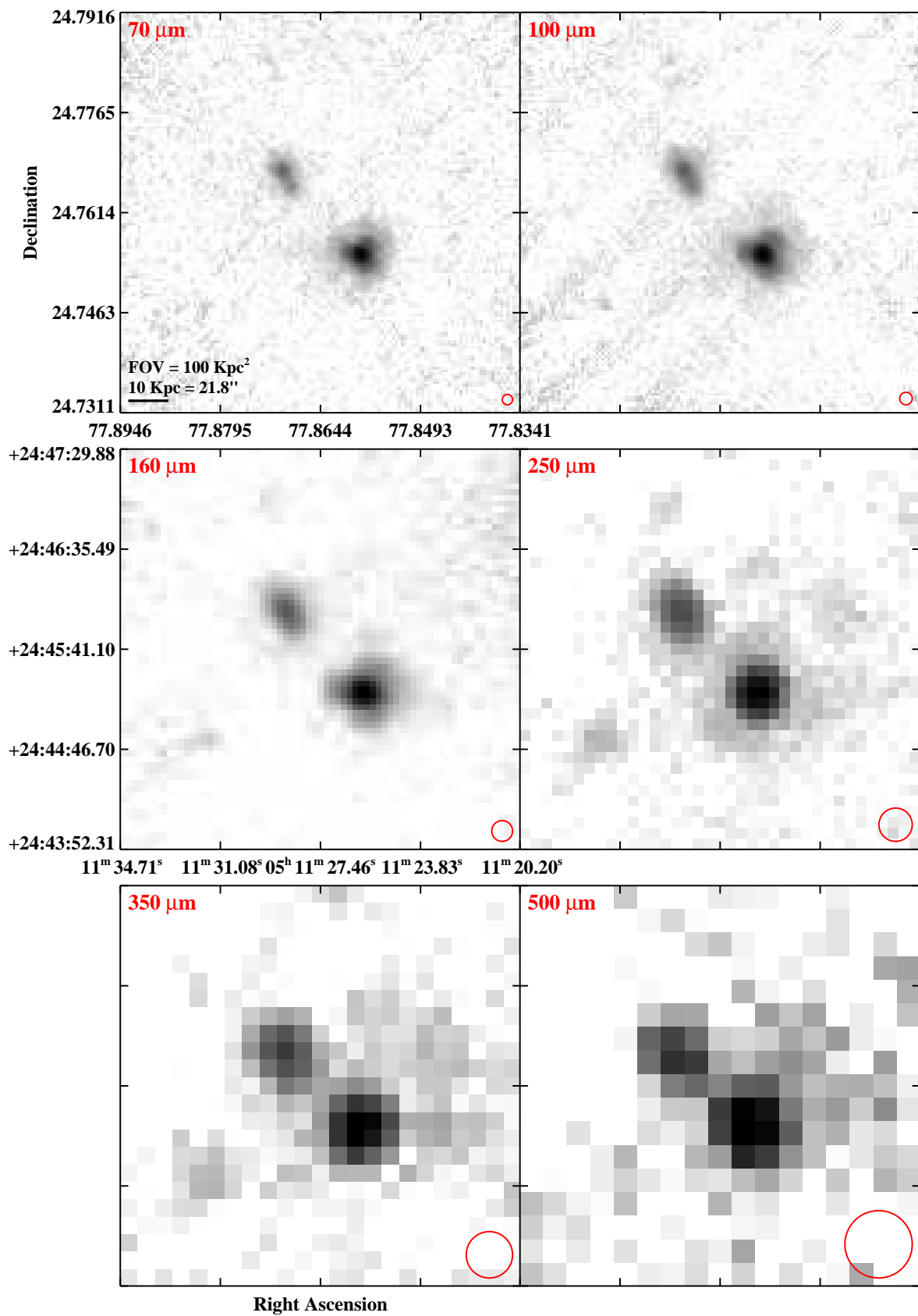


Fig. 3.— Continued (page 52 of 209).

IRAS F05081+7936 (VII Zw 031)

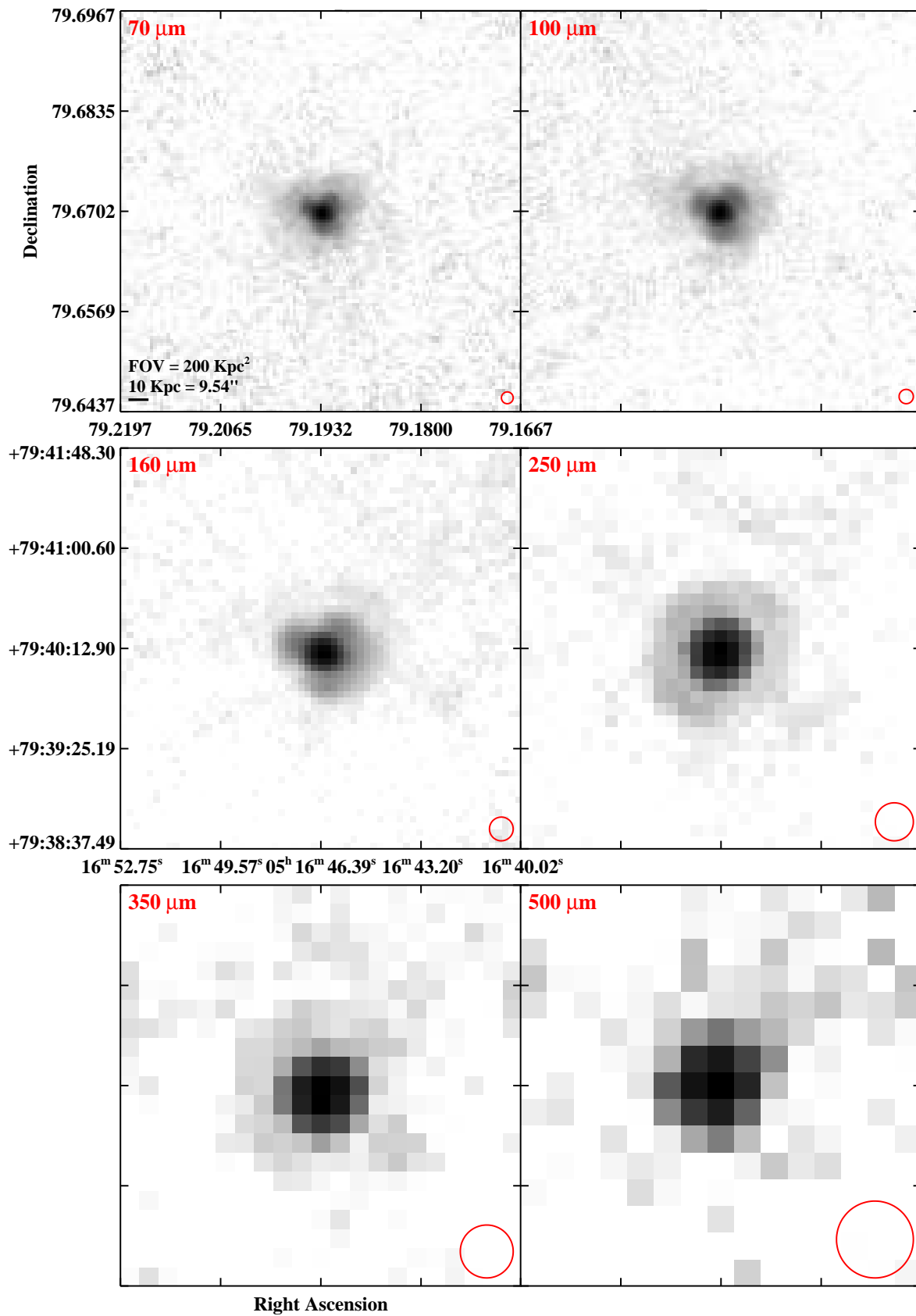


Fig. 3.— Continued (page 53 of 209).

IRAS 05129+5128

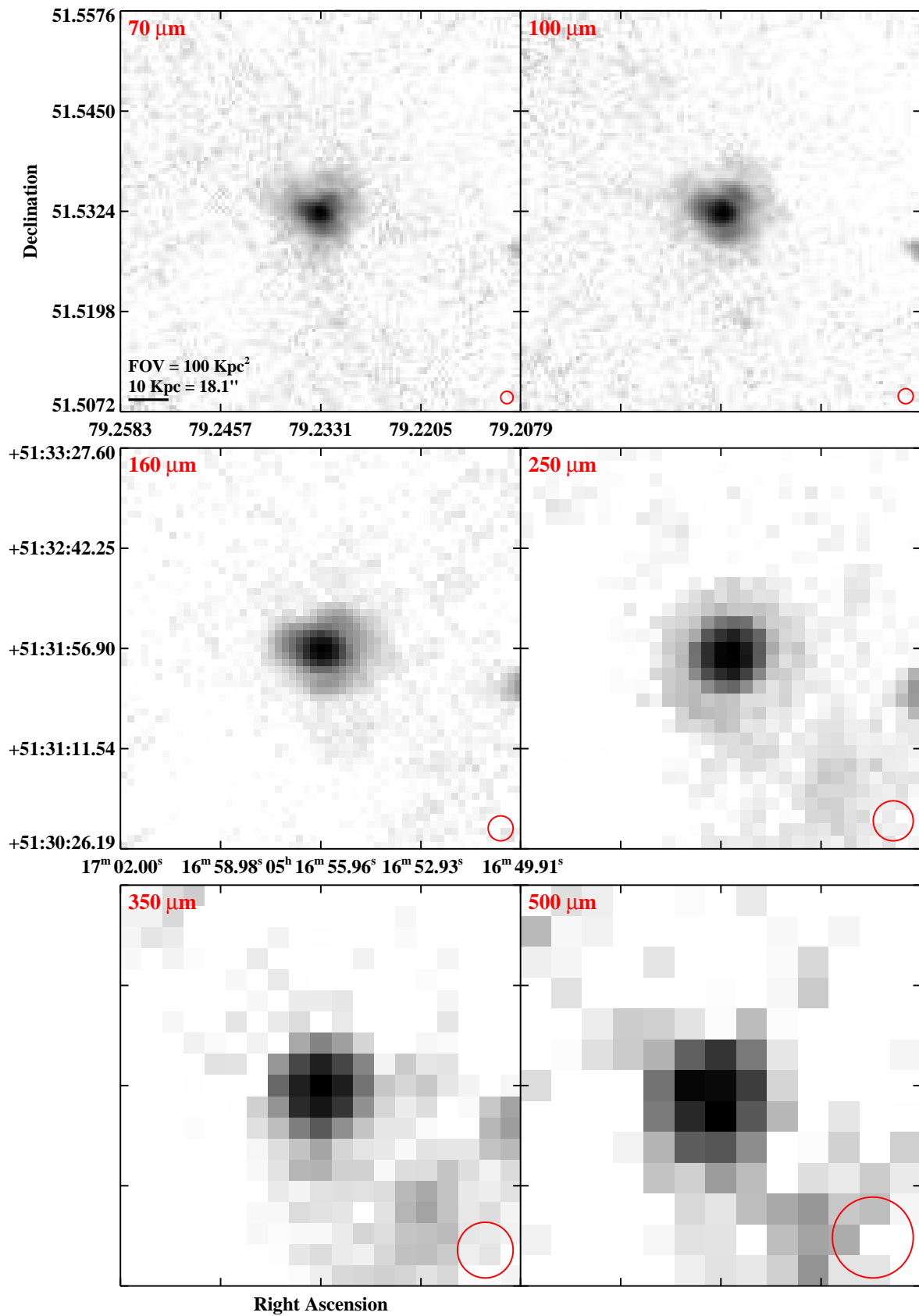


Fig. 3.— Continued (page 54 of 209).

IRAS F05189–2524

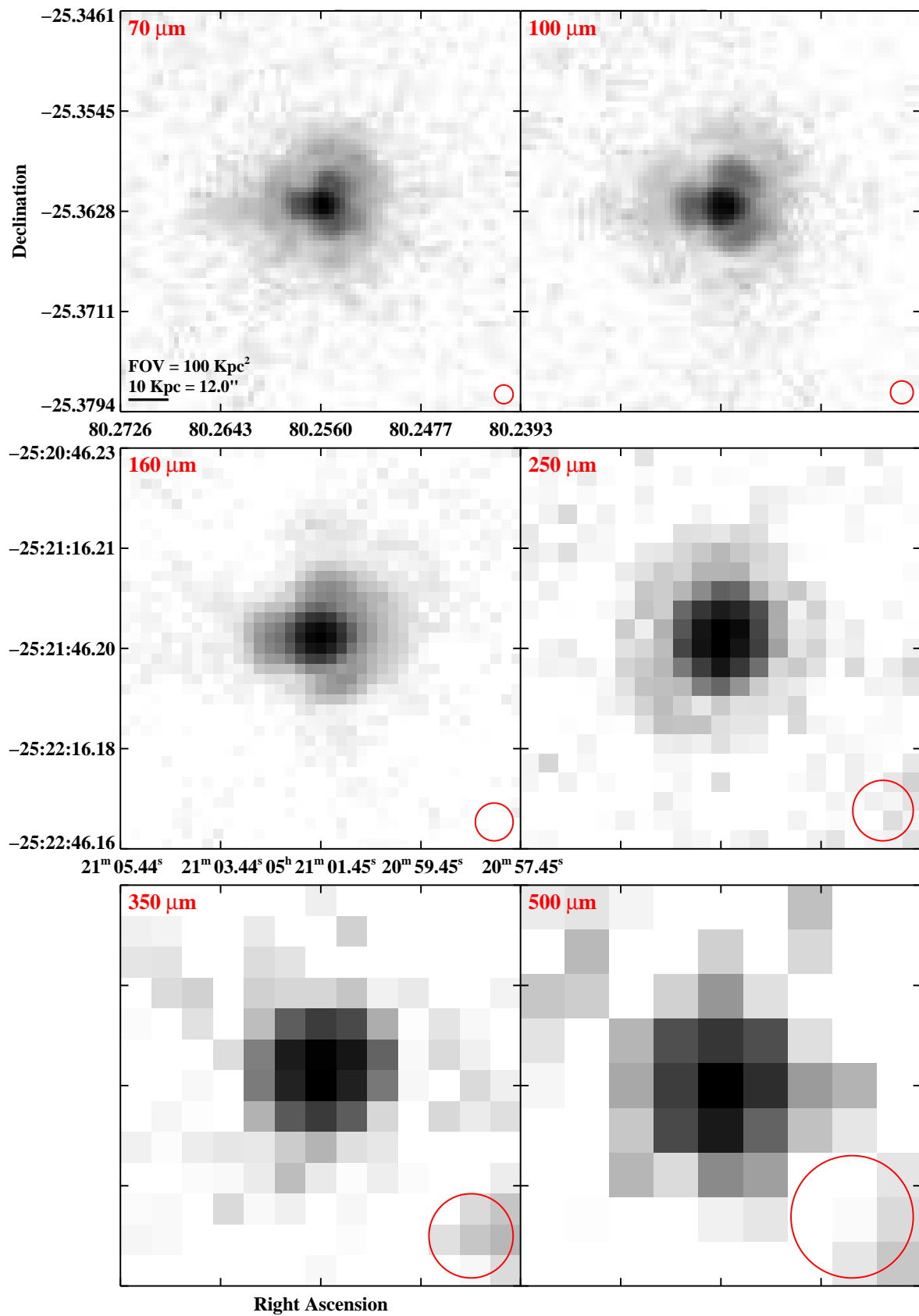


Fig. 3.— Continued (page 55 of 209).

IRAS F05187–1017

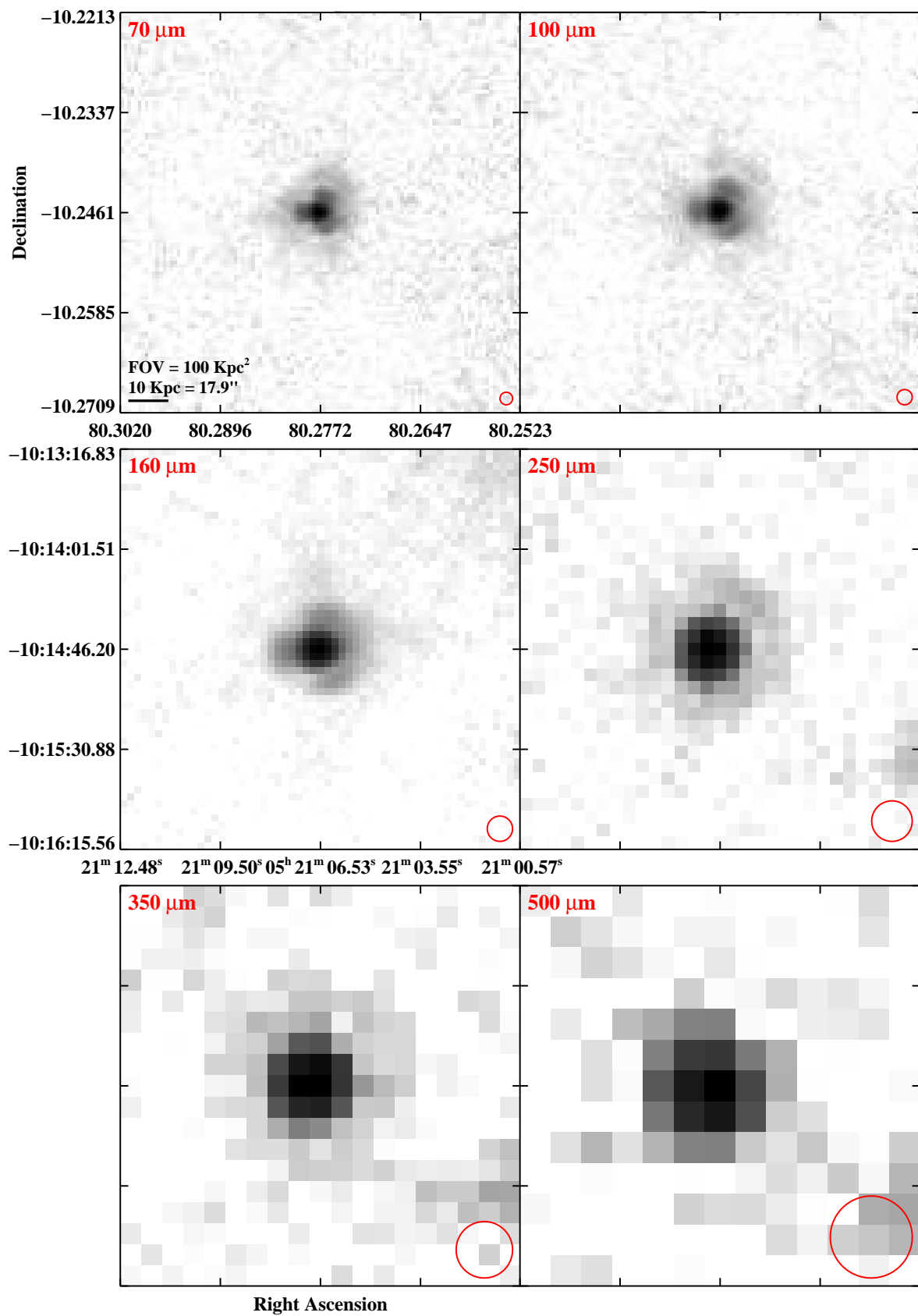


Fig. 3.— Continued (page 56 of 209).

IRAS 05368+4940 (MCG+08-11-002)

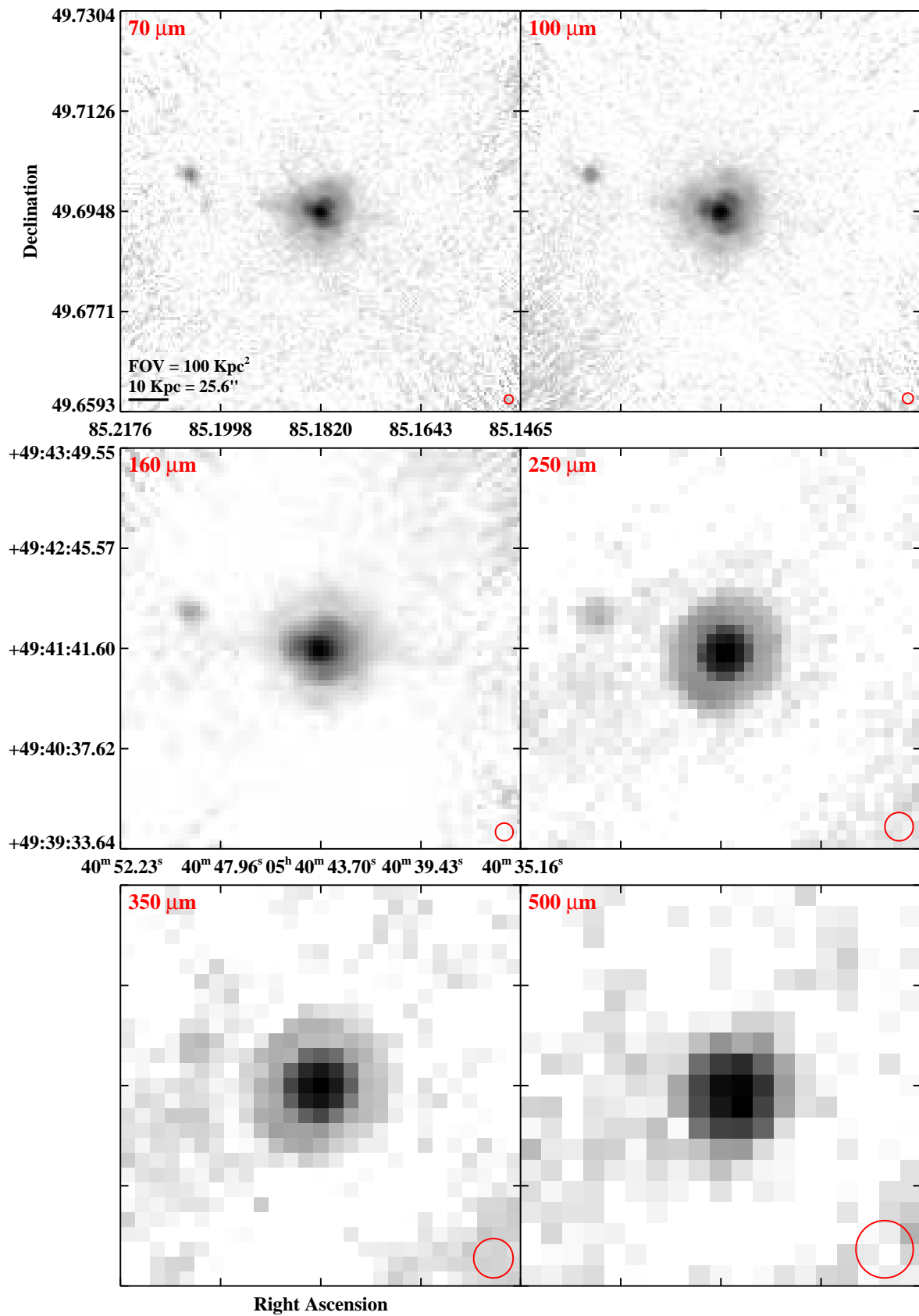


Fig. 3.— Continued (page 57 of 209).

IRAS F05365+6921 (NGC 1961)

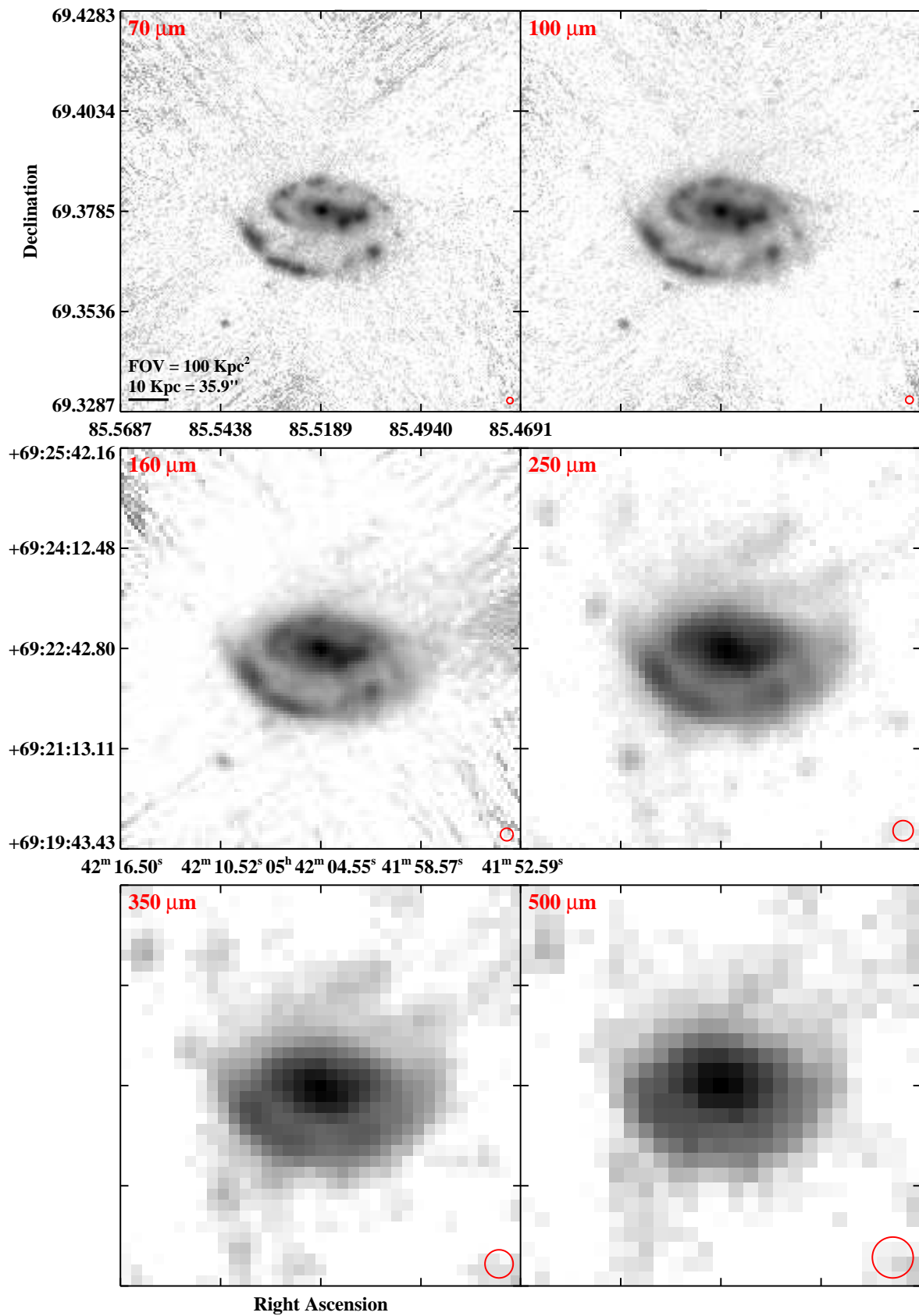


Fig. 3.— Continued (page 58 of 209).

IRAS F05414+5840 (UGC 03351)

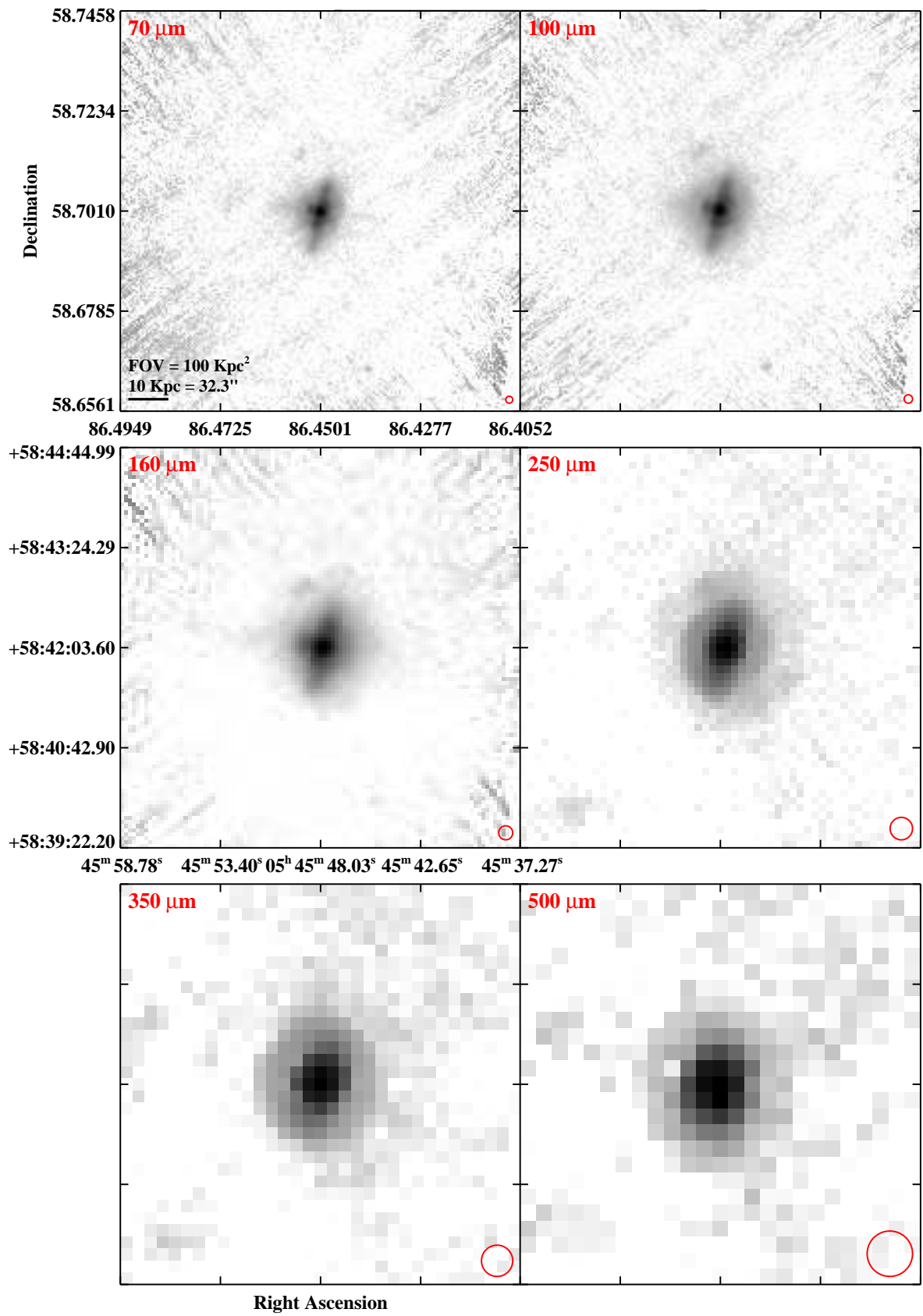


Fig. 3.— Continued (page 59 of 209).

IRAS 05442+1732

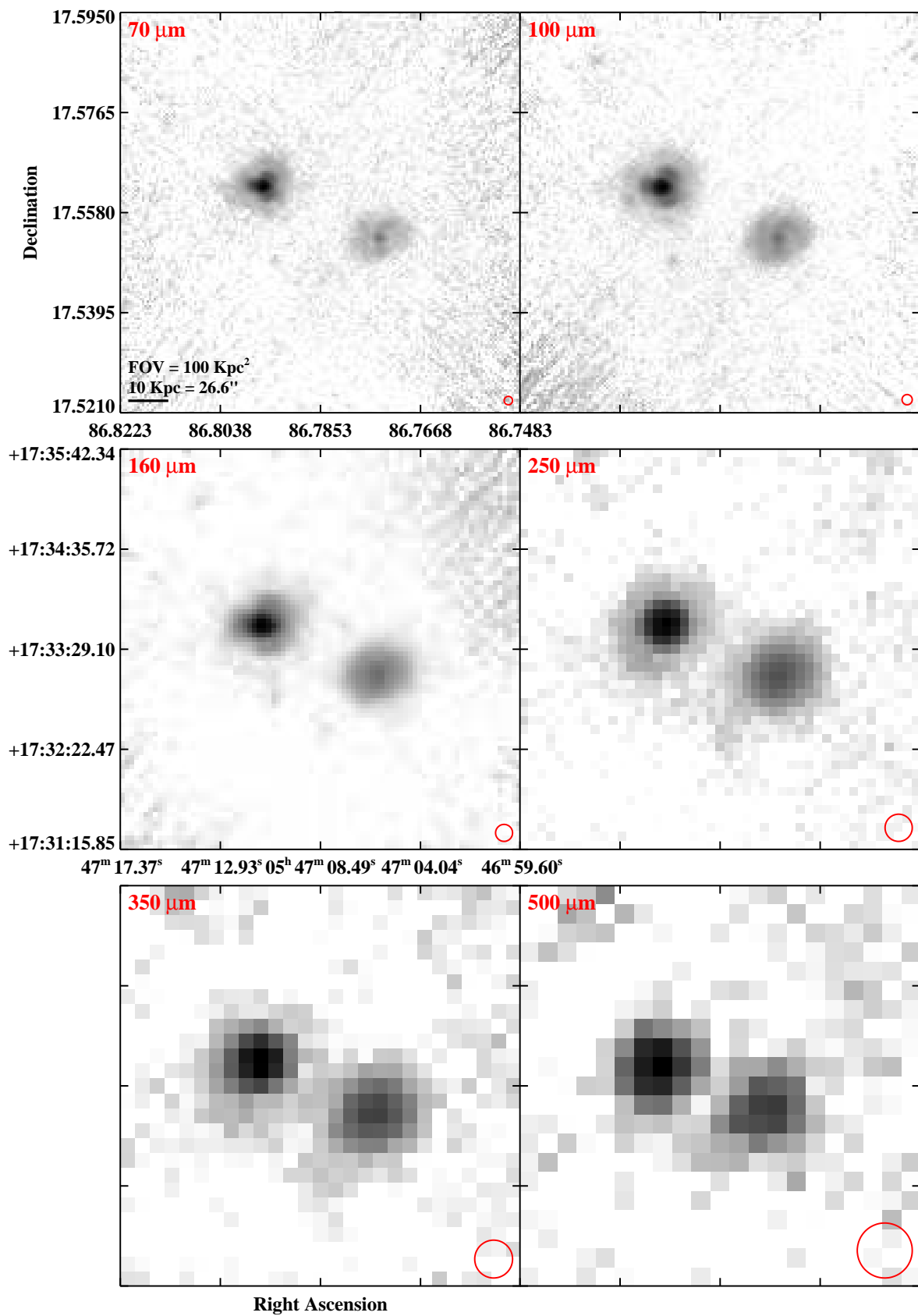


Fig. 3.— Continued (page 60 of 209).

IRAS F06076–2139

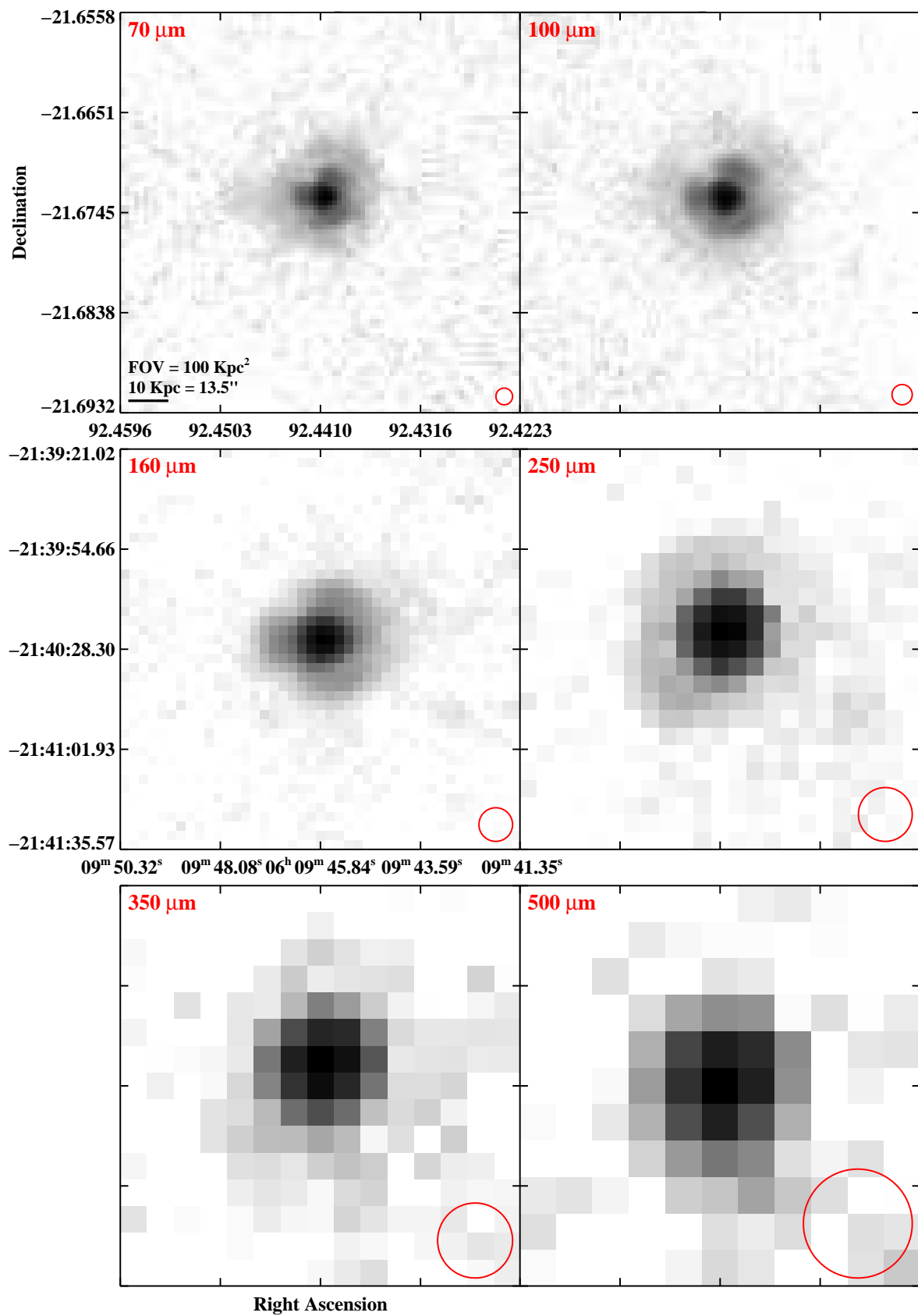


Fig. 3.— Continued (page 61 of 209).

IRAS F06052+8027 (UGC 03410)

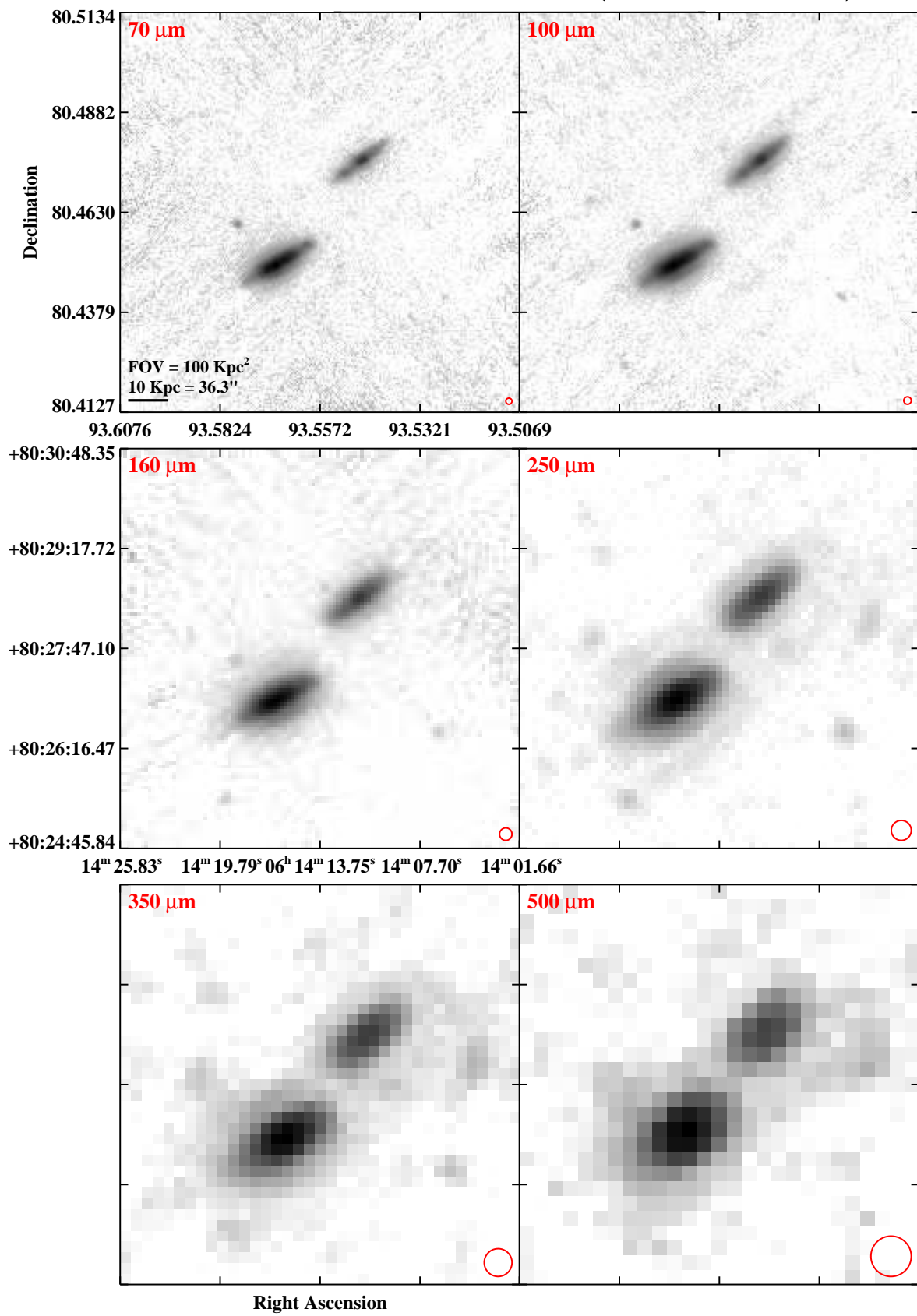
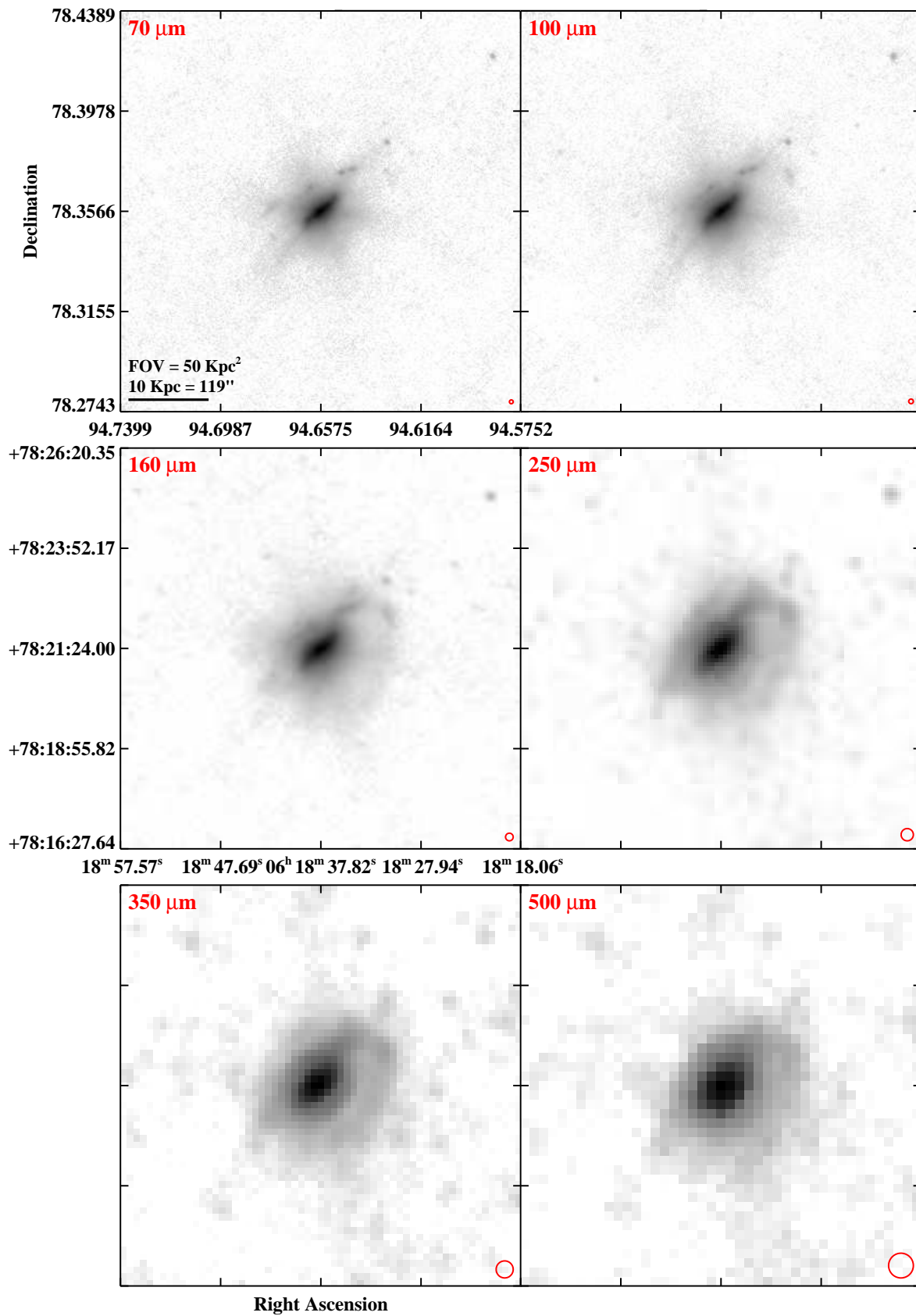


Fig. 3.— Continued (page 62 of 209).

IRAS F06107+7822 (NGC 2146)



90

Fig. 3.— Continued (page 63 of 209).

IRAS F06259–4708 (ESO 255–IG007)

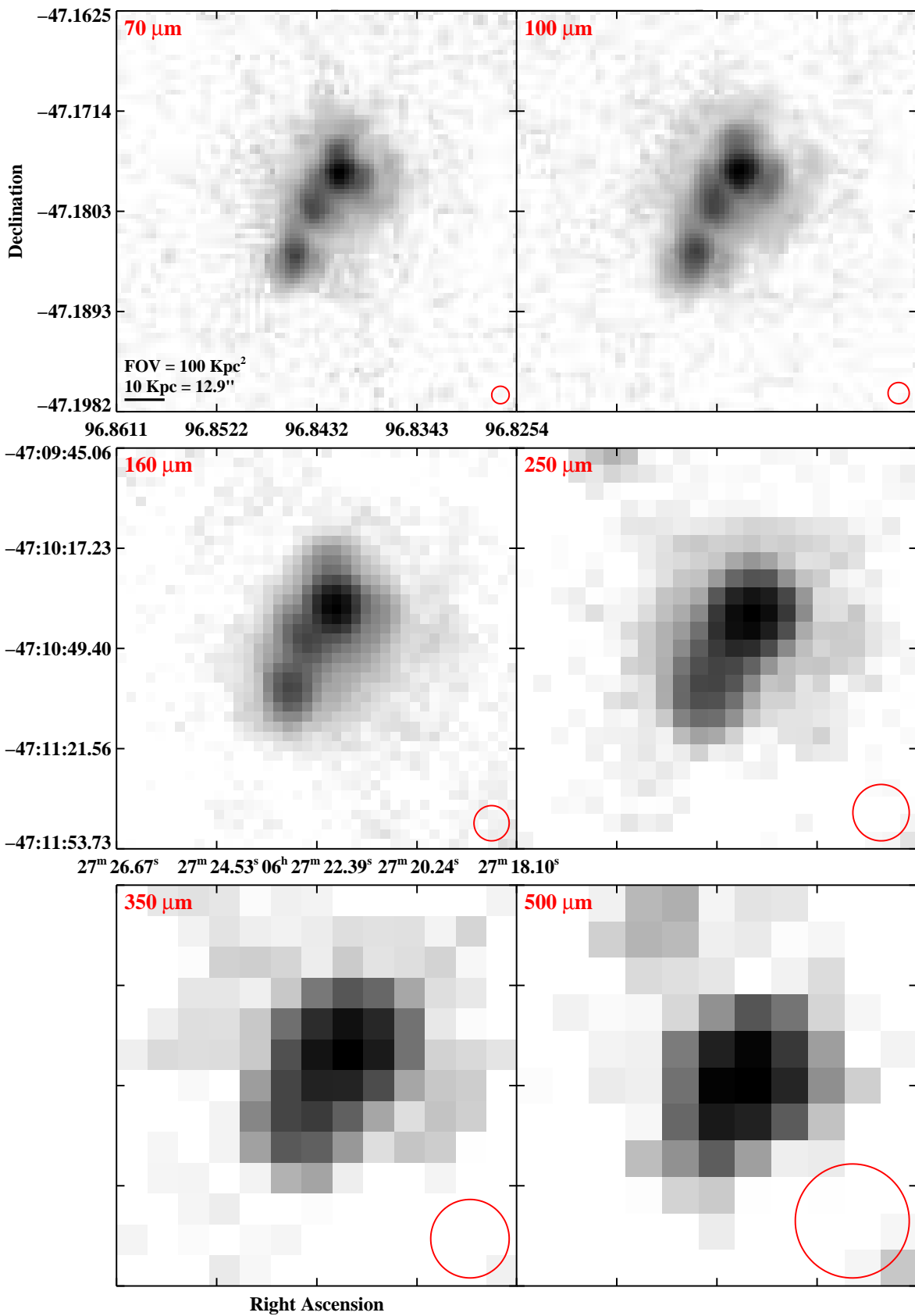


Fig. 3.— Continued (page 64 of 209).

IRAS F06295–1735 (ESO 557–G002)

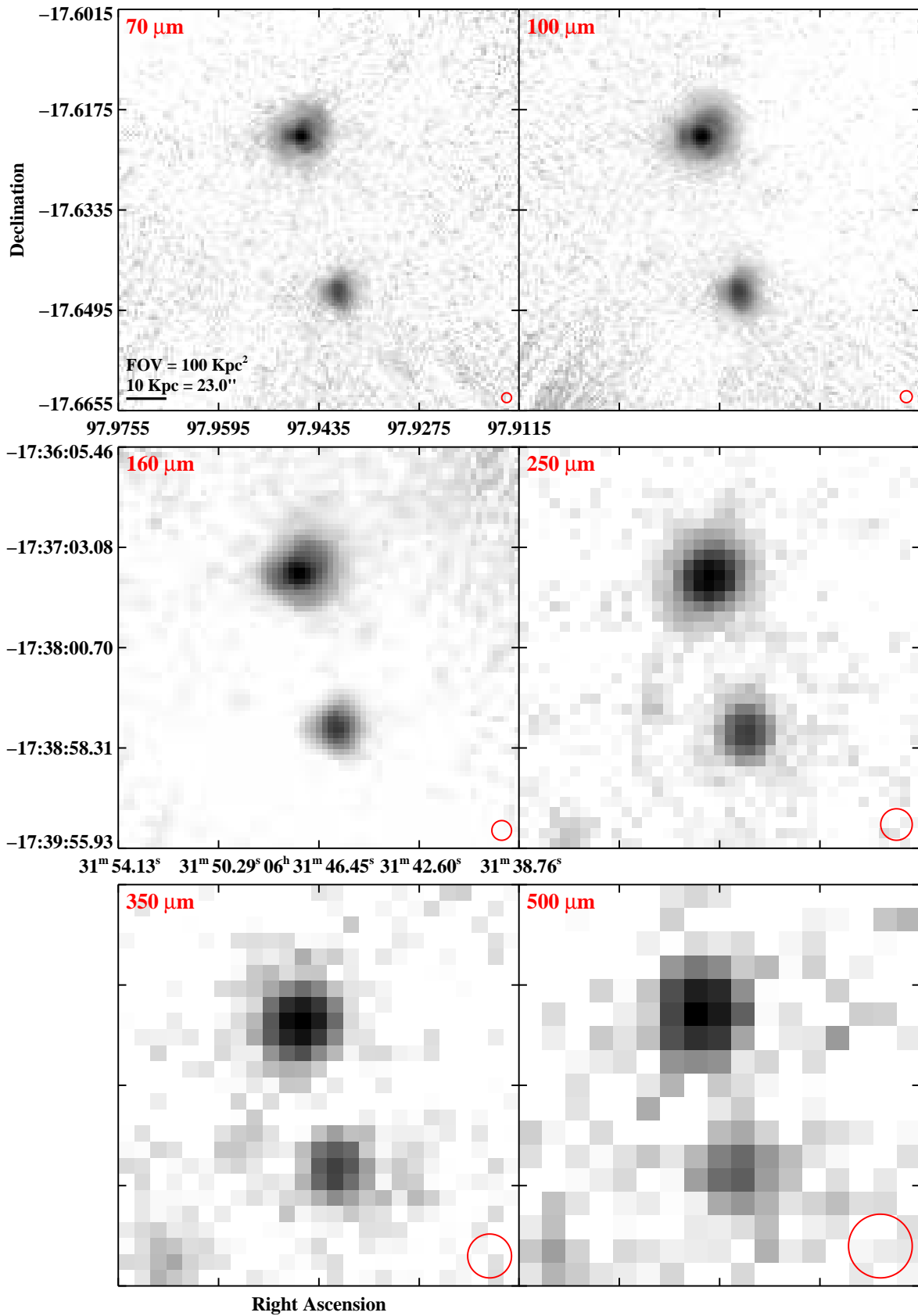


Fig. 3.— Continued (page 65 of 209).

IRAS F06538+4628 (UGC 03608)

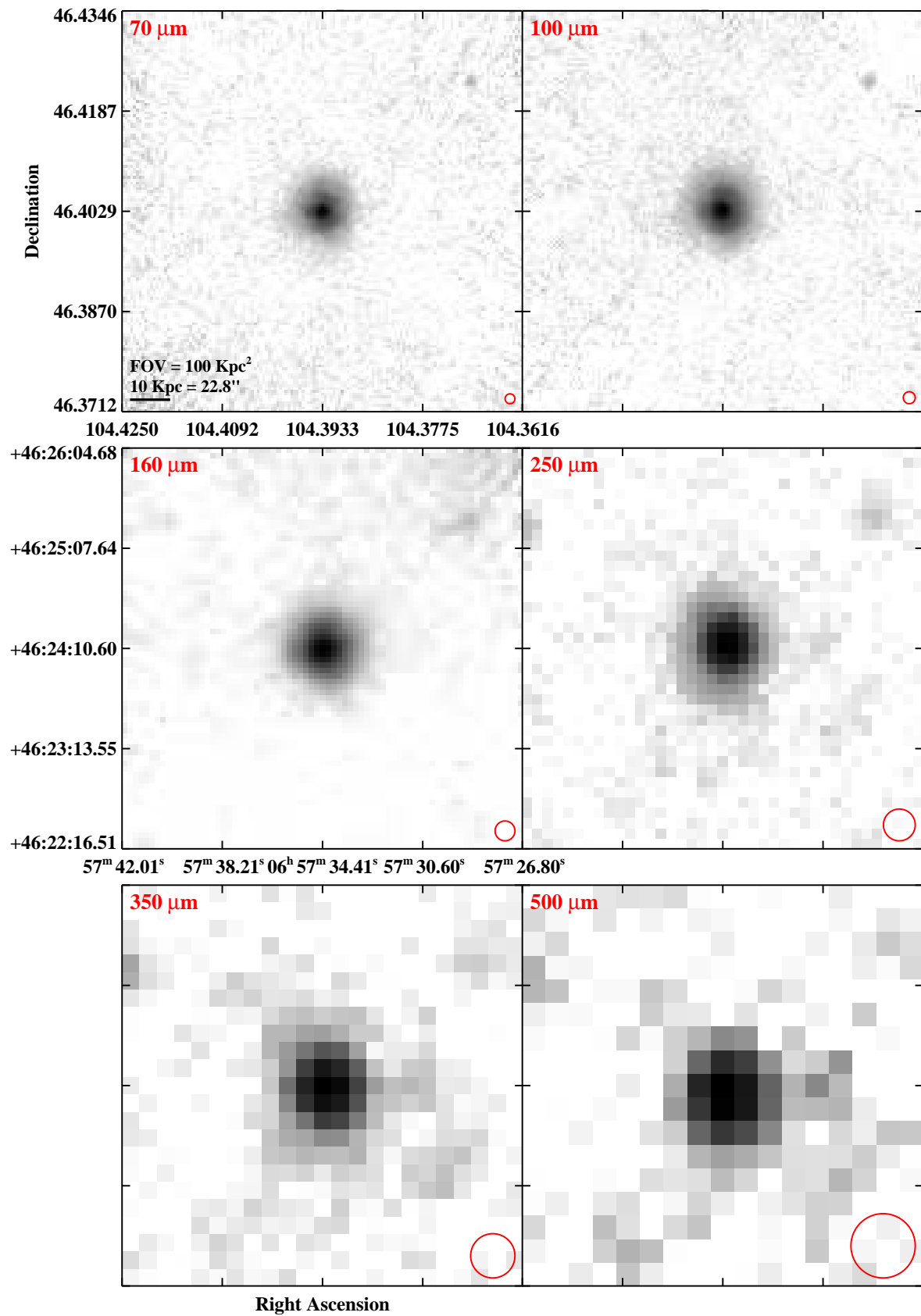


Fig. 3.— Continued (page 66 of 209).

IRAS F06592–6313

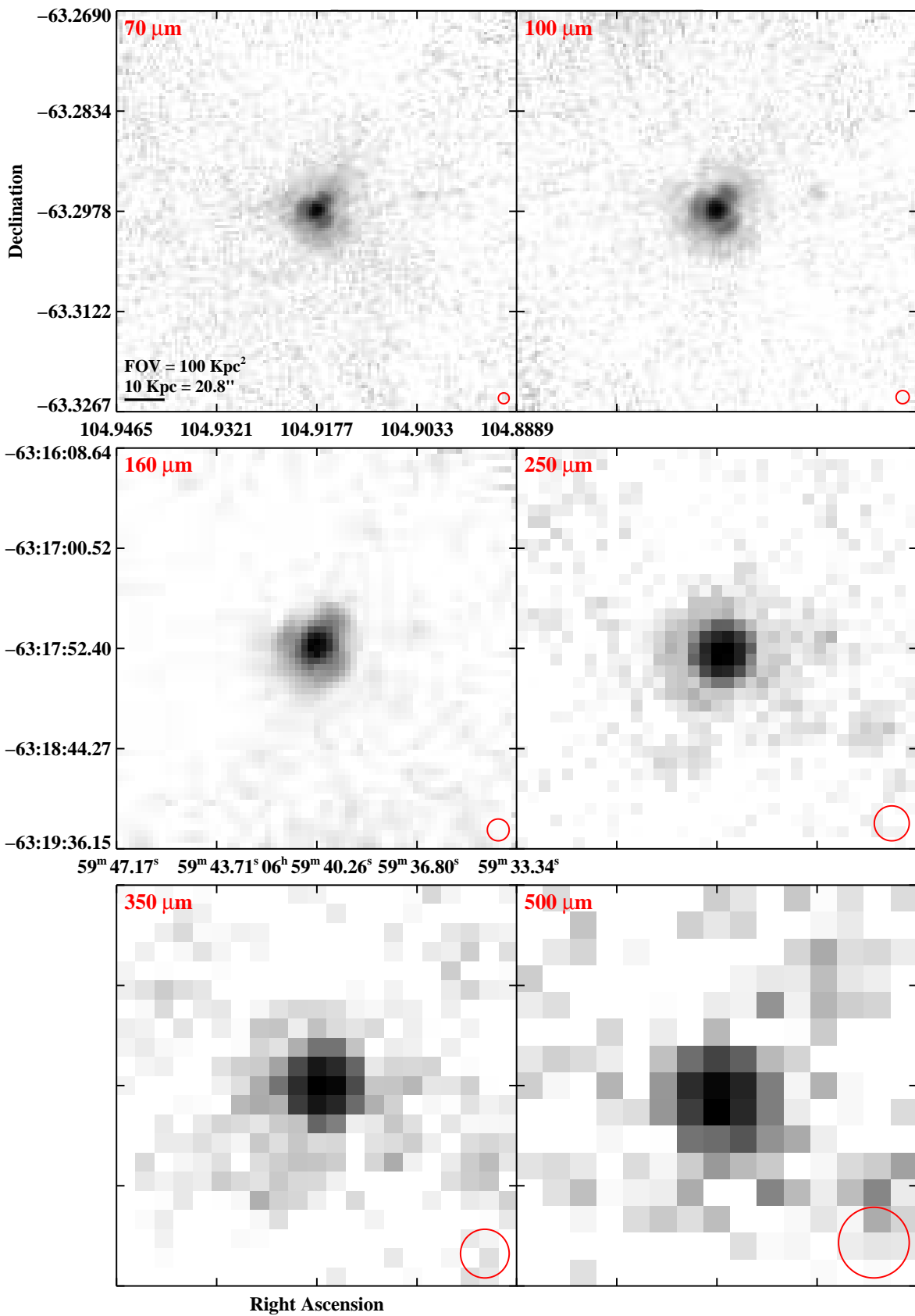


Fig. 3.— Continued (page 67 of 209).

IRAS F07027–6011 (AM 0702–601)

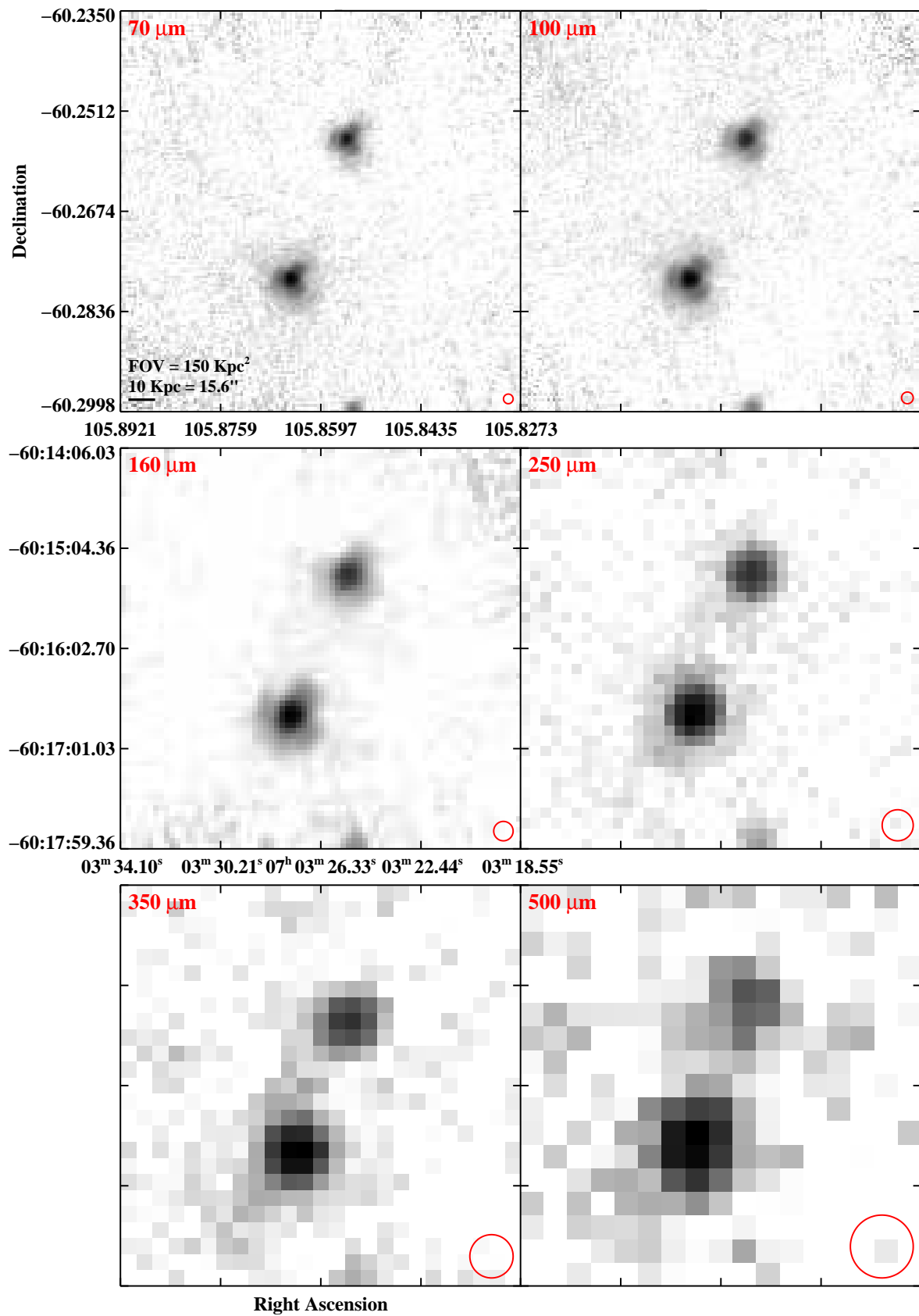


Fig. 3.— Continued (page 68 of 209).

IRAS 07063+2043 (NGC 2342)

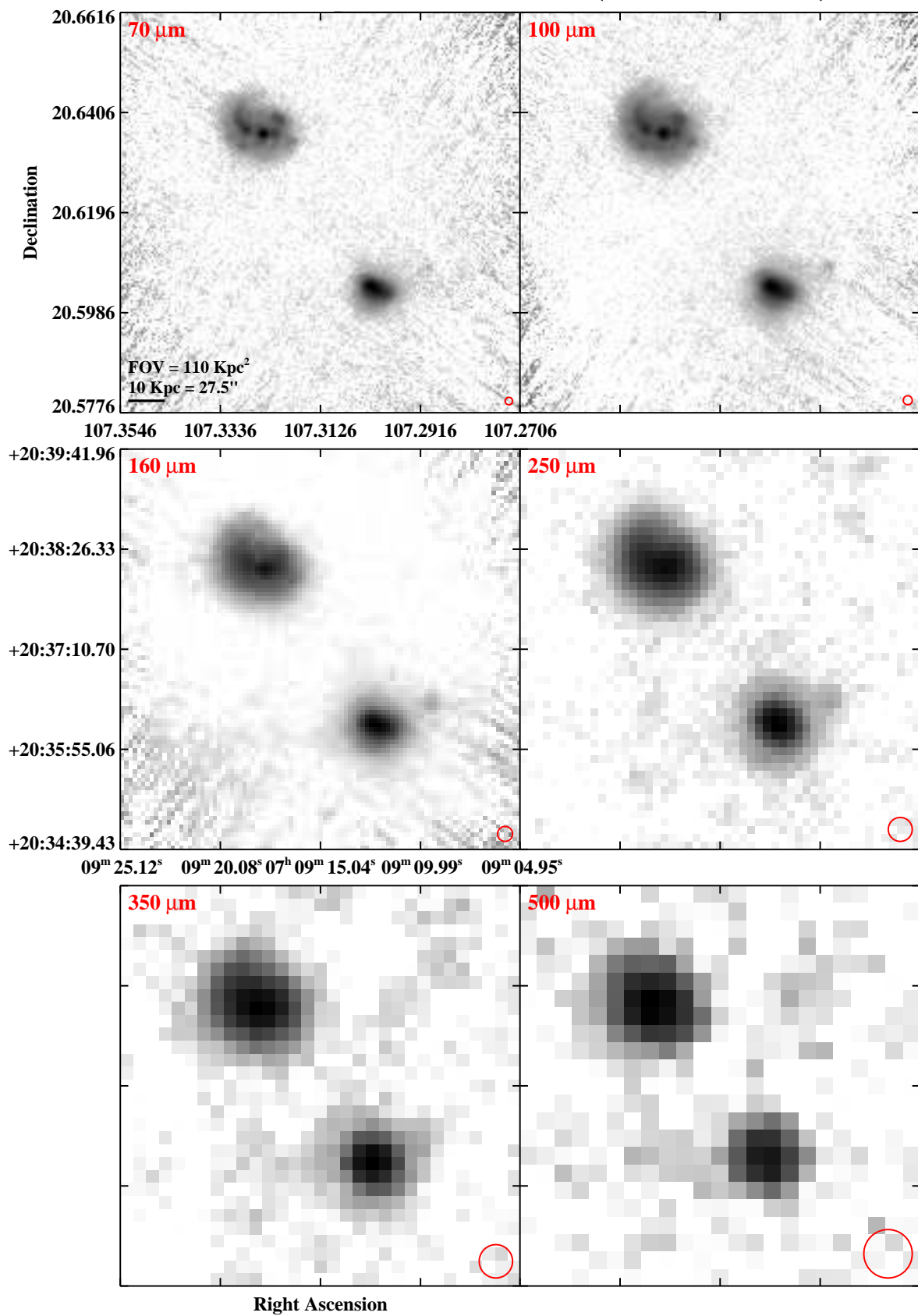


Fig. 3.— Continued (page 69 of 209).

IRAS F07160–6215 (NGC 2369)

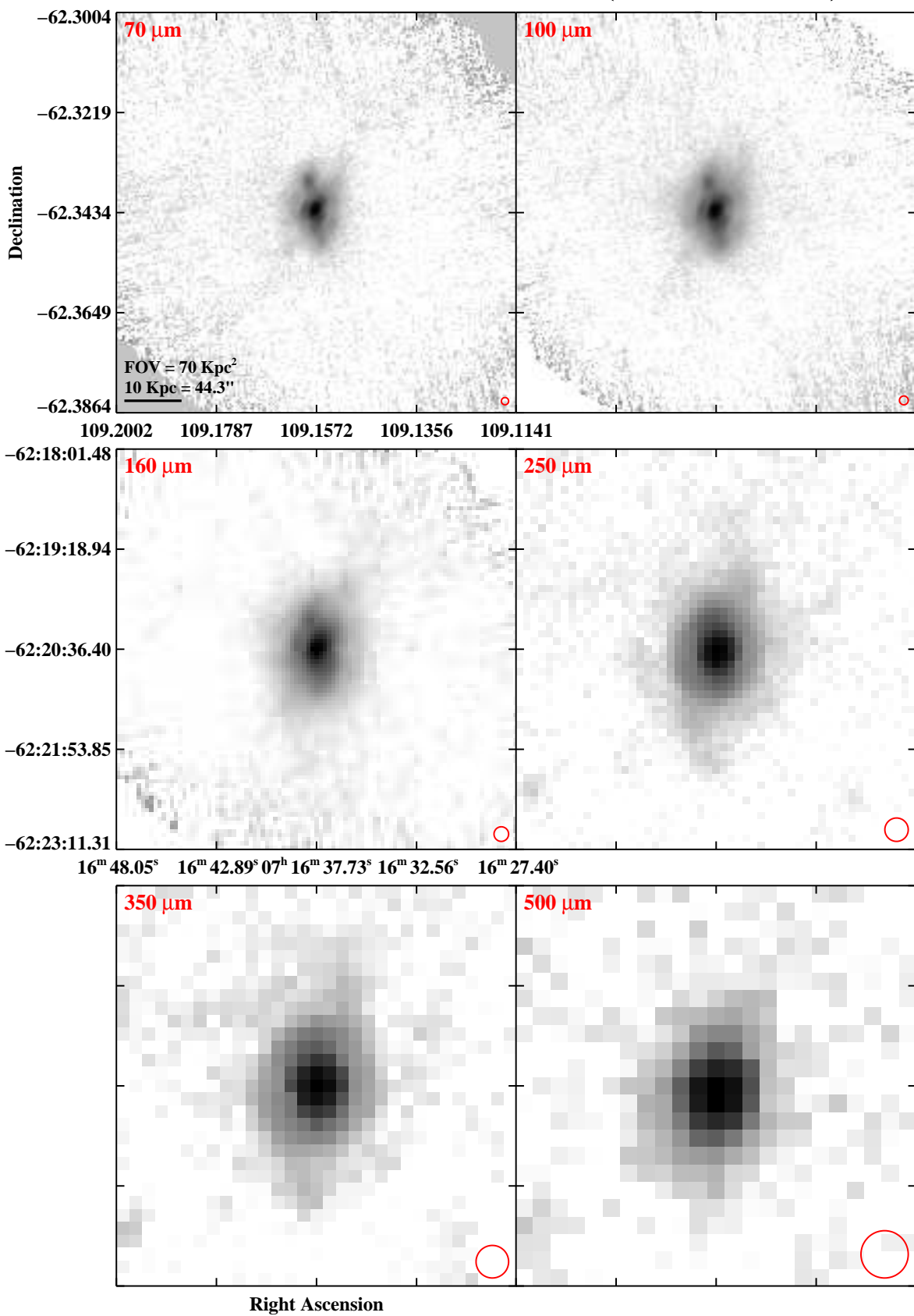


Fig. 3.— Continued (page 70 of 209).

IRAS 07251–0248

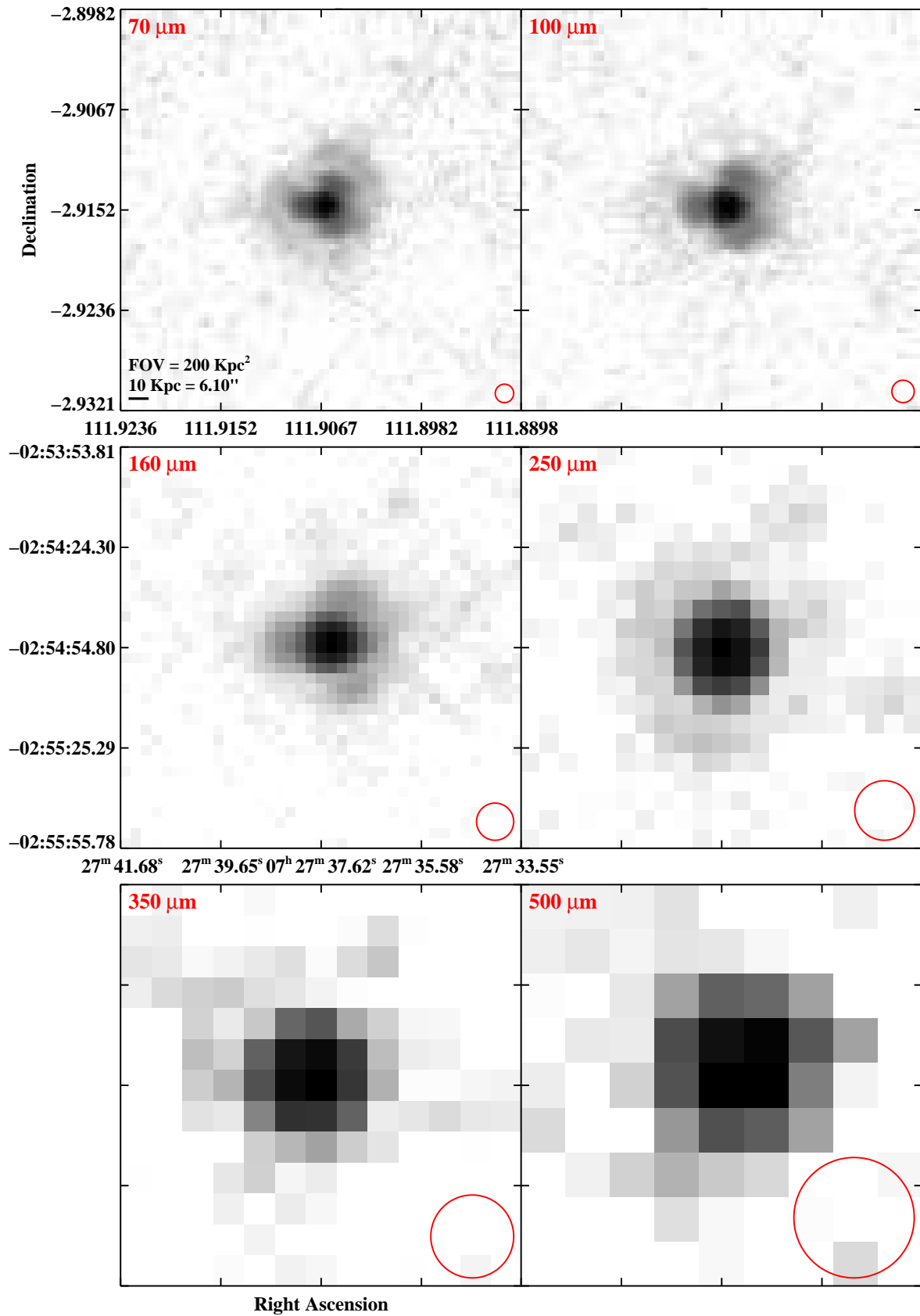


Fig. 3.— Continued (page 71 of 209).

IRAS F07256+3355 (NGC 2388)

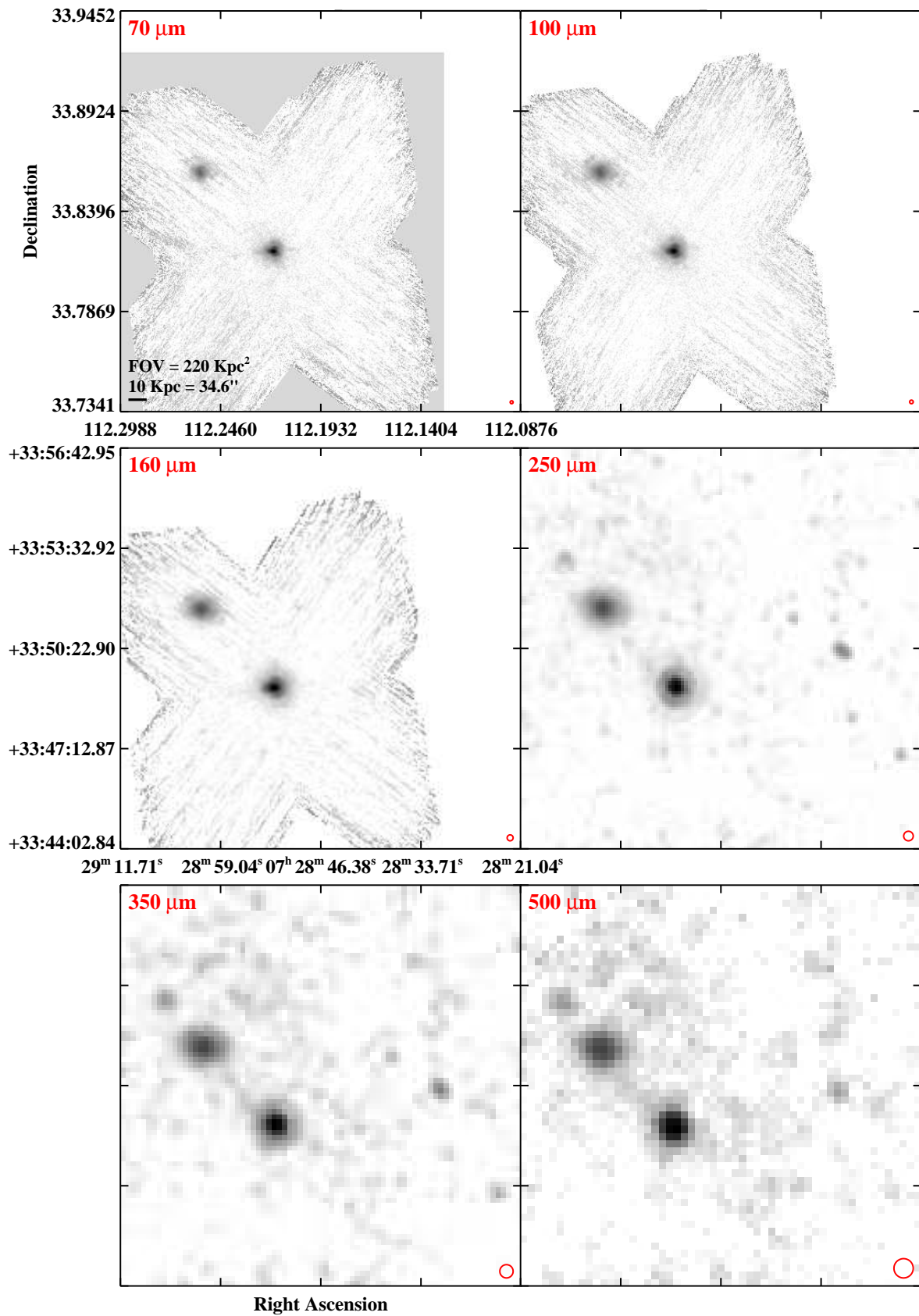


Fig. 3.— Continued (page 72 of 209).

IRAS F07329+1149 (MCG+02-20-003)

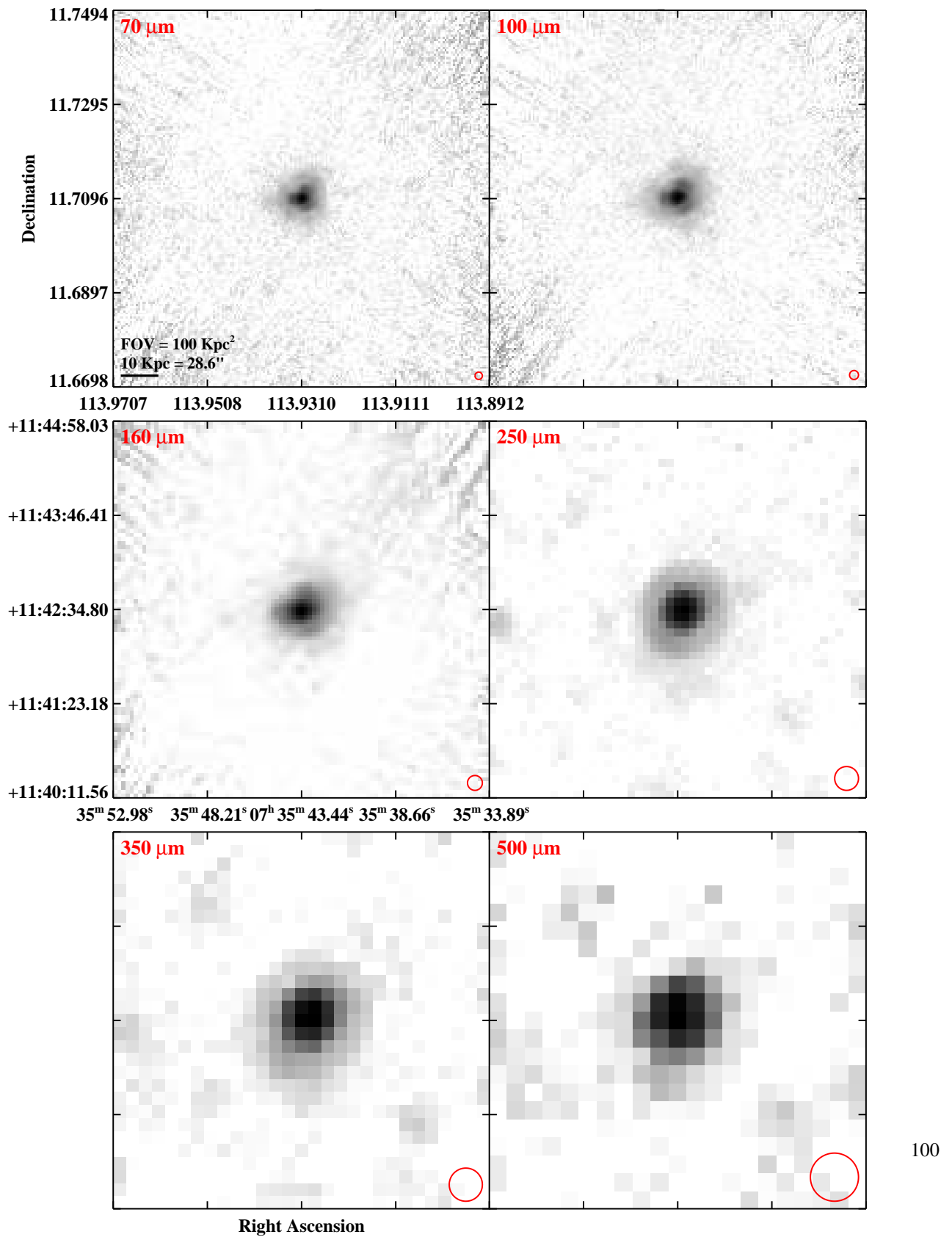


Fig. 3.— Continued (page 73 of 209).

IRAS F07329+1149 (NGC 2416)

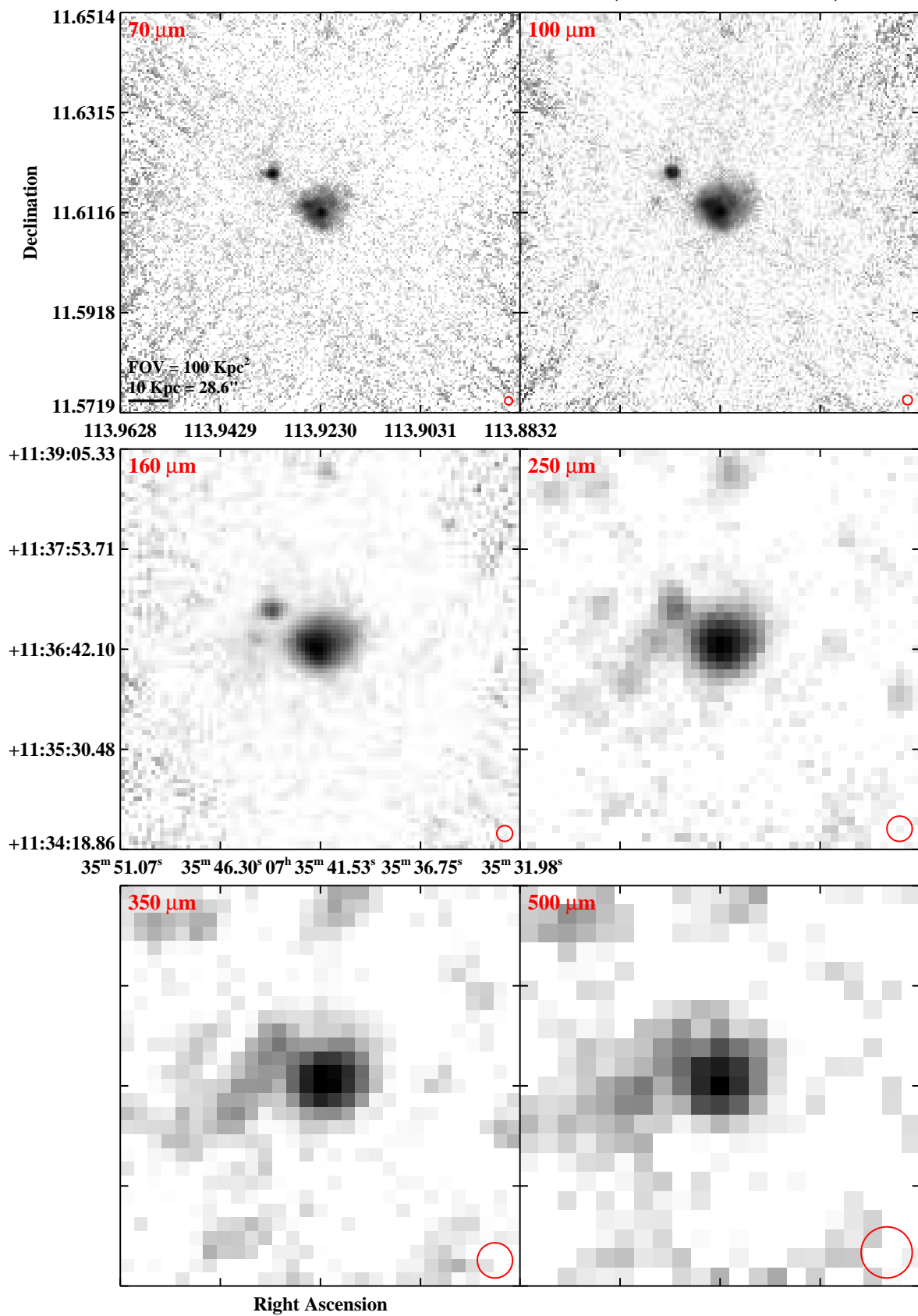


Fig. 3.— Continued (page 74 of 209).

IRAS 08355–4944

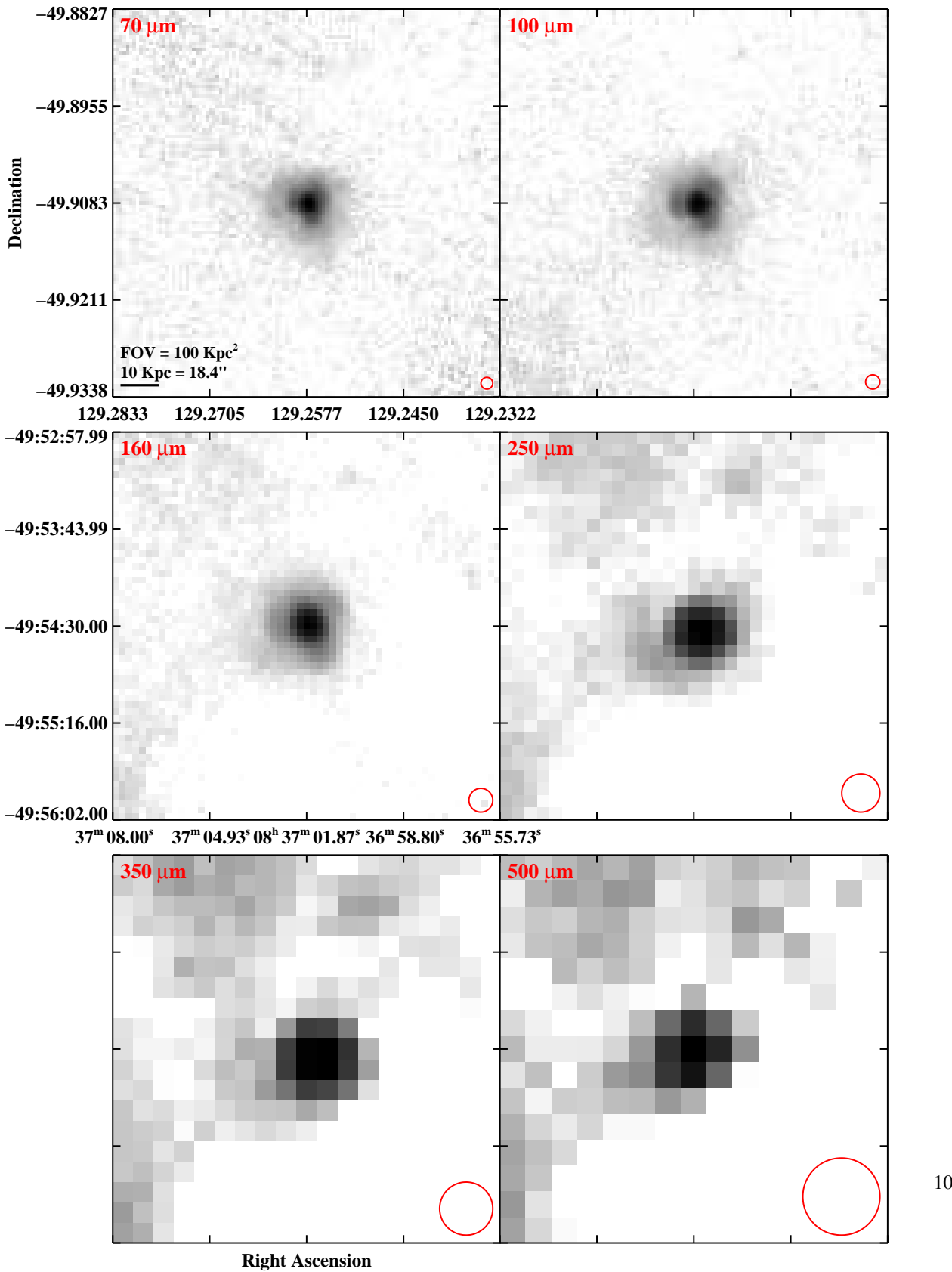


Fig. 3.— Continued (page 75 of 209).

IRAS F08339+6517

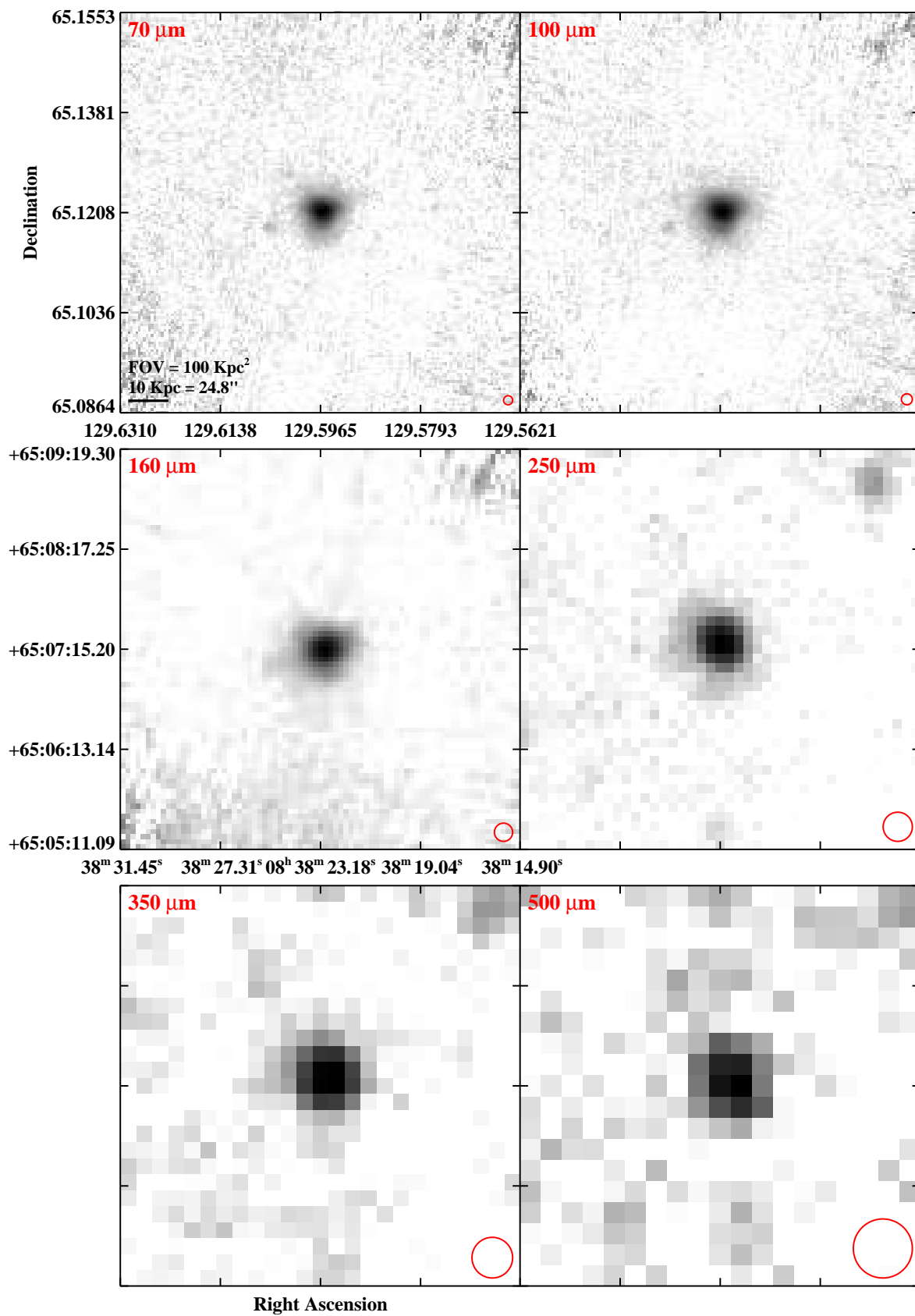


Fig. 3.— Continued (page 76 of 209).

IRAS F08354+2555 (NGC 2623)

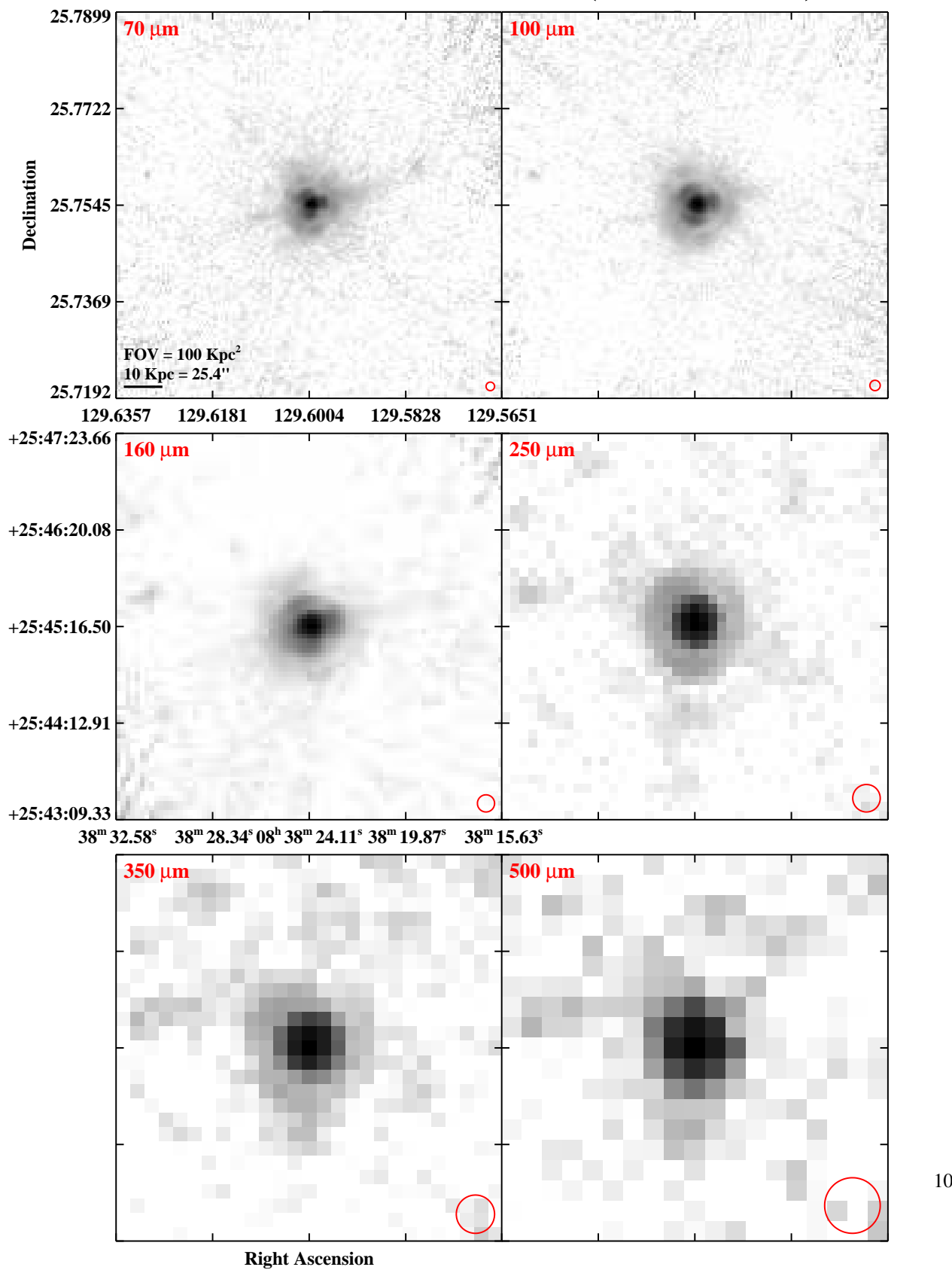


Fig. 3.— Continued (page 77 of 209).

IRAS 08424–3130 (ESO 432–IG006)

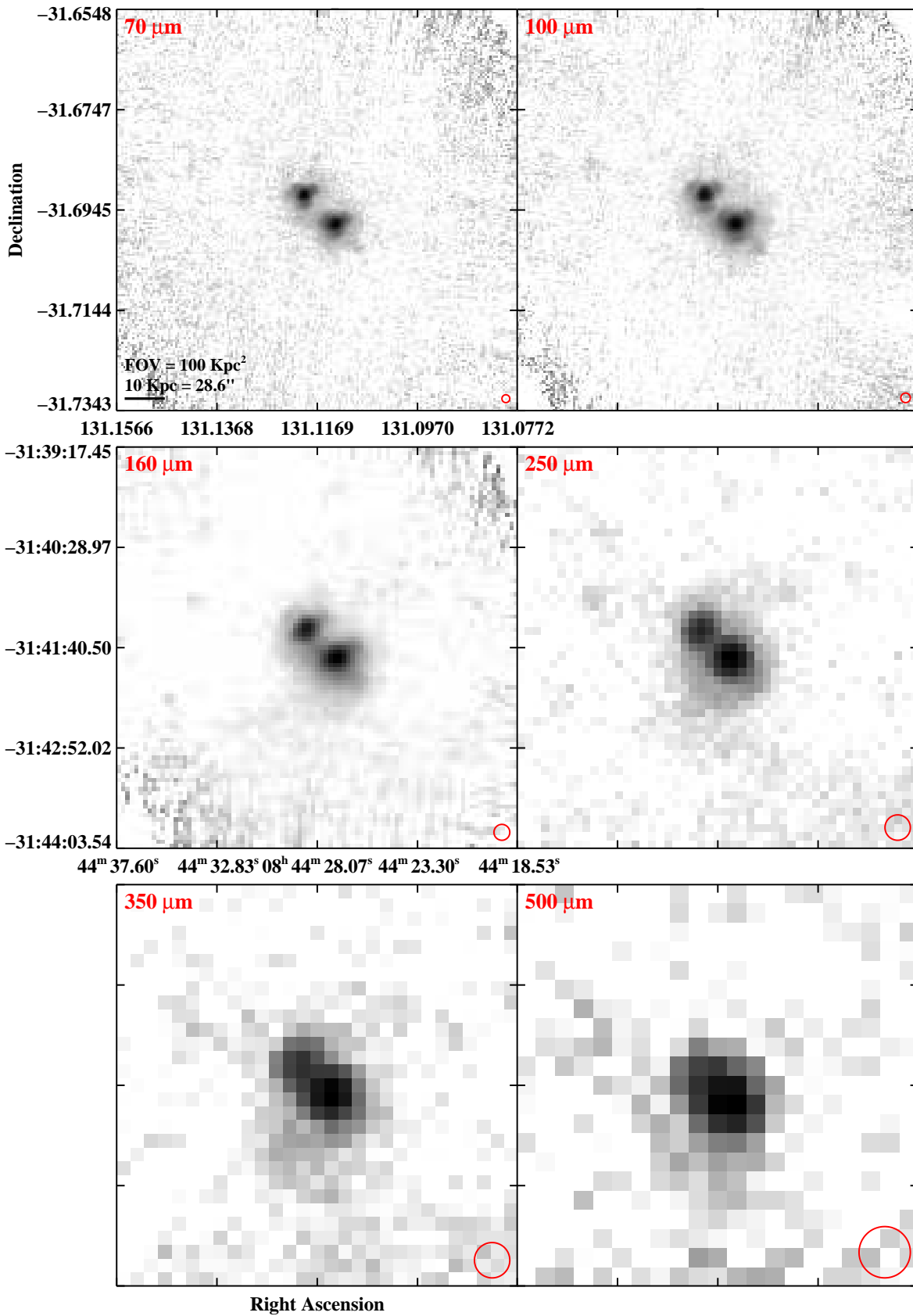


Fig. 3.— Continued (page 78 of 209).

IRAS F08520–6850 (ESO 060–IG016)

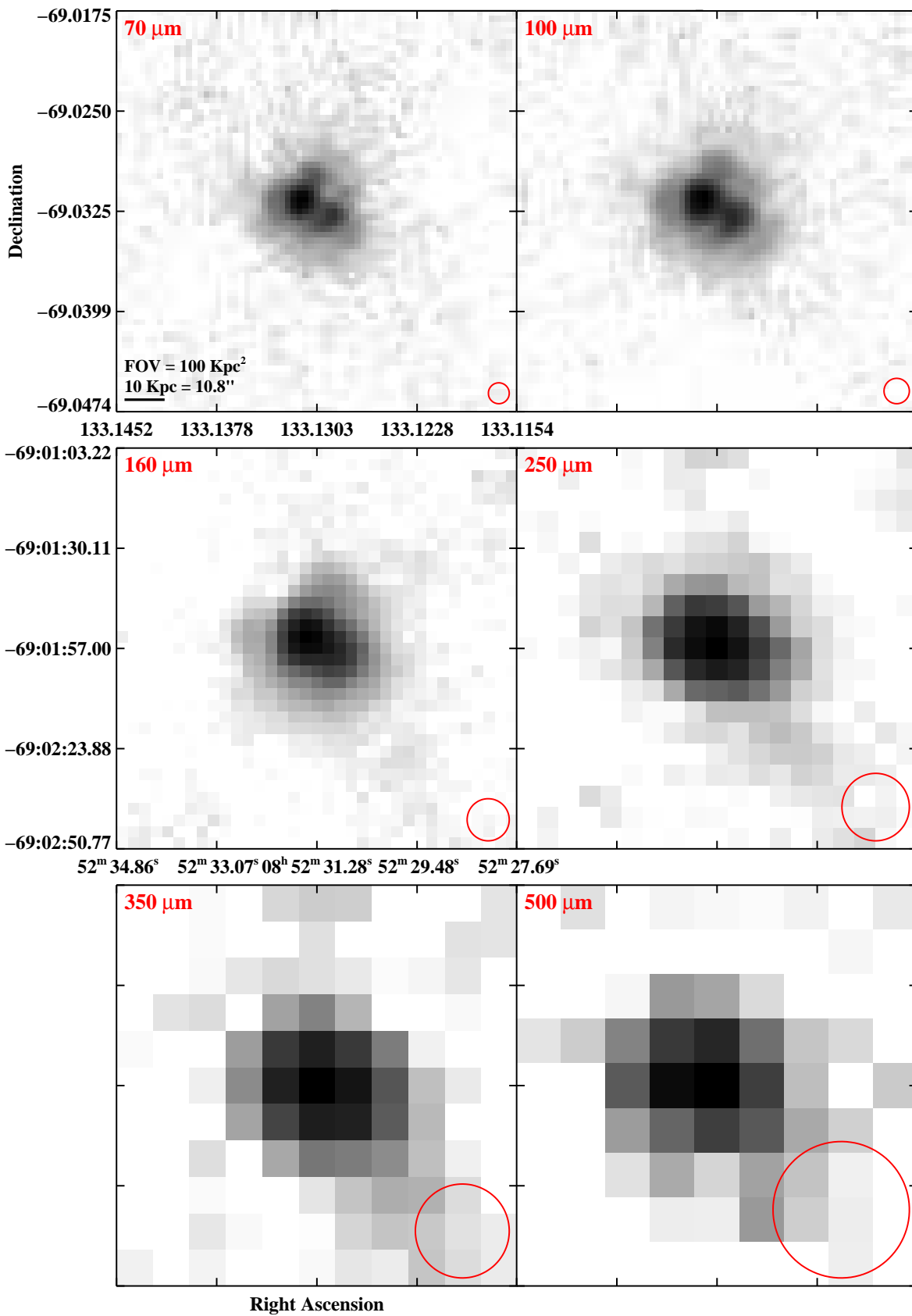


Fig. 3.— Continued (page 79 of 209).

IRAS F08572+3915

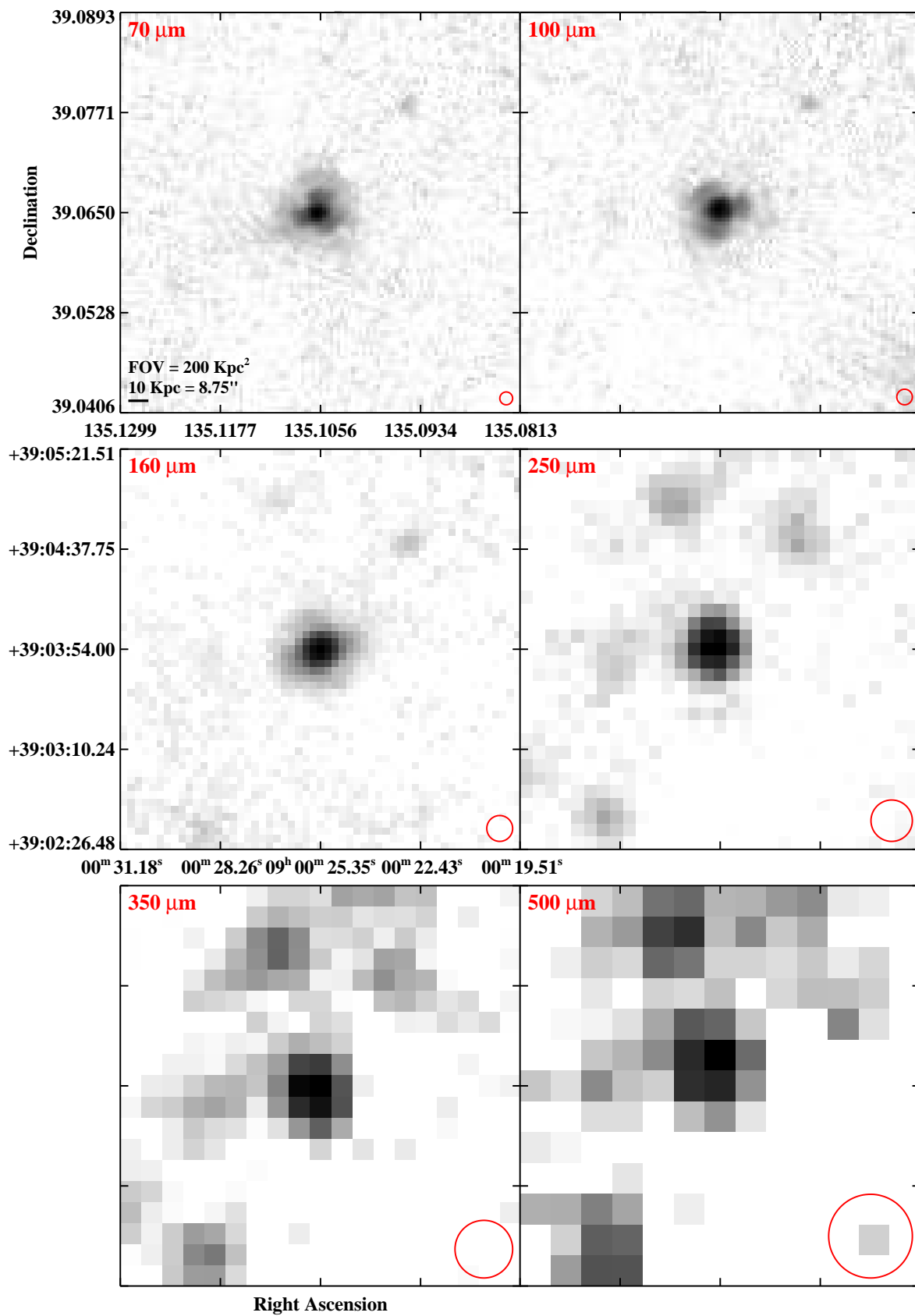


Fig. 3.— Continued (page 80 of 209).

IRAS 09022–3615

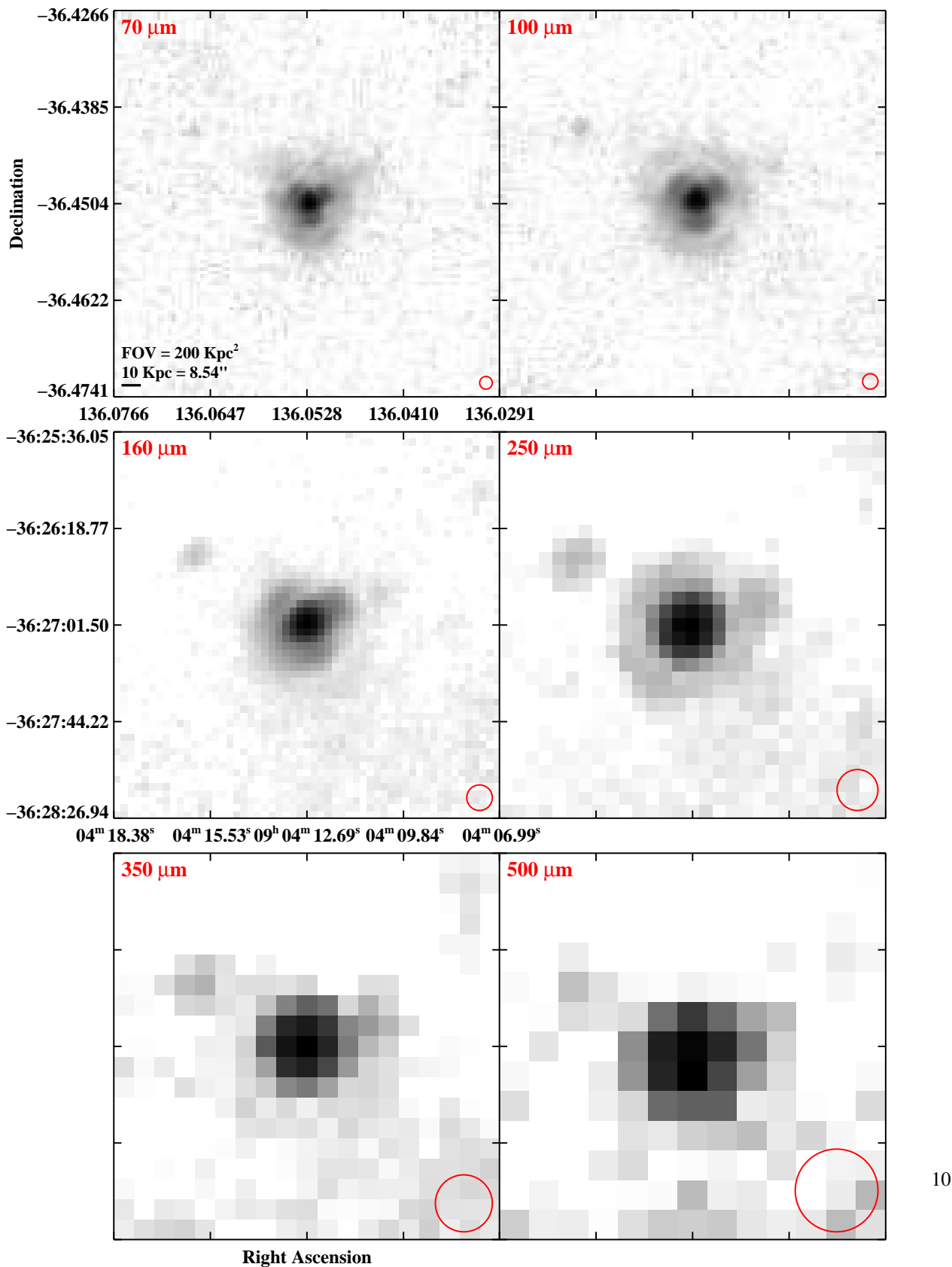


Fig. 3.— Continued (page 81 of 209).

IRAS F09111–1007

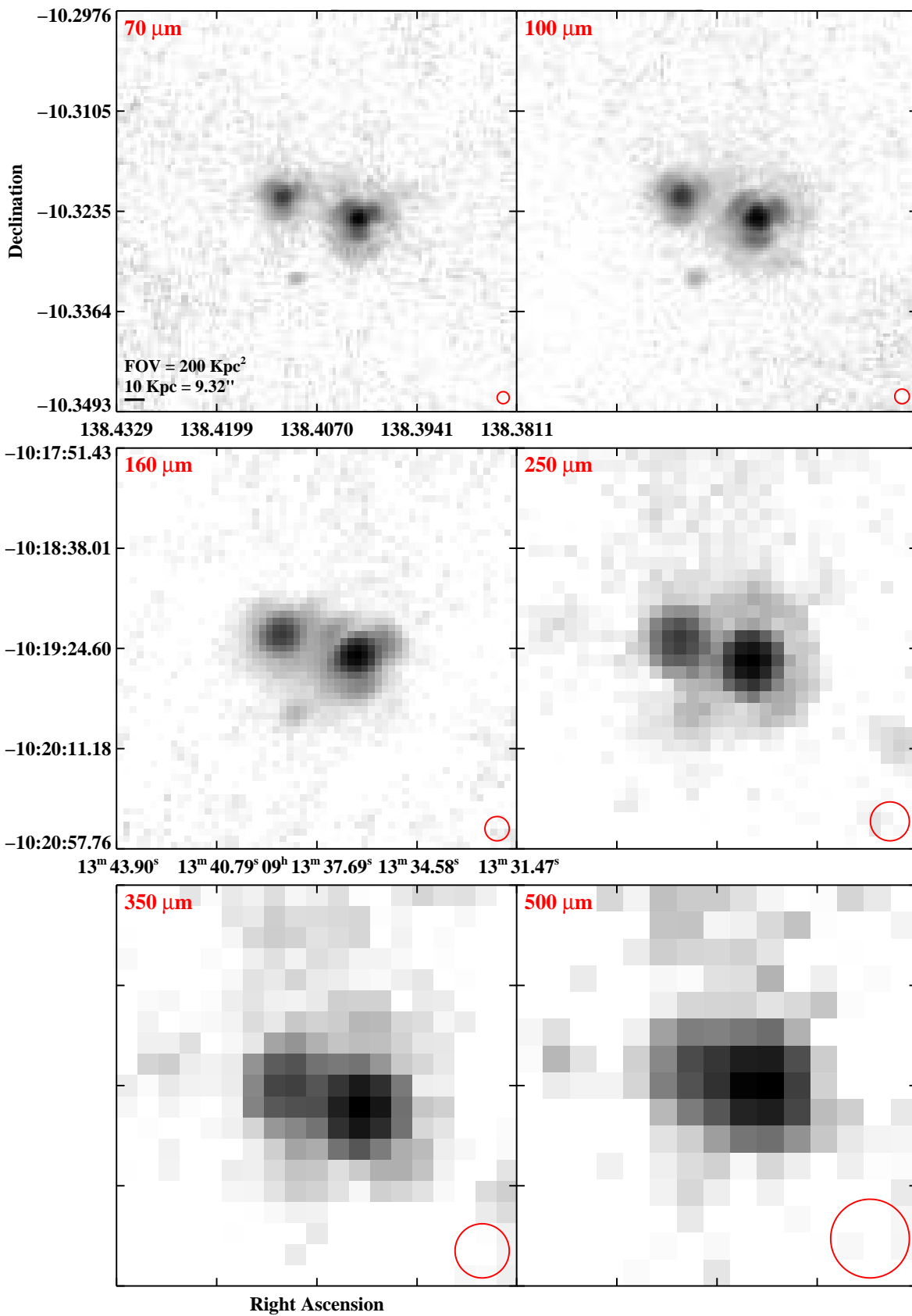


Fig. 3.— Continued (page 82 of 209).

IRAS F09126+4432 (UGC 04881)

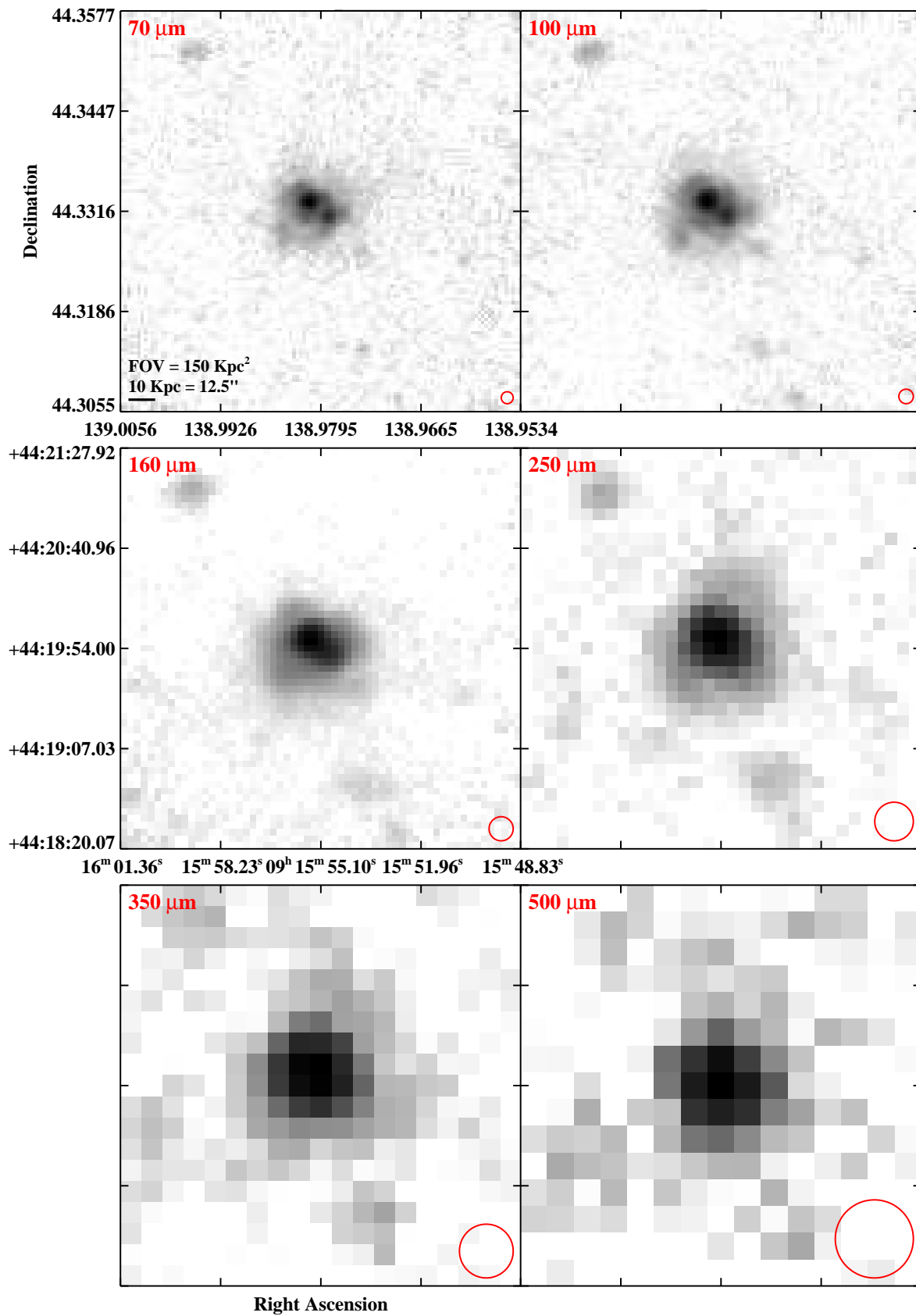


Fig. 3.— Continued (page 83 of 209).

IRAS F09320+6134 (UGC 05101)

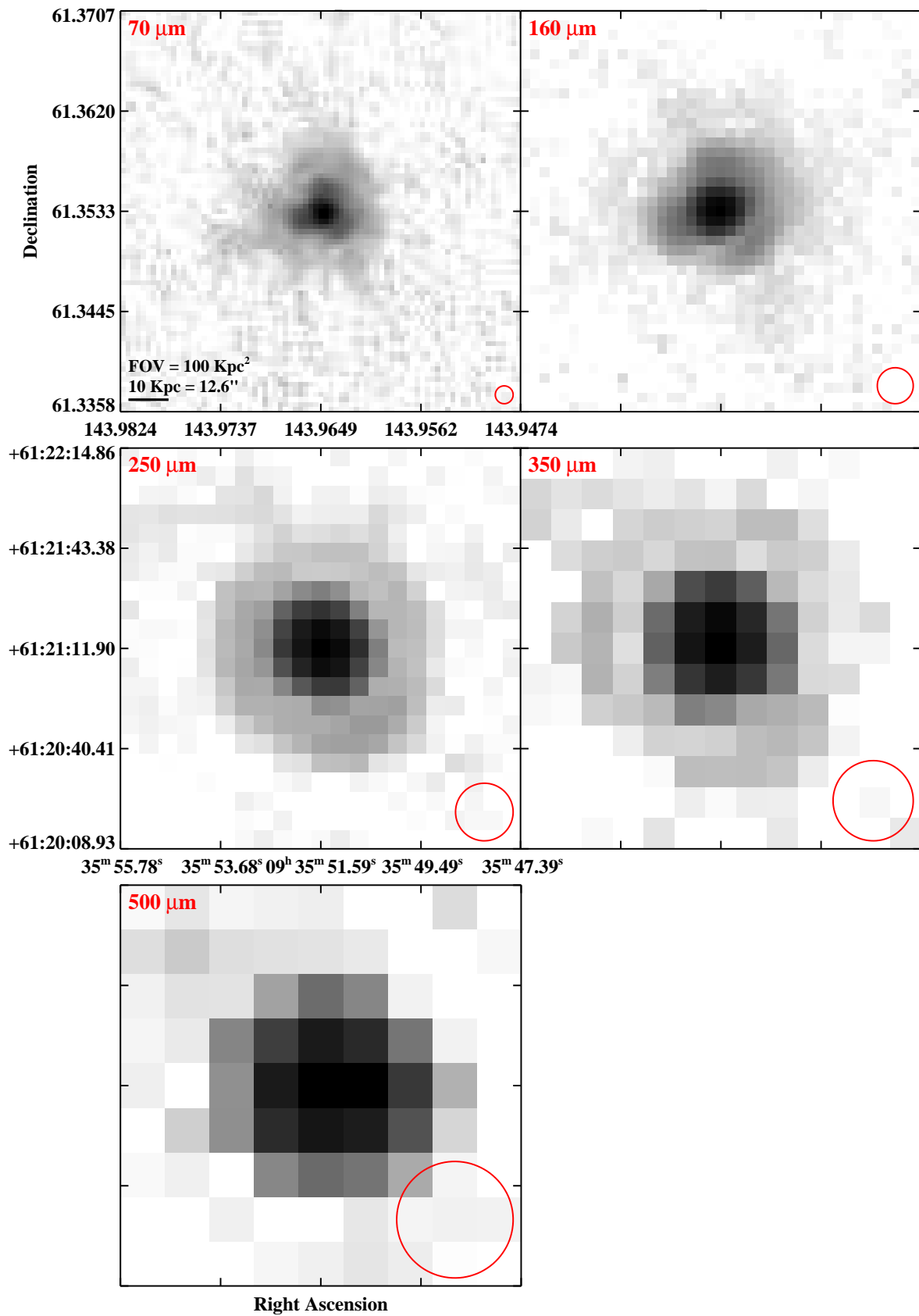


Fig. 3.— Continued (page 84 of 209).

IRAS F09333+4841 (MCG+08-18-013)

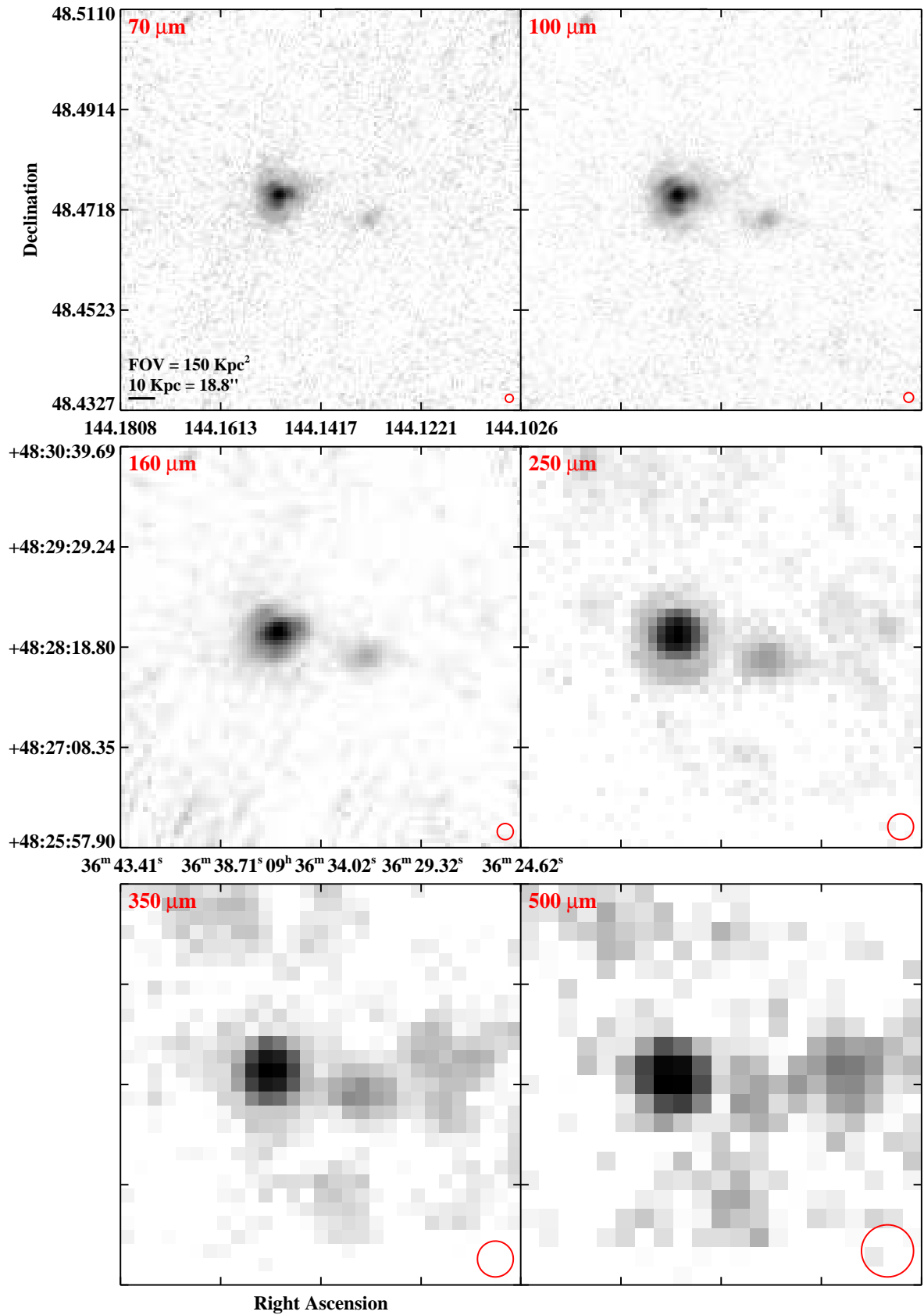


Fig. 3.— Continued (page 85 of 209).

IRAS F09437+0317 (Arp 303)

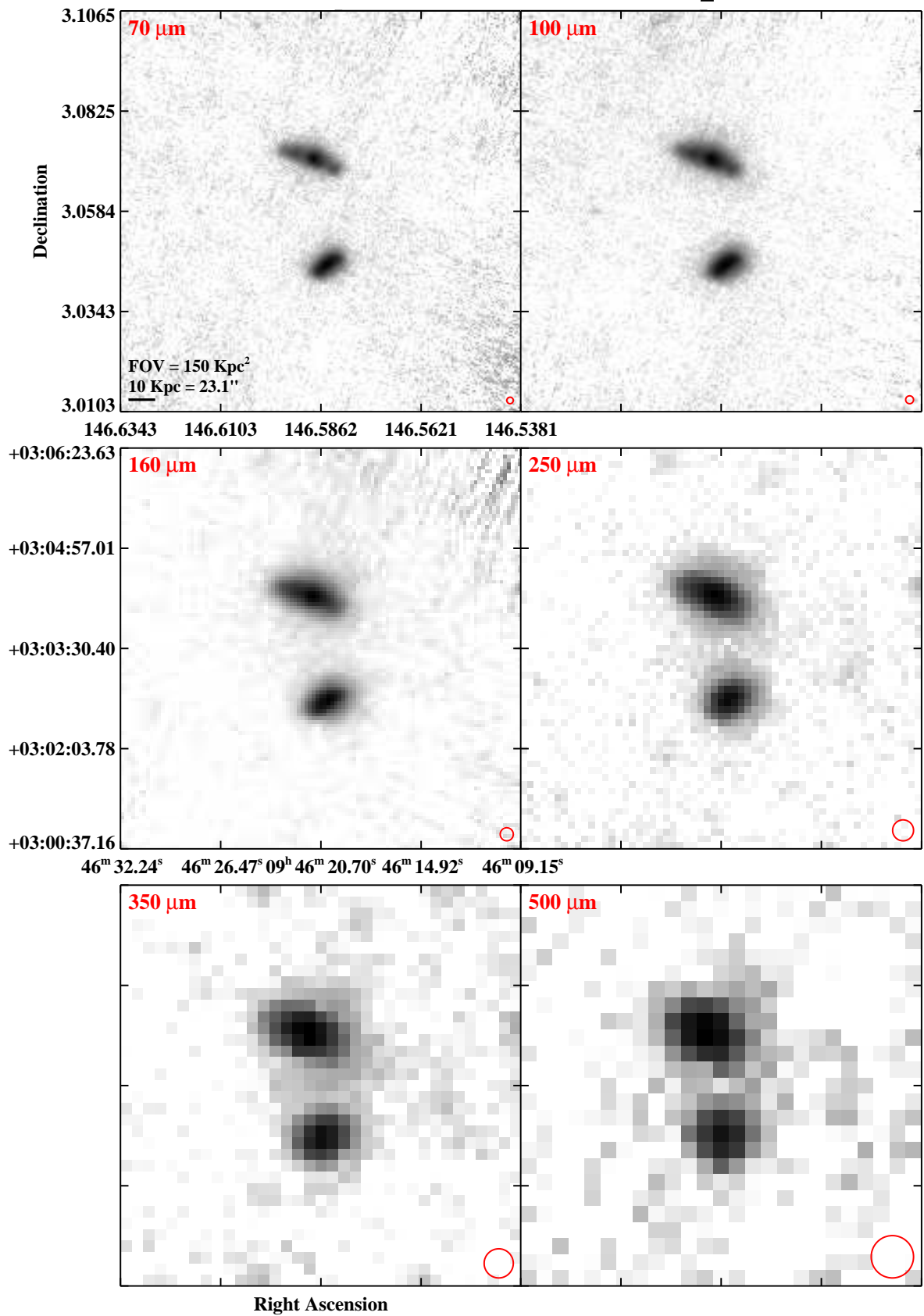


Fig. 3.— Continued (page 86 of 209).

IRAS F10015–0614 (NGC 3110)

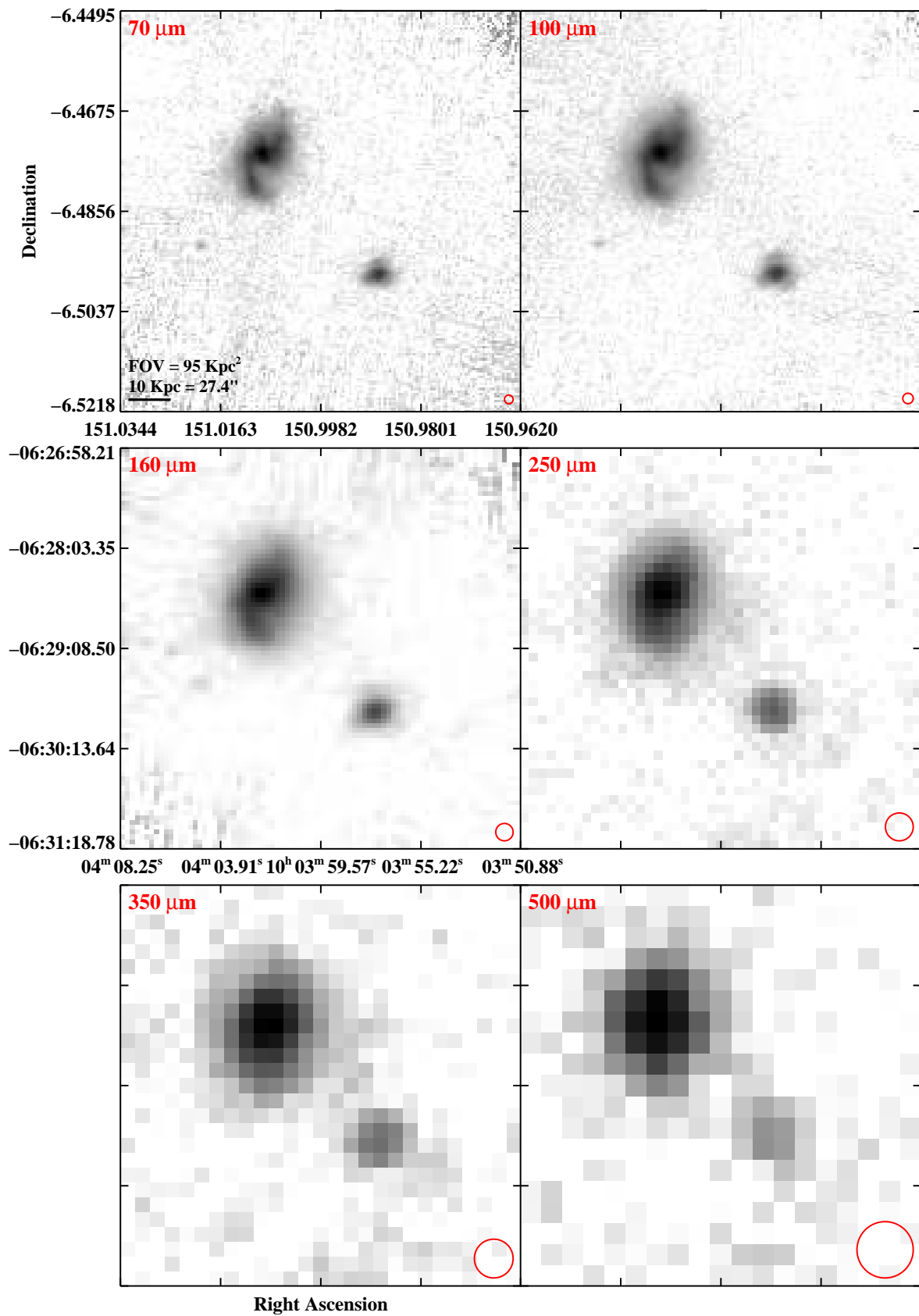


Fig. 3.— Continued (page 87 of 209).

IRAS F10038–3338 (ESO 374–IG 032)

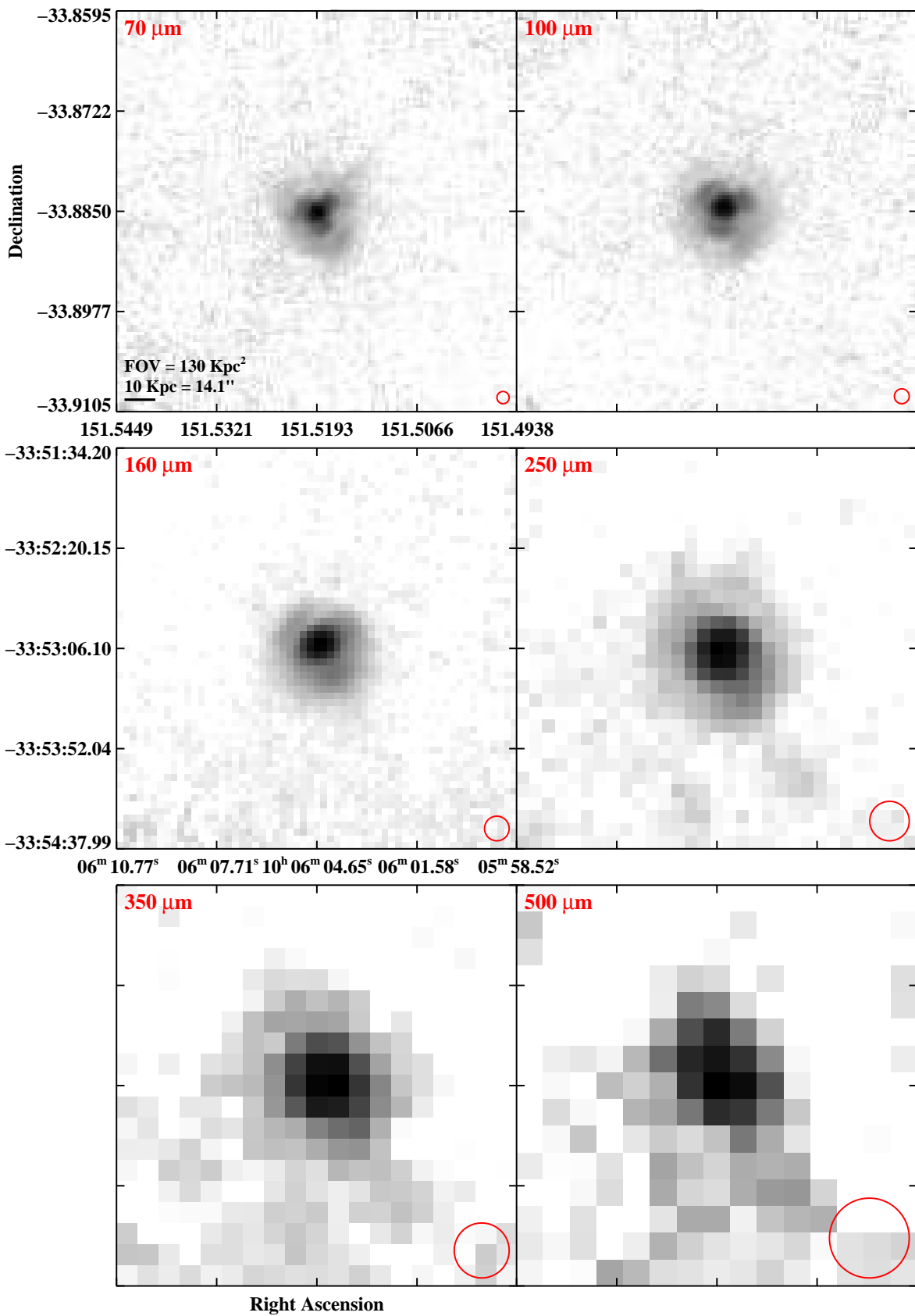


Fig. 3.— Continued (page 88 of 209).

IRAS F10173+0828

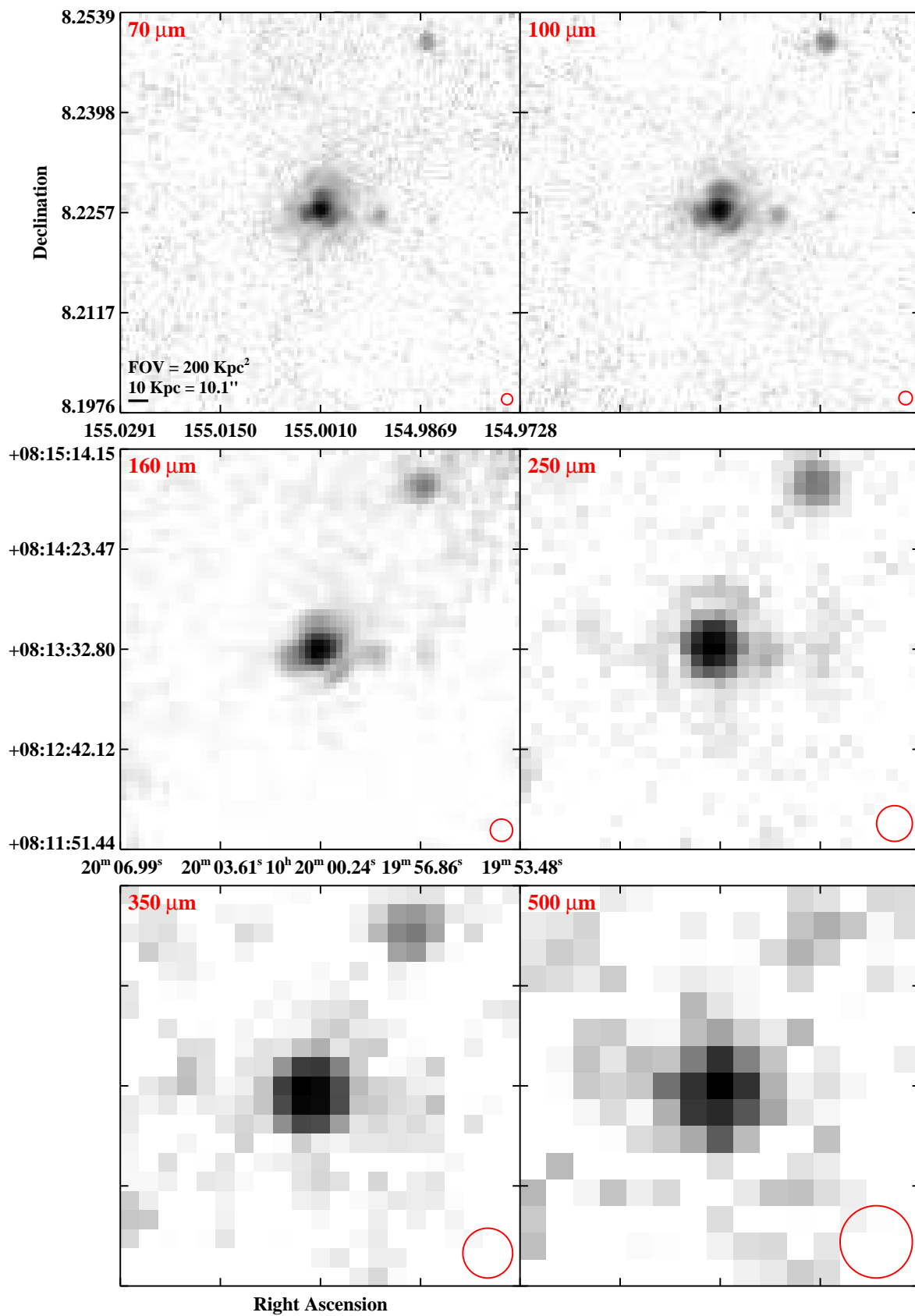


Fig. 3.— Continued (page 89 of 209).

IRAS F10196+2149 (NGC 3221)

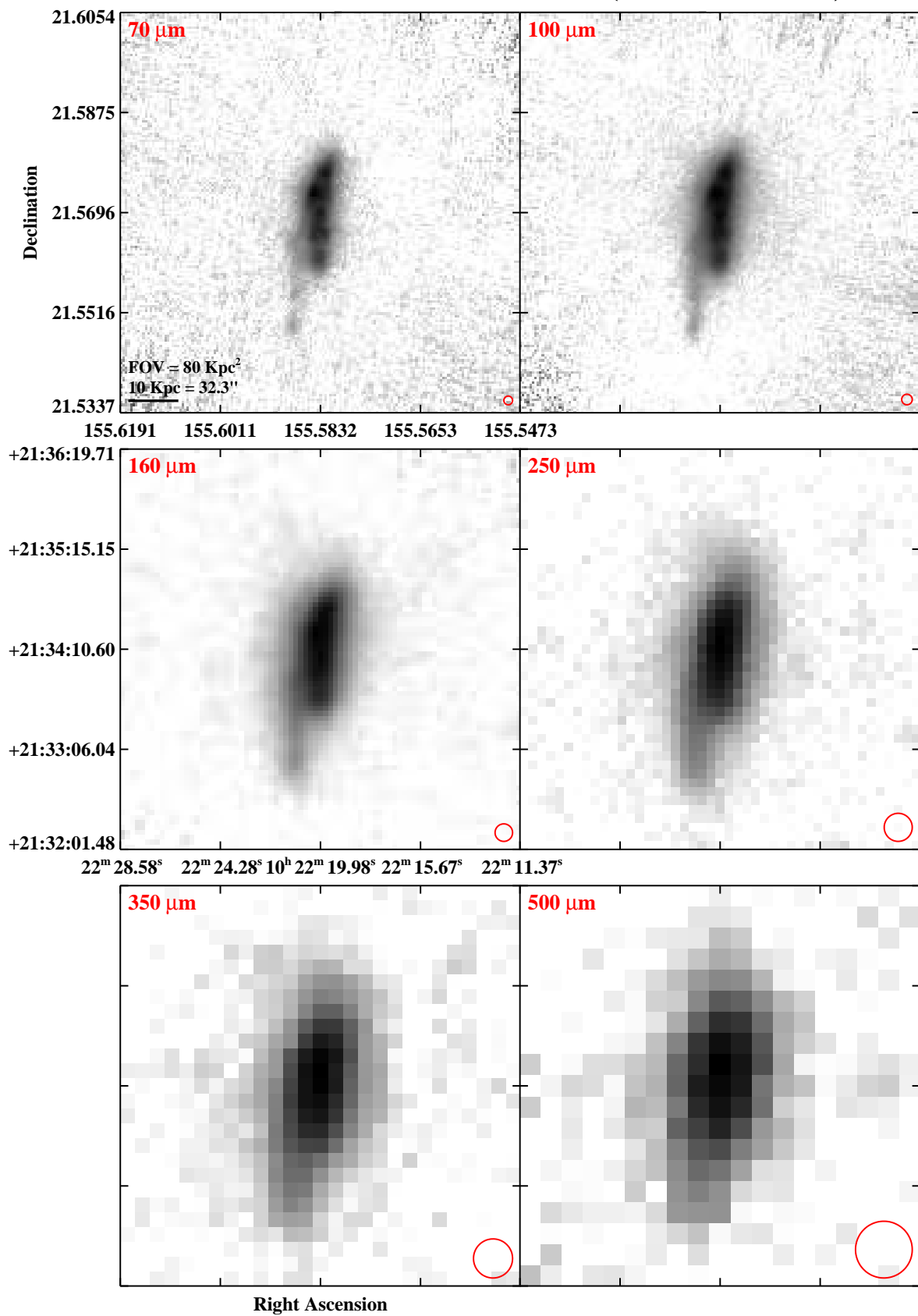


Fig. 3.— Continued (page 90 of 209).

IRAS F10257–4339 (NGC 3256)

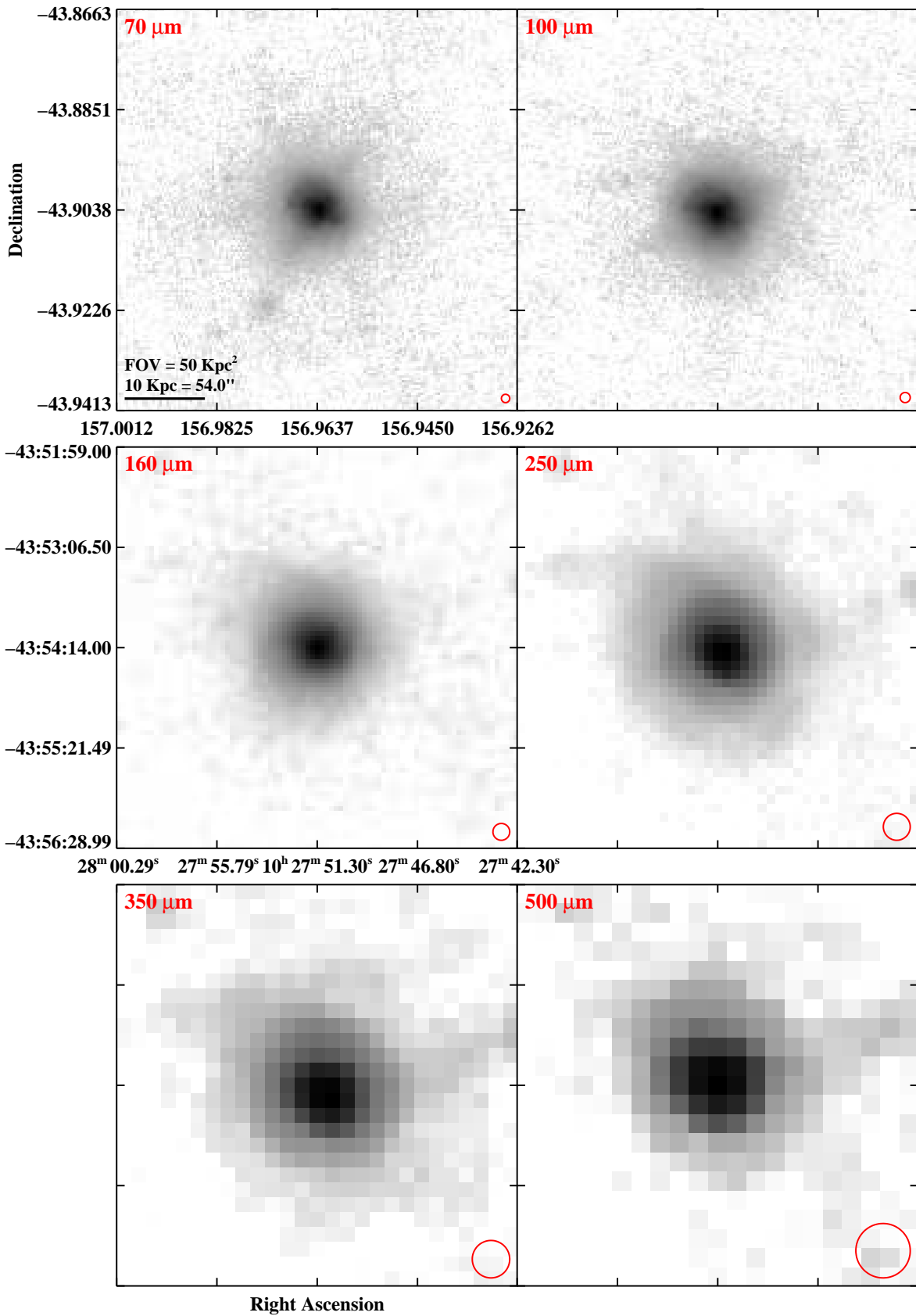


Fig. 3.— Continued (page 91 of 209).

IRAS F10409–4556 (ESO 264–G036)

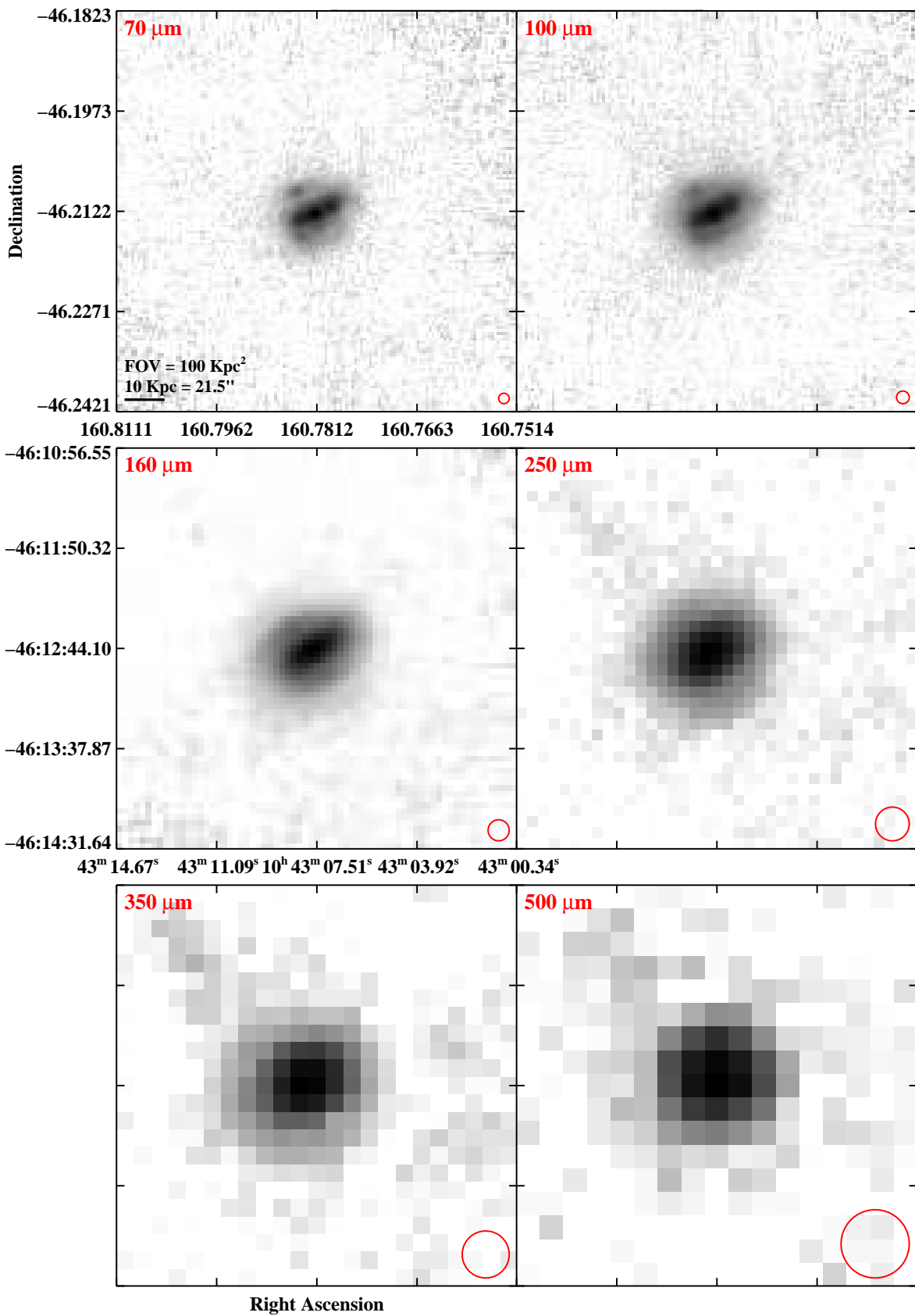


Fig. 3.— Continued (page 92 of 209).

IRAS F10567–4310 (ESO 264–G057)

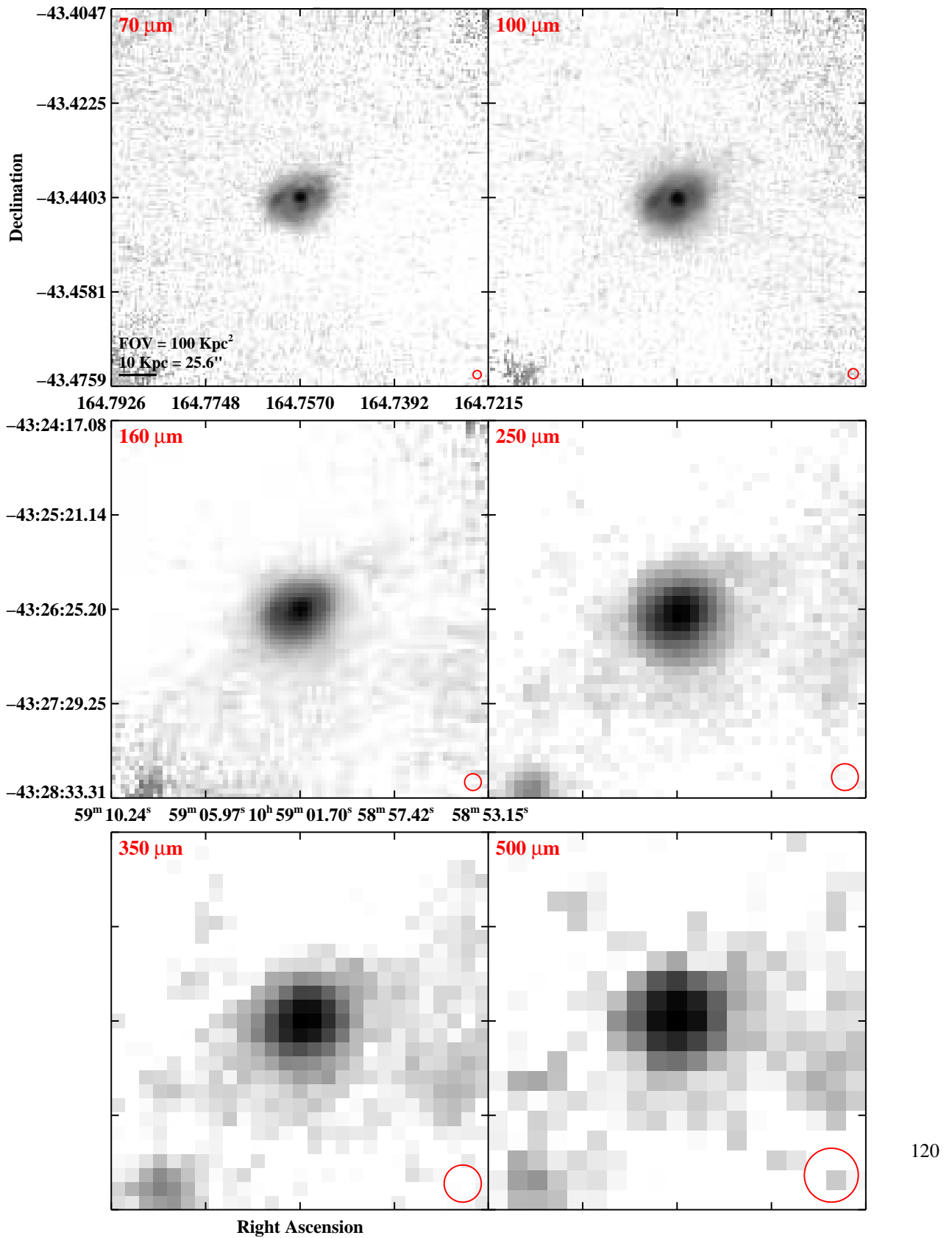


Fig. 3.— Continued (page 93 of 209).

IRAS F10565+2448

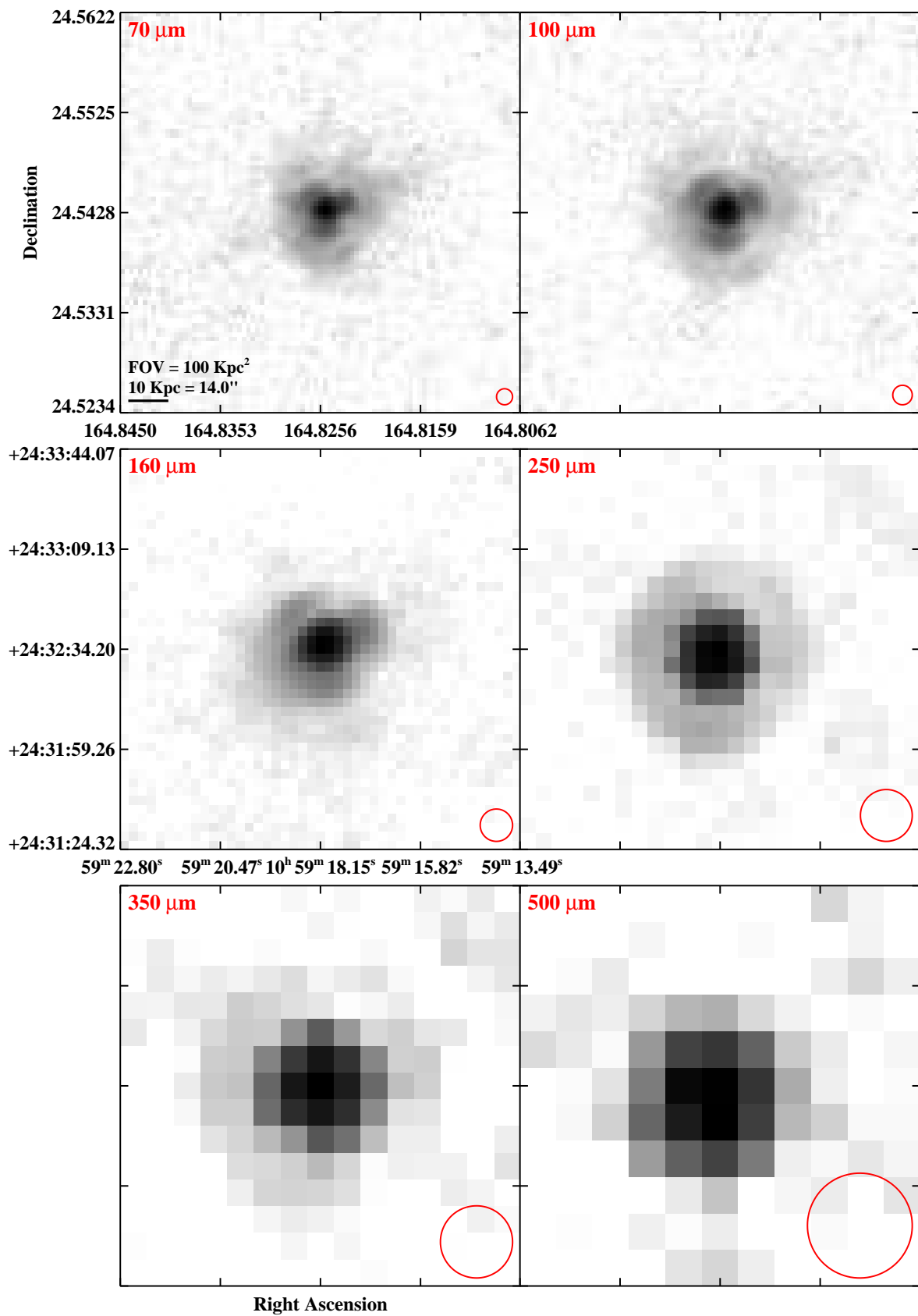


Fig. 3.— Continued (page 94 of 209).

IRAS F11011+4107 (MCG+07-23-019)

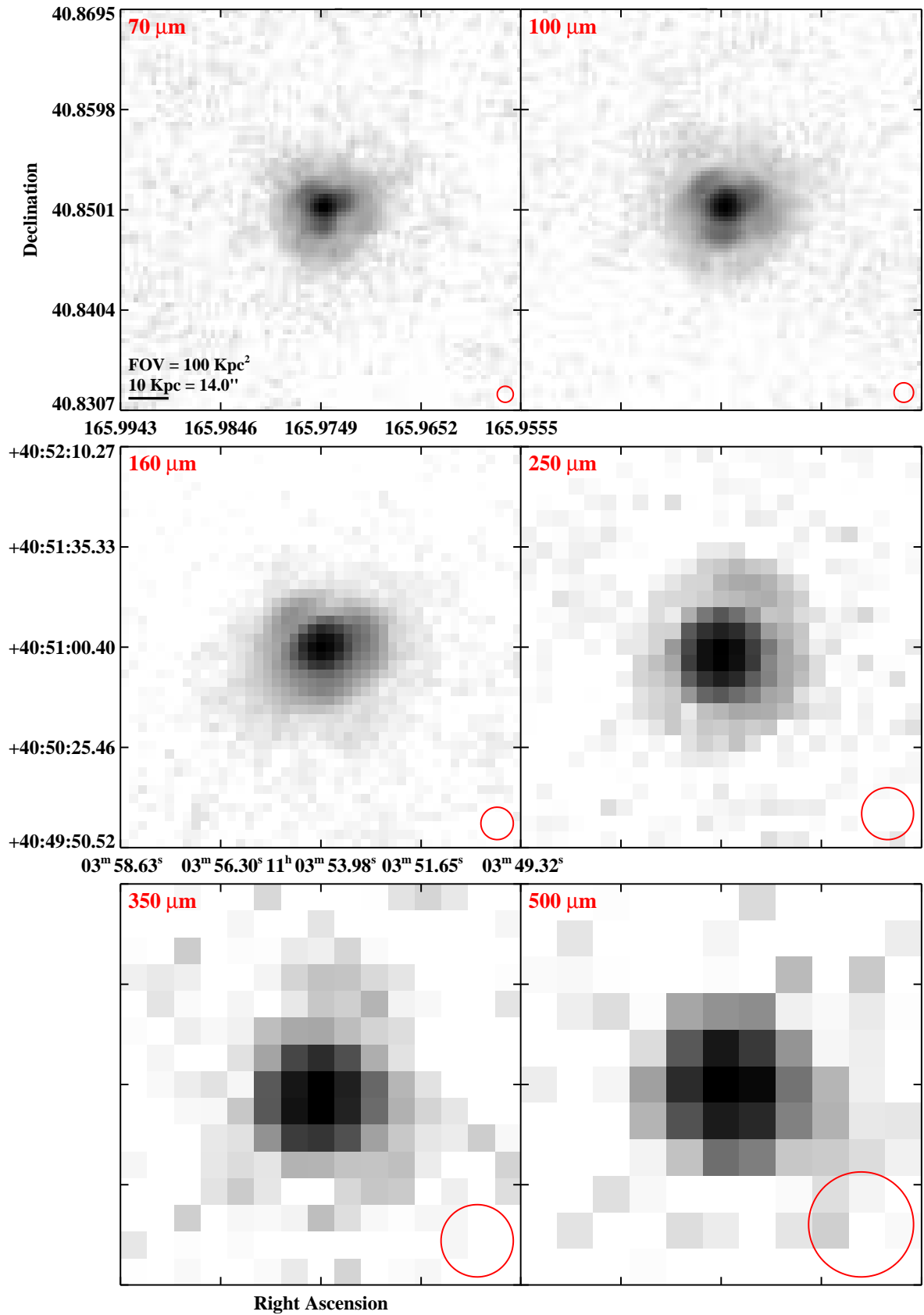


Fig. 3.— Continued (page 95 of 209).

IRAS F11186–0242 (CGCG 011–076)

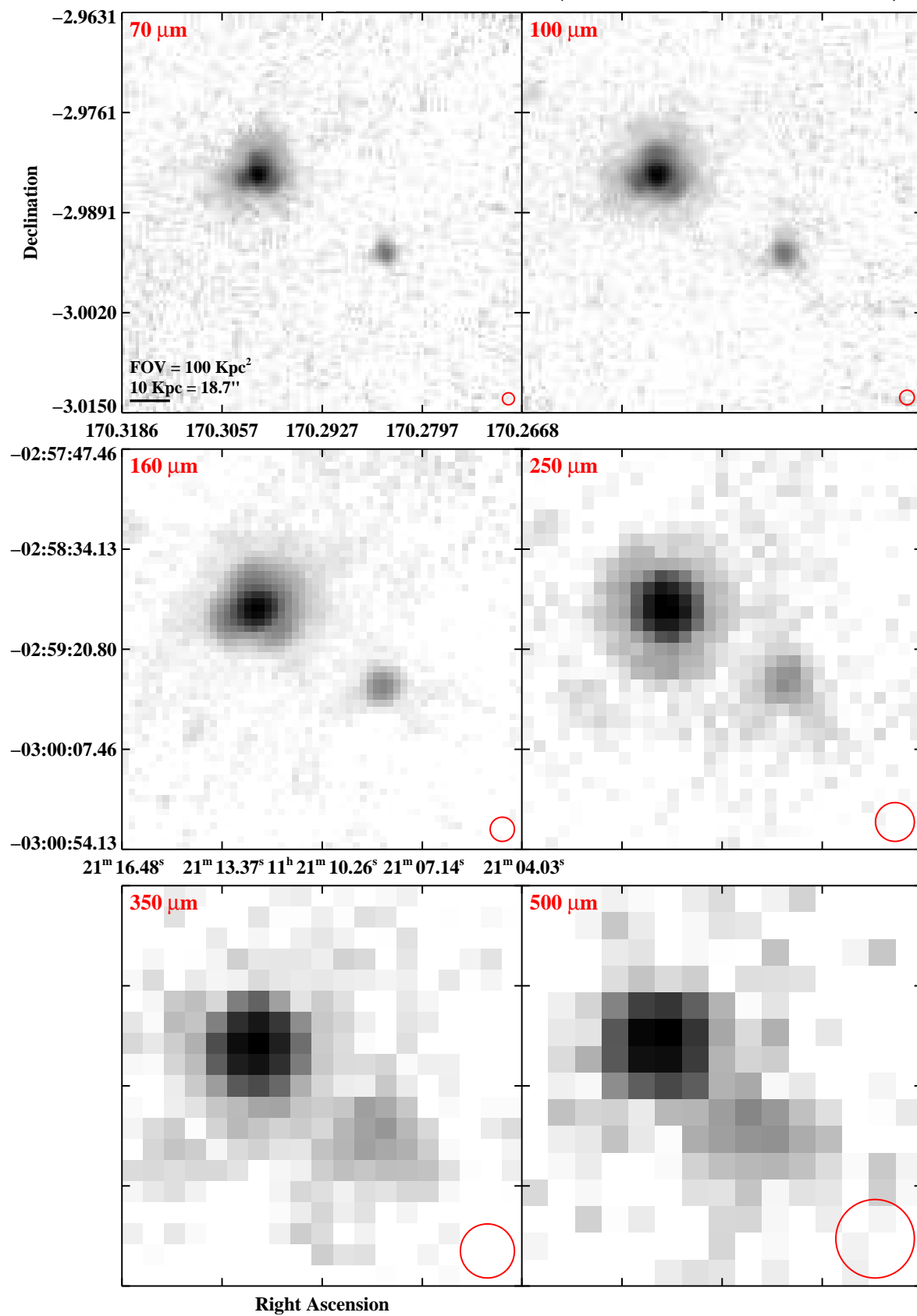


Fig. 3.— Continued (page 96 of 209).

IRAS F11231+1456 (IC 2810)

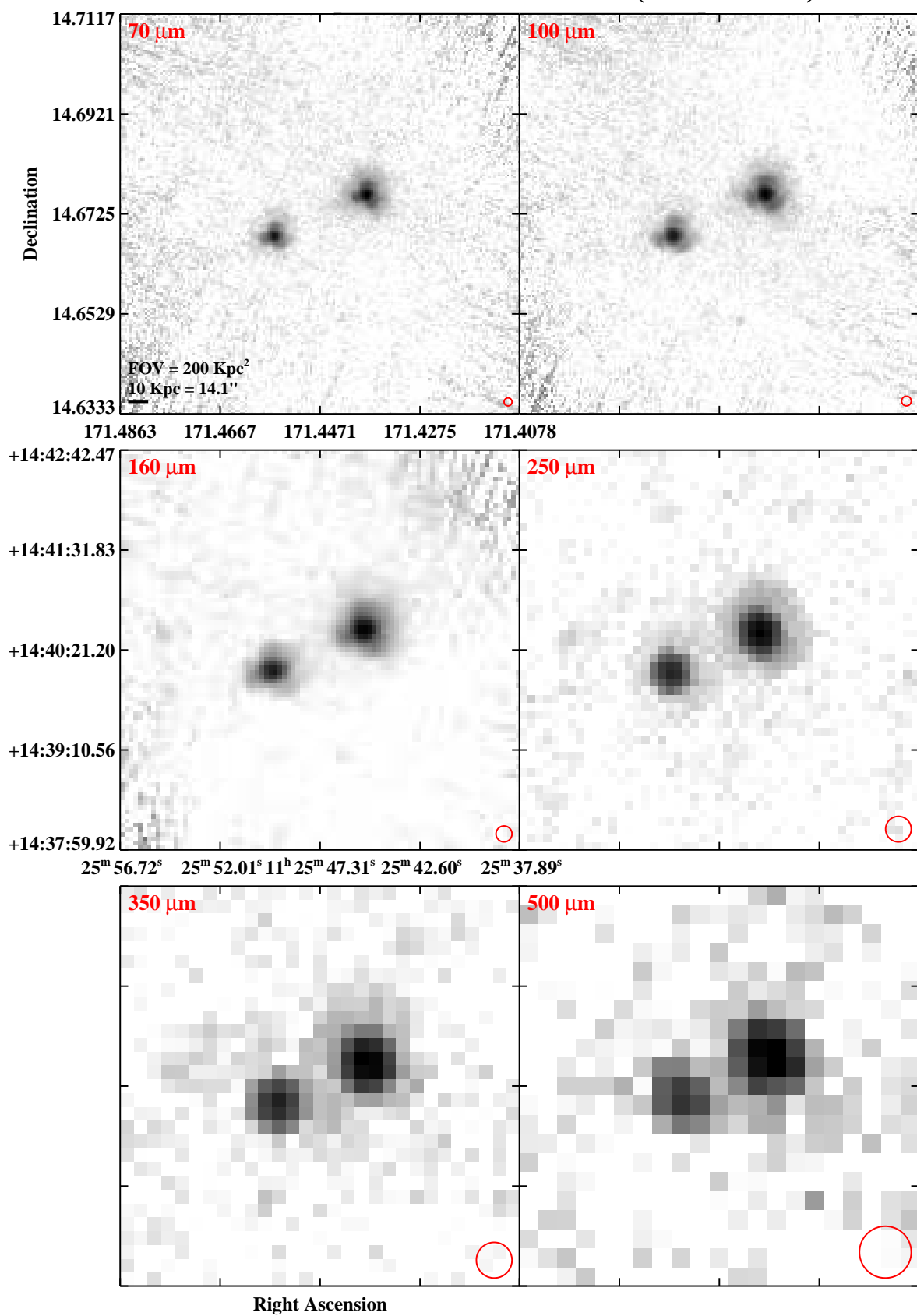


Fig. 3.— Continued (page 97 of 209).

IRAS F11255–4120 (ESO 319–G022)

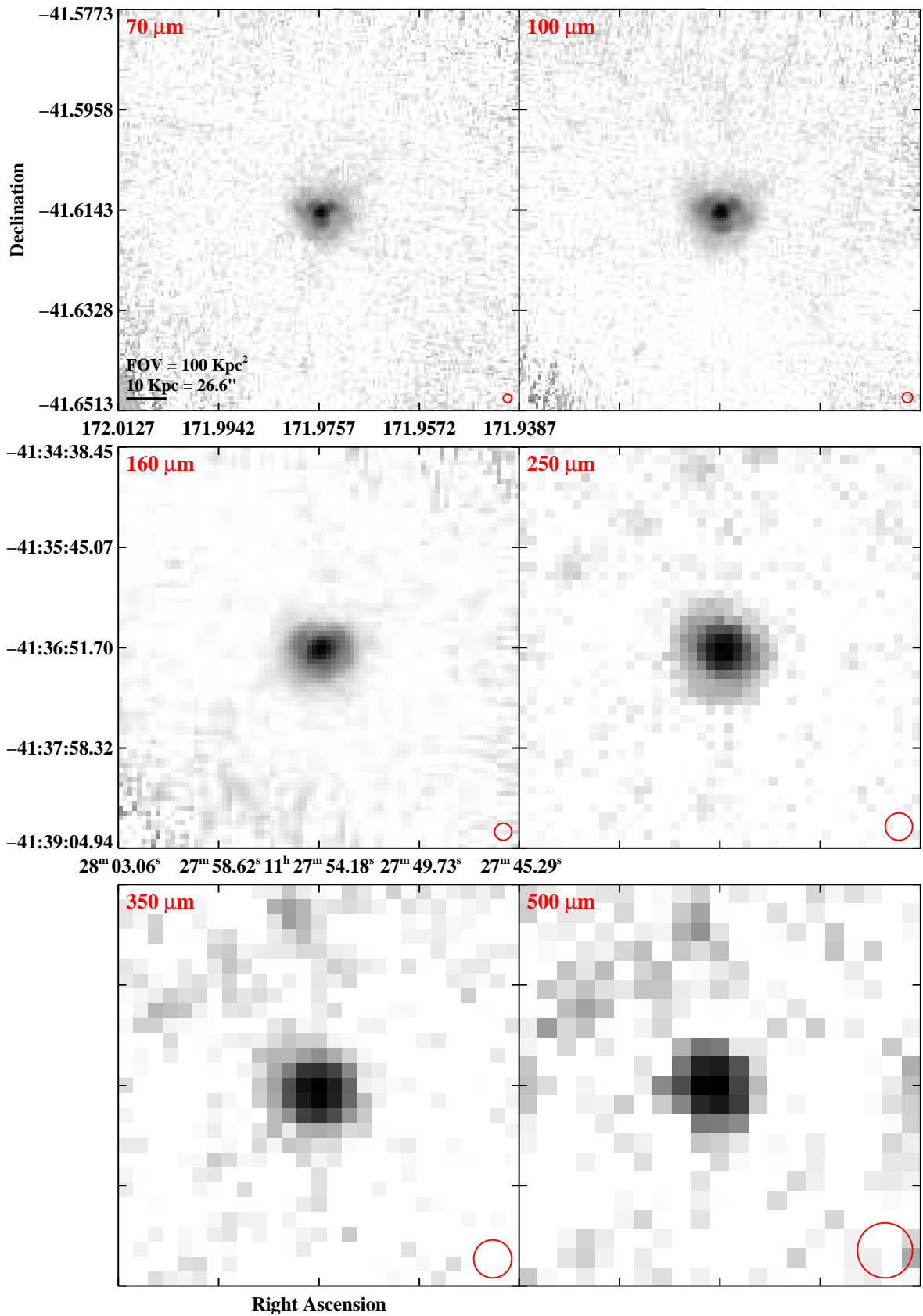


Fig. 3.— Continued (page 98 of 209).

IRAS F11257+5850 (NGC 3690)

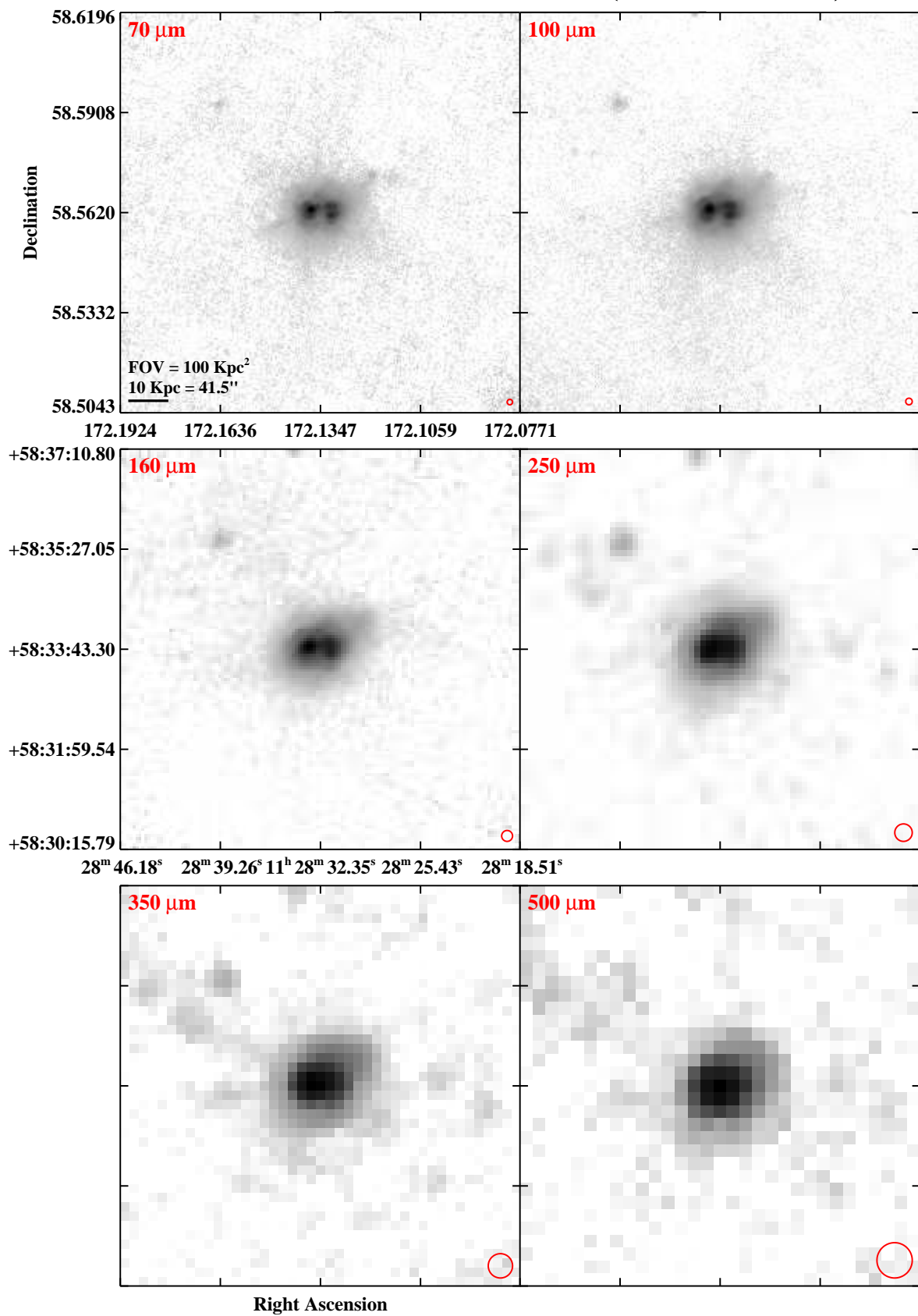


Fig. 3.— Continued (page 99 of 209).

IRAS F11506–3851 (ESO 320–G030)

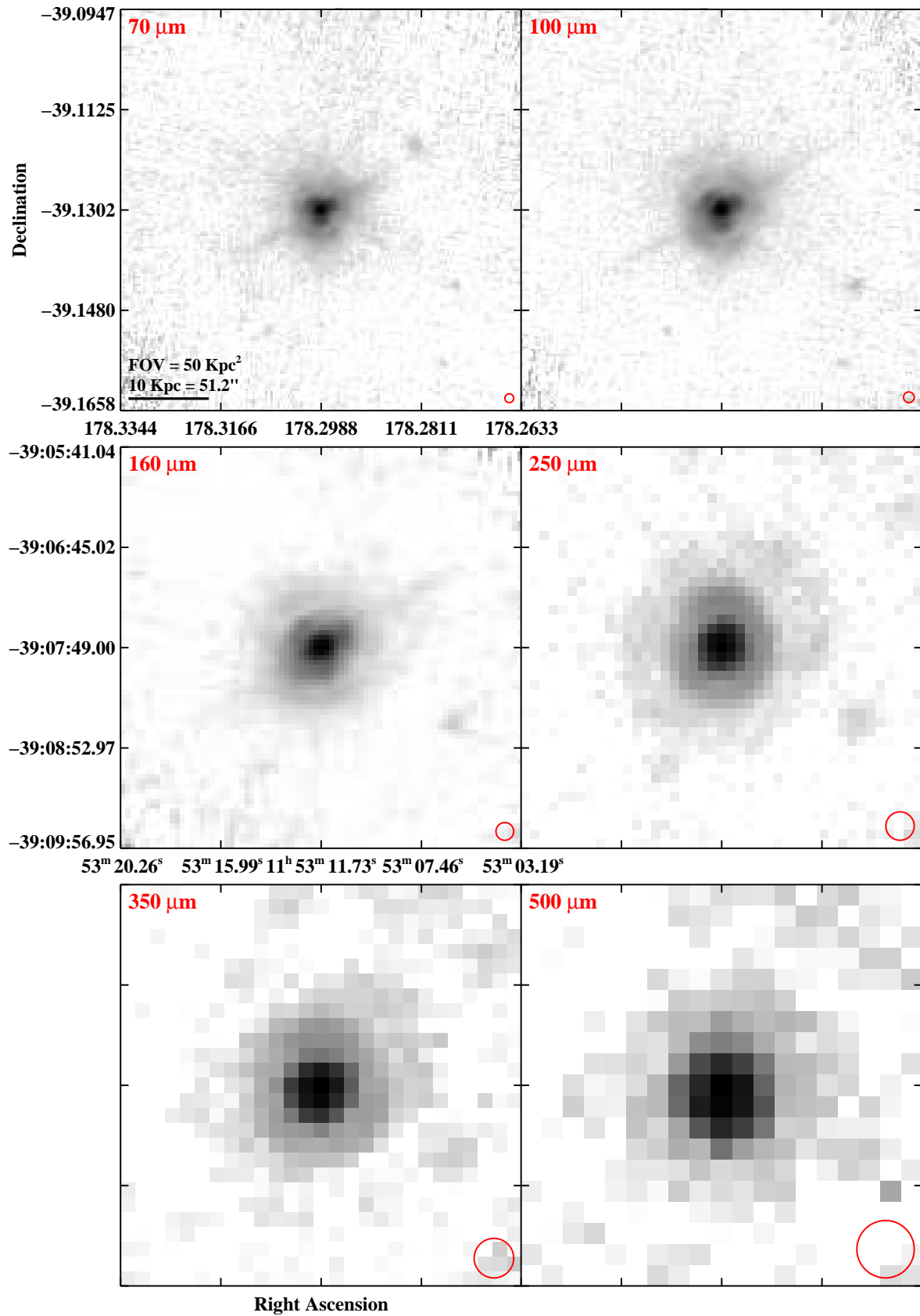


Fig. 3.— Continued (page 100 of 209).

IRAS F12043–3140 (ESO 440–IG058)

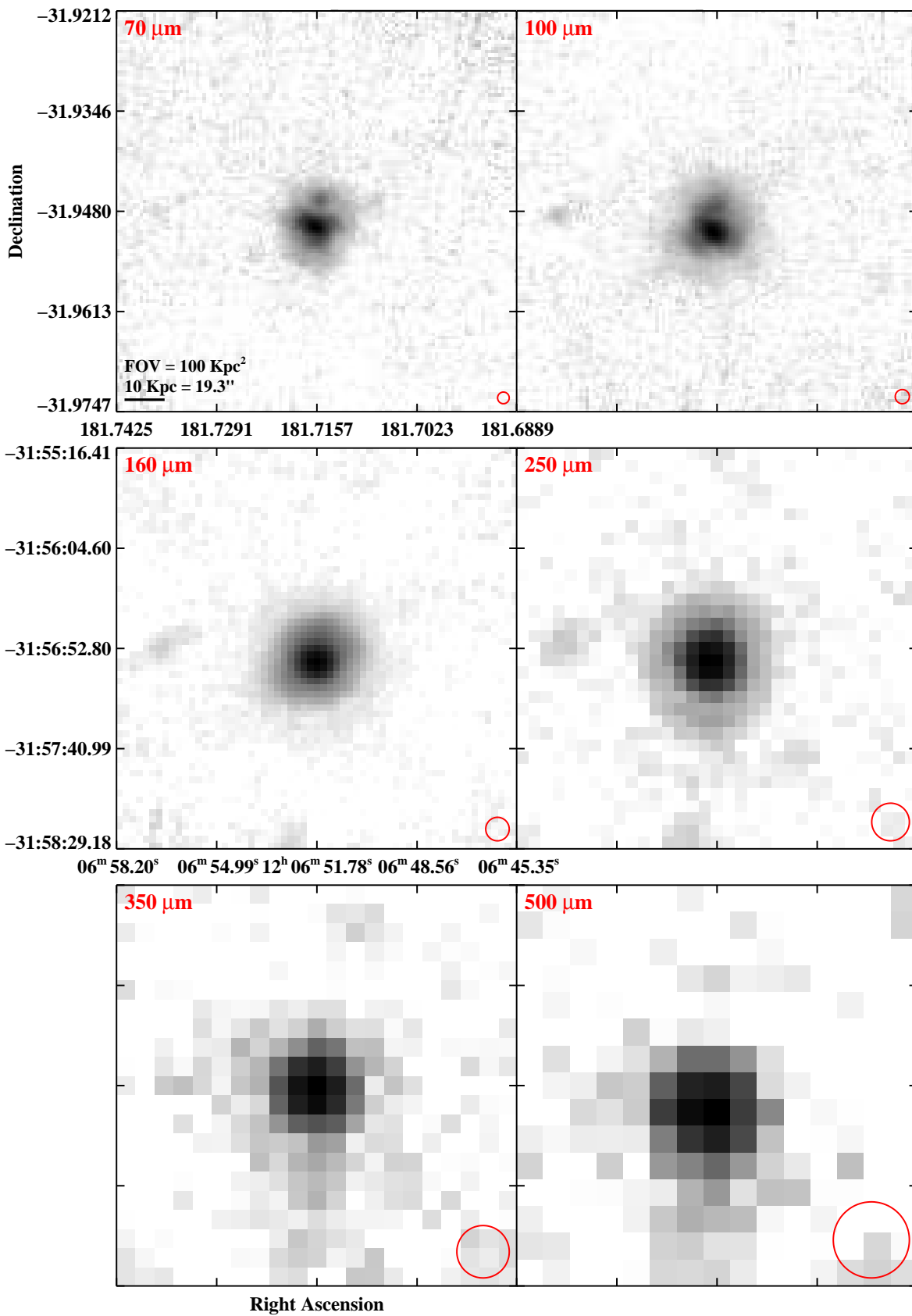


Fig. 3.— Continued (page 101 of 209).

IRAS F12112+0305

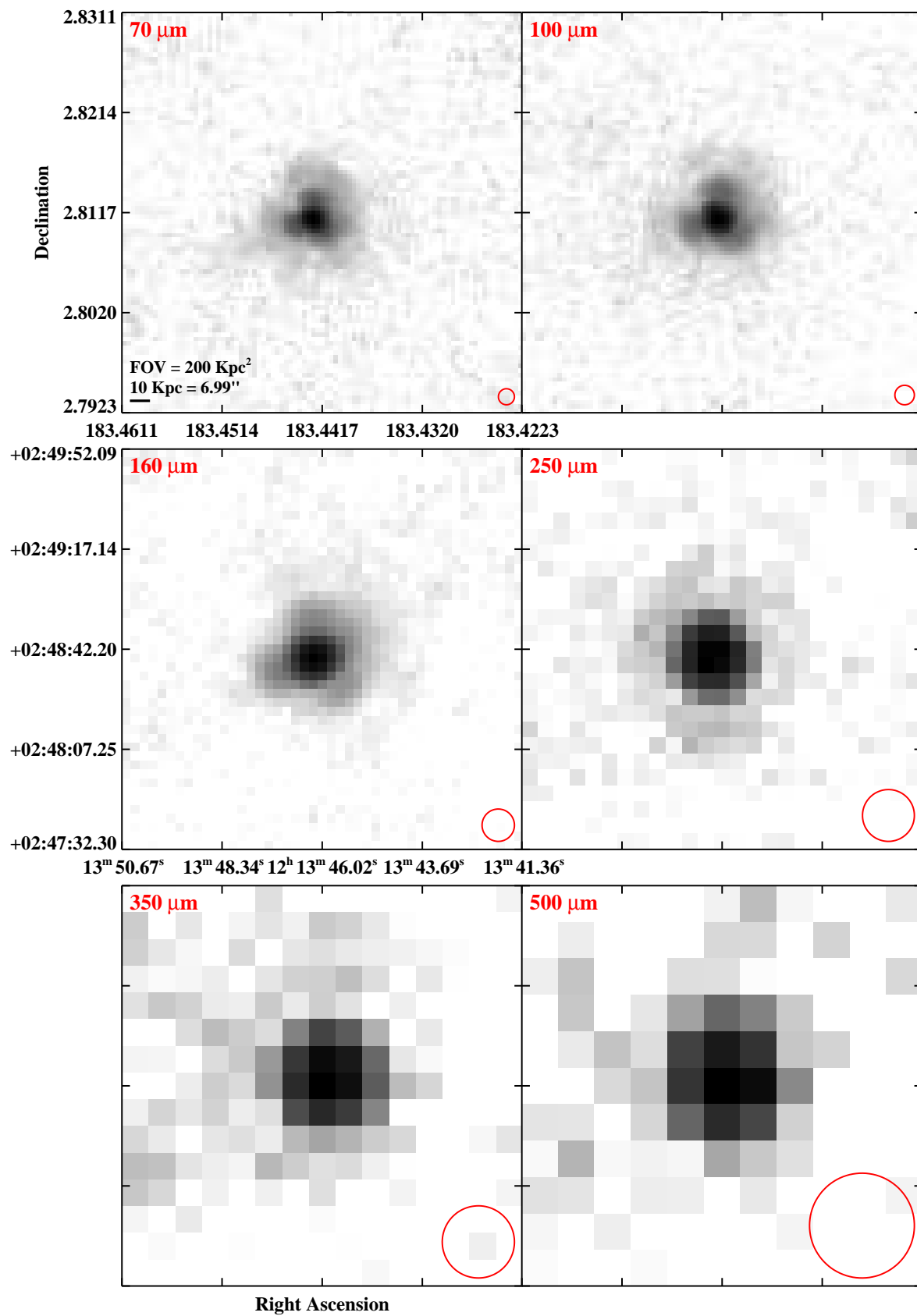


Fig. 3.— Continued (page 102 of 209).

IRAS F12116+5448 (NGC 4194)

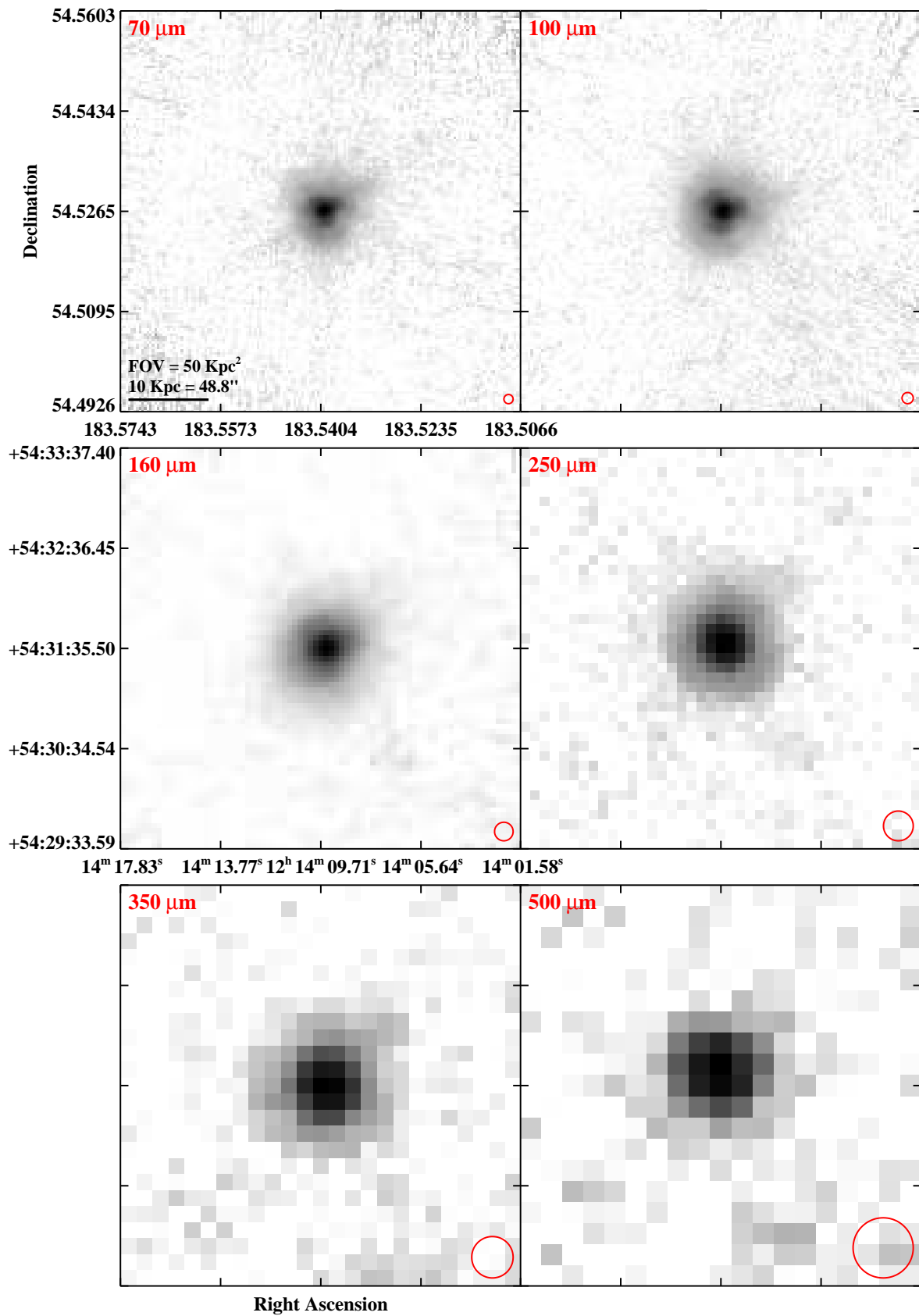


Fig. 3.— Continued (page 103 of 209).

IRAS F12115–4656 (ESO 267–G030)

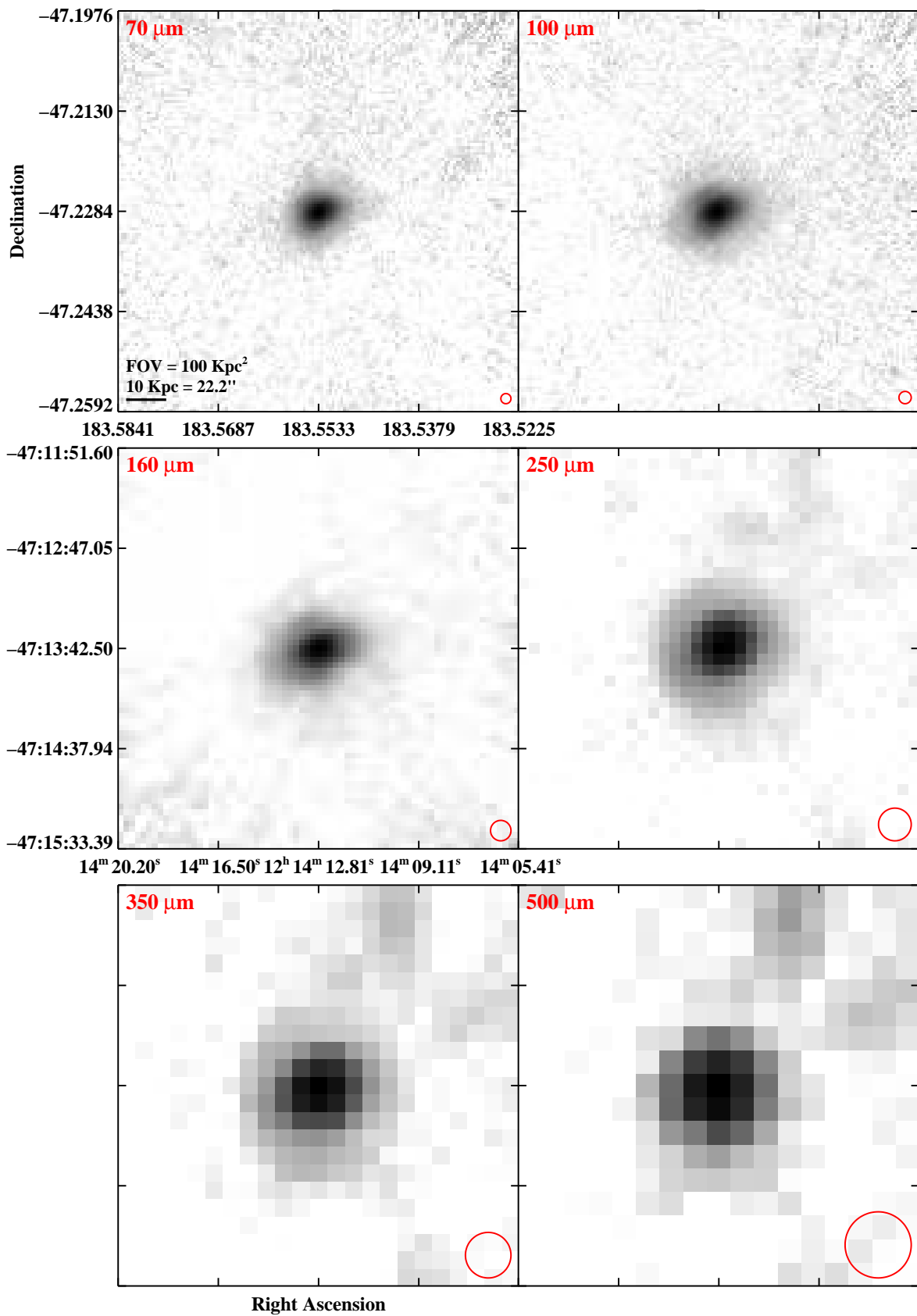


Fig. 3.— Continued (page 104 of 209).

IRAS F12115–4656 (ESO 267–G029)

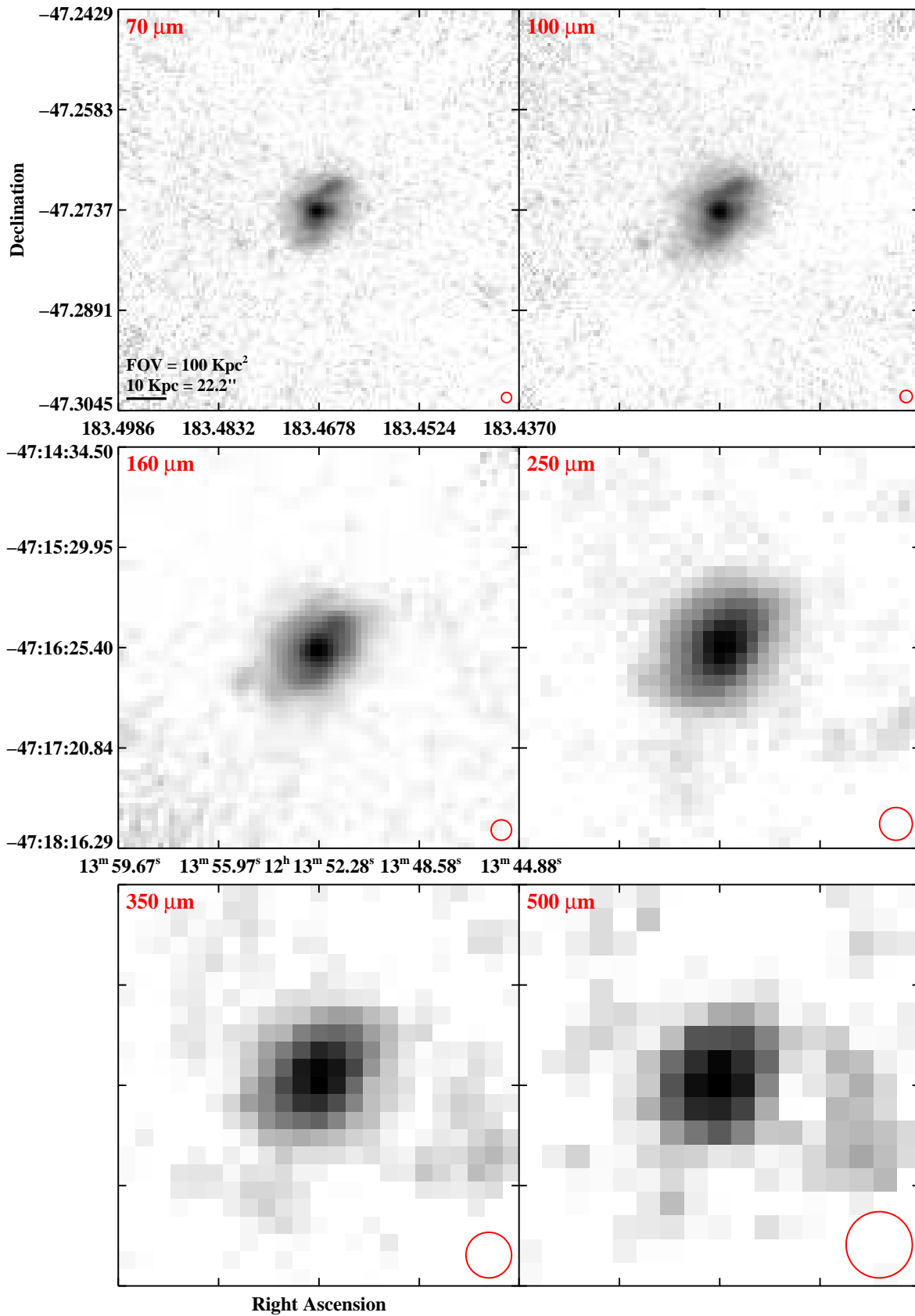


Fig. 3.— Continued (page 105 of 209).

IRAS 12116–5615

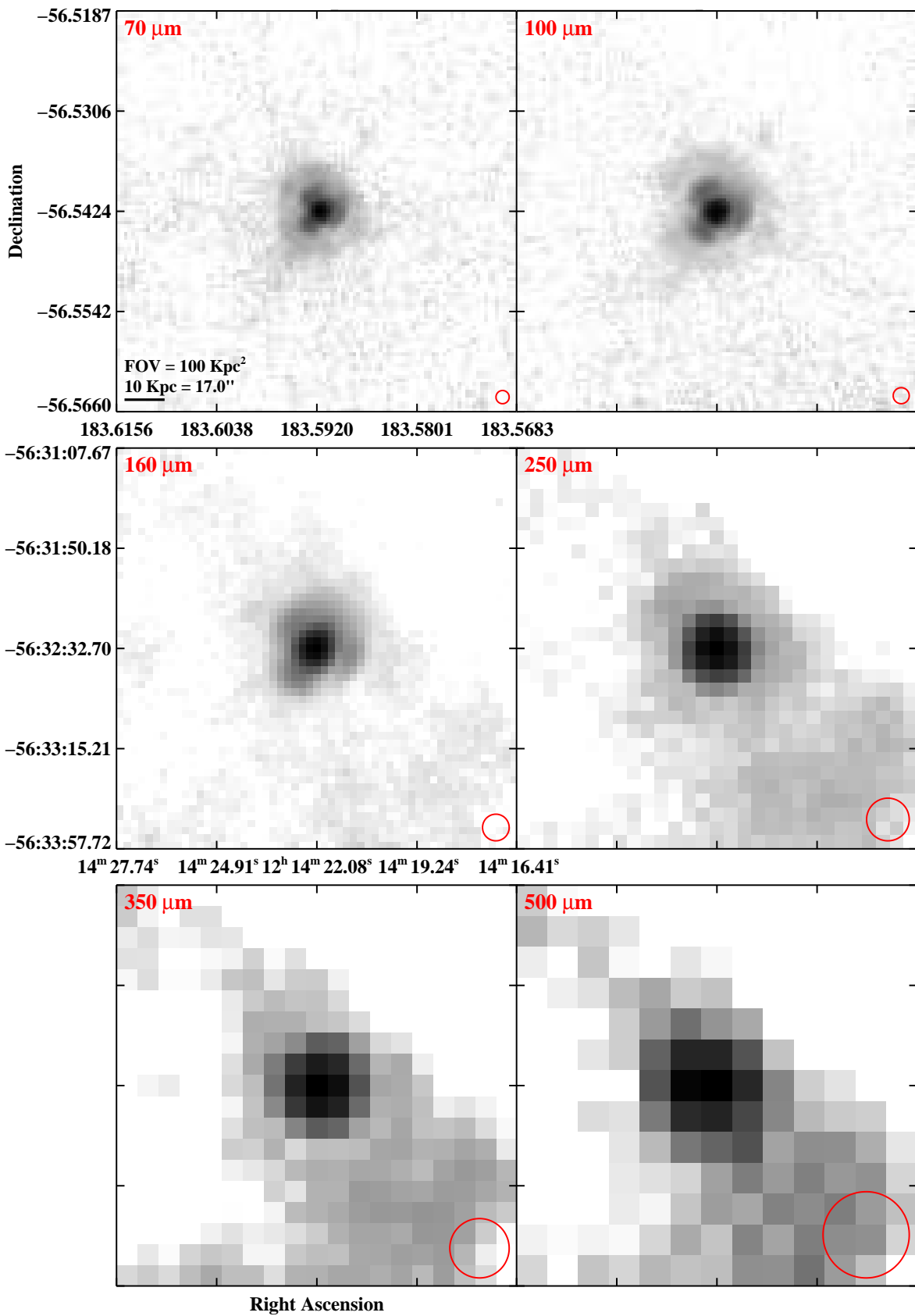


Fig. 3.— Continued (page 106 of 209).

IRAS F12224–0624

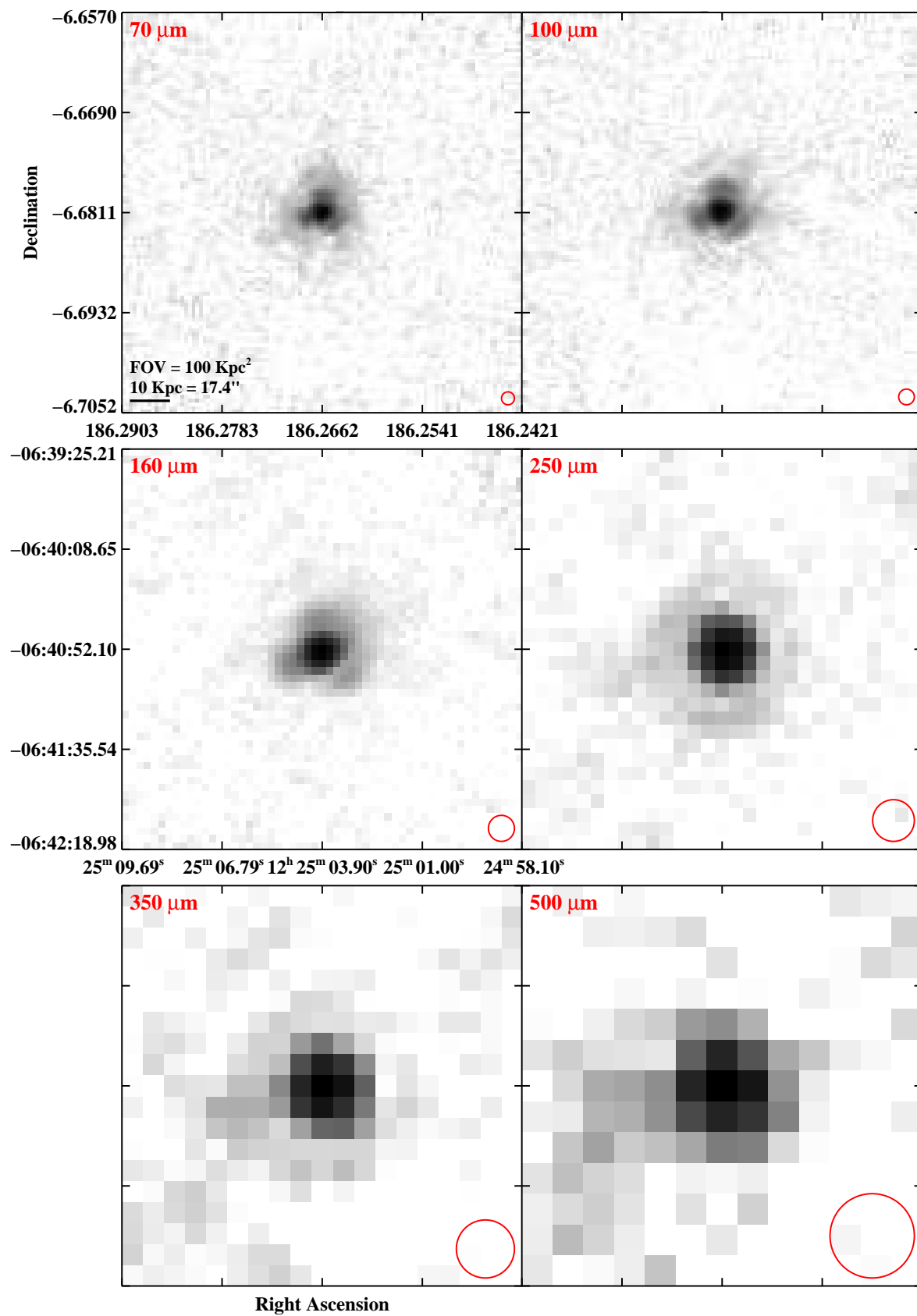


Fig. 3.— Continued (page 107 of 209).

IRAS F12243–0036 (NGC 4418)

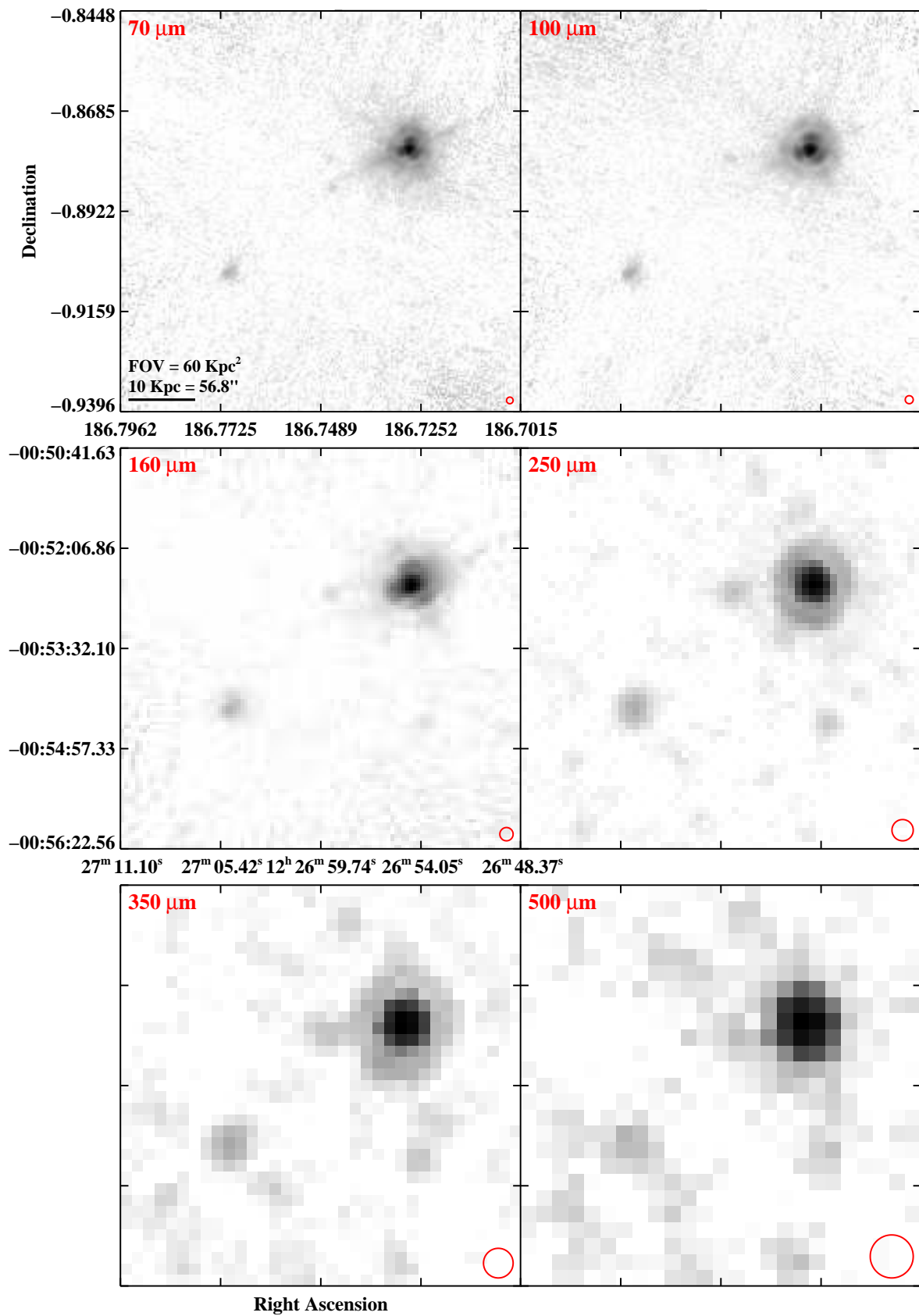


Fig. 3.— Continued (page 108 of 209).

IRAS F12540+5708 (Mrk 231/UGC 08058)

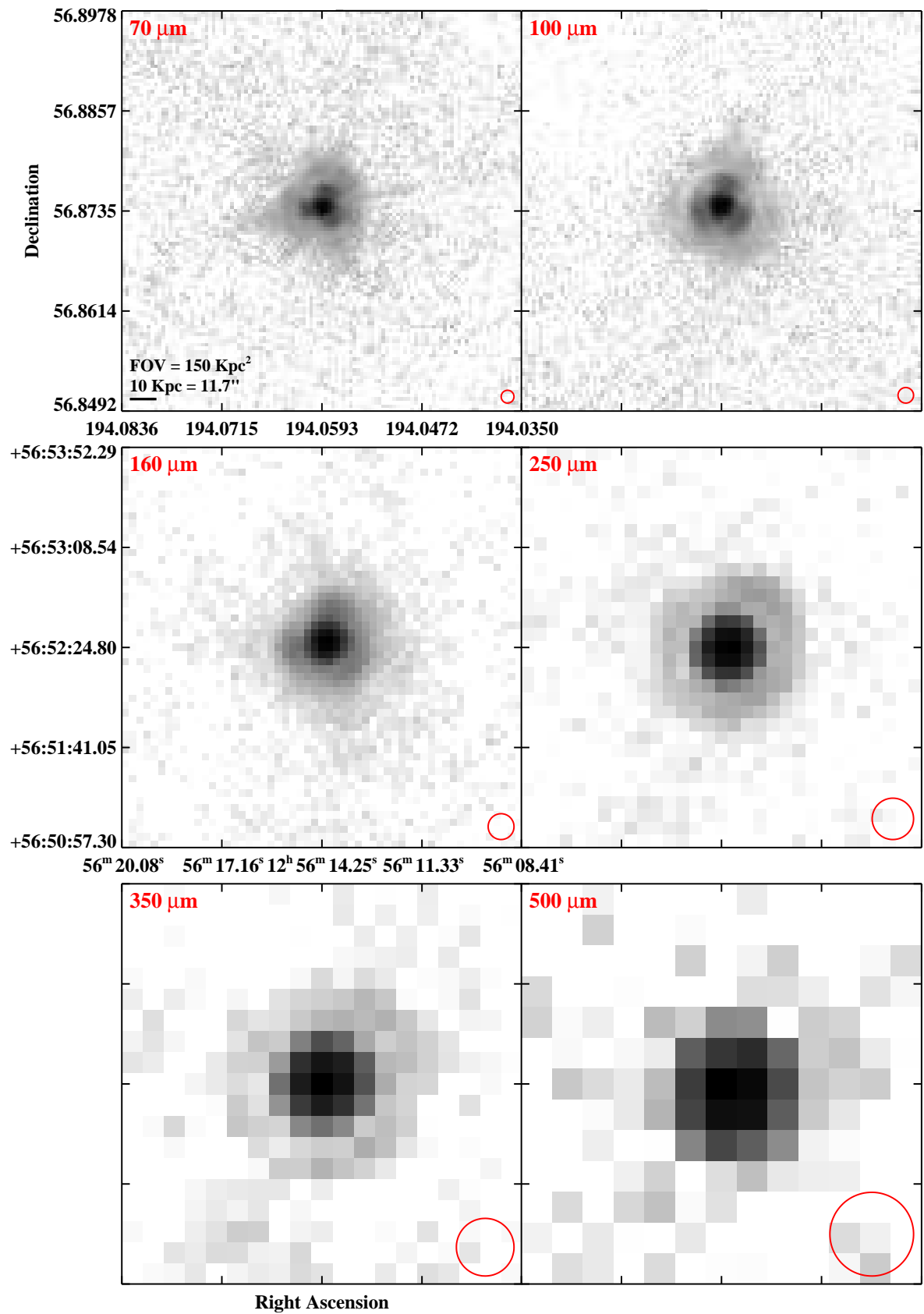


Fig. 3.— Continued (page 109 of 209).

IRAS F12590+2934 (NGC 4922)

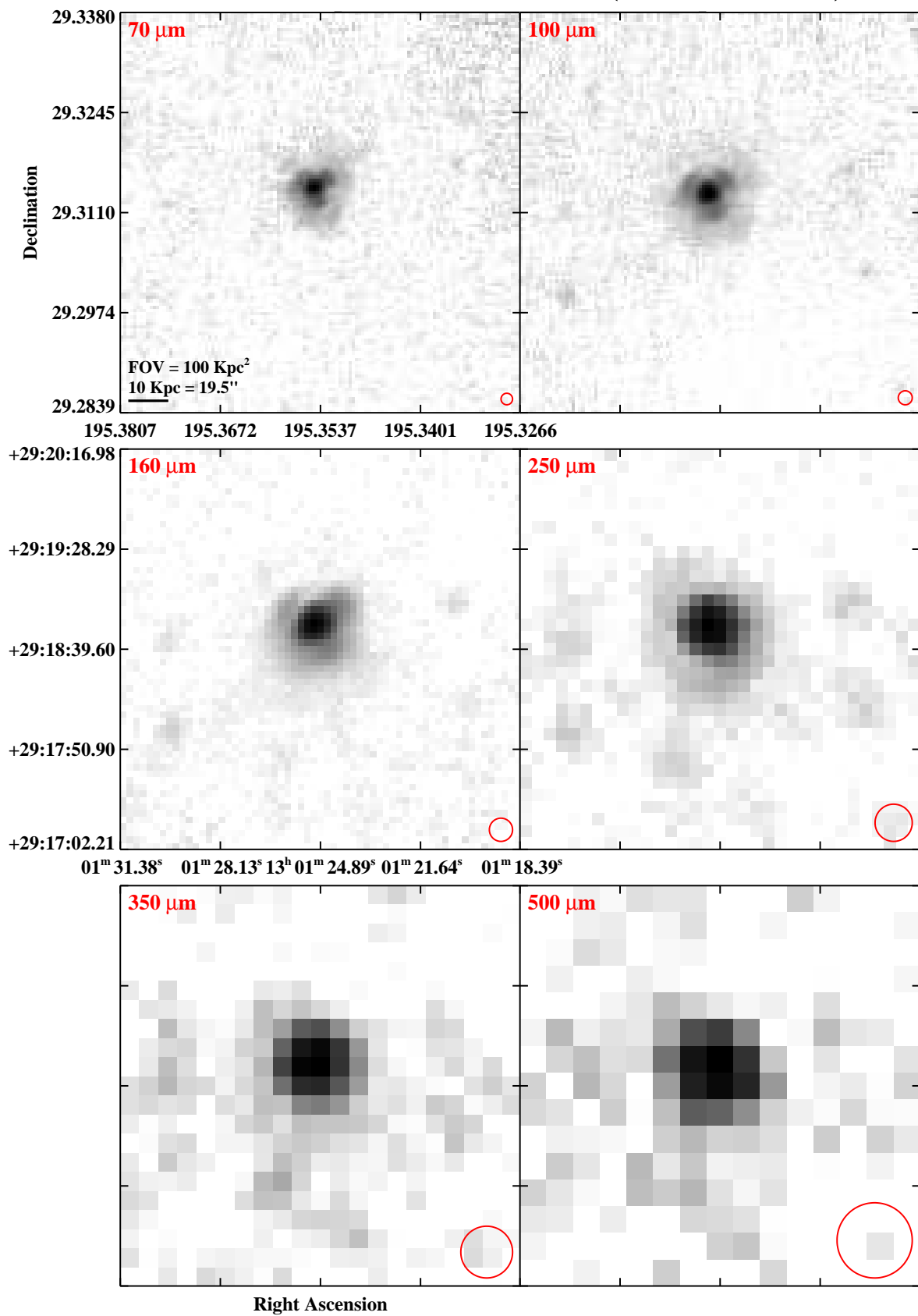


Fig. 3.— Continued (page 110 of 209).

IRAS F12592+0436 (CGCG 043-099)

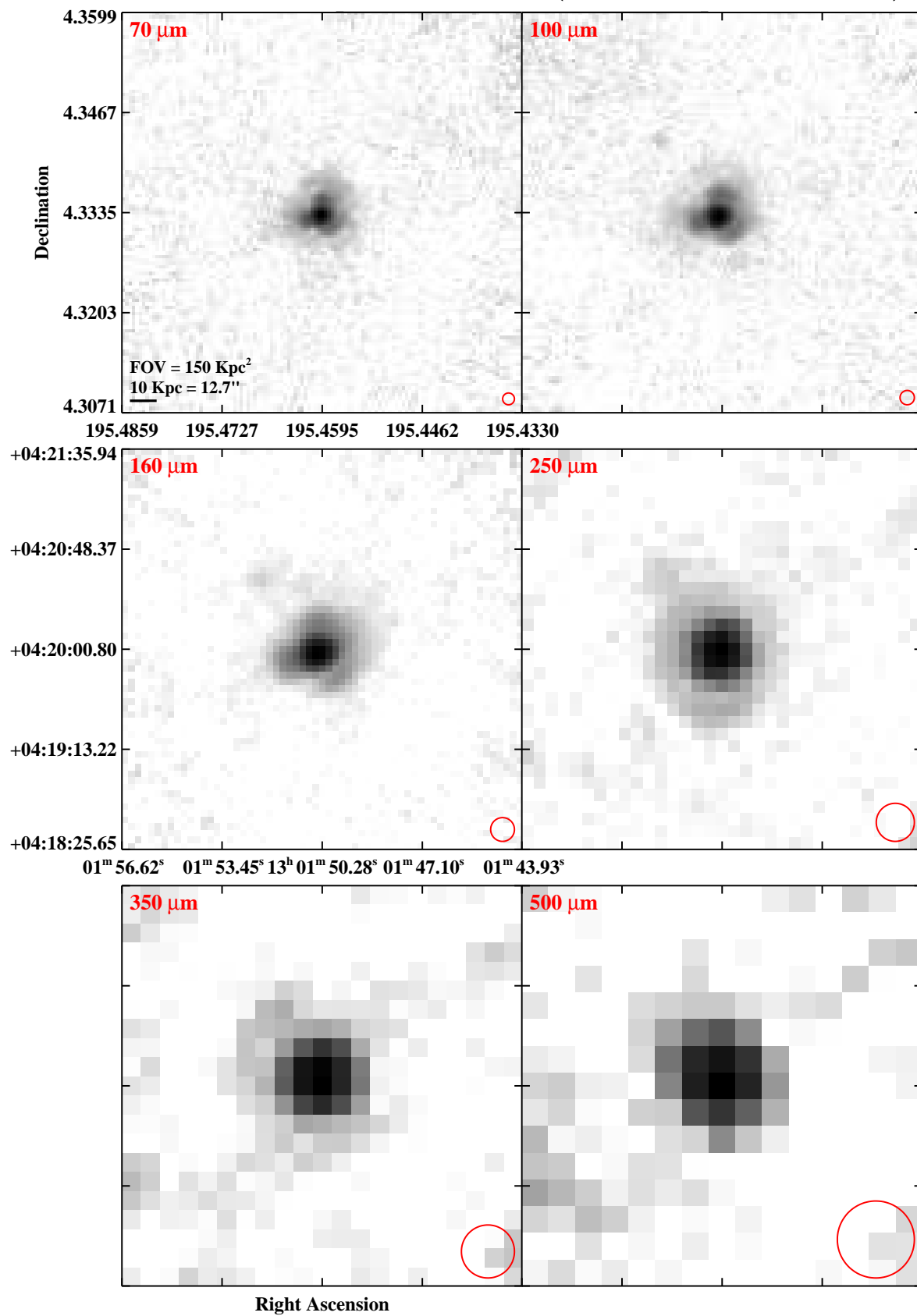


Fig. 3.— Continued (page 111 of 209).

IRAS F12596–1529 (MCG–02–33–098)

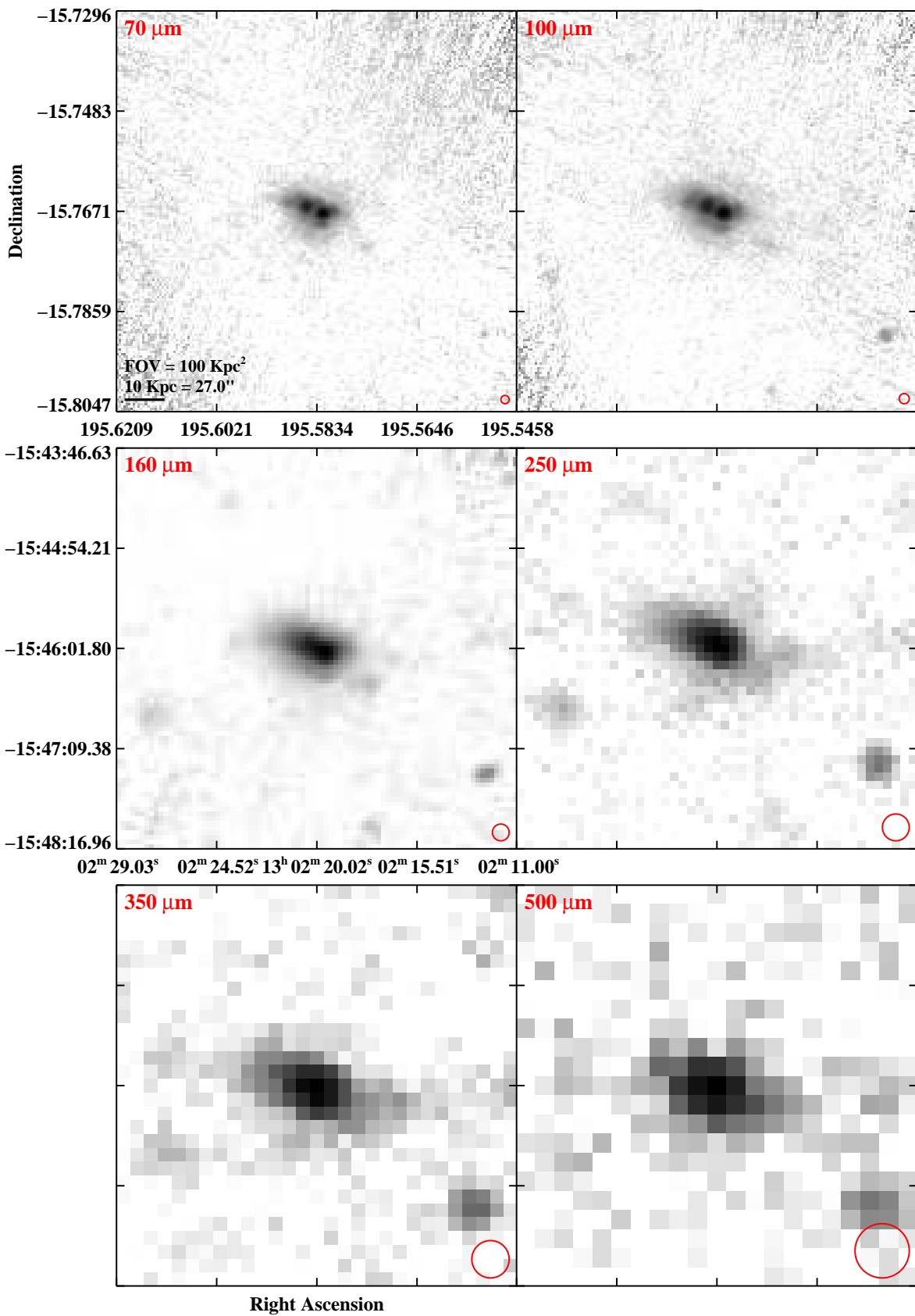


Fig. 3.— Continued (page 112 of 209).

IRAS F13001–2339 (ESO 507–G070)

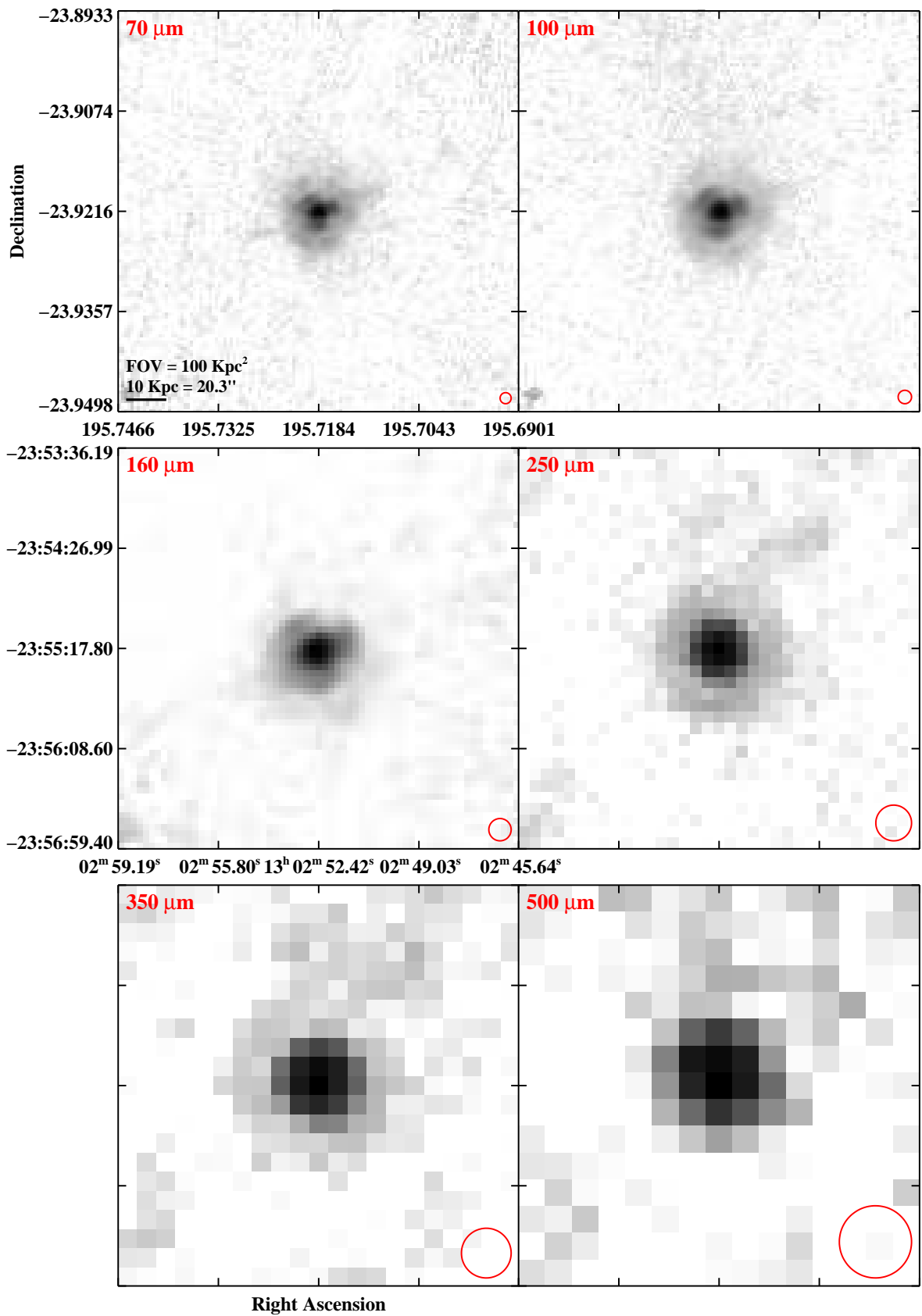


Fig. 3.— Continued (page 113 of 209).

IRAS 13052–5711

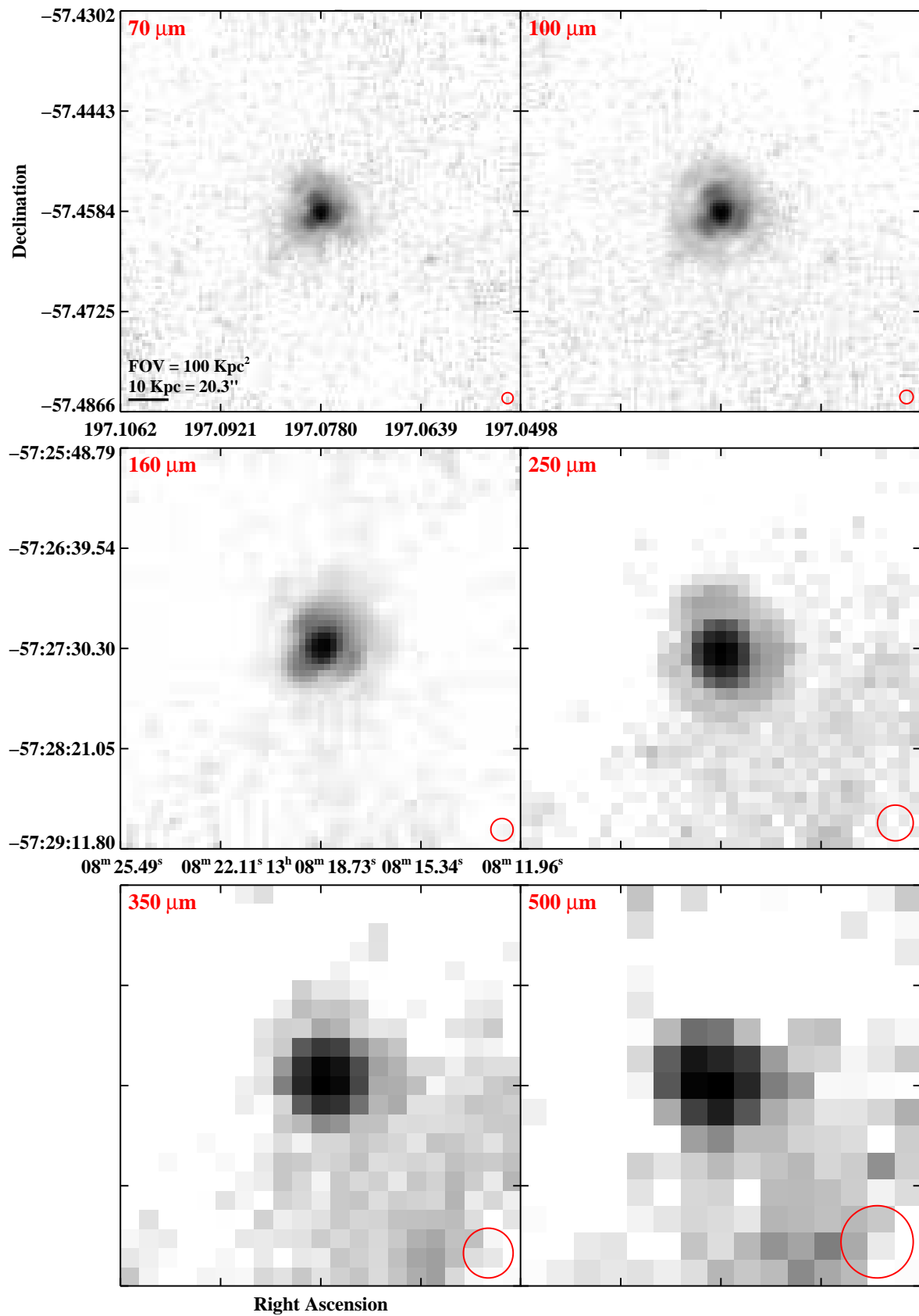


Fig. 3.— Continued (page 114 of 209).

IRAS F13126+2453 (IC 0860)

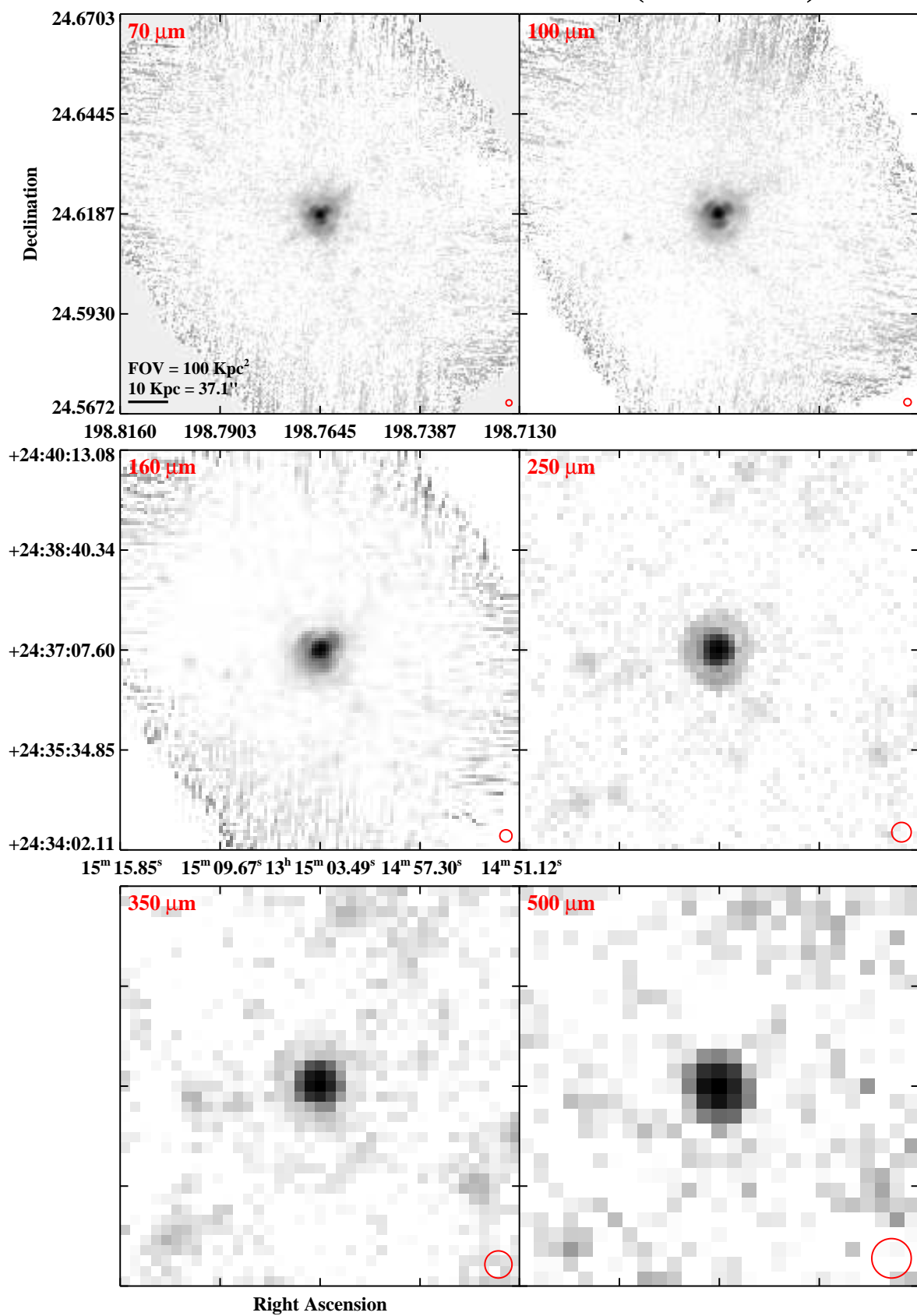


Fig. 3.— Continued (page 115 of 209).

IRAS 13120–5453

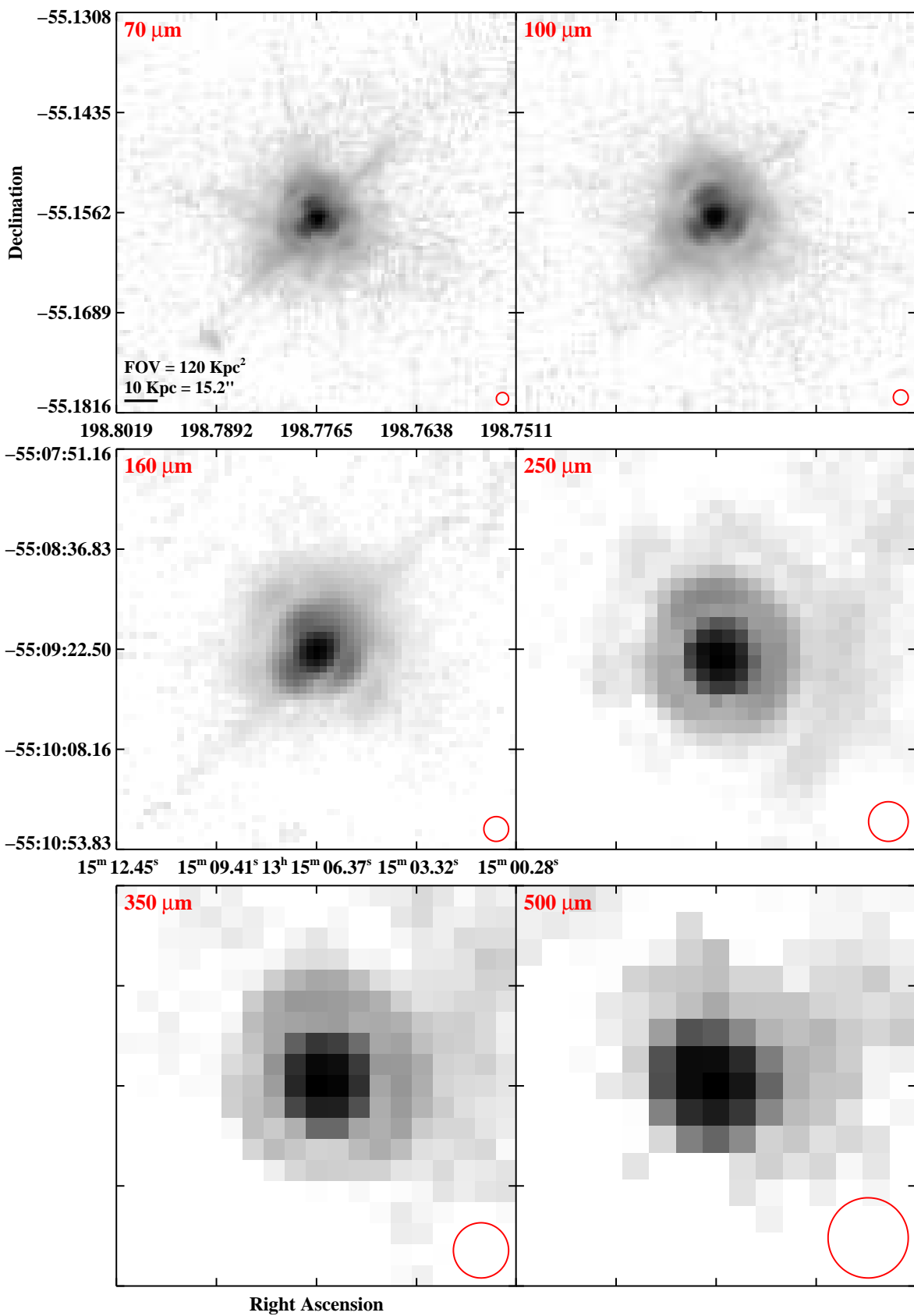


Fig. 3.— Continued (page 116 of 209).

IRAS F13136+6223 (VV 250a)

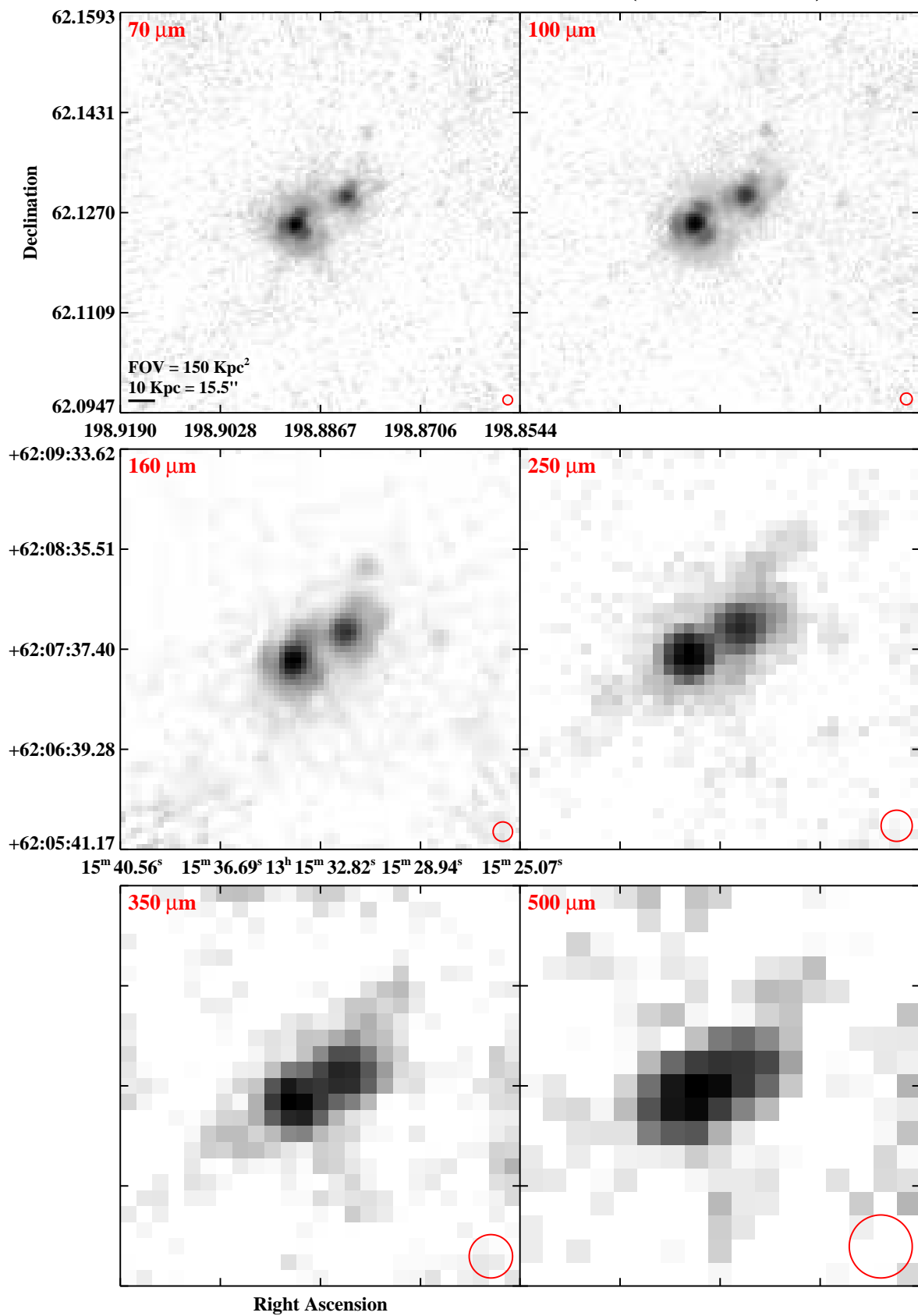


Fig. 3.— Continued (page 117 of 209).

IRAS F13182+3424 (UGC 08387)

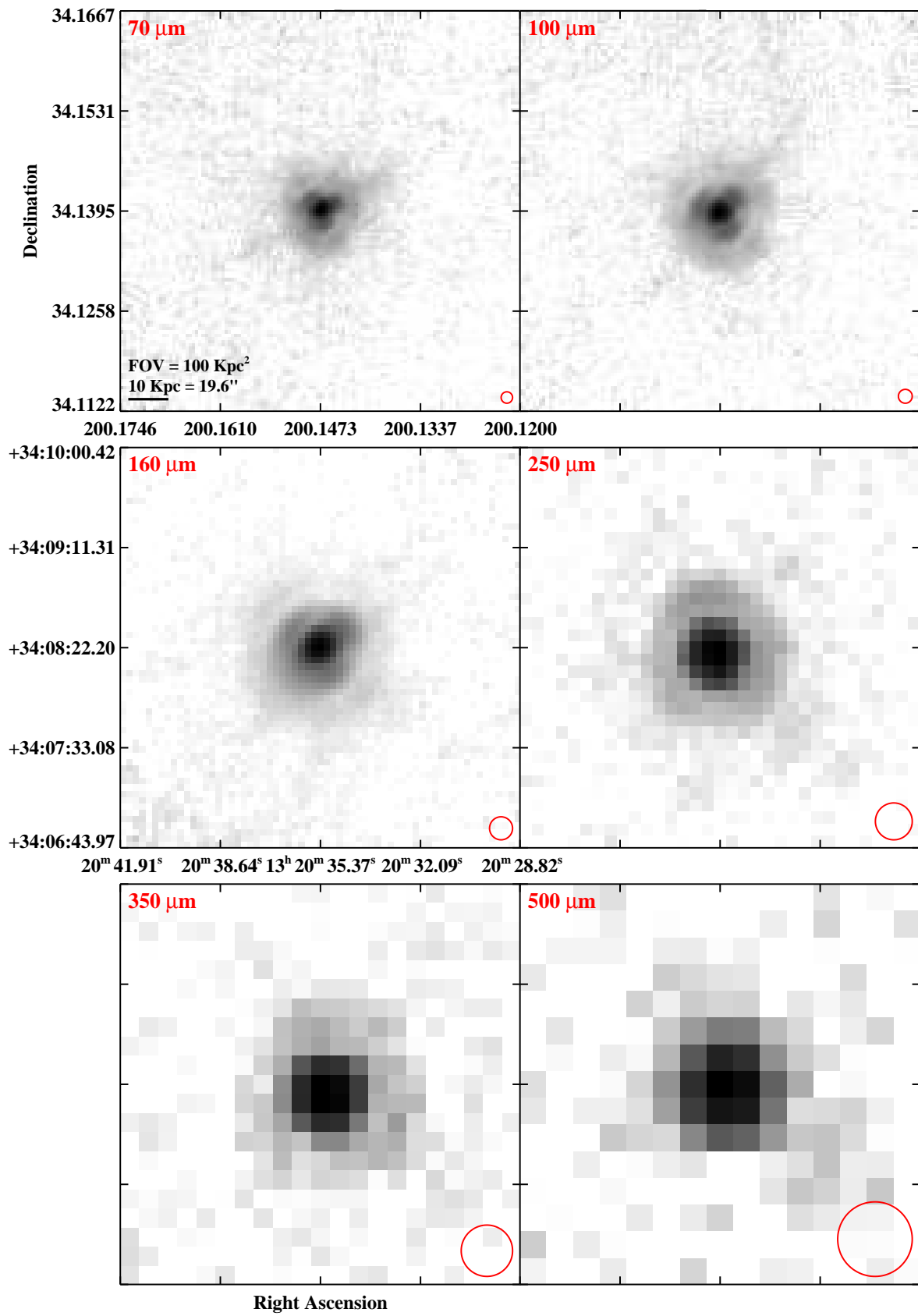


Fig. 3.— Continued (page 118 of 209).

IRAS F13188+0036 (NGC 5104)

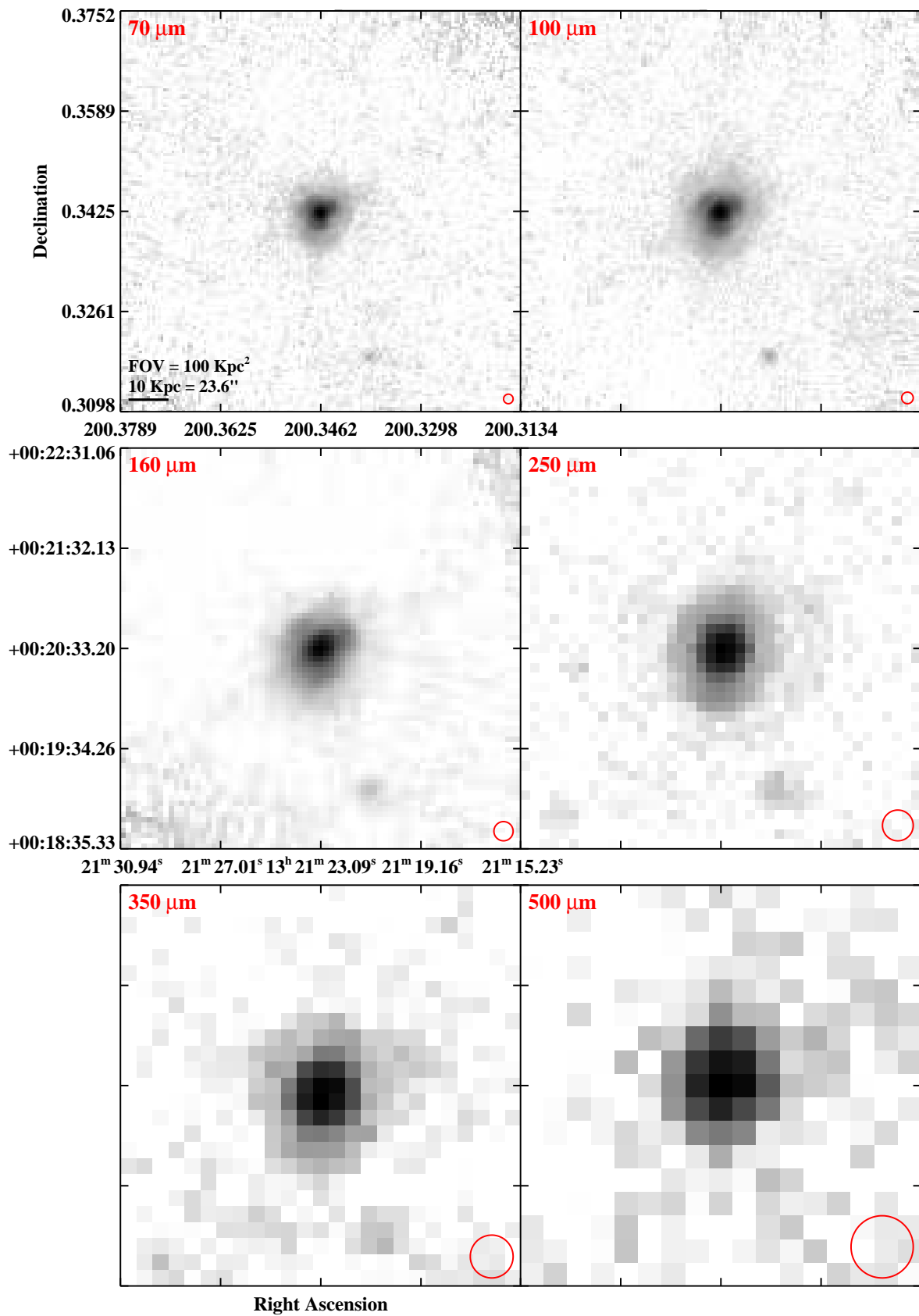


Fig. 3.— Continued (page 119 of 209).

IRAS F13197–1627 (MCG–03–34–064)

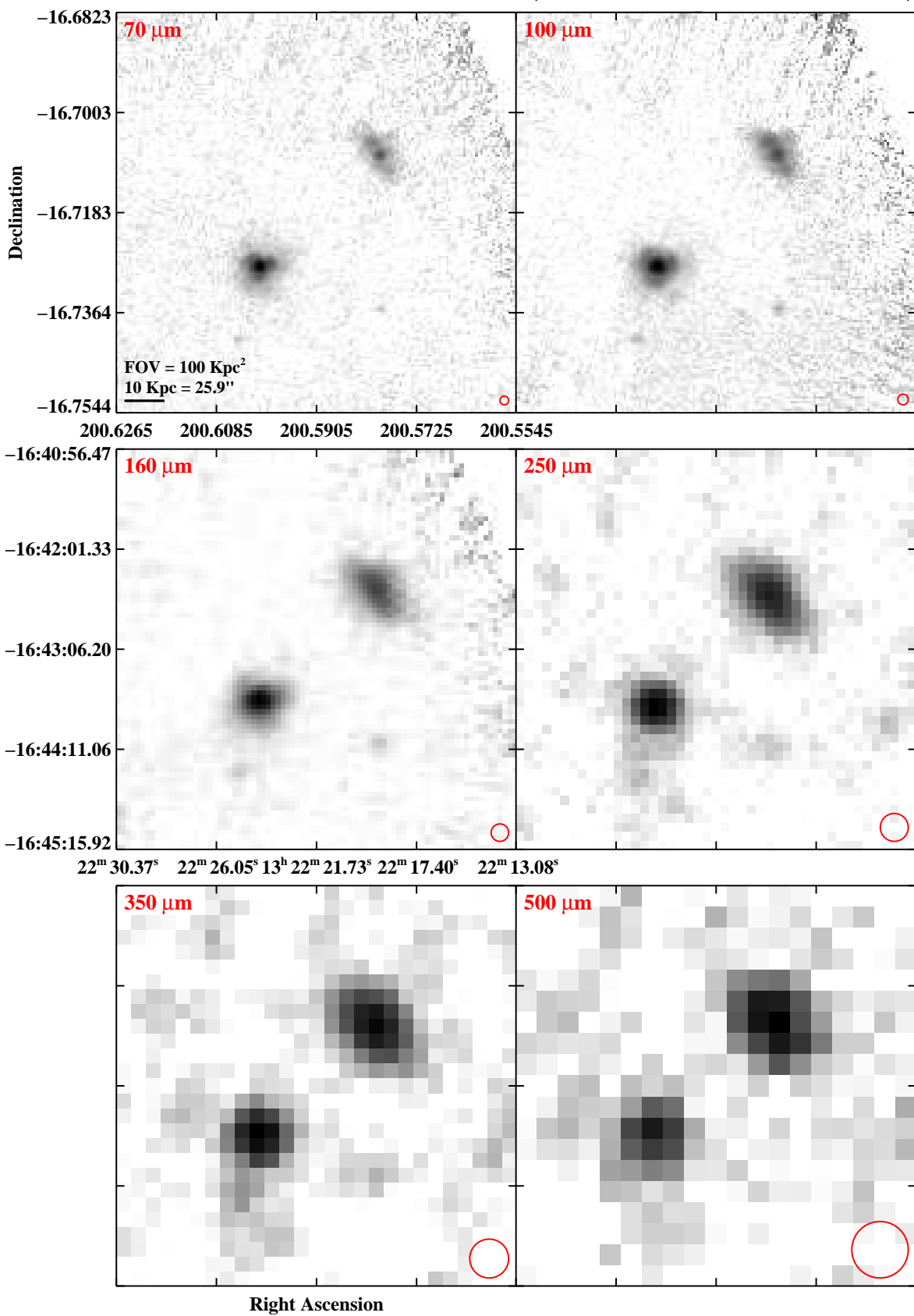


Fig. 3.— Continued (page 120 of 209).

IRAS F13229–2934 (NGC 5135)

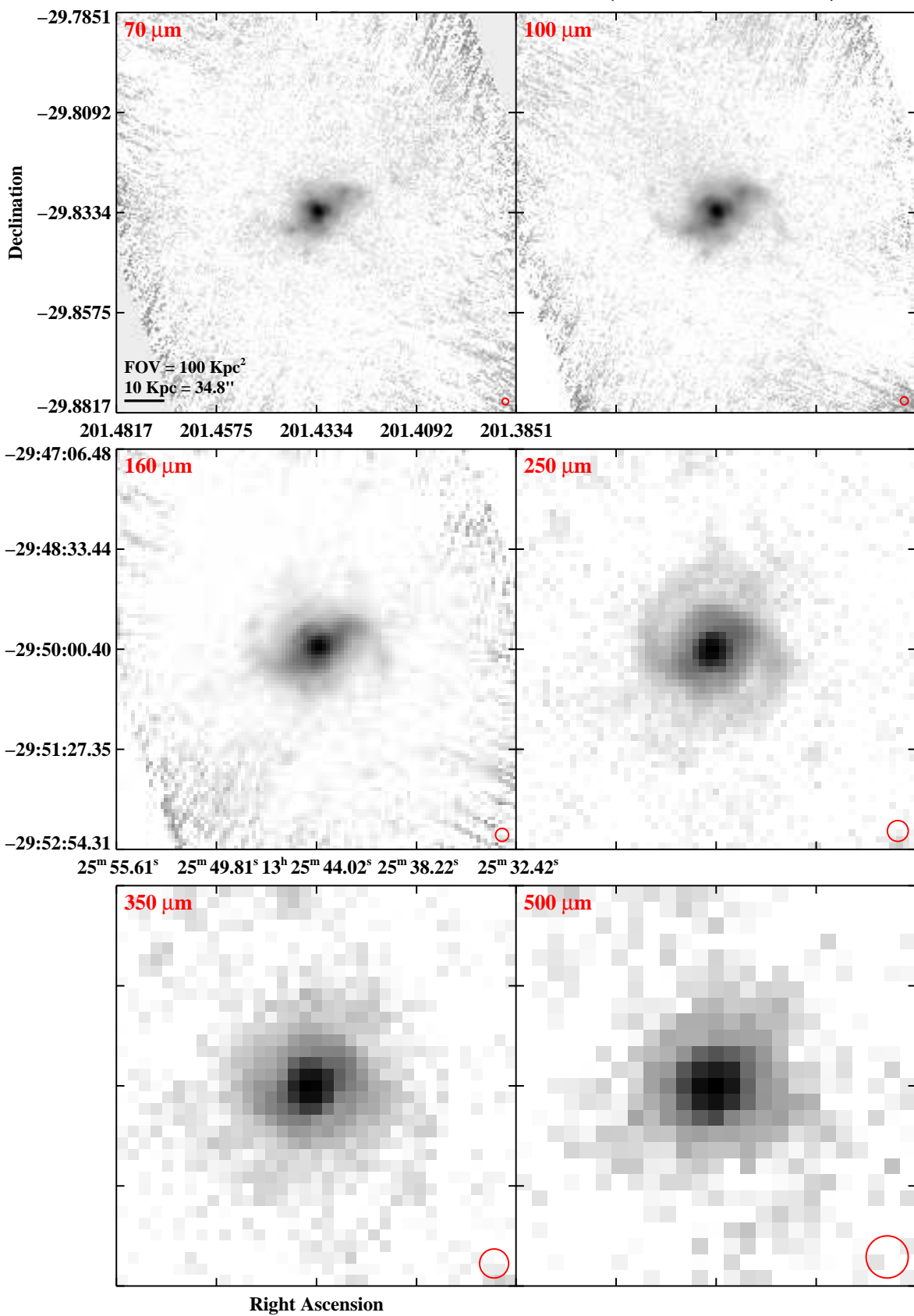


Fig. 3.— Continued (page 121 of 209).

IRAS 13242–5713 (ESO 173–G015)

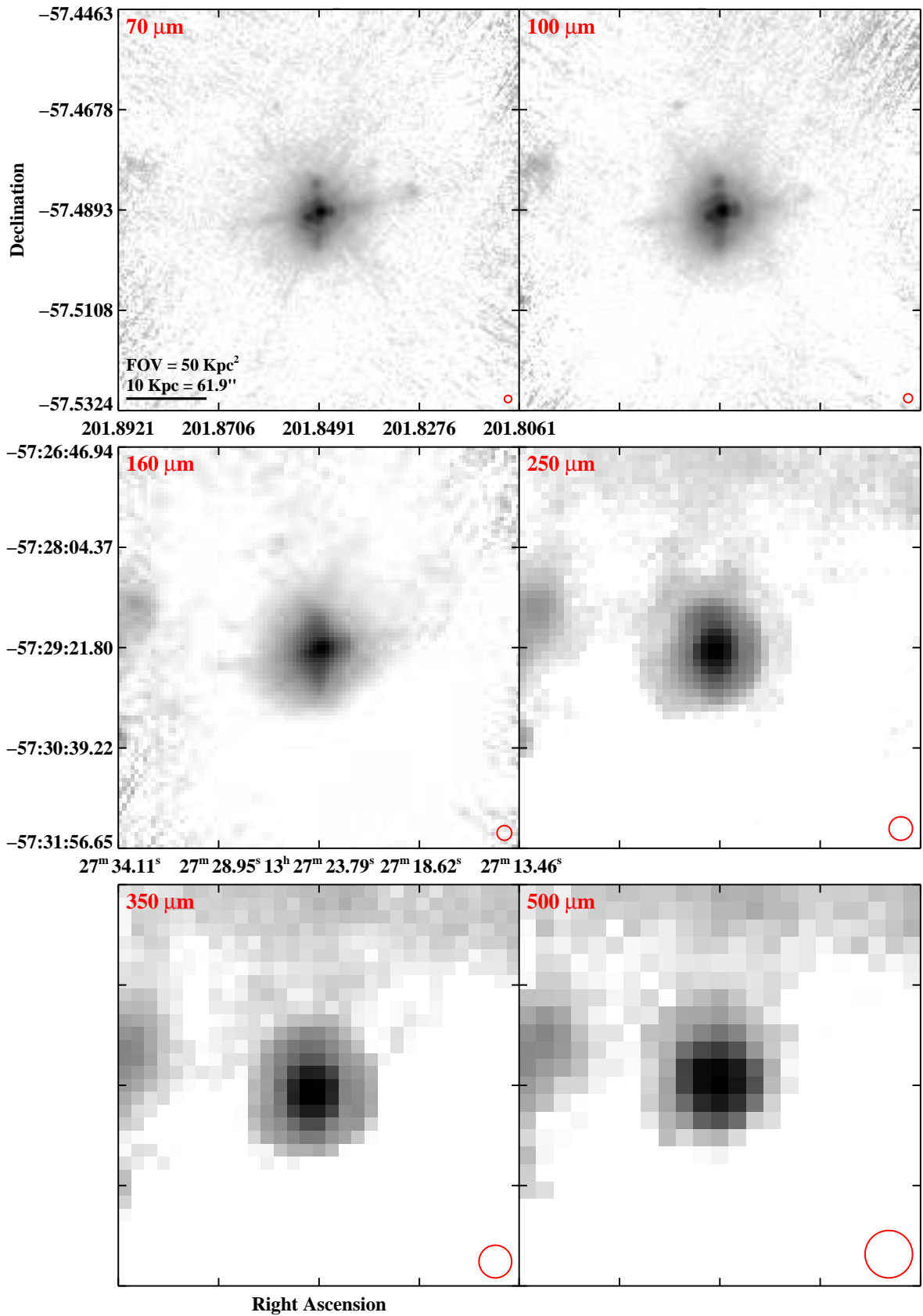


Fig. 3.— Continued (page 122 of 209).

IRAS F13301–2356 (IC 4280)

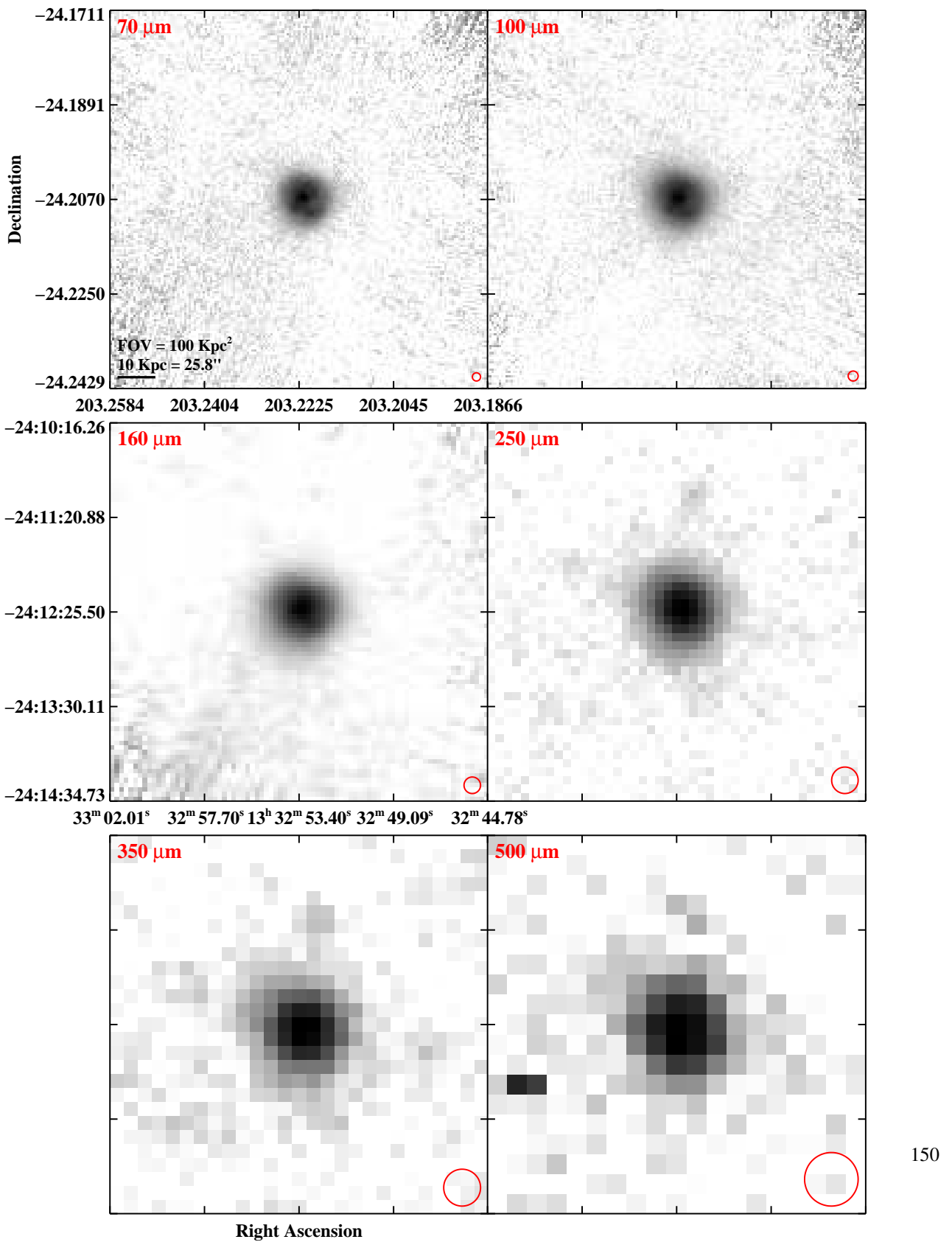


Fig. 3.— Continued (page 123 of 209).

IRAS F13362+4831 (NGC 5256)

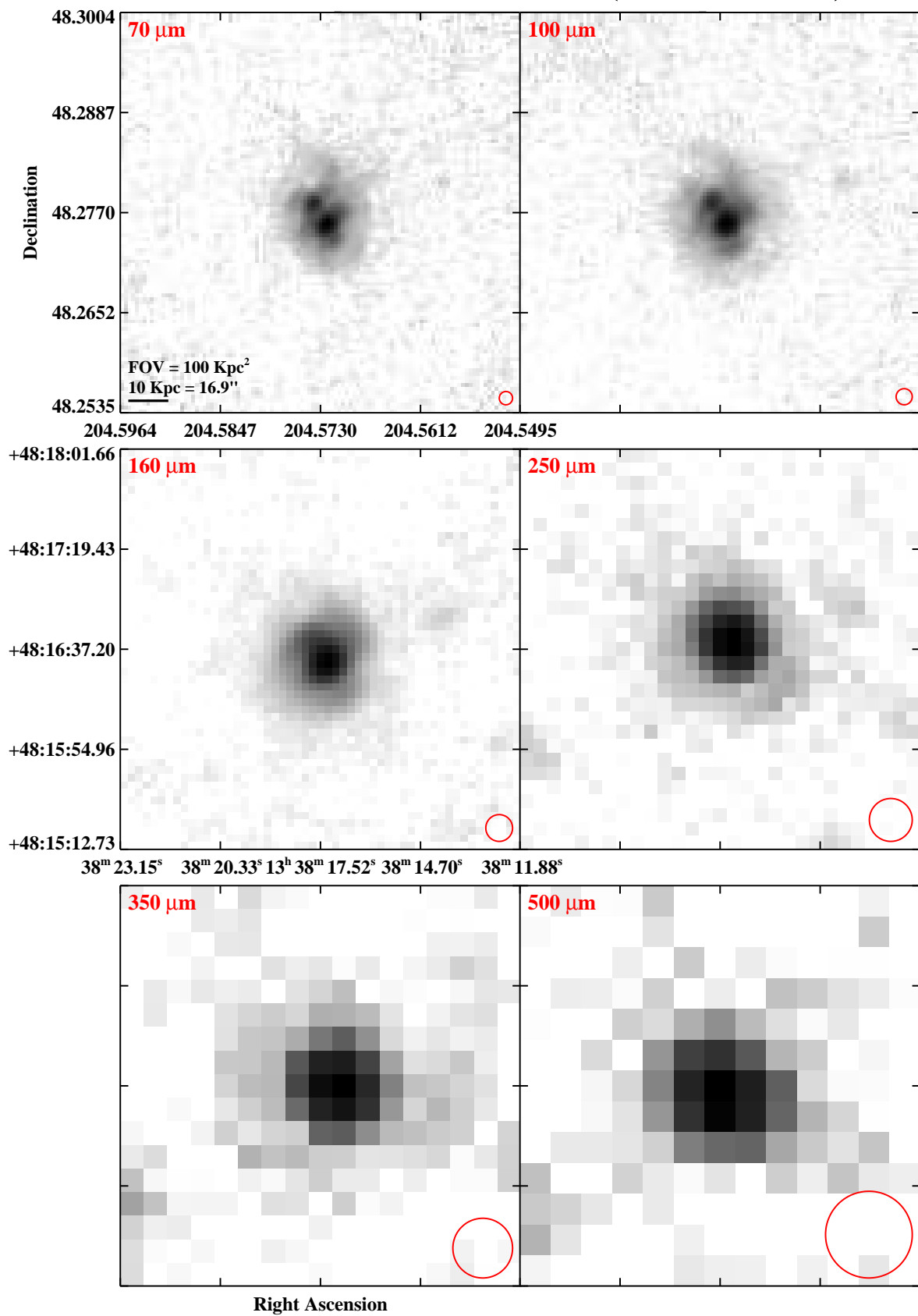


Fig. 3.— Continued (page 124 of 209).

IRAS F13373+0105 (Arp 240)

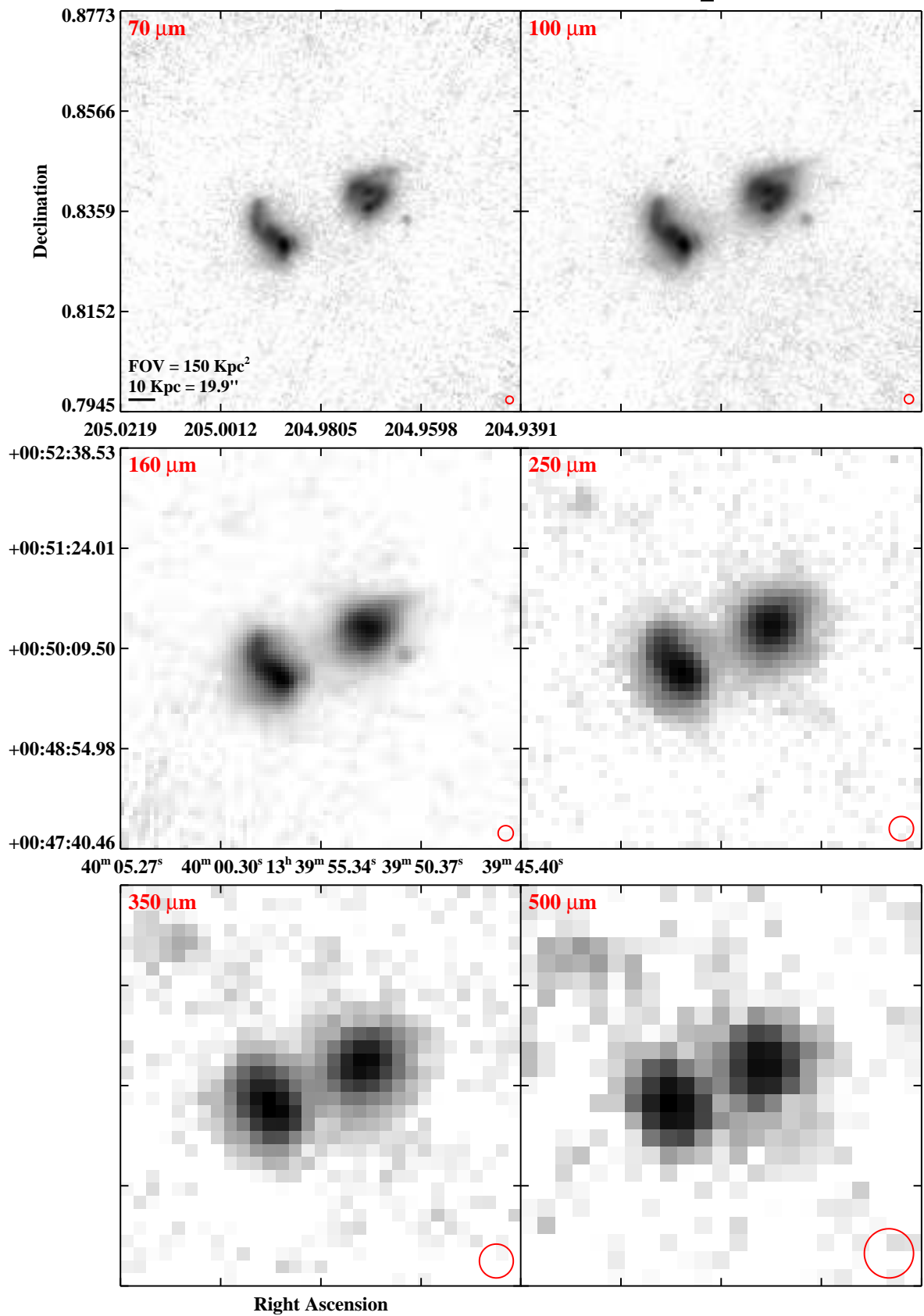


Fig. 3.— Continued (page 125 of 209).

IRAS F13428+5608 (Mrk 273/UGC 08696)

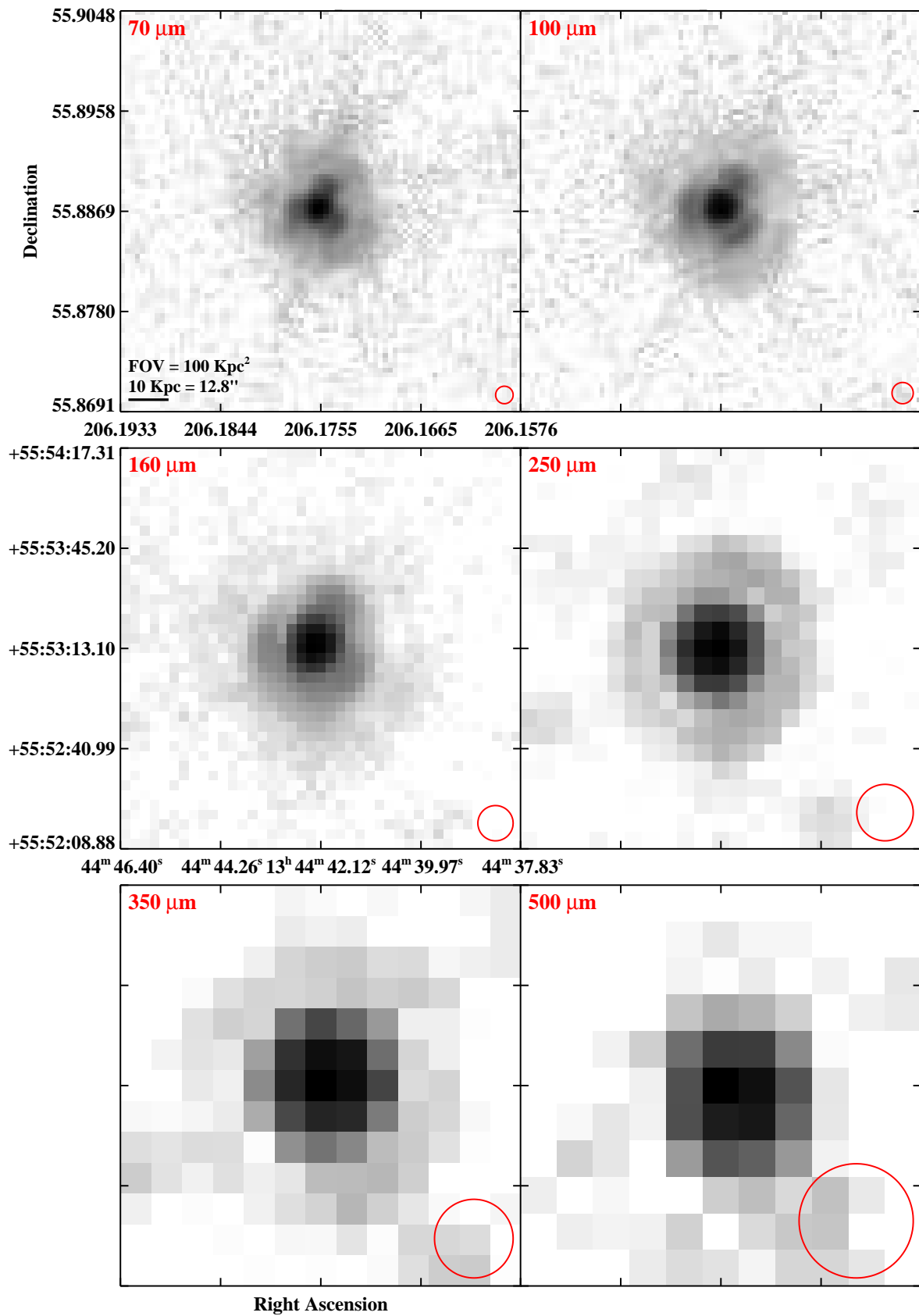


Fig. 3.— Continued (page 126 of 209).

IRAS F13470+3530 (UGC 08739)

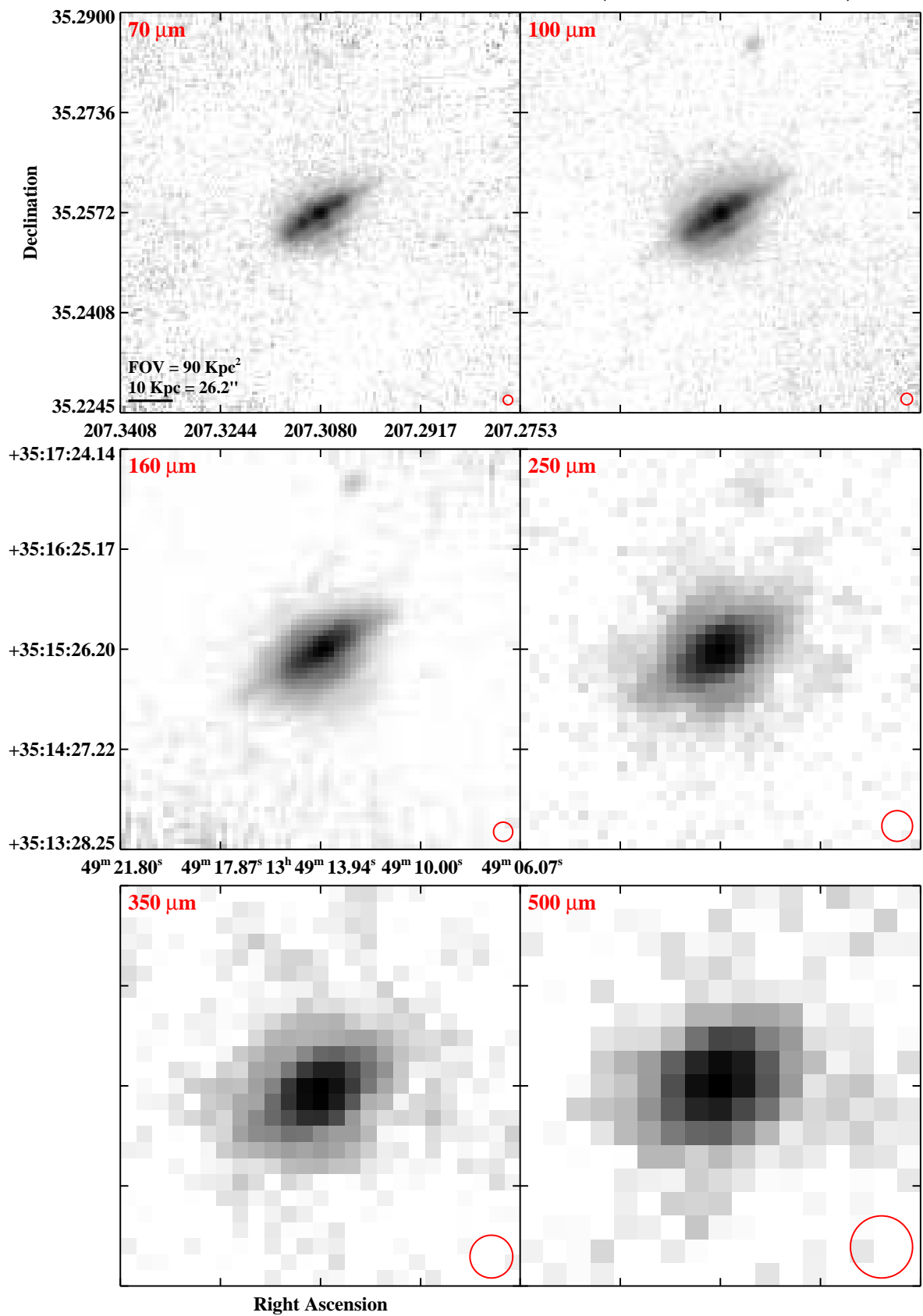


Fig. 3.— Continued (page 127 of 209).

IRAS F13478–4848 (ESO 221–IG010)

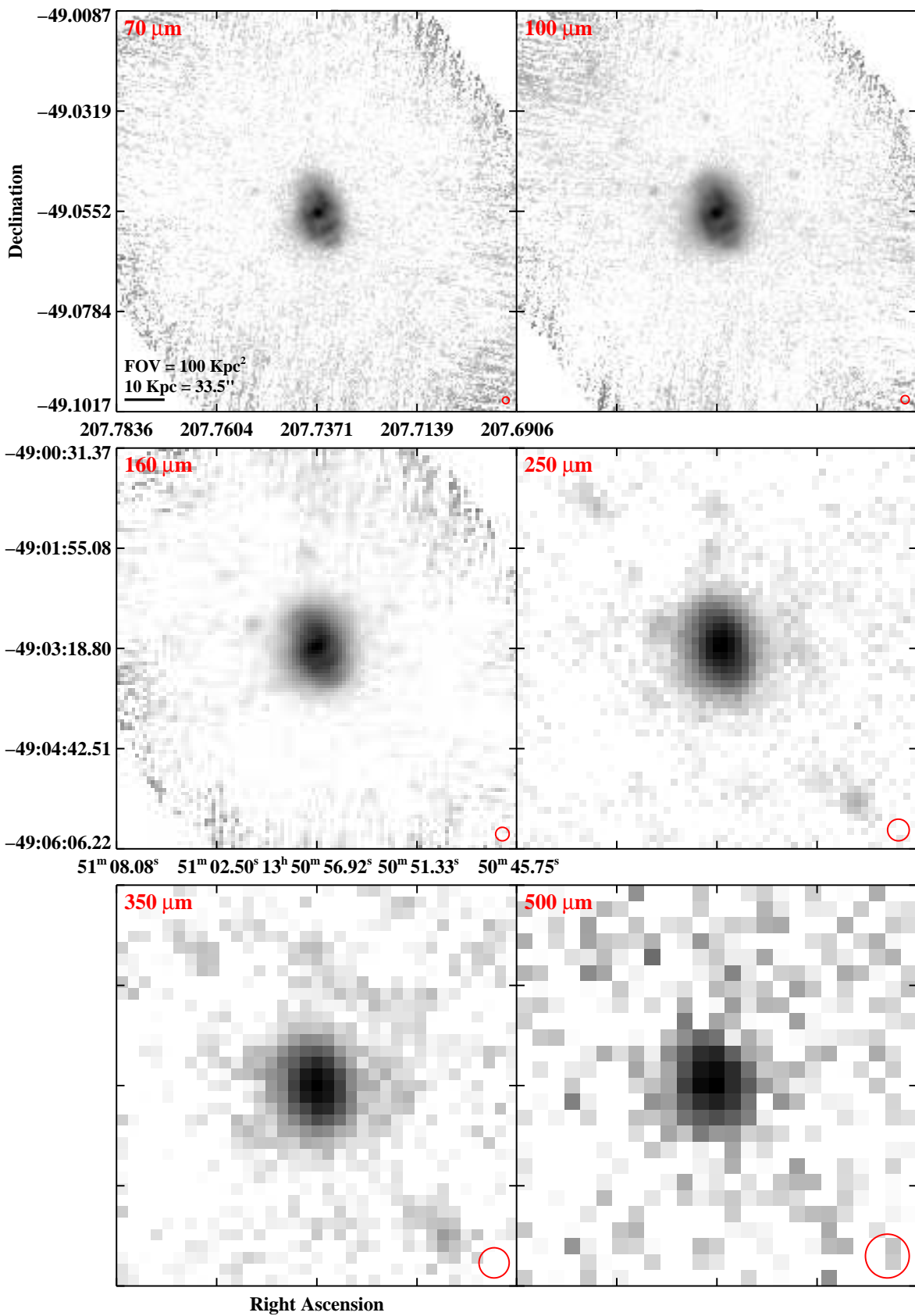


Fig. 3.— Continued (page 128 of 209).

IRAS F13497+0220 (NGC 5331)

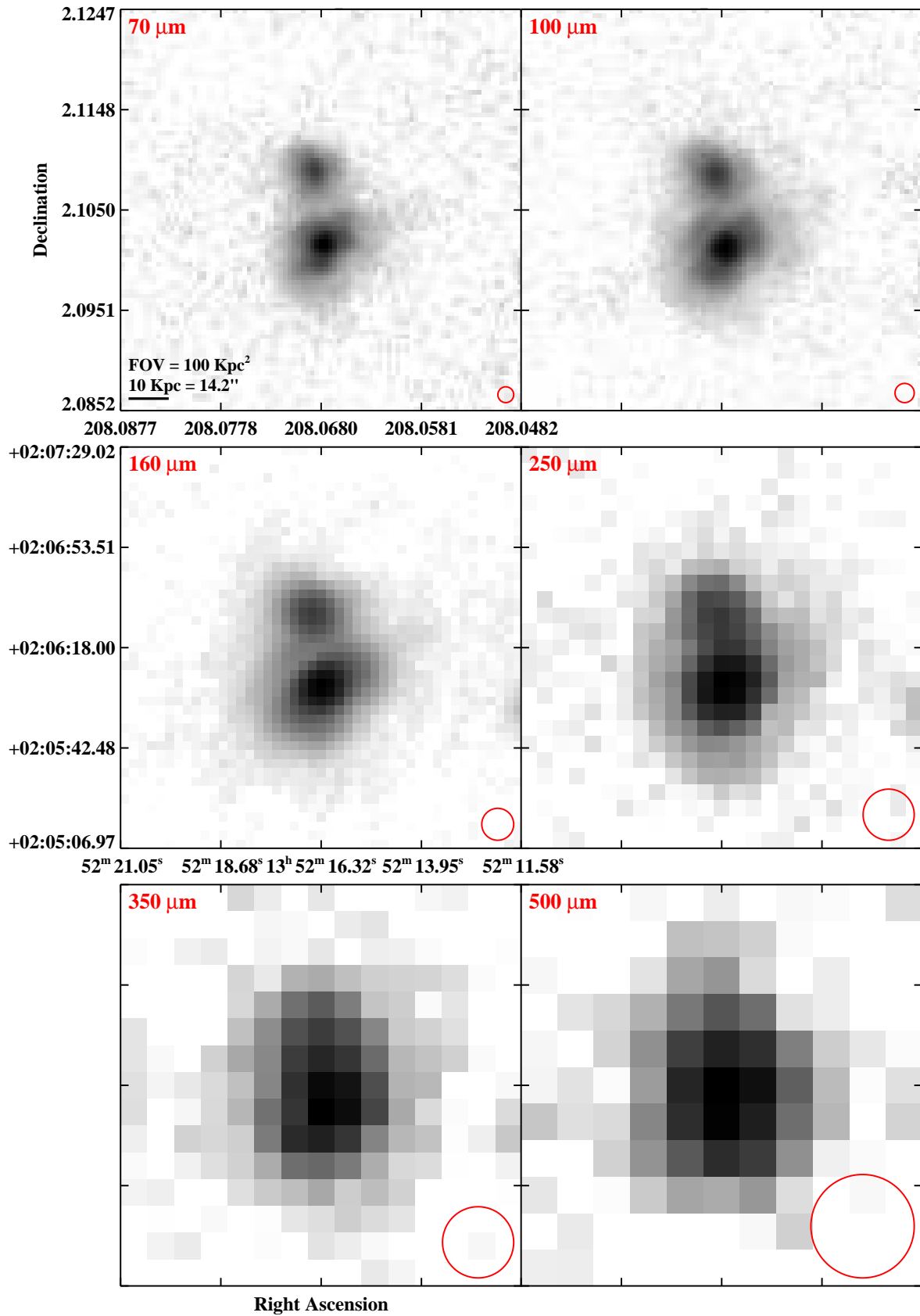


Fig. 3.— Continued (page 129 of 209).

IRAS F13564+3741 (Arp 84)

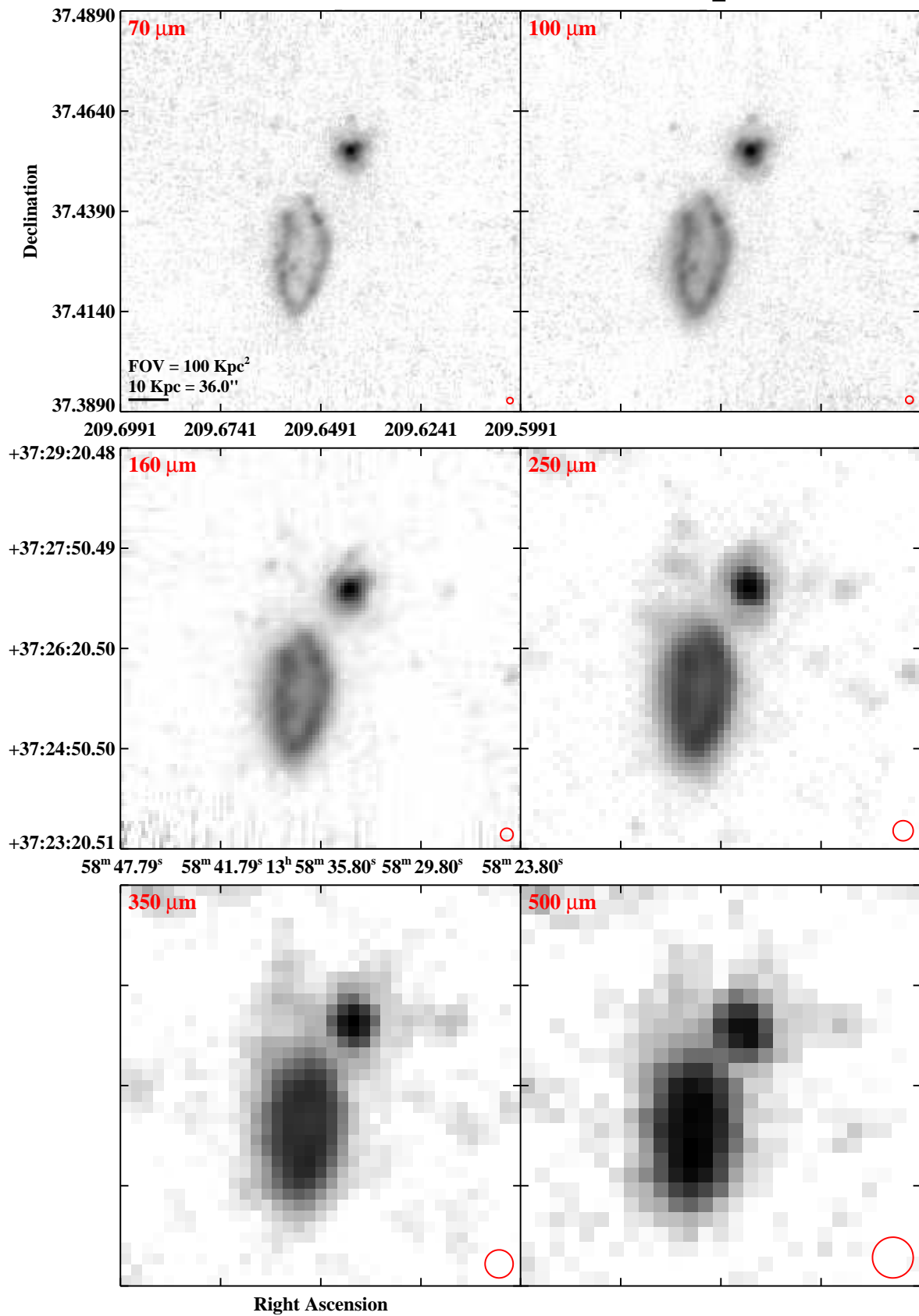


Fig. 3.— Continued (page 130 of 209).

IRAS F14179+4927 (CGCG 247-020)

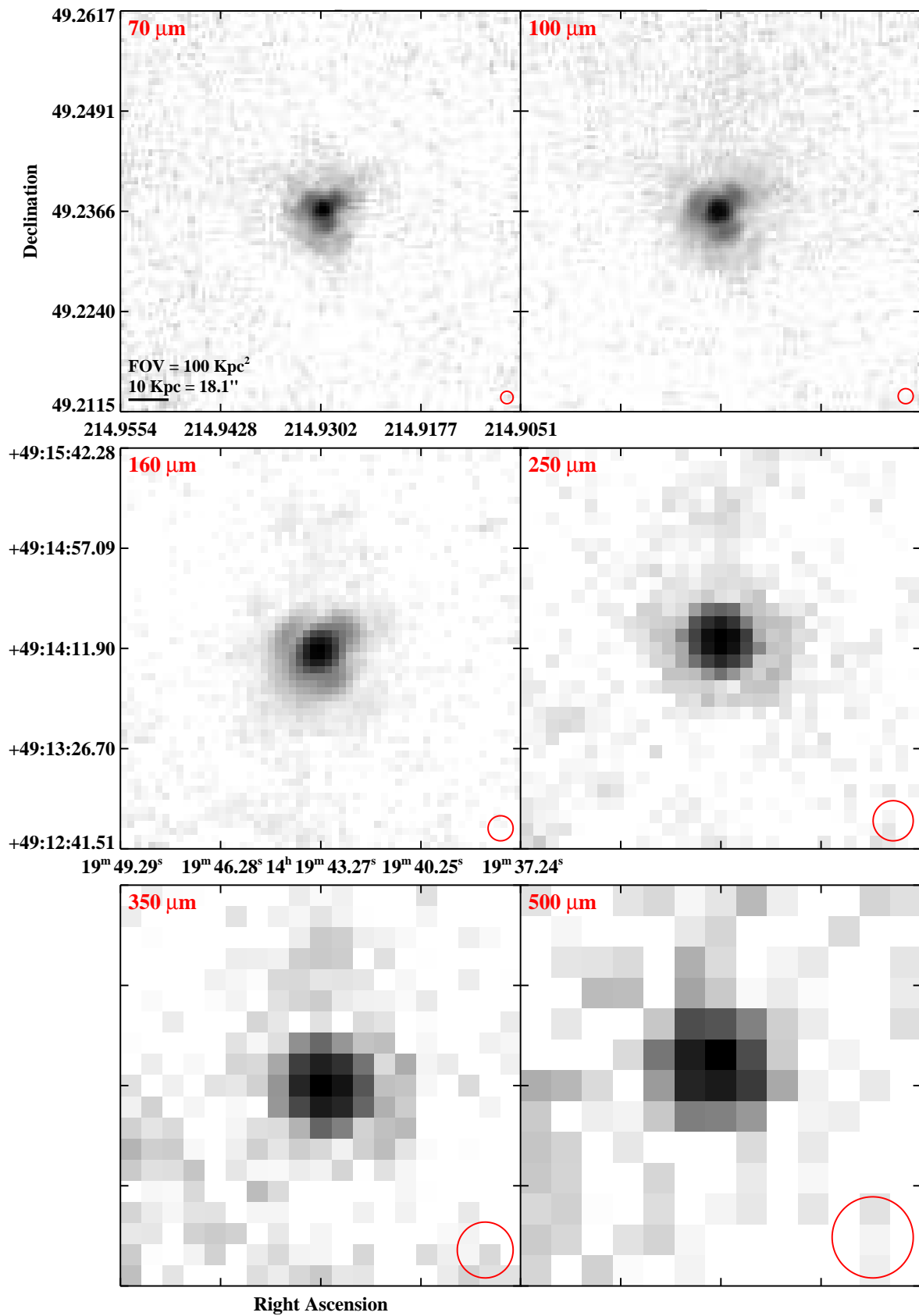


Fig. 3.— Continued (page 131 of 209).

IRAS F14280+3126 (NGC 5653)

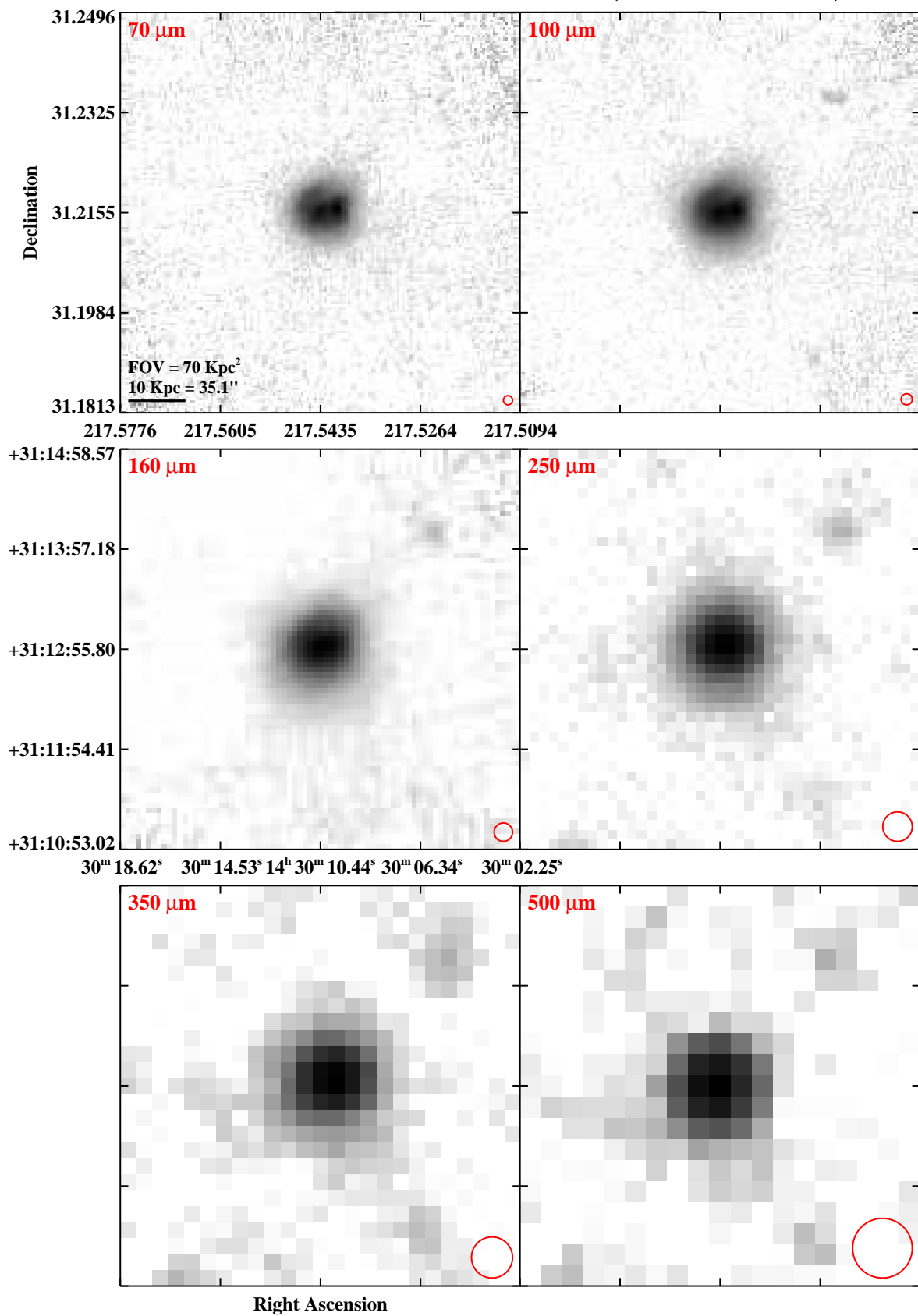


Fig. 3.— Continued (page 132 of 209).

IRAS F14348–1447

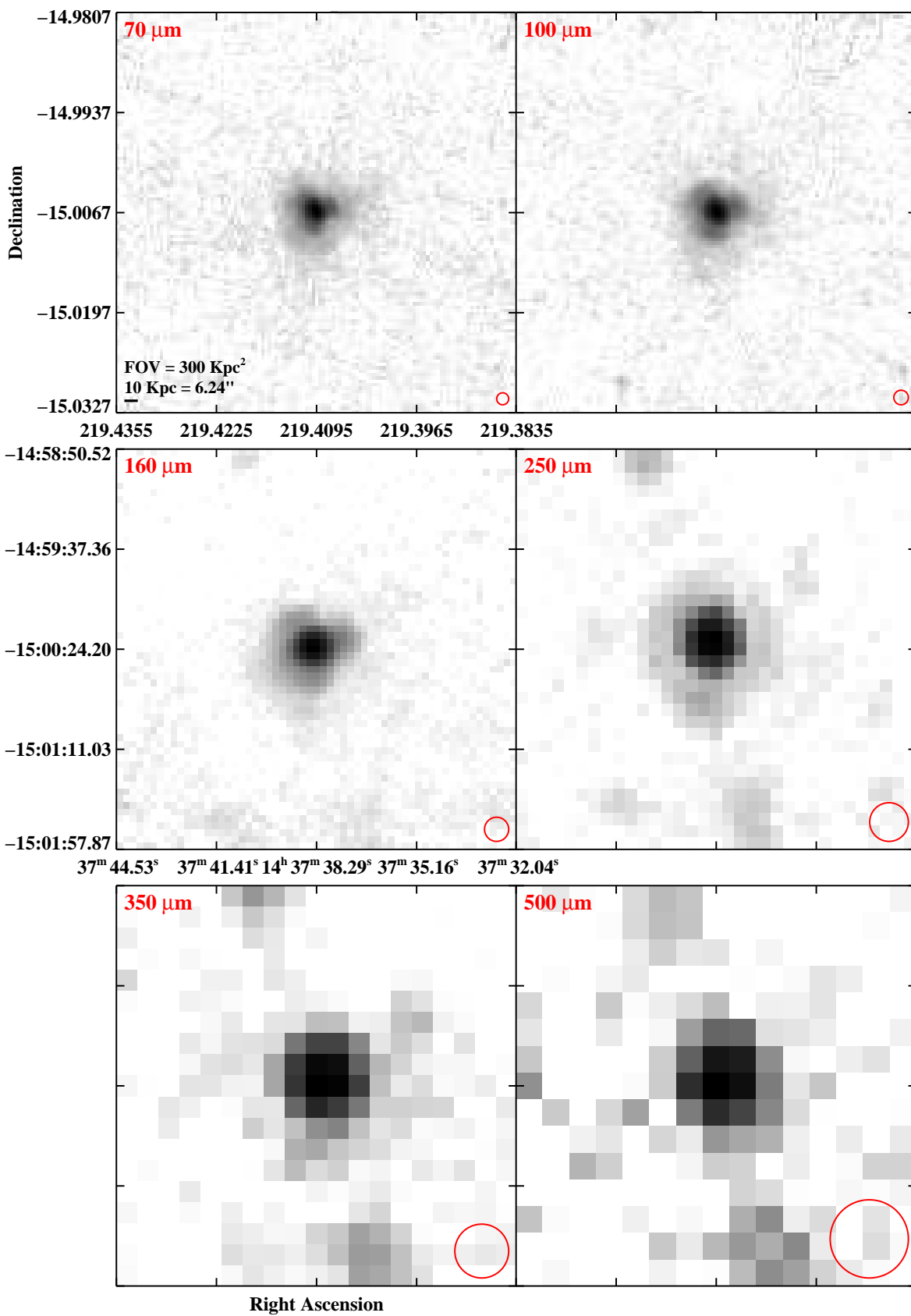


Fig. 3.— Continued (page 133 of 209).

IRAS F14378–3651

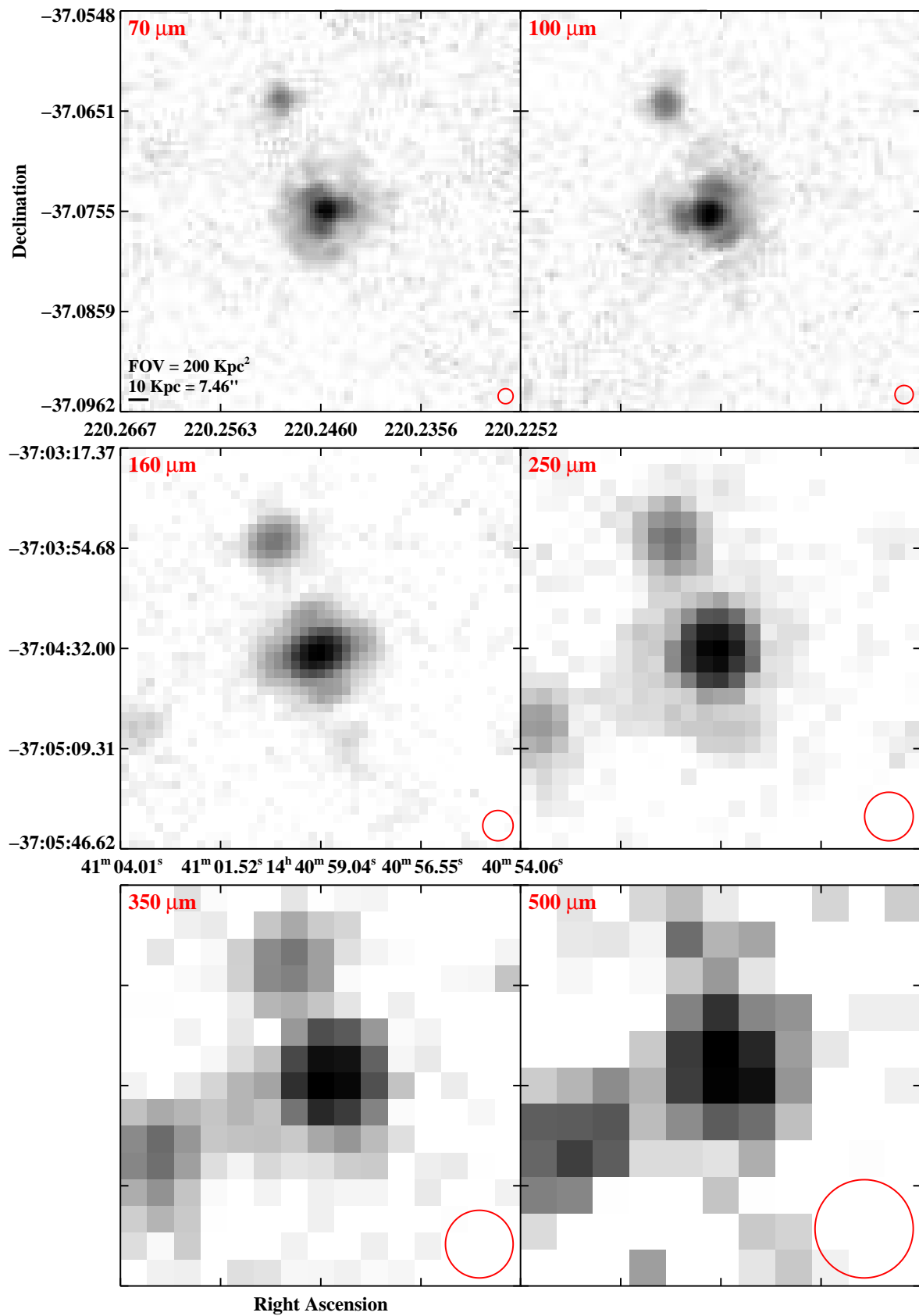


Fig. 3.— Continued (page 134 of 209).

IRAS F14423–2039 (NGC 5734)

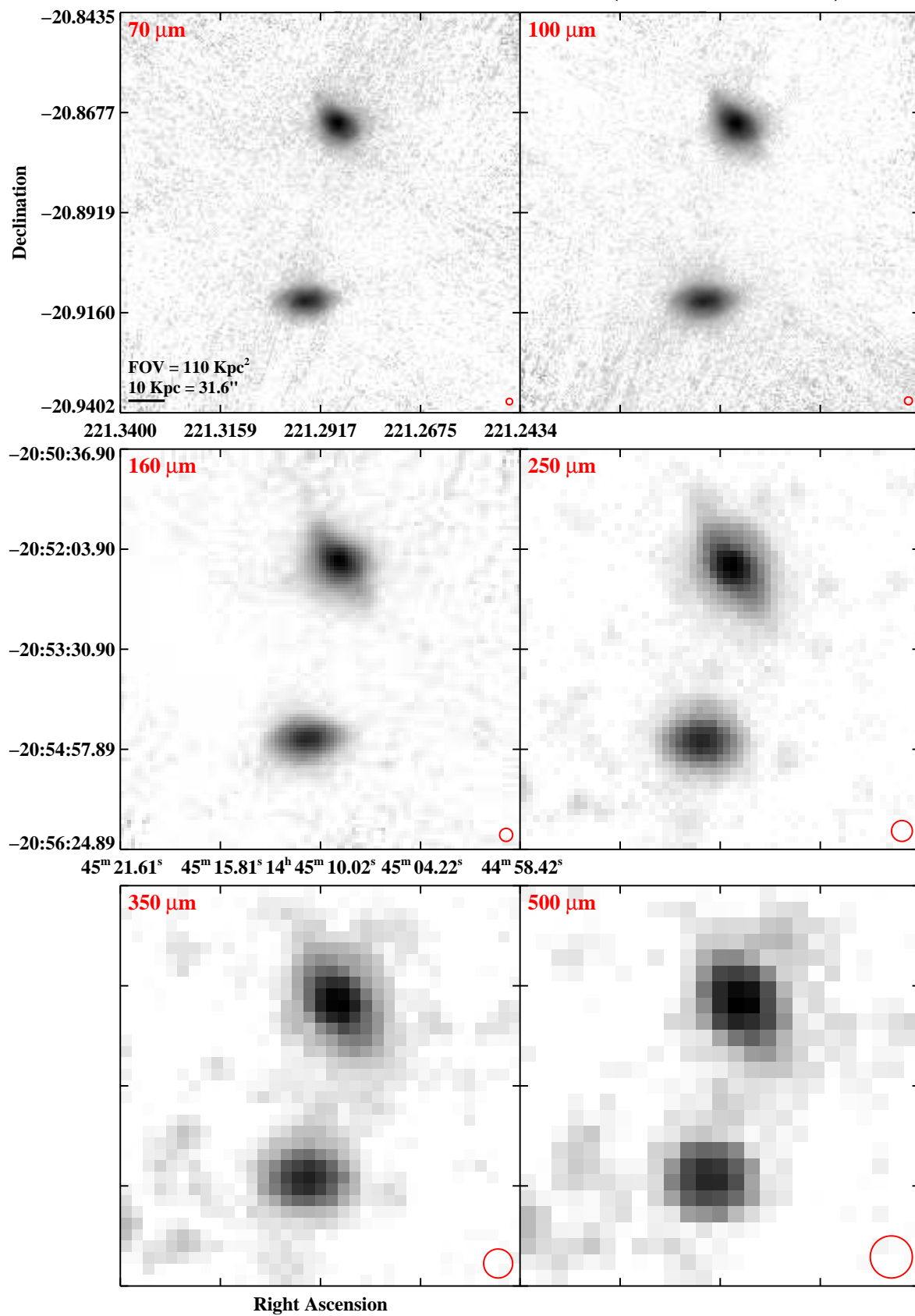


Fig. 3.— Continued (page 135 of 209).

IRAS F14547+2449 (VV 340a/Arp 302)

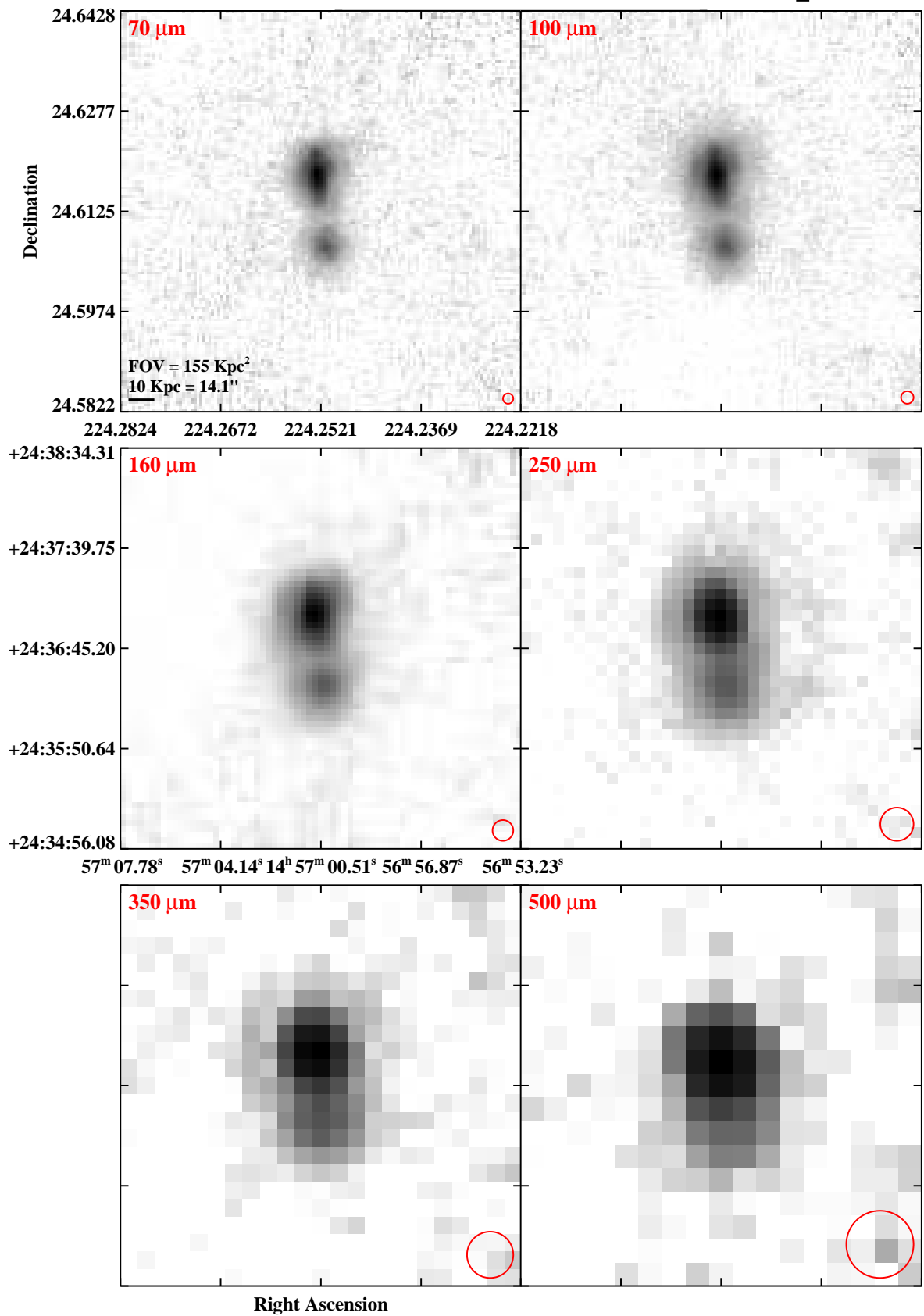


Fig. 3.— Continued (page 136 of 209).

IRAS F14544–4255 (IC 4518A/B)

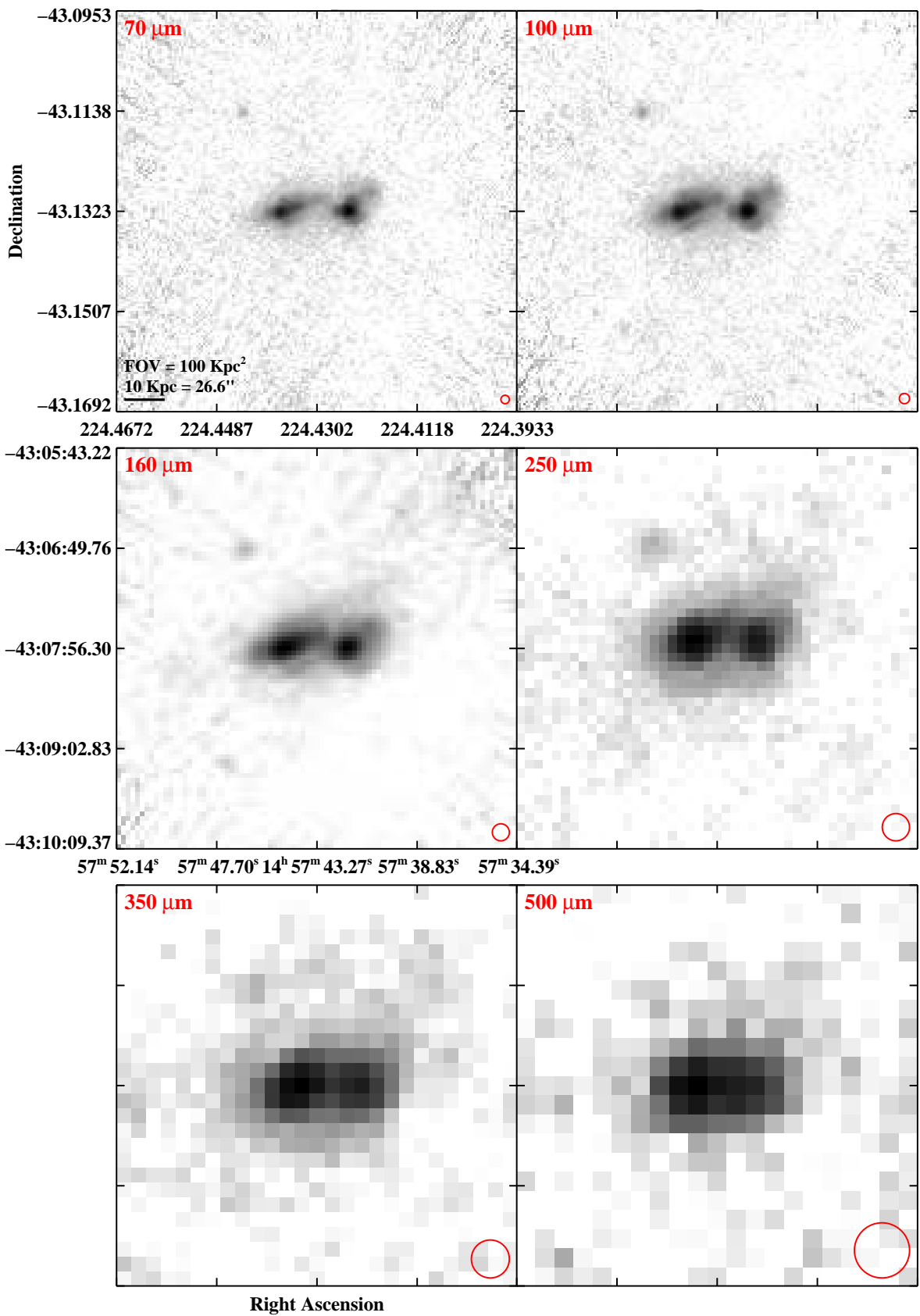


Fig. 3.— Continued (page 137 of 209).

IRAS F15107+0724 (CGCG 049–057)

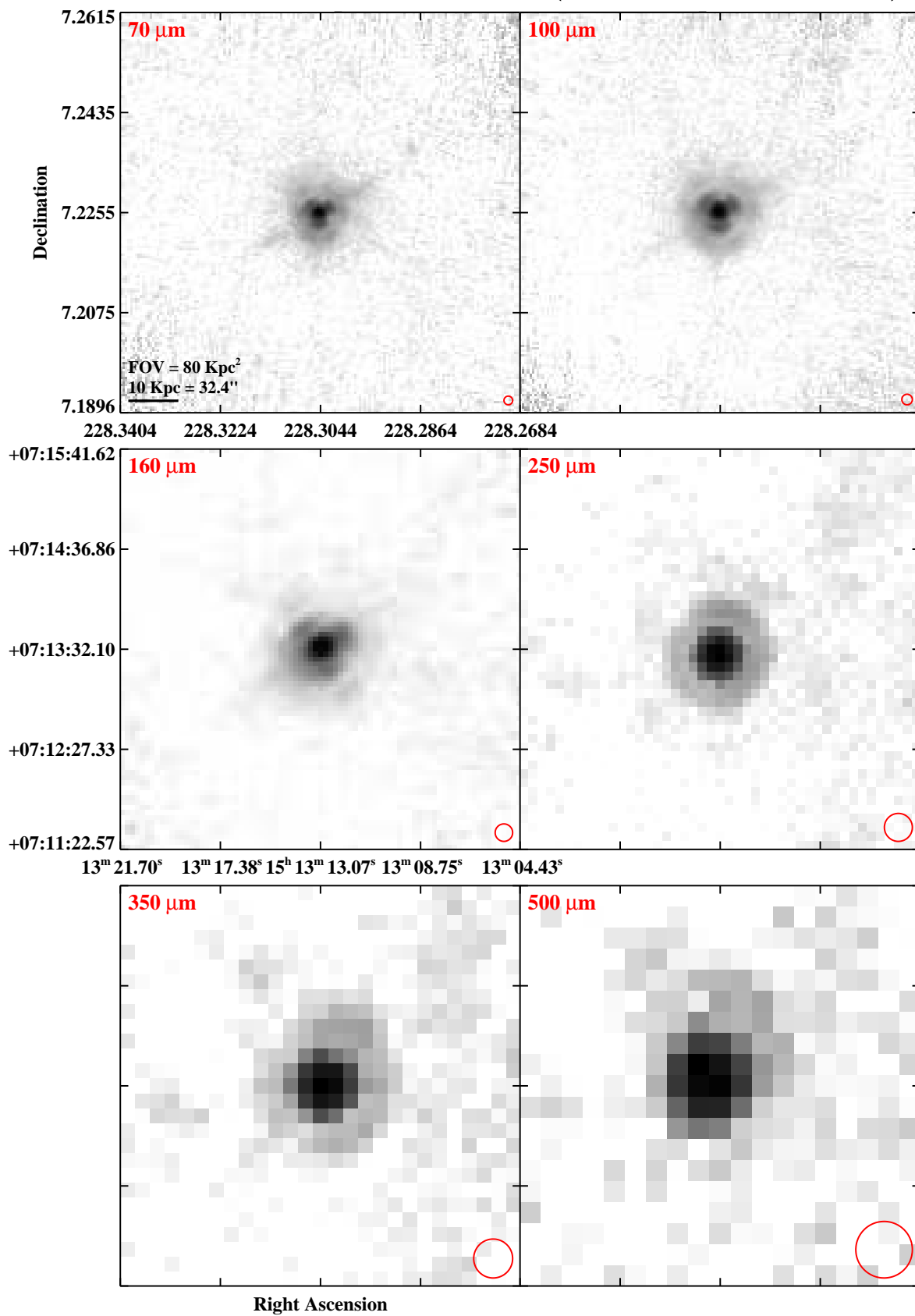


Fig. 3.— Continued (page 138 of 209).

IRAS F15163+4255 (VV 705)

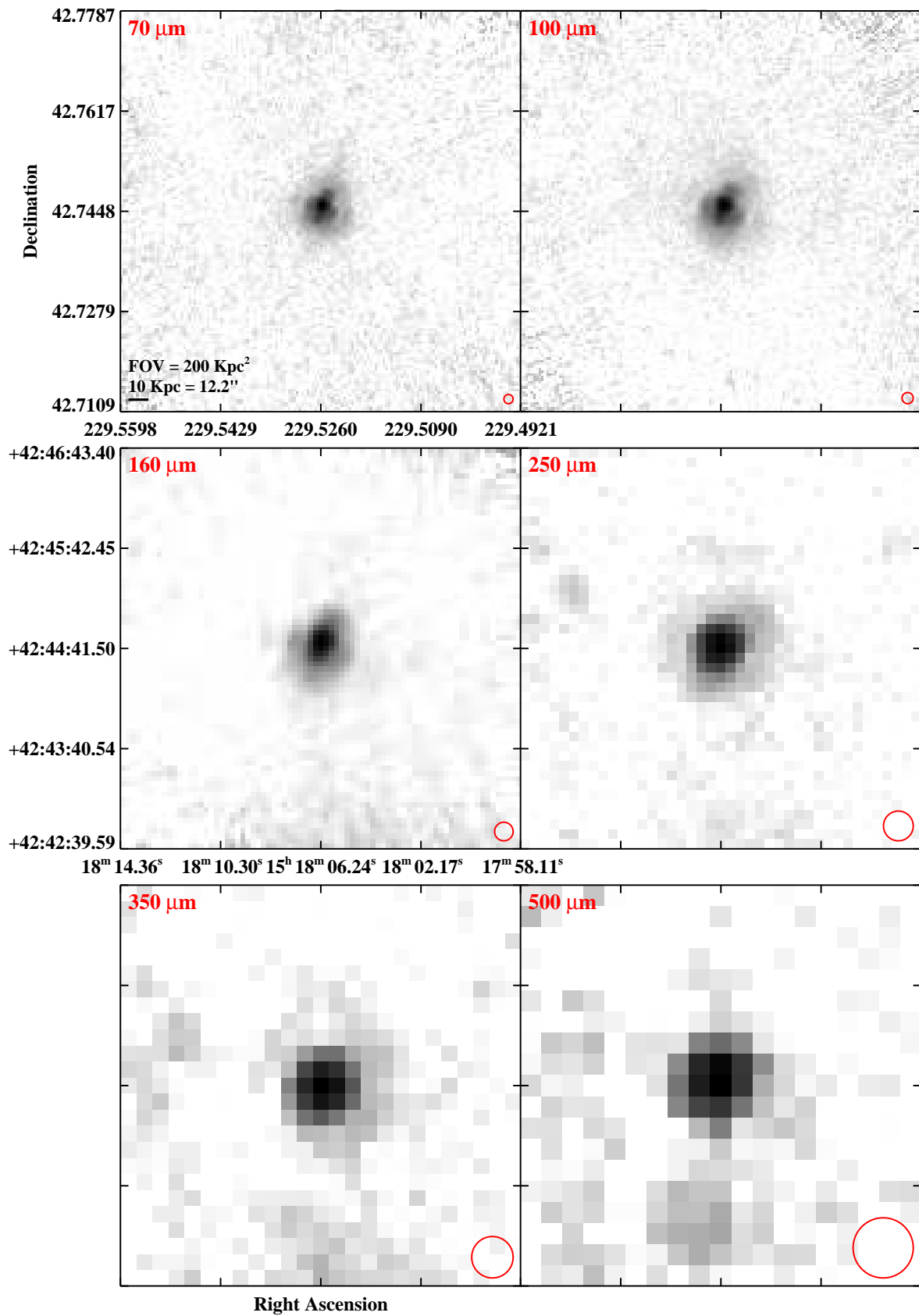


Fig. 3.— Continued (page 139 of 209).

IRAS 15206–6256 (ESO 099–G004)

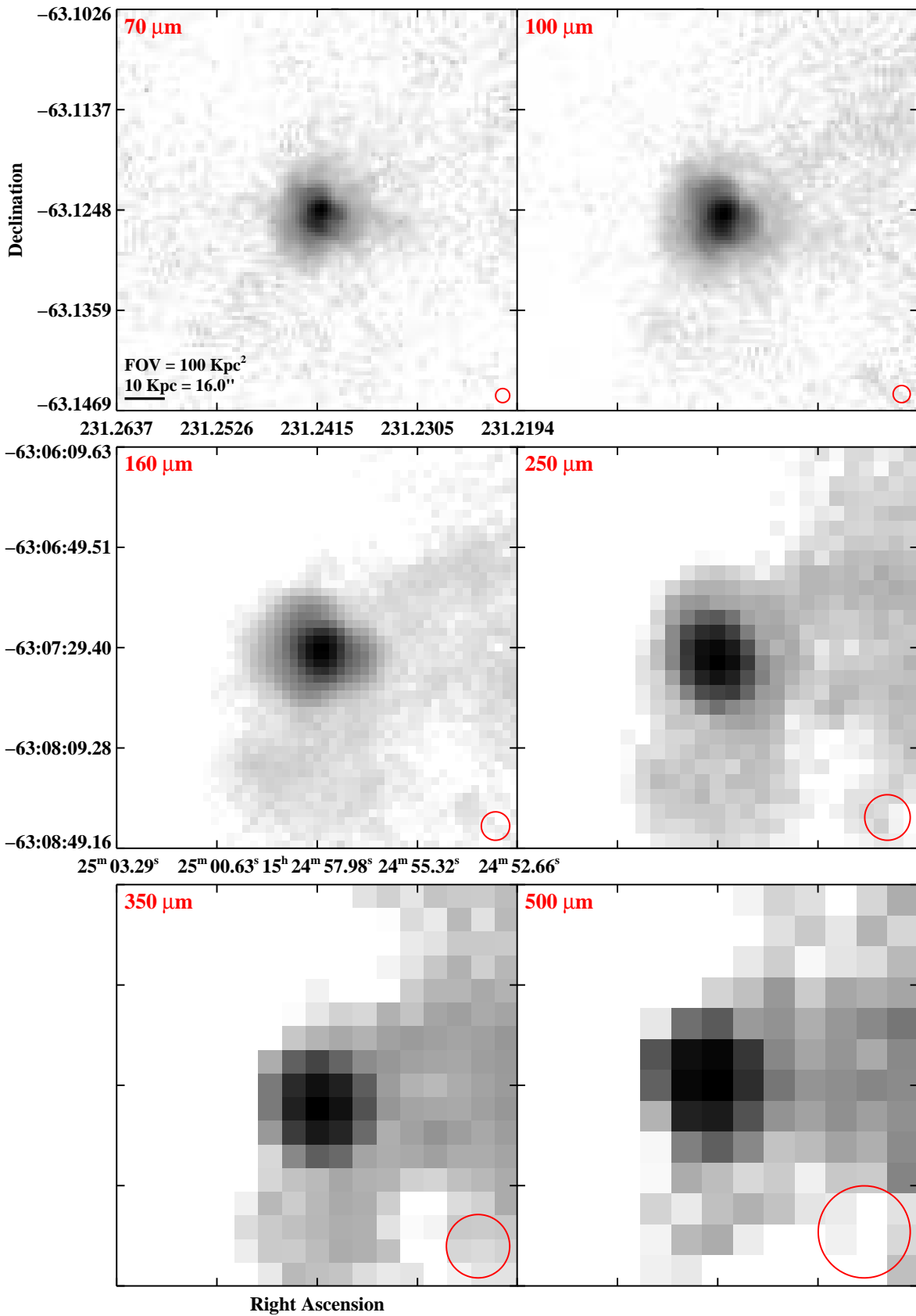


Fig. 3.— Continued (page 140 of 209).

IRAS F15250+3608

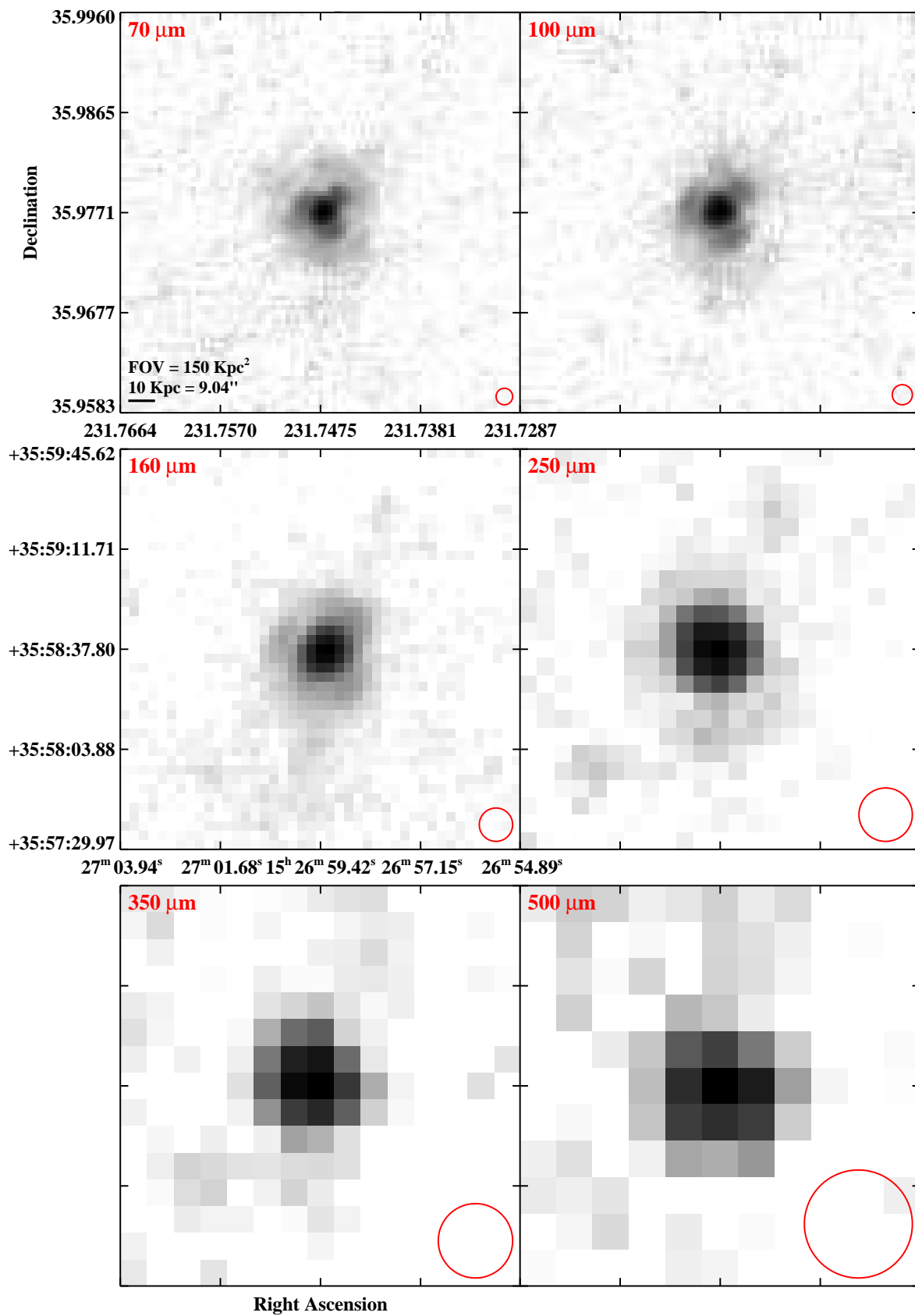


Fig. 3.— Continued (page 141 of 209).

IRAS F15276+1309 (NGC 5936)

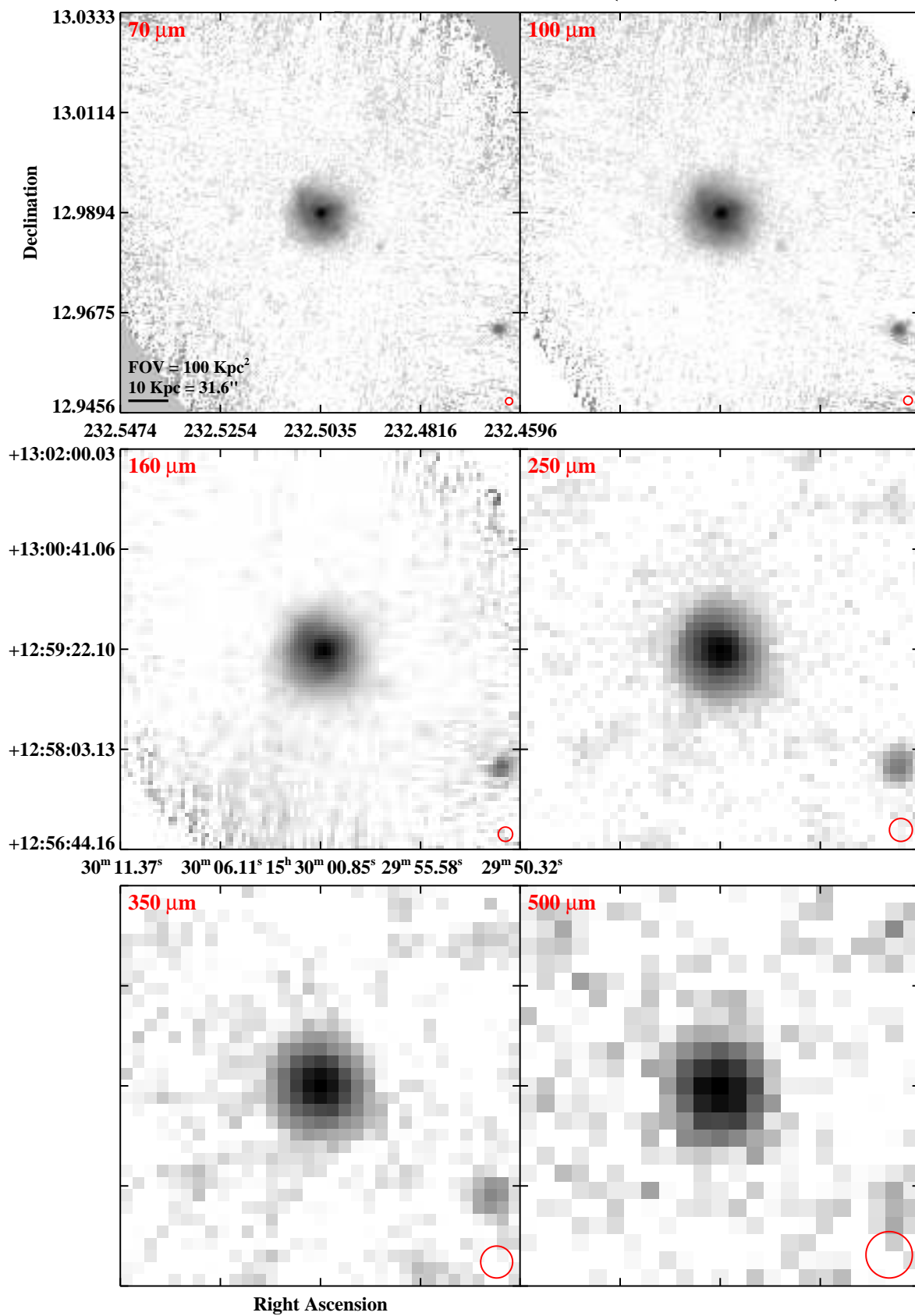


Fig. 3.— Continued (page 142 of 209).

IRAS F15327+2340 (Arp 220/UGC 09913)

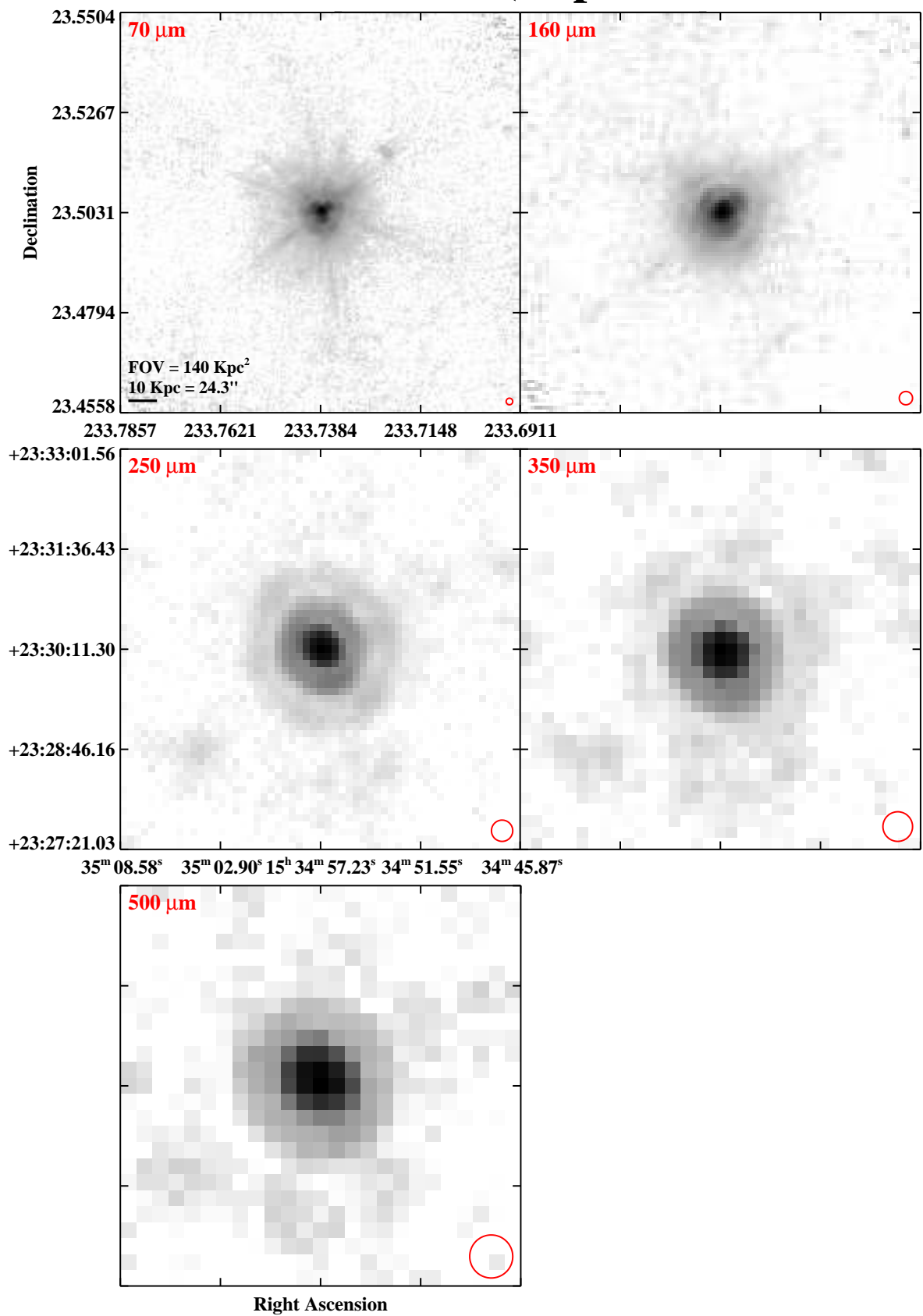


Fig. 3.— Continued (page 143 of 209).

IRAS F15437+0234 (NGC 5990)

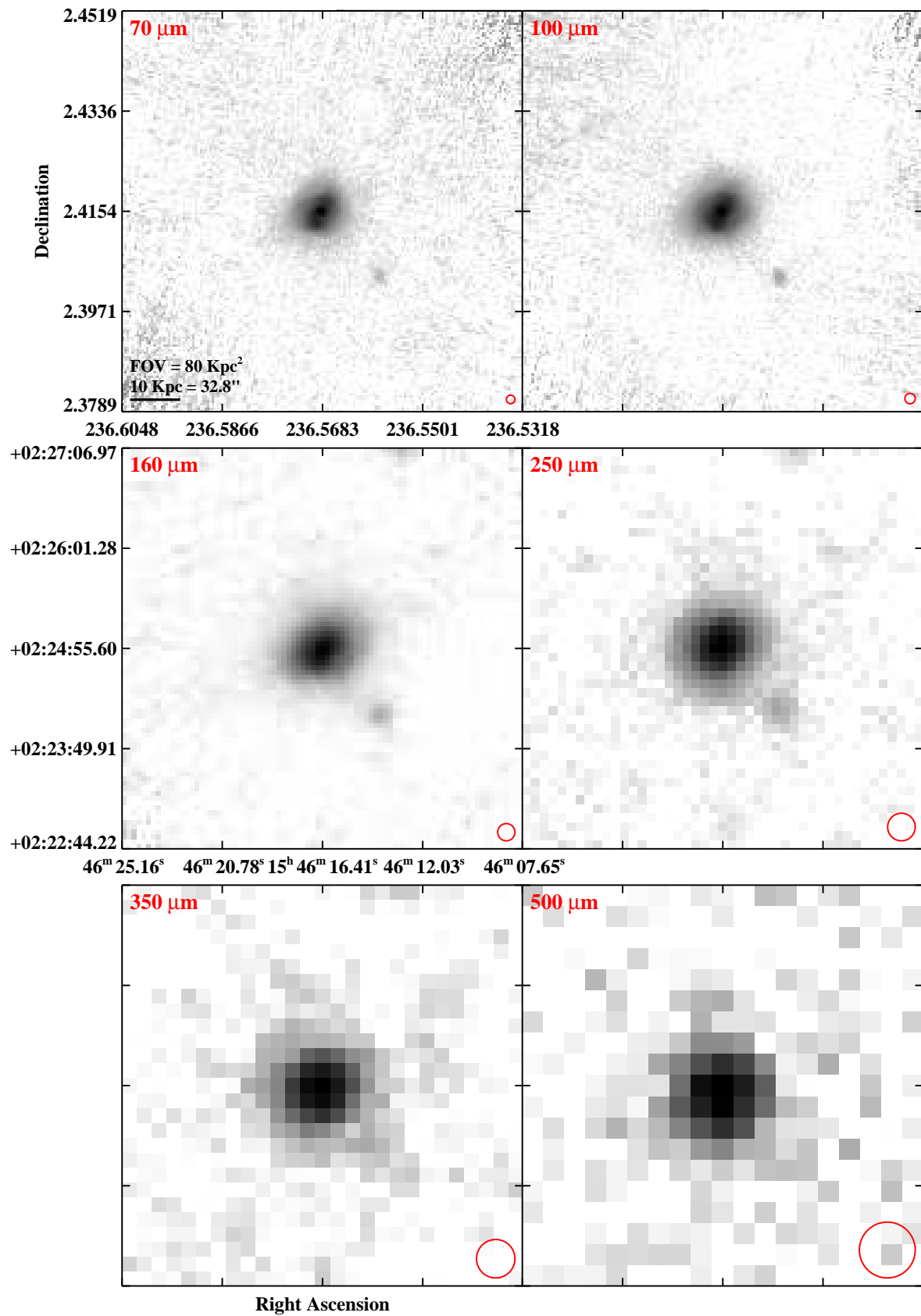


Fig. 3.— Continued (page 144 of 209).

IRAS F16030+2040 (NGC 6052)

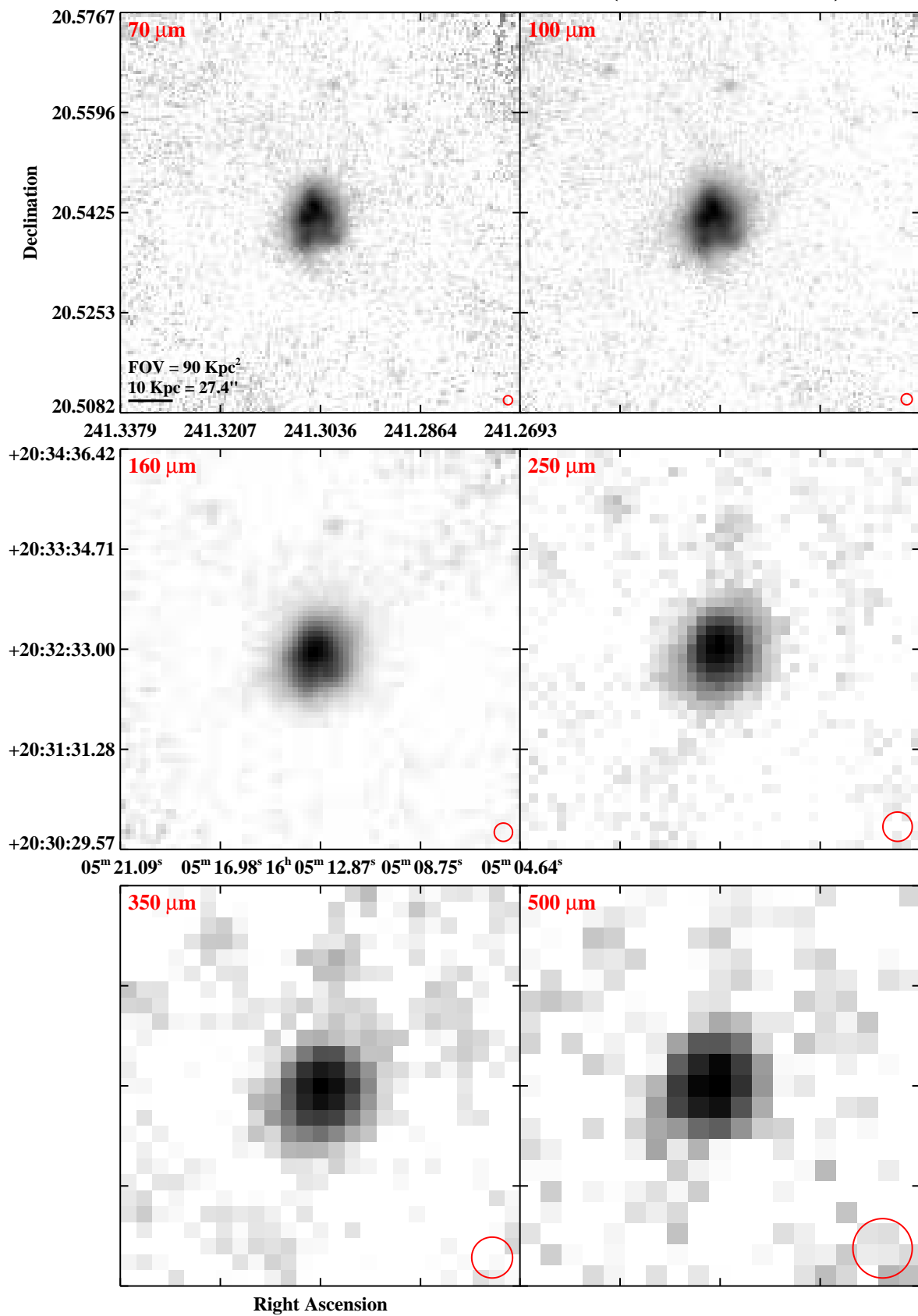


Fig. 3.— Continued (page 145 of 209).

IRAS F16104+5235 (NGC 6090)

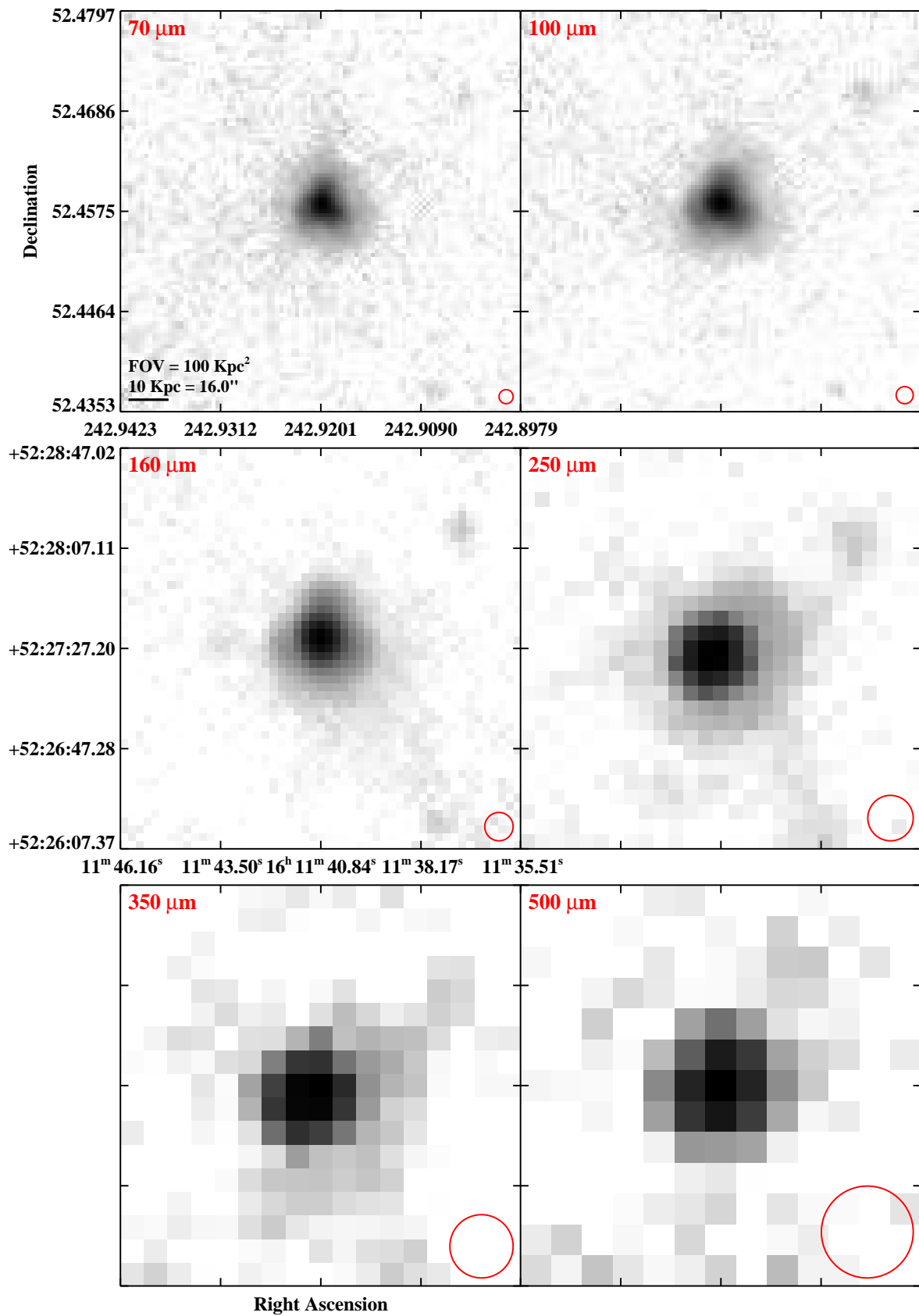


Fig. 3.— Continued (page 146 of 209).

IRAS F16164–0746

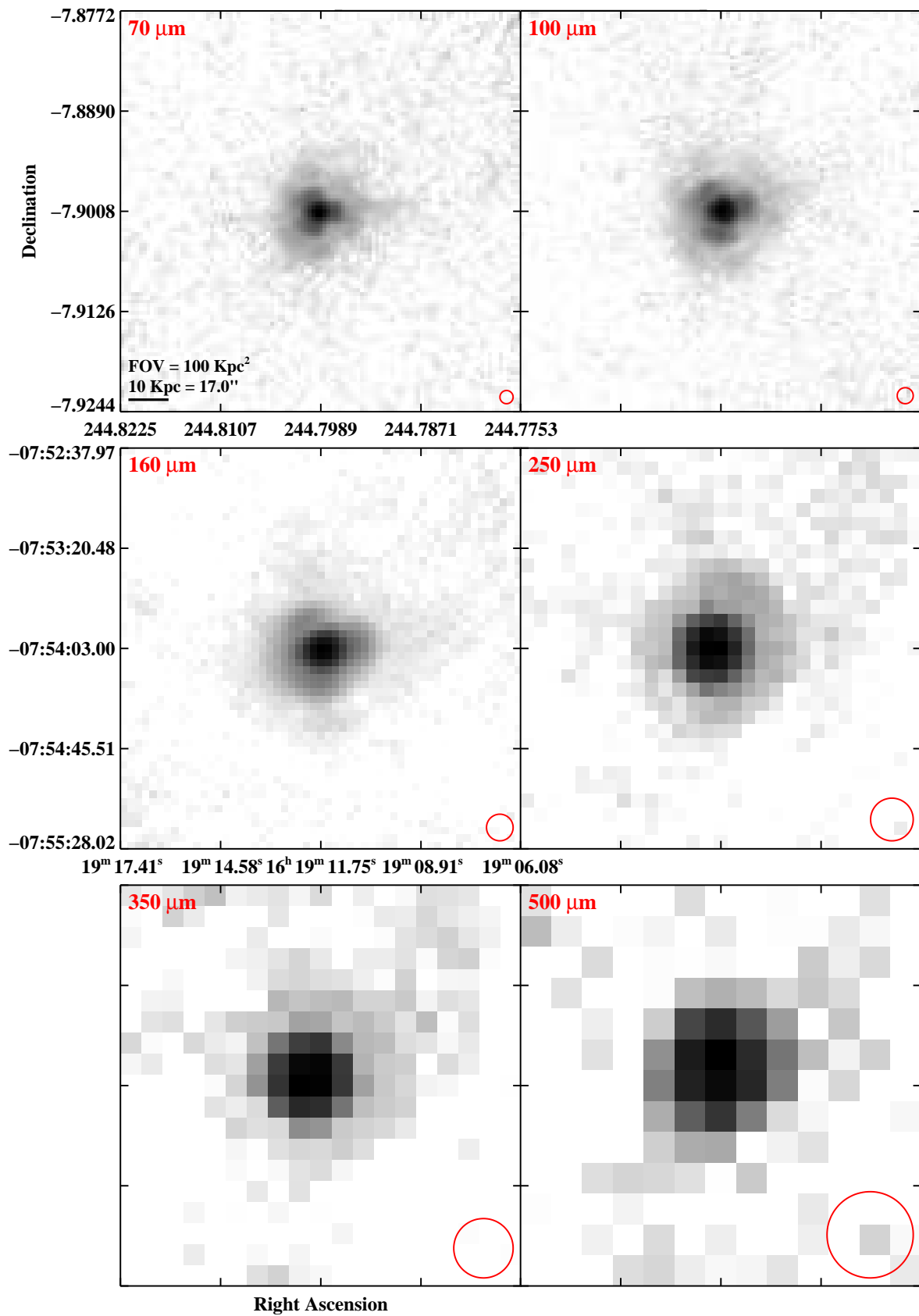


Fig. 3.— Continued (page 147 of 209).

IRAS F16284+0411 (CGCG 052-037)

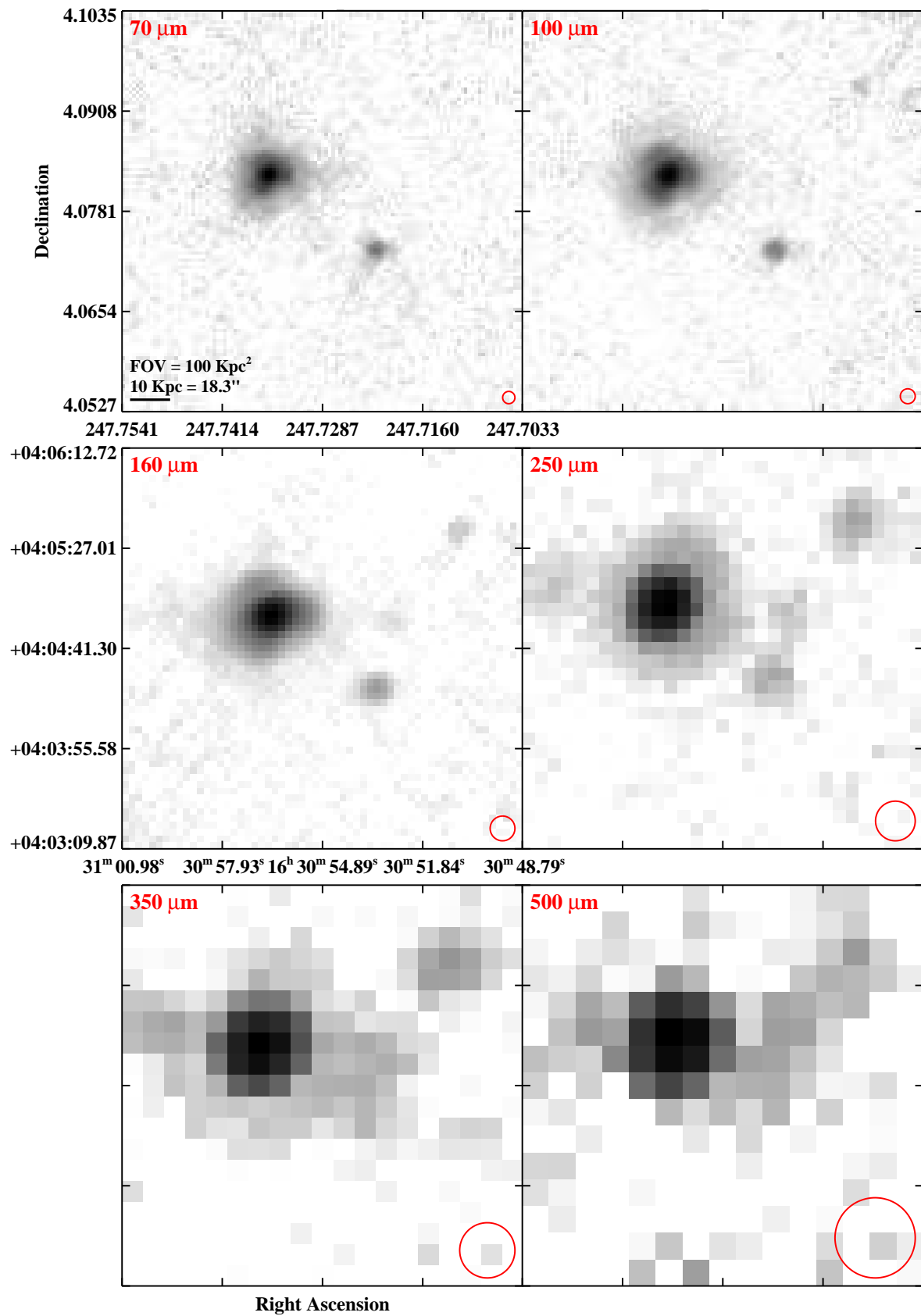


Fig. 3.— Continued (page 148 of 209).

IRAS 16304–6030 (NGC 6156)

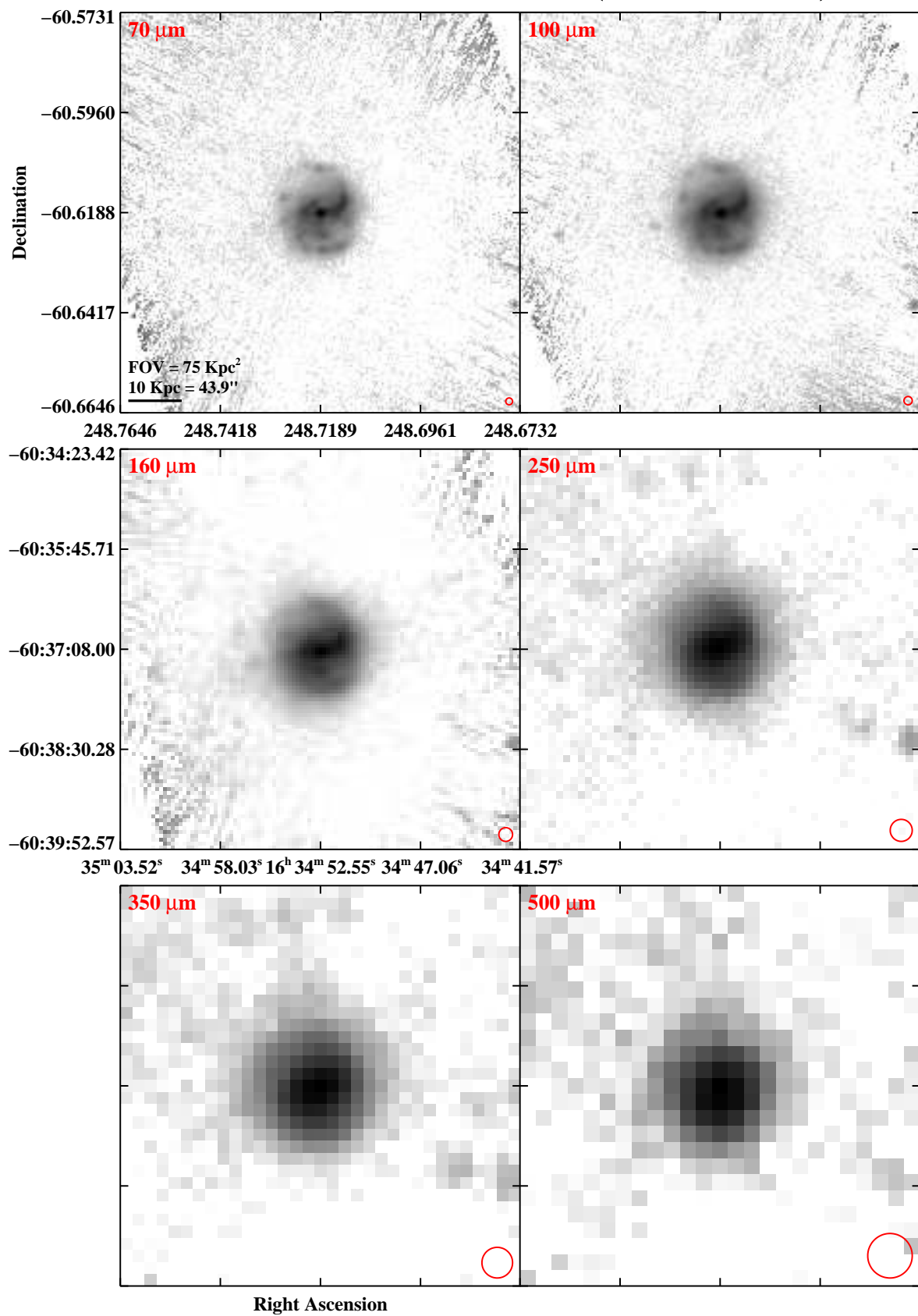


Fig. 3.— Continued (page 149 of 209).

IRAS F16330–6820 (ESO 069–IG006)

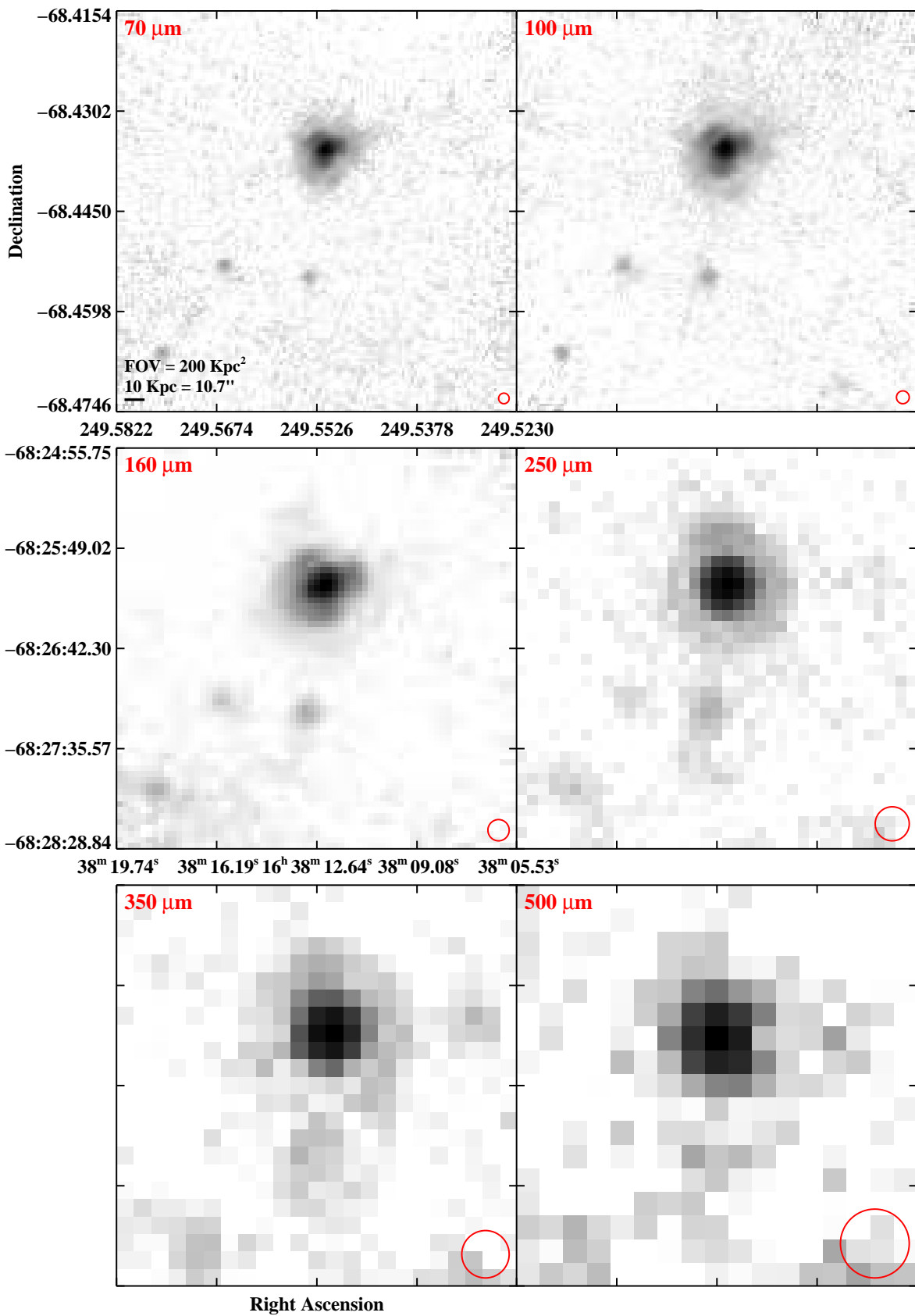


Fig. 3.— Continued (page 150 of 209).

IRAS F16399–0937

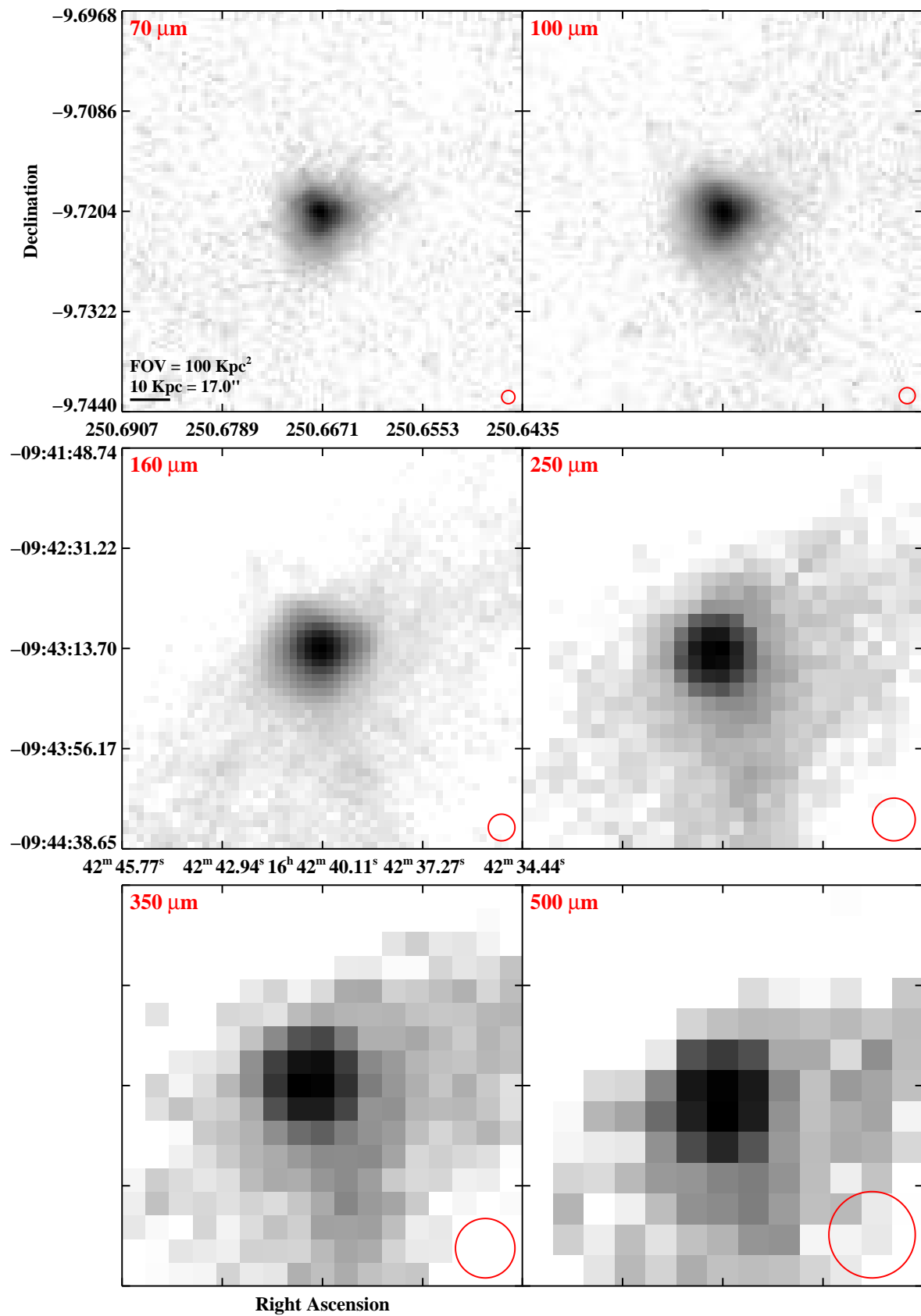


Fig. 3.— Continued (page 151 of 209).

IRAS F16443–2915 (ESO 453–G005)

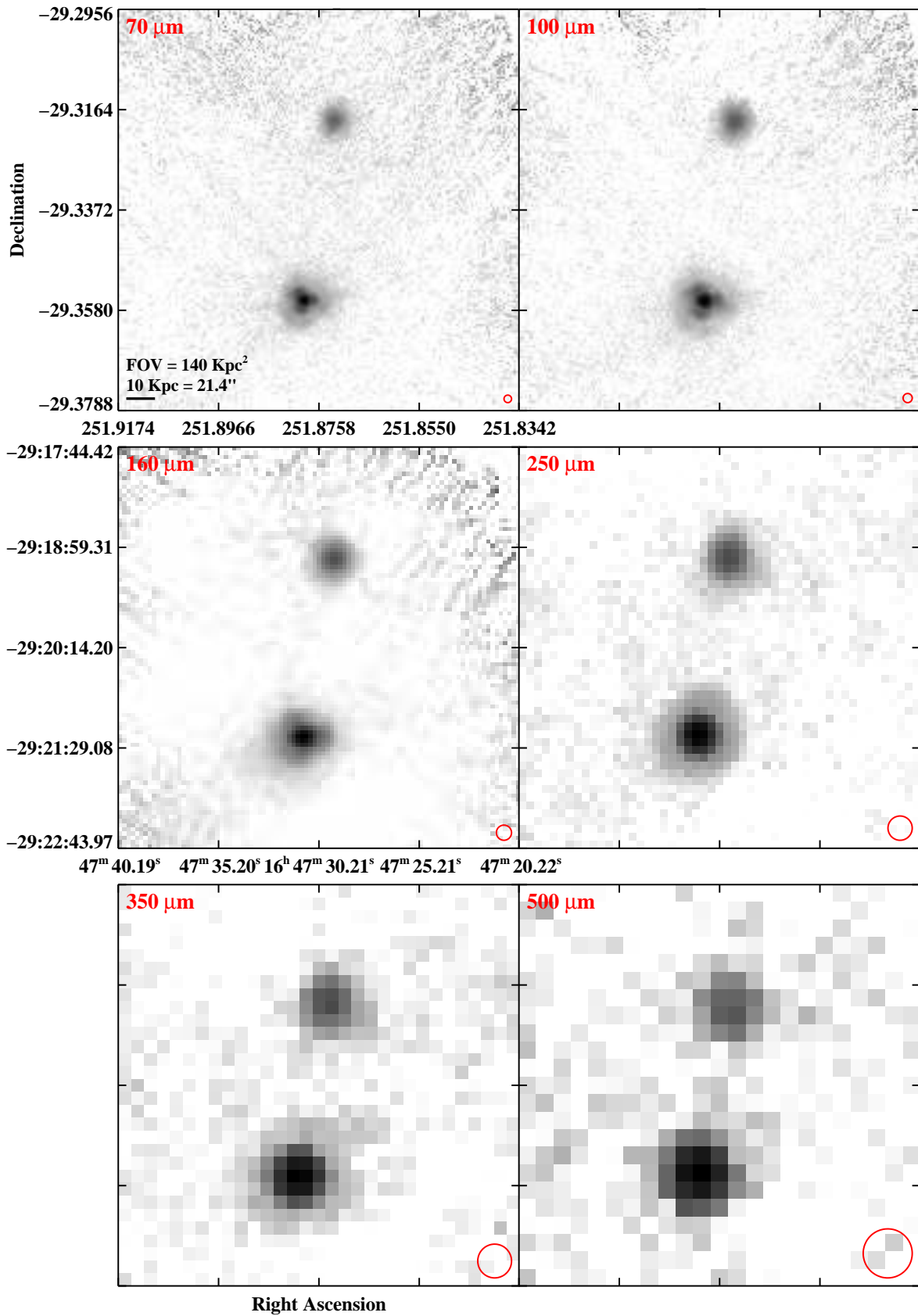
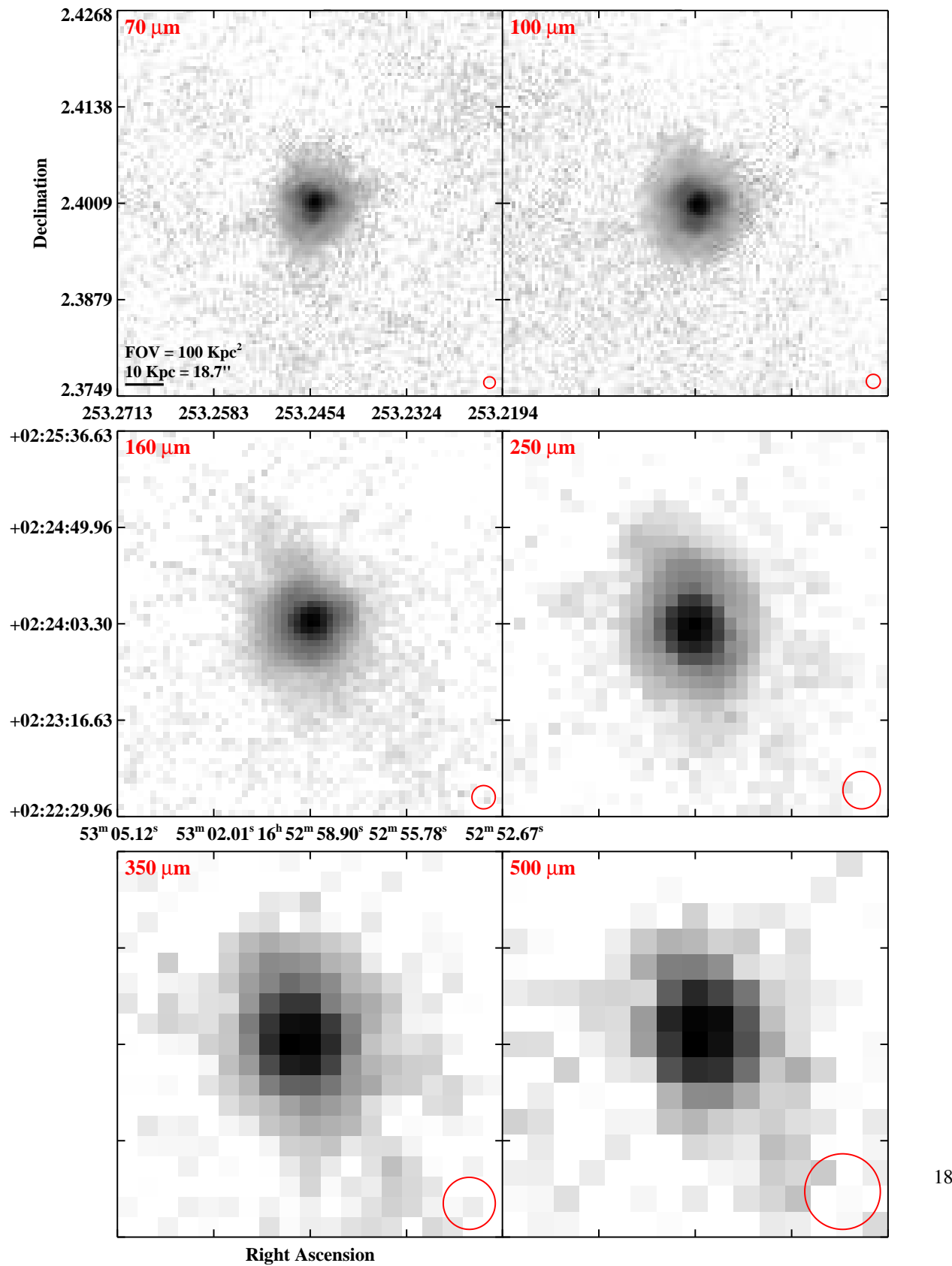


Fig. 3.— Continued (page 152 of 209).

IRAS F16504+0228 (NGC 6240)



180

Fig. 3.— Continued (page 153 of 209).

IRAS F16516–0948

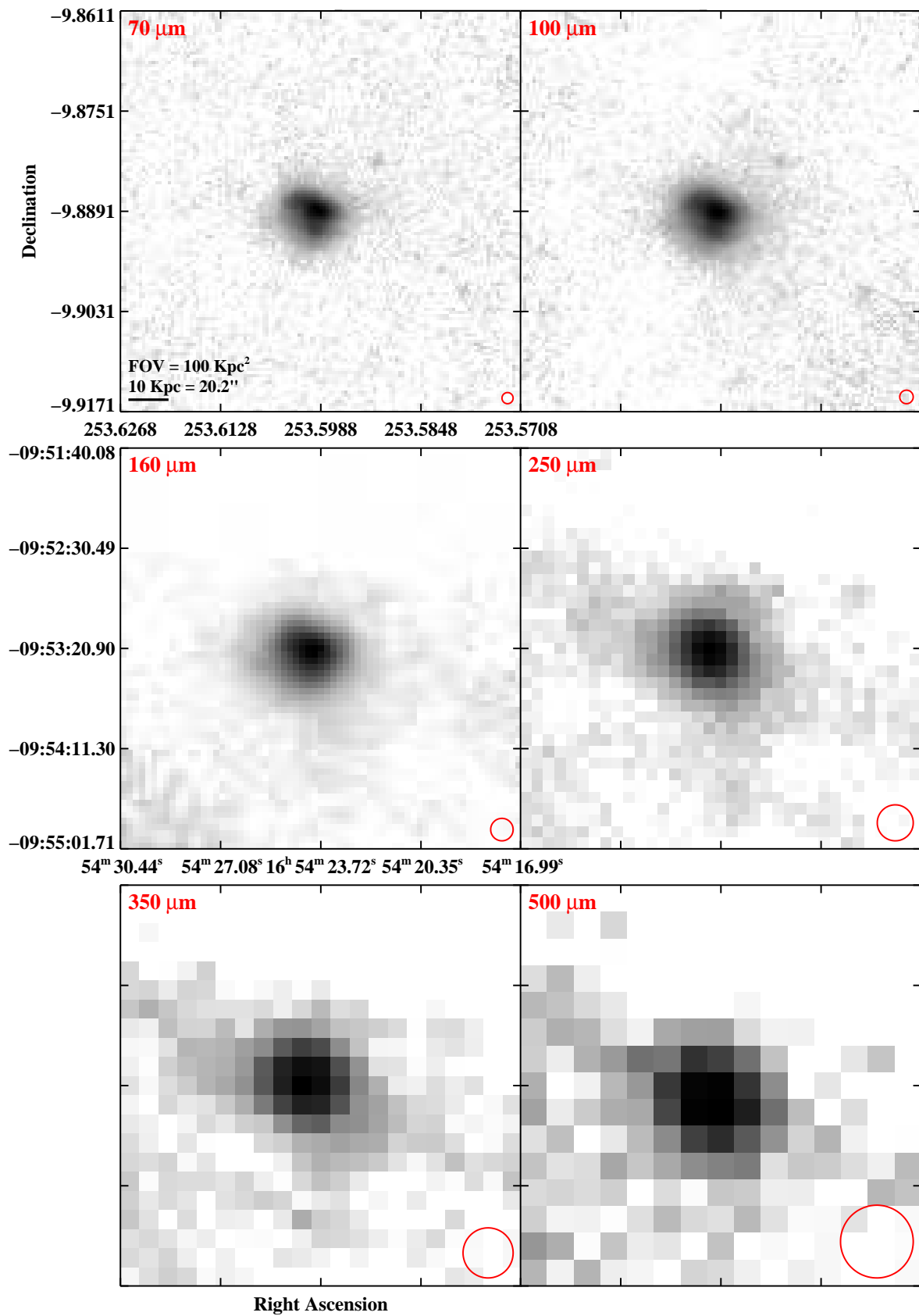


Fig. 3.— Continued (page 154 of 209).

IRAS F16577+5900 (Arp 293)

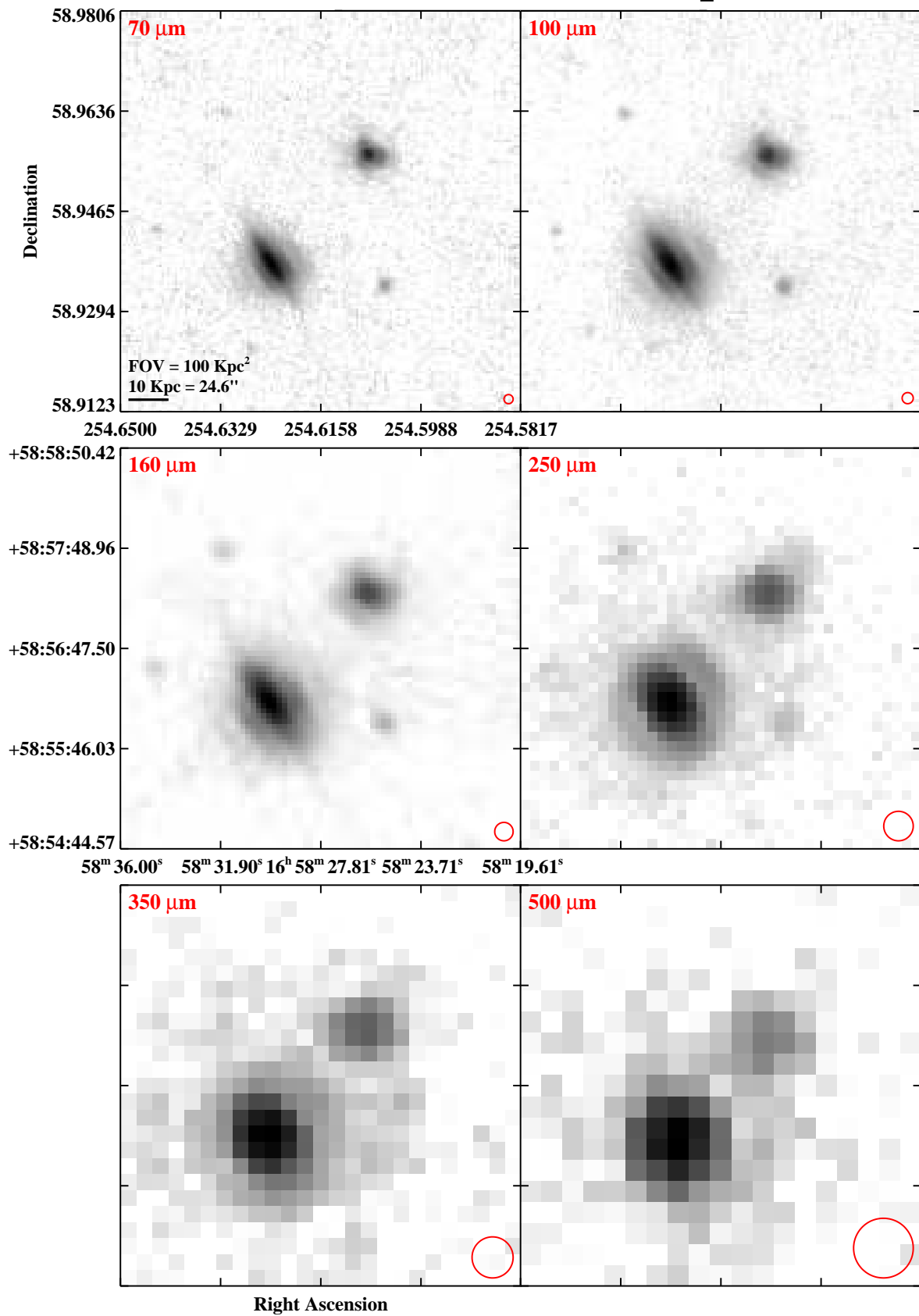


Fig. 3.— Continued (page 155 of 209).

IRAS F17132+5313

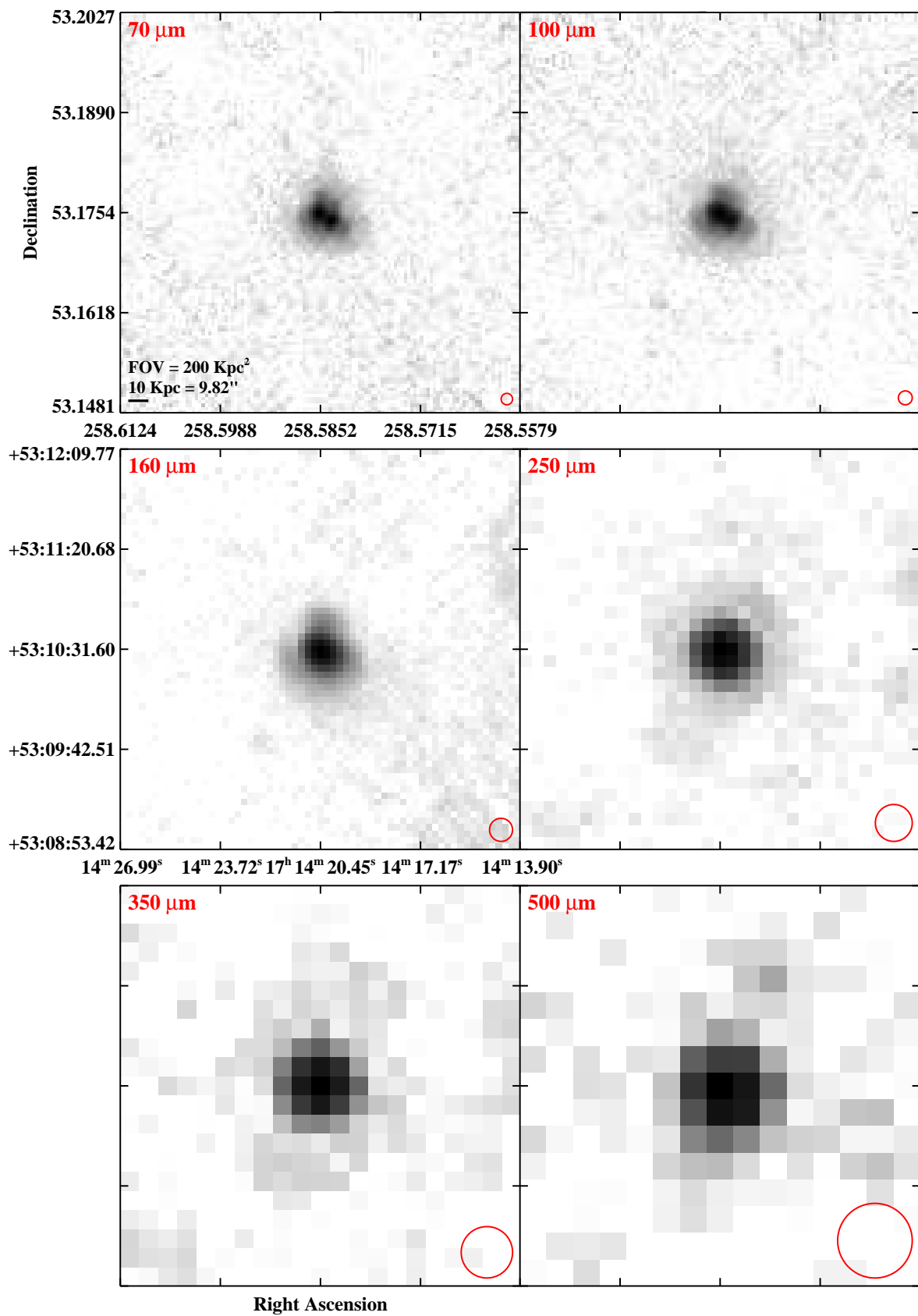


Fig. 3.— Continued (page 156 of 209).

IRAS F17138–1017

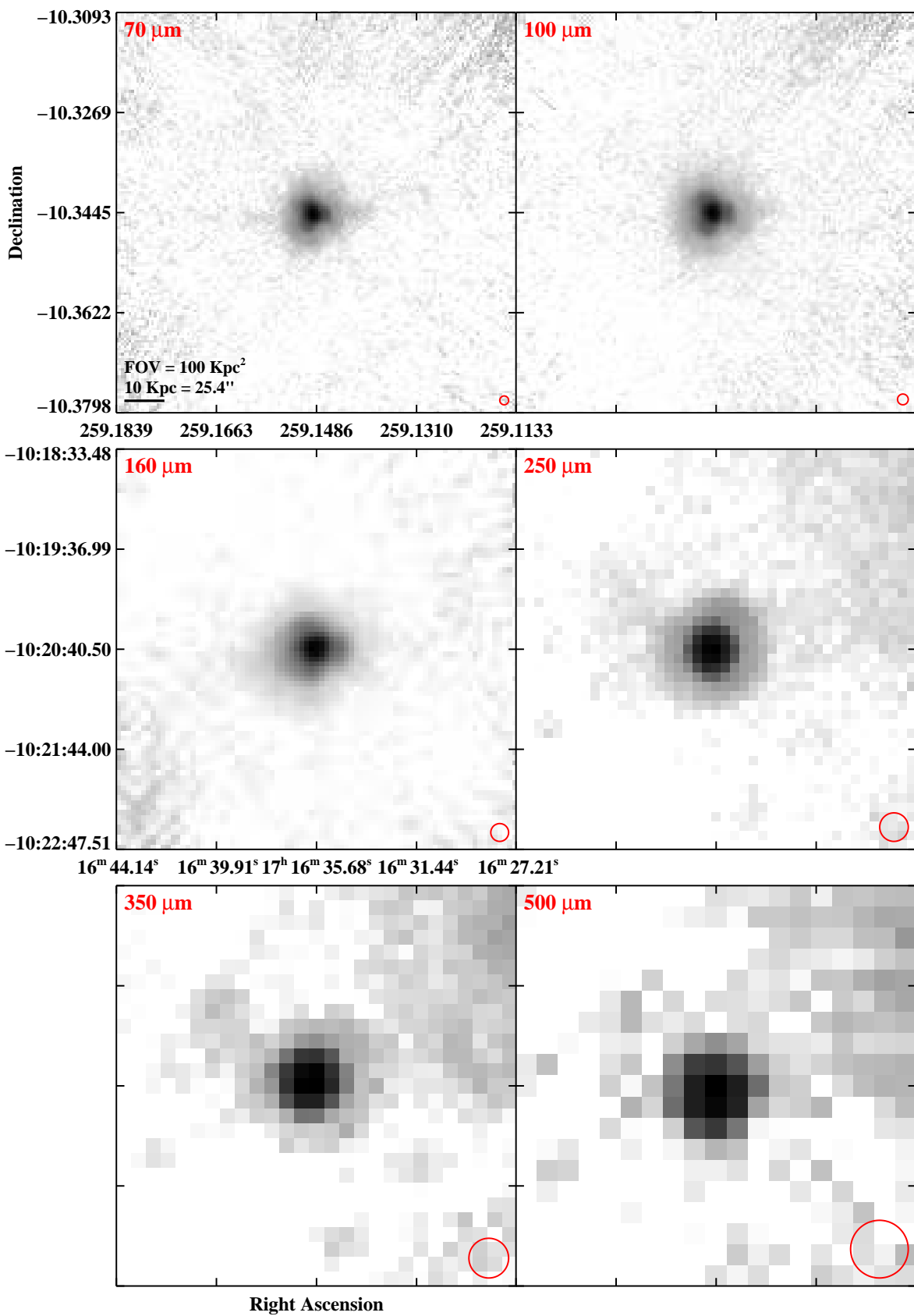


Fig. 3.— Continued (page 157 of 209).

IRAS F17207–0014

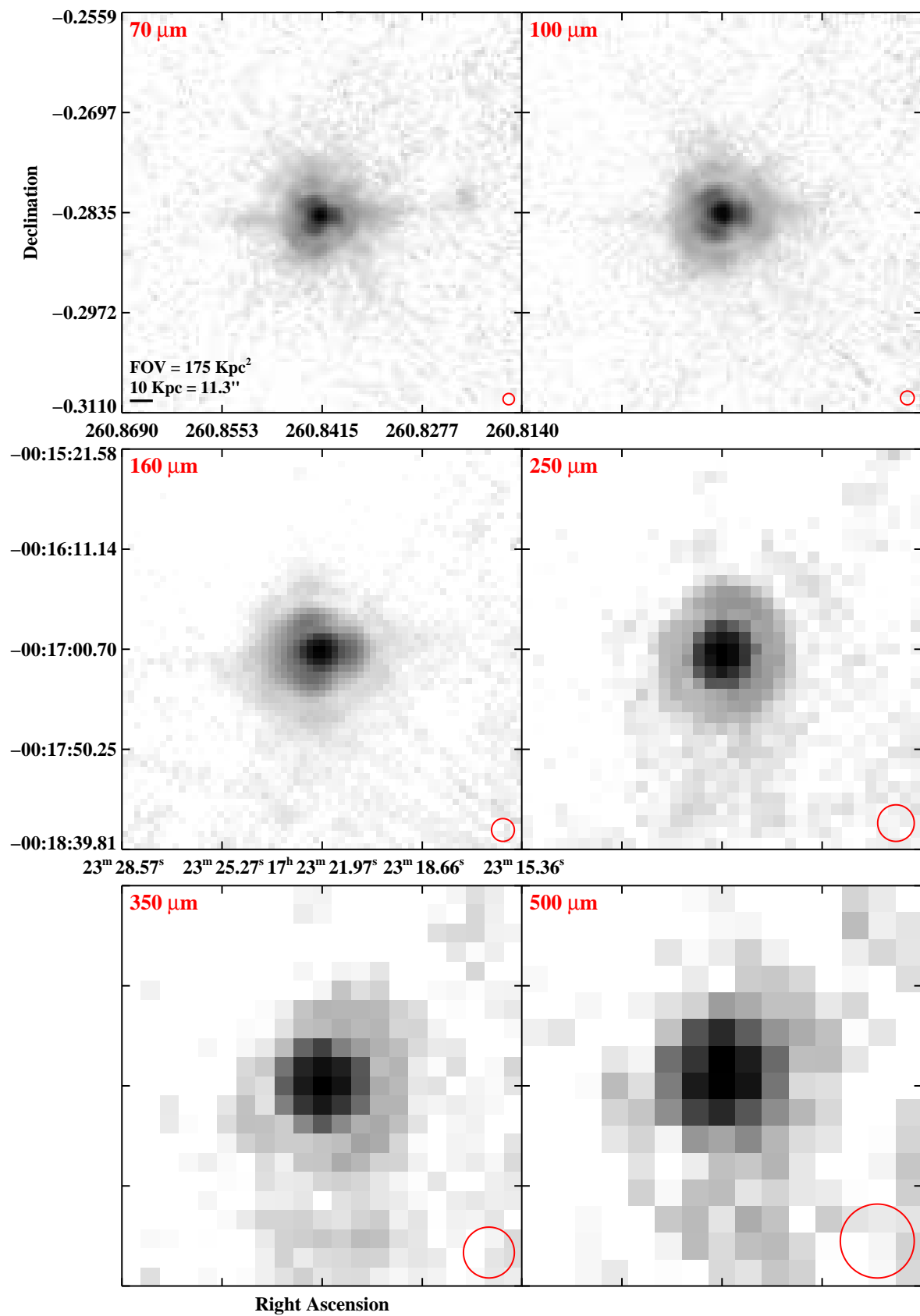


Fig. 3.— Continued (page 158 of 209).

IRAS F17222–5953 (ESO 138–G027)

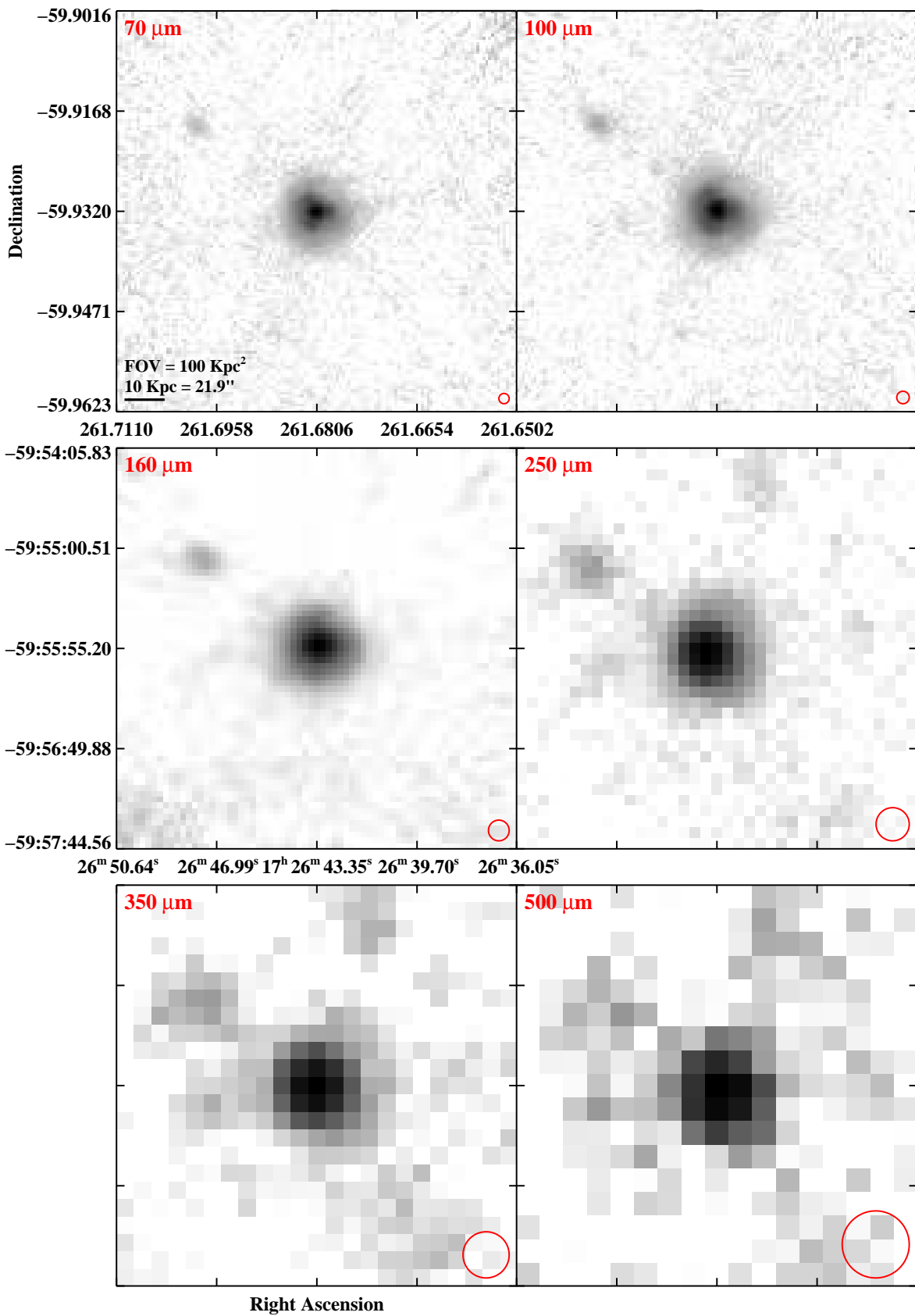


Fig. 3.— Continued (page 159 of 209).

IRAS F17530+3447 (UGC 11041)

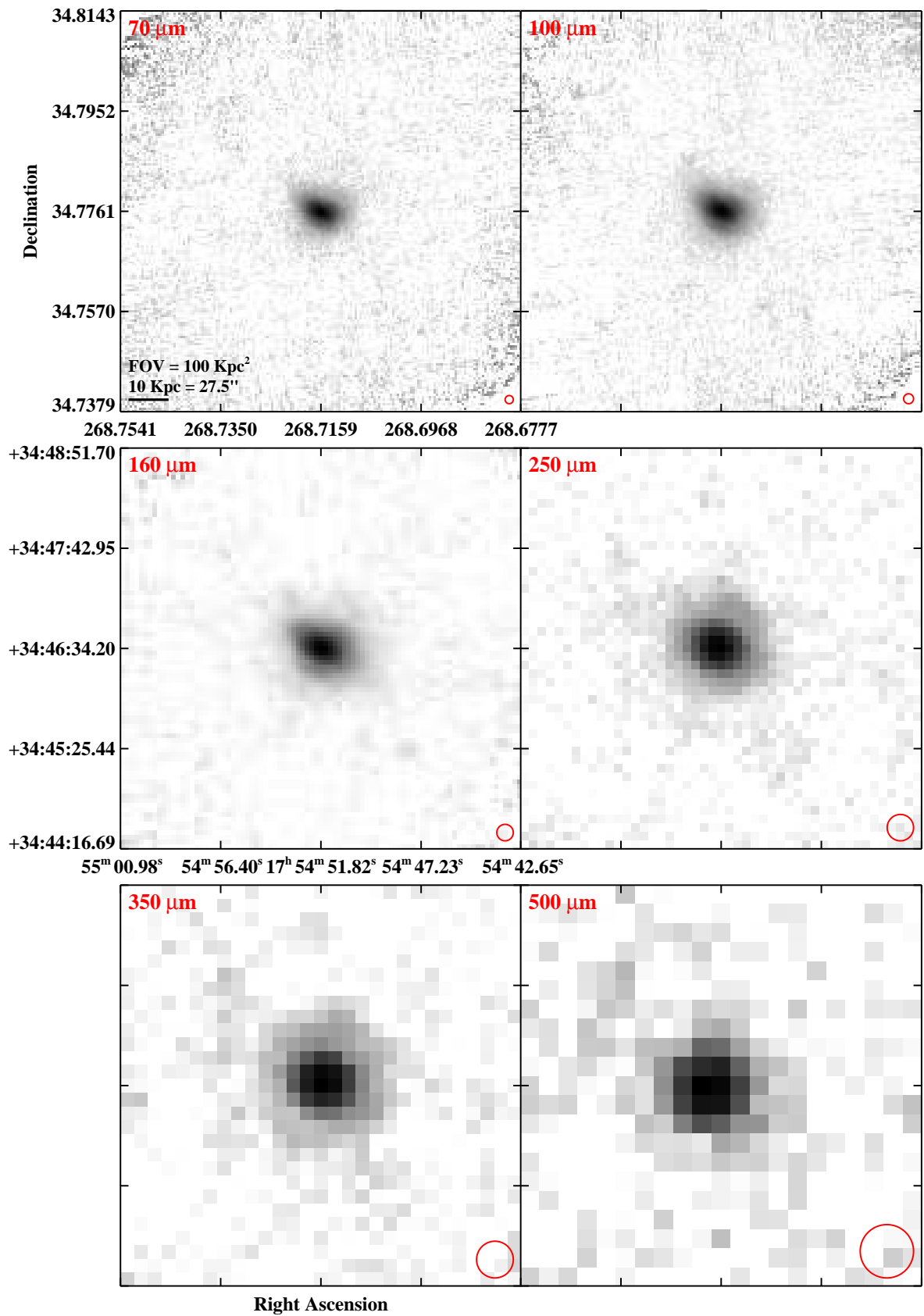


Fig. 3.— Continued (page 160 of 209).

IRAS F17548+2401 (CGCG 141-034)

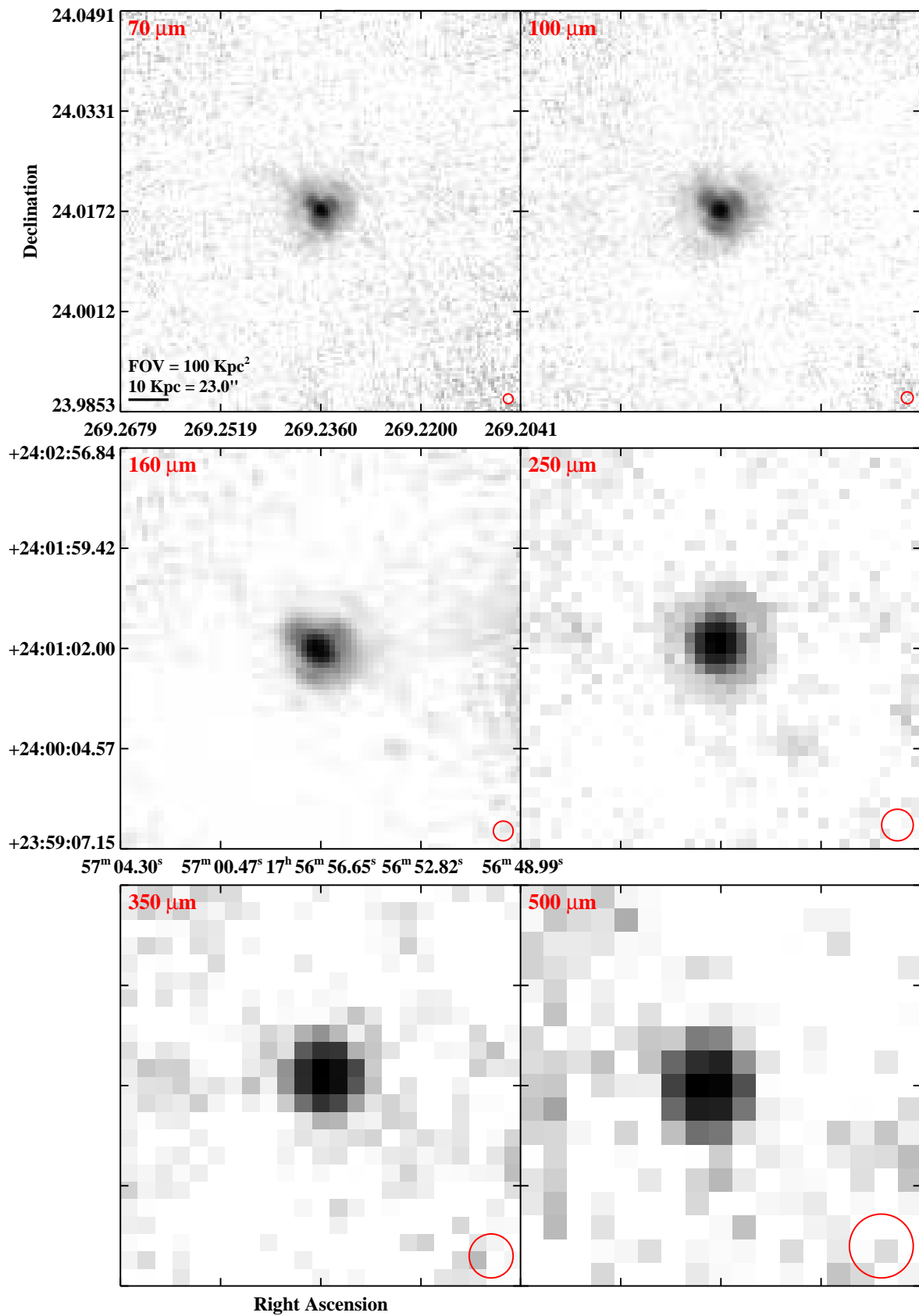


Fig. 3.— Continued (page 161 of 209).

IRAS 17578–0400

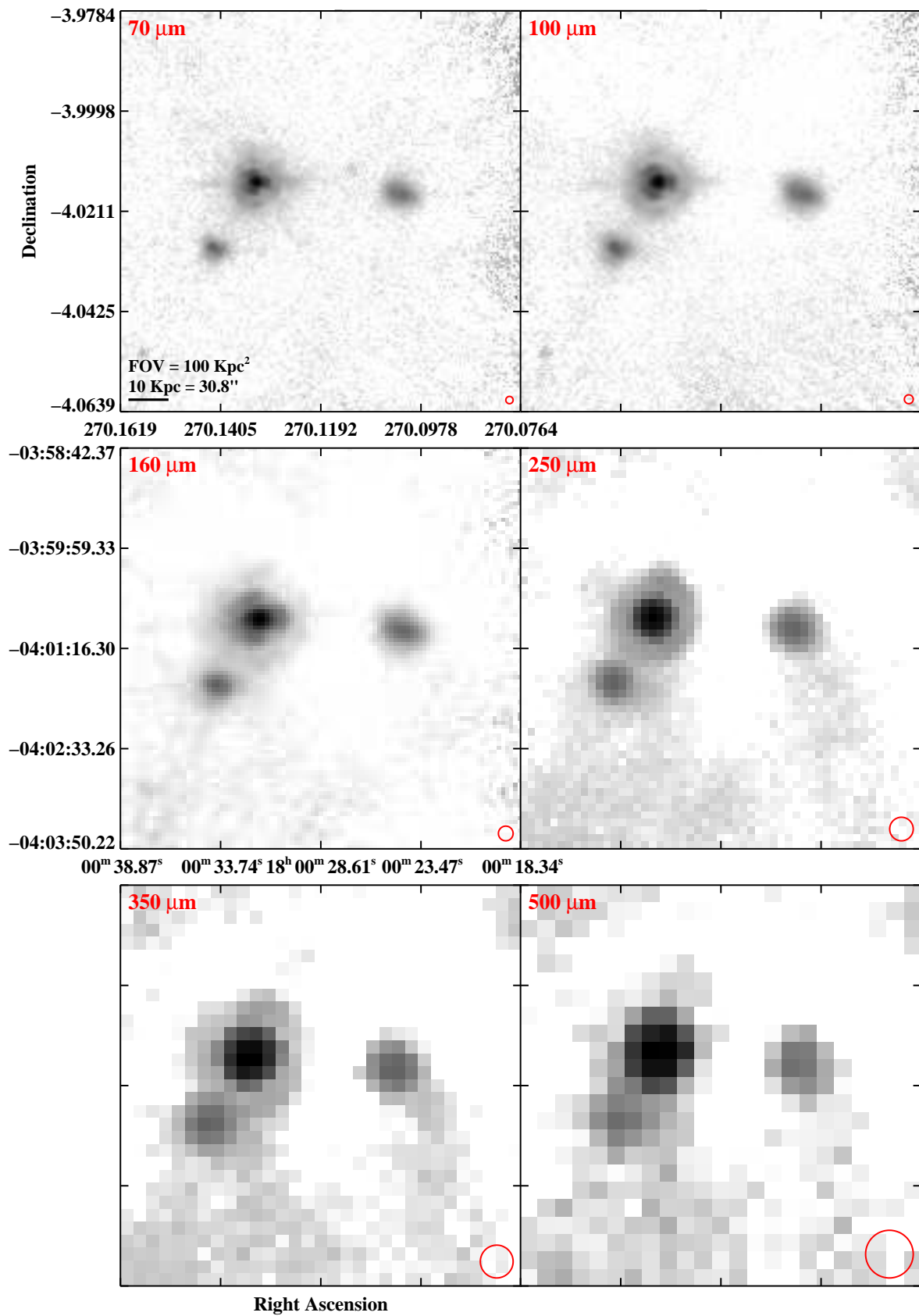


Fig. 3.— Continued (page 162 of 209).

IRAS 18090+0130

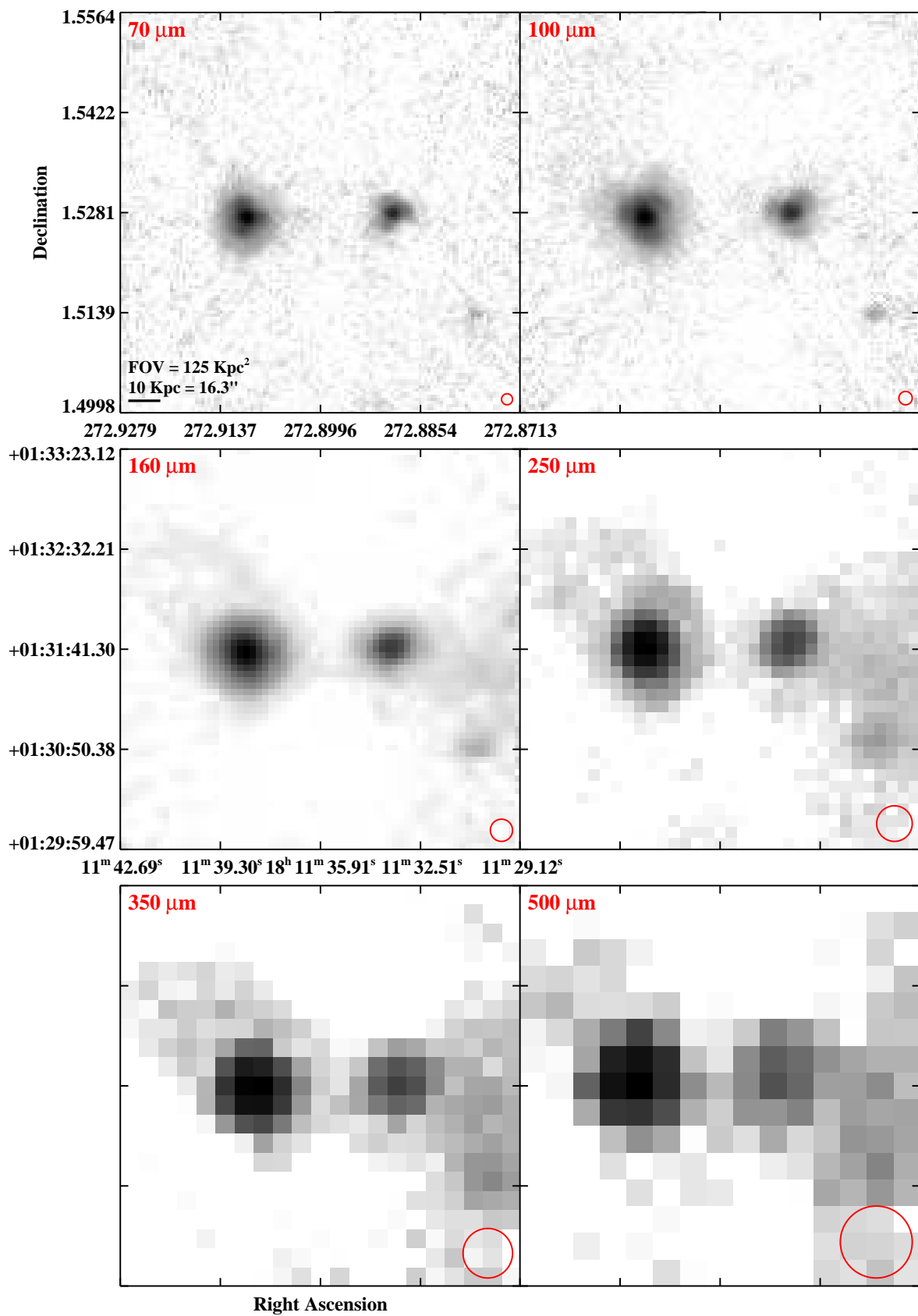


Fig. 3.— Continued (page 163 of 209).

IRAS F18131+6820 (NGC 6621)

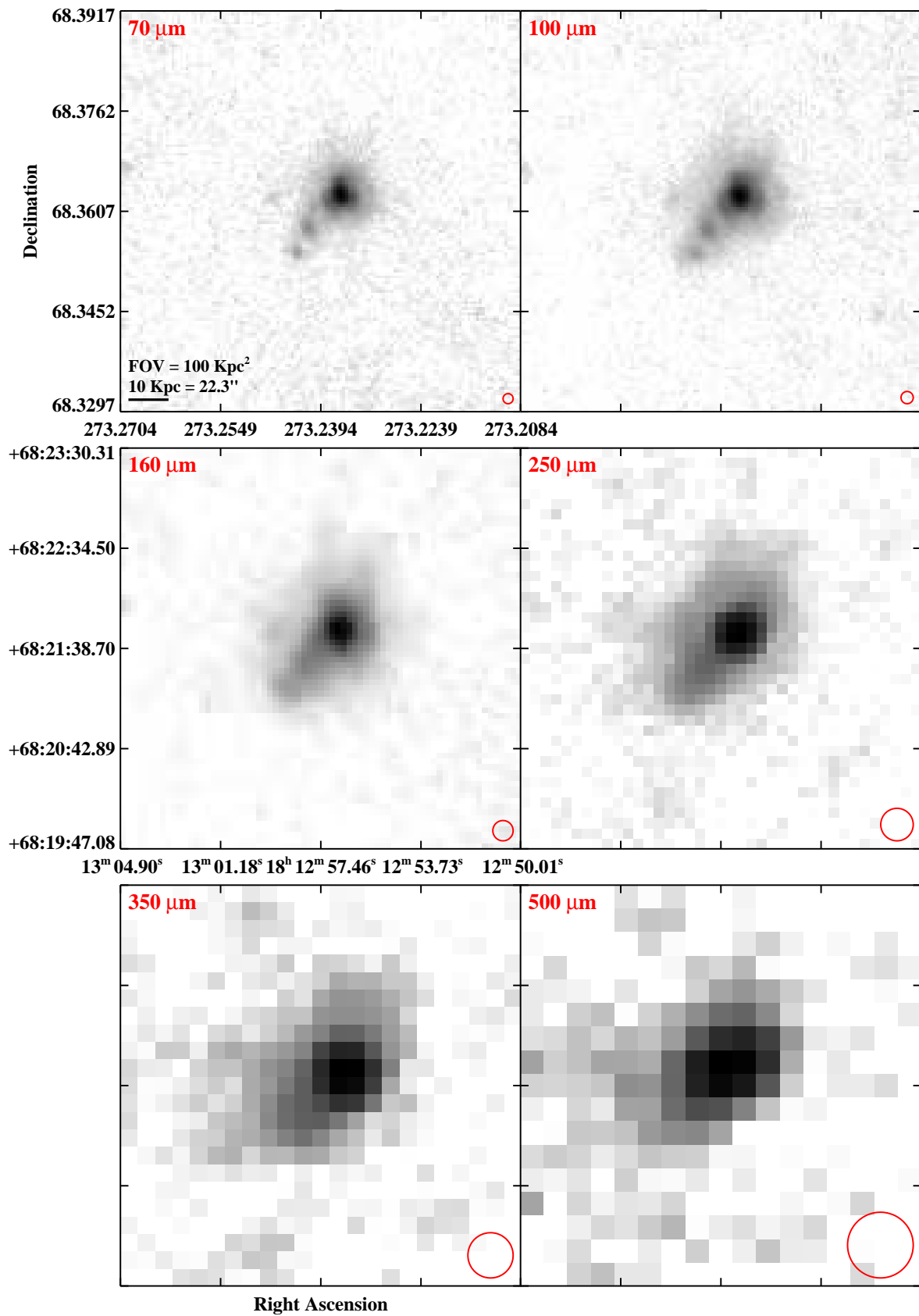


Fig. 3.— Continued (page 164 of 209).

IRAS F18093–5744 (IC 4687)

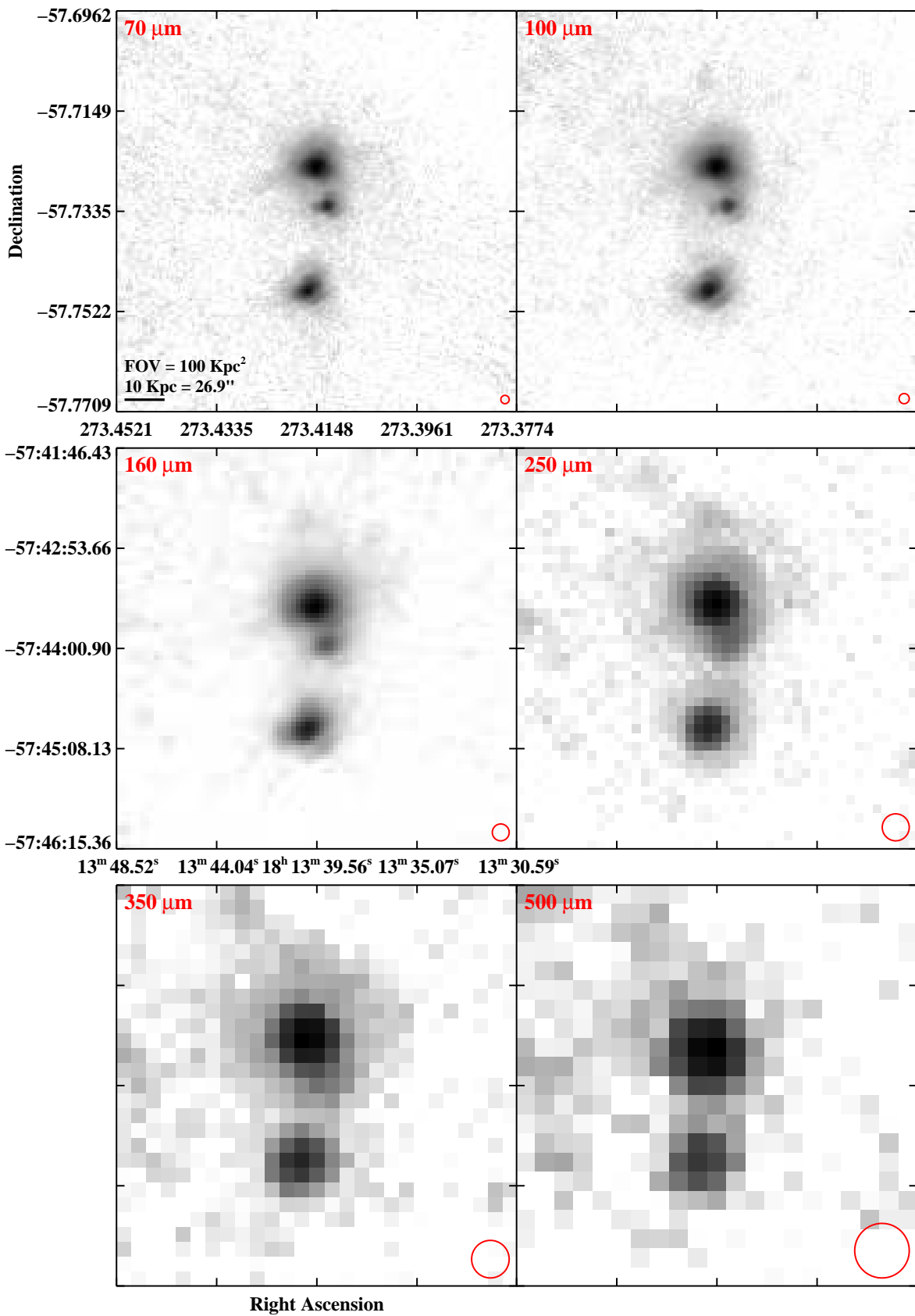


Fig. 3.— Continued (page 165 of 209).

IRAS F18145+2205 (CGCG 142-034)

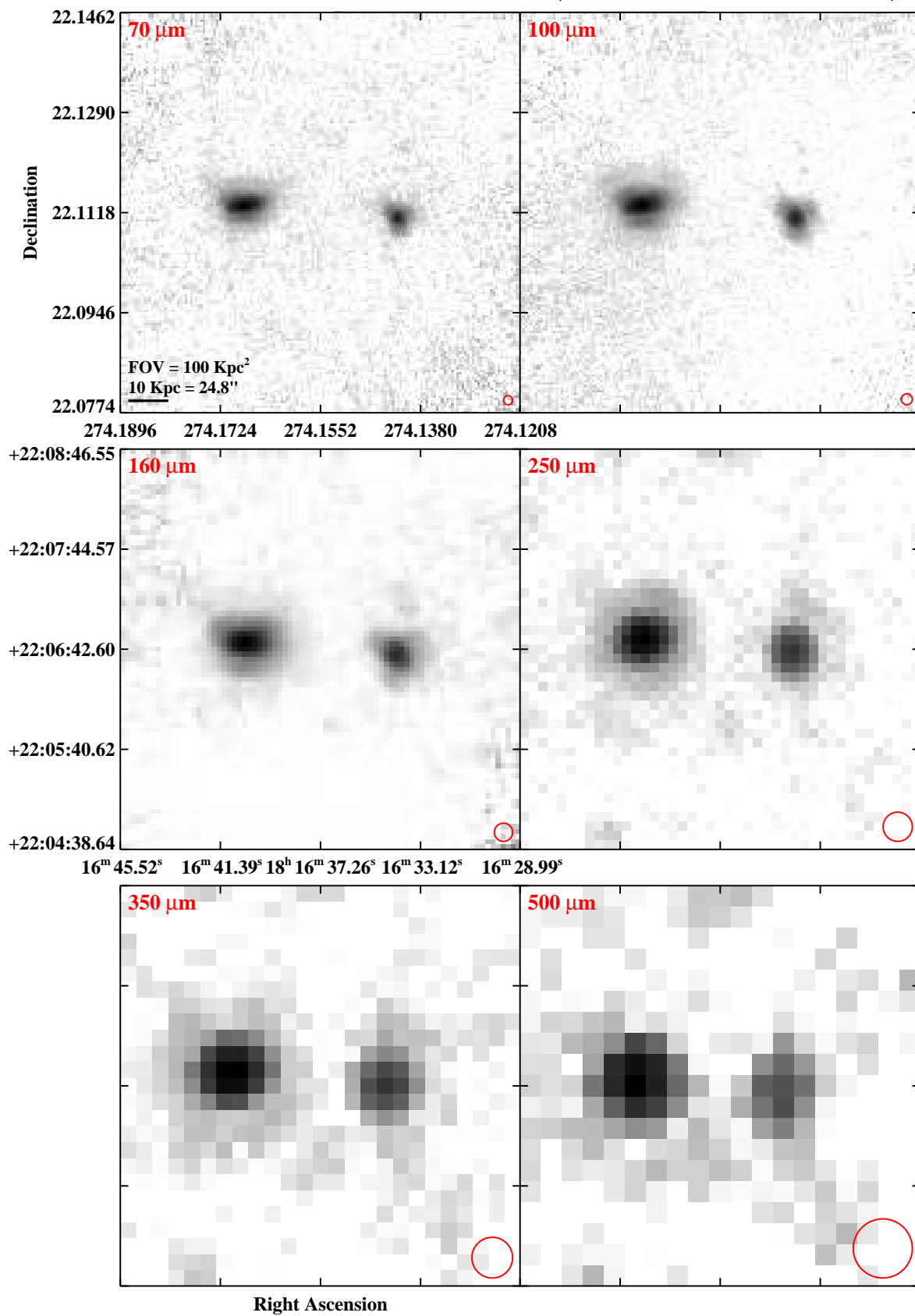


Fig. 3.— Continued (page 166 of 209).

IRAS F18293–3413

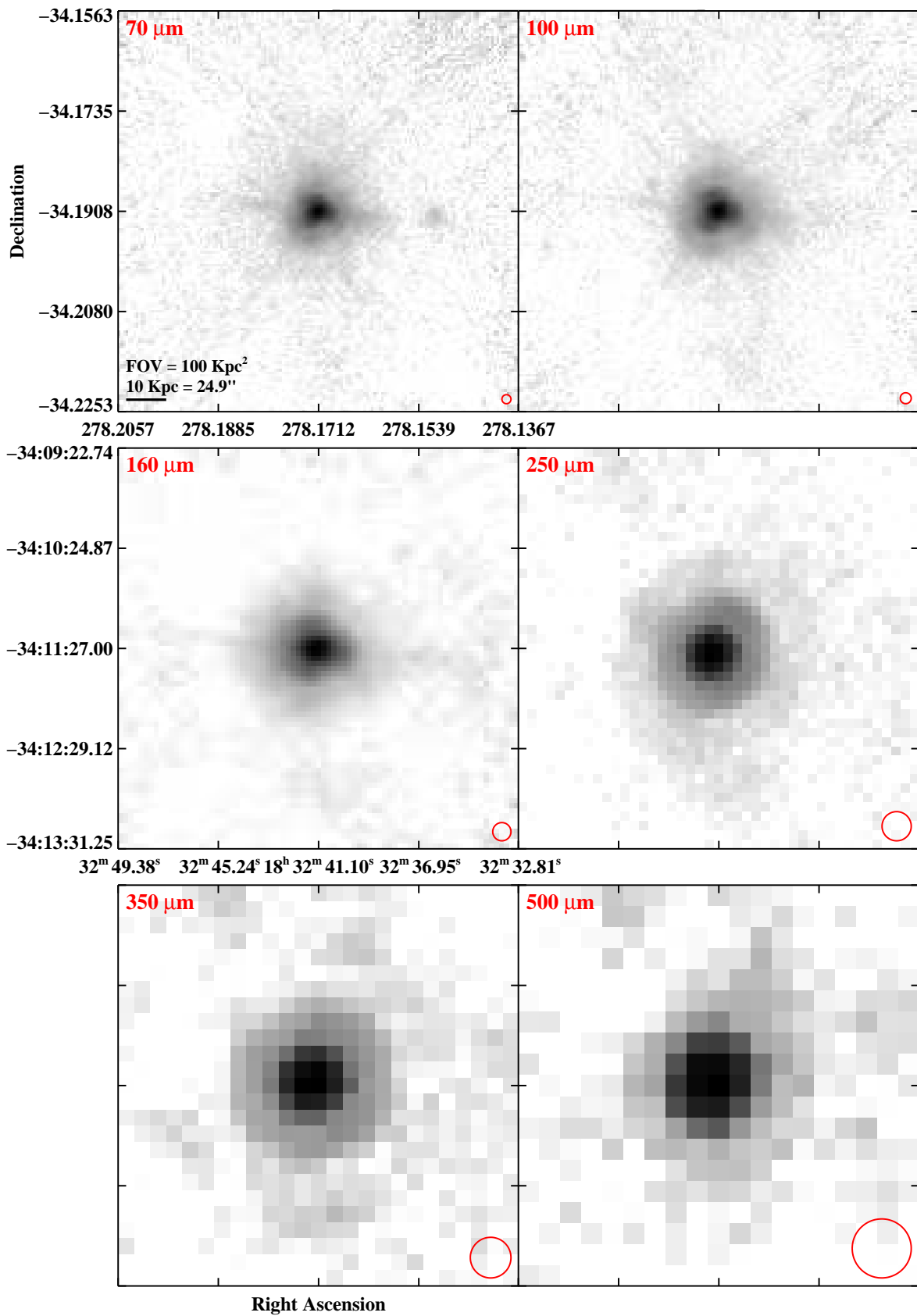


Fig. 3.— Continued (page 167 of 209).

IRAS F18329+5950 (NGC 6670A/B)

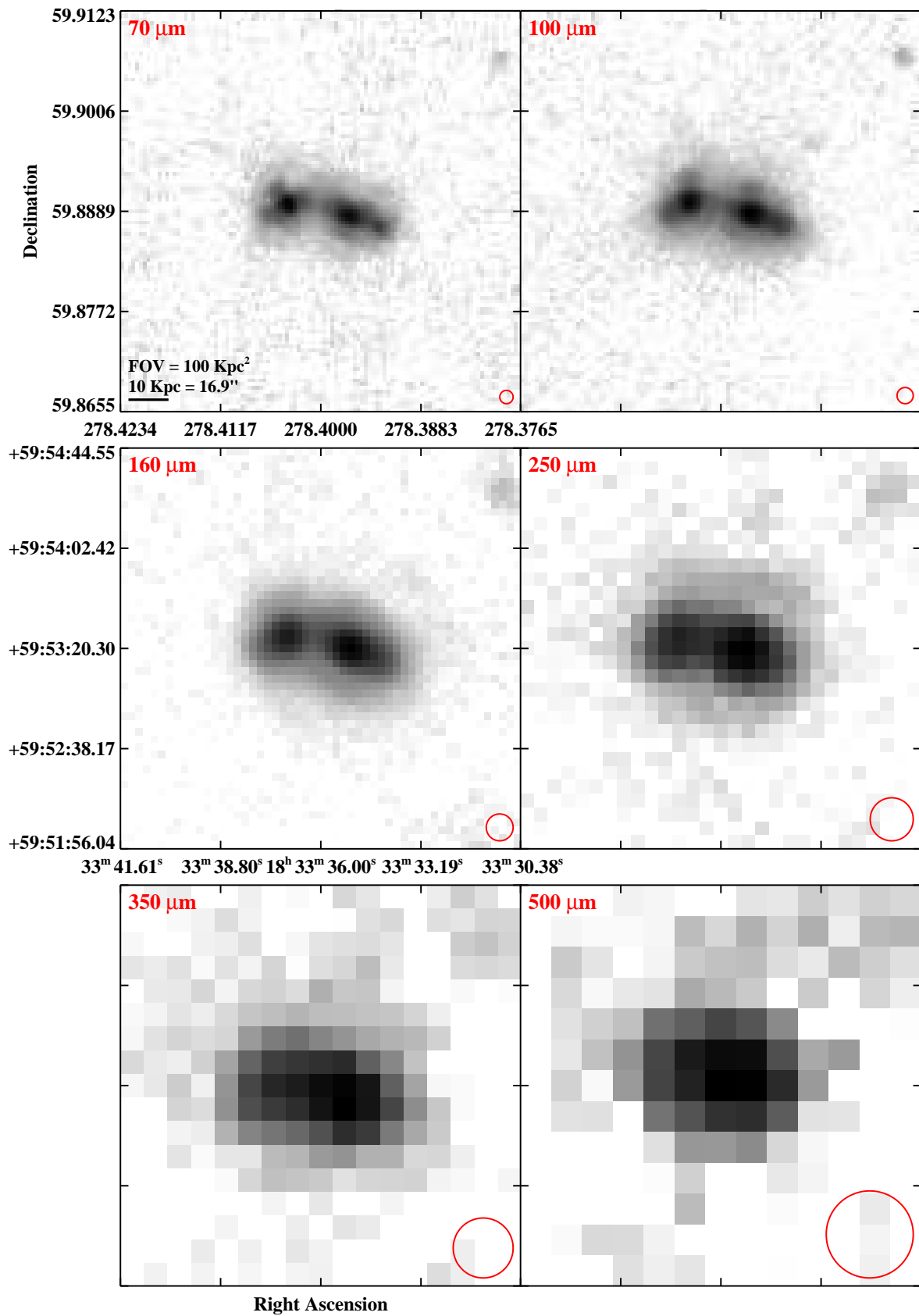


Fig. 3.— Continued (page 168 of 209).

IRAS F18341–5732 (IC 4734)

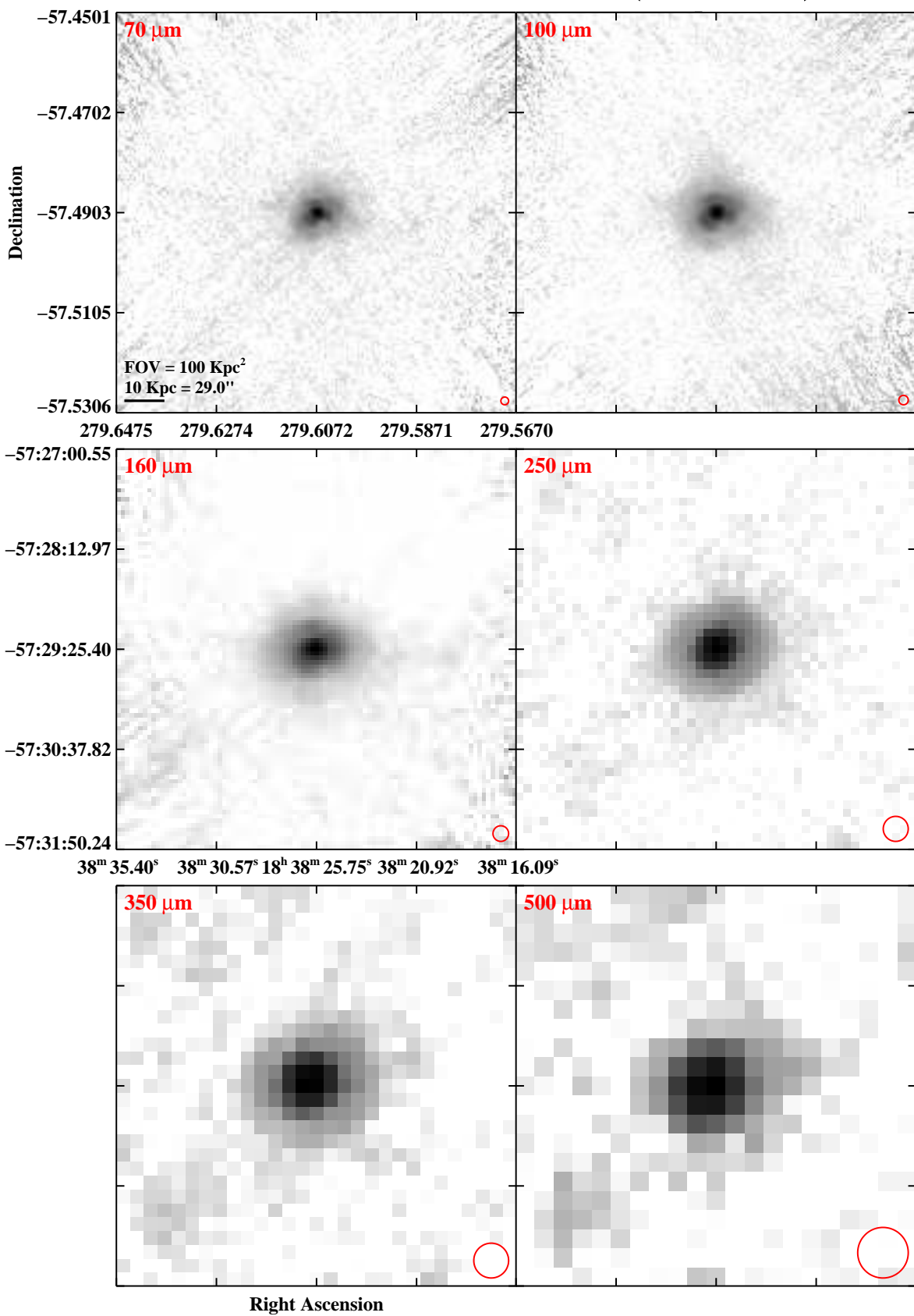


Fig. 3.— Continued (page 169 of 209).

IRAS F18425+6036 (NGC 6701)

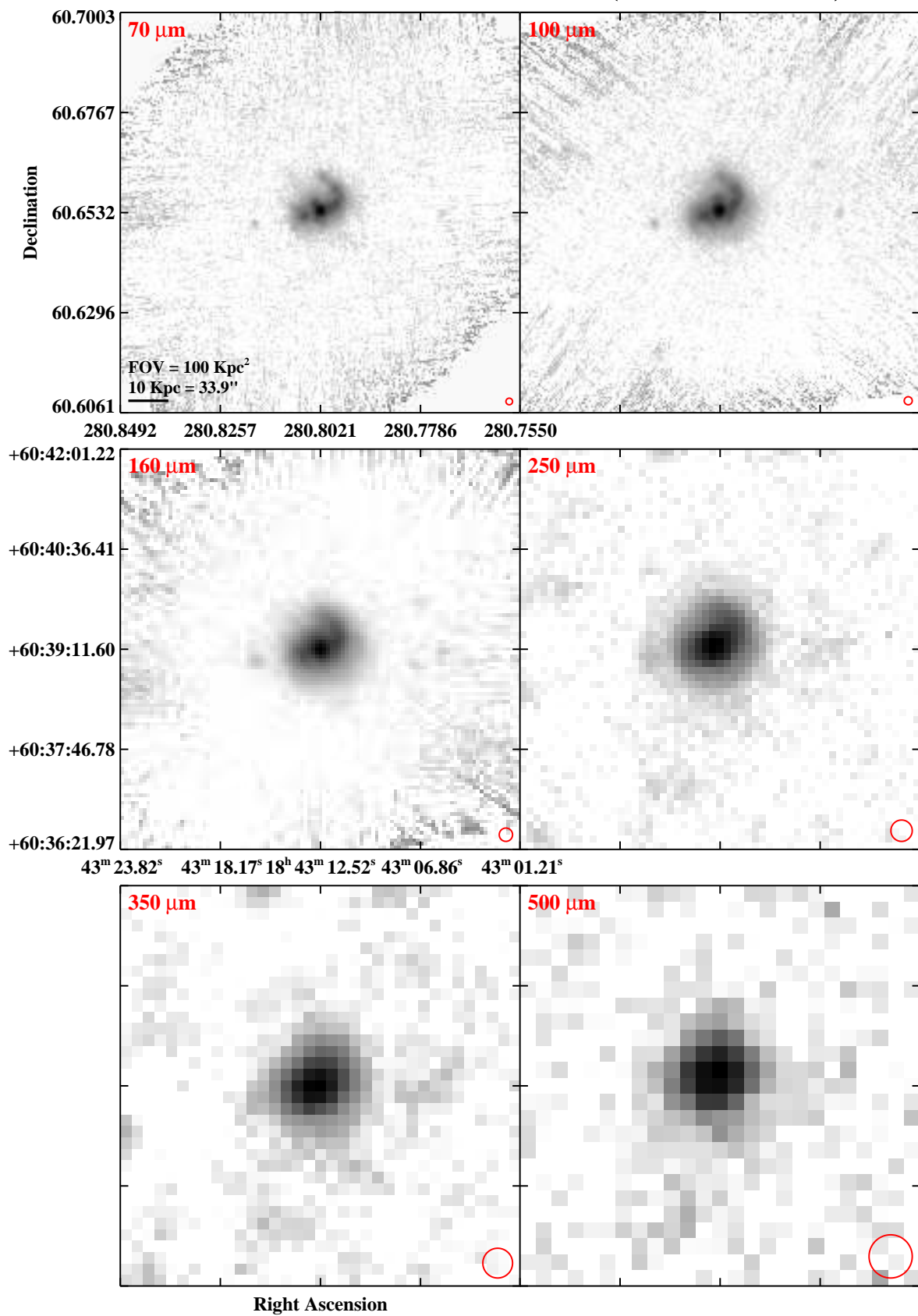


Fig. 3.— Continued (page 170 of 209).

IRAS F19120+7320 (VV 414/NGC 6786/UGC 11415)

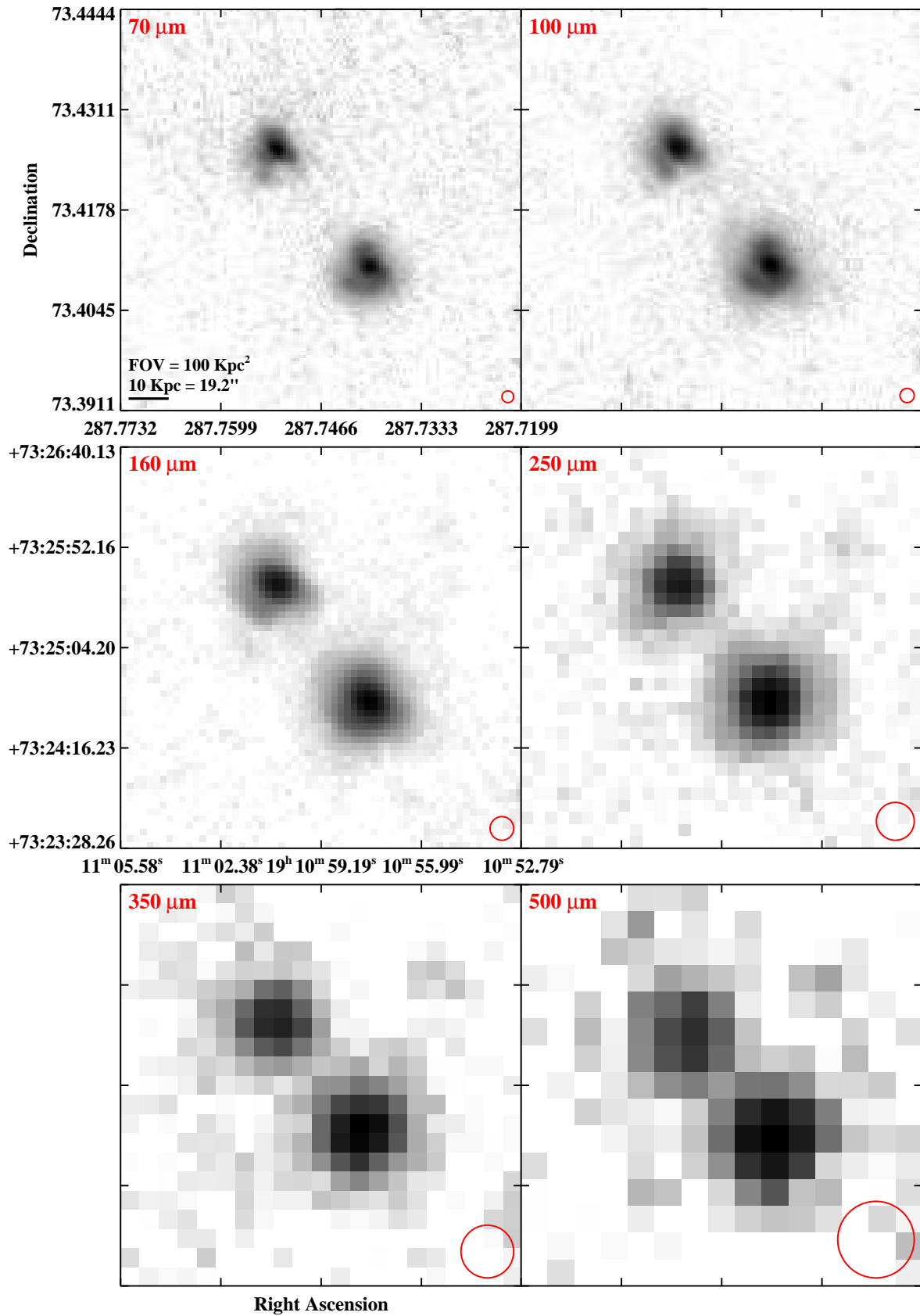


Fig. 3.— Continued (page 171 of 209).

IRAS F19115–2124 (ESO 593–IG008)

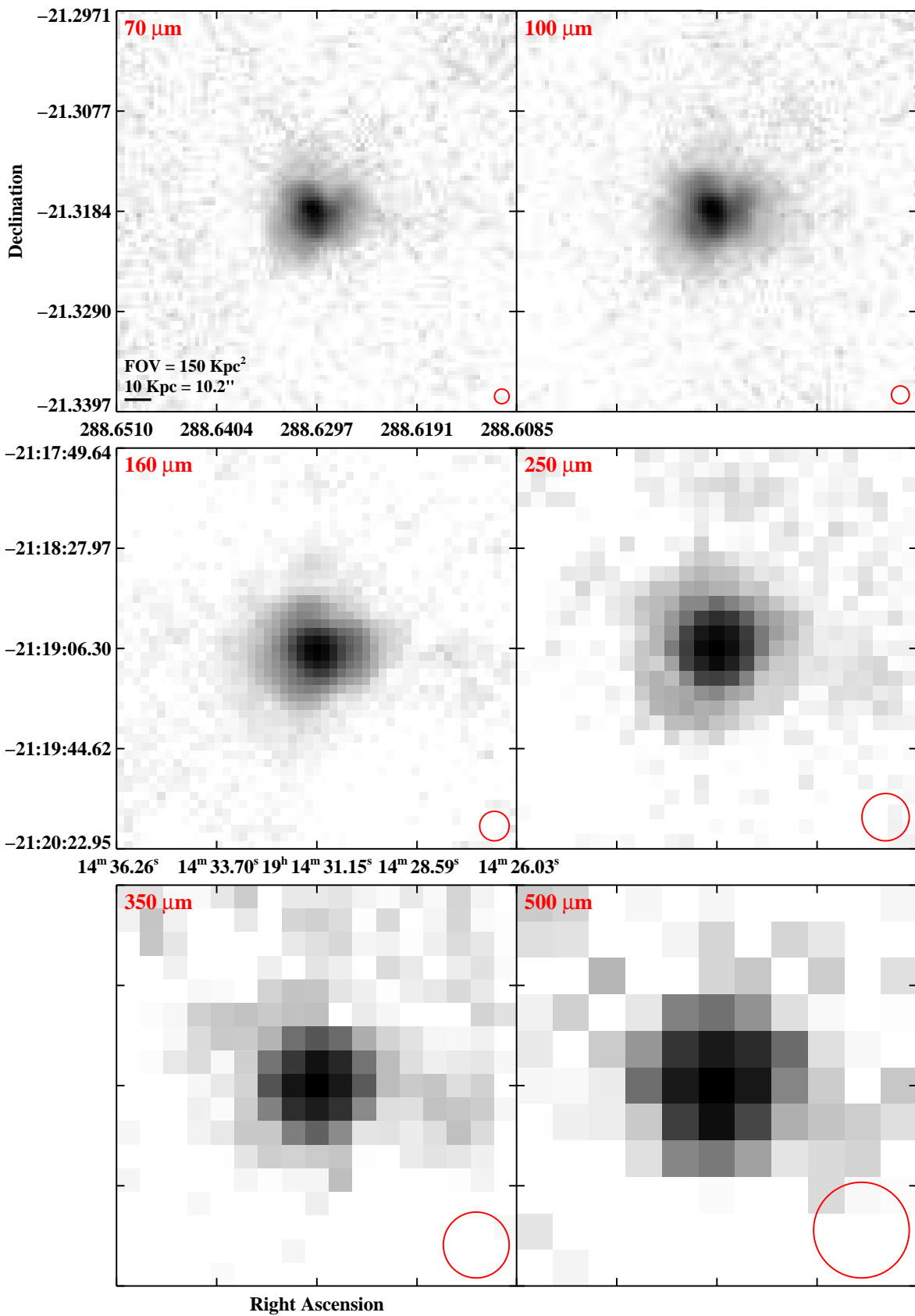


Fig. 3.— Continued (page 172 of 209).

IRAS F19297–0406

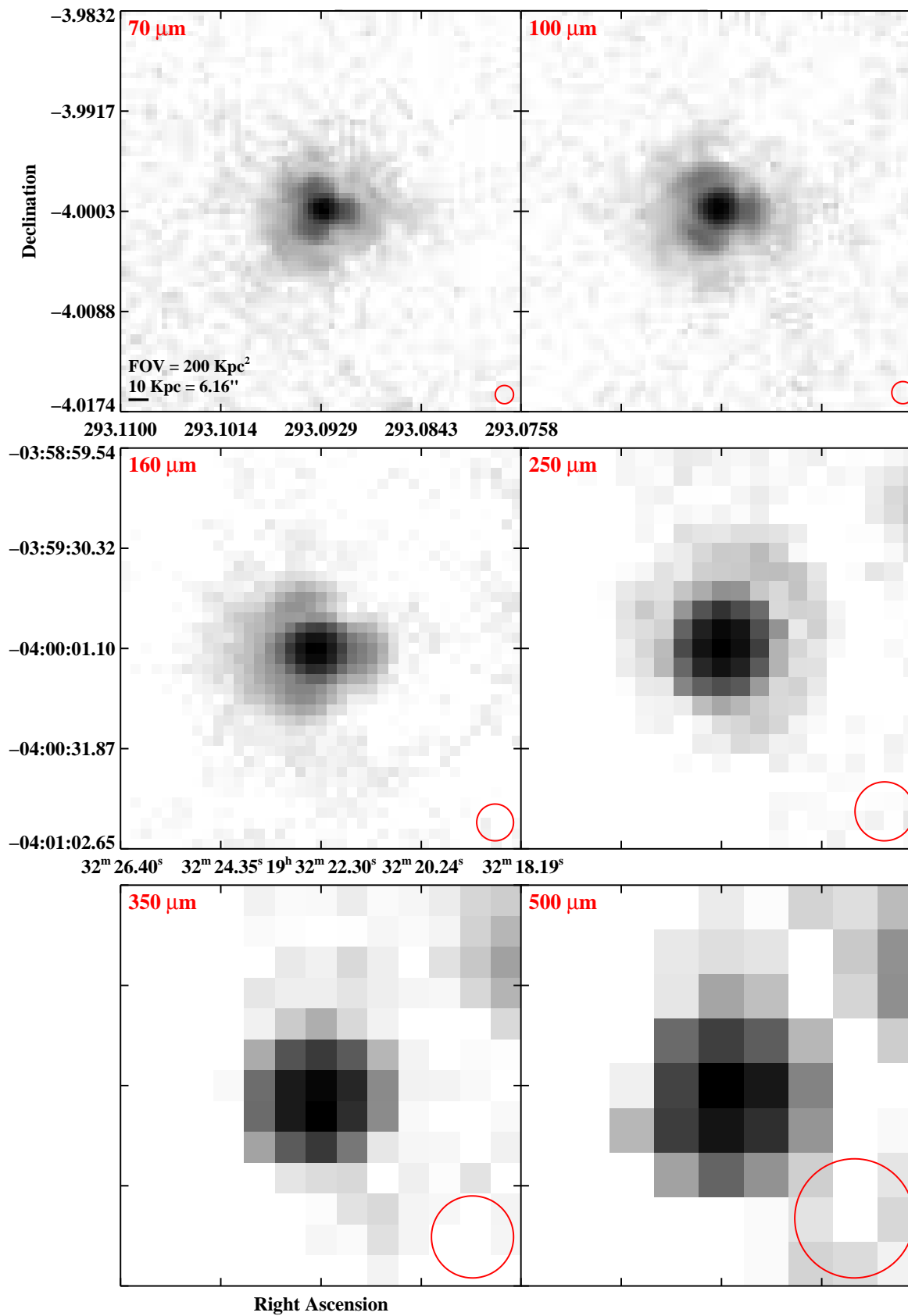


Fig. 3.— Continued (page 173 of 209).

IRAS 19542+1110

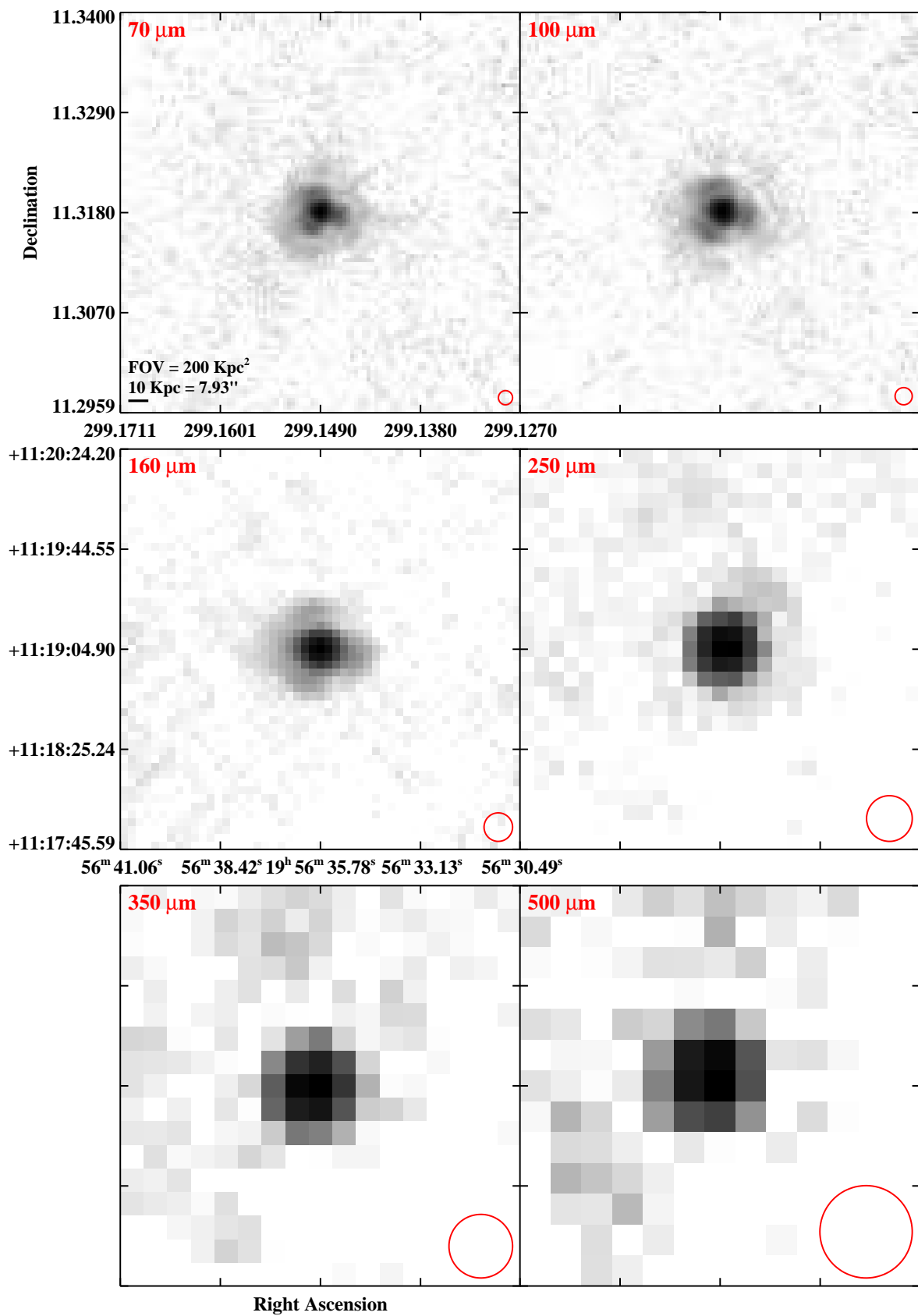


Fig. 3.— Continued (page 174 of 209).

IRAS F19542–3804 (ESO 339–G011)

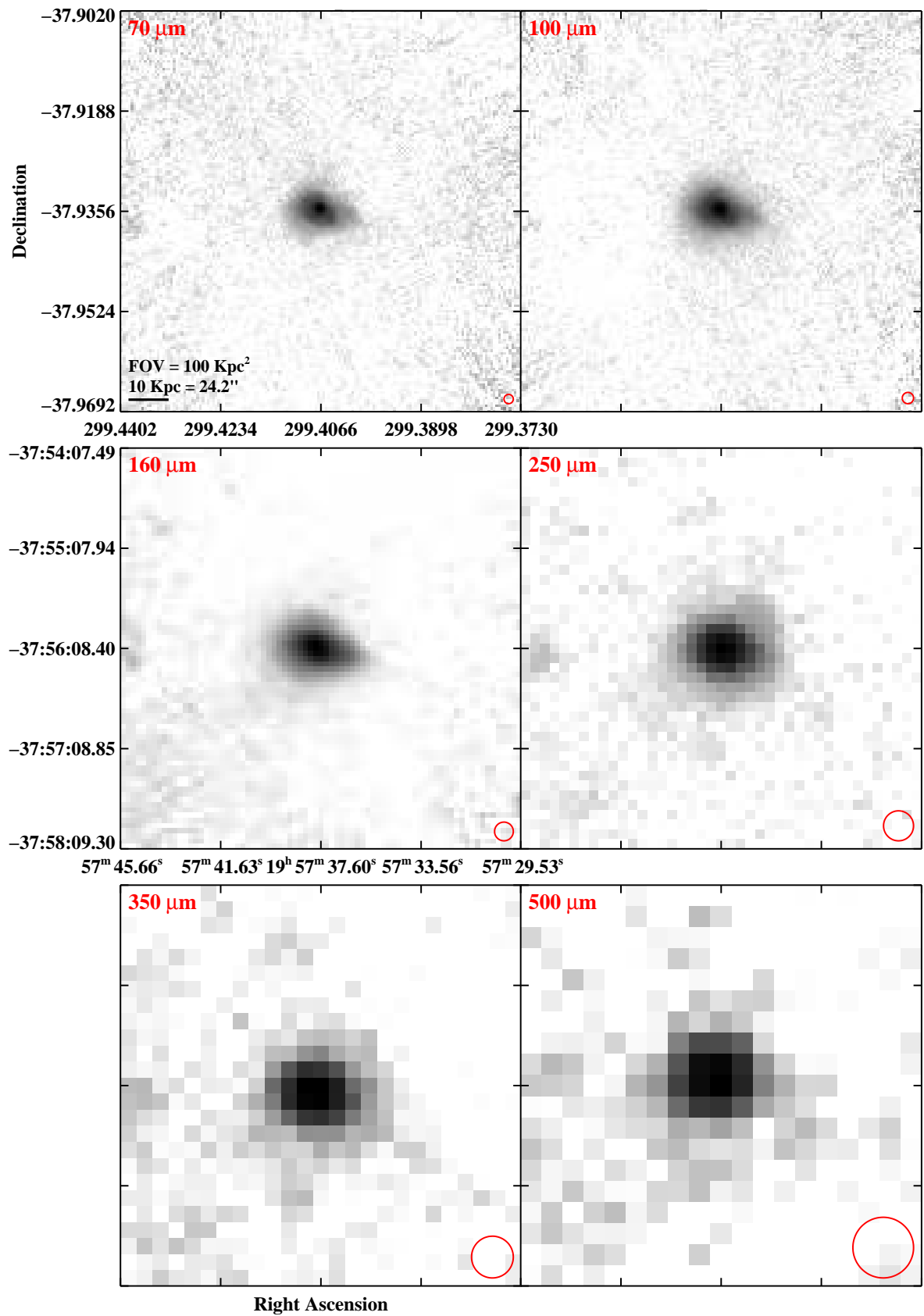


Fig. 3.— Continued (page 175 of 209).

IRAS F20221–2458 (NGC 6907)

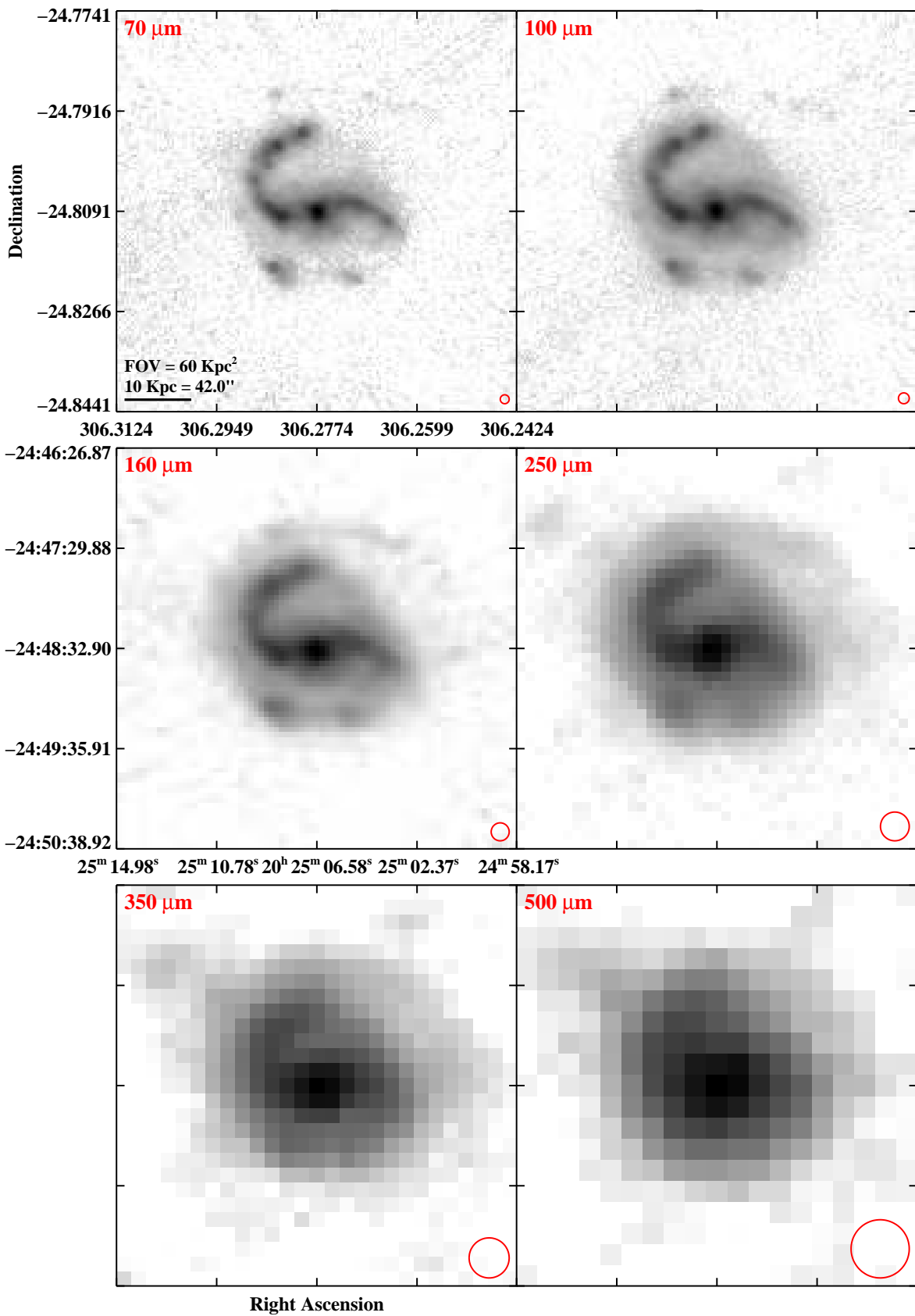


Fig. 3.— Continued (page 176 of 209).

IRAS 20264+2533 (MCG+04-48-002)

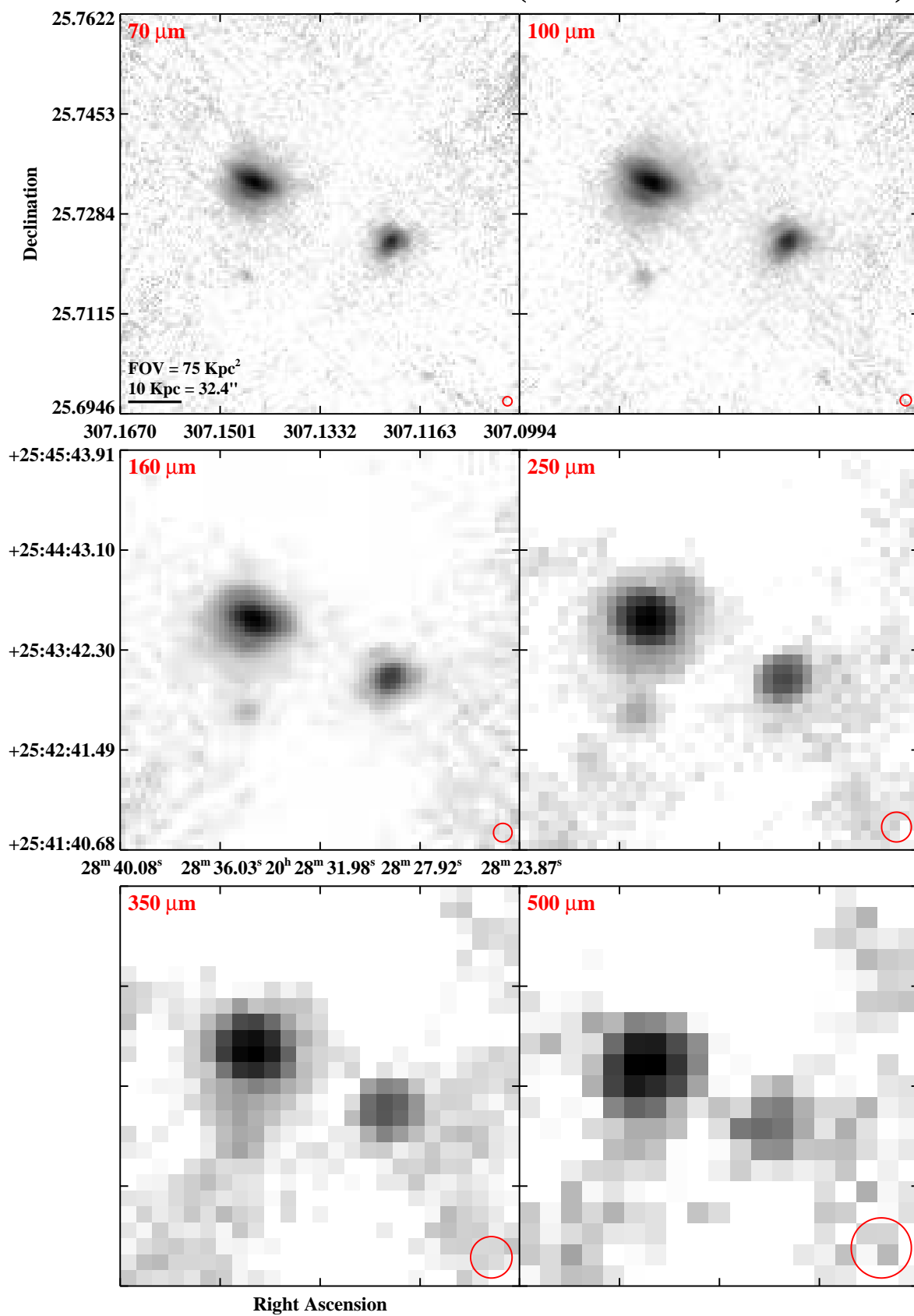


Fig. 3.— Continued (page 177 of 209).

IRAS F20304–0211 (NGC 6926)

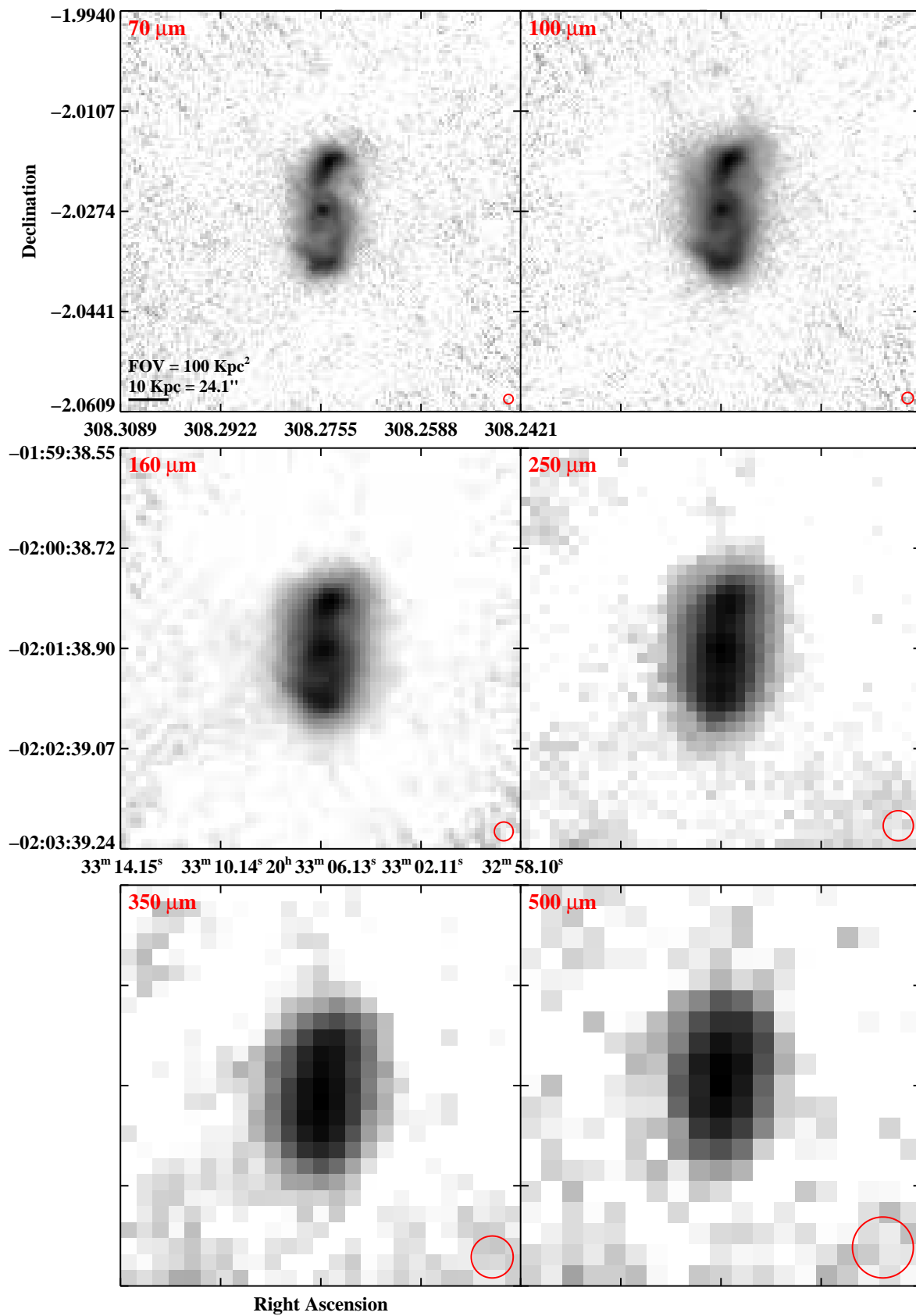


Fig. 3.— Continued (page 178 of 209).

IRAS 20351+2521

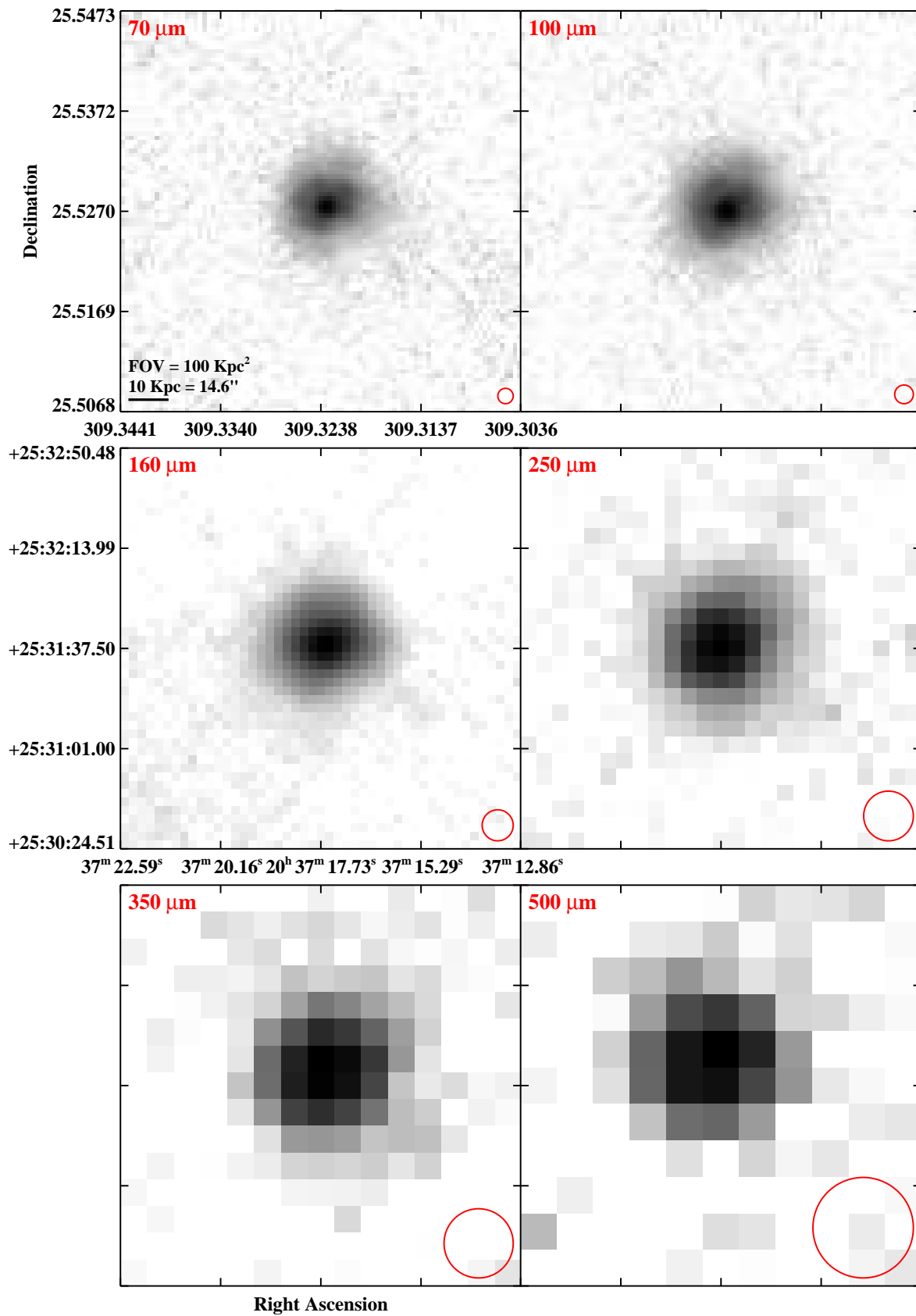


Fig. 3.— Continued (page 179 of 209).

IRAS F20550+1655 (CGCG 448–020/II Zw 096)

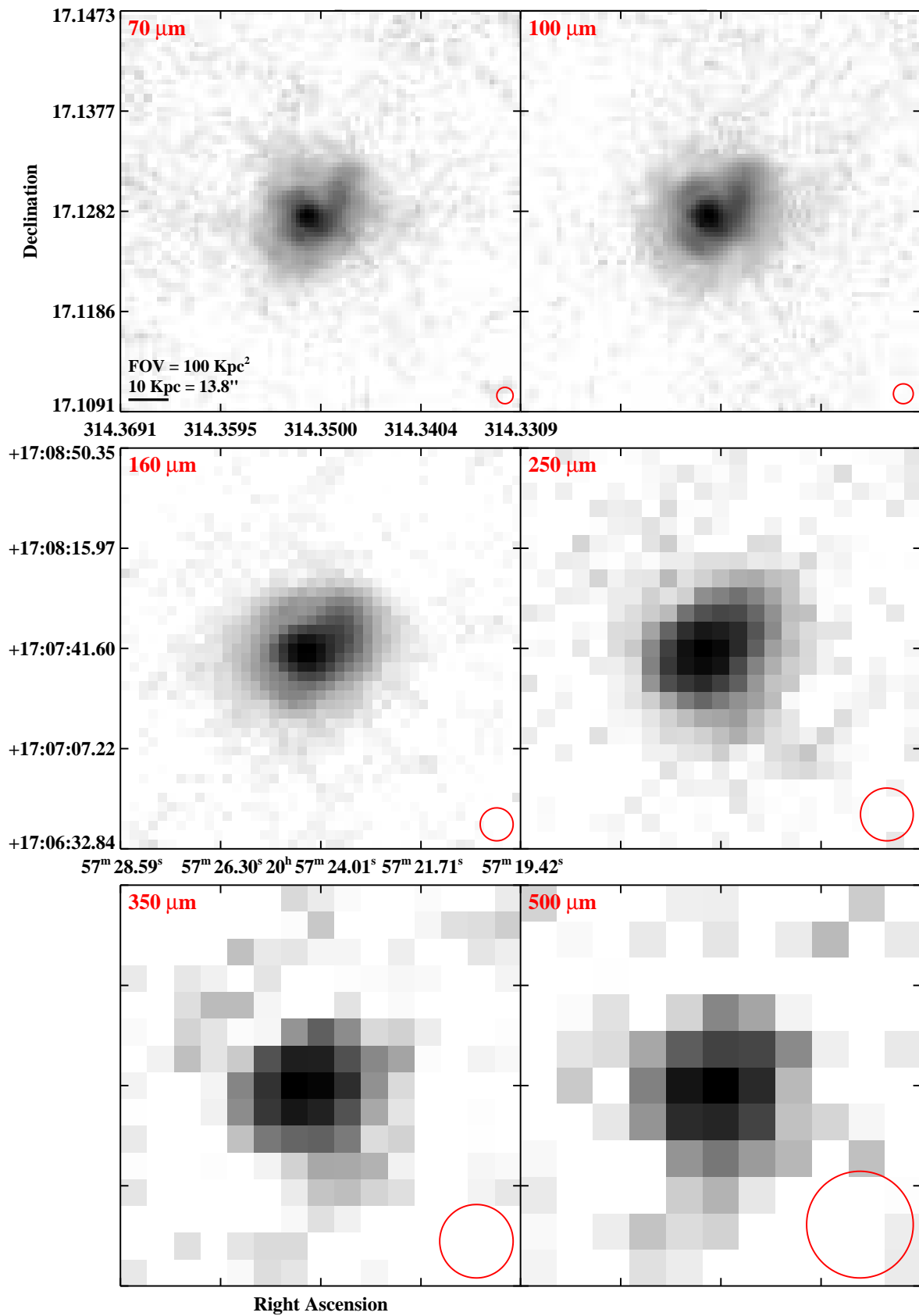


Fig. 3.— Continued (page 180 of 209).

IRAS F20551–4250 (ESO 286–IG019)

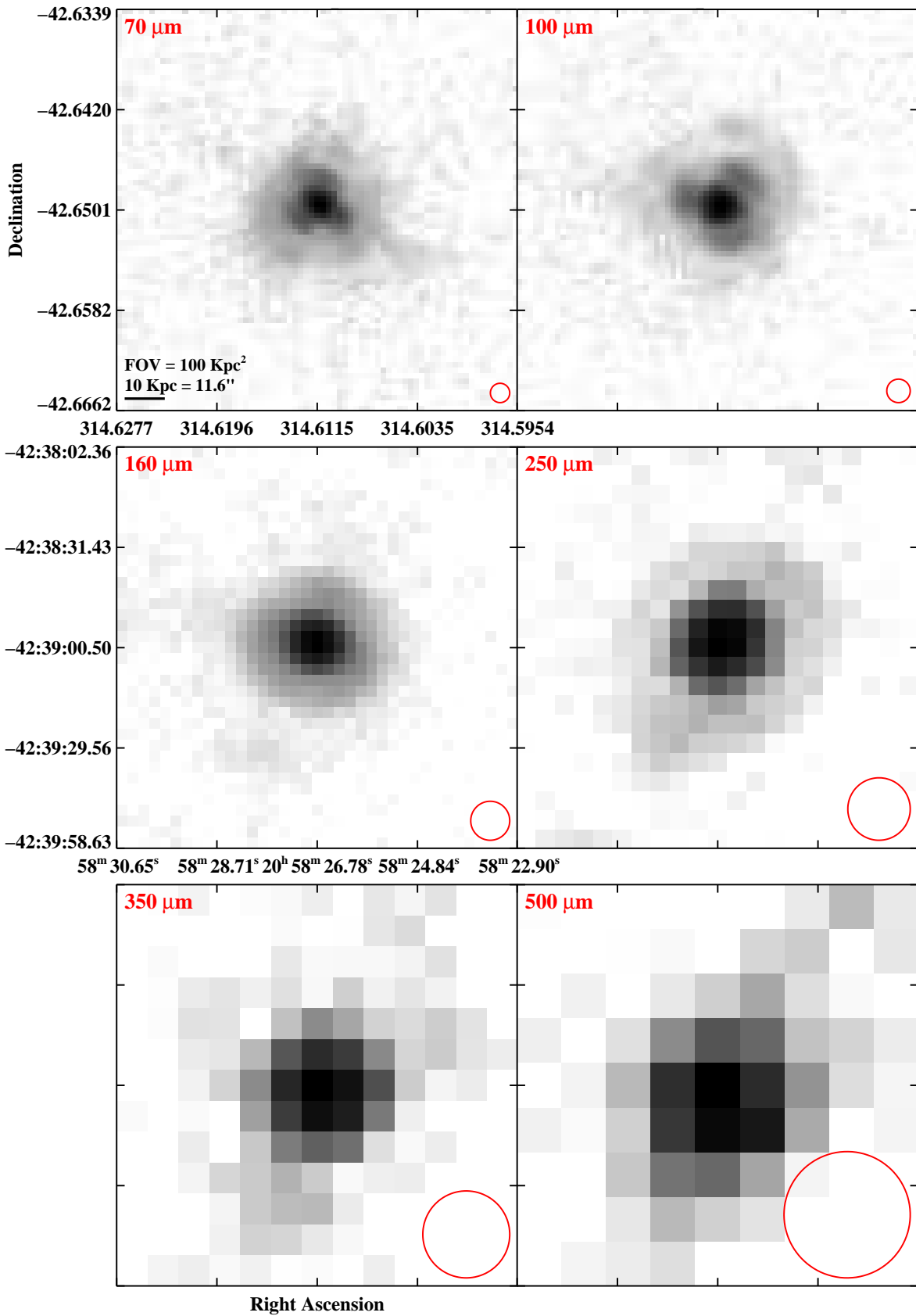


Fig. 3.— Continued (page 181 of 209).

IRAS F21008–4347 (ESO 286–G035)

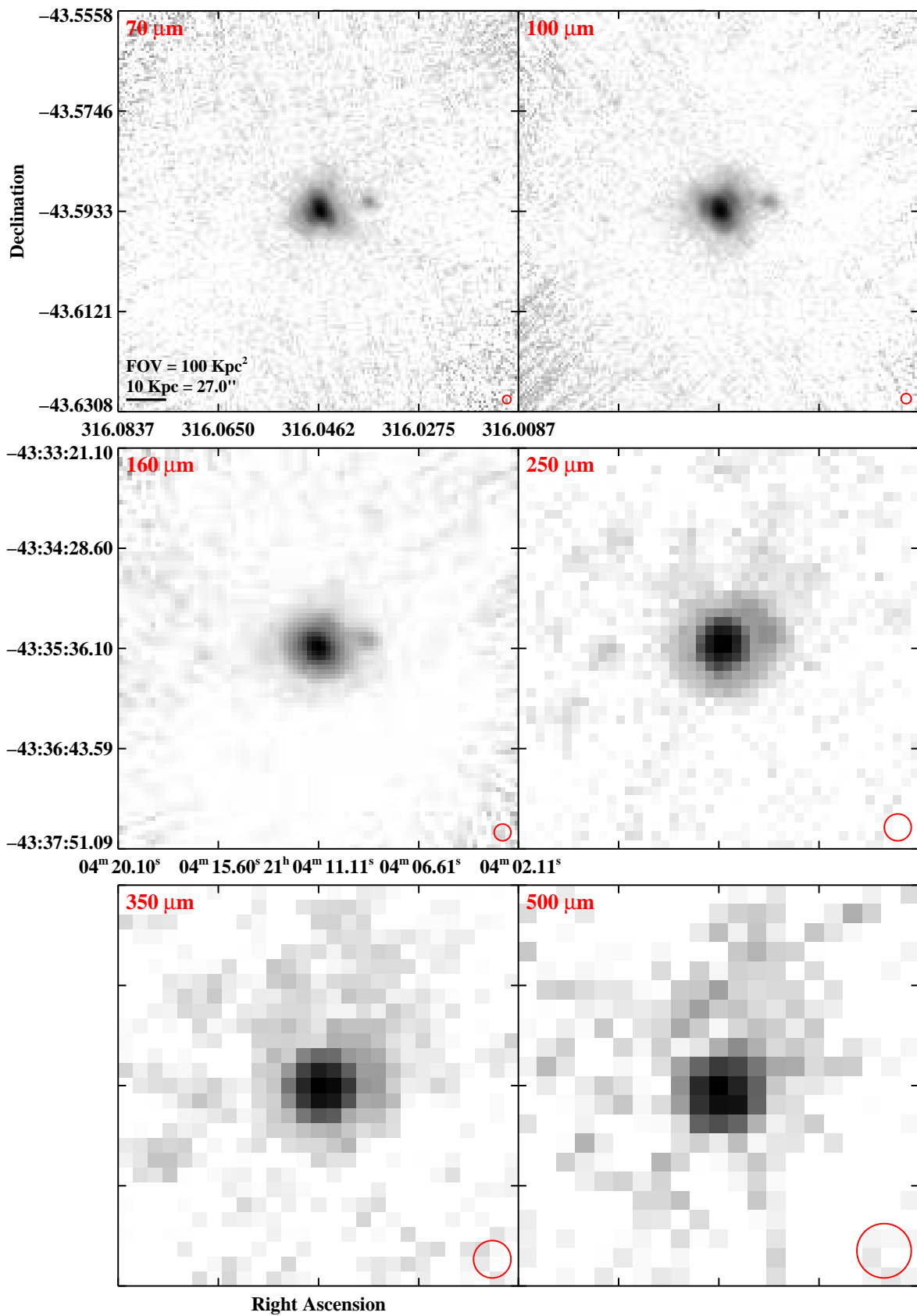


Fig. 3.— Continued (page 182 of 209).

IRAS 21101+5810

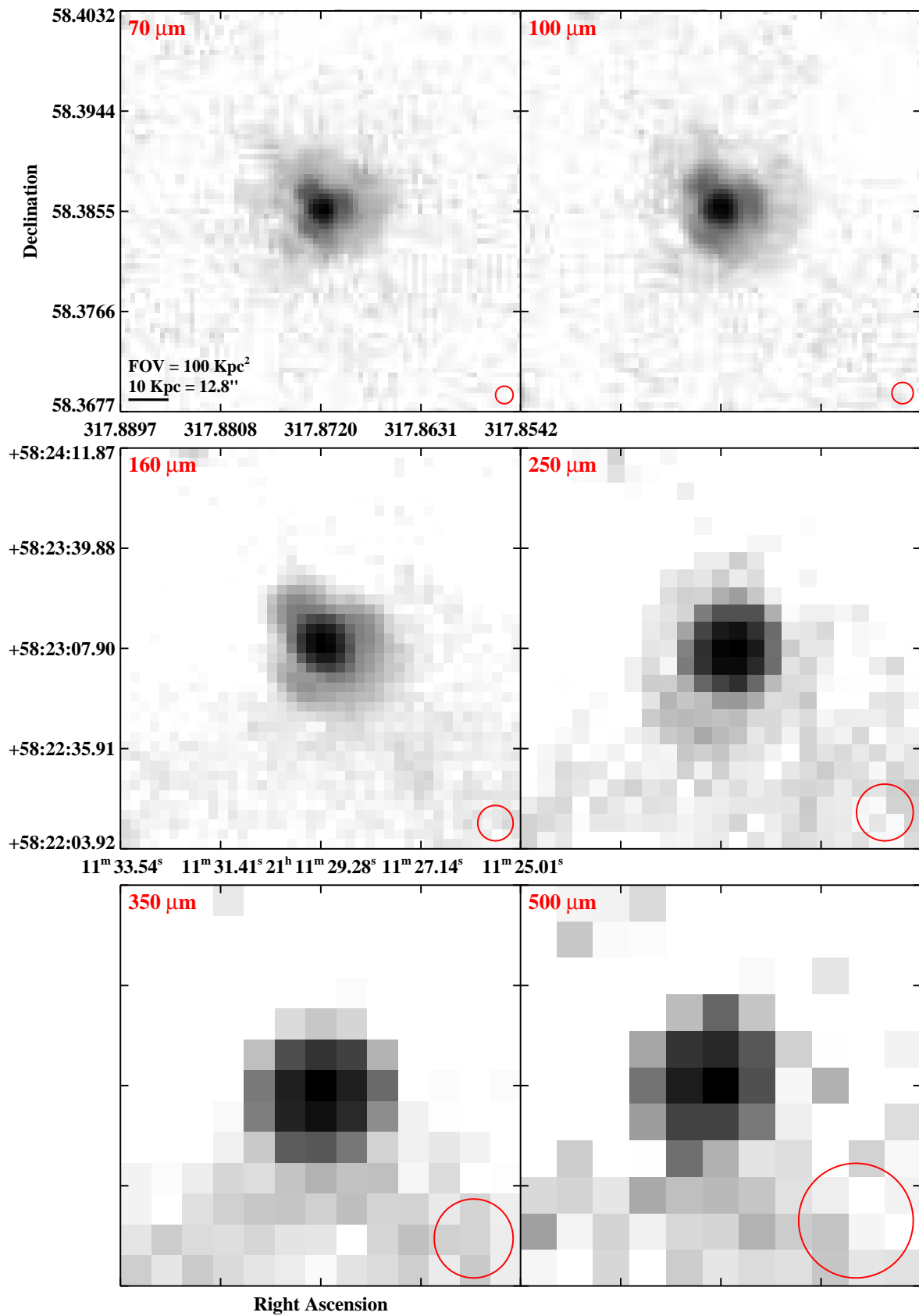


Fig. 3.— Continued (page 183 of 209).

IRAS F21330–3846 (ESO 343–IG013)

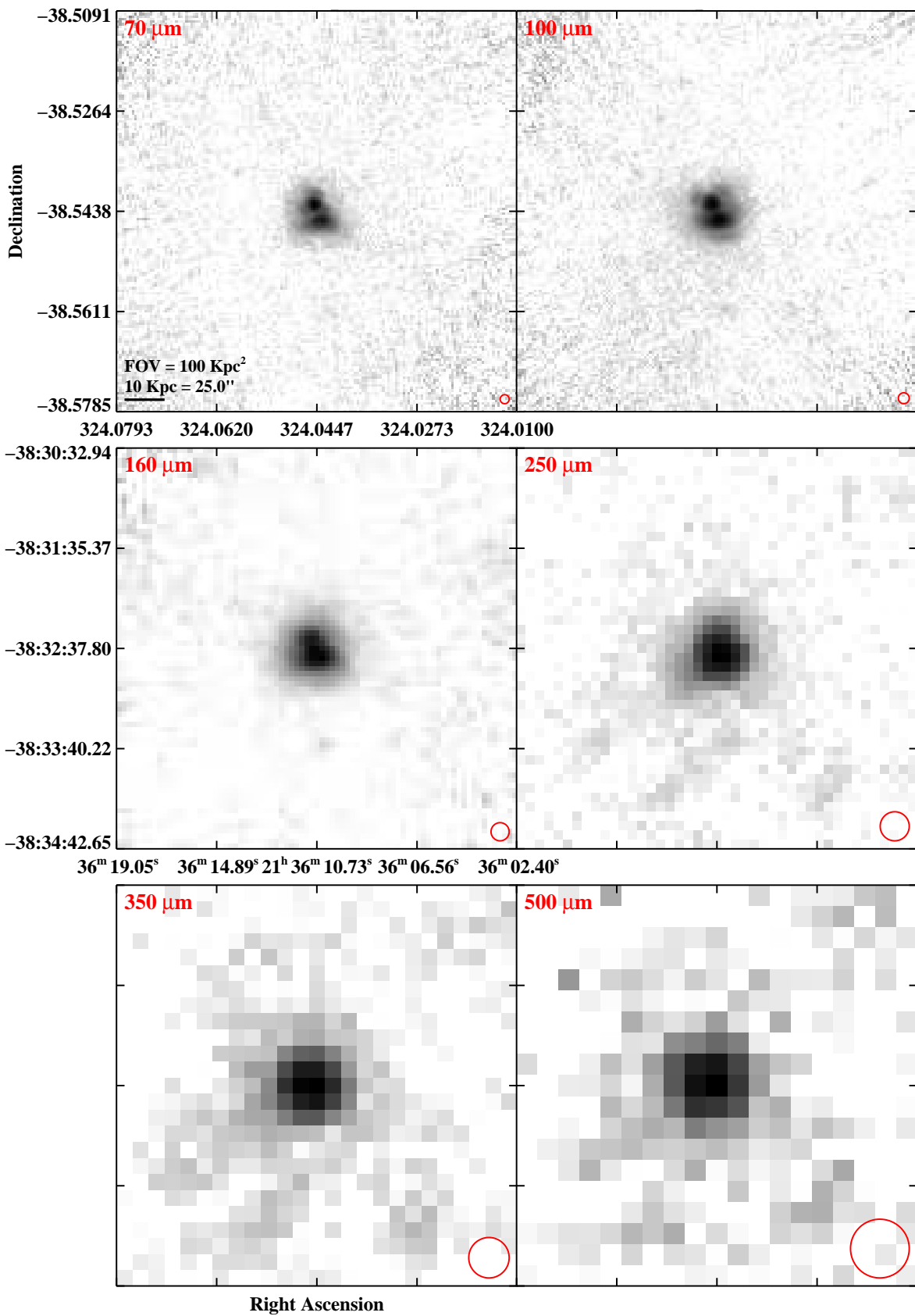


Fig. 3.— Continued (page 184 of 209).

IRAS F21453–3511 (NGC 7130)

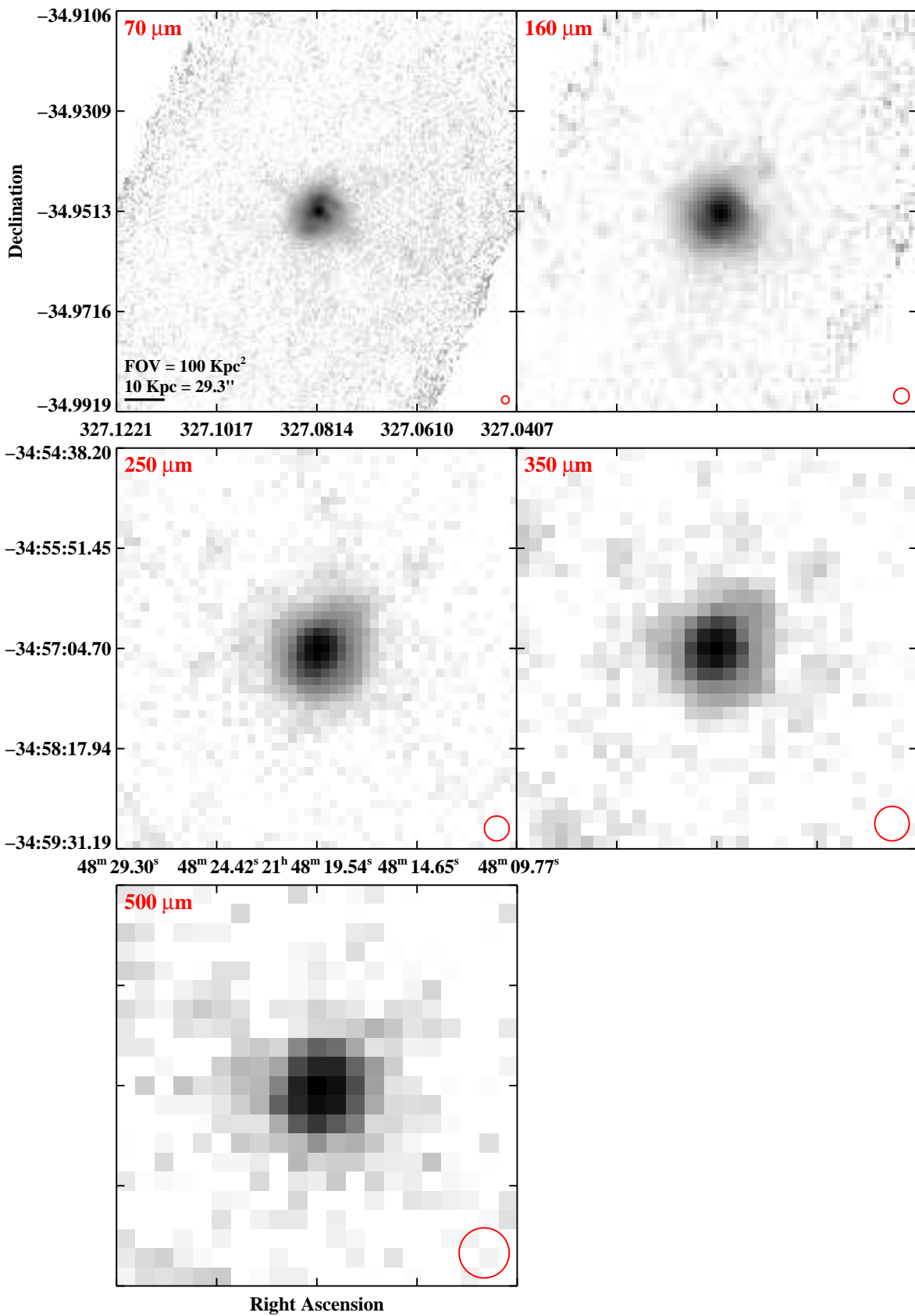


Fig. 3.— Continued (page 185 of 209).

IRAS F22118–2742 (ESO 467–G027)

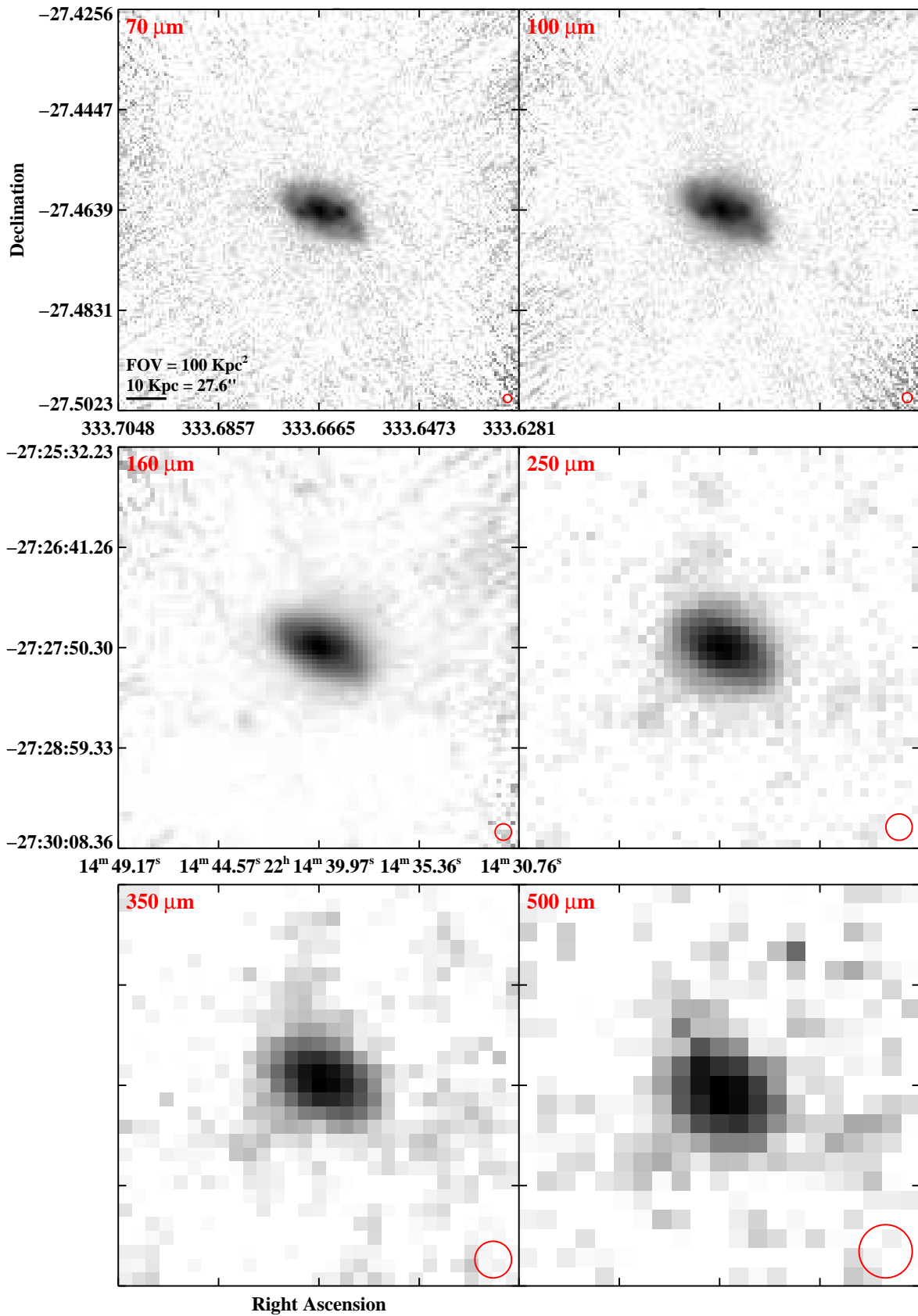


Fig. 3.— Continued (page 186 of 209).

IRAS F22132–3705 (IC 5179)

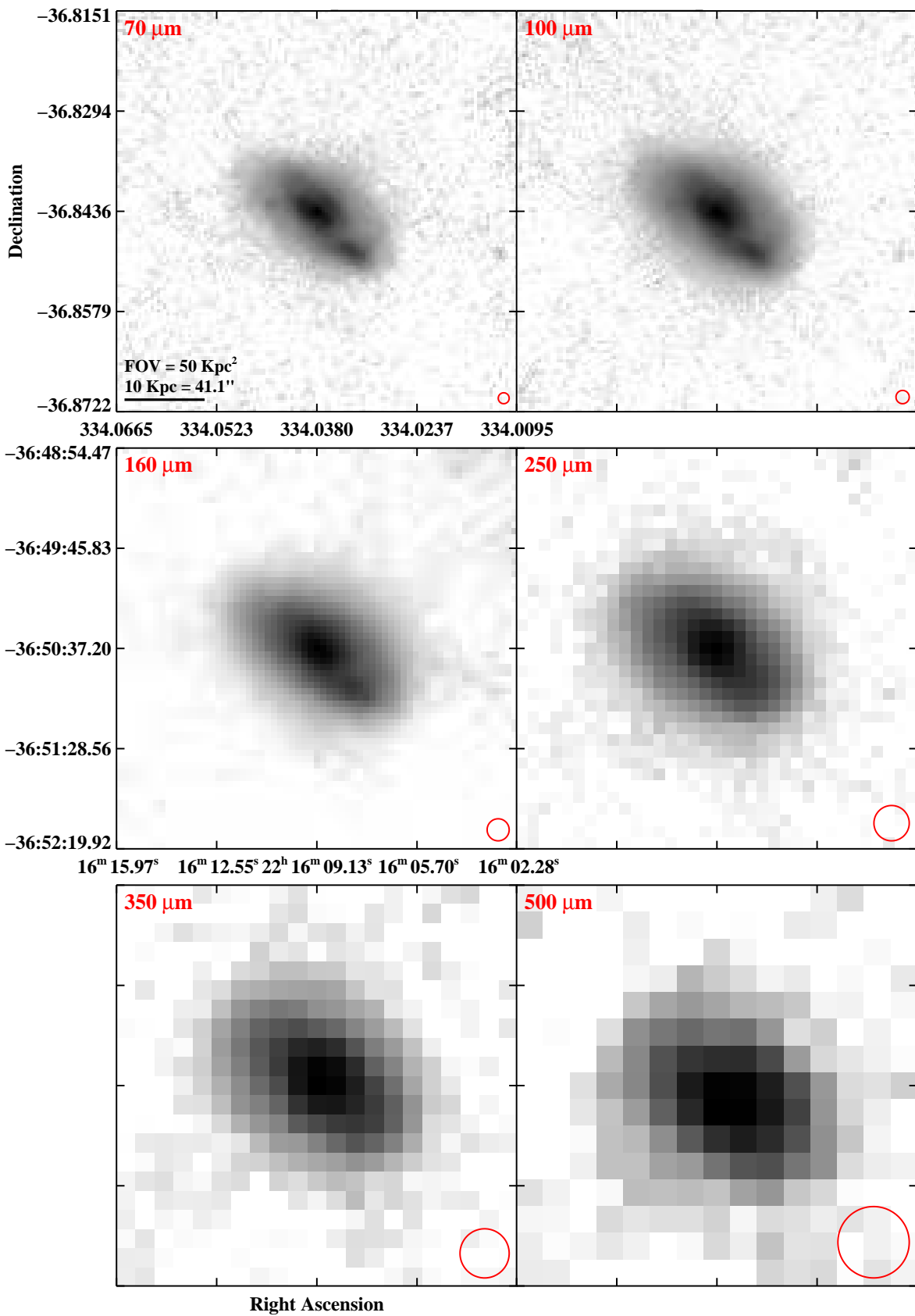


Fig. 3.— Continued (page 187 of 209).

IRAS F22287–1917 (ESO 602–G025)

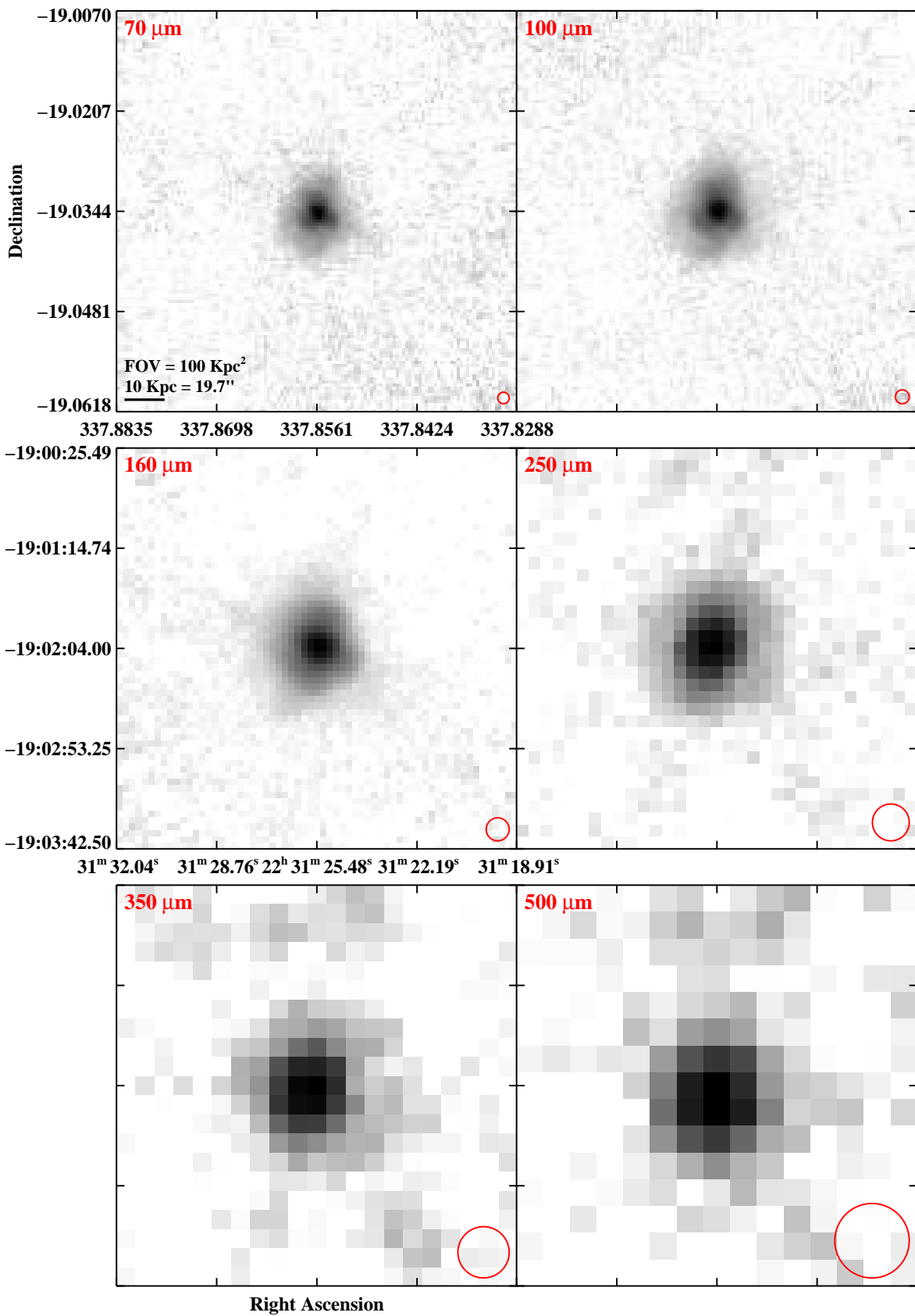


Fig. 3.— Continued (page 188 of 209).

IRAS F22389+3359 (UGC 12150)

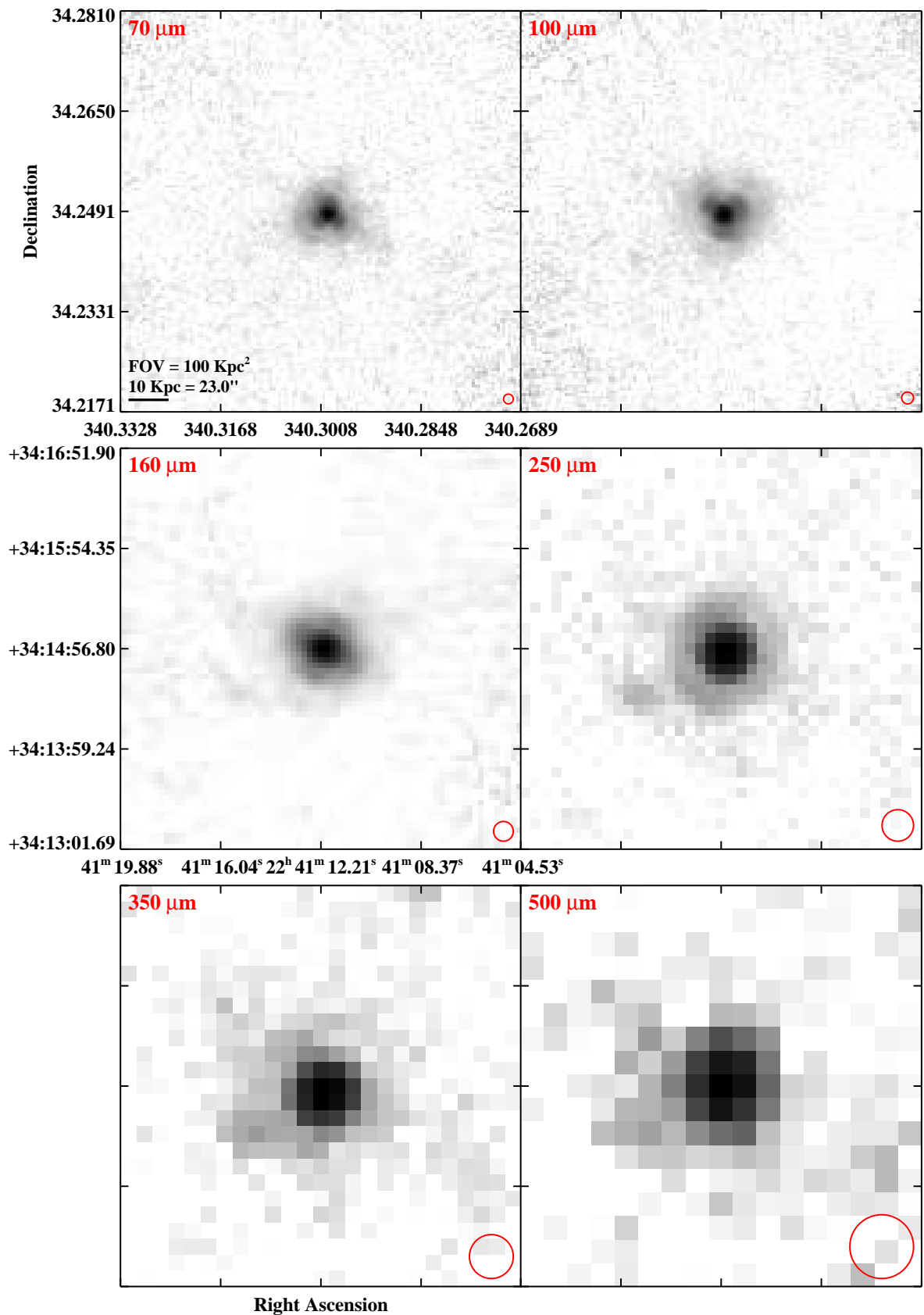


Fig. 3.— Continued (page 189 of 209).

IRAS F22467–4906 (ESO 239–IG002)

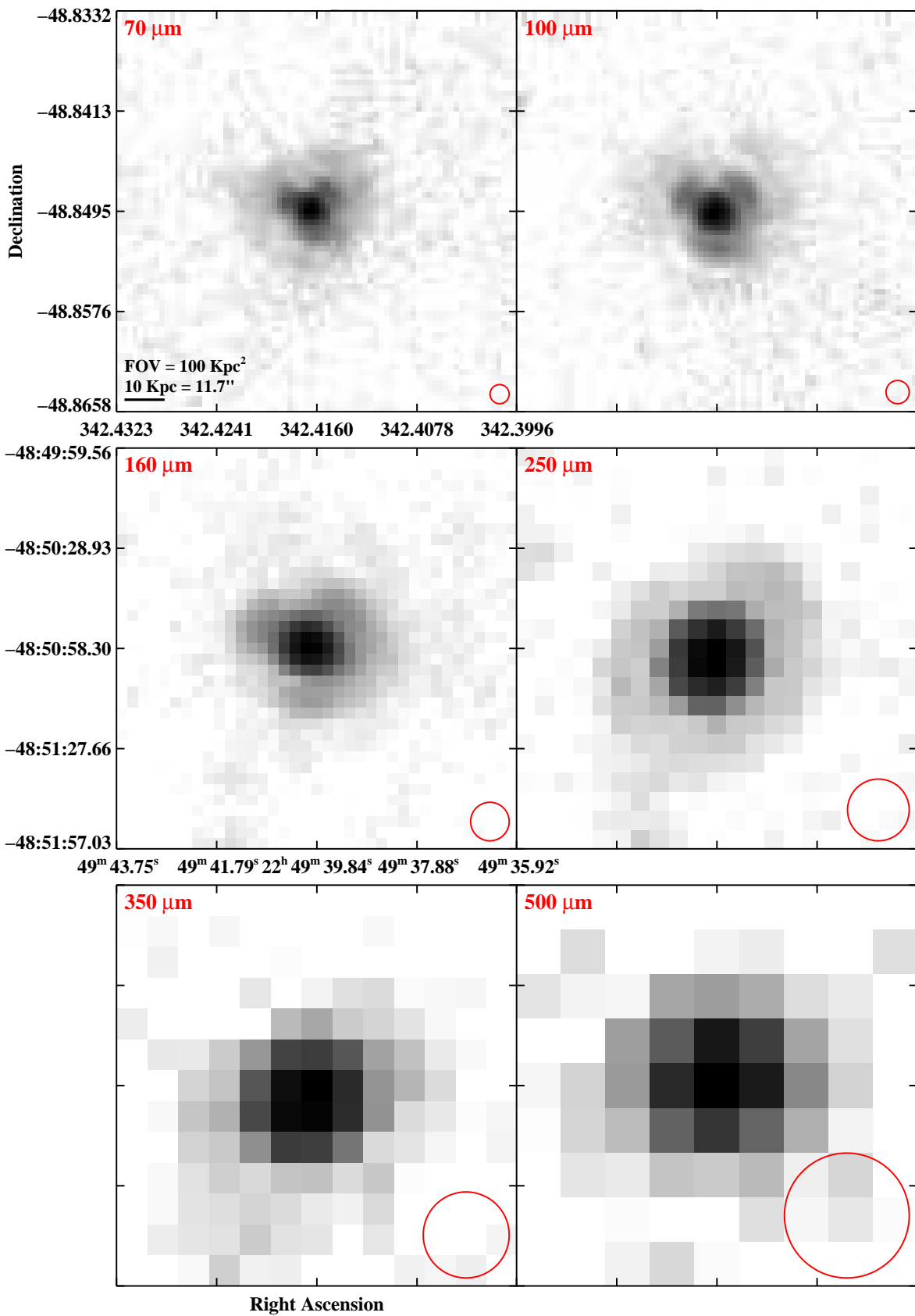


Fig. 3.— Continued (page 190 of 209).

IRAS F22491–1808

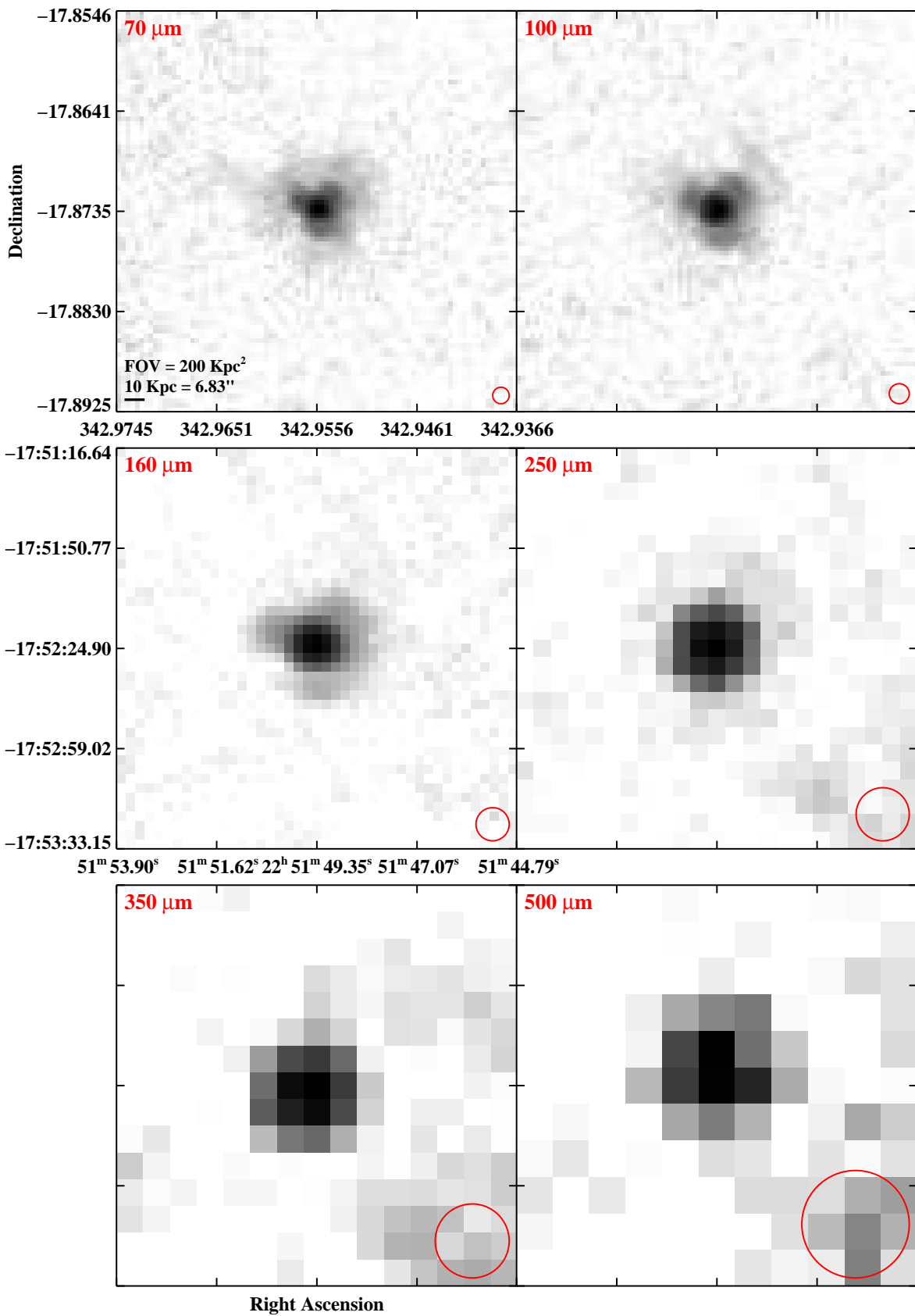


Fig. 3.— Continued (page 191 of 209).

IRAS F23007+0836 (NGC 7469/IC 5283/Arp 298)

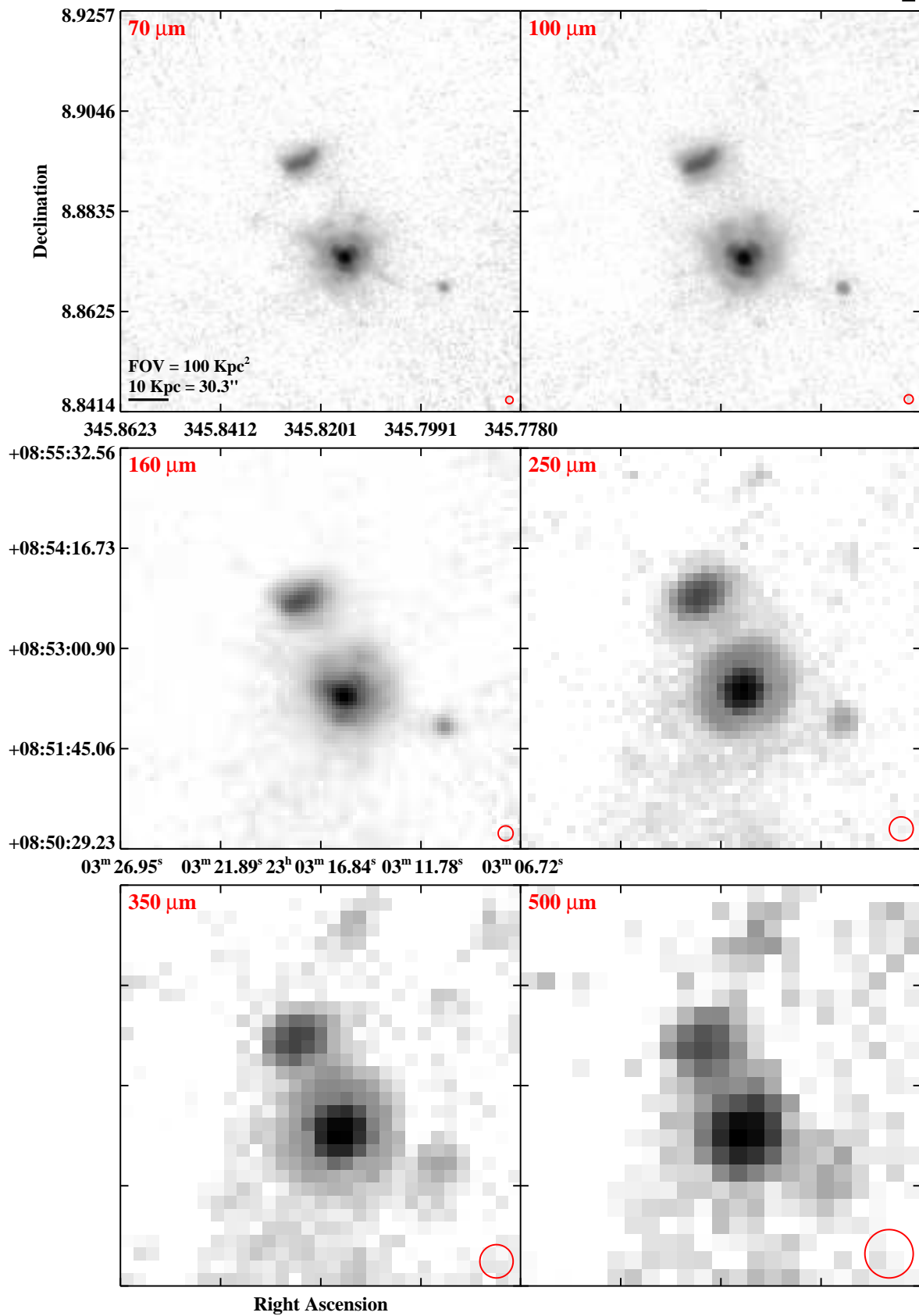


Fig. 3.— Continued (page 192 of 209).

IRAS F23024+1916 (CGCG 453-062)

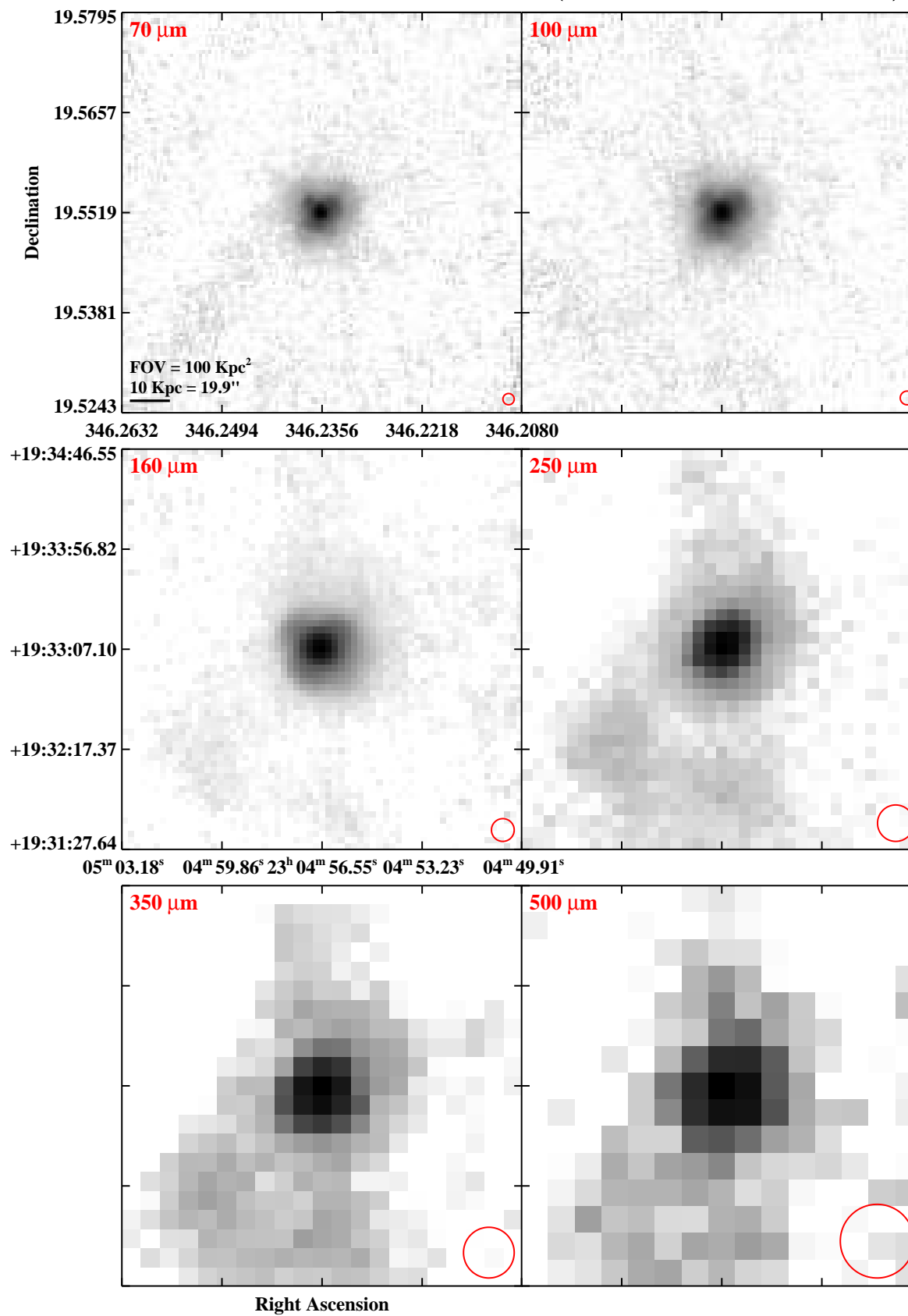


Fig. 3.— Continued (page 193 of 209).

IRAS F23128–5919 (ESO 148–IG002)

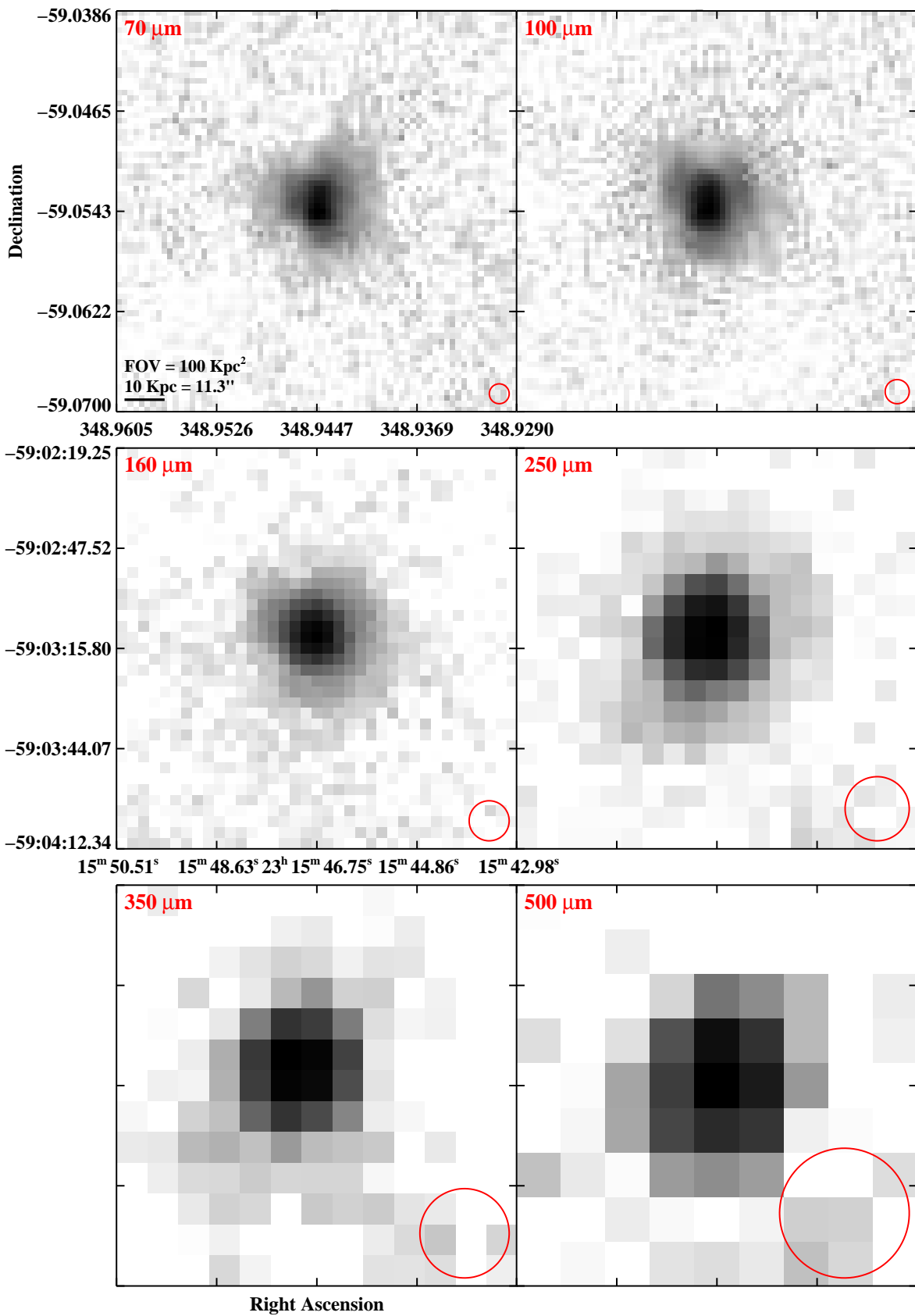


Fig. 3.— Continued (page 194 of 209).

IRAS F23135+2517 (IC 5298)

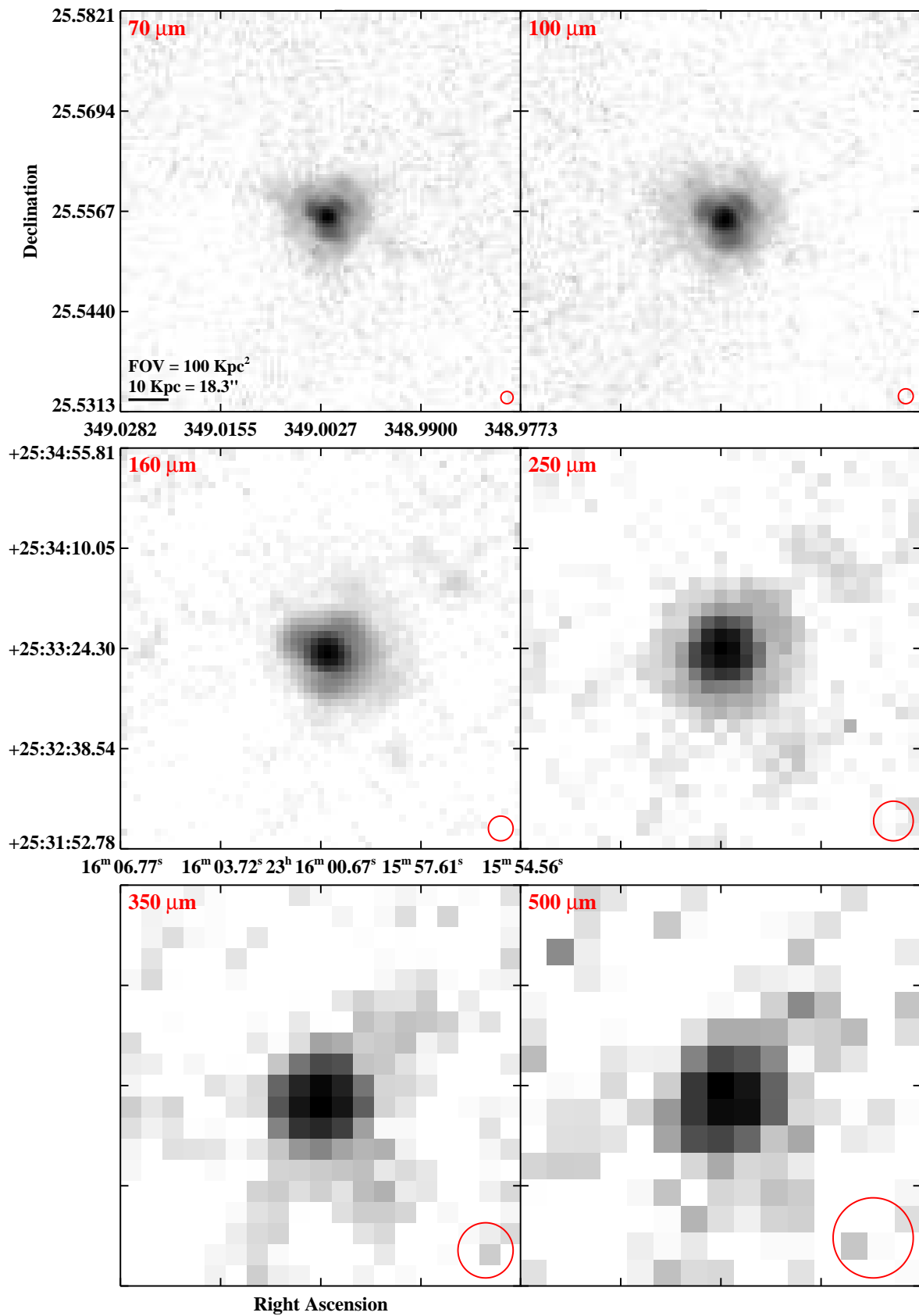


Fig. 3.— Continued (page 195 of 209).

IRAS F23133–4251 (NGC 7552)

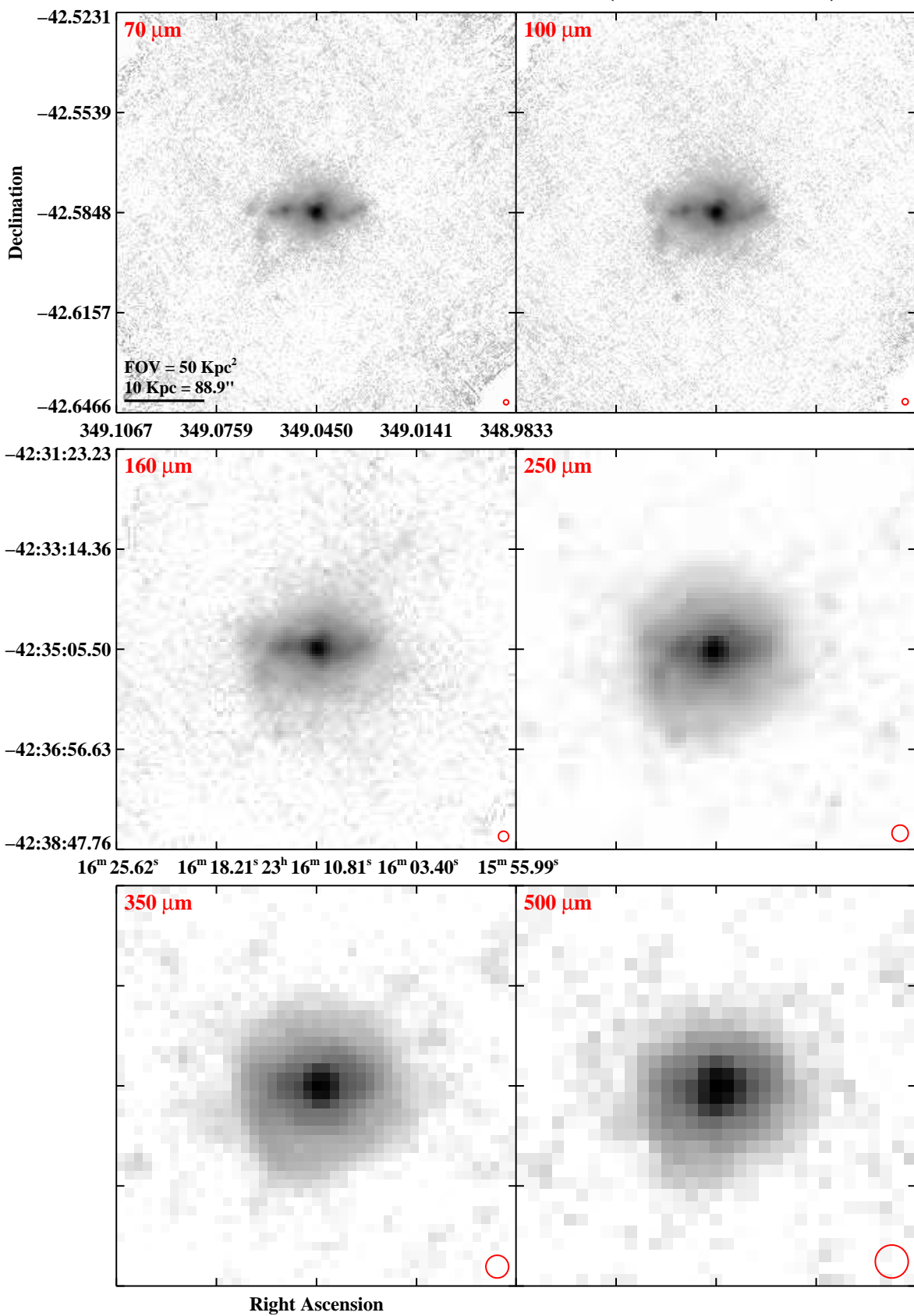


Fig. 3.— Continued (page 196 of 209).

IRAS F23157+0618 (NGC 7591)

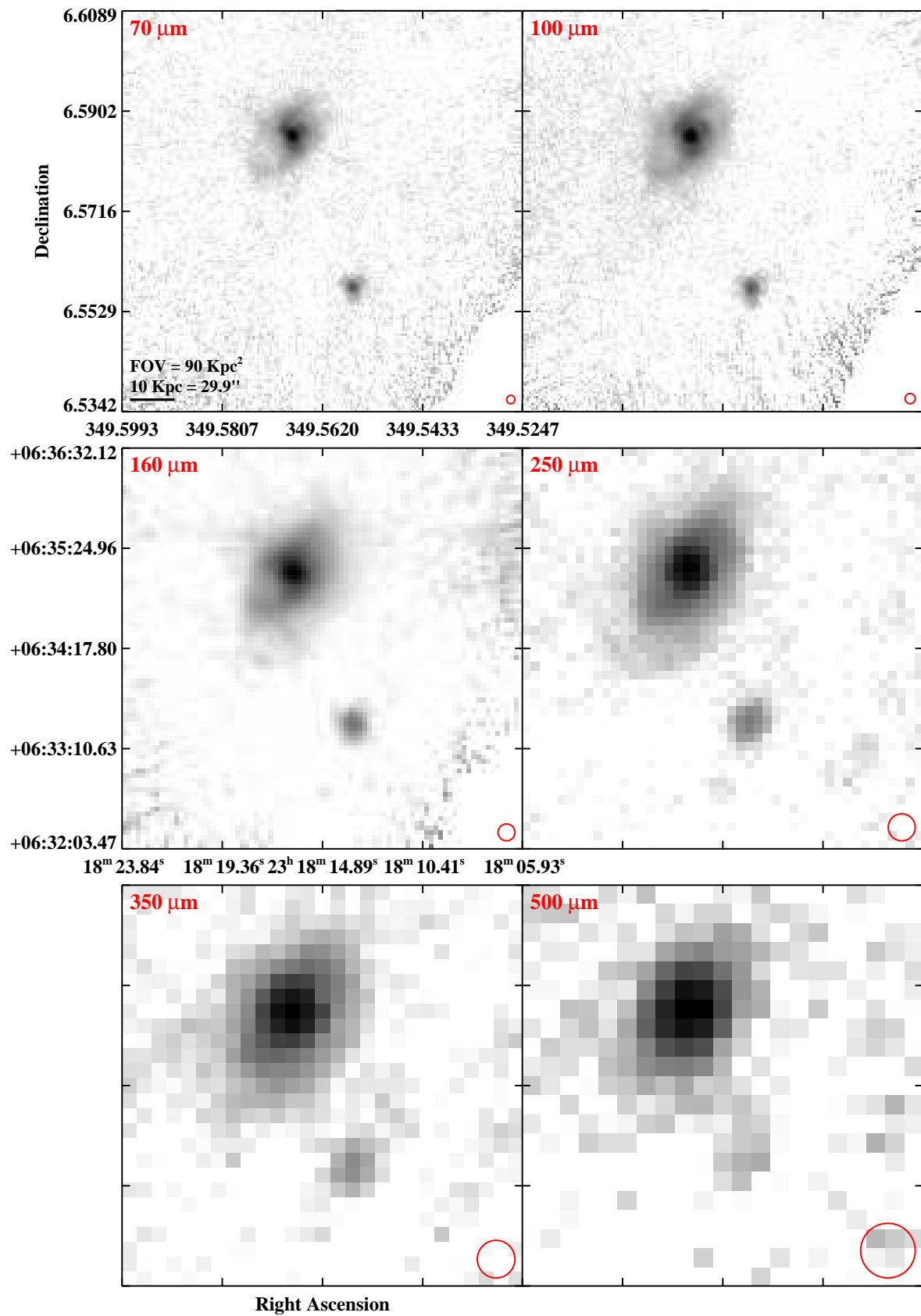


Fig. 3.— Continued (page 197 of 209).

IRAS F23157–0441 (NGC 7592)

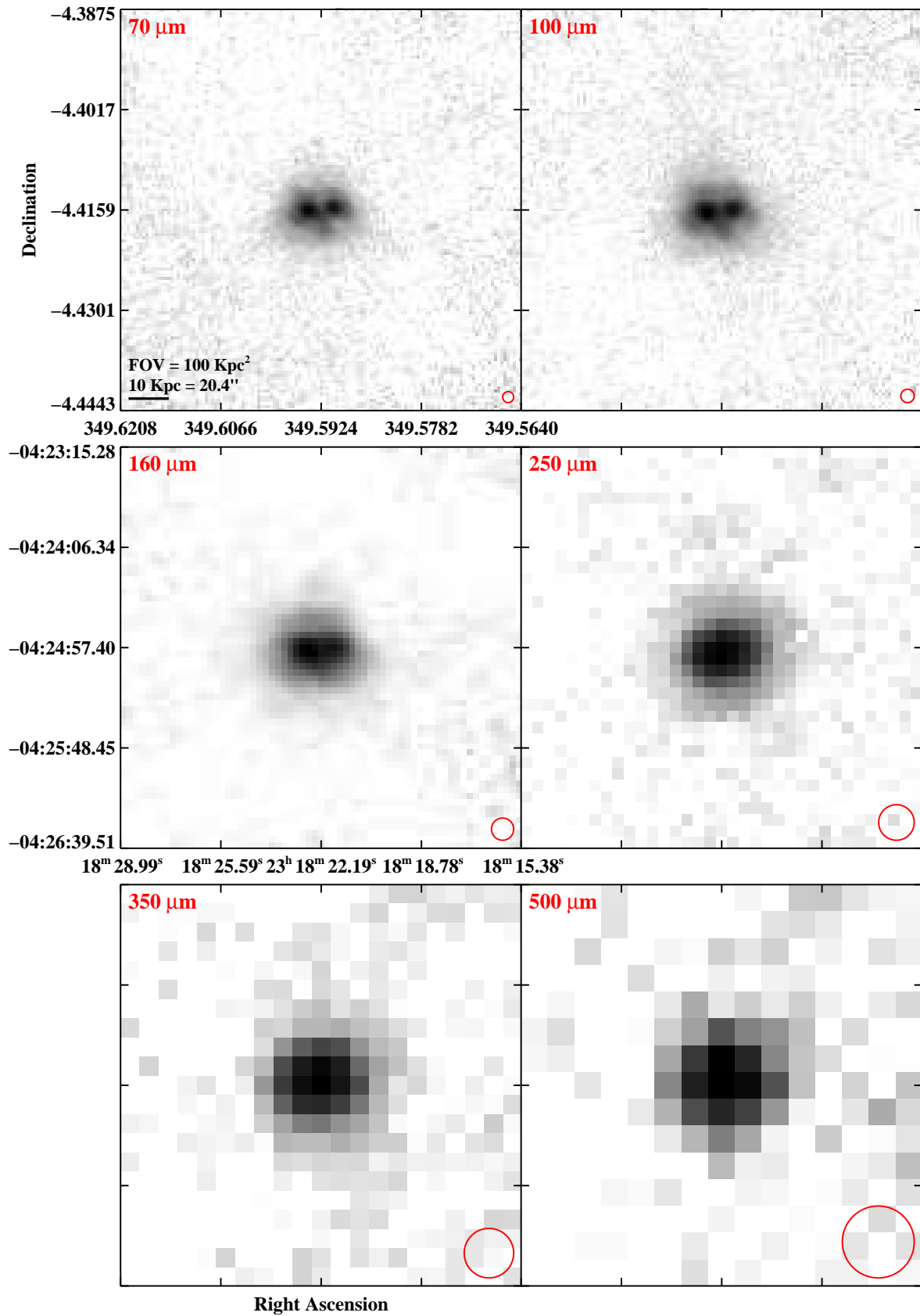


Fig. 3.— Continued (page 198 of 209).

IRAS F23180–6929 (ESO 077–IG014)

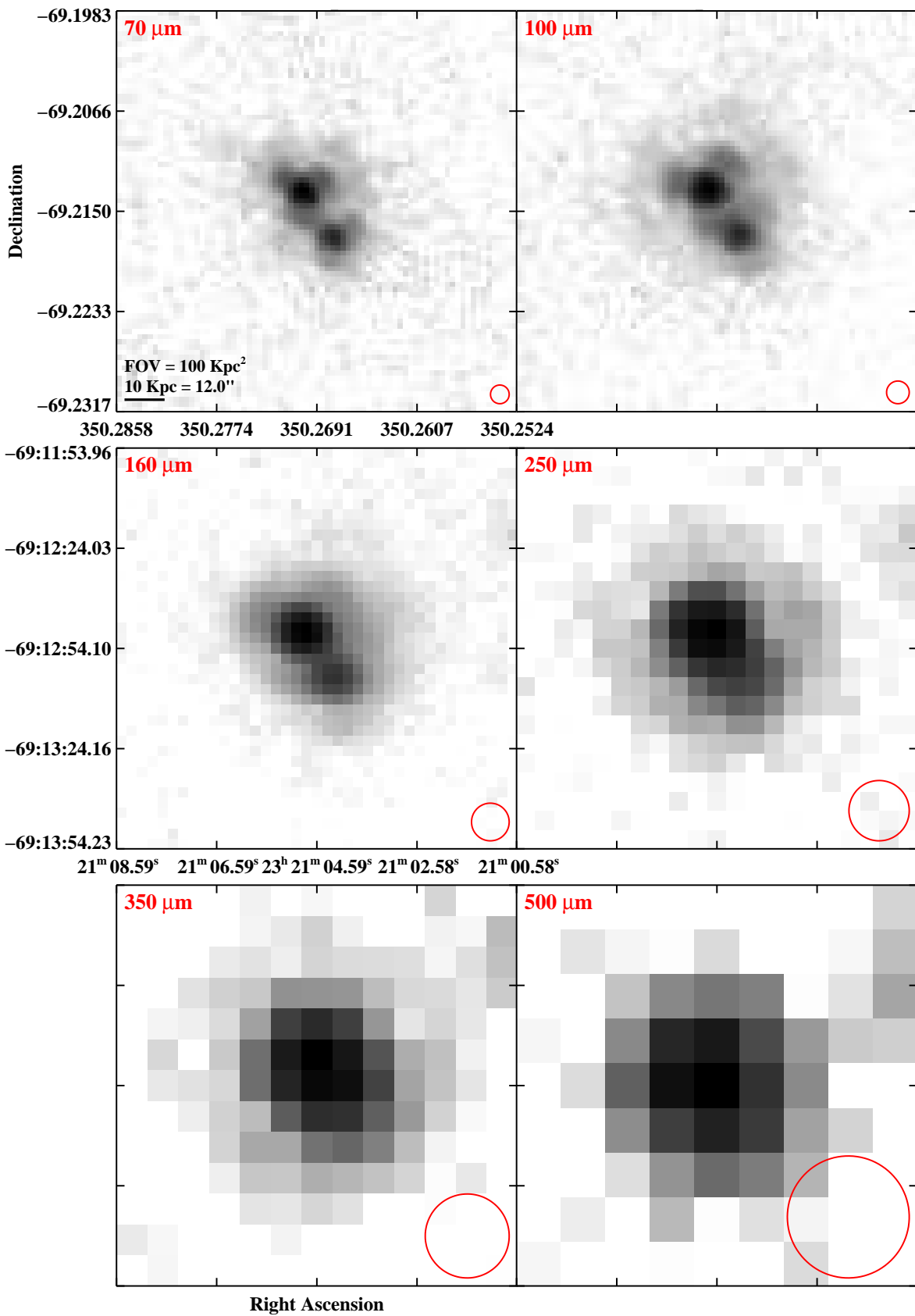


Fig. 3.— Continued (page 199 of 209).

IRAS F23254+0830 (NGC 7674)

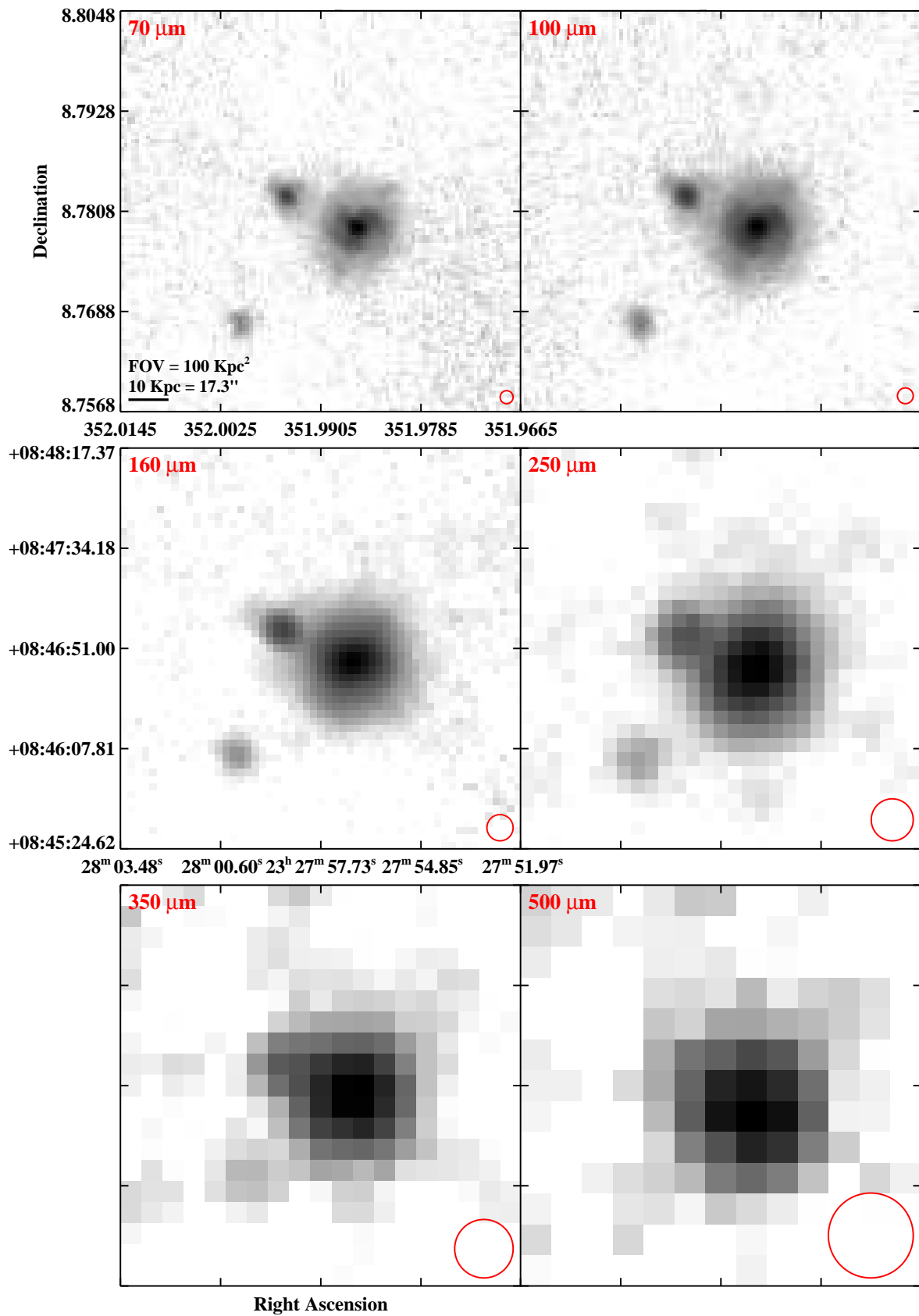


Fig. 3.— Continued (page 200 of 209).

IRAS 23262+0314 (NGC 7679)

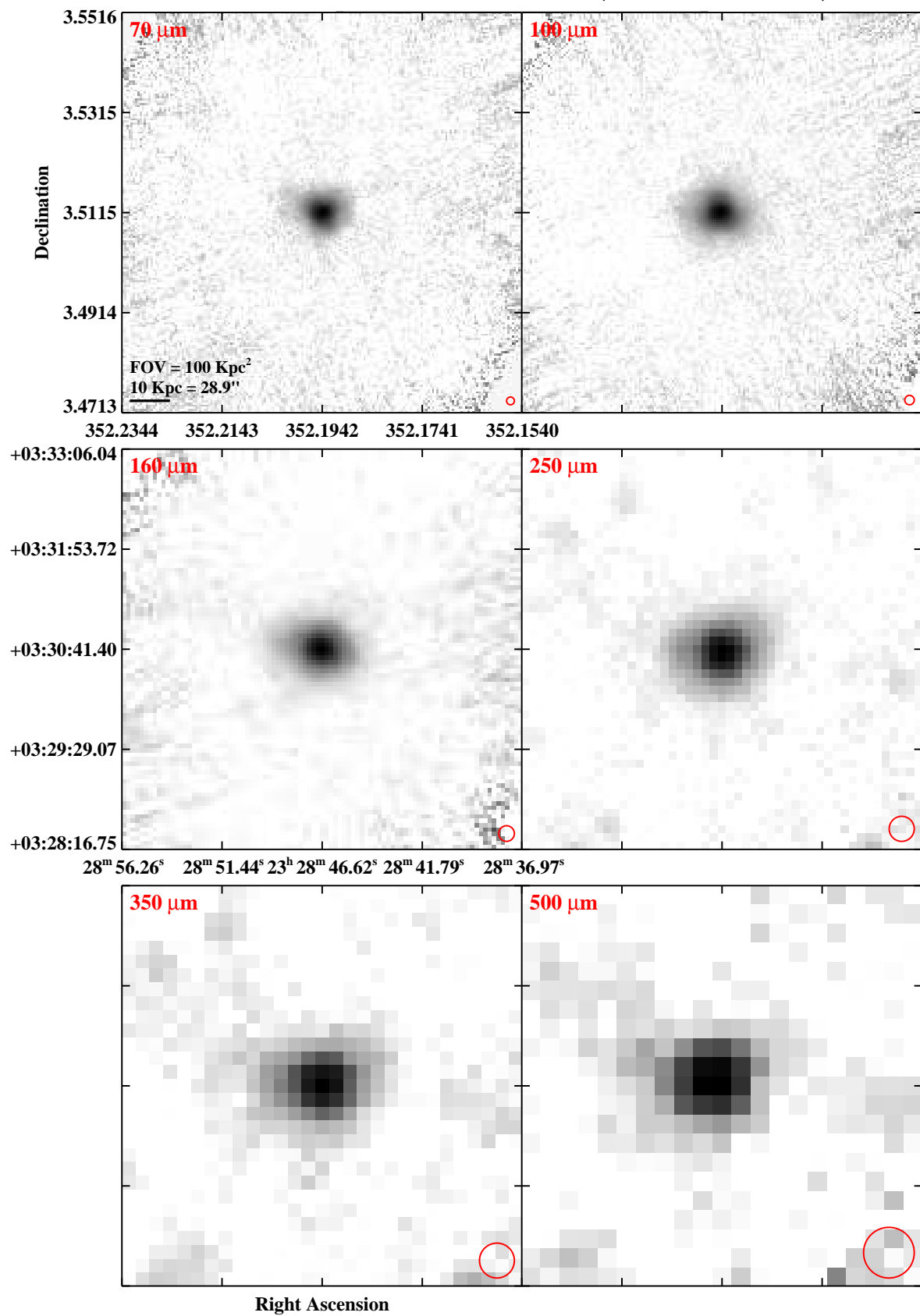


Fig. 3.— Continued (page 201 of 209).

IRAS 23262+0314 (NGC 7682)

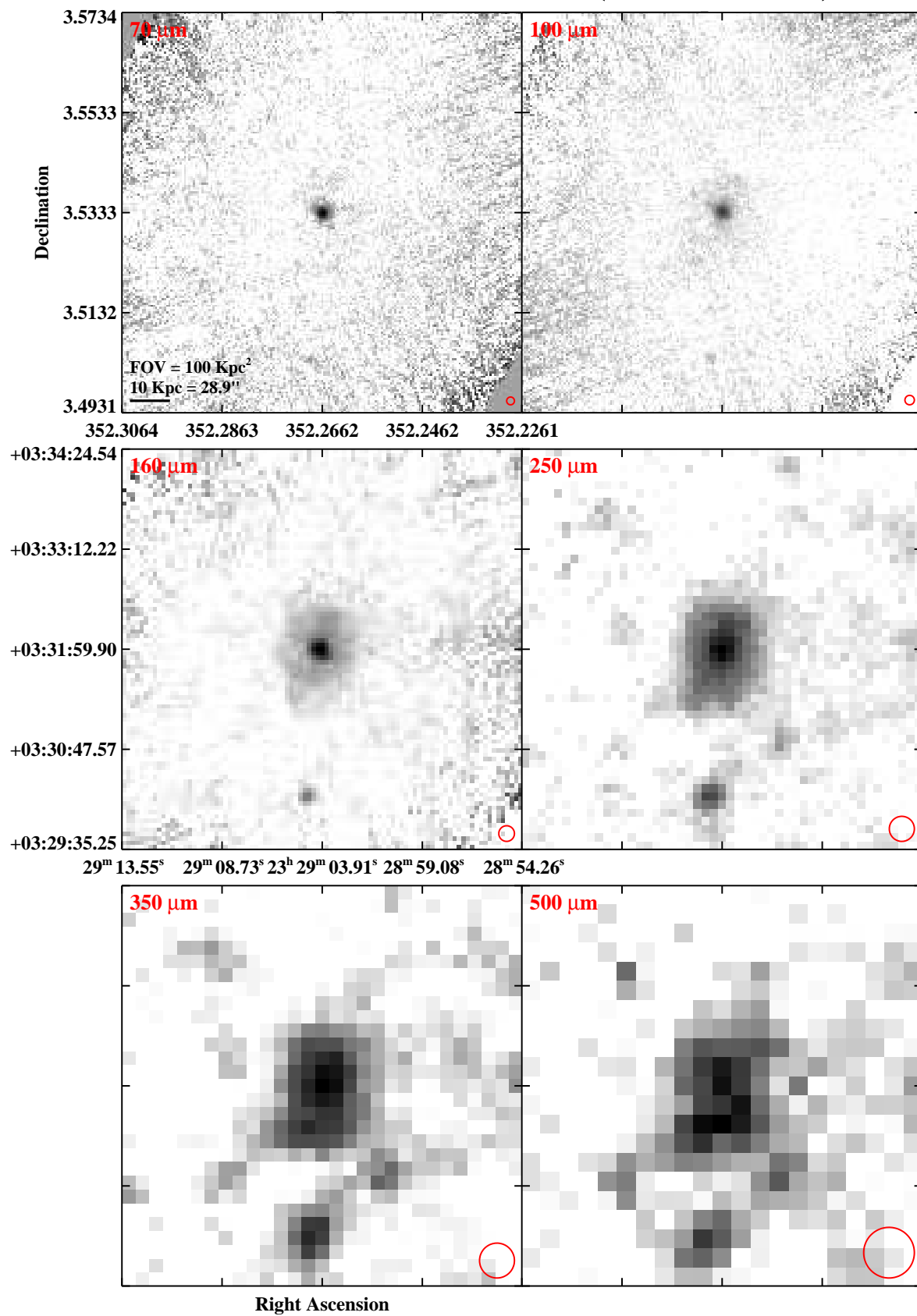


Fig. 3.— Continued (page 202 of 209).

IRAS F23365+3604

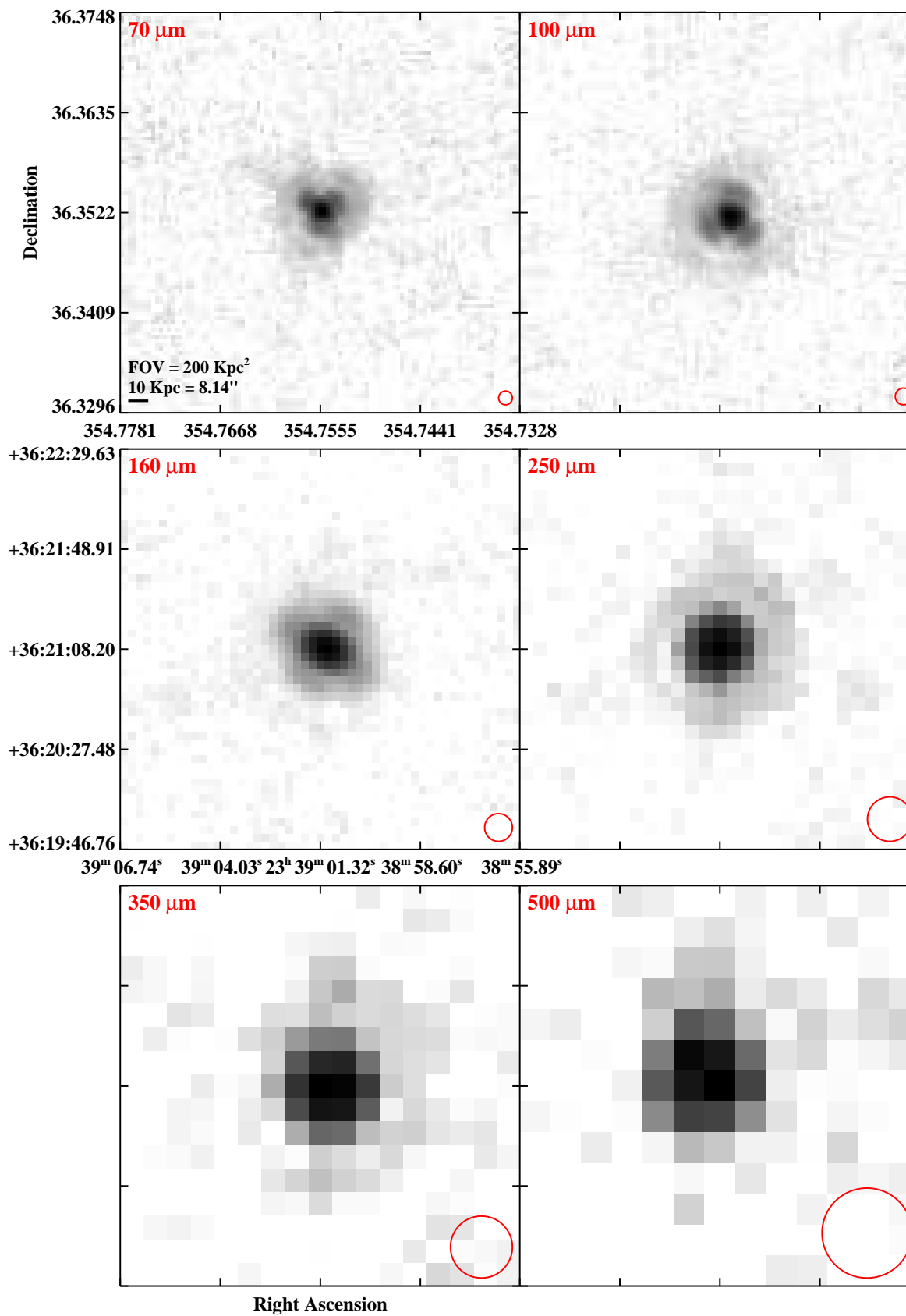


Fig. 3.— Continued (page 203 of 209).

IRAS F23394–0353 (MCG–01–60–022)

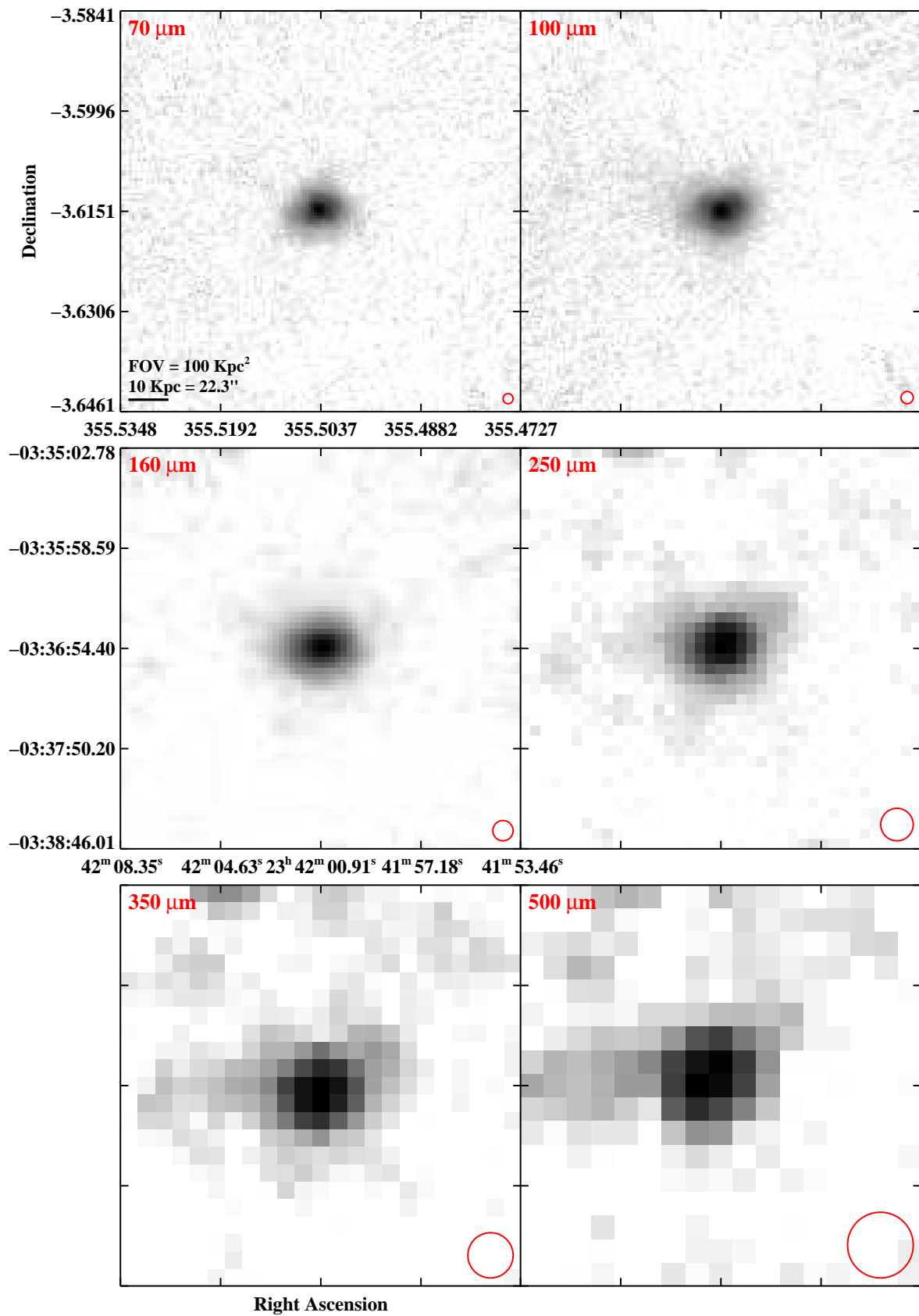


Fig. 3.— Continued (page 204 of 209).

IRAS F23394–0353 (MCG–01–60–021)

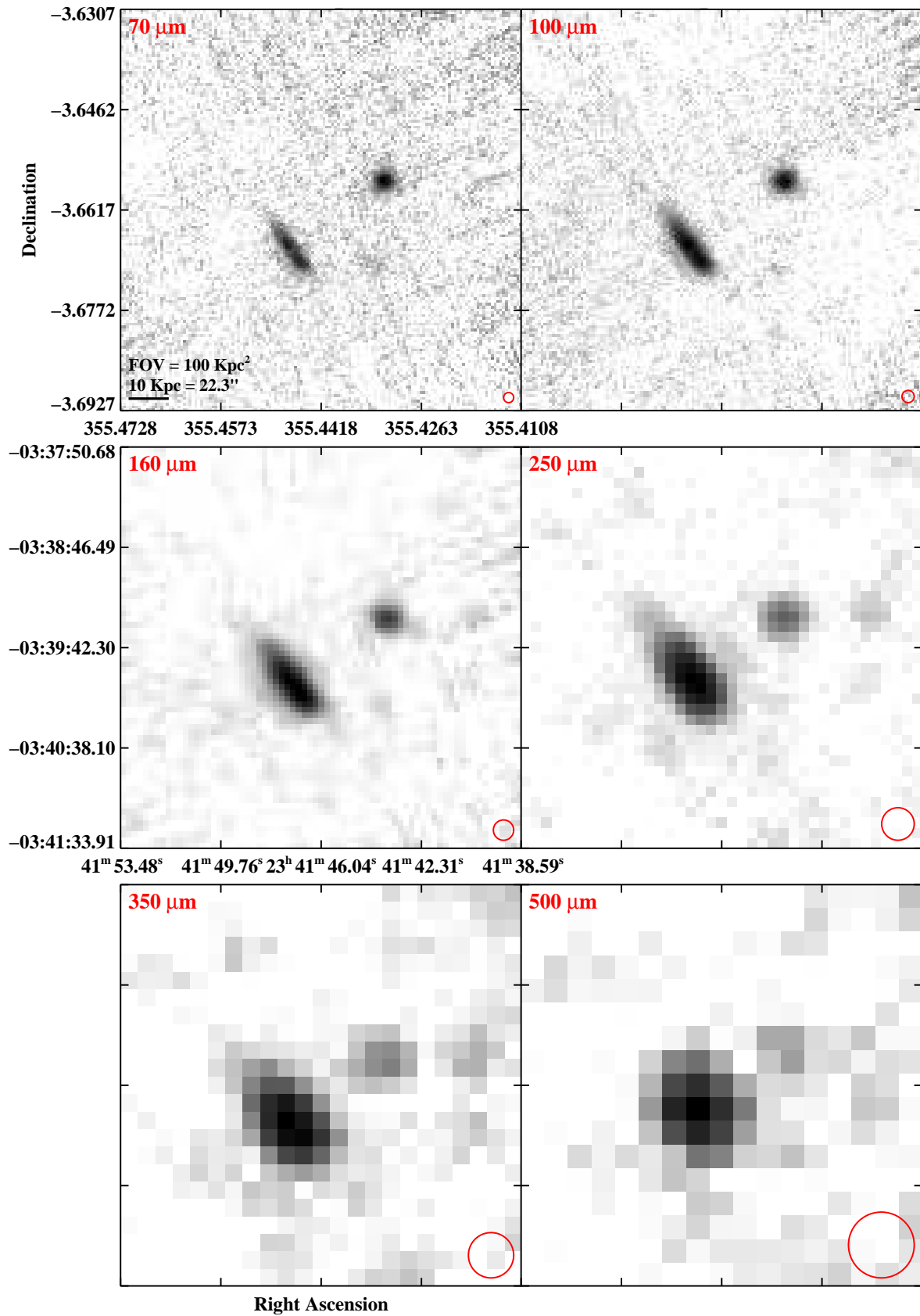


Fig. 3.— Continued (page 205 of 209).

IRAS 23436+5257

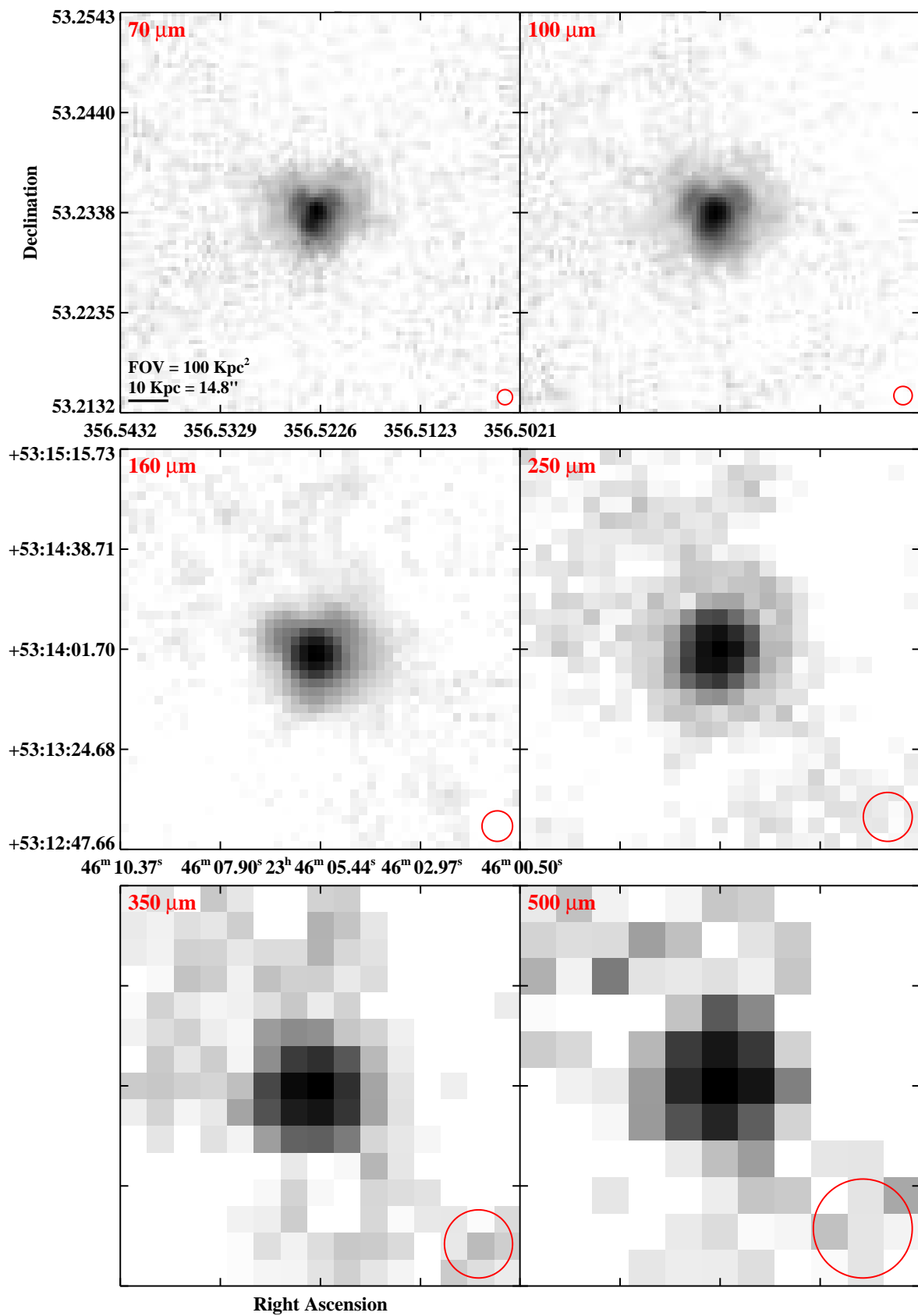
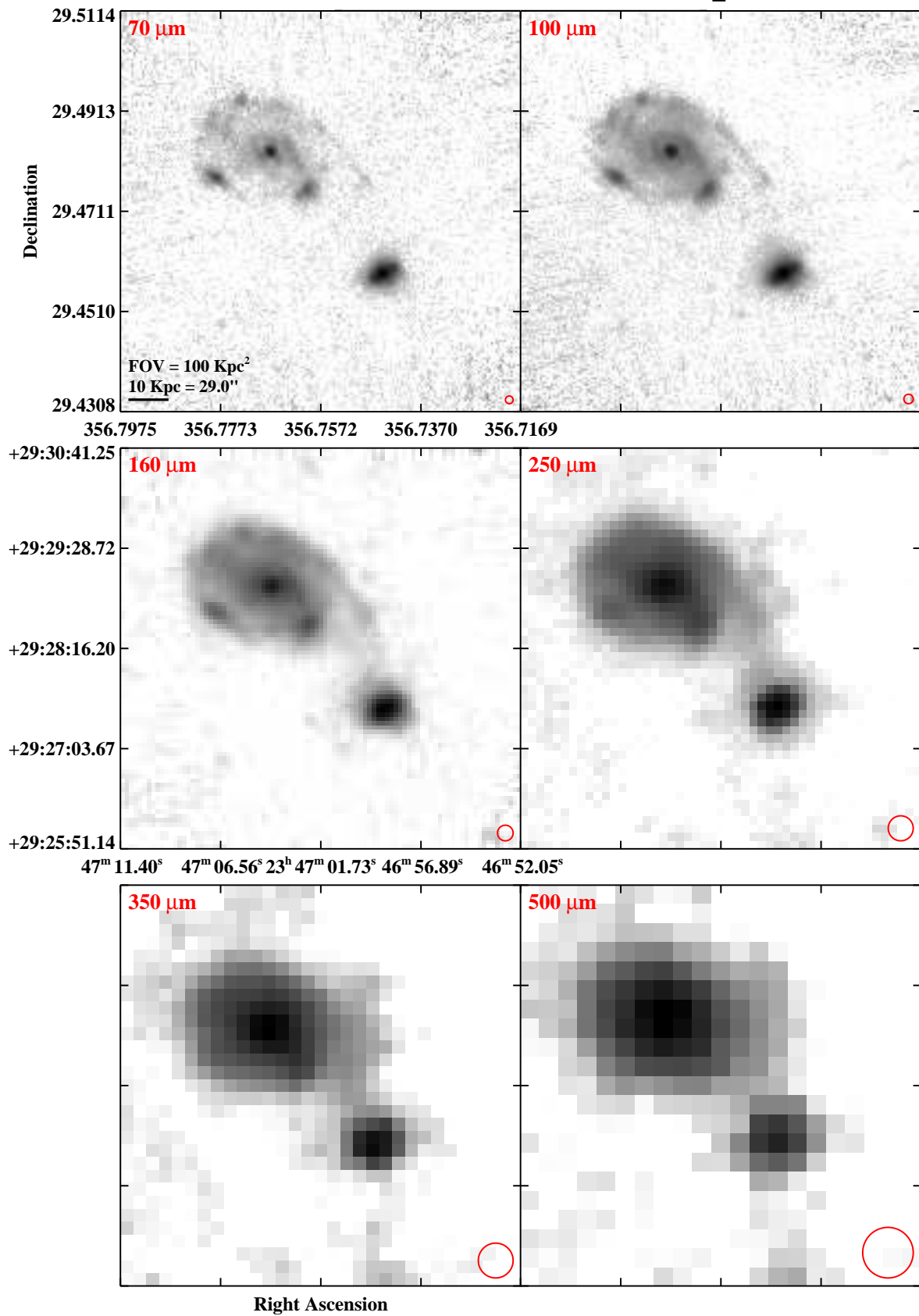


Fig. 3.— Continued (page 206 of 209).

IRAS F23444+2911 (Arp 86)



234

Fig. 3.— Continued (page 207 of 209).

IRAS F23488+1949 (NGC 7771)

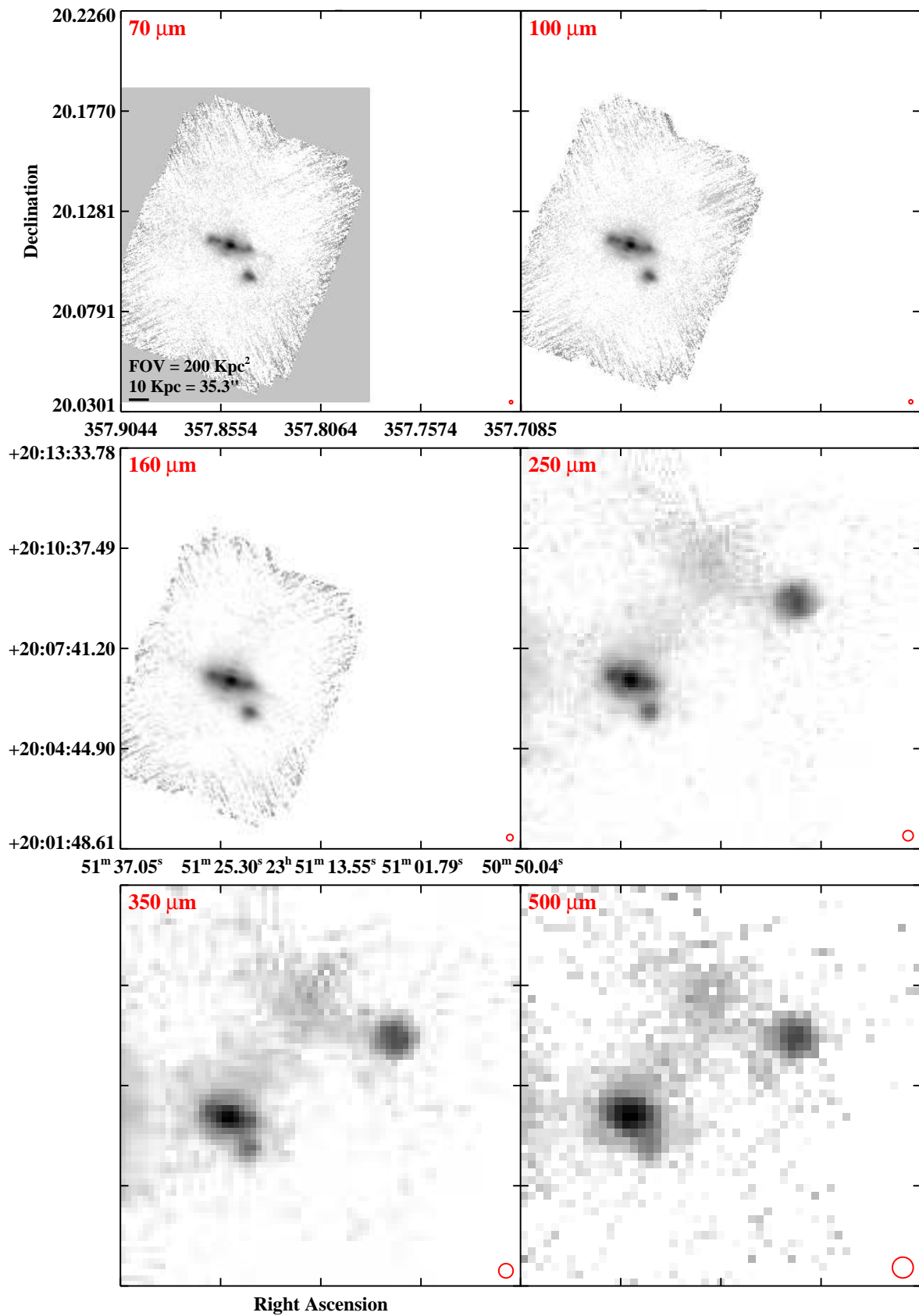


Fig. 3.— Continued (page 208 of 209).

IRAS F23488+2018 (Mrk 331)

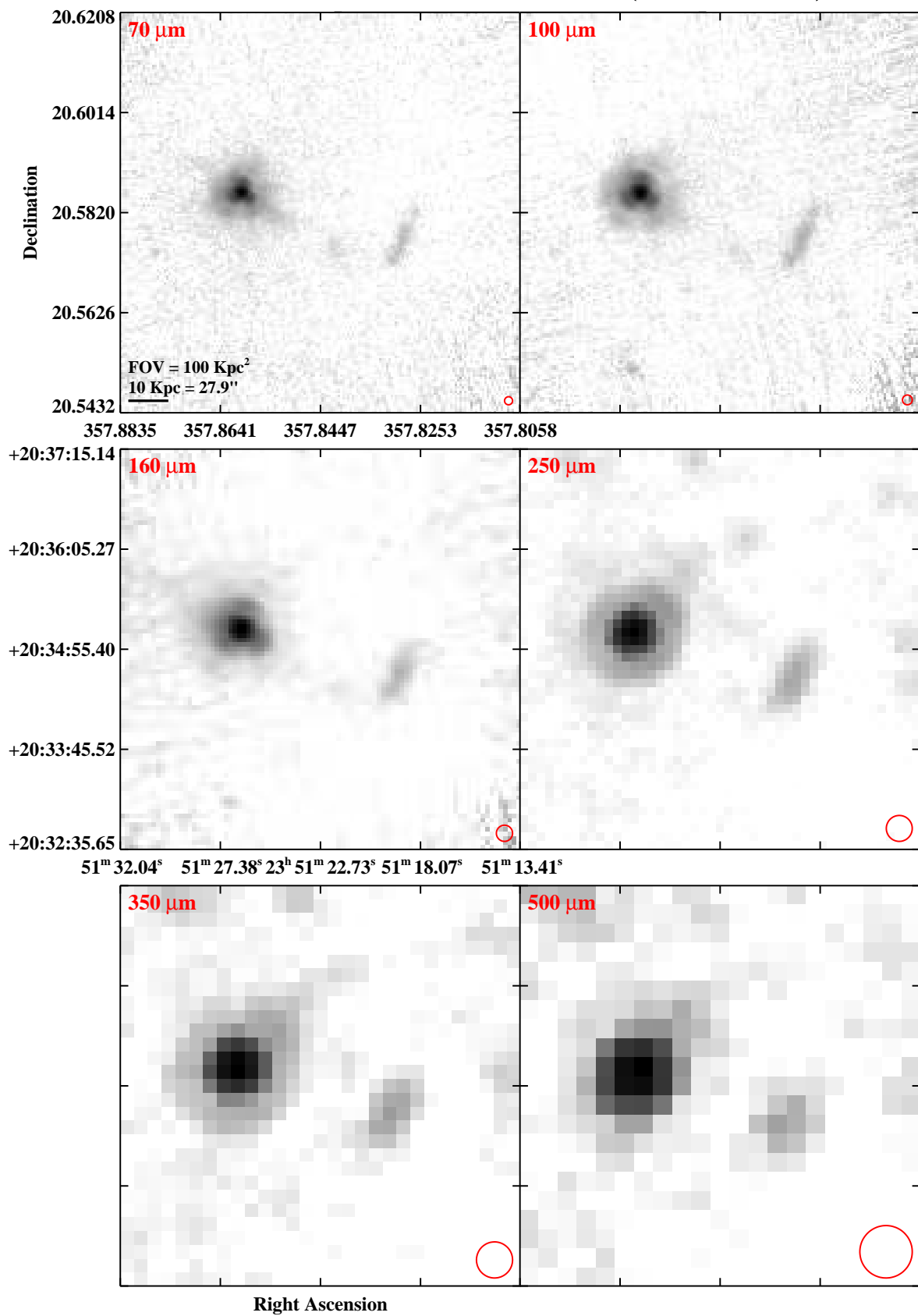


Fig. 3.— Continued (page 209 of 209).

6. *Herschel*-GOALS Aperture Photometry

In this section we discuss the manner in which the broadband photometry were determined for our sample. Both PACS and SPIRE photometry were obtained using the `annularSkyAperturePhotometry` routine found in HIPE. At first we attempted to measure fluxes by using an automated routine to determine the appropriate circular aperture sizes for each galaxy, based on data from the MIPS instrument on *Spitzer*. Unfortunately this approach does not work well for our sample, due to the extended nature of some GOALS systems and galaxies.

Instead we concluded that the best approach was to determine apertures by visual inspection, and subsequently check that we included all of the flux by plotting a curve of growth. We found that after subtracting any offset in the background levels, the curve of growth almost always flattens out at large radii, indicating a background flux contribution of zero. There are only a few small cases in the PACS data where the curve of growth does not flatten out, and in all cases this occurs when the object is very faint ($F_\lambda \lesssim 0.5$ Jy) and the background noise is more dominant. Curve of growth plots for the SPIRE data are also flat at large radii even for faint fluxes, again indicating robust background subtractions. In Figure 4 we show a set of representative curve-of-growth plots and apertures for IRAS F09111–1007 at different wavelengths. The photometry aperture is represented by the blue circle in the image and the blue line in the curve of growth plot below it. In order to facilitate comparison of matched aperture fluxes, all PACS aperture sizes are identical, while all SPIRE apertures are also identical, but larger than that of PACS. The aperture radius is typically set by the band with the largest beam size in which we can make a measurement for each instrument, which is usually the 160 μm channel for PACS and the 500 μm channel for SPIRE. We found that aperture radii encompassing approximately 95% of the total light gave the best tradeoff between including all of the flux but at the same time keeping the background error from getting too high. Although it is possible to use the same aperture size across all six bands (i. e. the SPIRE aperture size), the larger SPIRE aperture would encompass a significant amount of sky background for the higher resolution images (i. e. at 70 μm) and would introduce additional noise in our measurements. We therefore decided it was best to match the apertures for each instrument.

To accurately measure the flux of each galaxy the sky background must be subtracted from the measured flux. To do this we estimate the sky background in the annulus represented by the red circles in the image, which corresponds to the two red lines in the curve of growth plot. These background annuli were chosen to be as free from any source emission as possible. Within the `annularSkyAperturePhotometry` routine we used the sky estimation algorithm from DAOPhot⁷ to estimate the sky level, with the “fractional pixel” setting enabled. The background corrected flux density is then the total flux minus the product of the measured background level and the number of pixels within the target aperture.

We note that in some cases both component and total fluxes are measured for close pairs. These galaxies can be easily resolved and separated at shorter wavelengths, but become unresolved at longer wavelengths. In order to choose the best flux aperture, we carefully selected the radius at which the curve of growth was flattest. This is apparent in Figure 4 in the first two columns where the galaxy pair is easily resolved at 70 μm , but becomes marginally resolved at 160 μm . The third column in Figure 4 shows the curve of growth from a single large aperture encompassing the entire system, which includes faint extended flux missed by the individual component apertures. Finally since the galaxy pair is unresolved in the 350 μm and 500 μm SPIRE bands, we do not measure any component fluxes at those wavelengths. At 250 μm , component fluxes are still computed since they pair is still resolved. Every effort was made to measure as many marginally resolved systems as possible, while also providing a total flux measurement from one large aperture when necessary. We believe separately measuring component and total fluxes in cases such as this will be useful when the fractional flux contribution of each component is desired.

In Table 3 we present the table of monochromatic total flux density for each GOALS system in units of Jansky. Depending on the number of galaxies within a system, their apparent separation on the sky, and the beam size at that particular wavelength, the total *Herschel* flux for each system is calculated using one of three methods. In the simple case of single galaxy, the system flux is just the flux of that galaxy. In cases where there are two or more galaxies that are widely separated, the total flux is the sum of the component

⁷Adapted from the IDL AstroLib `mmm.pro` routine.

fluxes measured in separate apertures. Finally in cases where component galaxies are resolved but still overlapping (i. e. in Figure 4), the total system flux is obtained from a single large aperture encompassing all of the components. For triple and quadruple systems where two galaxies are close and a third (or fourth) is far away (i. e. IRAS F02071–1023), the total system flux is calculated using a hybrid method: a single large aperture for the two close components, plus a second (or third) aperture around the far component(s). Since all of the total fluxes are calculated differently, we omit the coordinate and aperture radius in Table 3, but we include it in Table 4 (see below).

In Table 3, Column (1) is the row reference number (corresponding to Tables 1, 2, and 4) while column (2) is the IRAS name of the galaxy, ordered by ascending RA. Galaxies with the “F” prefix originate from the *IRAS* Faint Source Catalog, and galaxies with no “F” prefix are from the Point Source Catalog. Column (3) lists common optical counterpart names to the galaxy systems. Columns (4) – (6) are the total fluxes from the PACS instrument in units of Jy. Note that the four galaxies which lack 100 μm measurements are IRAS F02401-0013 (NGC 1068), IRAS F09320+6134 (UGC 05101), IRAS F15327+2340 (Arp 220), and IRAS F21453-3511 (NGC 7130). Columns (7) – (9) are the total fluxes from the SPIRE instrument in units of Jy.

In Table 4 we present the table of monochromatic flux density in units of Jansky for each component measurable within each system, with the total system flux from Table 3 included for completeness on the last line for each system. For total fluxes that do not have an aperture size listed, the totals were calculated as the sum of the components. Likewise the RA and declination for these systems (on the totals line) represent the geometric midpoint between the companion galaxies. The column descriptions are (1) the row reference number, which corresponds to the same indices used in Tables 1–3. Column (2) is the IRAS name of the galaxy, ordered by ascending RA. Column (3) is the individual name to that galaxy component. Note that galaxies prefixed by IRGP are from the catalog of newly defined infrared galaxy pairs defined in the companion *Spitzer*-GOALS paper by Mazzarella et al. (2017). Columns (4) – (5) are the coordinates of the aperture centers used. Lines where coordinates are listed but have no aperture radii are cases where the total flux is the sum of two widely separated components. These are the same 8 μm coordinates adopted in

Mazzarella et al. (2017), however a few were slightly adjusted for the *Herschel* data. Columns (6) – (7) are the aperture radii used for PACS photometry, in arcsec and kpc respectively. Columns (8) – (10) are the fluxes from the PACS instrument in units of Jy. Galaxy components that do not have flux measurements are too close to a companion galaxy to be resolved by PACS. Columns (11) – (12) are the aperture radii used for SPIRE photometry, in arcsec and kpc respectively. Finally columns (13) – (15) are the fluxes from the SPIRE instrument in units of Jy. Galaxy components that do not have flux measurements are too close to a companion galaxy to be resolved by SPIRE.

6.1. PACS Aperture Photometry

In addition to measuring the flux, we must apply an aperture correction to account for flux outside of the aperture. The PACS aperture corrections are determined from observations of bright celestial standards, and the correction factors are included in the PACS calibration files distributed from the HSA. Within HIPE, the `photApertureCorrectionPointSource` task performs the aperture correction, where the input is the output product from the aperture photometry task. In addition a responsivity version must be specified, which for our data we used the most recent version (FM 7⁸). Since these aperture corrections are only applicable to point sources at each wavelength, we only apply the aperture correction to point sources within our sample. To identify the point sources, we performed PSF fitting of each source in our sample, and selected the objects with FWHM consistent with the corresponding point source FWHM in each PACS band. In Table 4 we denote the fluxes in which an aperture correction was applied by the superscript c. Typical (average) aperture correction values for the 70, 100, and 160 μm bands are 11.7%, 12.8%, and 15.5% of the uncorrected flux, respectively. The median values of the aperture correction values are less than a percent away from the averages. We do not flag aperture-corrected fluxes in Table 3 since many of the total fluxes are a combination of aperture-corrected and uncorrected fluxes.

We also experimented with applying these corrections to marginally resolved systems and systems with

⁸For a description, see section 2.3 of the PACS calibration framework document: http://hereschel.esac.esa.int/twiki/pub/Pacs/PacsCalibration/The_PACS_Calibration_Framework_-_issue_0.13.pdf

a point source and extended flux, however we found that the aperture corrections artificially boosted the flux by approximately 6% on average. This is because many of our objects have varying levels of flux contribution from the point source and extended component. Furthermore, the PACS team performed a careful surface brightness comparison⁹ of PACS data with that of *IRAS* and *Spitzer* MIPS data on the same fields. By convolving, converting, and re-gridding the higher resolution PACS 70 μm to that of *IRAS* 60 μm and MIPS 70 μm , and the PACS 100 μm maps to that of *IRAS* 100 μm it was shown that there is no need to apply any pixel-to-pixel gain corrections to the PACS data. They also conclude that their point-source based calibration scheme is applicable in the case for extended sources. A similar conclusion is reached for the PACS red array¹⁰. Meléndez et al. (2014) also found in their *Herschel* PACS observations of the *Swift* BAT sample that aperture corrections on extended sources were negligible (less than 3%). Therefore we leave sources appearing extended or semi-extended in our sample unaltered by any aperture correction.

The absolute flux calibration of PACS uses models of five different late type standard stars with fluxes ranging between 0.6–15 Jy in the three photometric bands (Balog et al. 2014). In addition, ten different asteroids are also used to establish the flux calibration over the range of 0.1–300 Jy (Müller et al. 2014). For the standard stars, the absolute flux accuracy is within 3% at 70 μm and 100 μm , and within 5% at 160 μm . In addition, Uranus and Neptune were also observed for validation purposes with fluxes of up to several hundred Jy, however a 10% reduction due to nonlinearity in the detector response was observed. Taken altogether, the error in flux calibration is consistent to within 5% of the measured flux and takes into account flat-fielding, responsivity correction which includes the conversion of engineering units from volts to Jy pixel^{-1} , and gain drift correction which corrects for small drifts in gain with time (PACS Observer’s Manual, and references therein). Since PACS did not perform absolute measurements over the course of the mission, the fluxes are only measured relative to the zero level calculated by the mappers which is arbitrary.

In addition to the flux calibration uncertainty, we must also take into account the error from the back-

ground subtraction as well as the instrumental error. The error from the background subtraction is calculated in the following manner: first using the HIPE implementation of DAOPhot the 1- σ dispersion is calculated from all the pixels within the background annulus surrounding the target aperture. This is then multiplied by the square root of the total number of pixels within photometry aperture, under the assumption that the error in background subtraction of individual pixels are not correlated. On the other hand the instrumental error is calculated as the quadrature sum of all error pixels within the target aperture, using the error maps produced by the mapmaker. The total flux uncertainty is then calculated as the quadrature sum of all three error components.

We note that only two of the three galaxies in IRAS F07256+3355 (NGC 2388) were observed by PACS due to the smaller field of view, while SPIRE observed all three. Consequently the total fluxes in Table 3 for this system is the sum of only the two galaxies observed by both instruments, however SPIRE photometry of the third galaxy to the west is provided in the component flux table (Table 4). The same is also true for IRAS F23488+1949, with the third galaxy to the NNW of the closer pair.

⁹For more details see the *Herschel* technical note PICC-NHSC-TN-029.

¹⁰See technical note PICC-NHSC-TR-034.

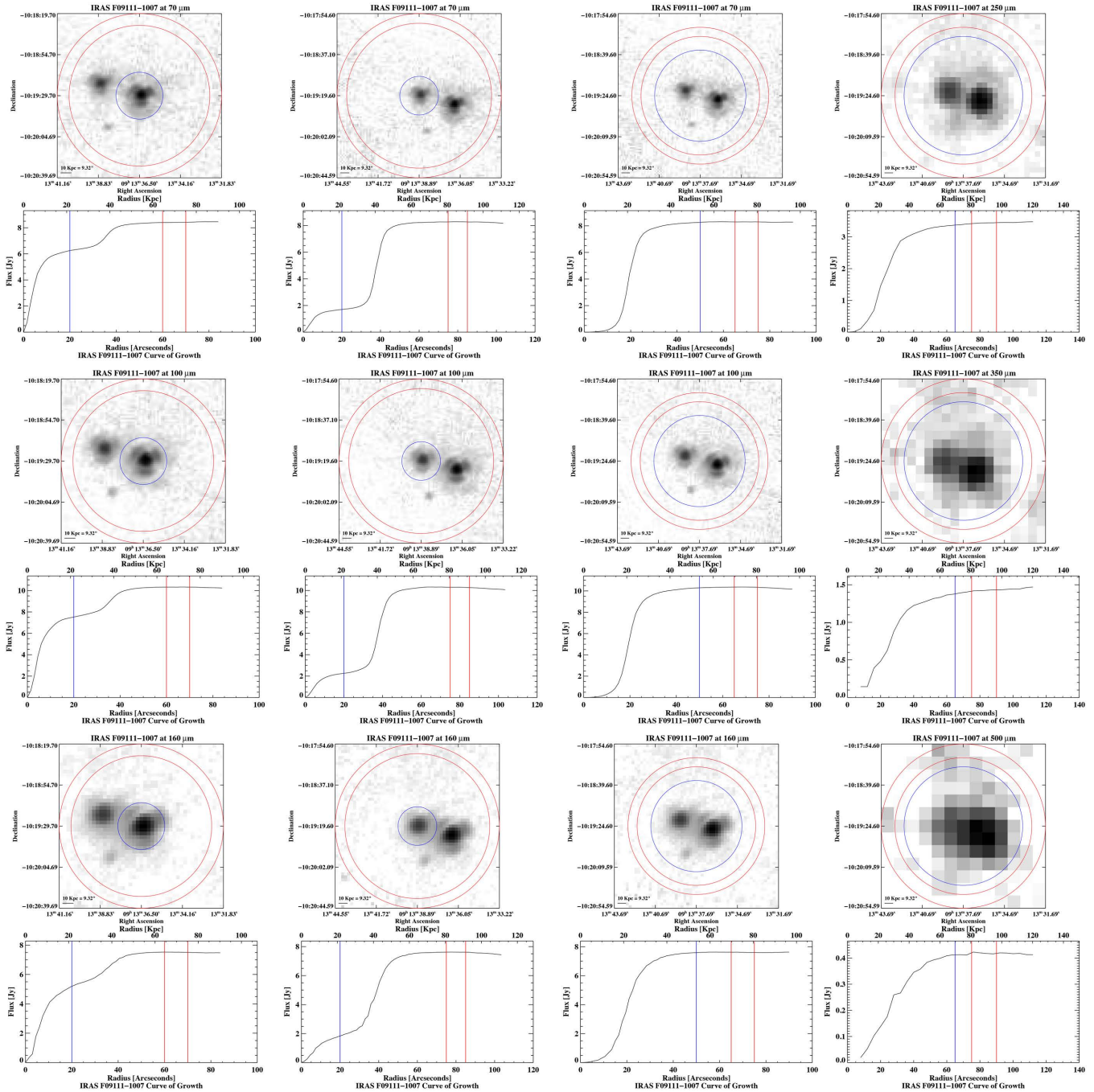


Fig. 4.— Twelve curve of growth plots for IRAS F09111–1007, which are representative for the entire GOALS sample. The blue circle in each image is the photometry aperture, while the red circles are the annuli from which the background is measured. These circles are represented in the curve of growth plot immediately below each image. The first column shows the PACS 70 μm , 100 μm , and 160 μm photometry apertures for the western component of the system. The second column shows the PACS photometry apertures for the eastern nucleus. The third column shows the PACS photometry apertures encompassing both galaxies which includes flux not in the component apertures, giving the total flux from this system. In the SPIRE bands, we only computed component fluxes at 250 μm since the galaxy pair is still resolved, however since the galaxies are essentially unresolved in the other two SPIRE bands, we only compute total fluxes at those two wavelengths. Note the fourth column only shows the total SPIRE apertures of both galaxies, and the individual 250 μm plots were omitted to keep the figure manageable.

TABLE 3
PACS AND SPIRE TOTAL FLUXES OF GOALS SYSTEMS

#	IRAS Name	Optical Name	PACS				SPIRE			
			(1)	(2)	(3)	F _{λ} (70 μ m) Jy (4)	F _{λ} (100 μ m) Jy (5)	F _{λ} (160 μ m) Jy (6)	F _{λ} (250 μ m) Jy (7)	F _{λ} (350 μ m) Jy (8)
1	F00073+2538	NGC 23	10.48 ± 0.52	14.26 ± 0.71	11.85 ± 0.59	5.311 ± 0.347	2.026 ± 0.134	0.718 ± 0.046		
2	F00085-1223	NGC 34, Mrk 938	18.21 ± 0.84	17.68 ± 0.81	10.65 ± 0.48	3.573 ± 0.214	1.239 ± 0.075	0.339 ± 0.021		
3	F00163-1039	Arp 256, MCG-02-01-051/2	8.038 ± 0.403	9.876 ± 0.495	7.496 ± 0.375	2.862 ± 0.189	1.209 ± 0.081	0.419 ± 0.033		
4	F00344-3349	ESO 350-IG 038, Haro 11	6.195 ± 0.276	5.096 ± 0.228	2.341 ± 0.101	0.639 ± 0.038	0.216 ± 0.014	0.067 ± 0.006		
5	F00402-2349	NGC 232	14.60 ± 0.56	20.00 ± 0.77	16.11 ± 0.60	6.397 ± 0.323	2.441 ± 0.124	0.703 ± 0.035		
6	F00506+7248	MCG+12-02-001	25.31 ± 1.27	29.07 ± 1.45	20.34 ± 1.02	7.968 ± 0.485	2.793 ± 0.174	0.896 ± 0.057		
7	F00548+4331	NGC 317B	10.91 ± 0.55	13.07 ± 0.65	9.945 ± 0.498	4.014 ± 0.266	1.600 ± 0.108	0.478 ± 0.039		
8	F01053-1746	IC 1623, Arp 236	25.56 ± 1.28	29.28 ± 1.47	21.46 ± 1.08	8.991 ± 0.546	3.277 ± 0.201	1.023 ± 0.062		
9	F01076-1707	MCG-03-04-014	8.996 ± 0.410	11.37 ± 0.51	8.758 ± 0.388	3.077 ± 0.187	1.181 ± 0.074	0.349 ± 0.023		
10	F01159-4443	ESO 244-G012	9.934 ± 0.498	10.88 ± 0.54	7.735 ± 0.387	2.948 ± 0.194	1.155 ± 0.077	0.341 ± 0.025		
11	F01173+1405	CGCG 436-030	11.71 ± 0.53	11.33 ± 0.51	6.907 ± 0.306	2.125 ± 0.128	0.770 ± 0.048	0.230 ± 0.015		
12	F01325-3623	ESO 353-G020	10.58 ± 0.49	16.43 ± 0.75	15.26 ± 0.68	6.565 ± 0.408	2.621 ± 0.163	0.881 ± 0.056		
13	F01341-3735	RR 032, ESO 297-G011/012	9.294 ± 0.300	12.45 ± 0.41	10.60 ± 0.36	4.107 ± 0.269	1.651 ± 0.110	0.522 ± 0.038		
14	F01364-1042		7.395 ± 0.334	6.845 ± 0.307	3.989 ± 0.174	1.336 ± 0.080	0.517 ± 0.032	0.158 ± 0.011		
15	F01417+1651	III Zw 035	14.74 ± 0.67	13.44 ± 0.61	7.770 ± 0.344	2.608 ± 0.156	0.995 ± 0.061	0.302 ± 0.019		
16	F01484+2220	NGC 695	9.303 ± 0.466	13.24 ± 0.66	11.20 ± 0.56	4.959 ± 0.302	1.942 ± 0.120	0.655 ± 0.047		
17	F01519+3640	UGC 01385	6.769 ± 0.302	8.267 ± 0.359	6.291 ± 0.253	2.537 ± 0.127	1.031 ± 0.055	0.279 ± 0.028		
18	F02071-1023	NGC 838	36.90 ± 1.04	44.00 ± 1.22	34.54 ± 0.96	14.72 ± 0.54	5.799 ± 0.216	1.837 ± 0.070		
19	F02070+3557	NGC 828	14.56 ± 0.73	24.95 ± 1.25	24.86 ± 1.24	12.78 ± 0.79	5.194 ± 0.324	1.621 ± 0.102		
20	F02114+0456	IC 214	5.922 ± 0.287	8.032 ± 0.379	6.672 ± 0.310	3.038 ± 0.166	1.261 ± 0.071	0.421 ± 0.039		
21	F02152+1418	NGC 877	16.11 ± 0.66	28.56 ± 1.21	31.25 ± 1.35	16.90 ± 1.10	7.291 ± 0.475	2.449 ± 0.162		
22	F02203+3158	MCG+05-06-036	9.069 ± 0.320	13.03 ± 0.45	11.30 ± 0.37	4.206 ± 0.277	1.651 ± 0.111	0.529 ± 0.042		
23	F02208+4744	UGC 01845	13.11 ± 0.59	17.48 ± 0.78	13.75 ± 0.60	5.036 ± 0.304	1.974 ± 0.121	0.563 ± 0.034		
24	F02281-0309	NGC 958	8.261 ± 0.415	16.78 ± 0.84	19.75 ± 0.99	10.46 ± 0.68	4.532 ± 0.297	1.614 ± 0.114		
25	F02345+2053	NGC 992	11.90 ± 0.60	16.25 ± 0.81	13.37 ± 0.67	5.906 ± 0.364	2.341 ± 0.145	0.734 ± 0.047		
26	F02401-0013	NGC 1068	28.8 ± 14.3	...	29.9 ± 14.5	11.79 ± 7.7	45.72 ± 2.97	14.40 ± 0.94		
27	F02435+1253	UGC 02238	9.946 ± 0.498	15.33 ± 0.77	13.48 ± 0.67	6.147 ± 0.375	2.380 ± 0.145	0.756 ± 0.052		
28	F02437+2122		6.927 ± 0.313	7.725 ± 0.347	5.027 ± 0.219	1.823 ± 0.106	0.658 ± 0.038	0.185 ± 0.012		
28	F02437+2123 ^a	2MASX J02464505+2133234	0.195 ± 0.014	0.541 ± 0.029	0.584 ± 0.031	0.491 ± 0.031	0.221 ± 0.015	0.079 ± 0.008		
29	F02512+1446	UGC 02369	8.701 ± 0.436	10.36 ± 0.52	7.659 ± 0.383	3.096 ± 0.204	1.197 ± 0.080	0.382 ± 0.024		
30	F03117+4151	UGC 02608	9.116 ± 0.456	11.57 ± 0.58	9.210 ± 0.461	4.135 ± 0.251	1.601 ± 0.099	0.518 ± 0.033		
30	F03117+4151 ^a	UGC 02612	0.575 ± 0.032	1.341 ± 0.069	1.660 ± 0.084	0.990 ± 0.061	0.429 ± 0.028	0.134 ± 0.012		
31	F03164+4119	NGC 1275	6.807 ± 0.343	7.490 ± 0.377	5.691 ± 0.286	3.506 ± 0.217	2.851 ± 0.176	2.739 ± 0.168		
32	F03217+4022		9.122 ± 0.412	10.84 ± 0.49	7.913 ± 0.345	3.134 ± 0.191	1.204 ± 0.075	0.358 ± 0.024		
33	F03316-3618	NGC 1365	1.376 ± 6.9	221.5 ± 11.1	209.7 ± 10.5	103.7 ± 6.7	43.94 ± 2.86	15.63 ± 1.02		

TABLE 3—Continued

#	IRAS Name	Optical Name	PACS			SPIRE		
			(1)	(2)	(3)	F _λ (70 μm) Jy (4)	F _λ (100 μm) Jy (5)	F _λ (160 μm) Jy (6)
34	F03359+1523	CGCG 465-012	7.170 ± 0.324	7.541 ± 0.339	4.878 ± 0.213	1.643 ± 0.099	0.599 ± 0.038	0.187 ± 0.013
35	F03514+1546	CGCG 465-011	6.673 ± 0.334	8.845 ± 0.443	6.946 ± 0.348	3.065 ± 0.186	1.130 ± 0.071	0.356 ± 0.025
35	F03514+1546 ^a	CGCG 465-011	2.255 ± 0.114	3.804 ± 0.191	4.015 ± 0.201	2.188 ± 0.135	0.867 ± 0.056	0.310 ± 0.024
36	03382+6012	5.685 ± 0.285	5.922 ± 0.296	3.745 ± 0.188	1.598 ± 0.098	0.659 ± 0.044	0.158 ± 0.014	
37	F04097+0525	UGC 02982	10.52 ± 0.53	16.86 ± 0.84	15.62 ± 0.78	7.324 ± 0.480	3.541 ± 0.223	1.068 ± 0.071
38	F04118-3207	ESO 420-G013	17.57 ± 0.81	22.28 ± 1.02	16.82 ± 0.75	6.401 ± 0.388	2.406 ± 0.148	0.669 ± 0.041
39	F04191-1855	ESO 550-JG 025	6.452 ± 0.323	8.676 ± 0.434	7.115 ± 0.356	3.273 ± 0.215	1.306 ± 0.087	0.449 ± 0.028
40	F04210-4042	NGC 1572	10.02 ± 0.50	16.45 ± 0.82	15.32 ± 0.77	7.368 ± 0.484	3.225 ± 0.199	1.028 ± 0.063
41	04271+3849	7.402 ± 0.371	10.97 ± 0.49	8.846 ± 0.385	3.815 ± 0.234	1.478 ± 0.093	0.453 ± 0.031	
42	F04315-0840	NGC 1614	36.74 ± 1.70	37.00 ± 1.70	22.96 ± 1.04	7.291 ± 0.452	2.650 ± 0.165	0.748 ± 0.049
43	F04326+1904	UGC 03094	8.159 ± 0.409	12.77 ± 0.64	11.93 ± 0.60	5.210 ± 0.341	2.114 ± 0.140	0.663 ± 0.047
44	F04454-4838	ESO 203-JG001	6.125 ± 0.272	5.284 ± 0.233	2.945 ± 0.125	0.918 ± 0.053	0.339 ± 0.020	0.091 ± 0.007
45	F04502-3304	MCG-05-12-006	9.169 ± 0.414	10.35 ± 0.46	6.949 ± 0.303	2.454 ± 0.153	0.905 ± 0.059	0.266 ± 0.021
46	F05053-0805	NGC 1797	11.00 ± 0.51	13.49 ± 0.62	10.83 ± 0.48	4.438 ± 0.270	1.670 ± 0.103	0.534 ± 0.034
46	F05053-0805 ^a	NGC 1799	0.402 ± 0.027	0.818 ± 0.044	0.954 ± 0.049	0.596 ± 0.044	0.315 ± 0.025	0.121 ± 0.014
47	F05054+1718	CGCG 468-002	10.43 ± 0.52	11.15 ± 0.56	7.394 ± 0.370	2.804 ± 0.185	1.015 ± 0.070	0.293 ± 0.024
48	05083+2441		7.576 ± 0.314	8.348 ± 0.333	5.716 ± 0.209	2.202 ± 0.146	0.824 ± 0.058	0.292 ± 0.024
49	F05081+7936	VII Zw 031	7.492 ± 0.338	10.12 ± 0.45	8.055 ± 0.351	3.130 ± 0.189	1.167 ± 0.072	0.349 ± 0.022
50	05129+5128	7.273 ± 0.329	7.655 ± 0.344	5.028 ± 0.219	1.771 ± 0.106	0.631 ± 0.038	0.196 ± 0.013	
51	F05189-2524	13.53 ± 0.61	11.39 ± 0.51	6.180 ± 0.269	1.975 ± 0.118	0.729 ± 0.044	0.199 ± 0.014	
52	F05187-1017	6.782 ± 0.309	8.595 ± 0.389	6.583 ± 0.292	2.721 ± 0.165	1.094 ± 0.064	0.327 ± 0.022	
53	05368+4940	MCG+08-11-002	19.40 ± 0.88	26.93 ± 1.22	21.56 ± 0.95	8.341 ± 0.507	3.223 ± 0.198	0.948 ± 0.056
54	F05365+6921	NGC 1961	11.59 ± 0.58	26.26 ± 1.31	34.08 ± 1.71	19.59 ± 1.27	8.715 ± 0.567	3.076 ± 0.201
55	F05414+5840	UGC 03351	19.02 ± 0.95	31.33 ± 1.57	28.88 ± 1.44	13.70 ± 0.90	5.817 ± 0.359	1.858 ± 0.114
56	05442+1732		11.86 ± 0.49	13.91 ± 0.55	10.18 ± 0.37	4.194 ± 0.276	1.639 ± 0.110	0.578 ± 0.043
57	F06076-2139	7.554 ± 0.338	8.405 ± 0.373	5.664 ± 0.242	2.157 ± 0.129	0.863 ± 0.053	0.271 ± 0.017	
58	F06052+8027	UGC 03410	12.42 ± 0.53	22.21 ± 0.92	23.59 ± 0.96	11.55 ± 0.60	4.528 ± 0.235	1.566 ± 0.077
59	F06107+7822	NGC 2146	1.98 ± 0.99	237.1 ± 11.9	174.4 ± 8.7	62.78 ± 4.08	22.89 ± 1.49	7.138 ± 0.465
60	F06259+4708	ESO 255-JG007	9.801 ± 0.491	10.67 ± 0.53	7.175 ± 0.359	2.764 ± 0.181	1.019 ± 0.068	0.289 ± 0.021
61	F06295-1735	ESO 557-G002	8.699 ± 0.335	10.29 ± 0.38	7.685 ± 0.279	3.006 ± 0.144	1.156 ± 0.057	0.345 ± 0.020
62	F06538+4628	UGC 03608	8.877 ± 0.444	10.62 ± 0.53	8.315 ± 0.416	3.593 ± 0.215	1.363 ± 0.083	0.429 ± 0.027
63	F06592-6313		6.904 ± 0.312	7.530 ± 0.338	5.027 ± 0.219	1.842 ± 0.113	0.755 ± 0.048	0.221 ± 0.017
64	F07027-6011	AM 0702-601	7.807 ± 0.260	9.229 ± 0.312	7.038 ± 0.228	2.540 ± 0.170	1.025 ± 0.072	0.309 ± 0.029
65	07063+2043	NGC 2342	17.64 ± 0.63	25.86 ± 0.93	22.26 ± 0.80	9.287 ± 0.443	3.761 ± 0.176	1.173 ± 0.057
66	F07160-6215	NGC 2369	26.90 ± 1.35	41.22 ± 2.06	37.55 ± 1.88	17.35 ± 1.14	7.181 ± 0.453	2.273 ± 0.143

TABLE 3—Continued

#	IRAS Name	Optical Name	PACS			SPIRE		
			F _λ (70 μm) Jy (1)	F _λ (100 μm) Jy (2)	F _λ (160 μm) Jy (3)	F _λ (250 μm) Jy (4)	F _λ (350 μm) Jy (5)	F _λ (500 μm) Jy (6)
67	07251-0248		7.024 ± 0.317	6.419 ± 0.288	3.878 ± 0.169	1.448 ± 0.087	0.561 ± 0.034	0.178 ± 0.012
68	F07256+3355	NGC 2388	24.48 ± 0.98 ^b	32.84 ± 1.26 ^b	27.76 ± 1.01 ^b	12.02 ± 0.57 ^b	4.632 ± 0.221 ^b	1.537 ± 0.072 ^b
69	F07329+1149	MCG+02-20-003	10.61 ± 0.48	13.13 ± 0.59	9.969 ± 0.437	4.071 ± 0.250	1.555 ± 0.095	0.503 ± 0.031
69	F07329+1149 ^a	NGC 2416	0.897 ± 0.047	1.705 ± 0.086	1.956 ± 0.098	1.008 ± 0.066	0.436 ± 0.029	0.154 ± 0.010
70	08355-4944		10.25 ± 0.46	9.529 ± 0.428	5.637 ± 0.246	1.758 ± 0.105	0.622 ± 0.040	0.173 ± 0.015
71	F08339+6517		5.865 ± 0.294	6.163 ± 0.309	3.979 ± 0.200	1.267 ± 0.084	0.506 ± 0.031	0.148 ± 0.010
72	F08354+2555	NGC 2623	27.92 ± 1.27	28.46 ± 1.29	17.65 ± 0.78	5.929 ± 0.358	2.124 ± 0.130	0.589 ± 0.035
73	08424-3130	ESO 432-IG006	7.597 ± 0.381	9.841 ± 0.493	7.663 ± 0.384	3.117 ± 0.205	1.227 ± 0.082	0.363 ± 0.027
74	F08520-6850	ESO 060-IG016	5.468 ± 0.274	5.560 ± 0.278	3.496 ± 0.175	1.318 ± 0.088	0.613 ± 0.040	0.170 ± 0.014
75	F08572+3915		6.398 ± 0.282	4.452 ± 0.194	1.997 ± 0.084	0.521 ± 0.031	0.188 ± 0.014	0.042 ± 0.007
76	09022-3615		12.81 ± 0.58	13.14 ± 0.59	8.057 ± 0.351	2.588 ± 0.152	0.880 ± 0.051	0.243 ± 0.014
77	F09111-1007		8.314 ± 0.417	10.35 ± 0.52	7.726 ± 0.387	3.434 ± 0.225	1.357 ± 0.090	0.434 ± 0.030
78	F09126+4432	UGC 04881	7.311 ± 0.366	9.282 ± 0.465	7.433 ± 0.372	3.296 ± 0.217	1.360 ± 0.092	0.435 ± 0.029
79	F09520+6134	UGC 05101	15.34 ± 0.69	...	15.29 ± 0.65	6.138 ± 0.371	2.403 ± 0.148	0.755 ± 0.045
80	F09333+4841	MCG+08-18-013	7.463 ± 0.334	8.835 ± 0.388	6.737 ± 0.282	2.302 ± 0.152	0.935 ± 0.063	0.266 ± 0.021
81	F09437+0317	Arp 303, IC 0563/4	6.876 ± 0.244	12.37 ± 0.44	13.41 ± 0.48	6.772 ± 0.443	2.876 ± 0.190	0.916 ± 0.064
82	F10015-0614	NGC 3110	15.41 ± 0.69	22.94 ± 1.04	20.76 ± 0.95	8.670 ± 0.567	3.373 ± 0.223	1.042 ± 0.072
83	F10038-3338	ESO 374-IG 032	10.14 ± 0.46	8.693 ± 0.390	5.048 ± 0.220	1.837 ± 0.111	0.784 ± 0.049	0.266 ± 0.018
84	F10173+0828		6.298 ± 0.287	5.677 ± 0.257	3.169 ± 0.141	1.132 ± 0.068	0.501 ± 0.031	0.144 ± 0.011
85	F10196+2149	NGC 3221	10.43 ± 0.52	20.96 ± 1.05	24.06 ± 1.20	12.52 ± 0.82	5.352 ± 0.350	1.809 ± 0.120
86	F10257+4339	NGC 3256	120.3 ± 6.0	135.4 ± 6.8	93.48 ± 4.68	33.91 ± 2.21	12.16 ± 0.79	3.929 ± 0.242
87	F10409-4556	ESO 264-G036	7.974 ± 0.399	13.09 ± 0.65	13.10 ± 0.66	6.560 ± 0.429	2.658 ± 0.163	0.860 ± 0.052
88	F10567-4310	ESO 264-G057	6.910 ± 0.346	11.10 ± 0.56	10.41 ± 0.52	5.057 ± 0.331	2.124 ± 0.131	0.690 ± 0.043
89	F10565+2448		14.26 ± 0.64	15.80 ± 0.71	10.45 ± 0.46	3.643 ± 0.215	1.337 ± 0.078	0.381 ± 0.022
90	F11011+4107	MCG+07-23-019	8.484 ± 0.387	10.52 ± 0.48	7.825 ± 0.346	2.862 ± 0.172	1.098 ± 0.066	0.325 ± 0.021
91	F11186-0242	CGCG 011-076	6.742 ± 0.295	9.474 ± 0.406	8.312 ± 0.350	3.795 ± 0.252	1.653 ± 0.112	0.562 ± 0.042
92	F11231+1456	IC 2810	8.456 ± 0.283	11.40 ± 0.38	9.348 ± 0.297	3.820 ± 0.252	1.610 ± 0.108	0.544 ± 0.041
93	F11255+4120	ESO 319-G022	9.086 ± 0.414	10.53 ± 0.48	7.785 ± 0.344	3.088 ± 0.186	1.144 ± 0.070	0.319 ± 0.021
94	F11257+5850	NGC 3690, Arp 299	130.3 ± 6.5	118.3 ± 5.9	68.77 ± 3.44	21.85 ± 1.42	7.688 ± 0.502	2.273 ± 0.149
95	F11506-3851	ESO 320-G030	41.98 ± 1.97	49.14 ± 2.28	34.81 ± 1.59	13.02 ± 0.81	5.182 ± 0.324	1.608 ± 0.101
96	F12043-3140	ESO 440-IG058	8.197 ± 0.410	10.89 ± 0.54	8.693 ± 0.435	3.607 ± 0.238	1.323 ± 0.089	0.388 ± 0.028
97	F12112+0305		9.283 ± 0.419	9.241 ± 0.415	5.831 ± 0.254	1.974 ± 0.119	0.796 ± 0.049	0.226 ± 0.016
98	F12116+5448	NGC 4194	26.20 ± 1.21	26.14 ± 1.20	16.60 ± 0.75	5.315 ± 0.324	1.867 ± 0.115	0.549 ± 0.034
99	F12115-4656	ESO 267-G030	6.914 ± 0.346	10.26 ± 0.51	9.280 ± 0.464	4.509 ± 0.272	1.757 ± 0.107	0.598 ± 0.035
99	F12115-4656 ^a	ESO 267-G029	5.725 ± 0.287	7.924 ± 0.397	7.143 ± 0.358	3.262 ± 0.213	1.350 ± 0.083	0.441 ± 0.028

TABLE 3—Continued

#	IRAS Name	Optical Name	PACS			SPIRE		
			F _{λ} (70 μ m) Jy (4)	F _{λ} (100 μ m) Jy (5)	F _{λ} (160 μ m) Jy (6)	F _{λ} (250 μ m) Jy (7)	F _{λ} (350 μ m) Jy (8)	F _{λ} (500 μ m) Jy (9)
100	12116-5615		11.76 ± 0.53	13.02 ± 0.58	8.808 ± 0.384	3.229 ± 0.195	1.268 ± 0.080	0.418 ± 0.028
101	F12224-0624		7.145 ± 0.323	7.761 ± 0.348	5.079 ± 0.221	1.972 ± 0.122	0.785 ± 0.050	0.271 ± 0.019
102	F12243-0036	NGC 4418	43.05 ± 1.98	34.46 ± 1.57	18.67 ± 0.83	6.631 ± 0.394	2.595 ± 0.152	0.930 ± 0.053
103	F12540+5708	UGC 08058, Mrk 231	34.87 ± 1.59	30.41 ± 1.37	16.93 ± 0.74	5.685 ± 0.343	2.007 ± 0.123	0.597 ± 0.036
104	F12590+2934	NGC 4922	6.763 ± 0.309	7.606 ± 0.345	5.283 ± 0.234	2.032 ± 0.122	0.727 ± 0.045	0.218 ± 0.015
105	F12592+0436	CGCG 043-099	6.538 ± 0.295	8.455 ± 0.379	6.675 ± 0.291	2.808 ± 0.171	1.055 ± 0.065	0.315 ± 0.020
106	F12596-1529	MCG-02-33-098	7.534 ± 0.377	8.490 ± 0.425	5.962 ± 0.299	2.654 ± 0.175	1.061 ± 0.072	0.330 ± 0.027
107	F13001-2339	ESO 507-G070	16.32 ± 0.75	16.90 ± 0.77	10.66 ± 0.47	3.747 ± 0.228	1.405 ± 0.087	0.451 ± 0.029
108	13052-5711		10.49 ± 0.48	13.55 ± 0.61	10.13 ± 0.45	3.819 ± 0.231	1.624 ± 0.101	0.422 ± 0.028
109	F13126+2453	IC 0860	19.67 ± 0.90	18.09 ± 0.82	10.66 ± 0.47	3.775 ± 0.228	1.523 ± 0.093	0.500 ± 0.030
110	13120-5453		50.72 ± 2.35	55.02 ± 2.53	34.97 ± 1.58	12.33 ± 0.75	4.396 ± 0.268	1.340 ± 0.079
111	F13136-6223	VV 250a	11.71 ± 0.59	11.16 ± 0.56	6.728 ± 0.337	2.429 ± 0.159	0.875 ± 0.059	0.273 ± 0.021
112	F13182+3424	UGC 08387	21.74 ± 1.00	25.82 ± 1.18	18.08 ± 0.81	6.356 ± 0.393	2.345 ± 0.146	0.646 ± 0.041
113	F13188+0036	NGC 5104	8.997 ± 0.410	13.54 ± 0.61	12.01 ± 0.53	5.266 ± 0.322	2.005 ± 0.124	0.658 ± 0.040
114	F13197-1627	MCG-03-34-064	6.179 ± 0.238	6.451 ± 0.234	5.199 ± 0.174	2.440 ± 0.108	1.016 ± 0.047	0.330 ± 0.017
115	F13229-2934	NGC 5135	21.44 ± 1.07	31.12 ± 1.56	26.86 ± 1.34	12.37 ± 0.81	5.058 ± 0.333	1.577 ± 0.106
116	13242-5713	ESO 173-G015	97.67 ± 4.89	105.8 ± 5.3	71.63 ± 3.58	26.51 ± 1.74	9.706 ± 0.642	3.092 ± 0.194
117	F13301-2356	IC 4280	7.647 ± 0.383	12.97 ± 0.65	12.52 ± 0.63	5.631 ± 0.369	2.431 ± 0.150	0.771 ± 0.048
118	F13362+4831	NGC 5256	8.113 ± 0.406	9.692 ± 0.485	7.069 ± 0.354	2.757 ± 0.182	1.070 ± 0.073	0.336 ± 0.026
119	F13373+0105	Atp 240, NGC 5257/8	13.98 ± 0.50	21.58 ± 0.77	20.37 ± 0.72	9.434 ± 0.615	3.759 ± 0.246	1.259 ± 0.084
120	F13428-5608	UGC 08696, Mrk 273	24.46 ± 1.11	22.32 ± 1.05	12.74 ± 0.56	4.177 ± 0.252	1.531 ± 0.094	0.427 ± 0.026
121	F13470+3530	UGC 08739	8.163 ± 0.409	14.94 ± 0.75	15.87 ± 0.79	8.243 ± 0.540	3.405 ± 0.225	1.162 ± 0.073
122	F13478-4848	ESO 221-IG010	15.78 ± 0.79	21.63 ± 1.08	17.97 ± 0.90	7.116 ± 0.465	2.771 ± 0.183	0.917 ± 0.066
123	F13497+0220	NGC 5331	7.484 ± 0.375	11.27 ± 0.56	10.31 ± 0.52	5.010 ± 0.329	1.892 ± 0.126	0.673 ± 0.044
124	F13564+3741	Atp 84, NGC 5394/5	12.88 ± 0.44	20.72 ± 0.70	22.65 ± 0.81	11.93 ± 0.78	5.187 ± 0.338	1.856 ± 0.122
125	F14179+4927	CGCG 247-020	6.514 ± 0.326	7.450 ± 0.373	4.904 ± 0.246	1.789 ± 0.120	0.688 ± 0.048	0.175 ± 0.015
126	F14280+3126	NGC 5653	15.03 ± 0.69	22.88 ± 1.05	21.09 ± 0.95	8.748 ± 0.538	3.369 ± 0.207	0.994 ± 0.062
127	F14348-1447		8.260 ± 0.373	8.385 ± 0.376	5.475 ± 0.239	1.967 ± 0.117	0.728 ± 0.044	0.217 ± 0.014
128	F14378-3651		6.857 ± 0.305	6.661 ± 0.294	3.917 ± 0.167	1.376 ± 0.076	0.547 ± 0.030	0.158 ± 0.010
129	F14423-2039	NGC 5734	16.94 ± 0.62	27.32 ± 1.00	25.93 ± 0.96	11.61 ± 0.56	4.630 ± 0.217	1.582 ± 0.070
130	F14547+2449	VV 340a, Arp 302	8.788 ± 0.440	14.70 ± 0.74	13.89 ± 0.69	6.588 ± 0.432	2.617 ± 0.173	0.911 ± 0.062
131	F14544-4255	IC 4518A/B	9.106 ± 0.457	12.89 ± 0.65	12.29 ± 0.62	6.015 ± 0.394	2.427 ± 0.161	0.803 ± 0.056
132	F15107+0724	CGCG 049-057	27.65 ± 1.28	31.67 ± 1.45	21.83 ± 0.99	8.430 ± 0.528	3.225 ± 0.204	1.059 ± 0.068
133	F15163+4255	VV 705	9.027 ± 0.452	9.120 ± 0.456	5.581 ± 0.279	2.284 ± 0.137	0.863 ± 0.053	0.254 ± 0.016
134	15206-6256	ESO 099-G004	12.54 ± 0.57	14.61 ± 0.66	10.87 ± 0.47	3.970 ± 0.242	1.674 ± 0.109	0.505 ± 0.039

TABLE 3—Continued

#	IRAS Name	Optical Name	PACS			SPIRE		
			F _λ (70 μm) Jy (1)	F _λ (100 μm) Jy (2)	F _λ (160 μm) Jy (3)	F _λ (250 μm) Jy (4)	F _λ (350 μm) Jy (5)	F _λ (500 μm) Jy (6)
135	F15250+3608	NGC 5936	7.158 ± 0.324	5.787 ± 0.260	3.031 ± 0.133	1.034 ± 0.061	0.385 ± 0.023	0.124 ± 0.008
136	F15276+1309	UGC 09913	10.75 ± 0.54	16.34 ± 0.82	14.97 ± 0.75	6.603 ± 0.431	2.715 ± 0.167	0.870 ± 0.056
137	F15327+2340	Arp 220, UGC 09913	139.2 ± 6.6	...	86.32 ± 3.99	30.87 ± 1.92	12.80 ± 0.80	3.865 ± 0.240
138	F15437+0234	NGC 5990	12.06 ± 0.60	16.81 ± 0.84	14.25 ± 0.71	6.071 ± 0.398	2.435 ± 0.150	0.831 ± 0.050
139	F16030+2040	NGC 6052	7.689 ± 0.385	10.16 ± 0.51	8.128 ± 0.407	3.317 ± 0.218	1.412 ± 0.088	0.483 ± 0.031
140	F16104+5235	NGC 6090	7.800 ± 0.352	9.269 ± 0.416	7.033 ± 0.307	2.666 ± 0.161	1.028 ± 0.063	0.288 ± 0.019
141	F16164-0746		13.29 ± 0.61	15.03 ± 0.68	10.21 ± 0.45	3.581 ± 0.220	1.266 ± 0.080	0.407 ± 0.028
142	F16284+0411	CGCG 052-037	9.151 ± 0.406	12.46 ± 0.55	10.04 ± 0.44	3.618 ± 0.240	1.423 ± 0.096	0.492 ± 0.036
143	16304+6030	NGC 6156	21.20 ± 1.06	32.32 ± 1.62	29.29 ± 1.47	12.91 ± 0.84	5.096 ± 0.334	1.678 ± 0.112
144	F16320-0820	ESO 069-IG006	9.444 ± 0.429	13.32 ± 0.60	10.75 ± 0.47	4.501 ± 0.266	1.788 ± 0.107	0.551 ± 0.033
145	F16399-0937		9.368 ± 0.436	10.80 ± 0.50	8.302 ± 0.379	3.527 ± 0.218	1.333 ± 0.088	0.435 ± 0.034
146	F16443-2915	ESO 453-G005	13.83 ± 0.56	16.54 ± 0.64	12.61 ± 0.45	5.356 ± 0.262	2.175 ± 0.107	0.773 ± 0.038
147	F16504+0228	NGC 6240	26.48 ± 1.22	28.03 ± 1.28	19.00 ± 0.85	7.026 ± 0.437	2.834 ± 0.177	0.874 ± 0.056
148	F16516-0948		5.698 ± 0.286	8.243 ± 0.413	7.099 ± 0.356	3.353 ± 0.203	1.232 ± 0.079	0.434 ± 0.030
149	F16577+5900	NGC 6286, Arp 293	12.94 ± 0.55	22.53 ± 0.98	22.71 ± 0.99	11.60 ± 0.76	4.599 ± 0.303	1.495 ± 0.101
150	F17132+5313		6.210 ± 0.311	6.980 ± 0.349	5.474 ± 0.239	2.009 ± 0.122	0.780 ± 0.048	0.226 ± 0.016
151	F17138-1017		18.51 ± 0.86	21.72 ± 1.00	15.62 ± 0.70	5.423 ± 0.332	1.875 ± 0.117	0.531 ± 0.035
152	F17207-0014		38.09 ± 1.74	37.91 ± 1.72	23.07 ± 1.02	7.959 ± 0.485	2.907 ± 0.180	0.890 ± 0.054
153	F17222-5953	ESO 138-G027	9.930 ± 0.497	11.00 ± 0.55	8.861 ± 0.386	3.340 ± 0.202	1.240 ± 0.077	0.370 ± 0.025
154	F17530+3447	UGC 11041	7.636 ± 0.382	11.71 ± 0.59	10.97 ± 0.55	5.299 ± 0.322	2.103 ± 0.130	0.689 ± 0.042
155	F17548+2401	CGCG 141-034	8.282 ± 0.374	10.45 ± 0.47	7.845 ± 0.342	2.961 ± 0.183	0.998 ± 0.064	0.302 ± 0.021
156	17578-0400		34.70 ± 1.62	39.78 ± 1.84	27.58 ± 1.26	11.12 ± 0.65	4.300 ± 0.250	1.306 ± 0.078
157	18090+0130		9.912 ± 0.367	14.19 ± 0.53	12.24 ± 0.45	5.010 ± 0.242	1.869 ± 0.094	0.590 ± 0.033
158	F18131+6820	NGC 6621, Arp 81	8.257 ± 0.414	12.08 ± 0.60	11.24 ± 0.56	5.331 ± 0.350	2.159 ± 0.143	0.661 ± 0.048
159	F18093-5744	IC 4687	23.87 ± 1.19	28.18 ± 1.41	20.08 ± 1.00	8.029 ± 0.526	2.935 ± 0.196	0.928 ± 0.065
160	F18145+2205	CGCG 142-034	7.918 ± 0.315	12.44 ± 0.49	11.56 ± 0.45	5.753 ± 0.273	2.229 ± 0.108	0.712 ± 0.035
161	F18293-3413		45.71 ± 2.11	59.13 ± 2.71	45.84 ± 2.07	17.22 ± 1.07	6.454 ± 0.400	1.987 ± 0.122
162	F18329+5950	NGC 6670A/B	10.33 ± 0.52	13.92 ± 0.70	11.25 ± 0.56	4.664 ± 0.305	1.782 ± 0.118	0.537 ± 0.038
163	F18345-5732	IC 4734	19.06 ± 0.88	25.41 ± 1.16	20.51 ± 0.92	8.450 ± 0.525	3.257 ± 0.203	1.051 ± 0.066
164	F18425+6036	NGC 6701	12.91 ± 0.65	19.13 ± 0.96	16.80 ± 0.84	7.422 ± 0.485	2.863 ± 0.188	0.945 ± 0.059
165	F19120+7320	VV 414, NGC 6786, UGC 11415	9.262 ± 0.296	11.90 ± 0.38	9.766 ± 0.309	4.003 ± 0.263	1.516 ± 0.102	0.568 ± 0.041
166	F19115-2124	ESO 593-IG008	7.972 ± 0.363	10.62 ± 0.48	8.597 ± 0.380	3.371 ± 0.203	1.278 ± 0.079	0.489 ± 0.030
167	F19297-0406		7.982 ± 0.400	8.114 ± 0.406	5.121 ± 0.257	1.833 ± 0.121	0.766 ± 0.046	0.225 ± 0.017
168	19542+1110		6.720 ± 0.300	6.516 ± 0.289	3.851 ± 0.165	1.265 ± 0.075	0.495 ± 0.030	0.126 ± 0.009
169	F19542-3804	ESO 339-G011	7.396 ± 0.340	10.69 ± 0.49	9.839 ± 0.440	4.448 ± 0.277	1.695 ± 0.108	0.591 ± 0.039

TABLE 3—Continued

#	IRAS Name	Optical Name	PACS			SPIRE		
			F _λ (70 μm) Jy (4)	F _λ (100 μm) Jy (5)	F _λ (160 μm) Jy (6)	F _λ (250 μm) Jy (7)	F _λ (350 μm) Jy (8)	F _λ (500 μm) Jy (9)
170	F20221-2458	NGC 6907	18.35 ± 0.92	31.39 ± 1.57	31.71 ± 1.59	16.38 ± 1.07	6.890 ± 0.448	2.378 ± 0.155
171	F20264+2533	MCG+04-48-002	12.92 ± 0.53	17.71 ± 0.73	13.35 ± 0.55	5.719 ± 0.291	2.085 ± 0.112	0.669 ± 0.040
172	F20304-0211	NGC 6926	8.895 ± 0.446	15.94 ± 0.80	16.62 ± 0.83	7.808 ± 0.509	3.102 ± 0.204	0.998 ± 0.067
173	F20351+2521	CGCG 448-020, II Zw 096	6.993 ± 0.350	9.142 ± 0.457	7.280 ± 0.364	3.280 ± 0.196	1.266 ± 0.077	0.347 ± 0.022
174	F20550+1655	ESO 286-IG019	11.79 ± 0.59	10.68 ± 0.53	6.199 ± 0.310	2.128 ± 0.140	0.810 ± 0.051	0.242 ± 0.018
175	F20551-14250	ESO 286-G035	12.64 ± 0.56	10.41 ± 0.46	5.749 ± 0.246	1.840 ± 0.111	0.631 ± 0.039	0.182 ± 0.013
176	F21008-4347	ESO 286-G035	9.498 ± 0.436	12.80 ± 0.58	10.42 ± 0.47	3.994 ± 0.242	1.470 ± 0.091	0.404 ± 0.026
177	21101+5810		8.068 ± 0.365	8.705 ± 0.391	5.753 ± 0.251	2.000 ± 0.122	0.749 ± 0.049	0.195 ± 0.015
178	F2130-3846	ESO 343-IG013	6.422 ± 0.322	8.031 ± 0.402	6.587 ± 0.330	2.721 ± 0.179	1.058 ± 0.072	0.354 ± 0.024
179	F21453-3511	NGC 7130	18.83 ± 0.94	...	19.98 ± 0.99	9.224 ± 0.571	3.549 ± 0.220	1.078 ± 0.068
180	F22118-2742	ESO 467-G027	7.027 ± 0.352	11.89 ± 0.59	5.478 ± 0.358	2.083 ± 0.138	0.773 ± 0.050	
181	F22132-3705	IC 5179	24.34 ± 1.22	37.57 ± 1.88	34.58 ± 1.73	14.97 ± 0.98	5.763 ± 0.377	1.892 ± 0.125
182	F22287-1917	ESO 602-G025	7.429 ± 0.339	10.36 ± 0.47	9.241 ± 0.409	3.991 ± 0.243	1.658 ± 0.103	0.488 ± 0.031
183	F22389+3359	UGC 12150	10.70 ± 0.48	14.70 ± 0.66	12.31 ± 0.54	5.086 ± 0.305	2.031 ± 0.121	0.611 ± 0.036
184	F22467-4906	ESO 239-IG002	8.041 ± 0.363	7.847 ± 0.352	4.975 ± 0.217	1.799 ± 0.107	0.700 ± 0.042	0.256 ± 0.016
185	F22491-1808		5.642 ± 0.252	4.975 ± 0.221	2.715 ± 0.116	0.841 ± 0.049	0.309 ± 0.018	0.082 ± 0.006
186	F23007+0836	NGC 7469, IC 5283, Arp 298	33.69 ± 1.43	40.18 ± 1.65	29.83 ± 1.16	11.16 ± 0.73	4.216 ± 0.278	1.266 ± 0.087
187	F23024+1916	CGCG 453-062	9.269 ± 0.422	11.42 ± 0.52	9.233 ± 0.409	4.418 ± 0.272	1.749 ± 0.111	0.609 ± 0.038
188	F23128-5919	ESO 148-IG002	11.97 ± 0.54	11.14 ± 0.50	6.028 ± 0.267	1.855 ± 0.110	0.655 ± 0.039	0.186 ± 0.013
189	F23135+2517	IC 5298	10.32 ± 0.47	11.53 ± 0.52	8.070 ± 0.357	3.042 ± 0.184	1.110 ± 0.069	0.336 ± 0.022
190	F23133-4251	NGC 7552	92.92 ± 4.65	116.3 ± 5.8	88.01 ± 4.40	35.64 ± 2.32	13.74 ± 0.90	4.226 ± 0.276
191	F23157+0618	NGC 7591	10.04 ± 0.47	14.49 ± 0.68	13.86 ± 0.65	7.067 ± 0.440	2.944 ± 0.186	0.973 ± 0.064
192	F23157-0441	NGC 7592	8.700 ± 0.435	10.44 ± 0.52	7.602 ± 0.380	2.916 ± 0.192	1.179 ± 0.073	0.355 ± 0.024
193	F23180-6929	ESO 077-IG014	6.716 ± 0.337	9.141 ± 0.458	7.056 ± 0.353	3.113 ± 0.205	1.254 ± 0.084	0.406 ± 0.025
194	F23254+0830	NGC 7674, HCG 96	5.865 ± 0.295	8.328 ± 0.418	7.663 ± 0.384	3.566 ± 0.232	1.424 ± 0.094	0.445 ± 0.031
195	23262-0314	NGC 7679	9.077 ± 0.413	11.74 ± 0.53	8.976 ± 0.397	3.367 ± 0.207	1.287 ± 0.079	0.496 ± 0.031
195	23262+0314 ^a	NGC 7682	0.409 ± 0.028	0.770 ± 0.043	0.971 ± 0.051	0.746 ± 0.051	0.384 ± 0.029	0.151 ± 0.014
196	F23365+3604		8.070 ± 0.365	8.315 ± 0.373	5.222 ± 0.228	1.901 ± 0.113	0.707 ± 0.042	0.195 ± 0.012
197	F23394-0353	MCG-01-60-022	6.181 ± 0.279	8.292 ± 0.372	6.863 ± 0.299	2.932 ± 0.180	1.226 ± 0.076	0.402 ± 0.026
198	F23394-0353 ^a	MCG-01-60-021, Mrk 933	0.722 ± 0.031	1.422 ± 0.056	1.988 ± 0.082	1.328 ± 0.087	0.555 ± 0.038	0.178 ± 0.014
198	23436+5257		6.576 ± 0.294	7.540 ± 0.335	5.213 ± 0.223	1.872 ± 0.112	0.684 ± 0.043	0.243 ± 0.017
199	F23444+2911	Arp 86, NGC 7752/3	7.612 ± 0.274	13.52 ± 0.50	15.05 ± 0.59	8.038 ± 0.524	3.524 ± 0.233	1.157 ± 0.080
200	F23488+1949	NGC 7771	27.61 ± 3.70 ^b	43.18 ± 4.66 ^b	40.13 ± 3.91 ^b	18.97 ± 1.24 ^b	7.501 ± 0.493 ^b	2.366 ± 0.157 ^b
201	F23488+2018	Mrk 331	21.31 ± 0.96	24.32 ± 1.08	17.46 ± 0.75	6.398 ± 0.375	2.410 ± 0.140	0.790 ± 0.044

NOTE.—The monochromatic flux density in units of Jansky for each of the three PACS and three SPIRE broadband filters. These are the total fluxes for each GOALS system. The column descriptions are (1) the row reference number, (2) The IRAS name of the galaxy, ordered by ascending RA. Galaxies with the “F” prefix originate from the *IRAS* Faint Source Catalog, and galaxies with no “F” prefix are from the Point Source Catalog. (3) Common optical counterpart names to the galaxy systems. Columns (4) – (6) are the fluxes from the PACS instrument in units of Jy. Note that the four galaxies which lack 100 μm measurements are IRAS F02401-0013 (NGC 1068), IRAS F09320+6134 (UGC 05101), IRAS F15327+2340 (Ap 220), and IRAS F21453-3511 (NGC 7130). Columns (7) – (9) are the fluxes from the SPIRE instrument in units of Jy.

^aThese are very widely separated galaxy pairs that required two *Herschel* PACS observations.

^bThis is a triple system, however only two component galaxies are visible in PACS due to its smaller field of view. The total flux for this system does *not* include the third galaxy not visible in PACS.

6.2. SPIRE Aperture Photometry

The SPIRE 2-pass pipeline (see §4.2.2) produces a point-source calibrated map as the main output. However since many of our objects appear extended or marginally extended in our sample, and following the recommendation from the NASA Herschel Science Center (NHSC), we opted to use the extended-source calibrated maps from which we measured all of the fluxes. Both sets of maps are produced nearly identically, however the extended-source calibrated maps have relative gain factors applied to each bolometer's signal, which accounts for the small differences between the peak and integral of each individual bolometer's beam profile. This method helps reduce residual striping in maps with extended sources, since the relative photometric gains between all of the bolometers is properly accounted for. In addition to applying the relative gains, the PMW and PLW channels are zero-point corrected by applying a constant offset based on the *Planck*-HFI maps (see §6.2.1). The overall calibration scheme for point and extended sources is described in Griffin et al. (2013).

The primary flux calibrator for SPIRE is Neptune, chosen because it has a well-understood submillimeter/FIR spectrum and is essentially a point source in the SPIRE beams. It is also bright enough from which high signal-to-noise measurements can be made, but not so bright that it would introduce non-linearity effects from the instrument. In order to calibrate the entire instrument, special ‘fine scan’ observations were taken such that each bolometer was scanned across Neptune in order to absolutely calibrate each bolometer. Repeated observations of Neptune also showed that there were no statistically significant changes in the detector responses over the mission. Further details on using Neptune as the primary SPIRE flux calibrator can be found in Bendo et al. (2013).

Since the vast majority of our sources have fluxes above 30 mJy, Pearson et al. (2014) recommends using either the timeline fitter or aperture photometry. Because a significant fraction of our sample contains marginally to very extended sources, as well as point sources, we opted to measure all of our SPIRE fluxes using the `annularSkyAperturePhotometry` task in HIPE in order to keep our measurements as uniform as possible. However this method results in the loss of flux outside the finite-sized aperture, for which an aperture correction is needed to fully account for all the flux. In the case of point sources, we

applied the aperture correction by dividing our fluxes by the encircled energy fraction (EEF) amount corresponding to the aperture radius and SPIRE channel. The EEFs can be found in the SPIRE calibration files (accessible from within HIPE), and represents the ratio of flux (energy) inside the aperture divided by the true flux of the point source. As with the PACS aperture corrections, SPIRE fluxes in which an aperture correction was applied are denoted by a superscript c in Table 4, with average corrections of 10.1%, 10.3%, and 14.8% for the 250, 350, and 500 μm channels respectively. Similarly the median correction values are less than a percent difference from the averages.

In order to check the validity of our point source fluxes, we measured our fluxes a second time using the timeline source fitter on a subset of 65 objects that are point sources in all three SPIRE bands. The timeline fitter is the preferred method of obtaining point source fluxes on the SPIRE maps, since it works on the baseline subtracted, destriped, and deglitched Level 1 timelines of the data (which are calibrated in Jy/beam¹¹). By using a Levenberg-Marquardt algorithm to fit a two dimensional circular or elliptical Gaussian function to the 2-D timeline data, the source can be modeled and the point source flux can be calculated from the 2-D fit. The advantage is it avoids any potential artifacts arising from the map-making process, such as smearing effects from pixelization. Because it does not use the Level 2 maps, source extraction is not necessary (i. e. aperture photometry), and there are no aperture corrections needed since the 2-D fit in principle takes into account all of the flux from the point source.

When we compared the aperture photometry results to the timeline fitter results, we found that they both agree very well at 250 μm and 350 μm with an average aperture/timeline flux ratio of 1.030 and 0.995 respectively, however the 500 μm channel had a slightly lower ratio of 0.93. To further check our results, we plotted the aperture/timeline flux ratio against the aperture photometry flux for all three bands, and found no statistically significant correlation in the flux ratio as a function of flux. However we do note in the 500 μm case, fluxes less than approximately 150 mJy appear to have a lower aperture/timeline flux ratio, whereas fluxes above that value have an average ratio close to unity. We believe this underestimation at faint fluxes is due to confusion noise, which was also observed in the SPIRE Map Making Test Report.

¹¹See Dowell et al. (2010), §5.

Furthermore we note that the discrepancy in the 500 μm fluxes are still consistent within the typical flux errors ($\sim 15\%$). As a final check we also plotted the aperture/timeline ratio against the aperture photometry radius, and we again found no statistically significant correlation. From these tests our point source aperture photometry fluxes appear to be in good agreement with the results from the timeline fitter.

In the case of semi-extended to extended sources, aperture corrections become more complex since the flux originates not from an unresolved source, but is seen instead as surface brightness distributed within an aperture. Although an aperture correction is needed for reasons similar to the point source case, Shimizu et al. (2016) found that their extended SPIRE fluxes for their *Swift* BAT sample did not need aperture corrections because they were negligible. To test this, they first convolved their 160 μm PACS data to the resolution of the three SPIRE bands, and then measured the fluxes on both the convolved and unconvolved images using the same SPIRE aperture sizes. Aperture corrections were then calculated as the ratio of the flux on the original PACS image divided by the flux obtained on the convolved image, with resulting median aperture corrections of 1.01, 0.98, and 0.98 for the 250 μm , 350 μm , and 500 μm channels respectively. This makes the assumption that the 160 μm and SPIRE fluxes originate from the same material within their galaxies. We also note that their aperture sizes are similar to ours, since their galaxy sample lies in the same redshift range. Ciesla et al. (2012) also showed by simulating in the worst-case scenario, a maximum aperture correction of 5% is needed at 500 μm . However this was done on an (intentionally) unphysical source that has a flat constant surface brightness, with a sharp drop to zero flux at a set radius. On more realistic sources they calculated aperture corrections of approximately $\lesssim 2\%$. As these corrections are very close to unity, we follow their precedent in only reporting the integrated, background subtracted flux for our extended sources.

To calculate the flux uncertainty for the SPIRE photometry, we follow a similar prescription we used for PACS. The first is a systematic error in the flux calibration related to the uncertainty in the models used for Neptune, which is the primary calibrator for SPIRE. These uncertainties, which are correlated across all three SPIRE bands, are currently quoted as 4%. The other source of uncertainty is a random uncertainty related to the ability to repeat flux density measurements of Neptune, which is 1.5% for all three bands. Alto-

gether, these two sources of uncertainty are added linearly for a total of 5.5% error in the point source flux calibration. However in the case of extended emission calibration, there is an additional error of 1% due to the current uncertainty in the measured beam area that is also added linearly. This error was recently improved from 4% with the release of the SPIRE calibration version 14.2. Therefore the total uncertainty in the extended source calibration scheme amounts to 6.5% of the background subtracted flux (Bendo et al. 2013).

To calculate our total flux uncertainties, we must also include any errors incurred from measuring and subtracting the background from the measured flux, as well as the instrumental error. To estimate the uncertainty from the background subtraction, we measure the $1-\sigma$ dispersion of the flux in each pixel within the annular area used for our background measurements. This is then multiplied by the square root of the number of pixels within the photometry aperture (which can be a fractional amount) to obtain the error in background measurement. The instrumental error is calculated by summing in quadrature the pixels within the aperture on the error map generated by the pipeline. We note this underestimates the error because the noise is correlated between pixels. Our final SPIRE flux uncertainties are then computed as the quadrature sum of all three sources of error. In the case where the total system flux is the sum of two (or more) components, the flux uncertainty is the quadrature sum of each galaxy component's flux error.

6.2.1. SPIRE Zero-Point Correction

Due to the large radiative contribution of *Herschel*'s optical components (230 Jy, 250 Jy, 270 Jy for the PSW, PMW, PLW channels respectively), SPIRE can only measure the relative flux on the sky, i. e. the flux of the target minus the background level. During data reduction the SPIRE maps are generated such that the background is approximately normalized to zero, which makes it impossible to determine the absolute flux of the target. However to recover the absolute flux we used the all-sky maps from the *Planck* mission (modified to have a spatial resolution of 8' FWHM), since the Planck-HFI 857 GHz and 545 GHz filters match fairly well to the *Herschel* 350 μm and 500 μm band passes respectively (see Fig. 5.16 in the SPIRE handbook). These corrections become more important in sources with very extended flux, since some of the diffuse low surface-brightness flux may be subtracted out.

Bertincourt et al. (2016) performed an in-depth analysis of SPIRE and HFI data on the same fields, and found a very high degree of linearity between the two datasets, as well as a good agreement in the relative calibrations between the two instruments. The zero-points of the *Planck* maps are derived assuming that the zero-point of the Galactic emission can be defined as zero dust emission for a null HI column density¹². The final step is to apply a slight gain correction to the *Planck* maps, which for our data we used the NHSC recommended gain factors of 0.989 and 1.02 for the 857 GHz and 545 GHz channels, respectively. The *Planck* calibration uncertainty for both channels is 10%. Using the all-sky *Planck* data, zero-point corrections are applied as flux offsets over the entire SPIRE map, and do not affect the SPIRE flux calibrations (which is background subtracted). We note that these zero point corrections were only applied to the 350 μm and 500 μm channels only, and the 250 μm maps were not corrected since there is no overlap with *Planck*.

¹²See the Explanatory Supplement to the Planck 2013 results:
http://wiki.cosmos.esa.int/plankpla/index.php/CMB_and_astrophysical_component_maps#Thermal_dust_emission

TABLE 4
PACS AND SPIRE TOTAL AND COMPONENT FLUXES OF GOALS SYSTEMS

#	IRAS Name	Individual Name	Aperture Center Coordinate						PACS						SPIRE											
			RA		Dec.		Ang. _{rr}		Phys. Ap.		F _λ (70 μm)		F _λ (100 μm)		F _λ (160 μm)		Ang. _{rr}		Phys. Ap.		F _λ (250 μm)		F _λ (350 μm)		F _λ (500 μm)	
			HH:MM:SS	DD:MM:SS	(4)	(5)	(6)	(7)	Jy	(8)	Jy	(9)	Jy	(10)	kpc	(11)	Jy	(12)	Jy	(13)	Jy	(14)	Jy	(15)		
1	F0073+2538	NGC 23	00 : 09 : 53.36	+ 25 : 55 : 27.7	45	13.81	10.48 ± 0.52	14.26 ± 0.71	11.85 ± 0.59	70	21.48	5.311 ± 0.347	2.026 ± 0.134	0.718 ± 0.046 ^c												
2	F0085+1223	NGC 34	00 : 11 : 06.56	- 12 : 06 : 28.2	45	17.78	18.21 ± 0.84 ^c	17.68 ± 0.81 ^c	10.65 ± 0.48 ^c	55	21.73	3.573 ± 0.214 ^c	1.239 ± 0.075 ^c	0.339 ± 0.021 ^c												
2	F0085+1223	NGC 35	00 : 11 : 10.51	- 12 : 01 : 14.9		
2	F0085+1223	IRGP J001108.5+120351	00 : 11 : 08.54	- 12 : 03 : 51.6		
3	F0163-1039	MCG-02-01-051	00 : 18 : 50.90	- 10 : 22 : 36.7	24	12.96	7.501 ± 0.329 ^c	8.382 ± 0.364 ^c	5.870 ± 0.244 ^c		
3	F0163-1039	MCG-02-01-052	00 : 18 : 49.85	- 10 : 21 : 34.0	38	20.52	1.206 ± 0.062	2.081 ± 0.105	1.960 ± 0.099		
3	F0163-1039	Ap 256	00 : 18 : 50.37	- 10 : 22 : 05.3	70	37.81	8.038 ± 0.403	9.876 ± 0.495	7.496 ± 0.375	80	43.21	2.862 ± 0.189	1.209 ± 0.081	0.419 ± 0.033												
4	F0344-3349	ESO 350-IG 038	00 : 36 : 52.49	- 33 : 33 : 17.2	27	11.18	6.195 ± 0.276 ^c	5.096 ± 0.228 ^c	2.341 ± 0.101 ^c	35	14.49	0.639 ± 0.038 ^c	0.216 ± 0.014 ^c	0.067 ± 0.006 ^c												
5	F0402-2349	NGC 232	00 : 42 : 45.83	- 23 : 33 : 41.0	35	15.49	12.23 ± 0.55 ^c	16.81 ± 0.75 ^c	13.53 ± 0.59 ^c	53	23.46	5.299 ± 0.317 ^c	2.011 ± 0.121 ^c	0.578 ± 0.033 ^c												
5	F0402-2349	NGC 235	00 : 42 : 52.82	- 23 : 32 : 27.8	35	15.49	2.371 ± 0.108 ^c	3.188 ± 0.144 ^c	2.581 ± 0.113 ^c	45	19.92	1.098 ± 0.065 ^c	0.431 ± 0.026 ^c	0.125 ± 0.035 ^c												
5	F0402-2349	RSGC 04	00 : 42 : 49.32	- 23 : 33 : 04.3		
6	F0506+7248	MCG+12-02-001	00 : 54 : 03.88	+ 73 : 05 : 05.9	50	16.41	25.31 ± 1.27	29.07 ± 1.45	20.34 ± 1.02	60	19.69	7.968 ± 0.485 ^c	2.793 ± 0.174 ^c	0.896 ± 0.057 ^c												
7	F0548+4331	NGC 317B	00 : 57 : 40.41	+ 43 : 47 : 32.5	28	10.06	11.63 ± 0.52 ^c	14.17 ± 0.63 ^c		
7	F0548+4331	NGC 317A	00 : 57 : 39.04	+ 43 : 48 : 03.1	10	3.592	0.061 ± 0.005	0.085 ± 0.006		
7	F0548+4331	NGC 317	00 : 57 : 39.72	+ 43 : 47 : 47.7	65	23.35	10.91 ± 0.55	13.07 ± 0.65	9.945 ± 0.498	75	26.94	4.014 ± 0.266	1.600 ± 0.108	0.478 ± 0.039												
8	F01053-1746	IC 1623A	01 : 07 : 46.79	- 17 : 30 : 27.4		
8	F01053-1746	IC 1623B	01 : 07 : 47.59	- 17 : 30 : 24.2		
8	F01053-1746	IC 1623	01 : 07 : 47.54	- 17 : 30 : 25.6	55	21.92	25.56 ± 1.28	29.28 ± 1.47	21.46 ± 1.08	60	23.91	8.991 ± 0.546 ^c	3.277 ± 0.201 ^c	1.023 ± 0.062 ^c												
9	F01076-1707	MCG-03-04-014	01 : 10 : 08.93	- 16 : 51 : 09.9	40	26.14	8.996 ± 0.410 ^c	11.37 ± 0.51 ^c	8.758 ± 0.388 ^c	53	34.64	3.077 ± 0.187 ^c	1.181 ± 0.074 ^c	0.349 ± 0.023 ^c												
10	F01159-4443	MCG-7-3-14	01 : 18 : 08.31	- 44 : 27 : 43.4		
10	F01159-4443	MCG-7-3-13	01 : 18 : 08.23	- 44 : 28 : 00.4		
10	F01159-4443	ESO 244-G012	01 : 18 : 08.27	- 44 : 27 : 51.9	45	19.13	9.934 ± 0.498	10.88 ± 0.54	7.735 ± 0.387	55	23.38	2.948 ± 0.194	1.155 ± 0.077	0.341 ± 0.025												
11	F01173+1405	GCGC 436-030	01 : 20 : 02.63	+ 14 : 21 : 42.3	40	15.94	11.71 ± 0.53 ^c	11.33 ± 0.51 ^c	6.907 ± 0.306 ^c	55	21.92	2.125 ± 0.128 ^c	0.770 ± 0.048 ^c	0.230 ± 0.015 ^c												
12	F01325-3623	ESO 353-G020	01 : 34 : 51.26	- 36 : 08 : 14.4	45	17.93	10.58 ± 0.49 ^c	16.43 ± 0.73 ^c	15.26 ± 0.68 ^c	70	27.90	6.565 ± 0.408 ^c	2.621 ± 0.163 ^c	0.881 ± 0.056 ^c												
13	F01341-3735	ESO 297-G 011	01 : 36 : 23.39	- 37 : 19 : 18.1	35	12.22	5.528 ± 0.250 ^c	8.316 ± 0.373 ^c	7.820 ± 0.341 ^c	40	13.96	3.446 ± 0.203 ^c		
13	F01341-3735	ESO 297-G 012	01 : 36 : 24.14	- 37 : 20 : 25.9	25	8.727	3.766 ± 0.166 ^c	4.130 ± 0.180 ^c	2.779 ± 0.116 ^c	25	8.727	0.969 ± 0.053 ^c		
13	F01341-3735	RR 032	01 : 36 : 23.76	- 37 : 19 : 51.9		
14	F01364-1042	IRAS F01364-1042	01 : 38 : 52.79	- 10 : 27 : 12.1	35	32.43	7.395 ± 0.334 ^c	6.845 ± 0.307 ^c	3.989 ± 0.174 ^c	45	41.69	1.336 ± 0.080 ^c	0.517 ± 0.032 ^c	0.158 ± 0.011 ^c												
15	F01417+1651	II Zw 035	01 : 44 : 30.56	+ 17 : 06 : 09.0	40	21.84	14.74 ± 0.67 ^c	13.44 ± 0.61 ^c	7.770 ± 0.344 ^c	50	27.30	2.608 ± 0.156 ^c	0.995 ± 0.061 ^c	0.302 ± 0.019 ^c												
16	F01484+2220	NGC 695	01 : 51 : 14.34	+ 22 : 34 : 56.0	45	28.45	9.303 ± 0.466	13.24 ± 0.66	11.20 ± 0.56	60	37.93	4.959 ± 0.302 ^c	1.942 ± 0.120 ^c	0.655 ± 0.047 ^c												
17	F01519+3640	UGC 01385	01 : 54 : 53.82	+ 36 : 55 : 04.3	45	16.78	6.542 ± 0.301 ^c	7.828 ± 0.358 ^c	5.595 ± 0.251 ^c	50	18.64	1.956 ± 0.120 ^c	0.811 ± 0.050 ^c	0.203 ± 0.022 ^c												
17	F01519+3640	KUG 0152+366	01 : 55 : 01.75	+ 36 : 55 : 11.6	30	11.18	0.227 ± 0.018	0.439 ± 0.026	0.697 ± 0.037	50	18.64	0.581 ± 0.043	0.221 ± 0.022	0.076 ± 0.017												
17	F01519+3640	IRGP J015457.8+365508	01 : 54 : 57.78	+ 36 : 55 : 07.9		

TABLE 4—Continued

#	IRAS Name	Individual Name	Aperture Center Coordinate			PACS						SPIRE					
			RA (4)	Dec. HH:MM:SS (5)	Ang. α , Ap. kpc (6)	F $_{\lambda}$ (70 μ m) Jy (8)	F $_{\lambda}$ (100 μ m) Jy (9)	F $_{\lambda}$ (160 μ m) Jy (10)	Ang. α , Ap. kpc (11)	F $_{\lambda}$ (250 μ m) Jy (12)	F $_{\lambda}$ (350 μ m) Jy (13)	F $_{\lambda}$ (500 μ m) Jy (14)	Phys. Ap. kpc (15)				
18	F02071-1023	NGC 839	02 : 09 : 42.81	- 10 : 11 : 02.0	50	12.92	13.70 ± 0.63 ^c	13.74 ± 0.63 ^c	8.861 ± 0.401 ^c	75	19.38	3.134 ± 0.193 ^c	1.145 ± 0.071 ^c	0.354 ± 0.023 ^c			
18	F02071-1023	NGC 838	02 : 09 : 38.66	- 10 : 08 : 47.2	60	15.50	15.35 ± 0.72 ^c	18.26 ± 0.85 ^c	14.24 ± 0.65 ^c	83	21.45	5.962 ± 0.348 ^c	2.293 ± 0.142 ^c	0.755 ± 0.047 ^c			
18	F02071-1023	NGC 835	02 : 09 : 24.64	- 10 : 08 : 09.3	40	10.34	7.041 ± 0.353	11.02 ± 0.55	10.19 ± 0.51	33	8.527	4.933 ± 0.278 ^c	1.916 ± 0.104 ^c	...			
18	F02071-1023	NGC 833	02 : 09 : 20.87	- 10 : 07 : 59.4	24	6.202	0.350 ± 0.027	0.590 ± 0.037	0.767 ± 0.043	27	6.977	0.448 ± 0.030	0.213 ± 0.015	...			
18	F02071-1023	NGC 835+0833	02 : 09 : 24.64	- 10 : 08 : 09.3	80	20.67	7.856 ± 0.397	11.99 ± 0.60	11.44 ± 0.57	85	21.96	5.629 ± 0.348 ^c	2.360 ± 0.146 ^c	0.728 ± 0.046 ^c			
18	F02071-1023	HCG 016	02 : 09 : 36.13	- 10 : 09 : 32.6	36.90 ± 1.04 ^c	44.00 ± 1.22 ^c	34.54 ± 0.96 ^c	14.72 ± 0.54 ^c	5.799 ± 0.216 ^c	1.837 ± 0.070 ^c			
19	F02070+3857	NGC 828	02 : 10 : 09.53	+ 39 : 11 : 24.7	50	17.84	14.56 ± 0.73	24.95 ± 1.25	24.86 ± 1.24	80	28.55	12.78 ± 0.79 ^c	5.194 ± 0.324 ^c	1.621 ± 0.102 ^c			
20	F02114+0456	IC 0214	02 : 14 : 05.56	+ 05 : 10 : 23.7	40	23.74	5.708 ± 0.286	7.558 ± 0.378	6.174 ± 0.309	60	35.60	2.659 ± 0.163 ^c	1.053 ± 0.068 ^c	0.352 ± 0.033 ^c			
20	F02114+0456	2MASX J02135594+0510043	02 : 13 : 55.99	+ 05 : 10 : 04.0	23	13.65	0.214 ± 0.015	0.474 ± 0.026	0.498 ± 0.027	45	26.70	0.379 ± 0.028 ^c	0.208 ± 0.019 ^c	0.069 ± 0.021 ^c			
20	F02114+0456	IRGP J021400.8+051014	02 : 14 : 00.77	+ 05 : 10 : 13.8	5.922 ± 0.287	8.032 ± 0.379	6.672 ± 0.310	0.338 ± 0.166 ^c	1.261 ± 0.071 ^c	0.421 ± 0.039 ^c			
21	F02152+1418	NGC 877	02 : 17 : 53.26	+ 14 : 31 : 18.4	48	12.31	3.303 ± 0.167	4.965 ± 0.249	4.741 ± 0.238	56	14.36	2.579 ± 0.168	1.138 ± 0.075	0.396 ± 0.028			
21	F02152+1418	NGC 876	02 : 17 : 59.68	+ 14 : 32 : 38.2	75	19.23	12.81 ± 0.64	23.60 ± 1.18	26.51 ± 1.33	85	21.80	13.91 ± 0.90	5.730 ± 0.373	1.962 ± 0.129			
21	F02152+1418	IRGP J021756.5+143158	02 : 17 : 56.46	+ 14 : 31 : 58.2	...	16.11 ± 0.66	28.56 ± 1.21	31.25 ± 1.35	150	38.47	16.90 ± 1.10	7.291 ± 0.475	2.449 ± 0.162				
22	F02203+3158	MCG+05-06-036	02 : 23 : 21.99	+ 32 : 11 : 48.8	30	19.74	6.814 ± 0.304 ^c	9.600 ± 0.426 ^c	8.152 ± 0.348 ^c	33	21.71	3.352 ± 0.192 ^c			
22	F02203+3158	MCG+05-06-035	02 : 23 : 18.97	+ 32 : 11 : 18.5	23	15.13	2.255 ± 0.099 ^c	3.426 ± 0.148 ^c	3.150 ± 0.130 ^c	24	15.79	1.390 ± 0.074 ^c			
22	F02203+3158	KPG 067	02 : 23 : 20.47	+ 32 : 11 : 33.6	...	9.069 ± 0.320 ^c	13.03 ± 0.45 ^c	11.30 ± 0.37 ^c	65	42.76	4.206 ± 0.277	1.651 ± 0.111	0.529 ± 0.042				
23	F02208+4744	UGC 01845	02 : 24 : 07.97	+ 47 : 58 : 11.9	35	11.03	13.11 ± 0.59 ^c	17.48 ± 0.78 ^c	13.75 ± 0.60 ^c	50	15.76	5.036 ± 0.304 ^c	1.974 ± 0.121 ^c	0.563 ± 0.034 ^c			
24	F02281-0309	NGC 958	02 : 30 : 42.84	- 02 : 56 : 20.5	75	28.22	8.261 ± 0.415	16.78 ± 0.84	19.75 ± 0.99	90	33.86	10.46 ± 0.68	4.532 ± 0.297	1.614 ± 0.114			
25	F02345+2053	NGC 992	02 : 37 : 25.46	+ 21 : 06 : 02.8	50	13.67	11.90 ± 0.60	16.25 ± 0.81	13.37 ± 0.67	70	19.14	5.906 ± 0.364 ^c	2.341 ± 0.145 ^c	0.734 ± 0.047 ^c			
26	F02401-0013	NGC 1068	02 : 42 : 40.72	- 00 : 00 : 47.9	170	13.02	285.8 ± 14.3	...	290.9 ± 14.5	200	15.32	117.9 ± 7.7	45.72 ± 2.97	14.40 ± 0.94			
27	F02435+1253	UGC 02238	02 : 46 : 17.46	+ 13 : 05 : 44.6	45	19.31	9.946 ± 0.498	15.33 ± 0.77	13.48 ± 0.67	60	25.74	6.147 ± 0.375 ^c	2.380 ± 0.148 ^c	0.756 ± 0.052 ^c			
28	F02437+2122	IRAS F02437+2122	02 : 46 : 39.13	+ 21 : 35 : 10.4	35	16.02	6.927 ± 0.313 ^c	7.725 ± 0.347 ^c	5.027 ± 0.219 ^c	35	16.02	1.823 ± 0.106 ^c	0.658 ± 0.038 ^c	0.185 ± 0.012 ^c			
28	F02437+2123 ^a	2MASX J02464505+2133234	02 : 46 : 45.05	+ 21 : 33 : 23.5	25	11.44	0.195 ± 0.014	0.541 ± 0.029	0.584 ± 0.031	40	18.31	0.491 ± 0.031 ^c	0.221 ± 0.015 ^c	0.079 ± 0.008 ^c			
29	F02512+1446	MCG+02-08-029	02 : 54 : 01.84	+ 14 : 58 : 15.7	
29	F02512+1446	MCG+02-08-030	02 : 54 : 01.75	+ 14 : 58 : 36.4	
29	F02512+1446	UGC 02369	02 : 54 : 01.79	+ 14 : 58 : 26.0	40	24.76	8.701 ± 0.436	10.36 ± 0.52	7.659 ± 0.383	50	30.96	3.096 ± 0.204	1.197 ± 0.080	0.382 ± 0.024 ^c			
30	F03117+4151 ^a	UGC 02608	03 : 15 : 01.47	+ 42 : 02 : 08.6	45	20.83	9.116 ± 0.456	11.57 ± 0.58	9.210 ± 0.461	60	27.78	4.135 ± 0.251 ^c	1.601 ± 0.099 ^c	0.518 ± 0.033 ^c			
30	F03117+4151 ^a	UGC 02612	03 : 15 : 14.58	+ 41 : 58 : 50.0	37	17.13	0.575 ± 0.032	1.341 ± 0.069	1.660 ± 0.084	45	20.83	0.990 ± 0.061 ^c	0.429 ± 0.028 ^c	0.134 ± 0.012 ^c			
31	F03164+1119	NGC 1275	03 : 19 : 48.18	+ 41 : 30 : 42.0	50	17.55	6.807 ± 0.343	7.490 ± 0.377	5.691 ± 0.286	75	26.33	3.506 ± 0.217 ^c	2.851 ± 0.176 ^c	0.739 ± 0.168 ^c			
32	F03217+4022	IRAS F03217+4022	03 : 25 : 05.37	+ 40 : 33 : 32.2	35	16.20	9.122 ± 0.412 ^c	10.84 ± 0.49 ^c	7.913 ± 0.345 ^c	55	25.46	3.134 ± 0.191 ^c	1.204 ± 0.075 ^c	0.358 ± 0.024 ^c			
33	F03316-3618	NGC 1365	03 : 33 : 36.40	- 36 : 08 : 25.9	320	27.46	137.6 ± 6.9	221.5 ± 11.1	209.7 ± 10.5	360	30.89	103.7 ± 6.7	43.94 ± 2.86	15.63 ± 1.02			
34	F03359+1523	IRAS F03359+1523	03 : 38 : 47.07	+ 15 : 32 : 54.1	35	24.06	7.170 ± 0.324 ^c	7.541 ± 0.339 ^c	4.878 ± 0.213 ^c	50	34.37	1.643 ± 0.099 ^c	0.599 ± 0.038 ^c	0.187 ± 0.013 ^c			

TABLE 4—Continued

#	IRAS Name	Individual Name	Aperture Center Coordinate			PACS						SPIRE					
			RA (4)	Dec. HH:MM:SS (5)	Ang. α , Ap. kpc (6)	F $_{\lambda}$ (70 μ m) Jy (8)	F $_{\lambda}$ (100 μ m) Jy (9)	F $_{\lambda}$ (160 μ m) Jy (10)	Ang. α , Ap. kpc (11)	F $_{\lambda}$ (250 μ m) Jy (12)	F $_{\lambda}$ (350 μ m) Jy (13)	F $_{\lambda}$ (500 μ m) Jy (14)	F $_{\lambda}$ (500 μ m) Jy (15)				
35	F03514+1546 ^a	GCGC 465-011	03 : 54 : 07.67	+ 15 : 59 : 24.3	40	17.47	2.255 ± 0.114	3.804 ± 0.191	4.015 ± 0.201	60	26.21	2.188 ± 0.135 ^c	0.867 ± 0.056 ^c	0.310 ± 0.024 ^c			
35	F03514+1546	GCGC 465-012	03 : 54 : 15.95	+ 15 : 55 : 43.4	35	15.29	6.673 ± 0.334	8.845 ± 0.443	6.946 ± 0.348	55	24.02	3.065 ± 0.186 ^c	1.130 ± 0.071 ^c	0.356 ± 0.025 ^c			
36	03582+6012	IRAS 03582+6012NE	04 : 02 : 32.99	+ 60 : 20 : 41.8		
36	03582+6012	IRAS 03582+6012SW	04 : 02 : 31.97	+ 60 : 20 : 38.3	33	19.76	5.685 ± 0.285	5.922 ± 0.296	3.745 ± 0.188	43	25.75	1.598 ± 0.098 ^c	0.659 ± 0.044 ^c	0.158 ± 0.014 ^c			
36	03582+6012	IRAS 03582+6012	04 : 02 : 32.47	+ 60 : 20 : 40.0	50	17.53	10.52 ± 0.53	16.86 ± 0.84	15.62 ± 0.78	90	31.55	7.324 ± 0.480	3.541 ± 0.223 ^c	1.068 ± 0.071 ^c			
37	F04097+40525	UGC 02982	04 : 12 : 22.68	+ 05 : 32 : 49.1	45	10.86	17.57 ± 0.81 ^c	22.28 ± 1.02 ^c	16.82 ± 0.75 ^c	55	13.28	6.401 ± 0.388 ^c	2.406 ± 0.148 ^c	0.669 ± 0.041 ^c			
38	F04118-3207	ESO 420-G013	04 : 13 : 49.70	- 32 : 00 : 25.3	10	6.303	2.671 ± 0.104 ^c	3.663 ± 0.133 ^c	3.110 ± 0.096 ^c		
39	F04191-1855	ESO 550-LG 025 NED01	04 : 21 : 20.08	- 18 : 48 : 57.4	8	5.042	4.438 ± 0.160 ^c	5.781 ± 0.195 ^c	4.736 ± 0.125 ^c		
39	F04191-1855	ESO 550-LG 025 NED02	04 : 21 : 20.02	- 18 : 48 : 39.6	40	25.21	6.452 ± 0.323	8.676 ± 0.434	7.115 ± 0.356	60	37.82	3.273 ± 0.215	1.306 ± 0.087	0.449 ± 0.028 ^c			
39	F04191-1855	ESO 550-LG 025	04 : 21 : 20.04	- 18 : 48 : 48.4	45	18.57	10.02 ± 0.50	16.45 ± 0.82	15.32 ± 0.77	65	26.82	7.368 ± 0.484	3.225 ± 0.199 ^c	1.028 ± 0.063 ^c			
40	F04210-4042	NGC 1572	04 : 22 : 42.81	- 40 : 36 : 03.1	35	13.20	7.402 ± 0.371	10.97 ± 0.49 ^c	8.846 ± 0.385 ^c	60	22.63	3.815 ± 0.234 ^c	1.478 ± 0.093 ^c	0.453 ± 0.031 ^c			
41	04271+3849	IRAS 04271+3849	04 : 30 : 33.09	+ 38 : 55 : 47.8	50	15.93	36.74 ± 1.70 ^c	37.00 ± 1.70 ^c	22.96 ± 1.04 ^c	70	22.30	7.291 ± 0.452 ^c	2.650 ± 0.165 ^c	0.748 ± 0.049 ^c			
42	F04315-0840	NGC 1614	04 : 33 : 59.95	- 08 : 34 : 46.6	50	24.46	8.159 ± 0.409	12.77 ± 0.64	11.93 ± 0.60	65	31.80	5.210 ± 0.341	2.114 ± 0.140	0.663 ± 0.047			
43	F04326+1904	UGC 03094	04 : 35 : 33.81	+ 19 : 10 : 18.0	28	28.78	6.125 ± 0.272 ^c	5.284 ± 0.233 ^c	3.945 ± 0.125 ^c	33	33.92	0.918 ± 0.033 ^c	0.339 ± 0.020 ^c	0.091 ± 0.007 ^c			
44	F04454-4838	ESO 203-IG001	04 : 46 : 49.55	- 48 : 33 : 30.6	35	13.29	9.169 ± 0.414 ^c	10.35 ± 0.46 ^c	6.949 ± 0.303 ^c	65	24.67	2.454 ± 0.153 ^c	0.905 ± 0.059 ^c	0.266 ± 0.021 ^c			
45	F04502-3304	MCG-05-12-006	04 : 52 : 04.96	- 32 : 59 : 26.0	45	13.44	11.00 ± 0.51 ^c	13.49 ± 0.62 ^c	10.83 ± 0.48 ^c	60	17.92	4.438 ± 0.270 ^c	1.670 ± 0.103 ^c	0.534 ± 0.034 ^c			
46	F05053-0805	NGC 1797	05 : 07 : 44.84	- 08 : 01 : 08.7	40	11.95	0.402 ± 0.027	0.818 ± 0.044	0.954 ± 0.049	60	17.92	0.596 ± 0.044	0.315 ± 0.025 ^c	0.121 ± 0.014 ^c			
46	F05053-0805 ^a	NGC 1799	05 : 07 : 44.59	- 07 : 58 : 09.0	15	5.461	2.389 ± 0.099 ^c	2.941 ± 0.121 ^c	2.375 ± 0.087 ^c		
47	F05054+1718	GCGC 468-002 NED01	05 : 08 : 19.71	+ 17 : 21 : 47.8	18	6.554	9.426 ± 0.402 ^c	9.891 ± 0.414 ^c	6.467 ± 0.251 ^c	50	18.20	2.804 ± 0.185	1.015 ± 0.070	0.293 ± 0.024			
47	F05054+1718	GCGC 468-002	05 : 08 : 21.21	+ 17 : 22 : 08.0	40	14.56	10.43 ± 0.52	11.15 ± 0.56	7.394 ± 0.370		
48	05083+2441	IRAS 05083+2441	05 : 11 : 25.88	+ 24 : 45 : 18.2	30	13.79	6.982 ± 0.312 ^c	7.413 ± 0.329 ^c	4.739 ± 0.203 ^c	37	17.01	1.672 ± 0.099 ^c	0.613 ± 0.036 ^c	0.198 ± 0.015 ^c			
48	05083+2441	2MASX J05112888+2445593	05 : 11 : 29.05	+ 24 : 46 : 04.0	30	13.79	0.594 ± 0.033	0.935 ± 0.049	0.977 ± 0.050	36	16.55	0.573 ± 0.040	0.290 ± 0.020 ^c	0.103 ± 0.011 ^c			
48	05083+2441	IRGP J051127.4+244539	05 : 11 : 27.46	+ 24 : 45 : 41.1	7.576 ± 0.314 ^c	8.348 ± 0.333 ^c	5.716 ± 0.209 ^c	70	32.17	2.202 ± 0.146	0.824 ± 0.058	0.292 ± 0.024			
49	F05081+7936	VII Zw 031	05 : 16 : 46.39	+ 79 : 40 : 12.9	35	36.69	7.492 ± 0.338 ^c	10.12 ± 0.45 ^c	8.055 ± 0.351 ^c	55	57.65	3.130 ± 0.189 ^c	1.167 ± 0.072 ^c	0.349 ± 0.022 ^c			
50	05129+5128	IRAS 05129+5128	05 : 16 : 55.96	+ 51 : 31 : 56.9	35	19.29	7.273 ± 0.329 ^c	7.655 ± 0.344 ^c	5.028 ± 0.219 ^c	45	24.81	1.771 ± 0.106 ^c	0.631 ± 0.038 ^c	0.196 ± 0.013 ^c			
51	F05189-2524	IRAS F05189-2524	05 : 21 : 01.45	- 25 : 21 : 46.2	35	29.19	13.53 ± 0.61 ^c	11.39 ± 0.51 ^c	6.180 ± 0.269 ^c	40	33.36	1.975 ± 0.118 ^c	0.729 ± 0.044 ^c	0.199 ± 0.014 ^c			
52	F05187-1017	IRAS F05187-1017	05 : 21 : 06.53	- 10 : 14 : 46.2	40	22.38	6.782 ± 0.309 ^c	8.595 ± 0.389 ^c	6.583 ± 0.292 ^c	50	27.97	2.721 ± 0.165 ^c	1.094 ± 0.068 ^c	0.327 ± 0.022 ^c			
53	05368+4940	MCG+08-11-002	05 : 40 : 43.70	+ 49 : 41 : 41.6	40	15.63	19.40 ± 0.88 ^c	26.93 ± 1.22 ^c	21.56 ± 0.95 ^c	55	21.49	8.341 ± 0.507 ^c	3.223 ± 0.198 ^c	0.948 ± 0.056 ^c			
54	F05365+6921	NGC 1961	05 : 42 : 04.55	+ 69 : 22 : 42.8	120	33.45	11.59 ± 0.58	26.26 ± 1.31	34.08 ± 1.71	140	39.03	19.59 ± 1.27	8.715 ± 0.567	3.076 ± 0.201			

TABLE 4—Continued

#	IRAS Name	Individual Name	RA HH:MM:SS (4)	Dec DD:MM:SS (5)	Ang. _{II} DD:MM:SS (6)	Ang. _{II} Phys. Ap. kpc (7)	PACS			SPIRE			
							F _λ (70 μm) Jy (8)	F _λ (100 μm) Jy (9)	F _λ (160 μm) Jy (10)	Ang. _{II} Phys. Ap. kpc (11)	F _λ (250 μm) Jy (12)	F _λ (350 μm) Jy (13)	F _λ (500 μm) Jy (14)
55	F05414+5840	UGC 03351	05:45:48.03	+58:42:03.6	53	16.42	19.02 ± 0.95	31.33 ± 1.57	28.88 ± 1.44	70	21.69	13.70 ± 0.90	5.817 ± 0.359 ^c
56	05442+1732	IRAS 05442+1732	05:47:11.20	+17:33:46.4	35	13.13	10.84 ± 0.49 ^c	11.95 ± 0.54 ^c	8.035 ± 0.350 ^c	43	16.14	2.878 ± 0.172 ^c	1.005 ± 0.061 ^c
56	05442+1732	UGC 03356	05:47:05.79	+17:33:11.9	35	13.13	1.026 ± 0.054	1.955 ± 0.099	2.141 ± 0.108	43	16.14	1.376 ± 0.091	0.577 ± 0.040
56	05442+1732	HIPASS J0547+17	05:47:47.08	+17:33:29.1	11.86 ± 0.49 ^c	13.91 ± 0.55 ^c	10.18 ± 0.37 ^c	90	33.77	4.194 ± 0.276	1.639 ± 0.110
57	F06076-2139	IRAS F06076-2139NW	06:09:45.74	-21:40:24.5
57	F06076-2139	IRAS F06076-2139SE	06:09:45.95	-21:40:32.1	30	22.30	7.554 ± 0.338 ^c	8.405 ± 0.373 ^c	5.664 ± 0.242 ^c	50	37.16	2.157 ± 0.129 ^c	0.863 ± 0.053 ^c
57	F06076-2139	IRAS F06076-2139	06:09:45.84	-21:40:28.3
58	F06052+8027	UGC 03410	06:14:29.61	+80:26:59.6	52	14.34	10.34 ± 0.52	17.92 ± 0.90	18.52 ± 0.93	68	18.76	8.771 ± 0.571	3.428 ± 0.223
58	F06052+8027	UGC 03405	06:13:57.90	+80:28:34.7	45	12.41	2.083 ± 0.106	4.294 ± 0.216	5.071 ± 0.255	50	13.79	2.782 ± 0.181	1.100 ± 0.072
58	F06052+8027	KPG 108	06:14:13.75	+80:27:47.1	...	12.42 ± 0.53	22.21 ± 0.92	23.59 ± 0.96	...	11.55 ± 0.60	4.528 ± 0.235	1.566 ± 0.077 ^c	
59	F06107+7822	NGC 2146	06:18:37.82	+78:21:24.0	120	10.12	198.7 ± 9.9	237.1 ± 11.9	174.4 ± 8.7	150	12.65	62.78 ± 4.08	22.89 ± 1.49
60	F06259-4708	ESO 255-IG 007 NED01	06:27:21.70	-47:10:36.2	7.138 ± 0.465
60	F06259-4708	ESO 255-IG 007 NED02	06:27:22.55	-47:10:47.3
60	F06259-4708	ESO 255-IG 007 NED03	06:27:23.09	-47:11:02.6
60	F06259-4708	ESO 255-IG 007	06:27:22.39	-47:10:49.4	45	34.97	9.801 ± 0.491	10.67 ± 0.53	7.175 ± 0.359	60	46.63	2.764 ± 0.181	1.019 ± 0.068
61	F06295-1735	ESO 557-G002	06:31:47.20	-17:37:16.6	40	17.36	7.144 ± 0.326 ^c	8.081 ± 0.366 ^c	6.001 ± 0.266 ^c	45	19.53	2.247 ± 0.135 ^c	0.857 ± 0.052 ^c
61	F06295-1735	ESO 557-G001	06:31:45.71	-17:38:44.9	30	13.02	1.555 ± 0.079	2.208 ± 0.111	1.684 ± 0.085	43	18.66	0.739 ± 0.052	0.299 ± 0.023
61	F06295-1735	IRGP J063146.5-173802	06:31:46.45	-17:38:00.7	8.699 ± 0.335 ^c	10.29 ± 0.38 ^c	7.685 ± 0.279 ^c	...	3.006 ± 0.144 ^c	1.156 ± 0.057 ^c	0.345 ± 0.020 ^c
62	F06538+4628	UGC 3608	06:57:34.41	+46:24:10.6	40	17.53	8.877 ± 0.444	10.62 ± 0.53	8.315 ± 0.416	50	21.91	3.533 ± 0.215 ^c	1.363 ± 0.083 ^c
63	F06592-6313	IRAS F06592-6313	06:59:40.26	-63:17:52.4	35	16.87	6.904 ± 0.312 ^c	7.530 ± 0.338 ^c	5.027 ± 0.219 ^c	55	26.50	1.842 ± 0.113 ^c	0.755 ± 0.048 ^c
64	F07027-6011	AM 0702-601 NED01	07:03:24.14	-60:15:21.9	28	18.00	2.554 ± 0.114 ^c	2.700 ± 0.120 ^c	2.081 ± 0.089 ^c	43	27.64	0.874 ± 0.054 ^c	0.344 ± 0.024 ^c
64	F07027-6011	AM 0702-601 NED02	07:03:28.52	-60:16:43.7	28	18.00	5.253 ± 0.234 ^c	6.529 ± 0.288 ^c	4.957 ± 0.210 ^c	50	32.14	1.991 ± 0.121 ^c	0.816 ± 0.051 ^c
64	F07027-6011	AM 0702-601	07:03:26.33	-60:16:02.7	7.807 ± 0.260 ^c	9.229 ± 0.312 ^c	7.038 ± 0.228 ^c	90	57.86	2.540 ± 0.170	1.025 ± 0.072
65	07063+2043	NGC 2342	07:09:18.07	+20:38:10.2	55	20.00	9.528 ± 0.477	14.86 ± 0.74	13.45 ± 0.67	65	23.63	5.856 ± 0.382	2.328 ± 0.153
65	07063+2043	NGC 2341	07:09:12.01	+20:36:11.2	35	12.73	8.112 ± 0.406	11.00 ± 0.55	8.818 ± 0.441	50	18.18	3.431 ± 0.225	1.433 ± 0.086 ^c
65	07063+2043	KPG 125	07:09:15.04	+20:37:10.7	17.64 ± 0.63	25.86 ± 0.93	22.26 ± 0.80	9.287 ± 0.443	3.761 ± 0.176 ^c
66	F07160-6215	NGC 2369	07:16:37.73	-62:20:36.4	60	13.56	26.90 ± 1.35	41.22 ± 2.06	37.55 ± 1.88	95	21.46	17.35 ± 1.14	7.181 ± 0.453 ^c
67	07251-0248	IRAS 07251-0248	07:27:37.62	-02:54:54.8	35	57.39	7.024 ± 0.317 ^c	6.419 ± 0.288 ^c	3.878 ± 0.169 ^c	45	73.78	1.448 ± 0.087 ^c	0.561 ± 0.034 ^c
68	F07256+3355	NGC 2389	07:29:04.59	+33:51:38.0	50	14.47	3.802 ± 0.194	6.412 ± 0.323	6.601 ± 0.332	78	22.58	3.538 ± 0.231	1.395 ± 0.091
68	F07256+3355	NGC 2388	07:28:53.44	+33:49:07.8	50	14.47	20.68 ± 0.96 ^c	26.43 ± 1.21 ^c	21.16 ± 0.96 ^c	85	24.60	8.484 ± 0.525 ^c	3.237 ± 0.201 ^c
68	F07256+3355	NGC 2385	07:28:28.17	+33:50:16.9	37	10.71	0.379 ± 0.025 ^b	0.184 ± 0.012 ^{b,c}
68	F07256+3355	WBL 142	07:28:46.38	+33:50:22.9	24.48 ± 0.98 ^c	32.84 ± 1.26 ^c	27.76 ± 1.01 ^c	...	12.02 ± 0.57 ^c	4.632 ± 0.221 ^c	1.537 ± 0.072 ^c
69	F07329+1149	MCG+02-20-003	07:35:43.44	+11:42:34.8	37	12.92	10.61 ± 0.48 ^c	13.13 ± 0.59 ^c	9.969 ± 0.437 ^c	70	24.43	4.071 ± 0.250 ^c	1.555 ± 0.095 ^c

TABLE 4—Continued

#	IRAS Name	Individual Name	Aperture Center Coordinate			PACS			SPIRE			
			RA HH:MM:SS (4)	Dec DD:MM:SS (5)	Ang. _{rr} kpc (6)	Phys. Ap. F _λ (70 μm) Jy (8)	Phys. Ap. F _λ (100 μm) Jy (9)	Phys. Ap. F _λ (160 μm) Jy (10)	Ang. _{rr} Ap. F _λ (250 μm) Jy (11)	Phys. Ap. F _λ (350 μm) Jy (12)	Phys. Ap. F _λ (500 μm) Jy (13)	
69	F07329+1149 ^a	NGC 2416	07 : 35 : 41.53	+ 11 : 36 : 42.1	32	11.17	0.897 ± 0.047	1.705 ± 0.086	1.956 ± 0.098	42	14.66	1.008 ± 0.066
70	08355-4944	IRAS 08355-4944	08 : 37 : 01.87	- 49 : 54 : 30.0	35	19.02	10.25 ± 0.46 ^c	9.529 ± 0.428 ^c	5.637 ± 0.246 ^c	40	21.74	1.758 ± 0.105 ^c
71	F08339+6517	IRAS F08339+6517	08 : 38 : 23.18	+ 65 : 07 : 15.2	45	18.13	5.865 ± 0.294	6.163 ± 0.309	3.979 ± 0.200	45	18.13	1.267 ± 0.084
72	F08354+2555	NGC 2623	08 : 38 : 24.11	+ 25 : 45 : 16.5	40	15.73	27.92 ± 1.27 ^c	28.46 ± 1.29 ^c	17.65 ± 0.78 ^c	50	19.66	5.929 ± 0.358 ^c
73	08424-3130	ESO 432-IG006SW	08 : 44 : 27.21	- 31 : 41 : 50.8	17	5.942	4.823 ± 0.204 ^c	6.700 ± 0.279 ^c	5.638 ± 0.211 ^c
73	08424-3130	ESO 432-IG006NE	08 : 44 : 28.93	- 31 : 41 : 30.3	14	4.894	3.469 ± 0.143 ^c	3.962 ± 0.160 ^c	2.783 ± 0.099 ^c
73	08424-3130	ESO 432-IG006	08 : 44 : 28.07	- 31 : 41 : 40.5	52	18.18	7.597 ± 0.381	9.841 ± 0.493	7.663 ± 0.384	65	22.72	3.117 ± 0.205
74	F08520-6850	ESO 060-IG 016 NED01	08 : 52 : 32.07	- 69 : 01 : 54.8
74	F08520-6850	ESO 060-IG 016 NED02	08 : 52 : 30.50	- 69 : 01 : 59.2
74	F08520-6850	ESO 060-IG 016	08 : 52 : 31.28	- 69 : 01 : 57.0	33	30.69	5.468 ± 0.274	5.560 ± 0.278	3.496 ± 0.175	60	55.79	1.318 ± 0.088
75	F08572+3915	IRAS F08572+3915	09 : 00 : 25.35	+ 39 : 03 : 54.0	25	28.57	6.398 ± 0.282 ^c	4.452 ± 0.194 ^c	1.997 ± 0.084 ^c	35	39.99	0.521 ± 0.031 ^c
76	09022-3615	IRAS 09022-3615	09 : 04 : 12.69	- 36 : 27 : 01.5	35	40.96	12.81 ± 0.58 ^c	13.14 ± 0.59 ^c	8.057 ± 0.351 ^c	40	46.81	2.588 ± 0.152 ^c
77	F09111-1007	2MASX J09113644-1019296	09 : 13 : 36.50	- 10 : 19 : 29.7	20	21.47	7.284 ± 0.315 ^c	8.923 ± 0.378 ^c	6.554 ± 0.262 ^c	20	21.47	2.615 ± 0.134 ^c
77	F09111-1007	2MASX J09138888-1019196	09 : 13 : 38.89	- 10 : 19 : 19.6	20	21.47	2.003 ± 0.087 ^c	2.674 ± 0.114 ^c	2.327 ± 0.093 ^c	20	21.47	1.001 ± 0.051 ^c
77	F09111-1007	IRAS F09111-1007	09 : 13 : 37.69	- 10 : 19 : 24.6	50	53.67	8.314 ± 0.417	10.35 ± 0.52	7.726 ± 0.387	65	69.77	3.434 ± 0.225
78	F09126-4432	CGCG 299-036	09 : 15 : 44.49	+ 44 : 14 : 09.6
78	F09126-4432	UGC 04881 NED01	09 : 15 : 55.52	+ 44 : 19 : 57.4
78	F09126-4432	UGC 04881 NED02	09 : 15 : 54.69	+ 44 : 19 : 50.8
78	F09126-4432	UGC 04881	09 : 15 : 55.10	+ 44 : 19 : 54.0	45	35.93	7.311 ± 0.366	9.282 ± 0.465	7.433 ± 0.372	60	47.91	3.296 ± 0.217
79	F09320+6134	UGC 05101	09 : 35 : 51.59	+ 61 : 21 : 11.9	30	23.82	15.34 ± 0.69 ^c	...	15.29 ± 0.65 ^c	53	42.09	6.138 ± 0.371 ^c
80	F09333+4841	MCG+08-18-013	09 : 36 : 37.20	+ 48 : 28 : 27.7	37	19.70	7.330 ± 0.333 ^c	8.600 ± 0.387 ^c	6.416 ± 0.282 ^c	37	19.70	2.320 ± 0.135 ^c
80	F09333+4841	MCG+08-18-012	09 : 36 : 30.86	+ 48 : 28 : 09.9	28	14.91	0.134 ± 0.023	0.235 ± 0.016	0.320 ± 0.019	28	14.91	0.187 ± 0.015
80	F09333+4841	CGCG 239-011	09 : 36 : 34.02	+ 48 : 28 : 18.8	7.463 ± 0.334 ^c	8.835 ± 0.388 ^c	6.737 ± 0.282 ^c	75	39.92	2.302 ± 0.152
81	F09437+0317	IC 0564	09 : 46 : 21.10	+ 03 : 04 : 16.3	50	21.65	3.334 ± 0.168	6.625 ± 0.332	7.802 ± 0.391	55	23.81	4.181 ± 0.274
81	F09437+0317	IC 0563	09 : 46 : 20.30	+ 03 : 02 : 44.7	40	17.32	3.542 ± 0.175	5.749 ± 0.288	5.604 ± 0.281	50	21.65	2.696 ± 0.177
81	F09437+0317	Ap 303	09 : 46 : 20.70	+ 03 : 03 : 30.4	...	6.876 ± 0.244	1.237 ± 0.44	1.341 ± 0.48	90	38.96	6.772 ± 0.443	
82	F10015-0614	NGC 3110	10 : 04 : 02.11	- 06 : 28 : 29.5	50	18.23	13.81 ± 0.69	20.79 ± 1.04	18.91 ± 0.95	67	24.43	7.794 ± 0.509
82	F10015-0614	MCG-01-26-013	10 : 03 : 57.03	- 06 : 29 : 47.7	30	10.94	1.597 ± 0.073 ^c	2.153 ± 0.097 ^c	1.852 ± 0.080 ^c	40	14.58	0.647 ± 0.041 ^c
82	F10015-0614	IRGP J100359.6-062908	10 : 03 : 59.57	- 06 : 29 : 08.5	...	15.41 ± 0.69 ^c	22.94 ± 1.04 ^c	20.76 ± 0.95 ^c	110	40.10	8.670 ± 0.567	
83	F10038-3338	ESO 374-IG 032	10 : 06 : 04.65	- 33 : 53 : 06.1	35	24.76	10.14 ± 0.46 ^c	8.693 ± 0.390 ^c	5.048 ± 0.220 ^c	55	38.90	1.837 ± 0.111 ^c
84	F10173+0828	IRASF10173+0828	10 : 20 : 00.24	+ 08 : 13 : 32.8	40	39.46	6.298 ± 0.287 ^c	5.677 ± 0.257 ^c	3.169 ± 0.141 ^c	45	44.40	1.132 ± 0.068 ^c
85	F10196+2149	NGC 3221	10 : 22 : 19.98	+ 21 : 34 : 10.6	95	29.43	10.43 ± 0.52	20.96 ± 1.05	24.06 ± 1.20	110	34.08	12.52 ± 0.82

TABLE 4—Continued

#	IRAS Name	Individual Name	Aperture Center Coordinate			PACS						SPIRE					
			RA HH:MM:SS (4)	Dec. DD:MM:SS (5)	Ang. α , Ap. kpc (6)	F $_{\lambda}$ (70 μ m) Jy (8)	F $_{\lambda}$ (100 μ m) Jy (9)	F $_{\lambda}$ (160 μ m) Jy (10)	F $_{\lambda}$ (350 μ m) Jy (11)	F $_{\lambda}$ (500 μ m) Jy (12)	Phys. Ap. kpc (13)	Phys. Ap. kpc (14)	Ang. α , Ap. Jy (15)				
86	F10257-4339	NGC 3256	10 : 27 : 51.30	-43 : 54 : 14.0	70	12.96	120.3 ± 6.0	135.4 ± 6.8	93.48 ± 4.68	85	15.74	33.91 ± 2.21	12.16 ± 0.79	3.929 ± 0.242 ^c			
87	F10409-4556	ESO 264-G036	10 : 43 : 07.51	-46 : 12 : 44.1	45	20.92	7.974 ± 0.399	13.09 ± 0.65	13.10 ± 0.66	60	27.90	6.560 ± 0.429	2.658 ± 0.163 ^c	0.860 ± 0.052 ^c			
88	F10567-4310	ESO 264-G057	10 : 59 : 01.70	-43 : 26 : 25.2	40	15.61	6.910 ± 0.346	11.10 ± 0.56	10.41 ± 0.52	60	23.42	5.057 ± 0.331	2.124 ± 0.131 ^c	0.690 ± 0.043 ^c			
89	F10565+2448	IRAS F10565+2448	10 : 59 : 18.15	+ 24 : 32 : 34.2	35	25.05	14.26 ± 0.64 ^c	15.80 ± 0.71 ^c	10.45 ± 0.46 ^c	43	30.77	3.643 ± 0.215 ^c	1.337 ± 0.078 ^c	0.381 ± 0.022 ^c			
90	F11011+4107	MCG+07-23-019	11 : 03 : 53.98	+ 40 : 51 : 00.4	40	28.62	8.484 ± 0.387 ^c	10.52 ± 0.48 ^c	7.8225 ± 0.346 ^c	45	32.20	2.862 ± 0.172 ^c	1.098 ± 0.066 ^c	0.325 ± 0.021 ^c			
91	F11186-0242	CGCG 011-076	11 : 21 : 12.24	- 02 : 59 : 02.5	40	21.43	6.460 ± 0.295 ^c	8.954 ± 0.405 ^c	7.885 ± 0.349 ^c	40	21.43	3.521 ± 0.209 ^c	1.382 ± 0.080 ^c	...			
91	F11186-0242	2MASX J11210825-0259399	11 : 21 : 08.29	- 02 : 59 : 39.2	27	14.46	0.281 ± 0.018 ^c	0.520 ± 0.026 ^c	0.427 ± 0.021 ^c	23	12.32	0.265 ± 0.016 ^c	0.121 ± 0.009 ^c	...			
91	F11186-0242	IRGP J112110.3-025922	11 : 21 : 10.26	- 02 : 59 : 20.8	6.742 ± 0.295 ^c	9.474 ± 0.406 ^c	8.312 ± 0.350 ^c	100	53.57	3.795 ± 0.252	1.653 ± 0.112	0.562 ± 0.042			
92	F11231+1456	IC 2810	11 : 25 : 45.07	+ 14 : 40 : 36.0	30	21.23	5.703 ± 0.235 ^c	7.671 ± 0.341 ^c	6.251 ± 0.267 ^c	44	31.14	2.713 ± 0.162 ^c	1.142 ± 0.068 ^c	...			
92	F11231+1456	MCG+03-29-044	11 : 25 : 49.55	+ 14 : 40 : 06.6	25	17.70	2.753 ± 0.122 ^c	3.734 ± 0.163 ^c	3.096 ± 0.139 ^c	37	26.19	1.324 ± 0.078 ^c	0.561 ± 0.033 ^c	...			
92	F11231+1456	IRAS F11231+1456	11 : 25 : 47.31	+ 14 : 40 : 21.2	...	8.456 ± 0.283 ^c	11.40 ± 0.38 ^c	9.348 ± 0.297 ^c	90	63.70	3.820 ± 0.252	1.610 ± 0.108	0.544 ± 0.041				
93	F12554-020	ESO 319-G022	11 : 27 : 54.18	- 41 : 36 : 51.7	40	15.01	9.086 ± 0.414 ^c	10.53 ± 0.48 ^c	7.785 ± 0.344 ^c	50	18.76	3.088 ± 0.186 ^c	1.144 ± 0.070 ^c	0.319 ± 0.021 ^c			
94	F11257+5850	UGC 6471	11 : 28 : 31.04	+ 58 : 33 : 40.5		
94	F11257+5850	UGC 6472	11 : 28 : 33.67	+ 58 : 33 : 46.1		
94	F11257+5850	NGC 3690	11 : 28 : 32.35	+ 58 : 33 : 43.3	75	18.07	130.3 ± 6.5	118.3 ± 5.9	68.77 ± 3.44	90	21.69	21.85 ± 1.42	7.688 ± 0.502	2.273 ± 0.149			
95	F11506-3851	ESO 320-G030	11 : 53 : 11.73	- 39 : 07 : 49.0	60	11.72	41.98 ± 1.97 ^c	49.14 ± 2.28 ^c	34.81 ± 1.59 ^c	80	15.63	13.02 ± 0.81 ^c	5.182 ± 0.324 ^c	1.608 ± 0.101 ^c			
96	F12043-3140	MCG-05-29-016	12 : 06 : 51.87	- 31 : 56 : 59.2		
96	F12043-3140	MCG-05-29-017	12 : 06 : 51.70	- 31 : 56 : 46.4		
96	F12043-3140	ESO 440-IG058	12 : 06 : 51.78	- 31 : 56 : 52.8	35	18.16	8.197 ± 0.410	10.89 ± 0.54 ^c	8.693 ± 0.435	50	25.94	3.607 ± 0.238	1.323 ± 0.089	0.388 ± 0.028			
97	F12112+0305	IRAS F12112+0305	12 : 13 : 46.02	+ 02 : 48 : 42.2	35	50.07	9.283 ± 0.419 ^c	9.241 ± 0.415 ^c	5.831 ± 0.254 ^c	45	64.38	1.974 ± 0.119 ^c	0.796 ± 0.049 ^c	0.226 ± 0.016 ^c			
98	F12116+5448	NGC 4194	12 : 14 : 09.71	+ 54 : 31 : 35.5	50	10.25	26.20 ± 1.21 ^c	26.14 ± 1.20 ^c	16.60 ± 0.75 ^c	60	12.30	5.315 ± 0.324 ^c	1.867 ± 0.115 ^c	0.549 ± 0.034 ^c			
99	F12115-4656	ESO 267-G030	12 : 14 : 12.81	- 47 : 13 : 42.5	40	18.04	6.914 ± 0.346	10.26 ± 0.51	9.280 ± 0.464	60	27.05	4.509 ± 0.272 ^c	1.757 ± 0.107 ^c	0.598 ± 0.035 ^c			
99	F12115-4656 ^a	ESO 267-G029	12 : 13 : 52.28	- 47 : 16 : 25.4	50	22.54	5.725 ± 0.287	7.924 ± 0.397	7.143 ± 0.358	70	31.56	3.262 ± 0.213	1.350 ± 0.083 ^c	0.441 ± 0.028 ^c			
100	I2116-5615	IRAS I2116-5615	12 : 14 : 22.08	- 56 : 32 : 32.7	35	20.58	11.76 ± 0.53 ^c	13.02 ± 0.58 ^c	8.808 ± 0.384 ^c	45	26.46	3.229 ± 0.195 ^c	1.268 ± 0.080 ^c	0.418 ± 0.028 ^c			
101	F12224-0624	IRAS F12224-0624	12 : 25 : 03.90	- 06 : 40 : 52.1	35	20.14	7.145 ± 0.323 ^c	7.761 ± 0.348 ^c	5.079 ± 0.221 ^c	65	37.41	1.972 ± 0.122 ^c	0.785 ± 0.050 ^c	0.271 ± 0.019 ^c			
102	F12243-0036	NGC 4418	12 : 26 : 54.60	- 00 : 52 : 39.6	50	8.799	4.281 ± 1.98 ^c	34.12 ± 1.57 ^c	18.32 ± 0.83 ^c	65	11.44	6.447 ± 0.393 ^c	2.498 ± 0.152 ^c	0.885 ± 0.053 ^c			
102	F12243-0036	MCG+00-32-013	12 : 27 : 04.88	- 00 : 54 : 24.7	25	4.400	0.233 ± 0.018	0.337 ± 0.021	0.357 ± 0.018 ^c	40	7.039	0.184 ± 0.013 ^c	0.097 ± 0.007 ^c	0.044 ± 0.006 ^c			
102	F12243-0036	KPG 337	12 : 26 : 59.74	- 00 : 53 : 32.1	43.05 ± 1.98 ^c	34.46 ± 1.57 ^c	18.67 ± 0.83 ^c	...	6.631 ± 0.394 ^c	2.595 ± 0.152 ^c	0.930 ± 0.053 ^c				
103	F12540+5708	UGC 08058	12 : 56 : 14.25	+ 56 : 52 : 24.8	35	30.00	34.87 ± 1.59 ^c	30.41 ± 1.37 ^c	16.93 ± 0.74 ^c	50	42.86	5.685 ± 0.343 ^c	2.007 ± 0.123 ^c	0.597 ± 0.036 ^c			
104	F12590+2934	2MASX J13012450+2918306	13 : 01 : 25.27	+ 29 : 18 : 49.5			
104	F12590+2934	FIRST J130125.2+291849	13 : 01 : 24.51	+ 29 : 18 : 29.8			

TABLE 4—Continued

#	IRAS Name	Individual Name	Aperture Center Coordinate			PACS						SPIRE					
			RA HH:MM:SS (4)	Dec DD:MM:SS (5)	Ang. _{''} kpc (6)	Phys. Ap. Jy (7)	F _λ (70 μm) Jy (8)	F _λ (100 μm) Jy (9)	F _λ (160 μm) Jy (10)	Ang. _{''} /Ap. kpc (11)	Phys. Ap. Jy (12)	F _λ (250 μm) Jy (13)	F _λ (350 μm) Jy (14)	F _λ (500 μm) Jy (15)			
104	F12590+2934	NGC 4922	13 : 01 : 24.89	+ 29 : 18 : 39.6	40	20.54	6.763 ± 0.309 ^c	7.606 ± 0.345 ^c	5.283 ± 0.234 ^c	50	25.67	2.032 ± 0.122 ^c	0.727 ± 0.045 ^c	0.218 ± 0.015 ^c			
105	F12592+0436	CGCG 043-099	13 : 01 : 50.28	+ 04 : 20 : 00.8	35	27.59	6.538 ± 0.295 ^c	8.455 ± 0.379 ^c	6.675 ± 0.291 ^c	60	47.30	2.808 ± 0.171 ^c	1.055 ± 0.065 ^c	0.315 ± 0.020 ^c			
106	F12596-1529	MCG-02-33-098SW	13 : 02 : 19.66	- 15 : 46 : 04.2		
106	F12596-1529	MCG-02-33-098NE	13 : 02 : 20.38	- 15 : 45 : 59.6	40	14.80	7.534 ± 0.377	8.490 ± 0.425	5.962 ± 0.299	70	25.89	2.654 ± 0.175	1.061 ± 0.072	0.330 ± 0.027			
106	F12596-1529	MCG-02-33-098	13 : 02 : 20.02	- 15 : 46 : 01.8	43	21.16	16.32 ± 0.75 ^c	16.90 ± 0.77 ^c	10.66 ± 0.47 ^c	55	27.06	3.747 ± 0.228 ^c	1.405 ± 0.087 ^c	0.451 ± 0.029 ^c			
107	F13001-2339	ESO 507-G070	13 : 02 : 52.42	- 23 : 55 : 17.8	38	18.72	10.49 ± 0.48 ^c	13.55 ± 0.61 ^c	10.13 ± 0.45 ^c	50	24.63	3.819 ± 0.231 ^c	1.624 ± 0.101 ^c	0.422 ± 0.028 ^c			
108	13052-5711	RAS 13052-5711	13 : 08 : 18.73	- 57 : 27 : 30.3	40	10.78	19.67 ± 0.90 ^c	18.09 ± 0.82 ^c	10.66 ± 0.47 ^c	50	13.48	3.775 ± 0.228 ^c	1.523 ± 0.093 ^c	0.500 ± 0.030 ^c			
109	F13126+2453	IC 0860	13 : 15 : 03.49	+ 24 : 37 : 07.6	50	32.85	50.72 ± 2.35 ^c	55.02 ± 2.53 ^c	34.97 ± 1.58 ^c	60	39.42	12.33 ± 0.75 ^c	4.396 ± 0.268 ^c	1.340 ± 0.079 ^c			
110	13120-5453	RAS 13120-5453	13 : 15 : 06.37	- 55 : 09 : 22.5	21	13.55	10.70 ± 0.46 ^c	9.771 ± 0.417 ^c	5.513 ± 0.223 ^c		
111	F13136+6223	VV 250a	13 : 15 : 34.96	+ 62 : 07 : 29.2	16	10.32	2.091 ± 0.088 ^c	2.730 ± 0.113 ^c	2.205 ± 0.082 ^c		
111	F13136+6223	VV 250b	13 : 15 : 30.69	+ 62 : 07 : 45.8	50	32.26	11.71 ± 0.59	11.16 ± 0.56	6.728 ± 0.337	70	45.17	2.429 ± 0.159	0.875 ± 0.059	0.273 ± 0.021			
112	F13182+3424	UGC 08387	13 : 20 : 35.37	+ 34 : 08 : 22.2	45	22.91	21.74 ± 1.00 ^c	25.82 ± 1.18 ^c	18.08 ± 0.81 ^c	65	33.09	6.356 ± 0.393 ^c	2.345 ± 0.146 ^c	0.646 ± 0.041 ^c			
113	F13188+0036	NGC 5104	13 : 21 : 23.09	+ 00 : 20 : 33.2	40	16.97	8.997 ± 0.410 ^c	13.54 ± 0.61 ^c	12.01 ± 0.53 ^c	60	25.45	5.266 ± 0.322 ^c	2.005 ± 0.124 ^c	0.658 ± 0.040 ^c			
114	F13197-1627	MCG-03-34-064	13 : 22 : 24.45	- 16 : 43 : 42.4	35	13.49	5.118 ± 0.232 ^c	4.863 ± 0.219 ^c	3.338 ± 0.146 ^c	40	15.42	1.235 ± 0.073 ^c	0.459 ± 0.028 ^c	0.120 ± 0.009 ^c			
114	F13197-1627	MCG-03-34-063	13 : 22 : 19.02	- 16 : 42 : 30.0	35	13.49	1.061 ± 0.057 ^c	1.588 ± 0.084	1.861 ± 0.095	55	21.20	1.205 ± 0.080	0.557 ± 0.038	0.210 ± 0.015 ^c			
114	F13197-1627	RAS F13197-1627	13 : 22 : 21.73	- 16 : 43 : 06.2	...	6.179 ± 0.238 ^c	6.451 ± 0.234 ^c	5.199 ± 0.174 ^c	2.440 ± 0.108 ^c	1.016 ± 0.047 ^c	0.330 ± 0.017 ^c				
115	F13229-2934	NGC 5135	13 : 25 : 44.02	- 29 : 50 : 00.4	70	20.12	21.44 ± 1.07	31.12 ± 1.56	26.86 ± 1.34	100	28.75	12.37 ± 0.81	5.058 ± 0.333	1.577 ± 0.106			
116	13342-5713	ESO 173-G015	13 : 27 : 23.79	- 57 : 29 : 21.8	70	11.30	97.67 ± 4.89	105.8 ± 5.3	71.63 ± 3.58	80	12.92	26.51 ± 1.74	9.706 ± 0.642	3.092 ± 0.194 ^c			
117	F13301-2356	IC 4280	13 : 32 : 53.40	- 24 : 12 : 25.5	45	17.41	7.647 ± 0.383	12.97 ± 0.65	12.52 ± 0.63	65	25.15	5.631 ± 0.369	2.431 ± 0.150 ^c	0.771 ± 0.048 ^c			
118	F13362+4831	KPG 388A	13 : 38 : 17.25	+ 48 : 16 : 32.9		
118	F13362+4831	KPG 388B	13 : 38 : 17.79	+ 48 : 16 : 41.6		
118	F13362+4831	NGC 5256	13 : 38 : 17.52	+ 48 : 16 : 37.2	40	23.68	8.113 ± 0.406	9.692 ± 0.485	7.069 ± 0.354	60	35.52	2.757 ± 0.182	1.070 ± 0.073	0.336 ± 0.026			
119	F13373+0105	NGC 5258	13 : 39 : 57.72	+ 00 : 49 : 53.0	45	22.65	7.311 ± 0.366	11.55 ± 0.58	11.03 ± 0.55	45	22.65	4.933 ± 0.323	1.954 ± 0.129	0.670 ± 0.039 ^c			
119	F13373+0105	NGC 5257	13 : 39 : 52.95	+ 00 : 50 : 25.9	43	21.64	6.664 ± 0.354	10.04 ± 0.50	9.350 ± 0.468	45	22.65	4.175 ± 0.273	1.649 ± 0.109	0.645 ± 0.037 ^c			
119	F13373+0105	Ap 240	13 : 39 : 55.34	+ 00 : 50 : 09.5	13.98 ± 0.50	21.58 ± 0.77	20.37 ± 0.72	90	45.29	9.434 ± 0.615	3.759 ± 0.246	1.259 ± 0.084			
120	F13428+5608	UGC 08696	13 : 44 : 42.12	+ 55 : 53 : 13.1	35	27.25	24.46 ± 1.11 ^c	22.32 ± 1.00 ^c	12.74 ± 0.56 ^c	55	42.82	4.177 ± 0.252 ^c	1.531 ± 0.094 ^c	0.427 ± 0.026 ^c			
121	F13470+3530	UGC 08739	13 : 49 : 13.94	+ 35 : 15 : 26.2	60	22.89	8.163 ± 0.409	14.94 ± 0.75	15.87 ± 0.79	80	30.52	8.243 ± 0.540	3.405 ± 0.225	1.162 ± 0.073 ^c			
122	F13478-4848	ESO 221-IG010	13 : 50 : 56.92	- 49 : 03 : 18.8	55	16.43	15.78 ± 0.79	21.63 ± 1.08	17.97 ± 0.90	75	22.40	7.116 ± 0.465	2.771 ± 0.183	0.917 ± 0.066			
123	F13497+0220	NGC 5331S	13 : 52 : 16.21	+ 02 : 06 : 05.1	17	12.32	6.750 ± 0.287 ^c	10.04 ± 0.42 ^c			
123	F13497+0220	NGC 5331N	13 : 52 : 16.43	+ 02 : 06 : 30.9	13	9.151	1.496 ± 0.061 ^c	2.538 ± 0.101 ^c			

TABLE 4—Continued

#	IRAS Name	Individual Name	Aperture Center Coordinate			PACS						SPIRE					
			RA HH:MM:SS (3)	Dec. DD:MM:SS (5)	Ang. η (6)	Phys. Ap. kpc (7)	F $_{\lambda}$ (70 μ m) Jy (8)	F $_{\lambda}$ (100 μ m) Jy (9)	F $_{\lambda}$ (160 μ m) Jy (10)	Ang. Ap. η (11)	Phys. Ap. kpc (12)	F $_{\lambda}$ (250 μ m) Jy (13)	F $_{\lambda}$ (350 μ m) Jy (14)	F $_{\lambda}$ (500 μ m) Jy (15)			
123	F1349+0220	NGC 5331	13 : 52 : 16.32	+ 02 : 06 : 18.0	50	35.20	7.484 ± 0.375	11.27 ± 0.56	10.31 ± 0.52	80	56.32	5.010 ± 0.329	1.862 ± 0.126	0.673 ± 0.044 ^c			
124	F13564+3741	NGC 5395	13 : 58 : 37.96	+ 37 : 25 : 28.1	82	22.78	4.972 ± 0.251	10.61 ± 0.53	14.71 ± 0.74	88	24.45	8.647 ± 0.562	3.819 ± 0.249	1.370 ± 0.090			
124	F13564+3741	NGC 5394	13 : 58 : 33.64	+ 37 : 27 : 12.9	37	10.28	7.904 ± 0.358 ^c	10.11 ± 0.46 ^c	7.938 ± 0.348 ^c	42	11.67	3.255 ± 0.191 ^c	0.173 ± 0.073 ^c	0.404 ± 0.023 ^c			
124	F13564+3741	Ap 84	13 : 58 : 35.80	+ 37 : 26 : 20.5	12.88 ± 0.44 ^c	20.72 ± 0.70 ^c	22.65 ± 0.81 ^c	140	38.89	11.93 ± 0.78	5.187 ± 0.338	1.856 ± 0.122			
125	F14179+4927	CGCG 247-020	14 : 19 : 43.27	+ 49 : 14 : 11.9	35	19.36	6.514 ± 0.326	7.450 ± 0.373	4.904 ± 0.246	45	24.89	1.789 ± 0.120	0.688 ± 0.048	0.175 ± 0.015			
126	F14280+3126	NGC 5653W	14 : 30 : 09.67	+ 31 : 12 : 56.7			
126	F14280+3126	NGC 5653E	14 : 30 : 10.44	+ 31 : 12 : 55.8			
126	F14280+3126	NGC 5653	14 : 30 : 10.44	+ 31 : 12 : 55.8	50	14.25	15.03 ± 0.69 ^c	22.88 ± 1.05 ^c	21.09 ± 0.95 ^c	70	19.95	8.748 ± 0.538 ^c	3.369 ± 0.207 ^c	0.994 ± 0.062 ^c			
127	F14348-1447	RAS F14378-1447 SW	14 : 37 : 38.28	- 15 : 00 : 24.2			
127	F14348-1447	RAS F14378-1447 NE	14 : 37 : 38.40	- 15 : 00 : 21.2			
127	F14348-1447	RAS F14348-1447	14 : 37 : 38.29	- 15 : 00 : 24.2	35	56.05	8.260 ± 0.373 ^c	8.385 ± 0.376 ^c	5.475 ± 0.239 ^c	45	72.06	1.967 ± 0.117 ^c	0.728 ± 0.044 ^c	0.217 ± 0.014 ^c			
128	F14378-3651	RAS F14378-3651	14 : 40 : 59.04	- 37 : 04 : 32.0	28	37.52	6.857 ± 0.305 ^c	6.661 ± 0.294 ^c	3.917 ± 0.167 ^c	30	40.20	1.376 ± 0.076 ^c	0.547 ± 0.030 ^c	0.158 ± 0.010 ^c			
129	F14423-2039	NGC 5734	14 : 45 : 09.04	- 20 : 52 : 13.2	55	17.39	10.70 ± 0.54	17.42 ± 0.87	16.78 ± 0.84	70	22.13	7.553 ± 0.492	2.869 ± 0.189	0.988 ± 0.060 ^c			
129	F14423-2039	NGC 5743	14 : 45 : 11.02	- 20 : 54 : 48.6	45	14.22	6.246 ± 0.313	9.899 ± 0.495	9.151 ± 0.458	60	18.97	4.055 ± 0.264	1.731 ± 0.105 ^c	0.593 ± 0.036 ^c			
129	F14423-2039	IRGP J144510.0-205331	14 : 45 : 10.02	- 20 : 53 : 30.9	16.94 ± 0.62	27.32 ± 1.00	25.93 ± 0.96	11.61 ± 0.56	4.630 ± 0.217 ^c	1.582 ± 0.070 ^c			
130	F14547+2449	VV 340a	14 : 57 : 00.70	+ 24 : 37 : 05.8	25	17.76	7.488 ± 0.375	12.28 ± 0.61	11.16 ± 0.56			
130	F14547+2449	VV 340b	14 : 57 : 00.32	+ 24 : 36 : 24.6	19	13.49	1.068 ± 0.054	1.873 ± 0.094	1.975 ± 0.099			
130	F14547+2449	VV 340	14 : 57 : 00.51	+ 24 : 36 : 45.2	50	35.51	8.788 ± 0.440	14.70 ± 0.74	13.89 ± 0.69	80	56.82	6.588 ± 0.432	2.617 ± 0.173	0.911 ± 0.062 ^c			
131	F14544-4255	IC 4518A	14 : 57 : 41.22	- 43 : 07 : 55.8	24	9.018	4.835 ± 0.242	5.842 ± 0.292			
131	F14544-4255	IC 4518B	14 : 57 : 45.33	- 43 : 07 : 57.0	30	11.27	4.503 ± 0.202 ^c	7.678 ± 0.341 ^c			
131	F14544-4255	IC 4518	14 : 57 : 43.27	- 43 : 07 : 56.3	65	24.42	9.106 ± 0.457	12.89 ± 0.65	12.29 ± 0.62	90	33.82	6.015 ± 0.394	2.427 ± 0.161	0.803 ± 0.056			
132	F15107+40724	CGCG 049-057	15 : 13 : 13.07	+ 07 : 13 : 32.1	50	15.44	27.65 ± 1.28 ^c	31.67 ± 1.45 ^c	21.83 ± 0.99 ^c	80	24.71	8.430 ± 0.528 ^c	3.225 ± 0.204 ^c	1.059 ± 0.068 ^c			
133	F15163+4255	VV 705 NED01	15 : 18 : 06.14	+ 42 : 44 : 45.0			
133	F15163+4255	VV 705 NED02	15 : 18 : 06.34	+ 42 : 44 : 38.1			
133	F15163+4255	VV 705	15 : 18 : 06.24	+ 42 : 44 : 41.5	35	28.71	9.027 ± 0.452	9.120 ± 0.456	5.581 ± 0.279	50	41.02	2.284 ± 0.137 ^c	0.863 ± 0.053 ^c	0.254 ± 0.016 ^c			
134	I5206-6256	ESO 099-G004	15 : 24 : 57.98	- 63 : 07 : 29.4	35	21.94	12.54 ± 0.57 ^c	14.61 ± 0.66 ^c	10.87 ± 0.47 ^c	45	28.21	3.970 ± 0.242 ^c	1.674 ± 0.109 ^c	0.505 ± 0.039 ^c			
135	F15254+3608	IRAS F15250+3608	15 : 26 : 59.42	+ 35 : 58 : 37.8	35	38.71	7.158 ± 0.324 ^c	5.787 ± 0.260 ^c	3.031 ± 0.133 ^c	40	44.23	1.034 ± 0.061 ^c	0.385 ± 0.023 ^c	0.124 ± 0.008 ^c			
136	F15276+309	NGC 5936	15 : 30 : 00.85	+ 12 : 59 : 22.1	50	15.83	10.75 ± 0.54	16.34 ± 0.82	14.97 ± 0.75	70	22.16	6.603 ± 0.431	2.715 ± 0.167 ^c	0.870 ± 0.056 ^c			
137	F15327+2340	UGC 09913	15 : 34 : 57.23	+ 23 : 30 : 11.3	70	28.78	139.2 ± 6.6 ^c	..	86.32 ± 3.99 ^c	90	37.00	30.87 ± 1.92 ^c	12.80 ± 0.80 ^c	3.865 ± 0.240 ^c			
138	F15437+0234	NGC 5990	15 : 46 : 16.41	+ 02 : 24 : 55.6	40	12.18	12.06 ± 0.60	16.81 ± 0.84	14.25 ± 0.71	60	18.27	6.071 ± 0.398	2.435 ± 0.150 ^c	0.831 ± 0.050 ^c			
139	F16030+2040	NGC 6052	16 : 05 : 12.87	+ 20 : 32 : 33.0	45	16.41	7.689 ± 0.385	10.16 ± 0.51	8.128 ± 0.407	60	21.87	3.317 ± 0.218	1.412 ± 0.088 ^c	0.483 ± 0.031 ^c			
140	F16104+5235	NGC 6090	16 : 11 : 40.84	+ 52 : 27 : 27.2	35	21.92	7.800 ± 0.352 ^c	9.269 ± 0.416 ^c	7.033 ± 0.307 ^c	55	34.45	2.666 ± 0.161 ^c	1.028 ± 0.063 ^c	0.288 ± 0.019 ^c			

TABLE 4—Continued

#	IRAS Name	Individual Name	Aperture Center Coordinate			PACS						SPIRE					
			RA HH:MM:SS (4)	Dec. DD:MM:SS (5)	Ang. α , Ap. kpc (6)	F $_{\lambda}$ (70 μ m) Jy (8)	F $_{\lambda}$ (100 μ m) Jy (9)	F $_{\lambda}$ (160 μ m) Jy (10)	F $_{\lambda}$ (350 μ m) Jy (11)	F $_{\lambda}$ (500 μ m) Jy (12)	Ang. α , Ap. kpc (13)	F $_{\lambda}$ (250 μ m) Jy (14)	F $_{\lambda}$ (350 μ m) Jy (15)				
141	F16164-0746	IRAS F16164-0746	16 : 19 : 11.75	-07 : 54 : 03.0	40	23.52	13.29 ± 0.61 ^c	15.03 ± 0.68 ^c	10.21 ± 0.45 ^c	60	35.28	3.581 ± 0.220 ^c	1.266 ± 0.080 ^c	0.407 ± 0.028 ^c			
142	F16284+0411	CGCG 052-037	16 : 30 : 56.53	+ 04 : 04 : 58.7	40	21.87	8.910 ± 0.406 ^c	12.17 ± 0.55 ^c	9.839 ± 0.435 ^c	40	21.87	3.771 ± 0.224 ^c			
142	F16284+0411	2MASX J16303264+04243	16 : 30 : 53.25	+ 04 : 04 : 23.9	20	10.94	0.241 ± 0.013 ^c	0.285 ± 0.015 ^c	0.204 ± 0.010 ^c	20	10.94	0.111 ± 0.008 ^c			
142	F16284+0411	RGP J163054.9+040441	16 : 30 : 54.89	+ 04 : 04 : 41.3	9.151 ± 0.406 ^c	12.46 ± 0.55 ^c	10.04 ± 0.44 ^c	70	38.28	3.618 ± 0.240	1.423 ± 0.096	0.492 ± 0.036			
143	I6304-6030	NGC 6156	16 : 34 : 52.55	-60 : 37 : 08.0	80	18.23	21.20 ± 1.06	32.32 ± 1.62	29.29 ± 1.47	100	22.79	12.91 ± 0.84	5.096 ± 0.334	1.678 ± 0.112			
144	F16330-6820	2MASX J16381190-6826080	16 : 38 : 11.85	-68 : 26 : 08.2	40	37.54	9.407 ± 0.429 ^c	13.21 ± 0.60 ^c	10.62 ± 0.47 ^c	55	51.62	4.374 ± 0.266 ^c	1.729 ± 0.107 ^c	0.527 ± 0.033 ^c			
144	F16330-6820	2MASX J16381338-6827170	16 : 38 : 13.43	-68 : 27 : 16.6	18	16.89	0.037 ± 0.007	0.110 ± 0.009	0.125 ± 0.008	25	23.46	0.128 ± 0.012	0.058 ± 0.008	0.024 ± 0.005			
144	F16330-6820	ESO 069-IG006	16 : 38 : 12.64	-68 : 26 : 42.3	9.444 ± 0.429 ^c	13.32 ± 0.60 ^c	10.75 ± 0.47 ^c	4.501 ± 0.266 ^c	1.788 ± 0.107 ^c	0.551 ± 0.033 ^c			
145	F16399-0937	IRAS F16399-0937	16 : 42 : 40.11	-09 : 43 : 13.7	55	32.37	9.368 ± 0.436 ^c	10.80 ± 0.50 ^c	8.302 ± 0.379 ^c	60	35.31	3.527 ± 0.218 ^c	1.333 ± 0.088 ^c	0.435 ± 0.034 ^c			
146	F16443-2915	ESO 453-G005	16 : 47 : 31.09	-29 : 21 : 21.6	35	16.36	12.19 ± 0.55 ^c	13.95 ± 0.63 ^c	10.04 ± 0.44 ^c	55	25.70	4.150 ± 0.252 ^c	1.635 ± 0.101 ^c	0.575 ± 0.035 ^c			
146	F16443-2915	2MASX J16472937-2919067	16 : 47 : 29.34	-29 : 19 : 06.8	30	14.02	1.645 ± 0.077 ^c	2.585 ± 0.117 ^c	2.569 ± 0.112 ^c	50	23.37	1.206 ± 0.074 ^c	0.539 ± 0.035 ^c	0.199 ± 0.015 ^c			
146	F16443-2915	RGP J164730.2-292014	16 : 47 : 30.21	-29 : 20 : 14.2	13.83 ± 0.56 ^c	16.54 ± 0.64 ^c	12.61 ± 0.45 ^c	5.356 ± 0.262 ^c	1.775 ± 0.107 ^c	0.773 ± 0.038 ^c			
147	F16504+0228	NGC 6240	16 : 52 : 58.90	+ 02 : 24 : 03.3	45	24.11	26.48 ± 1.22 ^c	28.03 ± 1.28 ^c	19.00 ± 0.85 ^c	80	42.86	7.026 ± 0.437 ^c	2.834 ± 0.177 ^c	0.874 ± 0.056 ^c			
148	F16516-0948	IRAS F16516-0948	16 : 54 : 23.72	-09 : 53 : 20.9	45	22.32	5.698 ± 0.286	8.243 ± 0.413	7.099 ± 0.356	55	27.28	3.353 ± 0.203 ^c	1.232 ± 0.079 ^c	0.434 ± 0.030 ^c			
149	F16577+5900	NGC 6286	16 : 58 : 31.63	+ 58 : 56 : 13.3	55	22.37	10.73 ± 0.54	19.32 ± 0.97	19.71 ± 0.99	50	20.34	9.311 ± 0.611	3.969 ± 0.239 ^c	1.307 ± 0.075 ^c			
149	F16577+5900	NGC 6285	16 : 58 : 23.99	+ 58 : 57 : 21.7	35	14.24	2.210 ± 0.100 ^c	3.206 ± 0.144 ^c	2.998 ± 0.131 ^c	40	16.27	1.435 ± 0.086 ^c	0.556 ± 0.034 ^c	0.189 ± 0.013 ^c			
149	F16577+5900	Ap 293	16 : 58 : 27.81	+ 58 : 56 : 47.5	12.94 ± 0.55 ^c	22.53 ± 0.98 ^c	22.71 ± 0.99 ^c	130	52.88	11.60 ± 0.76	4.599 ± 0.303	1.495 ± 0.101			
150	F17132+5313	IRAS F17132+5313	17 : 14 : 19.79	+ 53 : 10 : 29.0	
150	F17132+5313	IRAS F17132+5313	17 : 14 : 20.45	+ 53 : 10 : 32.1	
151	F17138-1017	RAS F17138-1017	17 : 16 : 35.68	-10 : 20 : 40.5	50	19.68	18.51 ± 0.86 ^c	21.72 ± 1.00 ^c	15.62 ± 0.70 ^c	60	23.62	5.423 ± 0.332 ^c	1.875 ± 0.117 ^c	0.531 ± 0.035 ^c			
152	F17207-0014	RAS F17207-0014	17 : 23 : 21.97	-00 : 17 : 00.7	40	35.31	38.09 ± 1.74 ^c	37.91 ± 1.72 ^c	23.07 ± 1.02 ^c	55	48.56	7.959 ± 0.485 ^c	2.907 ± 0.180 ^c	0.890 ± 0.054 ^c			
153	F17222-5953	ESO 138-G027	17 : 26 : 43.35	-59 : 55 : 55.2	35	16.00	9.930 ± 0.497	11.00 ± 0.55	8.861 ± 0.386 ^c	55	25.14	3.340 ± 0.202 ^c	1.240 ± 0.077 ^c	0.370 ± 0.025 ^c			
154	F17530+3447	UGC 11041	17 : 54 : 51.82	+ 34 : 46 : 34.2	45	16.36	7.636 ± 0.382	11.71 ± 0.59	10.97 ± 0.55	60	21.82	5.299 ± 0.322 ^c	2.103 ± 0.150 ^c	0.689 ± 0.042 ^c			
155	F17548+2401	CGCG 141-034	17 : 56 : 56.65	+ 24 : 01 : 02.0	35	15.24	8.282 ± 0.374 ^c	10.45 ± 0.47 ^c	7.845 ± 0.342 ^c	60	26.12	2.961 ± 0.183 ^c	0.998 ± 0.064 ^c	0.302 ± 0.021 ^c			
156	F17578-0400	IRAS F17578-0400	18 : 00 : 31.86	-04 : 00 : 53.4	38	12.34	33.39 ± 1.52 ^c	36.93 ± 1.67 ^c	25.04 ± 1.10 ^c	40	12.99	8.913 ± 0.529 ^c	3.443 ± 0.200 ^c	1.091 ± 0.062 ^c			
156	F17578-0400	2MASX J18003399-0401443	18 : 00 : 34.08	-04 : 01 : 43.9	25	8.121	1.889 ± 0.084 ^c	2.767 ± 0.121 ^c	2.520 ± 0.106 ^c	27	8.770	1.313 ± 0.072 ^c	0.531 ± 0.032 ^c	0.187 ± 0.012 ^c			
156	F17578-0400	2MASX J18002449-0401023	18 : 00 : 24.29	-04 : 01 : 03.8	30	9.745	2.356 ± 0.119	3.177 ± 0.160	2.596 ± 0.131 ^c	45	14.62	1.292 ± 0.080 ^c	0.575 ± 0.039 ^c	0.188 ± 0.016 ^c			
156	F17578-0400	2MASX J18003399-0401443	18 : 00 : 32.49	-04 : 01 : 13.1	65	21.11	32.34 ± 1.62	36.60 ± 1.83	24.98 ± 1.25	70	22.74	9.824 ± 0.647	3.725 ± 0.247	1.118 ± 0.077			
156	F17578-0400	IRGP J1800301-040113	18 : 00 : 28.61	-04 : 01 : 16.3	...	34.70 ± 1.62	39.78 ± 1.84	27.58 ± 1.26	11.12 ± 0.65 ^c	4.300 ± 0.250 ^c	1.306 ± 0.078 ^c				
157	18090+0130	2MASX J18113842+0131397	18 : 11 : 38.42	+ 01 : 31 : 40.3	40	24.55	7.775 ± 0.354 ^c	11.32 ± 0.51 ^c	9.853 ± 0.436 ^c	50	30.69	3.802 ± 0.229 ^c	1.451 ± 0.090 ^c	0.465 ± 0.030 ^c			
157	18090+0130	2MASX J18113342+0131427	18 : 11 : 33.41	+ 01 : 31 : 42.4	25	15.34	2.136 ± 0.095 ^c	2.865 ± 0.125 ^c	2.389 ± 0.101 ^c	40	24.55	1.208 ± 0.078 ^c	0.418 ± 0.029 ^c	0.124 ± 0.015 ^c			
157	18090+0130	IRAS 18090+0130	18 : 11 : 35.91	+ 01 : 31 : 41.3	...	9.912 ± 0.367 ^c	14.19 ± 0.53 ^c	12.24 ± 0.45 ^c	5.010 ± 0.242 ^c	1.869 ± 0.094 ^c	0.590 ± 0.033 ^c				

TABLE 4—Continued

#	IRAS Name	Individual Name	Aperture Center Coordinate			PACS						SPIRE					
			RA HH:MM:SS (4)	Dec. DD:MM:SS (5)	Ang. η (6)	Phys. Ap. kpc (7)	F $_{\lambda}$ (70 μ m) Jy (8)	F $_{\lambda}$ (100 μ m) Jy (9)	F $_{\lambda}$ (160 μ m) Jy (10)	Ang. Ap. η (11)	Phys. Ap. kpc (12)	F $_{\lambda}$ (250 μ m) Jy (13)	F $_{\lambda}$ (350 μ m) Jy (14)	F $_{\lambda}$ (500 μ m) Jy (15)			
158	F18131+6820	NGC 6621	18 : 12 : 55.39	+ 68 : 21 : 48.2	19	8.511	8.536 ± 0.366 ^c	11.77 ± 0.50 ^c	
158	F18131+6820	NGC 6621 SE	18 : 12 : 58.52	+ 68 : 21 : 29.4	9	4.032	0.273 ± 0.011 ^c	0.571 ± 0.020 ^c	
158	F18131+6820	NGC 6622	18 : 12 : 59.68	+ 68 : 21 : 15.1	9	4.032	0.110 ± 0.005 ^c	0.252 ± 0.010 ^c	
158	F18131+6820	Ap 81	18 : 12 : 57.46	+ 68 : 21 : 38.7	70	31.36	8.257 ± 0.414	12.08 ± 0.60	11.24 ± 0.56	85	38.08	5.331 ± 0.350	2.159 ± 0.143	0.661 ± 0.048	
159	F18093-5744	IC 4687	18 : 13 : 39.80	- 57 : 43 : 30.7	21	7.809	16.56 ± 0.72 ^c	19.76 ± 0.84 ^c	
159	F18093-5744	IC 4686	18 : 13 : 38.77	- 57 : 43 : 57.3	13	4.834	2.821 ± 0.115 ^c	2.559 ± 0.102 ^c	
159	F18093-5744	IC 4689	18 : 13 : 40.38	- 57 : 44 : 54.3	35	13.01	5.817 ± 0.263 ^c	7.494 ± 0.336 ^c	5.616 ± 0.245 ^c	38	14.13	2.154 ± 0.127 ^c	0.807 ± 0.047 ^c	0.252 ± 0.017 ^c	
159	F18093-5744	KTS 57	18 : 13 : 38.91	- 57 : 43 : 24.7	57	21.20	17.51 ± 0.88	20.08 ± 1.00	14.44 ± 0.72	55	20.45	5.488 ± 0.360	2.026 ± 0.135	0.585 ± 0.041	
159	F18093-5744	IRAS F18093-5744	18 : 13 : 39.56	- 57 : 44 : 00.9	90	33.47	23.87 ± 1.19	28.18 ± 1.41	20.08 ± 1.00	110	40.90	8.029 ± 0.526	2.935 ± 0.196	0.928 ± 0.065	
160	F18145+2205	CGCG 142-034	18 : 16 : 40.69	+ 22 : 06 : 46.4	35	14.12	6.075 ± 0.304	9.564 ± 0.479	8.625 ± 0.432	50	20.17	4.308 ± 0.259 ^c	1.637 ± 0.103 ^c	0.536 ± 0.033 ^c	
160	F18145+2205	CGCG 142-033	18 : 16 : 33.83	+ 22 : 06 : 38.9	25	10.08	1.842 ± 0.082 ^c	2.874 ± 0.126 ^c	2.938 ± 0.123 ^c	40	16.13	1.445 ± 0.087 ^c	0.542 ± 0.034 ^c	0.176 ± 0.013 ^c	
160	F18145+2205	RGP J1816372+220642	18 : 16 : 37.26	+ 22 : 06 : 42.6	7.918 ± 0.315 ^c	12.44 ± 0.49 ^c	11.56 ± 0.45 ^c	5.753 ± 0.273 ^c	2.229 ± 0.108 ^c	0.712 ± 0.035 ^c	
161	F18293-5413	IRAS F18293-5413	18 : 32 : 41.10	- 34 : 11 : 27.0	50	20.12	45.71 ± 2.11 ^c	59.13 ± 2.71 ^c	45.84 ± 2.07 ^c	70	28.17	17.22 ± 1.07 ^c	6.454 ± 0.400 ^c	1.987 ± 0.122 ^c	
162	F18329+5950	NGC 6670B	18 : 33 : 34.26	+ 59 : 53 : 17.9	18	10.68	5.462 ± 0.273	7.823 ± 0.391	6.439 ± 0.322	
162	F18329+5950	NGC 6670A	18 : 33 : 37.74	+ 59 : 53 : 22.8	13	7.714	4.247 ± 0.213	4.800 ± 0.240	3.101 ± 0.155	
162	F18329+5950	NGC 6670	18 : 33 : 36.00	+ 59 : 53 : 20.3	50	29.67	10.33 ± 0.52	13.92 ± 0.70	11.25 ± 0.56	60	35.60	4.664 ± 0.305	1.782 ± 0.118	0.537 ± 0.038	
163	F18341-5732	IC 4734	18 : 38 : 25.75	- 57 : 29 : 25.4	45	15.53	19.06 ± 0.88 ^c	25.41 ± 1.16 ^c	20.51 ± 0.92 ^c	75	25.89	8.450 ± 0.525 ^c	3.257 ± 0.203 ^c	1.051 ± 0.066 ^c	
164	F18425+6036	NGC 6701	18 : 43 : 12.52	+ 60 : 39 : 11.6	50	14.74	12.91 ± 0.65	19.13 ± 0.96	16.80 ± 0.84	70	20.63	7.422 ± 0.485	2.863 ± 0.188	0.945 ± 0.059 ^c	
165	F19120+7320	NGC 6786	19 : 10 : 54.01	+ 73 : 24 : 36.0	33	17.20	5.146 ± 0.231 ^c	7.238 ± 0.323 ^c	6.199 ± 0.268 ^c	45	23.45	2.685 ± 0.160 ^c	1.040 ± 0.063 ^c	0.360 ± 0.022 ^c	
165	F19120+7320	UGC 11415	19 : 11 : 04.37	+ 73 : 25 : 32.5	30	15.64	4.117 ± 0.184 ^c	4.666 ± 0.207 ^c	3.568 ± 0.153 ^c	33	17.20	1.487 ± 0.086 ^c	0.557 ± 0.034 ^c	0.219 ± 0.013 ^c	
165	F19120+7320	VV 414	19 : 10 : 59.19	+ 73 : 25 : 04.2	9.262 ± 0.296 ^c	11.90 ± 0.38	9.766 ± 0.309 ^c	90	46.91	4.003 ± 0.263	1.516 ± 0.102	0.568 ± 0.041	
166	F19151-2124	ESO 593-IG038	19 : 14 : 31.15	- 21 : 19 : 06.3	40	39.13	7.972 ± 0.363 ^c	10.62 ± 0.48 ^c	8.597 ± 0.380 ^c	50	48.92	3.371 ± 0.203 ^c	1.278 ± 0.079 ^c	0.489 ± 0.030 ^c	
167	F19297-0406	IRAS F19297-0406	19 : 32 : 22.30	- 04 : 00 : 01.1	40	64.98	7.982 ± 0.400	8.114 ± 0.406	5.121 ± 0.257	40	64.98	1.833 ± 0.121	0.766 ± 0.046 ^c	0.225 ± 0.017 ^c	
168	F19542+1110	IRAS 19542+1110	19 : 56 : 35.78	+ 11 : 19 : 04.9	30	37.83	6.720 ± 0.300 ^c	6.516 ± 0.289 ^c	3.851 ± 0.165 ^c	40	50.44	1.265 ± 0.075 ^c	0.495 ± 0.030 ^c	0.126 ± 0.009 ^c	
169	F19542-3804	ESO 339-G011	19 : 57 : 37.60	- 37 : 56 : 08.4	45	18.61	7.396 ± 0.340 ^c	10.69 ± 0.49 ^c	9.839 ± 0.440 ^c	80	33.08	4.448 ± 0.277 ^c	1.665 ± 0.108 ^c	0.591 ± 0.039 ^c	
170	F20221-2458	NGC 6907	20 : 25 : 06.58	- 24 : 48 : 32.9	80	19.04	18.35 ± 0.92	31.39 ± 1.57	31.71 ± 1.59	120	28.57	16.38 ± 1.07	6.890 ± 0.448	2.378 ± 0.155	
171	20264+2533	MCG+04-48-002	20 : 28 : 35.07	+ 25 : 44 : 00.3	40	12.33	10.36 ± 0.52	14.20 ± 0.71	10.81 ± 0.54	50	15.42	4.709 ± 0.284 ^c	1.724 ± 0.108 ^c	0.558 ± 0.038 ^c	
171	20264+2533	NGC 6921	20 : 28 : 28.90	+ 25 : 43 : 24.3	28	8.634	2.558 ± 0.114 ^c	3.510 ± 0.155 ^c	2.546 ± 0.108 ^c	40	12.33	1.009 ± 0.063 ^c	0.361 ± 0.027 ^c	0.111 ± 0.014 ^c	
171	20264+2533	IRGP J2028320+254342	20 : 28 : 31.98	+ 25 : 43 : 42.3	12.92 ± 0.53 ^c	17.71 ± 0.73 ^c	13.35 ± 0.55 ^c	...	5.719 ± 0.291 ^c	2.085 ± 0.112 ^c	0.669 ± 0.040 ^c		
172	F20304-0211	NGC 6926	20 : 33 : 06.13	- 02 : 01 : 38.9	60	24.93	8.895 ± 0.446	15.94 ± 0.80	16.62 ± 0.83	70	29.08	7.808 ± 0.509	3.102 ± 0.204	0.998 ± 0.067	
173	20351+2521	IRAS 20351+2521	20 : 37 : 17.73	+ 25 : 31 : 37.5	35	23.98	6.993 ± 0.350	9.142 ± 0.457	7.280 ± 0.364	50	34.25	3.280 ± 0.196 ^c	1.266 ± 0.077 ^c	0.347 ± 0.022 ^c	
174	F20550+1655	CGCG 448-020NW	20 : 57 : 23.65	+ 17 : 07 : 44.1	
174	F20550+1655	CGCG 448-020SEsw	20 : 57 : 24.09	+ 17 : 07 : 35.2	

TABLE 4—Continued

#	IRAS Name	Individual Name	RA HH:MM:SS (3)	Dec. DD:MM:SS (5)	Aperture Center Coordinate						PACS						SPIRE					
					Ang. _{rr} (6)	Ang. _{Ap.} kpc (7)	F _λ (70 μm) Jy (8)	F _λ (100 μm) Jy (9)	F _λ (160 μm) Jy (10)	Ang. _{rr} Ap. kpc (11)	Phys. Ap. kpc (12)	F _λ (250 μm) Jy (13)	F _λ (350 μm) Jy (14)	F _λ (500 μm) Jy (15)								
174	F20550+1655	CGCG 448-020SEne	20 : 57 : 24.38	+ 17 : 07 : 39.2	...	29.09	11.79 ± 0.59	10.68 ± 0.53	6.199 ± 0.310	...	50	36.36	2.128 ± 0.140	0.810 ± 0.051 ^c	0.242 ± 0.018 ^c	
174	F20550+1655	CGCG 448-020	20 : 57 : 24.01	+ 17 : 07 : 41.6	40	25.80	12.64 ± 0.56 ^c	10.41 ± 0.46 ^c	5.749 ± 0.246 ^c	55	47.30	1.840 ± 0.111 ^c	0.631 ± 0.039 ^c	0.182 ± 0.013 ^c	
175	F20551+4250	ESO 286-IG019	20 : 58 : 26.78	- 42 : 39 : 00.5	30	16.67	9.498 ± 0.436 ^c	12.80 ± 0.58 ^c	10.42 ± 0.47 ^c	55	20.37	3.994 ± 0.242 ^c	1.470 ± 0.091 ^c	0.404 ± 0.026 ^c	
176	F21008-4347	ESO 286-G035	21 : 04 : 11.11	- 43 : 35 : 36.1	35	27.35	8.068 ± 0.365 ^c	8.705 ± 0.391 ^c	5.753 ± 0.251 ^c	45	35.17	2.000 ± 0.122 ^c	0.749 ± 0.049 ^c	0.195 ± 0.015 ^c	
177	21101+5810	IRAS 21101+5810	21 : 11 : 29.28	+ 58 : 23 : 07.9		
178	F21330-3846	ESO 343-IG 013 NED01	21 : 36 : 10.53	- 38 : 32 : 42.8	...	18.02	6.422 ± 0.322	8.031 ± 0.402	6.587 ± 0.330	55	22.03	2.721 ± 0.179	1.058 ± 0.072	0.354 ± 0.024 ^c	
178	F21330-3846	ESO 343-IG013	21 : 36 : 10.93	- 38 : 32 : 33.0	45	13.65	18.83 ± 0.94	...	19.68 ± 0.99	75	25.60	9.224 ± 0.571 ^c	3.549 ± 0.220 ^c	1.078 ± 0.068 ^c	
178	F21330-3846	ESO 343-IG013	21 : 36 : 10.73	- 38 : 32 : 37.8	45	18.11	7.027 ± 0.352	11.89 ± 0.59	11.53 ± 0.58	70	25.35	5.478 ± 0.358	2.083 ± 0.138	0.773 ± 0.050 ^c	
179	F21453-3511	NGC 7130	21 : 48 : 19.54	- 34 : 57 : 04.7	50	15.82	24.34 ± 1.22	37.57 ± 1.88	34.58 ± 1.73	90	21.90	14.97 ± 0.98	5.763 ± 0.377	1.892 ± 0.125	
180	F22118-2742	ESO 467-G027	22 : 14 : 39.97	- 27 : 27 : 50.3	35	20.30	7.429 ± 0.339 ^c	10.36 ± 0.47 ^c	9.241 ± 0.409 ^c	60	30.46	3.991 ± 0.243 ^c	1.658 ± 0.103 ^c	0.488 ± 0.031 ^c	
181	F22132-3705	IC 5179	22 : 16 : 09.13	- 36 : 50 : 37.2	65	15.20	10.70 ± 0.48 ^c	14.70 ± 0.66 ^c	12.31 ± 0.54 ^c	45	19.55	5.086 ± 0.305 ^c	2.031 ± 0.121 ^c	0.611 ± 0.036 ^c	
182	F22287-1917	ESO 602-G025	22 : 31 : 25.48	- 19 : 02 : 04.0	40	29.80	8.041 ± 0.363 ^c	7.847 ± 0.352 ^c	4.975 ± 0.217 ^c	45	38.31	1.799 ± 0.107 ^c	0.700 ± 0.042 ^c	0.256 ± 0.016 ^c	
183	F22389+3359	UGC 12150	22 : 41 : 12.21	+ 34 : 14 : 56.8	35	43.95	5.642 ± 0.252 ^c	4.975 ± 0.221 ^c	2.715 ± 0.116 ^c	35	51.28	0.841 ± 0.049 ^c	0.309 ± 0.018 ^c	0.082 ± 0.006 ^c	
184	F22467-4906	ESO 239-IG002	22 : 49 : 39.84	- 48 : 50 : 58.3	35	10.88	33.69 ± 1.43 ^c	40.18 ± 1.65 ^c	29.83 ± 1.16 ^c	90	29.67	11.16 ± 0.73	4.216 ± 0.278	1.266 ± 0.087	
185	F22491-1808	IRAS F22491-1808	22 : 51 : 49.35	- 17 : 52 : 24.9	30	15.49	30.97 ± 1.43 ^c	35.76 ± 1.64 ^c	25.40 ± 1.14 ^c	52	17.14	9.561 ± 0.575 ^c	3.554 ± 0.216 ^c	1.084 ± 0.063 ^c	
186	F23007+40836	NGC 7469	23 : 03 : 15.64	+ 08 : 52 : 25.5	47	10.88	2.719 ± 0.137 ^c	4.421 ± 0.221	4.434 ± 0.222	35	11.54	1.997 ± 0.132	0.771 ± 0.053	0.235 ± 0.018	
186	F23007+40836	IC 5283	23 : 03 : 18.04	+ 08 : 53 : 36.5	33	90	14.62	35.64 ± 2.32	13.74 ± 0.90	4.226 ± 0.276	
187	F23024+1916	CGCG 453-062	23 : 04 : 56.55	+ 19 : 33 : 07.1	40	21.78	9.269 ± 0.422 ^c	11.42 ± 0.52 ^c	9.233 ± 0.409 ^c	60	30.17	4.418 ± 0.272 ^c	1.749 ± 0.111 ^c	0.609 ± 0.038 ^c	
188	F23128-5919	ESO 148-IG002	23 : 15 : 46.75	- 59 : 03 : 15.8	35	10.32	11.97 ± 0.54 ^c	11.14 ± 0.50 ^c	6.028 ± 0.267 ^c	40	35.37	1.855 ± 0.110 ^c	0.655 ± 0.039 ^c	0.186 ± 0.013 ^c	
189	F23135+2517	IC 5298	23 : 16 : 00.67	+ 25 : 33 : 24.3	40	21.86	9.046 ± 0.466	13.59 ± 0.68	13.07 ± 0.65	90	30.15	6.716 ± 0.440	2.813 ± 0.185	0.917 ± 0.063	
190	F23133-4251	NGC 7552	23 : 16 : 10.81	- 42 : 35 : 05.5	90	10.12	9.296 ± 0.466	11.63 ± 5.8	88.01 ± 4.40	130	11.73	0.351 ± 0.024 ^c	0.131 ± 0.012 ^c	0.056 ± 0.010 ^c	
191	F23157-40618	NGC 7591	23 : 18 : 16.25	+ 06 : 35 : 09.1	65	7.705	0.746 ± 0.035 ^c	0.897 ± 0.042 ^c	0.799 ± 0.035 ^c	35	41.57	3.113 ± 0.205	1.254 ± 0.084	0.406 ± 0.025 ^c	
191	F23157-40618	NGC 7591	23 : 18 : 13.52	+ 06 : 33 : 26.5	23	10.04 ± 0.47 ^c	14.49 ± 0.68 ^c	13.86 ± 0.65 ^c		
192	F23157-0441	NGC 7592E	23 : 18 : 22.60	- 04 : 24 : 58.0		
192	F23157-0441	NGC 7592W	23 : 18 : 21.78	- 04 : 24 : 57.0	40	19.59	8.700 ± 0.435	10.44 ± 0.52	7.602 ± 0.380	55	26.93	2.916 ± 0.192	1.179 ± 0.073 ^c	0.355 ± 0.024 ^c	
193	F23180-6929	ESO 077-IG 014 NED02	23 : 21 : 05.45	- 69 : 12 : 47.3	11	9.146	5.688 ± 0.225 ^c	7.545 ± 0.284 ^c		
193	F23180-6929	ESO 077-IG 014 NED01	23 : 21 : 03.47	- 69 : 13 : 02.2	9	7.483	2.067 ± 0.078 ^c	2.828 ± 0.099 ^c		
193	F23180-6929	ESO 077-IG014	23 : 21 : 04.59	- 69 : 12 : 54.1	40	33.26	6.716 ± 0.337	9.141 ± 0.458	7.056 ± 0.353	50	41.57	3.113 ± 0.205	1.254 ± 0.084	0.406 ± 0.025 ^c	

TABLE 4—Continued

#	IRAS Name	Individual Name	Aperture Center Coordinate			PACS			SPIRE					
			RA HH:MM:SS (4)	Dec. DD:MM:SS (5)	Ang. α (6)	Phys. Ap. kpc (7)	F $_{\lambda}$ (70 μ m) Jy (8)	F $_{\lambda}$ (100 μ m) Jy (9)	F $_{\lambda}$ (160 μ m) Jy (10)	Ang. Ap. α (11)	Phys. Ap. kpc (12)	F $_{\lambda}$ (250 μ m) Jy (13)	F $_{\lambda}$ (350 μ m) Jy (14)	F $_{\lambda}$ (500 μ m) Jy (15)
194	F22254+0830	NGC 7674	23 : 27 : 56.71	+ 08 : 46 : 44.3	28	16.21	5.489 ± 0.244 ^c	7.502 ± 0.331 ^c
194	F22254+0830	NGC 7674A	23 : 27 : 58.77	+ 08 : 46 : 57.9	11	6.368	0.718 ± 0.029 ^c	1.036 ± 0.039 ^c
194	F22254+0830	ARP 182	23 : 27 : 57.73	+ 08 : 46 : 51.0	70	40.52	5.895 ± 0.295	8.328 ± 0.418	7.663 ± 0.384	75	43.42	3.566 ± 0.232	1.424 ± 0.094	0.445 ± 0.031
195	23262+0314	NGC 7679	23 : 28 : 46.62	+ 03 : 30 : 41.4	40	13.83	9.077 ± 0.413 ^c	11.74 ± 0.53 ^c	8.976 ± 0.397 ^c	70	24.20	3.367 ± 0.207 ^c	1.287 ± 0.079 ^c	0.496 ± 0.031 ^c
195	23262+0314 ^a	NGC 7682	23 : 29 : 03.91	+ 03 : 31 : 59.9	45	15.56	0.409 ± 0.028	0.770 ± 0.043	0.971 ± 0.051	70	24.20	0.746 ± 0.051	0.384 ± 0.029	0.151 ± 0.014
196	F23365+3604	IRAS F23365+3604	23 : 39 : 01.32	+ 36 : 21 : 08.2	35	42.98	8.070 ± 0.365 ^c	8.315 ± 0.373 ^c	5.222 ± 0.228 ^c	45	55.26	1.901 ± 0.113 ^c	0.707 ± 0.042 ^c	0.195 ± 0.012 ^c
197	F23394+0353	MCG-01-60-022	23 : 42 : 00.91	- 03 : 36 : 54.4	35	15.68	6.181 ± 0.279 ^c	8.292 ± 0.372 ^c	6.863 ± 0.299 ^c	70	31.36	2.932 ± 0.180 ^c	1.226 ± 0.076 ^c	0.402 ± 0.026 ^c
197	F23394+0353 ^a	MCG-01-60-021	23 : 41 : 47.33	- 03 : 40 : 01.7	37	16.57	0.399 ± 0.025	0.978 ± 0.051	1.577 ± 0.080	38	17.02	1.074 ± 0.070	0.457 ± 0.030	0.177 ± 0.010 ^c
197	F23394+0353 ^a	MRK 0933	23 : 41 : 43.69	- 03 : 39 : 26.5	25	11.20	0.323 ± 0.018 ^c	0.444 ± 0.022 ^c	0.411 ± 0.019 ^c	32	14.33	0.184 ± 0.012 ^c	0.069 ± 0.006 ^c	0.023 ± 0.004 ^c
197	F23394+0353	MCG-01-60-021/MRK 0933	23 : 41 : 46.04	- 03 : 39 : 42.3	70	31.36	1.328 ± 0.087	0.555 ± 0.038	0.178 ± 0.014
198	23336+5257	IRAS 23336+5257	23 : 46 : 05.44	+ 53 : 14 : 01.7	30	20.26	6.576 ± 0.294 ^c	7.540 ± 0.335 ^c	5.213 ± 0.223 ^c	40	27.01	1.872 ± 0.112 ^c	0.684 ± 0.043 ^c	0.243 ± 0.017 ^c
199	F23444+2911	NGC 7752	23 : 47 : 04.84	+ 29 : 29 : 00.5	80	27.58	4.144 ± 0.211	8.625 ± 0.434	11.11 ± 0.56	90	31.02	6.964 ± 0.454 ^c	3.220 ± 0.211	1.102 ± 0.073
199	F23444+2911	NGC 7753	23 : 46 : 58.62	+ 29 : 27 : 32.0	35	12.06	3.468 ± 0.174	4.891 ± 0.245	3.943 ± 0.198	45	15.51	1.898 ± 0.113 ^c	0.717 ± 0.044 ^c	0.240 ± 0.015 ^c
199	F23444+2911	Ap 86	23 : 47 : 01.73	+ 29 : 28 : 16.2	...	7.612 ± 0.274	13.52 ± 0.50	15.05 ± 0.59	150	51.71	0.838 ± 0.524	3.524 ± 0.233	1.157 ± 0.080	
200	F23488+1949	NGC 7769	23 : 51 : 03.91	+ 20 : 09 : 01.7	55	15.60	5.017 ± 0.329 ^b	1.878 ± 0.128 ^b	0.703 ± 0.044 ^{b,c}
200	F23488+1949	NGC 7771	23 : 51 : 24.80	+ 20 : 06 : 42.2	47	13.33	24.12 ± 1.21	38.05 ± 1.95	36.67 ± 1.83	45	12.76	16.35 ± 1.07	6.181 ± 0.407	...
200	F23488+1949	NGC 7770	23 : 51 : 22.55	+ 20 : 05 : 49.2	30	8.508	3.493 ± 0.179	4.230 ± 0.215	3.451 ± 0.177	23	6.523	1.461 ± 0.077 ^c	0.500 ± 0.027 ^c	...
200	F23488+1949	KTG 82	23 : 51 : 23.67	+ 20 : 06 : 15.6	95	26.94	28.23 ± 1.41	43.77 ± 2.19	41.47 ± 2.07	100	28.36	18.97 ± 1.24	7.501 ± 0.493	2.366 ± 0.157
201	F23488+2018	MRK 0331	23 : 51 : 26.77	+ 20 : 35 : 10.5	40	14.31	21.05 ± 0.96 ^c	23.93 ± 1.08 ^c	17.03 ± 0.75 ^c	65	23.26	6.145 ± 0.375 ^c	2.282 ± 0.139 ^c	0.729 ± 0.044 ^c
201	F23488+2018	UGC 12812	23 : 51 : 18.69	+ 20 : 34 : 40.4	33	0.258 ± 0.022	0.387 ± 0.025	0.438 ± 0.026	45	16.10	0.253 ± 0.019	0.128 ± 0.011	0.061 ± 0.006 ^c	
201	F23488+2018	KPG 593	23 : 51 : 22.73	+ 20 : 34 : 55.4	...	21.31 ± 0.96 ^c	24.32 ± 1.08 ^c	17.46 ± 0.75 ^c	6.398 ± 0.375 ^c	2.410 ± 0.140 ^c	0.790 ± 0.044 ^c	

NOTE.—We present the table of monochromatic flux density in units of Jansky for each of the three PACS and three SPIRE broadband filters. These are the component fluxes measurable for each system, with the total system flux from Table 3 included for completeness on the last line for each system. For total fluxes that do not have an aperture size listed, the totals were calculated as the sum of the components. Likewise the RA and dec. for these systems represent the midpoint between the companion galaxies. The column descriptions are (1) the row reference number, which corresponds to the same indices used in Tables 1–3, (2) The IRAS name of the galaxy, ordered by ascending RA, Galaxies with the “F” prefix originate from the *IRAS Faint Source Catalog*, and galaxies with no ‘F’ prefix are from the Point Source Catalog. (3) The individual galaxy name of that component. Galaxies prefixed by IRGP (infrared galaxy pair) are defined in the companion *Spitzer-GOALS* paper by Mazzarella et al. (2017). Columns (4) – (5) are the coordinates of the aperture centers used. These are the same 8 μ m coordinates adopted in Mazzarella et al. (2017). Columns (6) – (7) are the aperture radii used for PACS photometry, in arcsec and kpc respectively. Columns (8) – (10) are the fluxes from the PACS instrument in units of Jy. Note that the four galaxies which lack 100 μ m measurements are IRAS F02401+0013 (NGC 1068), IRAS F09320+6134 (UGC 05101), IRAS F15327+2340 (Arp 220), and IRAS F21453+3511 (NGC 7130). Galaxy components that do not have flux measurements are too close to a companion galaxy to be resolved by PACS. Columns (11) – (15) are the fluxes from the PACS instrument in units of Jy. Galaxy components that do not have flux measurements are too close to a companion galaxy to be resolved by SPIRE.

^aThese are very widely separated galaxy pairs that required two *Herschel* PACS observations.

^bThis galaxy is part of a triple system, but is only visible in the SPIRE images. The total flux for this system does *not* include this galaxy.

^cThese fluxes have an aperture correction factor applied.

6.3. Distribution of *Herschel* Fluxes

In Figure 5 we show the distribution of fluxes from our *Herschel* program in each of the three PACS and SPIRE photometer bands. The histogram x -axis range and binning for each band was selected in order to meaningfully show the data. The fluxes shown here are all 1657 measured fluxes, comprising both component and total fluxes, and do not include total system fluxes that are the sum of the component fluxes. The x -axis of each panel is shown in units of $\log(\text{Jy})$ to encompass the wide dynamic range of fluxes measured within the data.

As expected the fluxes are generally higher in the three PACS bands, while they are lower in the SPIRE bands due to the Rayleigh-Jeans tail of the galaxy's SED. The number of measured fluxes and bin sizes are indicated for each band, as well as the minimum and maximum fluxes. The galaxies with the highest fluxes are all nearby (IRAS F02401–0013/NGC 1068, IRAS F03316–3618/NGC 1365, and IRAS F06107+7822/NGC 2146) and tend to be quite extended in the *Herschel* maps, with the exception of NGC 2146 which appears to be more concentrated than the other two in the PACS 70 μm and 100 μm channels. On the other hand the faintest measured fluxes in the PACS bands are well within the “faint” flux regime for PACS data reduction (see §4.1).

7. Discussion

7.1. Comparison of PACS Fluxes to Previous Missions

One important check is to compare our new PACS 100 μm fluxes to the legacy *IRAS* 100 μm fluxes published in Sanders et al. (2003), since the central wavelengths of both instruments are the same. In Figure 6 we show the filter transmission curves for PACS and *IRAS* in blue and red respectively. Before comparing the fluxes measured from each telescope, several constraints must be used to ensure a meaningful comparison. Importantly, we only selected objects that either appear as single galaxies in the PACS 100 μm maps, or have component galaxies close enough such that it is only marginally resolved (or not at all) by PACS. We note that the *IRAS* 100 μm channel has a FWHM beamsize of $\sim 4'$, which is significantly larger than the PACS 100 μm beamsize of $6''.8$, therefore any unresolved system in PACS would certainly appear unresolved to *IRAS*. Second, we also applied an aperture

correction for point source objects in the PACS 100 μm maps, however we did not apply a color correction to any of our fluxes (see §7.3.1). The latter point would be needed to stay in accordance with how Sanders et al. (2003) measured the *IRAS* RBGS fluxes (see also Soifer et al. 1989), to ensure as accurate of a comparison as possible¹³. Importantly, these objects span the entire range of 100 μm fluxes within the GOALS sample, and represent the entire spectrum of source morphology from point source to very extended objects.

In the upper panel of Figure 7 we plot the 100 μm PACS/*IRAS* flux ratio as a function of the *IRAS* 100 μm flux for 128 GOALS objects satisfying our criteria (corresponding to 64% of our sample). The red line represents the unweighted average of the ratio which is 1.012, with dashed lines representing the $1-\sigma$ scatter of 0.09. On the other hand the median of the PACS/*IRAS* ratio is 1.006. Additionally we see no variation in the flux ratio except for fluxes above ~ 100 Jy, where our PACS fluxes are slightly higher. The *IRAS* names of these six galaxies are F03316–3618, F06107+7822, F10257–4339, F11257+5850, 13242–5713, and F23133–4251. Of these six sources the two with the highest PACS/*IRAS* ratios, F03316–3618 (NGC 1365) and F06107+7822 (NGC 2146), are large galaxies with optical sizes of $11''.2 \times 6''.2$ and $6''.0 \times 3''.4$. Their fluxes could be underestimated by *IRAS* since they were computed assuming point source photometry, however once we exclude these two systems, there doesn't appear to be any PACS excess left in the bright sources. Overall, there is a broad agreement in fluxes between our *Herschel* data and the *IRAS* data, to within measurement errors ($\sim 5\text{--}10\%$ for PACS).

Additionally we also compared the PACS 70 μm fluxes to the *IRAS* 60 μm fluxes, however because of the difference in wavelength, we first had to interpolate the *IRAS* 60 μm measurement to 70 μm . To do this, we first estimated the power law index to the nearest whole number on the short-wavelength side of the SED bump using the *IRAS* 60 μm and PACS 70 μm fluxes¹⁴. To interpolate the *IRAS* 60 μm flux to 70 μm , we divided the *IRAS* 60 μm fluxes by multiplicative factors corresponding to each power law index found in Table 2 of the *Herschel* technical note PICC-ME-TN-038. These factors were calculated by

¹³The *IRAS* data reduction pipeline also assumes a power law spectral index of -1 , which is the same as PACS and SPIRE.

¹⁴We did not use the *IRAS* 100 μm flux as that is right on the peak of the SED, which would systematically underestimate the power law index.

the PACS team to convert PACS fluxes to other key wavelengths and vice versa based on SED shape. We then plotted the ratio of the PACS 70 μm flux to the interpolated *IRAS* 70 μm flux as a function of the *IRAS* flux, shown in the bottom panel of Figure 7. The average flux ratio represented by the red line is 1.001 with a 1- σ scatter of 0.04 (dashed lines), and the median ratio is 1.00. The agreement between the PACS and *IRAS* data in this case is exquisite, with an even tighter relation than the 100 μm comparison throughout the entire flux range.

Another comparison is to perform a similar analysis using GOALS data from the *Spitzer* MIPS instrument at 70 and 160 μm (Mazzarella et al. 2017, in prep). Unfortunately, many of the images from that program suffer from saturation and other image quality issues that make it impossible to draw a meaningful comparison. As a result we have agreed that the PACS 70 and 160 μm data will completely supersede the corresponding MIPS data.

The results here are also similar to the analysis done in the *Herschel* technical note SAP-PACS-MS-0718-11, where extended source fluxes were compared between PACS to *Spitzer*-MIPS and *IRAS*. Although they found an average PACS/*IRAS* 100 μm flux ratio of 1.32, their dispersion in the flux ratio is very similar to our results in Figure 7. We note that their analysis was done on HIPE 6, where the PACS responsivity was not well understood resulting in much higher flux ratios than our result.

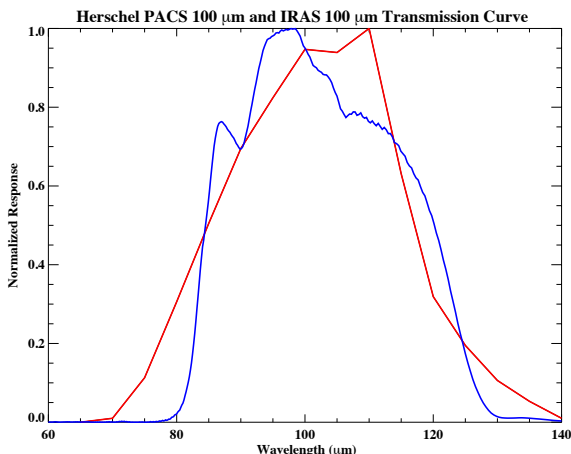


Fig. 6.— The normalized transmission curves of the 100 μm band passes for *Herschel*-PACS in blue and *IRAS* in red.

7.2. Comparison of SPIRE Fluxes Measured From Different Calibration Versions

To check the consistency of our SPIRE fluxes we compared the measured fluxes of our SPIRE data reduced using three different SPIRE calibrations: SPIRECAL_10_1, SPIRECAL_13_1, and the latest version SPIRECAL_14_2. In Figure 8 we show six histograms of the fractional percentage change in flux between each calibration version for each of the bands. In order to facilitate as direct of a comparison as possible, we use the uncorrected fluxes computed directly by the annularSkyAperturePhotometry task in HIPE, which are not aperture or color corrected. The histograms show a general trend towards longer wavelengths, a larger variance in the percent change in flux. This is again due to the long wavelength Rayleigh-Jeans tail of the galaxy’s SED, where the fainter fluxes are affected more by instrument uncertainties.

In the histogram comparing SPIRECAL_10_1 and SPIRECAL_13_1 (Fig. 8, first column), the general trend is an increase in the measured flux by an unweighted average of approximately 1.45%, 0.91%, and 1.19% of the SPIRECAL_13_1 flux, for the 250 μm , 350 μm , and 500 μm channels. The shape of the histogram distribution is very close to Gaussian in each case, however the 250 μm channel shows a slight positive skewness. The main updates in the calibration and data reduction pipeline are improved absolute flux calibrations of Neptune, and a better algorithm in de-striping the data and removal of image artifacts.

In the second column of Figure 8 we show the histogram of measured fluxes between SPIRECAL_13_1, and the latest version SPIRECAL_14_2. The only change was an update to the absolute flux calibration of the instrument, which resulted in an even smaller change in the average flux: 0.24%, -0.19%, and 0.25% for the 250 μm , 350 μm , and 500 μm channels respectively. SPIRE maps reduced using the two previous calibration versions are available upon request.

7.3. Caveats

In this section we detail several cautionary notes on using the data presented in this paper.

7.3.1. Color Corrections

By convention both of the PACS and SPIRE data reduction packages consider a flux calibration of the form $\nu F_\nu = \text{constant}$ (i.e. a spectral index of -1).

Since the *Herschel* photometry for the GOALS sample covers a wide range of wavelengths, and therefore different parts of the galaxy’s SED, the color correction factor changes as a function of wavelength, as well as weaker dependence on infrared luminosity (due to a change in the dust temperature). This is because the effective beam area of each instrument changes slightly for different spectral indices. For PACS the color correction factors are listed on the NHSC website¹⁵, and are applied to the fluxes by *dividing* the factor for the appropriate power law exponent. The SPIRE color correction factors are listed in the online SPIRE data reduction guide¹⁶ in Table 6.16 and are to be *multiplied*.

For this paper, we have decided to forego applying a color correction for both PACS and SPIRE fluxes. This would otherwise require a detailed analysis involving a multi-component SED fit for each galaxy to derive the spectral slope at each observed *Herschel* band, which is outside the current scope of this paper. This decision was agreed upon for both the *Herschel* and *Spitzer* (Mazzarella et al. 2017) data for the GOALS sample. Flux changes due to color corrections for PACS bands are up to $\sim 3\%$, and for SPIRE bands up to $\sim 6\%$ for extended sources, which is less than or equal to the absolute calibration uncertainty of both instruments. However we note for point sources, the SPIRE color correction can be higher, which we estimate to be $\sim 15\%$ for a spectral index of $\alpha = 4$. If a photometric precision of within a few percent is desired, we strongly recommend users of the *Herschel*-GOALS data to include color corrections to the aperture photometry presented in this paper.

7.3.2. PACS Saturation Limits

Since galaxies within GOALS sample are very bright in the far-infrared, there is a small chance that some of our images exhibit saturation issues in a few of our *Herschel* maps. For the PACS photometer there are two types of saturations. Hard saturation occurs when the signal after the readout electronics are outside the dynamic range of the analog-to-digital converter. On the other hand soft saturation arises from saturation of the readout electronics itself. Taking into account both effects, the point source saturation limits are 220 Jy,

¹⁵https://nhscsci.ipac.caltech.edu/pacs/docs/PACS_photometer_colorcorrectionfactors.txt

¹⁶http://hercshel.esac.esa.int/hcss-doc-14.0/print/spire_drg/spire_drg.pdf

510 Jy, and 1125 Jy for the 70 μm , 100 μm , and 160 μm passbands respectively.

Fortunately for our sample, the latter two passbands have saturation limits well above our maximum measured fluxes of 248 Jy and 301 Jy for the 100 μm and 160 μm channels. For the 70 μm channel, the nearby galaxy F02401–0013 has a total measured flux of 290 Jy which is above the saturation limit, and F06107+7822 which has a flux of 205 Jy and is close to the saturation limit. However both appear very extended at 70 μm , and in checking the saturation masks in the time-ordered data cubes we found no significant number of pixels were masked due to saturation.

7.3.3. Correlated Noise in PACS Data

Nine of our PACS maps exhibit residual correlated noise resembling low-level ripples in both the scan and cross-scan directions for only the blue camera (70 μm and 100 μm). Of these maps three of them only have this effect on the edges of the map, and do not affect the photometry or map quality. Unfortunately for the other six maps the current processing techniques in Jscanam, Unimap, and MADMap fail to remove it. One example of this is the 100 μm map of F03316–3618. However we emphasize that these are very low-level effects, and do not significantly affect the quality of the photometry¹⁷, which we estimate to be on the few percent level. This was calculated by first placing ten random apertures on empty sky on each map, then measuring the standard deviation in the flux per pixel on the affected maps. This is then multiplied by the number of pixels within the photometry aperture.

8. Summary

In this paper we have presented broad band *Herschel* imaging for the entire GOALS sample in Figure 3. Total system fluxes, and component fluxes (where possible) are also computed in all six *Herschel* bands in Tables 3 and 4 respectively. Particular care was taken in producing archival quality atlas maps using the best data reduction codes and algorithms available at the time. The data presented here are thus far the highest resolution, most sensitive and comprehensive far-infrared imaging survey of the nearest luminous infrared galaxies. For many of these objects, this paper presents the first imaging data and reliable photometry

¹⁷These image artifacts are taken into account when calculating the uncertainty in flux.

at wavelengths beyond $\sim 200 \mu\text{m}$ in the submillimeter regime.

1) All 201 GOALS objects were detected in all three *Herschel* PACS (70, 100, and 160 μm) and all three SPIRE (250, 350, 500 μm) bands. The FOV of the PACS and SPIRE images are sufficient and sensitive enough to detect the full extent of the far-infrared emission for even the widest pair separations. Only two GOALS systems have full SPIRE coverage but lack PACS coverage of a third distant component (NGC 2385 in F07256+3355, and NGC 7769 in F23488+1949). In addition, four galaxies observed outside of our *Herschel* program lack 100 μm data since they were not observed by those programs.

2) The image quality of the data are superb and were cleaned using the most up to date reduction routines and calibration files from the *Herschel* Science Center. None of the images suffer from any saturation effects, major striping, or other image quality issues that may arise from scan-based observations. Aperture corrections were applied only to point sources, while no color corrections were applied to any objects. Furthermore the SPIRE 350 μm and 500 μm maps were zero-point corrected using data from the *Planck* observations.

3) The resolution is sufficient to resolve individual components of many pairs and interacting/merging systems in our sample, particularly at the shorter wavelengths where the PACS 70 μm FWHM band has a beamsize of 5''.6. On the other hand wider pairs can still be resolved even at the longer wavelength SPIRE bands.

4) Comparing our PACS 70 and 100 μm fluxes to the legacy *IRAS* 60 and 100 μm measurements respectively, we found an excellent agreement (to within error) across our flux range as well as object morphologies ranging from point sources to extended systems.

5) The PACS 70 μm and 160 μm data within this paper supersede the reported fluxes and maps from the MIPS instrument on *Spitzer* (see Mazzarella et al. 2017, in prep.) due to the better sensitivity, resolution, and lack of image artifacts in the *Herschel* data.

In conjunction with datasets from other infrared telescopes (i. e. *Spitzer*, WISE), the *Herschel* data from this paper will allow us for the first time to construct accurate spectral energy distributions in the infrared ($\sim 3\text{--}500 \mu\text{m}$) for the entire GOALS sample, which will be presented in several forthcoming papers. The FITS files for the image mosaics constructed and pre-

sented in this atlas are being made available in the Infrared Science Archive (IRSA)¹⁸. Metadata for the images are also being folded into the NASA/IPAC Extragalactic Database (NED)¹⁹ to simplify searches in context with other data in NED, including links to the FITS files at IRSA.

9. Acknowledgments

J. Chu gratefully acknowledges Laurie Chu for proofreading the manuscript, and Thomas Shimizu for discussions on reducing the *Herschel* data. D.S. acknowledges the hospitality of the Aspen Center for Physics, which is supported by the National Science Foundation Grant No. PHY-1066293. D.S. and K.L. also acknowledge the Distinguished Visitor Program at the Research School for Astronomy and Astrophysics, Australian National University for their generous support while they were in residence at the Mount Stromlo Observatory, Weston Creek, NSW. J.B., J.C., K.L. and D.S. gratefully acknowledge funding support from NASA grant NNX11AB02G. G.C.P. was supported by a FONDECYT Postdoctoral Fellowship (No. 3150361). Support for this research was provided by NASA through a GO Cycle 1 award issued by JPL/Caltech. We thank the Observer Support group of the NASA *Herschel* Science Center for patiently handling revisions and refinements of our AORs before execution of the observations, and for their expert assistance in reducing the data. This paper has used data from the *Planck* mission, which is a project of the European Space Agency in cooperation with the scientific community. ESA led the project, developed the satellite, integrated the payload into it, and launched and operated the satellite. This research has made extensive use of the NASA/IPAC Extragalactic Database (NED) which is operated by the Jet Propulsion Laboratory, California Institute of Technology, under contract with the National Aeronautics and Space Administration. We thank the anonymous referee whose comments helped us further improve our manuscript.

Facilities: *Herschel* (PACS), *Herschel* (SPIRE), *Planck* (HFI).

¹⁸<http://irsa.ipac.caltech.edu/data/Herschel/GOALS/>

¹⁹<http://ned.ipac.caltech.edu/>

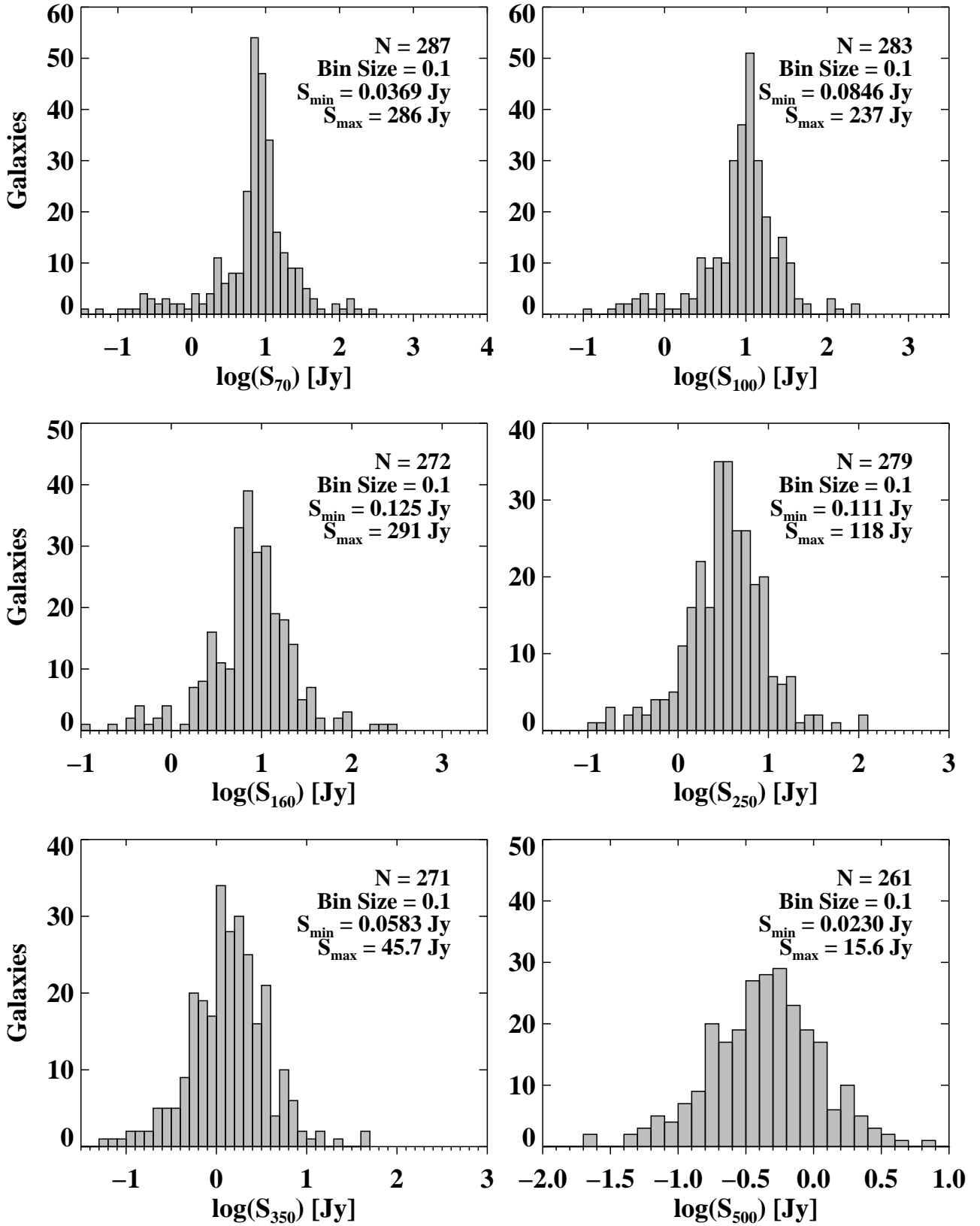


Fig. 5.— Histogram plot of the *Herschel* PACS and SPIRE fluxes from our sample. The histogram range for each band was fine tuned in order to meaningfully show the data. The fluxes shown here are all the actual measured fluxes, consisting of component and total fluxes. The x -axis of each panel is shown in units of $\log(\text{Jy})$ to encompass the wide dynamic range of fluxes measured within the data.

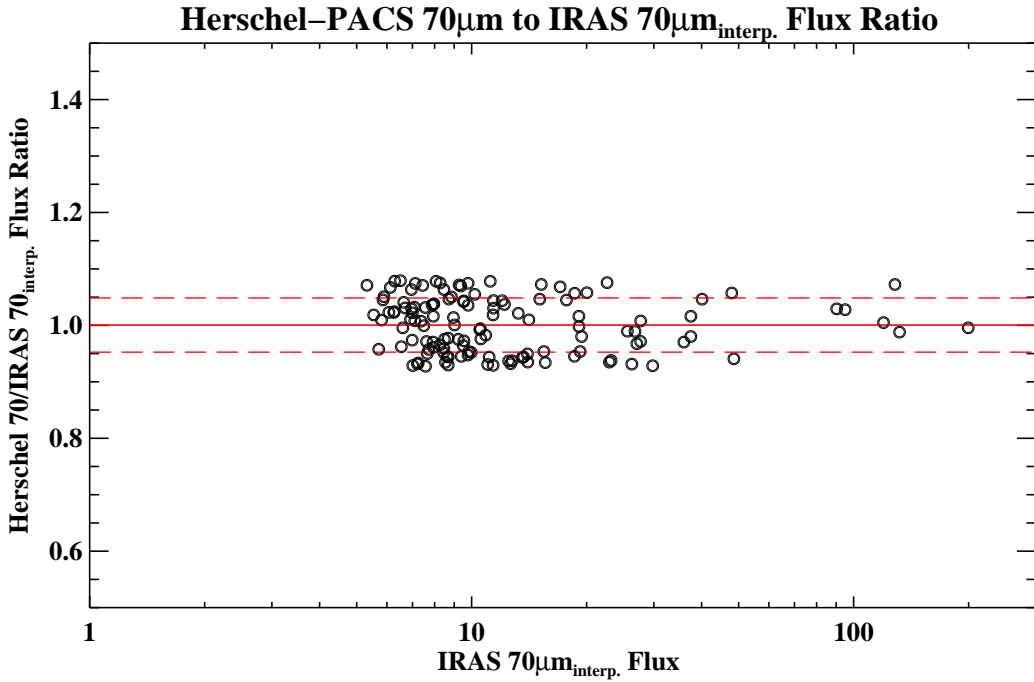
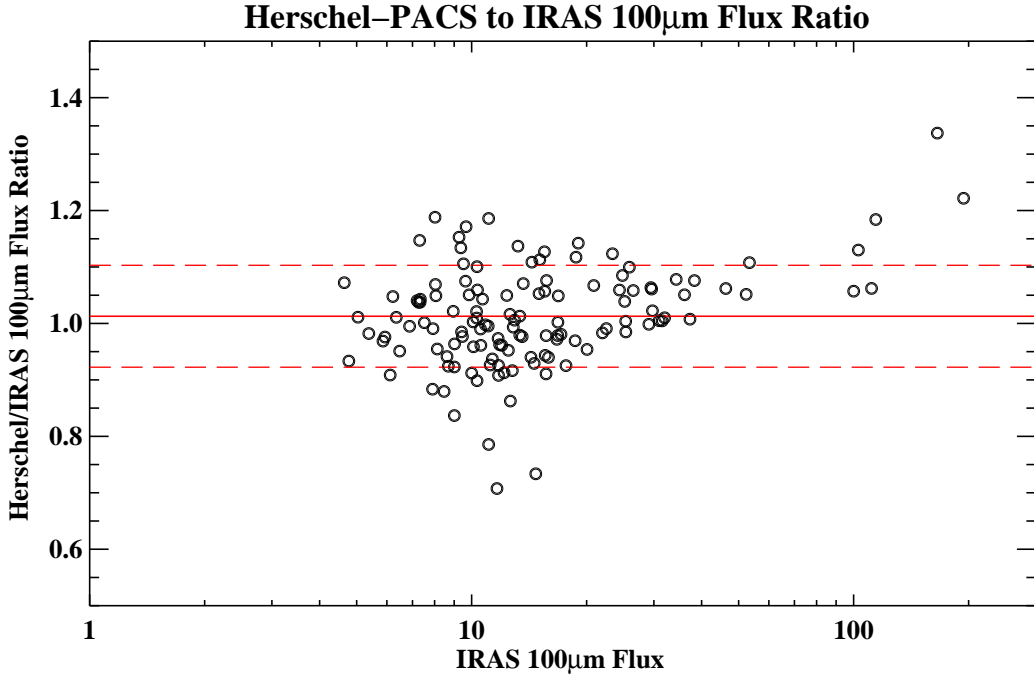


Fig. 7.— *Upper panel:* The *Herschel-PACS* 100 μ m to *IRAS* 100 μ m flux ratio plotted as a function of the *IRAS* 100 μ m flux for 128 of our galaxies carefully chosen to be single objects, or if the system has multiple components they are too close to be distinguishable by PACS at 100 μ m. These galaxies represent the entire spectrum of very extended emission, to point sources as seen by PACS. The mean ratio represented by the red line is 1.012, with the dashed red lines representing the 1- σ scatter of 0.09. The median ratio is 1.006. There appears to be no significant systematic offset, nor is there any evidence of a slope signifying a change in the flux ratio at different *IRAS* 100 μ m flux. Error bars were omitted to keep the plot readable. *Lower panel:* Same as the upper panel but for the *Herschel-PACS* 70 μ m data compared to the interpolated *IRAS* 70 μ m flux. The mean ratio is 1.001 with a 1- σ scatter of 0.04, and a median ratio of 1.00. The agreement between the PACS 70 μ m and interpolated *IRAS* 70 μ m fluxes is excellent.

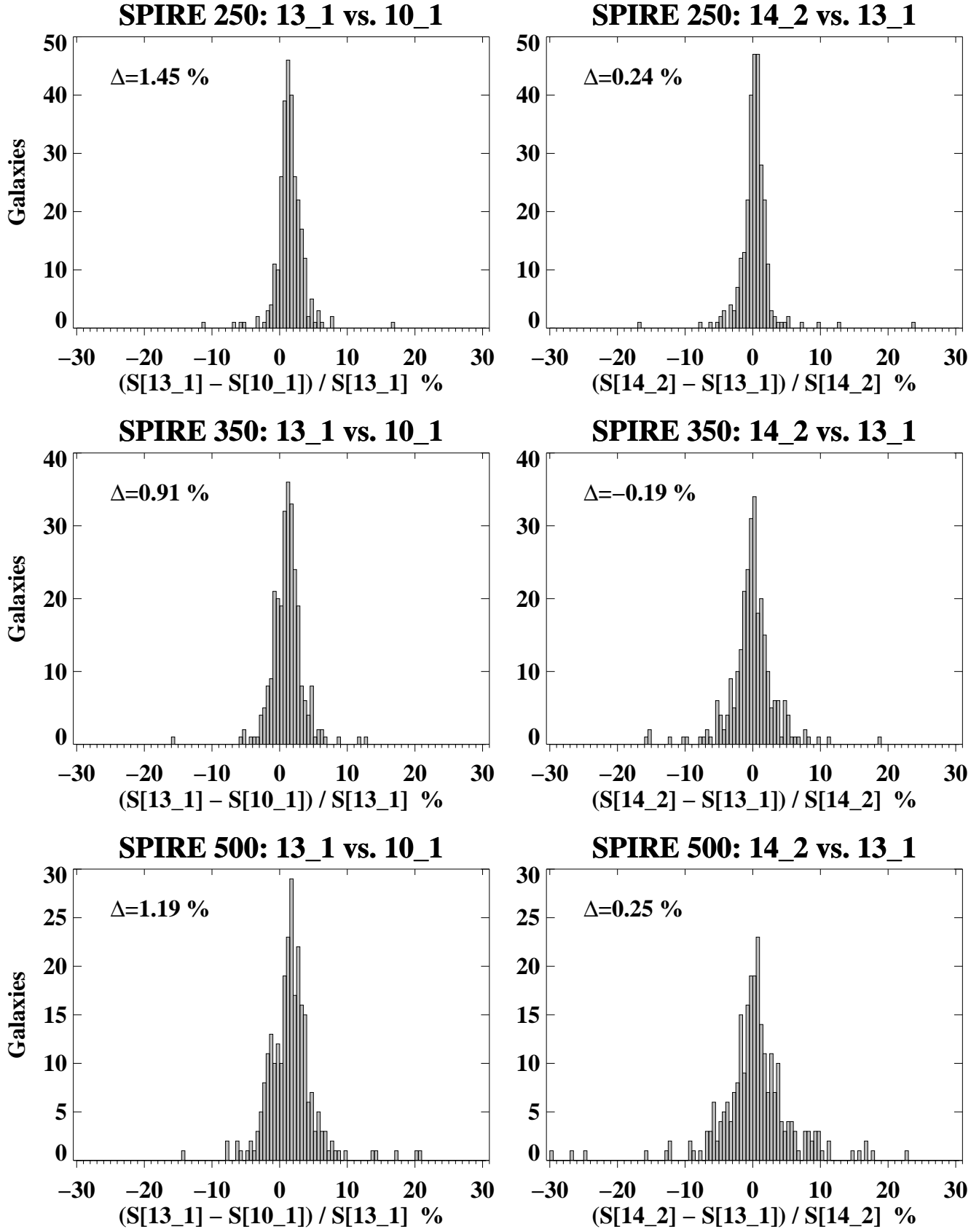


Fig. 8.— Histogram plots comparing the percent change in flux between SPIRECAL_10_1 vs. SPIRECAL_13_1 in the first column, and SPIRECAL_13_1 vs. SPIRECAL_14_2 in the second column. The values in each panel represent the unweighted average percent change between each calibration version.

REFERENCES

- Armus, L., et al. 2009, PASP, 121, 559
- Balog, Z., et al. 2014, Experimental Astronomy, 37, 129
- Barbey, N., Sauvage, M., Starck, J.-L., Ottensamer, R., & Chanial, P. 2011, A&A, 527, A102
- Bendo, G. J., et al. 2013, MNRAS, 433, 3062
- Bertincourt, B., et al. 2016, A&A, 588, A107
- Cantalupo, C. M., Borrill, J. D., Jaffe, A. H., Kisner, T. S., & Stompor, R. 2010, ApJS, 187, 212
- Ciesla, L., et al. 2012, A&A, 543, A161
- Condon, J. J., Helou, G., Sanders, D. B., & Soifer, B. T. 1990, ApJS, 73, 359
- Condon, J. J., Helou, G., Sanders, D. B., & Soifer, B. T. 1996, ApJS, 103, 81
- Díaz-Santos, T., et al. 2013, ApJ, 774, 68
- Díaz-Santos, T., et al. 2014, ApJ, 788, L17
- Dowell, C. D., et al. 2010, in Proc. SPIE, Vol. 7731, Space Telescopes and Instrumentation 2010: Optical, Infrared, and Millimeter Wave, 773136
- Dunne, L., Eales, S., Edmunds, M., Ivison, R., Alexander, P., & Clements, D. L. 2000, MNRAS, 315, 115
- Griffin, M. J., et al. 2010, A&A, 518, L3
- Griffin, M. J., et al. 2013, MNRAS, 434, 992
- Howell, J. H., et al. 2010, ApJ, 715, 572
- Ishida, C. M. 2004, PhD thesis, UNIVERSITY OF HAWAII
- Iwasawa, K., et al. 2011, A&A, 529, A106
- Kim, D., Sanders, D. B., Veilleux, S., Mazzarella, J. M., & Soifer, B. T. 1995, ApJS, 98, 129
- Lu, N., et al. 2014, ApJ, 787, L23
- Lu, N., et al. 2015, ApJ, 802, L11
- Meléndez, M., Mushotzky, R. F., Shimizu, T. T., Barger, A. J., & Cowie, L. L. 2014, ApJ, 794, 152
- Miville-Deschénes, M.-A., & Lagache, G. 2005, ApJS, 157, 302
- Mould, J. R., et al. 2000, ApJ, 528, 655
- Müller, T., et al. 2014, Experimental Astronomy, 37, 253
- Nguyen, H. T., et al. 2010, A&A, 518, L5
- Ott, S. 2010, in Astronomical Society of the Pacific Conference Series, Vol. 434, Astronomical Data Analysis Software and Systems XIX, ed. Y. Mizumoto, K.-I. Morita, & M. Ohishi, 139
- Patanchon, G., et al. 2008, ApJ, 681, 708
- Pearson, C., et al. 2014, Experimental Astronomy, 37, 175
- Piazzo, L., Calzoletti, L., Faustini, F., Pestalozzi, M., Pezzuto, S., Elia, D., di Giorgio, A., & Molinari, S. 2015, MNRAS, 447, 1471
- Pilbratt, G. L., et al. 2010, A&A, 518, L1
- Poglitsch, A., et al. 2010, A&A, 518, L2
- Roussel, H. 2013, PASP, 125, 1126
- Sanders, D. B., Mazzarella, J. M., Kim, D., Surace, J. A., & Soifer, B. T. 2003, AJ, 126, 1607
- Sanders, D. B., Scoville, N. Z., & Soifer, B. T. 1991, ApJ, 370, 158
- Shimizu, T. T., Meléndez, M., Mushotzky, R. F., Koss, M. J., Barger, A. J., & Cowie, L. L. 2016, MNRAS, 456, 3335
- Skrutskie, M. F., et al. 2006, AJ, 131, 1163
- Soifer, B. T., Boehmer, L., Neugebauer, G., & Sanders, D. B. 1989, AJ, 98, 766
- Stierwalt, S., et al. 2013, ApJS, 206, 1
- Zhao, Y., et al. 2013, ApJ, 765, L13
- Zhao, Y., et al. 2016, ApJ, 819, 69